# THE EFFECTS OF ANCILLARY LIGAND PROPERTIES ON THE REACTIONS OF RHODIUM DIPHOSPHINE ALKOXO ALKENE COMPLEXES

BY

CASSEDAY P RICHERS

DISSERTATION

Submitted in partial fulfillment of the requirements
for the degree of Doctor of Philosophy in Chemistry
in the Graduate College of the
University of Illinois at Urbana-Champaign, 2013

Urbana, Illinois

Doctoral Committee:
Professor John F. Hartwig, Chair
Professor Thomas B. Rauchfuss
Professor Gregory S. Girolami
Professor Jeffrey S. Moore

**ABSTRACT**

Rhodium diphosphine alkoxo alkene complexes were synthesized by the addition of unsaturated alcohols to rhodium diphosphine silylamido complexes at -78 °C. The alkoxo alkene complexes were characterized by NMR spectroscopy at 50 °C and allowed to react at either 35 °C or 70 °C. The reactions produced tetrahydrofurans and rhodium hydrido complexes by a mechanism involving alkene insertion into the rhodium alkoxo bond and β-hydrogen elimination. The reactions were monitored by $^{1}H$ NMR spectroscopy, and the rate constants for insertion of the alkene ligand into the alkoxo ligand were determined by fitting the exponential curves to the data. The effects of the ancillary ligand on the rates for alkene insertion were determined by systematically varying the electronic, steric, and bite angle properties of the diphosphine ligand and observing how these changes affect the rates for alkoxo alkene complex decomposition and furan formation. The data show that the properties of the ancillary ligand do affect the rates for alkene insertion into rhodium-alkoxo bonds, and that certain characteristics or properties are desirable for promoting this reaction.

**TABLE OF CONTENTS**


**CHAPTER 1: Metal-Catalyzed Aminations and Alkoxylations of Alkenes ..... 1**

1.1 Introduction ..... 1

1.2 Metal Catalyzed Hydroaminations ..... 1

1.3 Oxidative Aminations ..... 19

1.4 Hydroalkoxylations ..... 28

1.5 Oxidative Alkoxylations ..... 34

1.6 Summary and Objectives ..... 38

**CHAPTER 2: Alkene Insertions into Metal-Amido and -Alkoxo Bonds ..... 42**

2.1 Background ..... 42

2.2 Present Research: The Reactions of Rhodium Diphosphine Amido and Alkoxo Alkene Complexes ..... 67

2.3 Experimental ..... 89

**CHAPTER 3: The Effects of Ancillary Ligand Properties on Metal-Mediated Reactions ..... 116**

3.1 Background ..... 116

3.2 Present Research: The Effects of Ancillary Ligand Properties on the Reactions of Rhodium Diphosphine Alkoxo Alkene Complexes ..... 172

3.3 Experimental ..... 189

3.4 NMR Spectra and Kinetic Data. ..... 234

**CHAPTER 4: The Reactions of Less Electron-Rich Rhodium Alkoxo Alkene Complexes ..... 350**

4.1 Background ..... 350

4.2 Present Research: The Reactions of Rhodium Diphosphonite, Diphosphite, and Bis-Bis(Trifluoromethyl) Phosphino Complexes. ..... 350

4.3 Experimental ..... 360

## CHAPTER 1: Metal-Catalyzed Aminations and Alkoxylations of Alkenes

### 1.1 Introduction

Alkene functionalizations are an important class of reactions. Simple alkenes, such as ethene, propene, butenes, and higher alkyl alkenes are derived from petroleum through cracking reactions, and are used in the production of commodity chemicals. More complex alkenes, such as those used in the production of pharmaceuticals, dyes, and agrochemicals often serve as substrates in carbon-carbon bond-forming reactions and as precursors to carbon stereocenters. Reactions that functionalize alkenes include alkene polymerizations, hydrogenations, hydroformylations, hydrocyanations, Diels Alder and Friedel-Crafts reactions, the alkylations of arenes with alkenes, ammoxidations, oxychlorinations, hydroborations, hydrochlorinations, epoxidations, dihydroxylations, and the Mizoroki-Heck reaction.

While several methods have been developed for the direct conversion of alkenes into alcohols, aldehydes, ketones, epoxides, alkyl halides, alkyl boranes, esters, and alkenes, only a few methods have been developed for the direct conversion of alkenes into amines and ethers. Acid-catalyzed additions of amines and alcohols to alkenes are used in the production of *tert*-butylamine and methyl *tert*-butyl ether, but these reactions require strong acids and suffer from low conversions. Base-catalyzed aminations of alkenes are also known, but these reactions require harsh conditions and are not performed on an industrial scale. Other methods to synthesize alkyl amines and ethers require two or more steps and the intermediacy of alcohols, alkyl halides, nitriles, ketones or aldehydes. These methods include the direct conversion of alcohols to amines via dehydration catalysts, the reductive aminations of aldehydes and ketones, the catalytic reductions of nitriles and nitroalkanes with $H_2$, the reactions of ammonia and amines with alkyl halides in the presence of base, the catalytic dehydration of alcohols to form symmetric ethers, and the additions of alcohols to alkyl halides under basic conditions to form un-symmetric ethers (Williamson Ether Synthesis). In each case, the substrates for these reactions are formed in separate reactions from hydrocarbon feedstocks, and as a result, additional solvents and reagents are required. More direct routes to simple amines and ethers are the direct conversion of hydrocarbon feedstocks to amines and ethers, but these methods are limited to only a few reactions.

This chapter summarizes research on metal-catalyzed aminations and alkoxylations of alkenes. The purpose of this review is to provide a general background on metal-catalyzed aminations and alkoxylations. The material is organized according to transformation. Hydroaminations are presented first, followed by oxidative aminations, hydroalkoxylations, and oxidative alkoxylations. Hydrations and Wacker oxidations are omitted, as are reactions of allenes and alkynes and solvomercurations.

### 1.2 Metal Catalyzed Hydroaminations

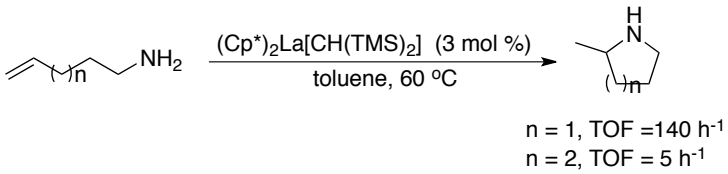
Hydroaminations are the additions of N-H bonds across carbon-carbon multiple bonds. Metal-catalyzed hydroaminations of alkenes have been reported with a variety of metal complexes.[1] The complexes can be organized according to the location of the metal on the Periodic table. Non-transition metal catalysts include lanthanides, actinides and alkaline earth metals. These complexes react primarily through insertion pathways. Early transition metal catalysts include titanium and zirconium complexes. These catalysts react through insertion mechanisms and by [2+2] cycloadditions. Late transition metal catalysts include complexes of ruthenium, iridium,

rhodium, platinum, palladium, nickel, and gold. These complexes react primarily through nucleophilic attacks onto coordinated alkenes, but may also react through an insertion mechanism or by nucleophilic attacks onto $\eta^3$-benzyl and -allyl complexes and $\eta^6$-arene complexes. The present section highlights a few of the metal catalysts that have been reported for the hydroaminations of alkenes and the mechanisms by which the react. The scope of these reactions is limited primarily to amino alkenes, activated alkenes such as norbornene or other strained alkenes and Michael acceptors, or more acidic amine derivatives, such as tosylamides and carboxamides. High barriers for the hydroaminations of alkenes are thought to arise from electron-electron repulsions between the alkene and the lone pair of electrons on the amine nitrogen.

### 1.2.1 Rare Earth Metal-Catalyzed Hydroaminations

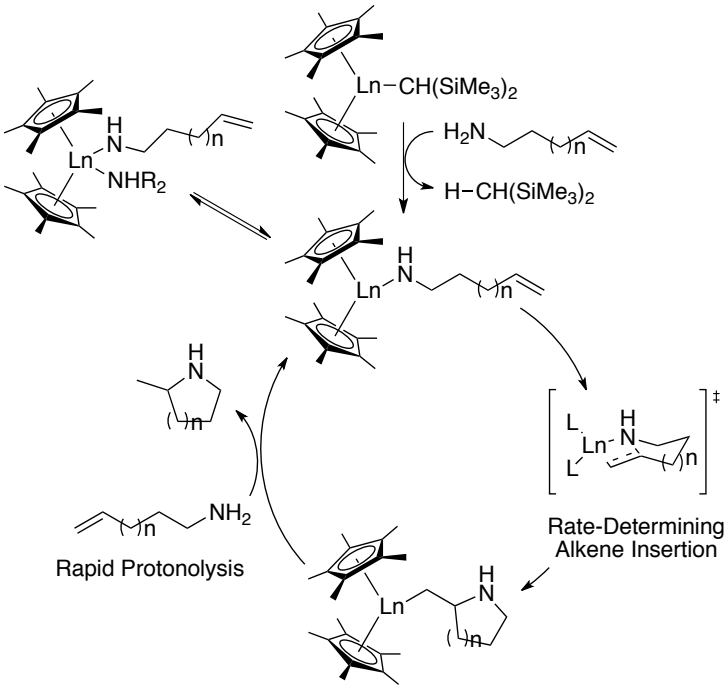
Several groups have reported rare earth metal catalysts for the hydroaminations of alkenes and amino alkenes.[1b] These catalysts are some of the most active for the hydroaminations of alkenes.[1b] Both intra- and intermolecular reactions are reported. Rates are generally higher for intramolecular reactions. Rates are also higher with metals having larger radii and with complexes having less bulky ligands.

Some of the first rare-earth metal catalysts for the hydroaminations of alkenes were reported by Marks and co-workers (Scheme 1).[2]



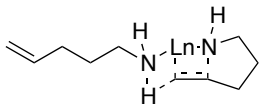

**Scheme 1: A rare earth metal-catalyzed hydroaminations of aminoalkenes. The reaction was originally reported by Marks and co-workers in 1989.**

The mechanisms for these reactions were studied in detail. The rate expressions for the intramolecular hydroaminations of amino alkenes show a first-order dependence on catalyst concentration and a zero-order dependence on aminoalkene concentration.[2,3] The data are consistent with a mechanism involving rapid protonolysis of rare earth metal-alkyl bonds and rate-limiting insertions of alkene into metal-amido bonds (Scheme 2).[2]



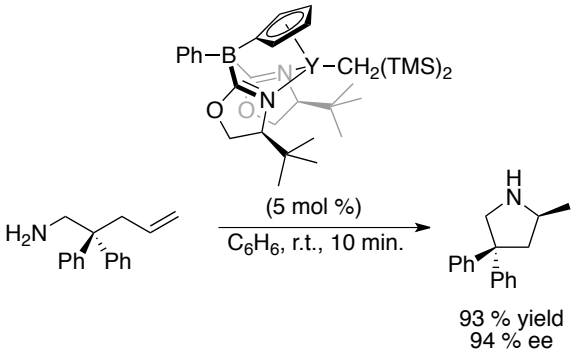

**Scheme 2: The mechanism proposed by Marks and co-workers for the rare earth metal-catalyzed hydroaminations of aminoalkenes with lanthanocenes.**

Reactions with N-deutero amino alkenes show a primary kinetic isotope effect between 2.7 and 5.2. This observation suggests that N-H bond cleavage also occurs during the rate-limiting step. To account for this observation, a transition state for insertion was proposed in which a proton from a second amine is transferred to the alkene in concert with C-N bond formation (Scheme 3).



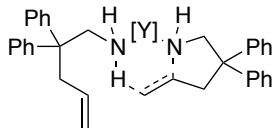

**Scheme 3: Transition state proposed for C-N bond formation in the rare earth metal-catalyzed hydrogaminations of amino alkene developed by Marks and co-workers.**

A different rate-law and mechanism was recently reported by Sadow and co-workers in the case of an yttrium-catalyzed hydroamination of amino alkenes (Scheme 4).[4]




**Scheme 4: An yttrium-catalyzed a intramoledular hydroaminations of amnioalkenes. The reaction was reported by Sadow and co-workers in 2011.**

In this case, a first-order dependence on amino alkene concentration was observed in addition to a first-order dependence on catalyst concentration. Moreover, no products formed when exactly one equivalent of amino alkene was added to the metal catalyst. To account for these observations, a non-insertive mechanism was proposed in which a proton from a second amino alkene is transferred to the alkene in concert with C-N bond formation (Scheme 5).

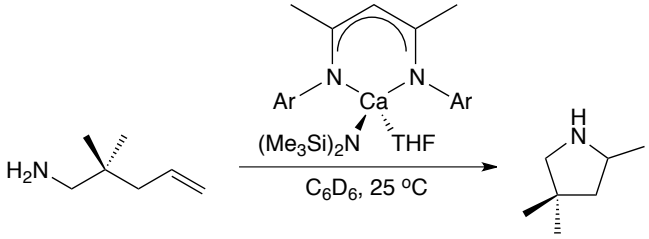



**Scheme 5: The transition state proposed by Sadow and co-workers for C-N and C-H bond formation in a rare earth metal-catalyzed hydroamination of aminoalkenes.**

The difference between this mechanism and the mechanism proposed by Marks and co-workers is subtle. In the mechanism proposed by Marks, the alkene interacts directly with the metal, and in the mechanism proposed by Sadow, the alkene does not.

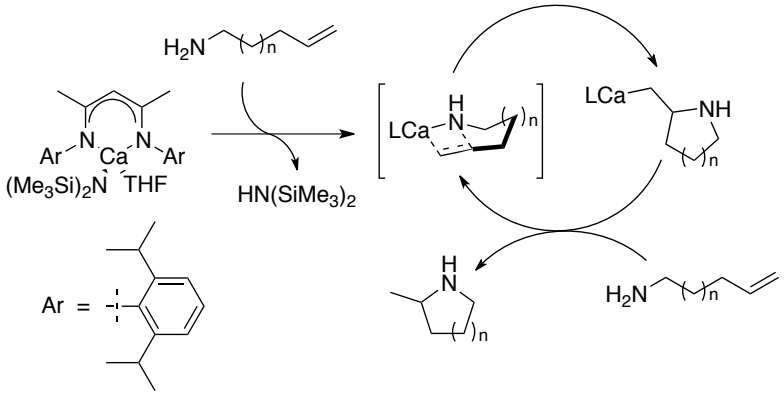
### 1.2.2 Alkaline Earth Metal-Catalyzed Hydroaminations

Alkaline earth metal catalysts for the hydroaminations of amino alkenes were developed by Hill and co-workers (Scheme 6).[5]



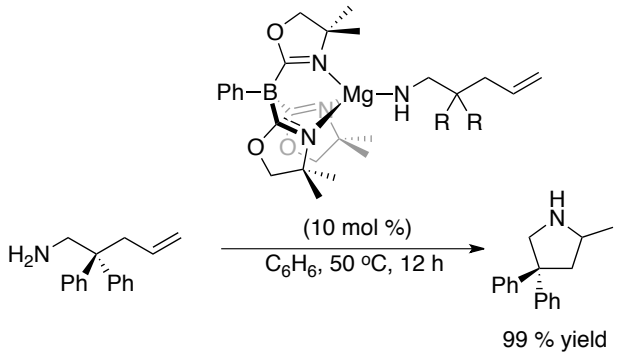

**Scheme 6: A calcium-catalyzed hydroamination of aminoalkenes. The reaction was reported by Hill and co-workers in 2005.**

The reactions show a first-order dependence on catalyst concentration and an inverse order dependence on aminoalkene concentration. A mechanism involving rate-limiting alkene insertion into a metal-amido bond was proposed based upon similarities between this system and the lanthanide catalysts of Marks and co-workers (Scheme 7). These similarities include a lack of d-electrons and a strong preference for a single oxidation state. The inverse dependence on amino alkene concentration was subsequently attributed to a competition between alkene coordination and coordination of a second amino alkene molecule.



**Scheme 7: The mechanism proposed by Hill and co-workers for the calcium-catalyzed hydroaminations of alkenes with Ca(nacnac)[N(SiMe$_3$)$_2$](THF).**

A different mechanism was proposed by Sadow and co-workers in the case of a magnesium-catalyzed hydroamination of amino alkenes (Scheme 8).[6]

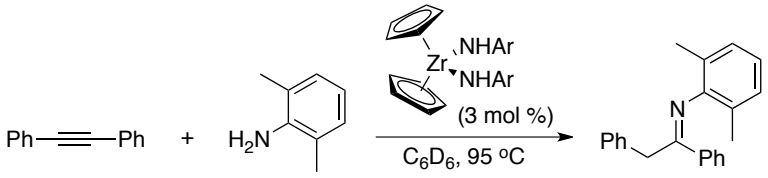


**Scheme 8: A magnesium-catalyzed hydroamination of aminoalkenes. The reaction was reported by Sadow and co-workers in 2010.**

In this case, the rates for amino alkene cyclization show a first-order dependence on both catalyst and amino alkene concentration. A kinetic isotope effect of 4.6 was observed with N-deutero amino alkenes. A mechanism involving "non-insertive" transfer of both an amido group and a proton to the alkene was initially proposed. DFT calculations, however, have shown this mechanism to be less favorable than a mechanism involving alkene insertion into a magnesium amido bond.[7]

### 1.2.3 Group IV Metal-Catalyzed Hydroaminations

Bergman and co-workers developed group IV metal catalysts for the intermolecular hydroaminations of alkynes with primary amines (Scheme 9).[8]

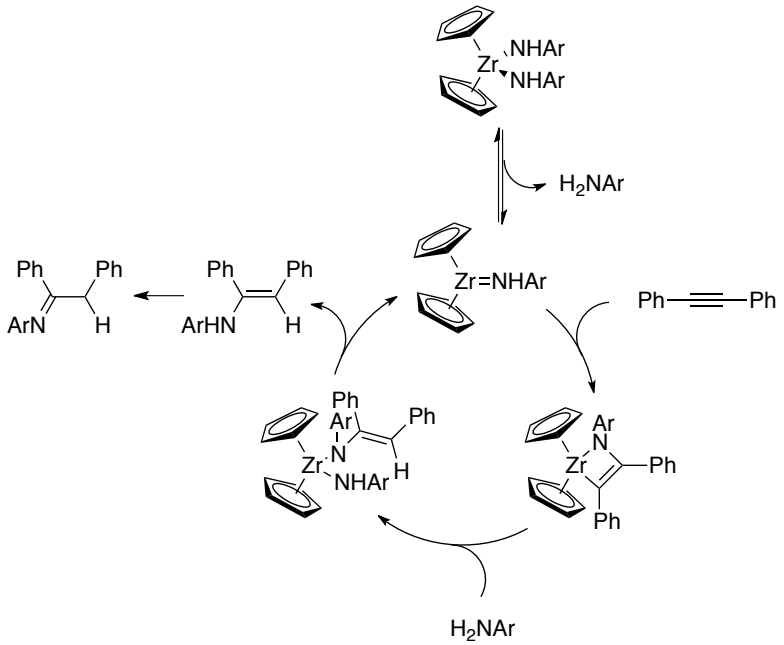


**Scheme 9: A Group IV metal-catalyzed intermolecular hydroaminations of alkynes with anilines. The reaction was originally reported by Bergman and co-workers in 1992.**

The mechanisms for these reactions involve the formation metal imido complexes through the successive deprotonations of the primary amine. These imido complexes proceed to react with alkynes to generate

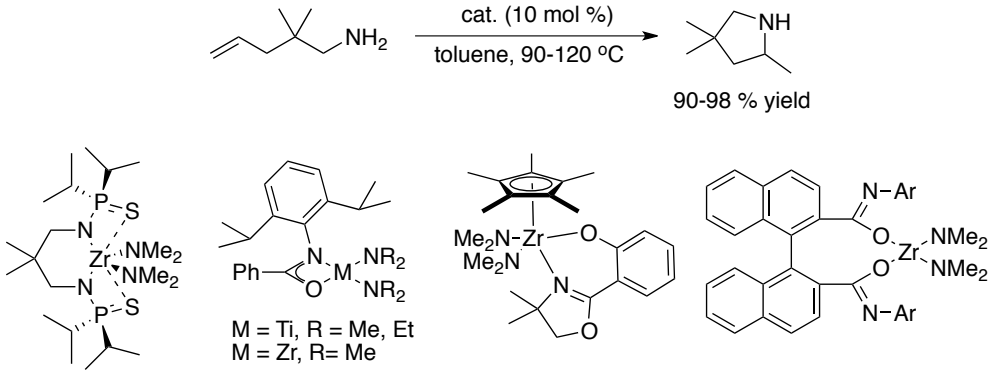
azametallocyclobutene intermediates (Scheme 10). Protonation of this azametallocyclobutene intermediate by a second primary amine molecule forms an amido enamide complex and eventually liberates the enamine.

The rate expressions for these $Cp_2Zr$-catalyzed reactions show a first-order dependence on catalyst concentration, a first-order dependence on alkyne concentration, and an inverse first-order dependence on amine concentration. The rate-limiting step is thought to be protonation of the enamide ligand formed by initial protonation of the metallocyclobutene intermediate. The inhibitive effect of amine concentration was attributed to a non-productive coordination of the amine to the metal catalyst prior to alkyne coordination and insertion. Attempts to realize the intermolecular hydroaminations of alkenes with these catalysts were unsuccessful.



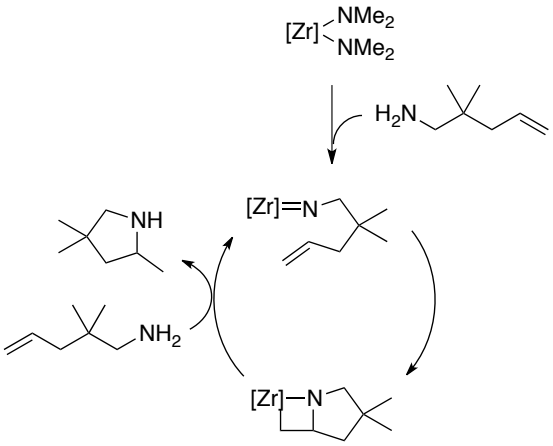

**Scheme 10: The mechanism proposed by Bergman and co-workers for the Group IV metal-catalyzed hydroaminations of alkynes with anilines.**

Intramolecular hydroaminations of primary amino alkenes are reported by the groups of Livinghouse,[9] Schafer,[10] Scott,[11] and Hultzsch (Scheme 11).[12]




**Scheme 11: Group IV metal-catalyzed hydroaminations of amino alkenes. The first reactions were reported by the groups of Livinghouse, Schafer in 2005.**

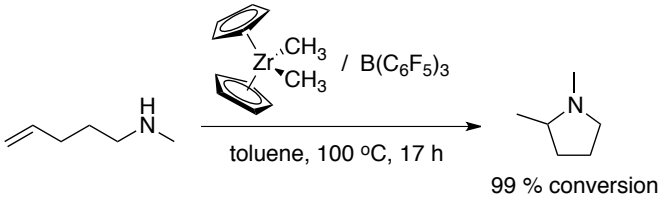
The reactions use neutral Group IV metal catalysts. The mechanisms for these reactions are thought to involve [2+2] cycloadditions (Scheme 12).



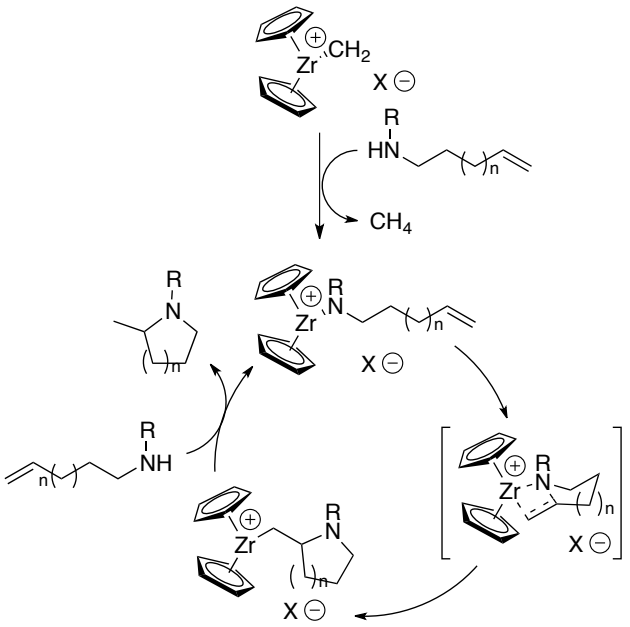

**Scheme 12: The mechanism proposed by the groups of Livinghouse, Schafer, Scott, and Hultzsch for the Group IV metal-catalyzed hydroaminations of aminoslkenes with netural Group IV metal catalysts.**

Indirect support for this mechanism is provided by the fact that secondary amino alkenes do not form hydroamination products. The reactions reported by Schafer and Hultzsch show a first-order dependence on catalyst concentration and a first-order dependence on amino alkene concentration. The data support a mechanism in which protonation of the metallocyclobutane intermediate, formed by [2+2] cycloadditions, is the rate-limiting step. In contrast to these reports, the reactions reported by Scott and co-workers show a first-order dependence on catalyst concentration and a zero-order dependence on amino alkene concentration. In this case, the data support a mechanism in which formation of the imido complex is rate-limiting. The difference between these two rate expressions was attributed, by Scott and co-workers, to the steric properties of the ancillary ligand. Bulkier ligands are thought to favor a mechanism in which the formation of the metal imido complex is rate-limiting.

Cationic Group IV metal catalysts for the intramolecular hydroaminations of secondary amino alkenes were reported by the groups of Scott[13] and Hultzsch (Scheme 13).[14]

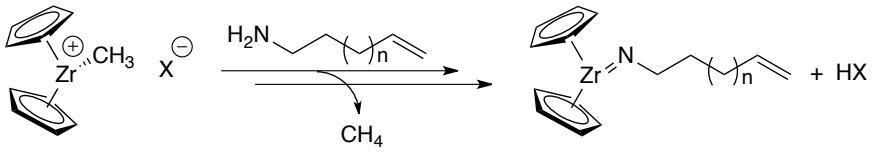



**Scheme 13: Group IV metal-catalyzed hydroaminations of aminoalkenes with cationic catalysts. Separate reactions were reported by the groups of Scott and Hutlzsch in 2004.**



**Scheme 14: The mechanism proposed by the groups of Scott and Hultzsch for the Group IV metal-catalyzed hydroaminations of aminoalkenes using cationic Group IV metal catalysts.**

In this case, the reactions are thought to involve alkene insertions into metal-amido bonds (Scheme 14). Support for this mechanism comes primarily from the fact that secondary amino alkenes, which cannot undergo successive deprotonations to form metal imido complexes, react to form hydroamination products. Interestingly, primary amino alkenes do not form hydroamination products with these catalysts. A possible explanation for this observation is that primary amino alkenes form metal-imido complexes, which are inactive towards hydroamination (Scheme 15), although it is not clear why these metal-imido complexes would be catalytically inactive.

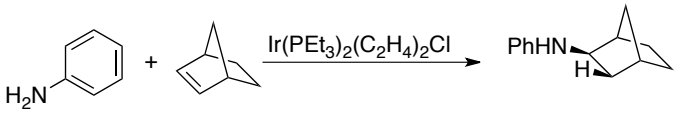


**Scheme 15: The formation of a zirconium imido complex from the reaction of a primary aminoalkene with $[(Cp)_2ZrMe]X$. The formation of catalytically inactive zirconium imido complexes has been proposed for the absence of alkene amination products in the reactions of primary aminoalkenes with cationic zirconium catalysts. It is not clear how the formation of zirconium imido complexes prevent the formation of alkene amination products.**

### 1.2.4 Late Transition Metal-Catalyzed Hydroaminations

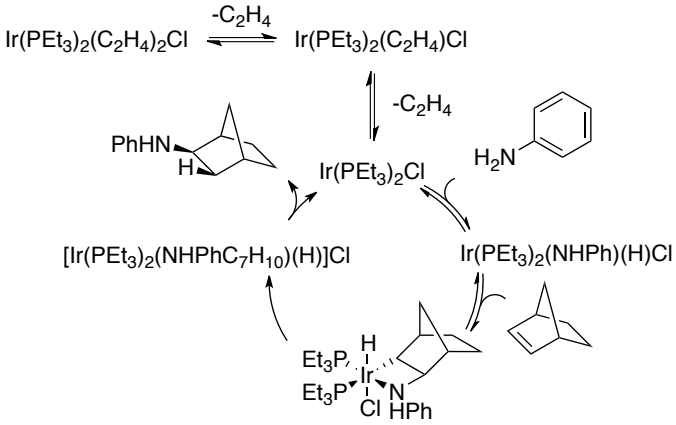
#### 1.2.4.1 Iridium Catalysts

An iridium catalyst for the intermolecular hydroaminations of ethene with secondary amines was reported by Coulson in 1971.[15] No details for this reaction are given. The hydroamination of norbornene with aniline by Ir-based catalysts was subsequently described by Milstein and co-workers (Scheme 16).[16]



**Scheme 16: An iridium-catalyzed intermolecular hydroamintion of norbornene with aniline. The reaction was reported by Milstein and co-workers in 1988.**

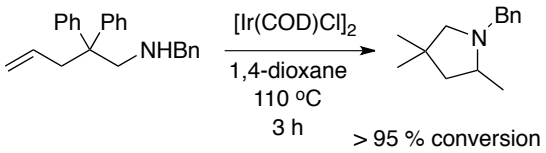
In this case, the mechanism was investigated by a series of stoichiometric reactions. Observations from these reactions are consistent with a mechanism involving N-H oxidative addition of aniline to an unsaturated iridium(I) complex, followed by norbornene insertion, and rate-limiting C-H reductive elimination (Scheme 17).




**Scheme 17: The mechanism proposed by Milstein and co-workers. for the iridium-catlayzed hydroamination norbornene with aniline.**

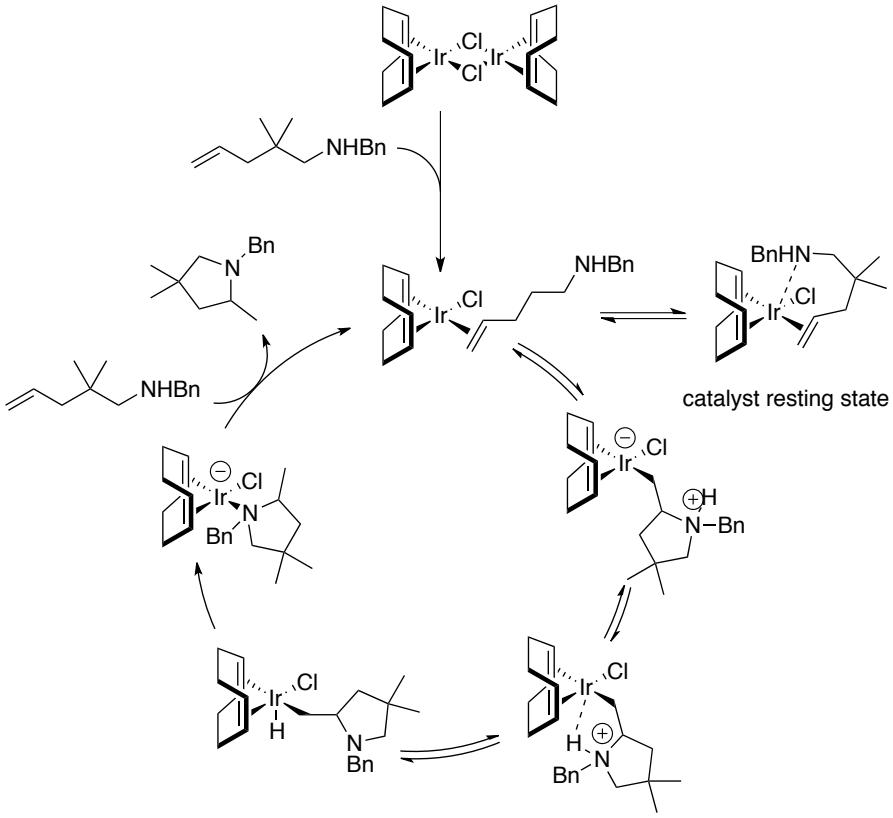
Both N-H oxidative addition and norbornene insertion are reversible under the reaction conditions. The addition of $ZnCl_2$ to the reaction promotes C-H reductive elimination from the iridium(III) norbornyl aniline hydride complex by an unknown mechanism. The overall reaction is unique among metal-catalyzed hydroaminations of alkenes in that it involves N-H oxidative addition of the amine and alkene insertion into a late transition metal-amido bond.

More recently, Stradiotto and co-workers reported an iridium-catalyzed hydroamination of amino alkenes (Scheme 18).[17]




**Scheme 18: An iridium-catalyzed hydroamination of aminoalkenes. The reaction was reported by Stradiotto and co-workers in 2009.**

The reactions show a first-order dependence on catalyst concentration and an inverse first-order dependence on both amino alkene substrate and amine product. A kinetic isotope effect of 3.4 was observed with N-deutero aminoalkene substrates. The data support a mechanism in which alkene coordination to iridium is followed by intramolecular nucleophilic attack and rate-limiting protonolysis (Scheme 19).



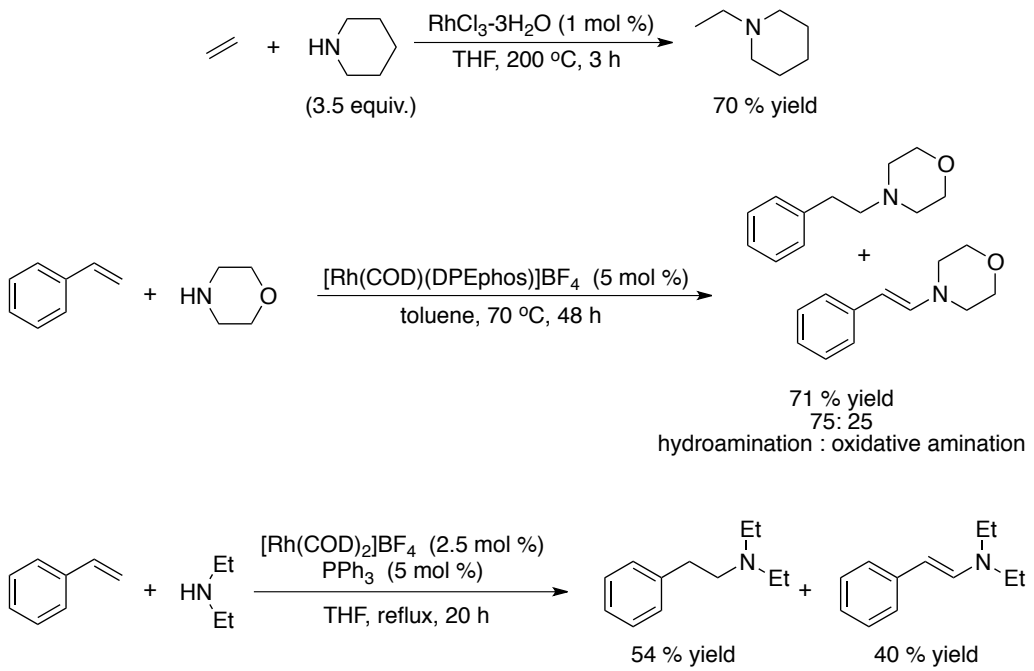

**Scheme 19: The mechanism proposed by Stradiotto and co-workers for the iridium-catalyzed hydroamination of aminoalkenes with $[Ir(COD)Cl]_2$.**

The inhibitory effect of substrate (and product) concentration was attributed to the basicity of these compounds. In this case, the presence of basic compounds is thought to inhibit protonolysis by removing protons from solution. The rate expressions and kinetic isotope effect is similar to what is observed by Michael and co-workers for intramolecular hydroaminations catalyzed by cationic palladium(II) complexes (vide infra).[18]

DFT calculations performed on these reactions suggest that protonolysis occurs by the formation of an iridium(III) hydride complex and subsequent C-H reductive elimination. The calculations also suggest that the inhibitory effects of substrate and product are due to deprotonations of the zwitterionic ammonium complexes formed immediately by nucleophilic attack of the amine onto the coordinated alkene. In this case, deprotonation of the ammonium nitrogen hinders the formation of the iridium (III) hydride complex required for product elimination.

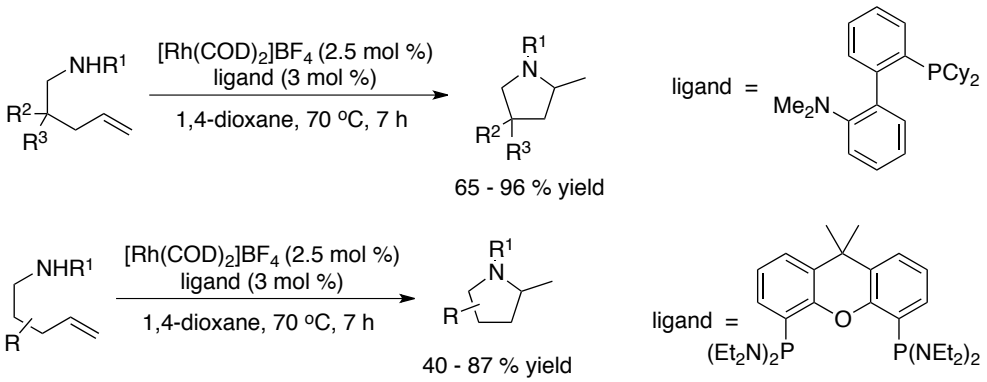
### 1.2.4.2 Rhodium Catalysts

Intermolecular hydroaminations of ethene and vinyl arenes were reported by Coulson[15] and by the groups of Beller[19] and Hartwig[20] (Scheme 20). The mechanisms for these reactions are unclear. The reactions occur with anti-Markovnikov regiochemistry, but are limited to vinyl arenes.



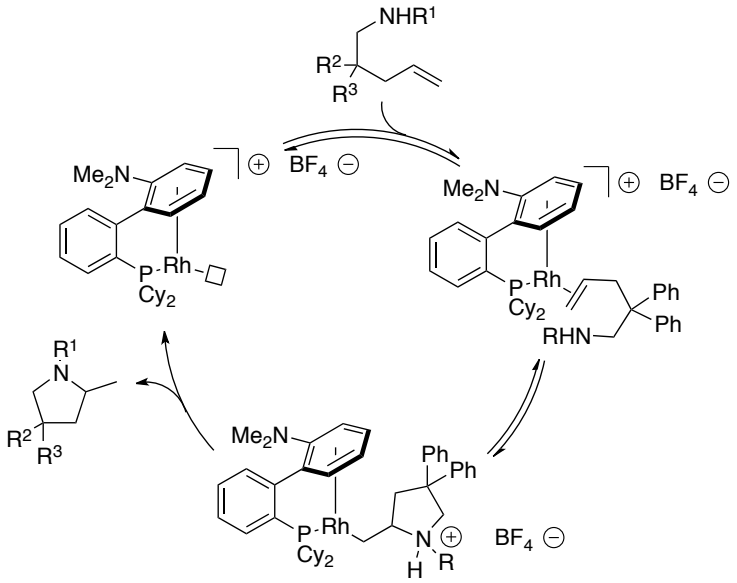

**Scheme 20: Rhodium-catalyzed hydroamintations of ethene and vinyl arenes rerported by the groups of Coulson, Beller, and Hartwig.**

In addition to these catalysts, two separate rhodium catalysts for the intramolecular hydroaminations of primary and secondary amino alkenes (Scheme 21).[21] The catalysts differ by their ancillary ligands.



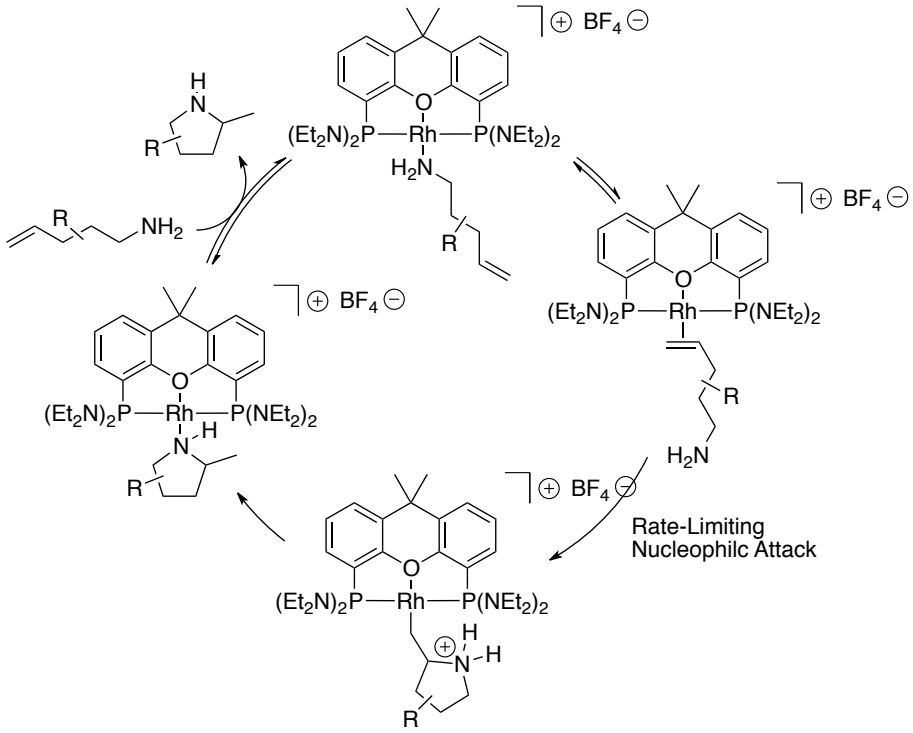

**Scheme 21: Rhodium-catalyzed hydroaminations of aminoalkenes reported by Hartwig and co-workers. The top reaction was reported 2008, while the bottom reaction was reported in 2008 and 2010.**

Reactions preformed with 2-(N,N-dimethylamino)-2'-(dicyclohexylphosphino)-1,1'-biphenyl as the ancillary ligand show a first-order dependence on catalyst concentration and a zero-order dependence on amino alkene concentration.[22] A primary kinetic isotope effect of 2.5 was measured with N-deutero amino alkenes. Moreover, the resting state of the catalyst was identified as a cationic rhodium alkene complex, in the case of secondary amino alkenes and as a cationic rhodium amino alkene complex in the case of primary amino alkenes. The data are consistent with a mechanism involving alkene coordination to rhodium, followed by reversible nucleophilic attack and rate-limiting protonolysis of the rhodium-carbon bond (Scheme 22).




**Scheme 22: The mechanism proposed by Hartwig and co-workers for the rhodium-catalyzed hydroaminations of aminoalkenes with rhodium 2-(N,N-dimethylamino)-2'-(dicyclohexylphosphino)-1,1'-biphenyl..**

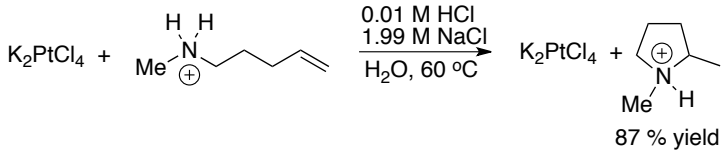
The stereochemistry of amine addition was investigated using a N-deutero cyclohexenyl amine. The stereochemistry of the resulting product is consistent with an *anti*-addition pathway for aminometallation. This mechanism is similar to those proposed for platinum, palladium, and iridium complexes. Reactions performed with the 9,9-dimethyl-4,5-bis[bis(diethylamino)phosphino]xanthene as the ancillary ligand show a kinetic isotope effect of 1.16 with N-deutero amino alkenes and cationic rhodium amine and alkene resting states.[23] The data suggest a mechanism in which nucleophilic attack onto a coordinated alkene is rate-limiting (Scheme 23).




**Scheme 23: The mechanism proposed by Hartwig and co-workers for the rhodium-catalyzed hydroaminations of aminoalkenes with rhodium 9,9-dimethyl-4,5-bis[bis(diethylamino)phosphino]xanthene.**

### 1.2.4.3 Platinum Catalysts

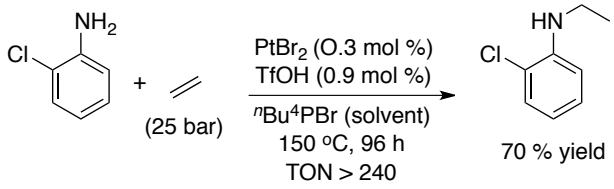
A platinum-mediated hydroamination of amino alkenes was reported by Venanzi and co-workers in 1978 (Scheme 24).[24]




**Scheme 24: A platinum-catalyzed intramolecular hydroaminstion of aminoalkenes under acidic aqeuous conditions. The reaction was reported by Venanzi and co-workers in 1978.**

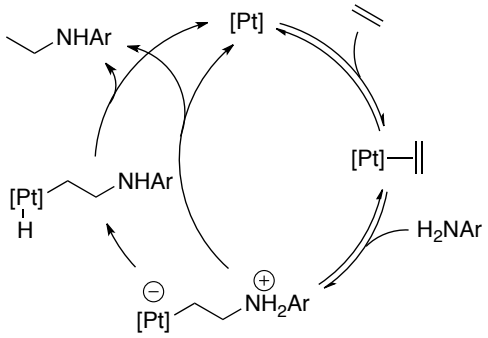
The reactions occur in aqueous solutions under acidic conditions. Although catalytic reactions were not reported, the platinum salts used in these reactions could be recovered at the end of the reaction. A mechanism involving alkene coordination and nucleophilic attack was proposed based on stoichiometric reactions that demonstrated each step.[25]

A platinum-catalyzed hydroaminations of ethene and hexene was reported by Brunet and co-workers in 2005 (Scheme 25).[26]



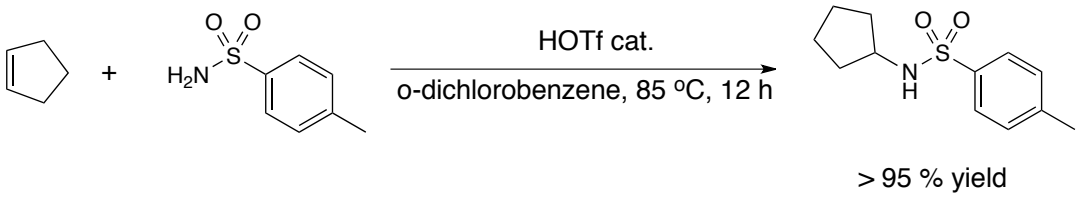

**Scheme 25: A platinum-catalyzed hydroamination of ethene with aniline. The reaction was developed by Brunet and co-workers in 2005.**

A mechanism involving nucleophilic attack onto a coordinated alkene was proposed (Scheme 26). In this case, both alkene coordination to the metal complex, and nucleophilic attack onto the coordinated alkene are thought to be reversible, and protonolysis of the platinum-carbon bonds is considered to be the rate-limiting step. The reactions are inhibited by N-ethyl aniline and added $PEt_3$ and promoted by triflic acid.



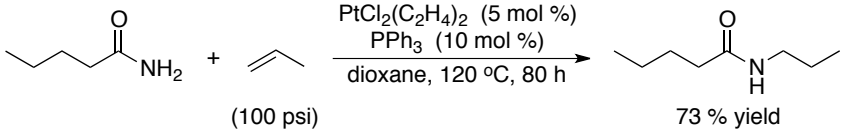

**Scheme 26: The mechanism proposed by Brunet and co-workers for the platinum-catalyzed hydroamination of ethene with anilines.**

Tilley and co-workers reported a platinum complex for the intermolecular hydroamination of simple alkenes using aryl sulfonamides (Scheme 27).[27] Further investigations into this system, however, revealed that actual catalyst is triflic acid generated in situ.



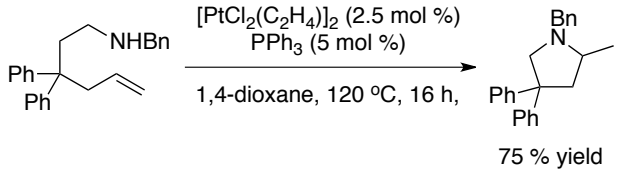

**Scheme 27: A platinum-catalyzed intermolecular hydroamination of simple alkenes with sulfonamides.**

Widenhoefer reported intermolecular hydroaminations of ethene and propene with carboxamides and carbamates and co-workers (Scheme 28).[28]

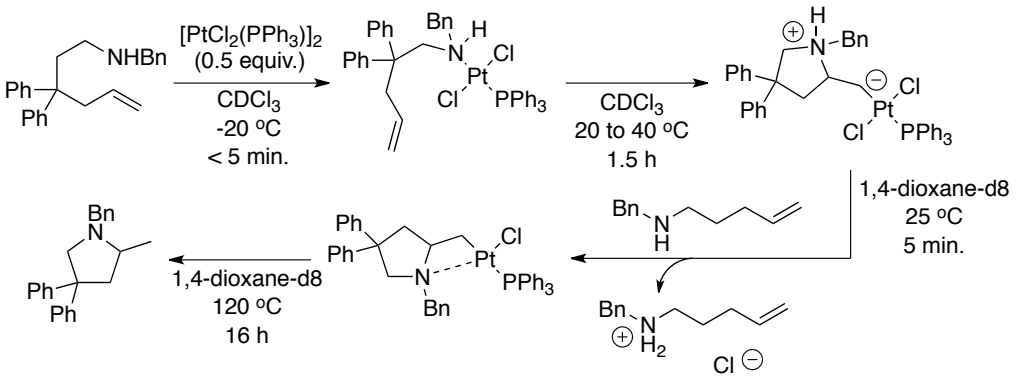



**Scheme 28: A platinum-catalyzed intermolecular hydroamination of ethene and propene with carboxamides and carbamates.**

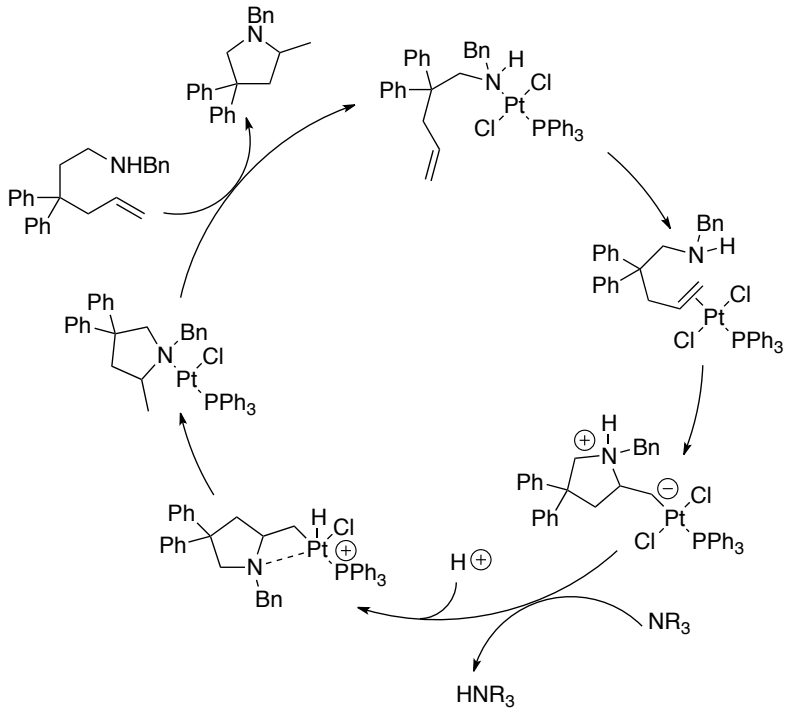
The same catalyst was also reported for the intramolecular hydroaminations of secondary amino alkenes (Scheme 29).[29] In this case, the mechanism was investigated by a series of stoichiometric reactions (Scheme 30). The results suggest a mechanism involving nucleophilic attack onto a coordinated alkene, but do not reveal the rate-limiting step (Scheme 31).




**Scheme 29: A platinum-catalyzed hydroamination of aminoalkenes using $[PtCl_2(C_2H_4)]_2$ / $PPh_3$ as catalyst. The reaction was reported by Widenhoefer and co-workers in 2005.**



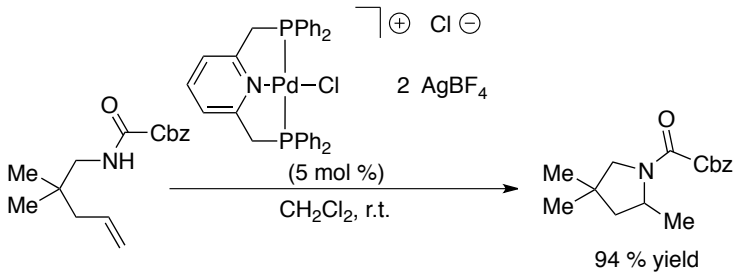

**Scheme 30: The sotichiometric hydroamiatnion of aminoalkenes with $[PtCl_2(PPh_3)]_2$**




**Scheme 31: The mechanism proposed by Widenhoefer for the platinum-catalyzed hydroamination of aminoalkenes with $PtCl_2(C_2H_4)_2$ / $PPh_3$ as catalyst.**

### 1.2.4.4 Palladium Catalysts

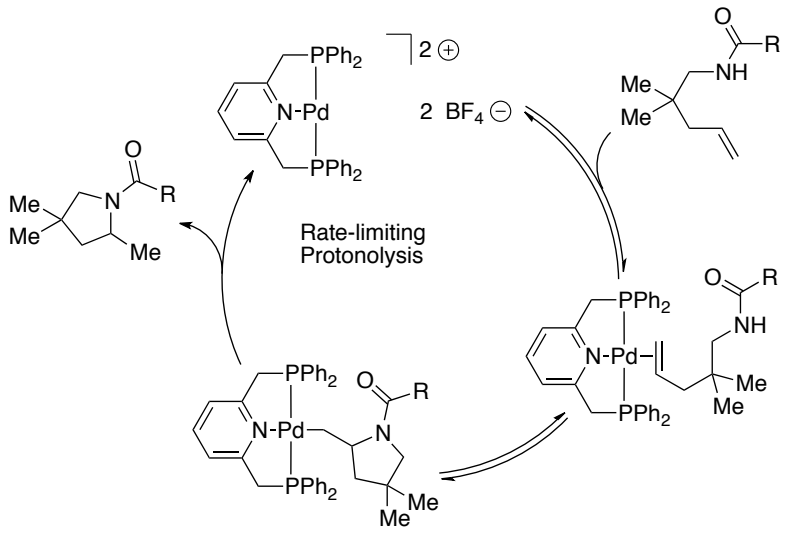
A palladium catalyst for the intramolecular hydroaminations of amino alkenes was reported by Michael and co-workers (Scheme 32).[18]




**Scheme 32: A palladium-catalyzed hydroaminaion of aminoalkenes with PNP pincer catalysts. The reaction was reported by Michael and co-workers in 2008.**

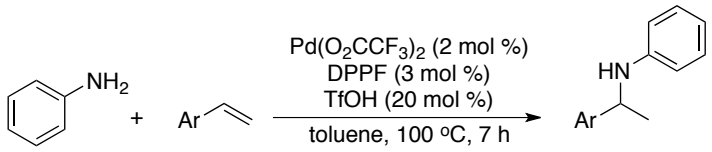
The reactions are unusual in the sense that most palladium-catalyzed additions of amines to alkenes result in the formation of oxidative products. In this case, the lack of oxidative was attributed to the PNP-pincer ancillary ligand, which was shown to stabilize palladium alkyl complexes from β-hydride elimination.[18] The reactions occur at room temperature in $CH_2Cl_2$ solvents. Coordinating solvents completely inhibit the reaction. Electron-withdrawing groups (CBz, Boc, toluoyl) on nitrogen are required for cyclization to occur, however, gem-disubstitution on the amino alkene substrate is not. Only terminal alkenes are reported.

Mechanistic studies on these reactions revealed a first-order dependence on catalyst concentration and an inverse first-order dependence on amino alkene concentration. The resting state of the catalyst was identified as a palladium alkyl complex formed by aminopalladation of the alkene. Aminopalladation was shown to be reversible. The data are consistent with a mechanism in which alkene coordination and reversible nucleophilic attack precede rate-limiting protonolysis of the palladium-carbon bond (Scheme 33). The inhibitory effect of substrate (and product) concentration was attributed to the basicity of these reagents. In this case, the removal of protons from the reaction solution reduces the rate of protonolysis, which determines the overall rate of reaction. Stradiotto and co-workers observed a similar effect for an iridium-catalyzed hydroamination of amino alkenes (vide supra).



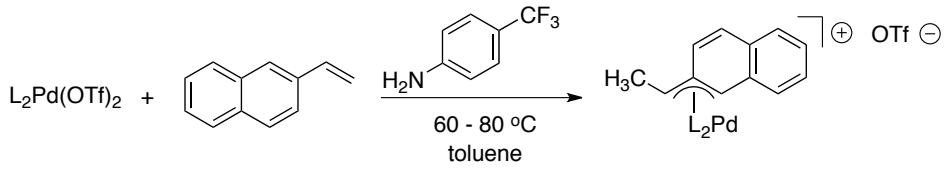

**Scheme 33: The mechanism proposeed by Michael and co-workers for the palladium-catalyzed hydroamination of aminoalkenes with cationic PNP-pincer palladium catalysts.**

Palladium-catalysts for the hydroaminations of 1,3-dienes and vinylarenes with arylamines were reported Hartwig and co-workers (Scheme 34).[30]



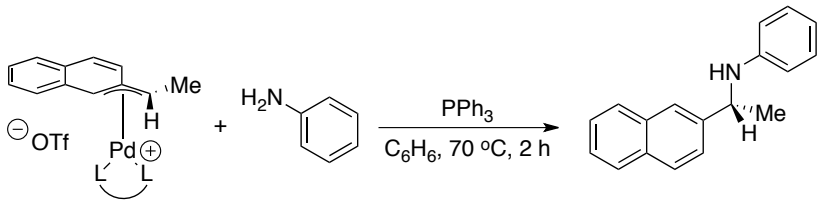

**Scheme 34: A palladium-catalyzed hydroamination of vinylarenes with anilines. The reaction was reported by Hartwig and co-workers in 2001.**

In this case, the reactions occur by nucleophilic attacks onto $\eta^3$-benzyl and $\eta^3$-allyl complexes. The mechanism for these reactions was established by a series of NMR experiments and stoichiometric reactions. During the course of these studies, an $\eta^3$-benzyl complex, {Pd[(*R*)-Tol-(BINAP)][1-(2-napthyl)-ethyl]}(OTf), was observed and isolated from the reaction of vinylnaphthalene with aniline (Scheme 35). [31]



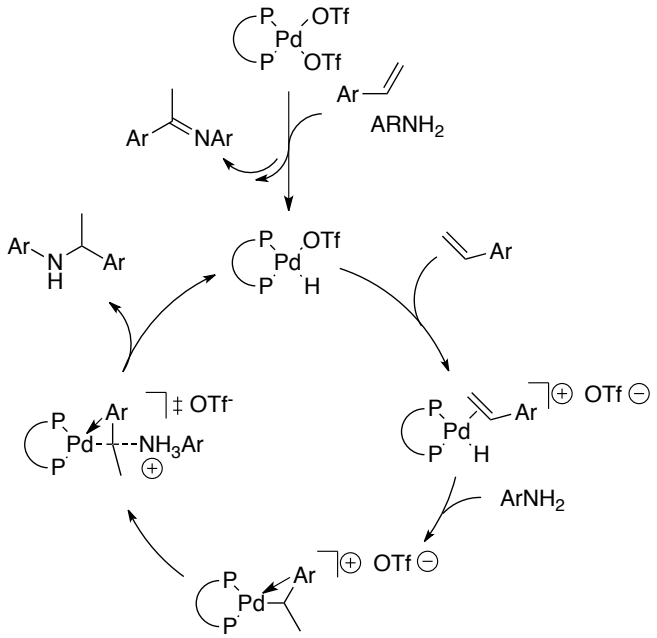

**Scheme 35: The reaction of vinylnaphthalene with aniline in the presence of {Pd[(*R*)-Tol-(BINAP)]}(OTf)$_2$**

This complex reacts with excess aniline to form *N*-(1-naphthyl)ethylaniline (Scheme 36).




**Scheme 36: The reaction of aniline with , {Pd[(*R*)-Tol-(BINAP)][1-(2-napthyl)-ethyl]}(OTf).**

To show that the formation *N*-(1-naphthyl)ethylaniline occurs by direct addition of aniline to an $\eta^3$-benzyl complex and not by extrusion of alkene to form the active catalysts, stoichiometric reactions were performed on isolated $\eta^3$-benzyl complexes. The data support a mechanism in which the formation of an $\eta^3$-benzyl complex is followed by rate-limiting nucleophilic attack (Scheme 37).

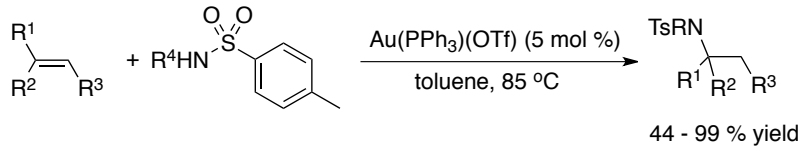


**Scheme 37: The mechanism proposed for the hydroamination of vinyl arenes with aniline using {Pd[(*R*)-Tol-(BINAP)]}$(OTf)_2$ as catalyst.**

Similar mechanisms are proposed for the hydroaminations of 1,3-dienes and vinyl arenes catalyzed by nickel complexes.[32]

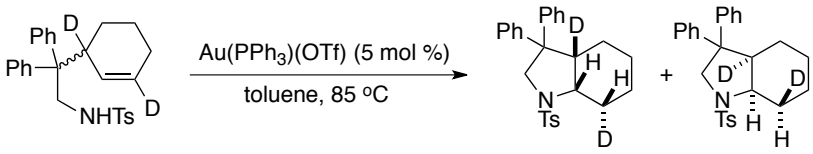
### 1.2.4.5 Gold Catalysts

Gold-catalyzed hydroaminations are reported by He and co-workers (Scheme 38).[33]



**Scheme 38: A gold-catalyzed hydroamination of alkenes with sulfonamides. The reaction was reported by He and co-workers in 2006.**

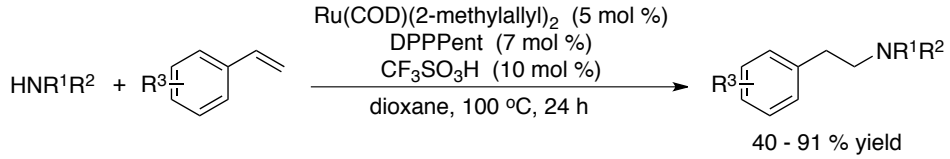
In this case, the reactions are thought to involve nucleophilic attacks onto coordinated alkenes, but there is little evidence to support this mechanism. Reactions with N-deutero cyclohexenyl amines, show that nitrogen and hydrogen add to different faces of the alkene (Scheme 39), but do not show the involvement of the metal complex in the reactions. It is possible that the reaction is catalyzed by trace amounts of acid generated in solution.[34]



**Scheme 39: The stereochemistry of C-N and C-H bond formation in the gold-catalyzed hydroaminations of aminoalkenes developed by He and co-workers.**

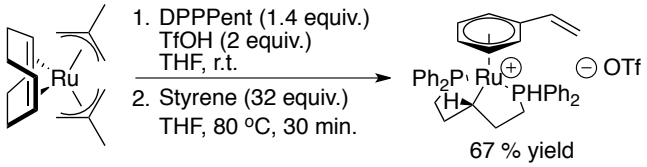
### 1.2.4.6 Ruthenium Catalysts

Ruthenium-catalyzed anti-Markovnikov hydroaminations of styrenes were reported by Hartwig and co-workers (Scheme 40).[35]

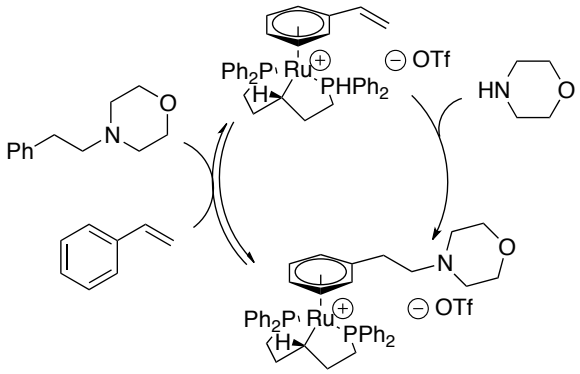



**Scheme 40: A ruthenium-catalyzed anti-Markovnikov hydroamination of vinylarenes with Rh(COD)(2-methylallyl)$_2$ / DPPPent as catalyst. Harwtig and co-workers reported the reaction in 2004.**

The mechanisms for these reactions were investigated by a series of NMR experiments. Ruthenium arene complexes were identified as the major ruthenium species in solution (Scheme 41). This observation, along with the rates for arene exchange at ruthenium, support a mechanism in which nucleophilic attack occurs at the terminal alkenyl position of a $\eta^6$-bound styrene (Scheme 42). So far, this mechanism remains unique among reported hydroaminations.




**Scheme 41: An independent synthesis of the $\eta^6$-arene complex observed by Hartwig and co-workers in the ruthenium-catalyzed anti-Markovnikov hydroaminaiton of vinylarenes with amines.**




**Scheme 42: The mechanism proposed by Hartwig and co-workers for the ruthenium-catalyzed anti-Markovnikov hydroaminations of vinylarenes.**

## 1.3 Oxidative Aminations

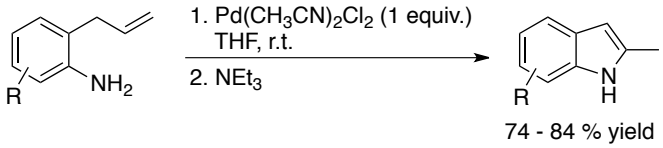
Oxidative aminations are the additions of amines to alkenes (or other substrates) with the formal loss of $H_2$ from the combined substrates. Nearly all of the catalysts reported for these reactions are palladium(II) complexes. The mechanisms for these reactions involve aminopalladations of the alkene substrates followed by β-hydride elimination from the resulting palladium(II) alkyl complexes. The palladium hydrides generated by this sequence of steps can eliminate acids to form palladium(0), which is inactive towards oxidative aminations. AS a result, oxidants or hydrogen acceptors have to be added to the reactions to induce catalyst turnover. Common oxidants include copper(II) salts, benzoquinone, and $O_2$. Like metal-catalyzed hydroaminations, the substrate scope for oxidative aminations is limited primarily amino alkenes, activated alkenes, and more-acidic amine derivatives, such as tosylamides and phthalimide. The present section summarizes a few examples of the metal-catalyzed oxidative aminations of alkenes along with their mechanisms, where available. Particular emphasis is placed on reactions that

reveal the stereochemistry of the aminometallation step. Both *anti* and *syn* additions have been observed. The mechanism by which the amine adds to the alkene has been the subject of several investigations. Early studies suggested that an *anti* addition pathway occurred in most cases. More recent studies have shown that both *anti* and *syn* additions can occur and that a *syn* addition pathway dominates in many cases. Moreover, the mechanism depends on the catalyst, substrate, and reaction conditions.

### 1.3.1 Intramolecular Reactions

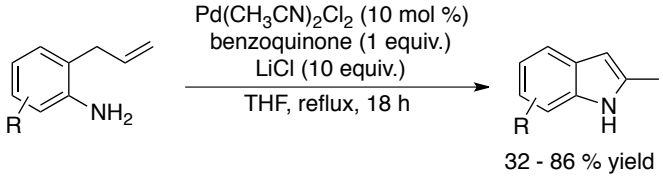
#### 1.3.1.1 Oxidative Aminations of 2-Allylanilines

Intramolecular oxidative aminations of 2-allylaniline were reported by Hegedus and co-workers in 1976 (Scheme 43).[36] The reactions use stoichiometric amounts of $Pd(CH_3CN)_2Cl_2$. The procedure requires two steps. In the first step, 2-allylaniline is added to the palladium(II) salt. In the second step, triethylamine is added to the reaction to liberate the 2-methylindole products. The precise mechanism for this transformation is unclear. Nucleophilic attack onto a coordinated alkene was proposed based on prior precedent of this reaction, but the mechanism was not investigated. The reactions are performed in the absence of any additives, such as LiCl.



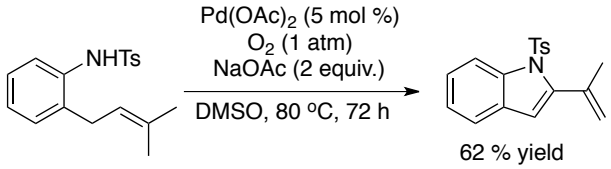

**Scheme 43: A stoichiometric intramolecular oxidative amination of 2-allylanilines with $Pd(CH_3CN)_2Cl_2$. Hegedus and co-workers reported the reaction in 1976.**

Two years later, a catalytic oxidative amination of 2-allylaniline was reported (Scheme 44).[37] In this case, catalyst turnover was achieved by the addition of either benzoquinone or $CuCl_2$ to the reaction. While both oxidants provided moderate to good yields of 2-methylindoles, $CuCl_2$ impeded product work-up. Consequently, benzoquinone was used preferentially. The reactions are carried out in the presence of 10 equivalents of LiCl. The mechanism for these reactions is assumed to involve nucleophilic attacks onto coordinated alkenes, but was not investigated.



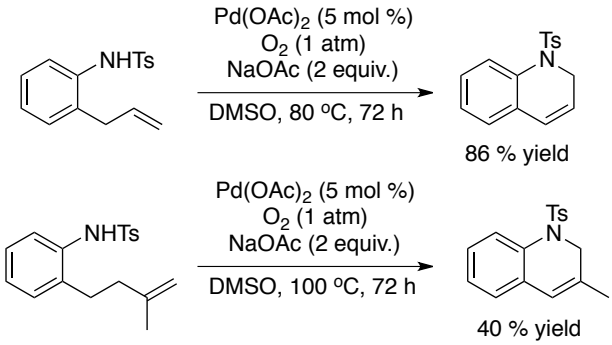

**Scheme 44: A palladium-catalyzed intramolecular oxidative amination of 2-allylanilines using $Pd(CH_3CN)_2Cl_2$ as the catalyst and benzoquinone as the oxidant. The reaction was reported by Hegedus and co-workers in 1978.**

In 1996, Larock and co-workers reported oxidative aminations of 2-allylanilines using $O_2$ as the oxidant (Scheme 45). The reactions occur with moderate to good yield. The same reaction conditions were used by Larock and co-workers for the intramolecular oxidative lactonization of unsaturated carboxylic acids and for the intramolecular oxidative aminations of unsaturated tosylamides (vide infra).




**Scheme 45: A palladium-catalyzed intramolecular oxidative amination of *N*-sulfonyl-2-allylanilines with $O_2$ as the oxidant. $Pd(OAc)_2$ was employed as the catalyst. Larock and co-workers reported the reactions in 1996.**

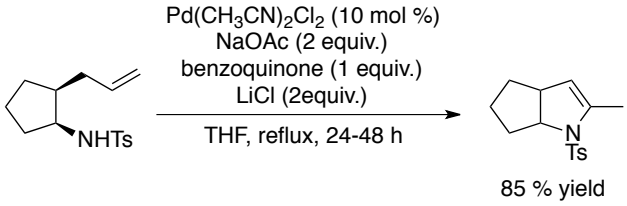
In several cases, the reactions occur with anti-Markovnikov regioselectivity (Scheme 46). To account for this regiochemistry, the authors proposed the formation of π-allyl intermediates, but did not investigate this possibility further.




**Scheme 46: A palladium-catalyzed anti-Markovnikov hydroamination of *N*-sulfonyl-2-allylanilines with $O_2$ as the oxidant and $Pd(OAc)_2$ as the catalyst. Larock and co-workers reported the reactions in 1996.**

### 1.3.1.2 Oxidative Aminations of Unsaturated Tosylamides

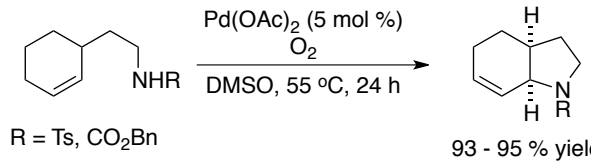
In 1982, Hegedus and co-workers reported palladium-catalyzed intramolecular oxidative aminations of unsaturated tosylamides using the same catalyst system used for the oxidative aminations of 2-allylanilnes (Scheme 47).[38]




**Scheme 47: A palladium-catalyzed intranolecular hydroamination of *N*-sulfonyl aminoalkenes with $Pd(CH_3CN)_2Cl_2$ as catalyst and benzoquinone as oxidant.. The reaction was reported by Hegedus and co-workers in 1982.**

The authors note that oxidative aminations of the analogous unsaturated amines do not occur under these conditions. The lack of amination products, in this latter case, was attributed to the increased basicities of the amines relative to their tosylamides. More basic amines are thought to result in unproductive coordination of the metal complex. This hypothesis, however, was not investigated further.

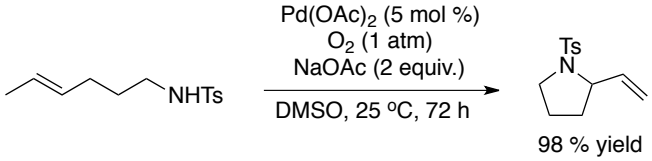
In 1995, Andersson and co-workers reported intramolecular oxidative aminations of unsaturated carboxamides and sulfonamides using $O_2$ as the oxidant (Scheme 48).[39]




**Scheme 48: A palladium intranolecular hydroamination of *N*-sulfonyl aminoalkenes with $Pd(CH_3CN)_2Cl_2$ as catalyst and benzoquinone as oxidant. The reaction was reported by Andersson and co-workers in 1995.**

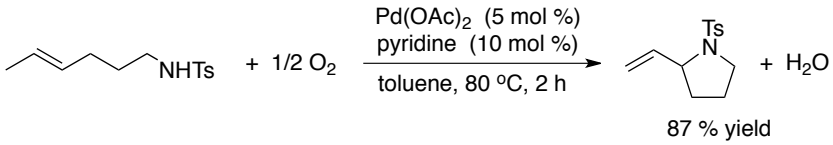
The reactions were performed in DMSO in the absence of other additives. Although the yields of pyrrole products are good, only two reactions were reported.

In 1996, Larock and co-workers published intramolecular oxidative aminations of unsaturated tosylamides using a slightly different catalysts system (Scheme 49).[40] In this case, 2 equivalents of NaOAc are added to the reaction. The same conditions were used for the intramolecular oxidative aminations of 2-allylanilines (vide supra) and for the intramolecular oxidative lactonization of unsaturated carboxylic acids. The reaction conditions were not re-screened for this reaction.




**Scheme 49: A palladium-catalyzed intramolecular hydroamination of *N*-sulfonyl alkylamines with $O_2$ as the oxidant and $Pd(OAc)_2$ as the catalysts. The reaction was reported by Larock and co-workers in 1996.**

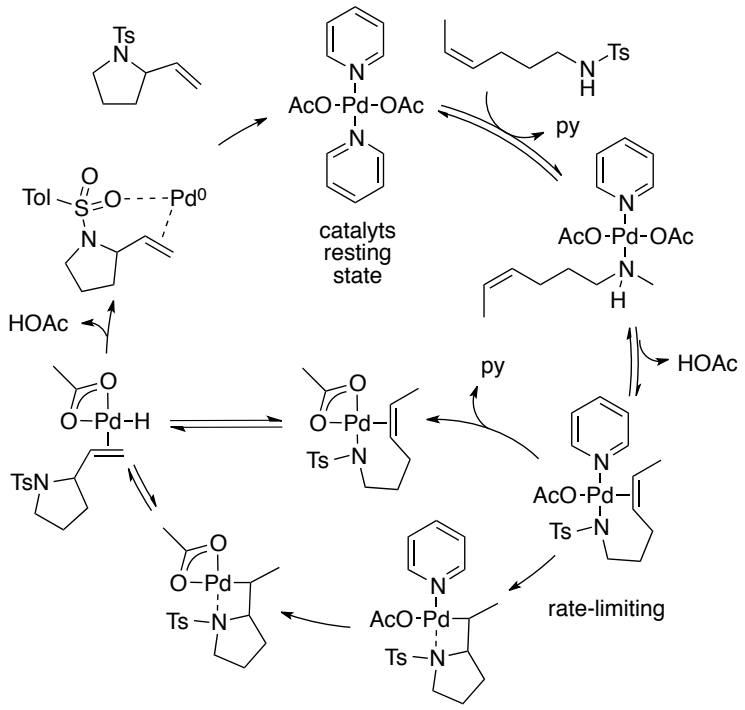
In 2004, Stahl and co-workers reported palladium-catalyzed intramolecular oxidative aminations of unsaturated tosylamides using a mixture of $Pd(OAc)_2$ and pyridine as catalyst (Scheme 50).[41]




**Scheme 50: A palladium-catalyzed intramolecular hydroamination of *N*-sulfonyl alkylamines with $O_2$ as the oxidant and $Pd(OAc)_2$ as the catalysts. The reaction was reported by Stahl and co-workers in 2004.**

The rates and turnover numbers for these catalysts are greater those obtained with $Pd(OAc)_2$ and NaOAc. The rates are strongly dependent on the palladium-to-pyridine ratio. A 1:1 palladium-to-pyridine ratio provided the fastest rates for oxidative amination, but also resulted in significant amounts of catalyst decomposition. A 1:2 palladium-to-pyridine ratio resulted in a slower rate of aminopalladation, but also a longer catalyst lifetime.

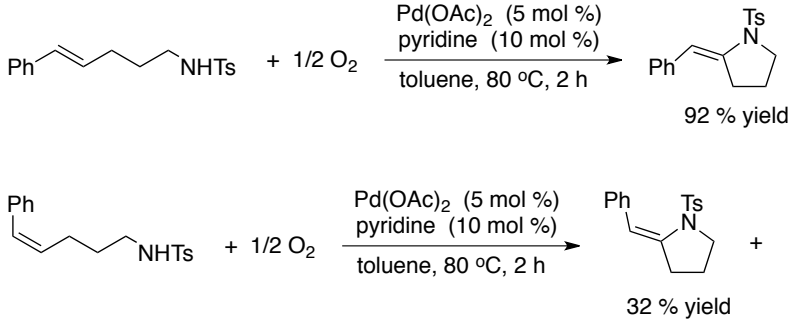
Mechanistic studies were performed with a 1:4 palladium-to-pyridine ratio. The rate expression obtained with this palladium-to-pyridine ratio shows a saturation dependence on both catalyst concentration and amino alkene concentration and a zero-order dependence on the partial pressure of $O_2$. The catalyst resting state in this system was identified as $Pd(OAc)_2(C_5H_5N)_2$. Moreover β-Hydride elimination was shown to be reversible A kinetic isotope effect of 1.15 was measured with N-deutero tosylamides. The data are consistent with a mechanism involving rate-limiting aminopalladation (Scheme 51).



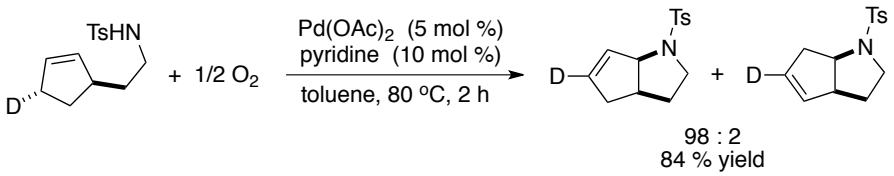

**Scheme 51: The mechanism proposed for the palladium-catalyzed intramolecular hydroamination of *N*-sulfonyl alkylamines with $O_2$ as the oxidant and $Pd(OAc)_2$ as the catalyst. The reaction was developed by Stahl and co-workers in 2004.**

When a 1:2 palladium-to-pyridine ratio is used the rate expression changes, and a positive dependence on the partial pressure of $O_2$ is observed. In this case, the rate data are consistent with a mechanism in which oxidation of palladium(0) to palladium(II) is the rate-limiting step.

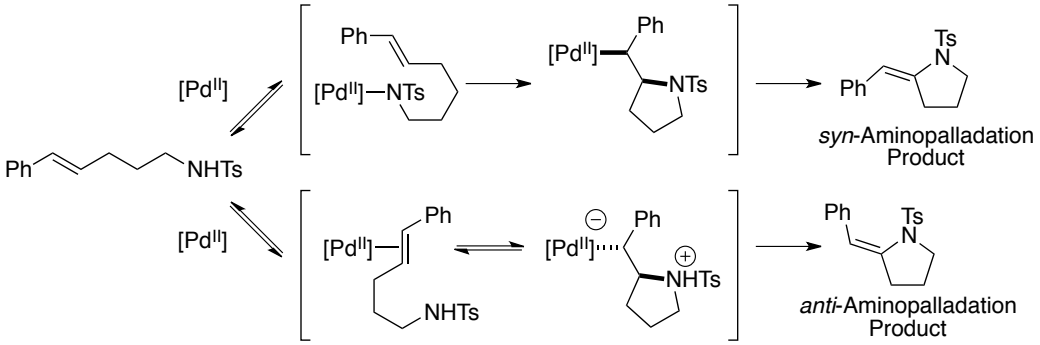
The stereochemistry of the aminopalladation step, was determined from the reactions of enantiopure N-tosyl-5-phenyl-4-penten-1-amines and deuterated cyclohexenyl tosylamides (Scheme 52 and Scheme 53).[42] The reactions indicate that both *syn*- and *anti*-aminopalladations occur, and that *syn*-aminopalladation is generally preferred, but that the mechanism depends on both the substrate and the reaction conditions (Scheme 54 and Scheme 55). Reactions performed with other palladium show similar results.



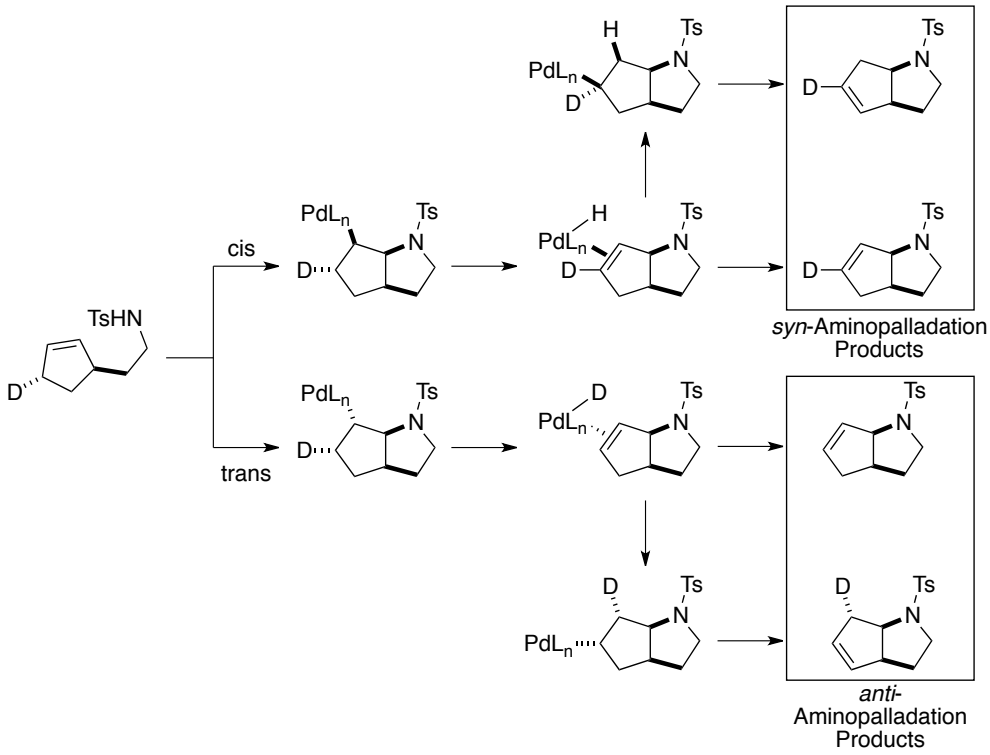

**Scheme 52: The stereochemistry of the palladium-catalyzed oxidative amination of of *N*-sulfonyl alkylamines with $O_2$ as the oxidant and $Pd(OAc)_2$ as the catalyst. The reaction was reported by Stahl and co-workers in 2007.**




**Scheme 53: The stereochemistry of the palladium-catalyzed oxidative amination of of *N*-sulfonyl alkylamines with $O_2$ as the oxidant and $Pd(OAc)_2$ as the catalyst. The reaction was reported by Stahl and co-workers in 2007.**



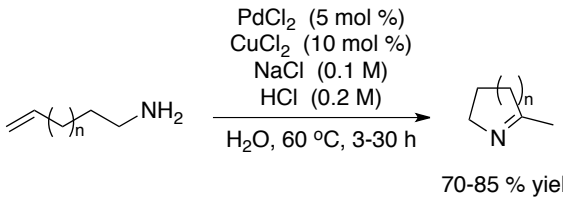

**Scheme 54: The stereochemistry of the palladium-catalyzed oxidative amination of of *N*-sulfonyl alkylamines with $O_2$ as the oxidant and $Pd(OAc)_2$ as the catalyst. The reaction was reported by Stahl and co-workers in 2007.**




**Scheme 55: The stereochemistry of the palladium-catalyzed oxidative amination of of *N*-sulfonyl alkylamines with $O_2$ as the oxidant and $Pd(OAc)_2$ as the catalyst. The reaction was reported by Stahl and co-workers in 2007.**

### 1.3.1.3 Oxidative Aminations of Unsaturated Amines

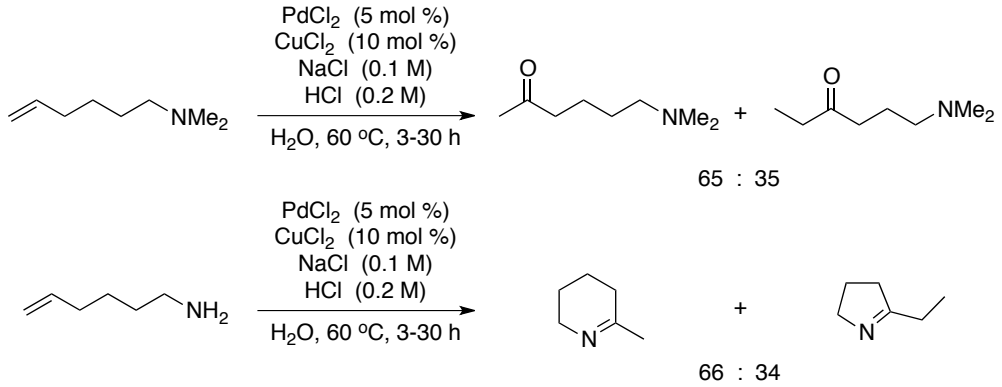
Palladium-catalyzed oxidative aminations of unsaturated amines were reported by Venanzi and co-workers in 1983 (Scheme 56).[43]




**Scheme 56: A palladium-catalyzed oxidative amination of unsaturated amines with $PdCl_2$ as the catalyst. The reaction was developed by Venanzi and co-workers in 1983.**

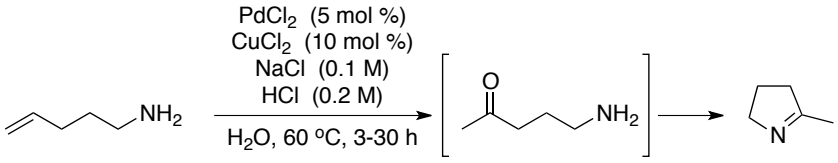
In this case, $O_2$ serves as the oxidant. The reactions are conducted in water in the presence of strong acids. The reactions conditions are nearly identical to those used in Wacker oxidations of alkenes. Not surprisingly, a mixture of oxidative amination products and Wacker products was observed.

To determine the mechanism for these reactions, the oxidation of *N,N*-dimethyl-5-hexen-1-amine was performed (Scheme 57).




**Scheme 57: The reactions of *N,N*-dimethyl-5-hexen-1-amine and 5-hexenyl-1-amine with $PdCl_2$ (5 mol %), $CuCl_2$ (10 mol %), NaCl (0.1 M), and HCl (0.2 M) in water. The relative ratio of ketone and imine products suggests a similar mechanism for the formation of both reactions.**

The ratio of ketone products obtained from this reaction matches the ratio of imine products obtained from the oxidative amination of 5-hexen-1-amine. The data suggest a mechanism involving intermolecular Wacker oxidation of the alkene to the corresponding ketone followed by intramolecular imine condensation.

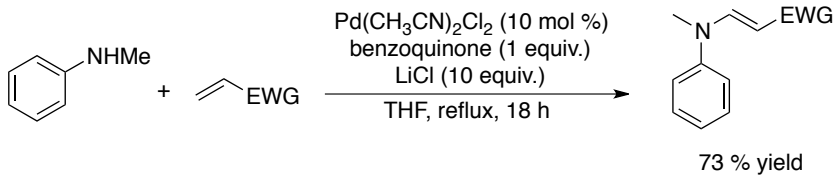



**Scheme 58: The mechanism proposed for the palladium-catalyzed intramolecular oxidative aminations of unsaturated amines with $PdCl_2$ (5 mol %), $CuCl_2$ (10 mol %), NaCl (0.1 M), and HCl (0.2 M).**

### 1.3.2 Intermolecular Oxidative Aminations

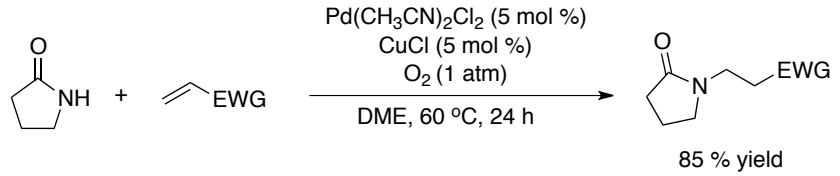
#### 1.3.2.1 Oxidative Aminations of Activated Alkenes

Intermolecular oxidative aminations of α,β-unsaturated esters, ketones, and nitriles were reported by Hegedus and Bozell in 1981 (Scheme 59).[44] The reactions use the same catalyst and reaction conditions as those reported previously for the intramolecular oxidative aminations of 2-allylanilines. Only activated alkenes are reported.



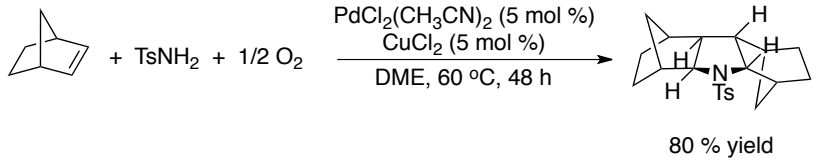

**Scheme 59: A palladium-catalyzed intermolecular oxidative amination of α,β-unsaturated esters, ketones, and nitriles with anilines using $Pd(CH_3CN)_2Cl_2$ as catalyst and benzoquinone as oxidant. The reaction was reported by Hegedus and Bozell in 1981.**

Similar oxidative aminations of unsaturated α,β-unsaturated esters, ketones, and aldehydes were reported by Murahashi and co-workers using $O_2$ as the oxidant. (Scheme 60). [45]

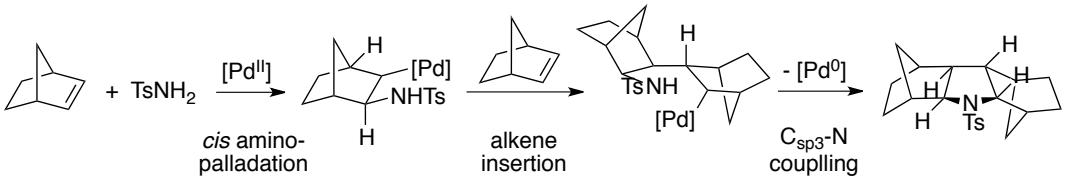



**Scheme 60: A palladium-catalyzed intermolecular oxidative amination of α,β-unsaturated esters, ketones, and aldehydes with carboxamides using $Pd(CH_3CN)_2Cl_2$ as catalyst a combination of $CuCl_2$ and $O_2$ as oxidant. The reaction was reported by Murahashi and co-workers in 1992.**

Oxidative aminations of norbornene with tosylamides were reported by Stahl and co-workers in 2005 (Scheme 61).[41a] In this case $C_2$-symmetric pyrrolidines were formed. To rationalize this result, Stahl proposed a sequence of steps involving *syn*-aminopalladation, followed norbornene insertion into the resulting palladium-carbon bond, and finally $C_{sp3}$-N reductive elimination (Scheme 62).



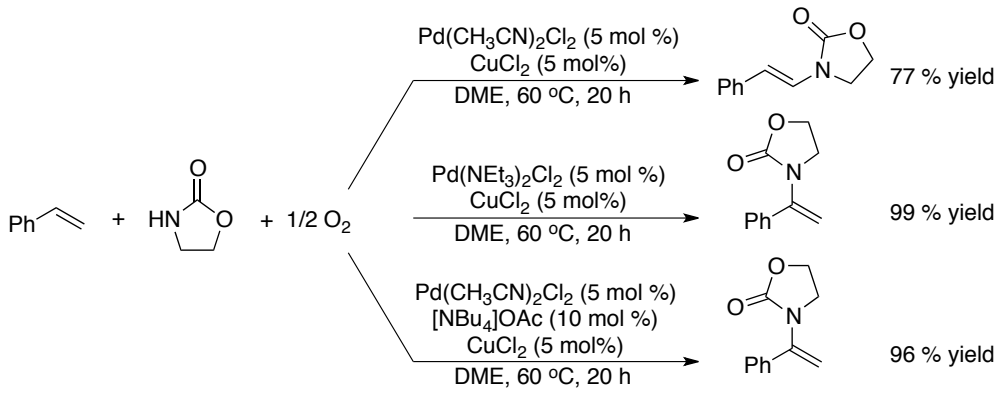

**Scheme 61: A palladium-catalyzed intermolecular oxidative amination of norbornene with sulfonamides. The reaction was reported by Stahl and co-workers in 2005.**




**Scheme 62: The mechanism proposed by Stahl and co-workers for the palladium-catalyzed intermolecular oxidative amination of norbornene with sulfonamides.**

### 1.3.2.2 Oxidative Aminations with Tosylamides, Carboxamides, Phthalimides, and Carbamates

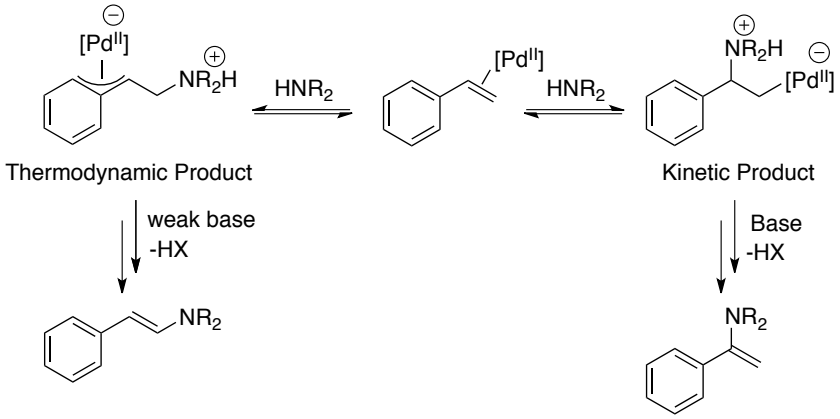
Two different palladium catalysts for the oxidative aminations of styrene with carboxamides were reported by Stahl and co-workers.[46] The catalysts are distinguished by their rates, ancillary ligands, and the regioselectivities they impart. Reactions catalyzed by $Pd(CH_3CN)_2Cl_2$ occur with slower rates and result in products with anti-Markovnikov regiochemistry. Reactions catalyzed by $Pd(NEt_3)_2Cl_2$ occur with faster rates and result in products with Markovnikov regiochemistry. Markovnikov regiochemistry is also observed when reactions are catalyzed by $Pd(CH_3CN)_2Cl_2$ in the presence of an inorganic base (Scheme 63).




**Scheme 63: An intermolecular oxidative amination of sytene with carbamates using $Pd(CH_3CN)_2$ as the catalyst and $CuCl_2$ as a co-catalyst. The reaction was reported by Stahl and co-workers in 2003.**

The origin of these differences was investigated by a series of kinetic experiments.[47] Reactions catalyzed by $Pd(CH_3CN)_2Cl_2$ show a first order dependence on oxazolidinone concentration and a saturation dependence on the concentration of styrene. Reactions catalyzed by $Pd(NEt_3)_2Cl_2$ show a saturation dependence on oxazolidinone concentration and a first-order dependence on styrene concentration. Kinetic isotope effects were measured with N-deutero oxazolidinone. A kinetic isotope effect of 3.0 was measured with $Pd(CH_3CN)_2Cl_2$ and a kinetic isotope effect of 1.1 was measured with $Pd(NEt_3)_2Cl_2$.

The data are consistent with a mechanism in which the kinetic product of aminopalladation displays Markovnikov regiochemistry and the thermodynamic product displays anti-Markovnikov regiochemistry (Scheme 64). Under base-free conditions, aminopalladation is reversible and the thermodynamic (anti-Markovnikov) product forms. The rate-limiting step is deprotonation of the zwitterionic intermediate formed by aminopalladation. Under basic conditions, deprotonation is no longer the rate-limiting step, and the kinetic product of aminopalladation is trapped. Aminopalladation is the rate-limiting step.



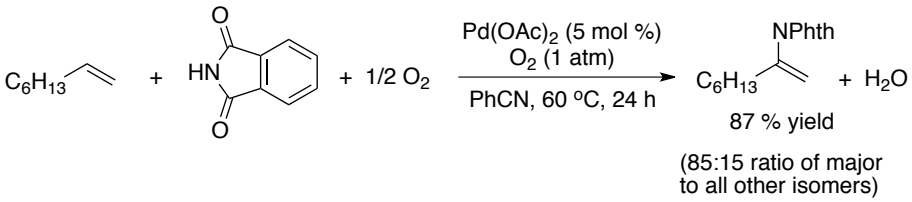

**Scheme 64: A mechanistic rationale for the different regioselectivities observed for the palladium-catalyzed intermolecular oxidative aminations of vinyl arenes with carbamates using $Pd(CH_3CN)_2Cl_2$ as the catalyst.**

Oxidative aminations of styrene with phthalimide, cyclic carboxamides, and sulfonamides were also reported by Stahl and co-workers at this time (Scheme 65).[46] The mechanism for these reactions was not reported. The reactions were performed in the presence of base.




**Scheme 65: A palladium-catalyzed intermolecular hydroamination of vinylamines with tosylamides. The reaction was developed by Stahl and co-workers in 2003.**

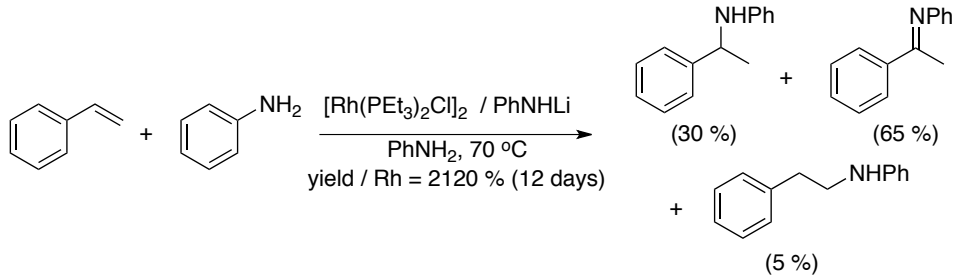
Oxidative aminations of unactivated alkenes with phthalimide were also reported by Stahl and co-workers. In this case, $Pd(OAc)_2$ serves as the catalyst and $O_2$ is the oxidant (Scheme 66).[41a]




**Scheme 66: A palladium-catalyzed intermolecular hydroamination of simple alkenes with phthalimide using $Pd(OAc)_2$ as the catalyst and $O_2$ as the oxidant. The reaction was reported by Stahl and co-workers in 2005.**

### 1.3.2.3 Rhodium-Catalyzed Oxidative Aminations

Rhodium-catalyzed oxidative aminations of styrene with aniline were reported by Brunet and co-workers in 1993 (Scheme 67).[48]




**Scheme 67: A rhodium-catalyzed oxidative aminaiton of styrene with anilines. The reaction was reported by Brunet and co-workers in 1993.**

In this case a mixture of hydroamination and oxidative amination products are observed. Excess styrene serves as the oxidant or hydrogen acceptor. The oxidative amination of 1-hexene was also reported at this time, but quantitative data was not provided. The mechanism is unknown. The reactions are a rare example of an oxidative amination that occurs with a metal other than palladium.

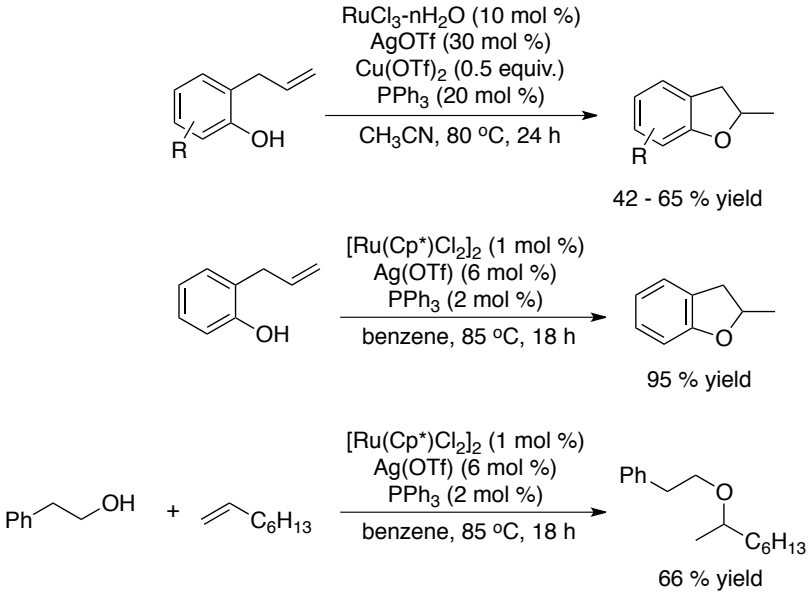
## 1.4 Hydroalkoxylations

Hydroalkoxylations, the additions of RO-H bonds across carbon-carbon multiple bonds have been reported with a variety of metal complexes.[49] The mechanisms for these reactions are not always clear. Several studies have shown that small amounts of acid, generated by the metal complex in solution, actually catalyze the observed hydroxylation reactions. [34,49-50] This observation seems especially true when metal triflates are involved. Characteristics of acid-catalyzed hydroalkoxylations include a strong preference for Markovnikov regioselectivity and faster rates with more-substituted alkenes relative to less-substituted alkenes. Hartwig and co-workers

developed a simple diagnostic test to determine whether a reaction is catalyzed by an acid or by a metal complex. In this case, two tethered alkenes, one mono-substituted and one tri-substituted are attached to the same alcohol (or amine). If the reaction occurs at the more-substituted alkene, the reaction is most likely catalyzed by acids generated in situ, and if the reaction occurs at the less-substituted alkene the reaction is most likely catalyzed by the metal. Simple additions of acids to the substrate are not always telling. The present section summarizes a few of the metal complexes that have been reported for the catalyzed additions of alcohols to alkenes.

### 1.4.1 Ruthenium-Catalyzed Hydroalkoxylations

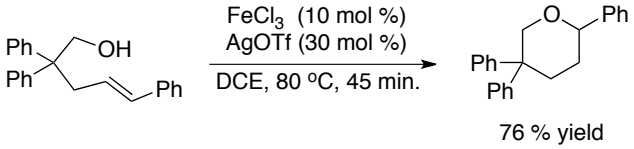
Ruthenium catalysts for the intramolecular hydroalkoxylations of 2-allylphenols, and for the intermolecular hydroalkoxylations of styrene, octene, and norbornene with 2-phenylethanol were reported by Oe and co-workers (Scheme 68).[51] The catalysts are formed by either the combination of $RuCl_3 \bullet 3H_2O$, $Cu(OTf)_2$, Ag(OTf), and $PPh_3$ or by the combination of $[RuCp^*Cl_2]_2$, Ag(OTf), and $PPh_3$. The mechanism for these reactions is unclear. Hydroaminations are not observed when $Cu(OTf)_2$ is replaced with $CuCl_2$, or when $AgBF_4$ is used in place of Ag(OTf). The data suggest the involvement of acid-catalyzed reactions, but do not confirm it. Reactions that might distinguish between these two pathways were not performed.




**Scheme 68: A ruthenium-catalyzed hydroalkoxylation of 2-allylphenols and simple alkenes. The reaction was reported by Oe and co-workers in 1998, and may actually occur by an acid-catalyzed mechanism.**

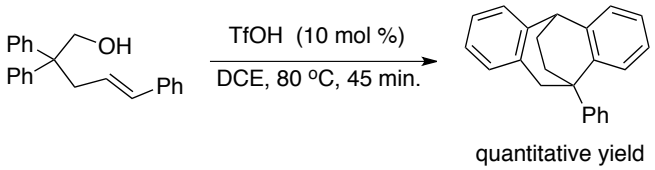
### 1.4.2 Iron-Catalyzed Hydroalkoxylations

An Iron catalyst for the hydroalkoxylations of unsaturated alcohols was reported by Takaki and co-workers (Scheme 69).[52]




**Scheme 69: An iron-catalyzed hydroalkoxylation of unsaturated alcohols with $FeCl_3$ / AgOTf as catalyst. The reaction was reported by Takaki and co-workers in 2007, and may actually occur by an acid-catalyzed mechanism.**

In this case, the catalyst is formed by a mixture of $FeCl_3$ and AgOTf. While the yields of the corresponding furans are good, the reported substrate scope is narrow. Reactions performed with catalytic amounts of triflic acid in place of $FeCl_3$ and AgOTf gave varying results. When 5 mol % triflic acid was used in place of $FeCl_3$ and AgOTf furans were obtained in good yield. When 10 mol % of triflic acid was used in place of $FeCl_3$ and AgOTf the formation of a bicyclic compound was observed (Scheme 70).

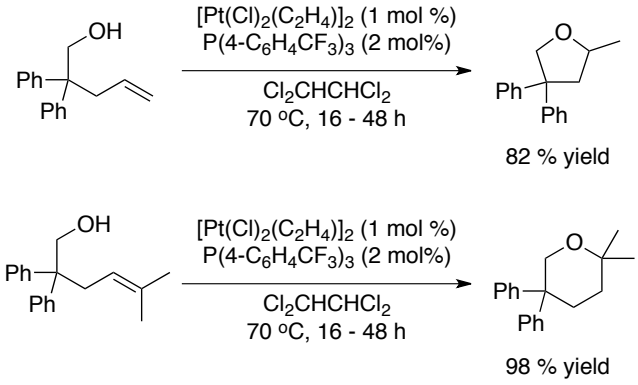



**Scheme 70: The reaction of triflic acid with (*E*)-2,2,5-triphenylpent-4-en-1-ol**

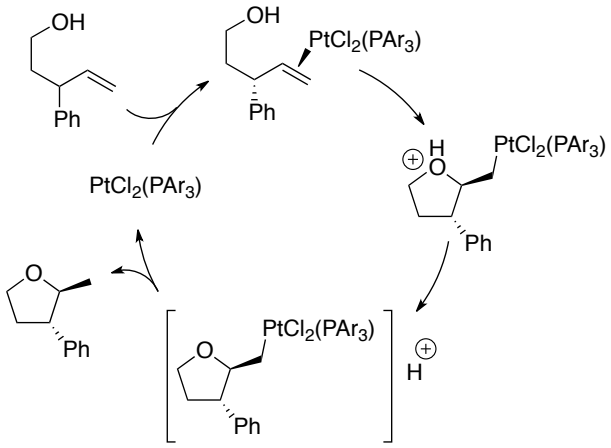
This bicyclic compound is presumably formed by an acid-catalyzed dehydrative isomerization and subsequent Friedel-Crafts cyclizations. While the authors argue for an iron-catalyzed process, the results suggest a mechanism in which a small amount of triflic acid is responsible for furan formation. The occurrence of an acid-catalyzed process is supported by studies that show that AgOTf and 1,2-dichloroethane (DCE) react to form triflic acid at elevated temperatures.[50]

### 1.4.3 Platinum-Catalyzed Hydroalkoxylations

Platinum catalysts for the intramolecular hydroalkoxylation of unsaturated alcohols were reported by Widenhoefer and co-workers using a 1:2 mixture of $Pt(C_2H_4)(Cl)_2$ and tri-arylphosphine, $P(4\text{-}CF_3C_6H_4)_3$ (Scheme 71).[53] The reactions generate the corresponding cyclic ethers in good yields (47-98 %) and with Markovnikov regiochemistry. While the authors propose a mechanism involving nucleophilic attack onto a coordinated alkene (Scheme 72), they did not rule out the possibility of an acid catalyzed reaction.



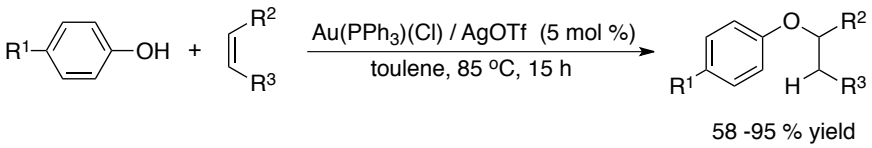

**Scheme 71: A platinum-catalyzed hydroalkoxylation of unsaturated alcohols with $Pt(C_2H_4)(Cl)_2$ / $P(4\text{-}CF_3C_6H_4)_3$ as catalyst. Widenhoefer and co-workers reported the reaction in 2004.**



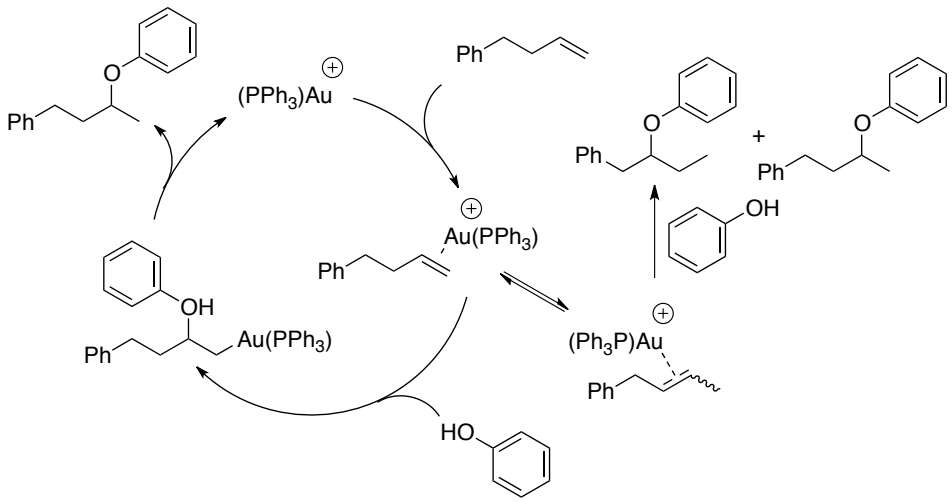

**Scheme 72: The mechanism proposed by Widenhoefer and co-workers for the hydroalkoxylation of unsaturated alcohols with $Pt(C_2H_4)(Cl)_2$ / $P(4\text{-}CF_3C_6H_4)_3$ as catalyst.**

### 1.4.4 Gold-Catalyzed Hydroalkoxylations

Gold-catalyzed intermolecular hydroalkoxylations of alkenes with phenols were reported by He and co-workers (Scheme 73).[54] The reactions are catalyzed by combination of $Au(PPh_3)Cl$ and Ag(OTf). Although a mechanism involving alkene coordination and nucleophilic attack was proposed (Scheme 74), it is not clear if this is the actual mechanism.[49]



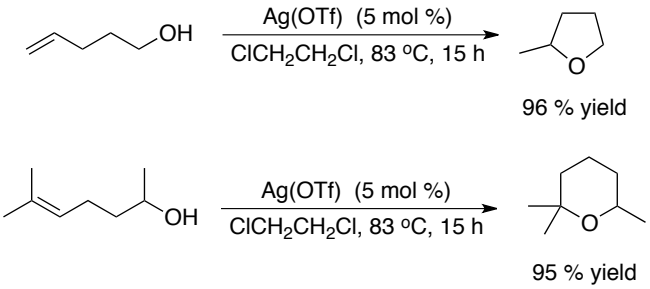

**Scheme 73: A gold-catalyzed hydroalkoxylation of simple alkenes with phenols. The reation was reported by He and co-workers in 2005.**




**Scheme 74: The mechanism proposed for the gold-catalyzed hydroalkoxylations of simple alkenes with $Au(PPh_3)Cl$ / AgOTf as catalyst.**

### 1.4.5 Silver-Catalyzed Hydroalkoxylations

Silver-catalyzed intramolecular hydroalkoxylations were reported by He and co-workers (Scheme 75). [55]



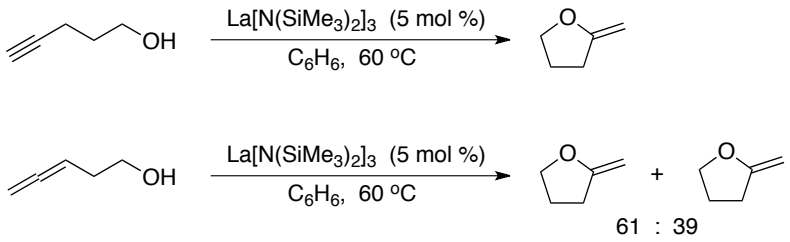

**Scheme 75: A silver-catalyzed intramolecular hydroalkoxylation of unsaturated alcohols with Ag(OTf) as catalyst. The reaction was reported by He and co-workers in 2005, and most likely occurs by an acid-catalyzed mechanism.**

The reactions were monitored by 1H NMR spectroscopy. Significant shifts in the vinyl protons of the alkene suggest alkene coordination to silver. In addition, the cyclizations of hydroxyl alkenes bearing acid-sensitive functional groups suggest that an acid-catalyzed process is not operative. When 5 mol % triflic acid was added to the same hydroxyl alkenes little to no cyclization was observed. The data suggest a mechanism in which alkene coordination to silver is followed by nucleophilic attack onto the coordinated alkene, but do not completely rule out an acid-catalyzed process. More recent studies by Hintermann and co-workers show that triflic acid is generated by the reactions of AgOTf with 1,2-dichloroethane (DCE).[50]

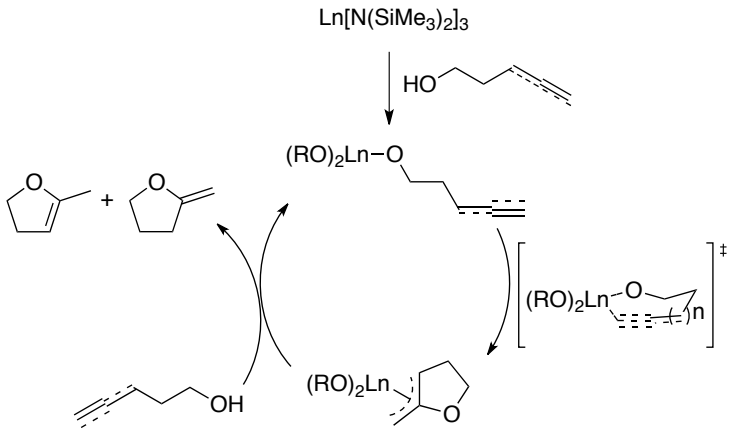
### 1.4.6 Rare Earth Metal-Catalyzed Hydroalkoxylations

Rare earth metal-catalyzed intramolecular hydroalkoxylations of hydroxyl alkynes and allenes were reported by Marks and co-workers in 2007 (Scheme 76).[56]

The reactions are thought to occur by alkene insertions into lanthanide-alkoxo bonds. The mechanism is similar to the mechanisms proposed for rare-earth metal-catalyzed hydroaminations of amino alkenes (Scheme 77).[56a,56c]

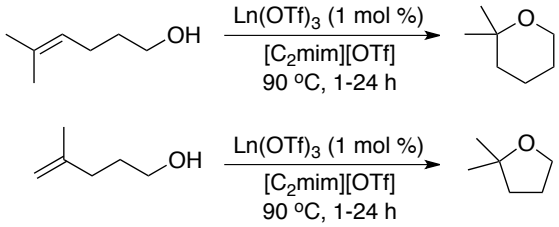



**Scheme 76: A rare earth metal-catalyzed hydroalkoxylation of alkynyl alcohols with $La[N(SiMe_3)_2]_3$ as catalyst. The reaction was reported by Marks and co-workers in 2007.**



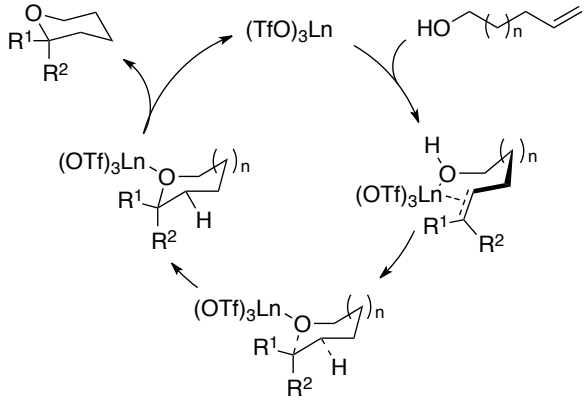

**Scheme 77: The mechanism proposed for the rare earth metal-catalyzed hydroalkoxylation of alkynyl alcohols developed by Marks and co-workers.**

In contrast, rare earth metal-catalyzed hydroalkoxylations of hydroxyl alkenes (Scheme 78) are thought to proceed by Lewis acid catalysis (Scheme 79).[56b,56d]




**Scheme 78: A rare earth metal-catalyzed hydroalkoxylation of alkenyl alcholos with Ln(OTF)$_3$ as catalyst. The reaction was reported by Marks and co-workers in 2009.**

In this case, coordination of the unsaturated alcohol to the metal through the oxygen atom acidifies the hydroxyl group sufficiently enough to protonate the alkene. The resulting carbocation is then attacked by the coordinated alkoxide to generate the cyclic ether product. The rate-limiting step in this mechanism is thought to involve concerted substrate coordination and proton transfer. The rate expressions for these reactions show a first-order dependence on catalyst concentration and a first-order dependence on hydroxyl alkene concentration Moreover a kinetic isotope effect of 2.48 is observed with O-deutero alcohols. Rates are faster with smaller, more Lewis-acidic metal ions, and inhibited by proton traps and sponges. The reactions are performed in ionic liquids.



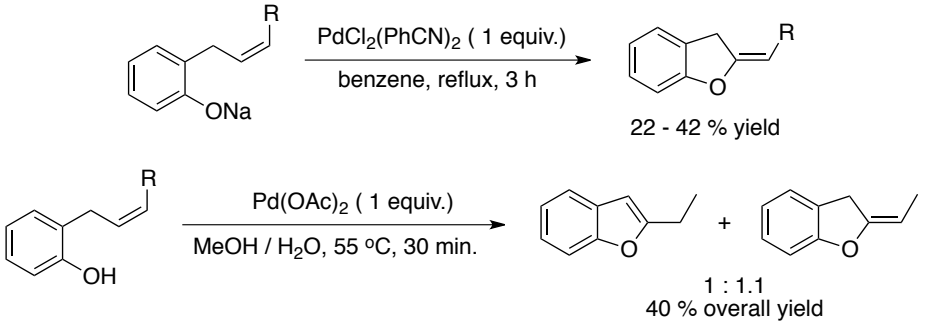

**Scheme 79: The mechanism proposed by Marks and co-workers for the rare earth metal-catalyzed hydroalkoxylation of alkenyl alcohols.**

## 1.5 Oxidative Alkoxylations

Oxidative alkoxylations involve the additions of alcohols to alkenes (and other substrates) with the formal loss of $H_2$ from the combined substrates. The reactions are similar to both oxidative aminations and Wacker oxidations. The differences between these reactions lie primarily with the identity of the nucleophile that adds to the alkene. With oxidative aminations, amines and amine derivatives add to the alkene. With oxidative alkoxylations, alcohols add to the alkene, and with Wacker oxidations, water adds to the alkene. Like oxidative aminations and Wacker oxidations, oxidative alkoxylations are catalyzed by palladium(II) complexes. The reactions involve the formations of metal alkyl complexes through the alkoxymetallations of alkenes. Subsequent β-hydride elimination generates the enol product and a palladium(II) hydride which can eliminate acid to form a palladium(0) complex. Common oxidants for the oxidative alkoxylations of alkenes include, copper(II) salts, benzoquinone, and $O_2$. The reactions are limited primarily to intramolecular reactions. The additions of alcohols to alkenes under normal Wacker conditions produce ketals and acetals. In contrast, the oxidative alkoxylations of unsaturated alcohols afford cyclic enol ethers.

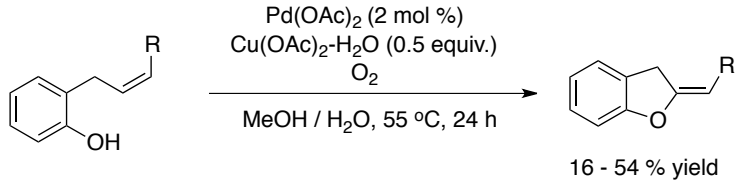
### 1.5.1 Intramolecular Oxidative Alkoxylations of 2-Allylphenols

Palladium-promoted oxidative alkoxylations of 2-allylphenoxides and 2-allylphenols were reported by Hosokawa and co-workers in 1973 (Scheme 80).[57] In this case, the reactions use stoichiometric amounts of $PdCl_2(PhCN)_2$ and result in low to moderate yields of benzofuran products.



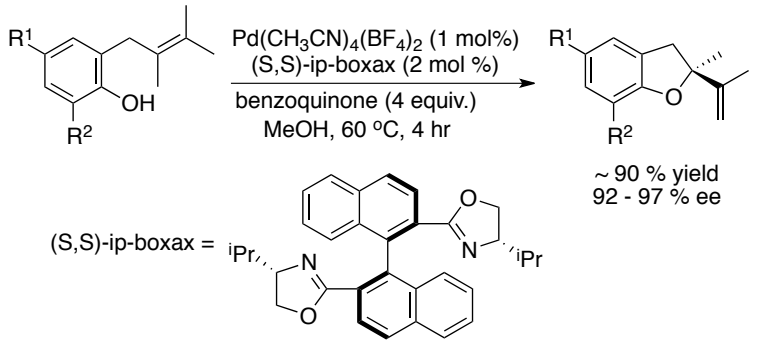

**Scheme 80: A stoichiometric intramolcular oxidative alkoxylation of 2-allylphenols and phenoxides using $PdCl_2(PhCN)_2$ and $Pd(OAc)_2$. Hosokawa and co-workers reported the reactions in 1973.**

Shortly thereafter, Hosokawa and co-workers reported palladium-catalyzed oxidative alkoxylations using a combination of $Cu(OAc)_2$ and $O_2$ as the oxidant (Scheme 81).[58] The same conditions are used in palladium-catalyzed Wacker oxidations (oxidative hydrations). Interestingly, the authors note that exocyclic furanyl alkenes are formed almost exclusively in these catalytic reactions. This contrasts with stoichiometric reactions, in which a 1 to 1.1 mixture of endocyclic to exocyclic alkenes are observed (Scheme 80). The authors attribute the greater selectivity for exocyclic alkenes to lower amounts of alkene isomerization. The authors also postulate that syn-alkoxypalladation reactions occur in these reactions, but later recanted this suggestion.[59]

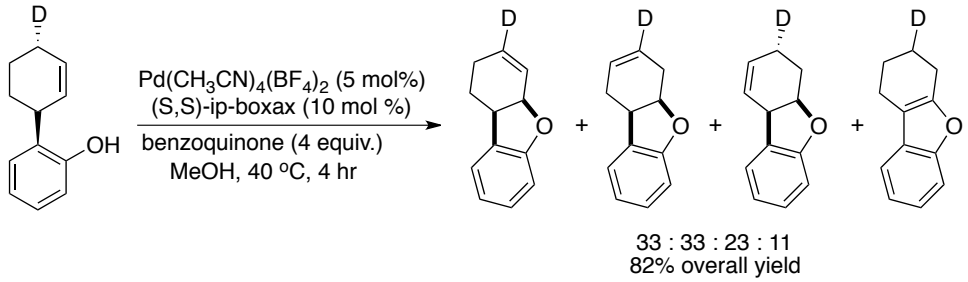



**Scheme 81: A palladium-catalyzed oxidative alkoxylation of 2-allylphenols with $Pd(OAc)_2$ as catalyst, $Cu(OAc)_2$-$H_2O$ as co-catalyst, and $O_2$ as oxidant. The reaction was reported by Hosokawa and co-workers in 1975.**

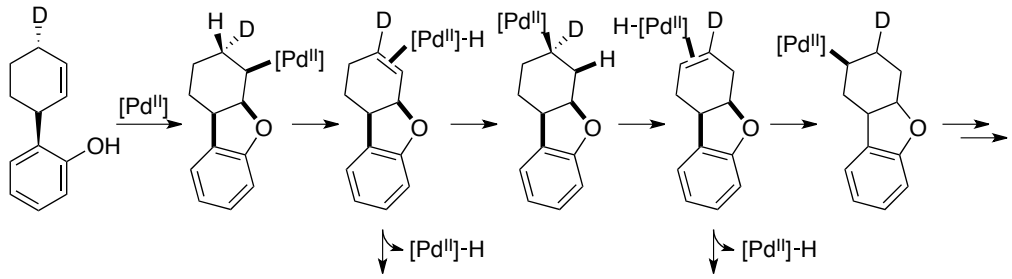
In 2004, Hayashi and co-workers reported oxidative alkoxylations of 2-allylphenols under slightly different conditions (Scheme 82).[60] In this case, a combination of $Pd(CH_3CN)_4(BF_4)_2$ and (S,S)-ip-boxax is used as catalyst, and benzoquinone serves as the oxidant. The mechanism for the C-O bond formation (alkoxypalladation) was investigated using a series of enantiopure deuterated cyclohexenyl phenols (Scheme 83). The stereochemistries of the resulting benzofurans are consistent with a mechanism involving *syn*-alkoxypalladation (assuming syn-specific β-hydride elimination) (Scheme 84).




**Scheme 82: A palladium-catalyzed oxidative alkoxylation of 2-allylphenols with $Pd(CH_3CN)_4(BF_4)_2$ / (S,S)-ip-boxax as the catalyst, and benzoquinone as the oxidant. Hayashi and co-workers reported the reaction in 2004.**



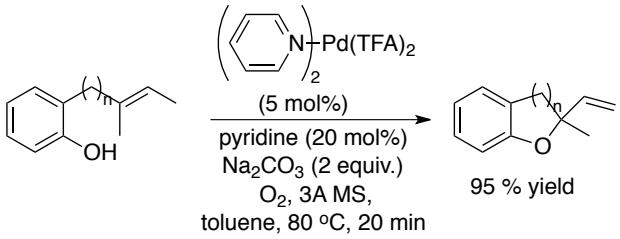

**Scheme 83: The stereochemistry of the palladium-catalyzed oxidative alkoxylation of 2-allylphenols developed by Hayashi and co-workers.**




**Scheme 84: The mechanism proposed for the palladium-catalyzed oxidative alkoxylation of 2-allylphenols developed by Hayashi and co-workers.**

When the same reactions were performed in the presence of added LiCl (2 equiv.), the stereochemistries of the resulting benzofurans change and are consistent with a mechanism involving outer sphere nucleophilic attack onto a coordinated alkene. [60] The results mirror those obtained by Henry and co-workers for Wacker oxidations of alkenes (vide infra).

Intramolecular oxidative alkoxylations of 2-allylphenols were also reported by Stoltz and co-workers (Scheme 85).[61]

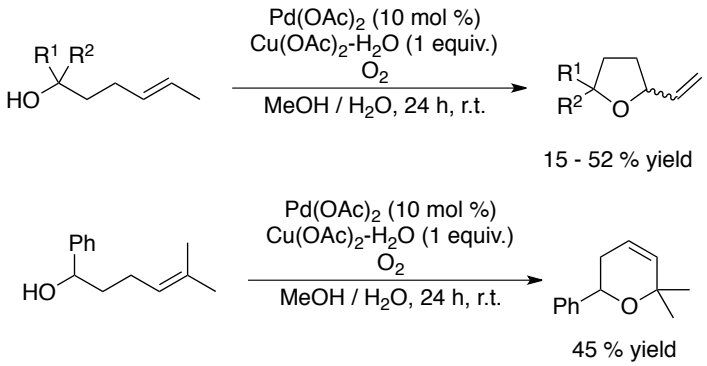



**Scheme 85: A palladium-catalyzed intramolecular oxidative alkoxylation of 2-allylphenols with $Pd(pyridine)_2(TFA)_2$ as catalyst and $O_2$ as oxidant. Stoltz and co-workers reported the reaction in 2005.**

While the mechanism for aminopalladation was not investigated with this system, the same catalyst was shown to effect the oxidative alkoxylations of unsaturated alcohols by a mechanisms involving alkene insertion into a palladium-alkoxo bond (vide infra).

### 1.5.2 Intramolecular Oxidative Alkoxylations of Unsaturated Alcohols.

Palladium-catalyzed oxidative alkoxylations of γ,δ-unsaturated alcohols were also reported by Hosokawa in 1976 (Scheme 86).[62] The reactions occur with Markovnikov regiochemistry. When two methyl groups are located at to the δ position, pyran derivatives are formed. The mechanism for these reactions, the formation of furans and the formation of pyrans, is unclear.




**Scheme 86: A palladium-catalyzed intramolecular oxidative alkoxylation of unsaturated alcohols with $Pd(OAc)_2$ as catalyst, $Cu(OAc)_2$-$H_2O$ as co-catalyst and $O_2$ as oxidant. Hosokawa and co-workers reported the reaction ins 1976.**

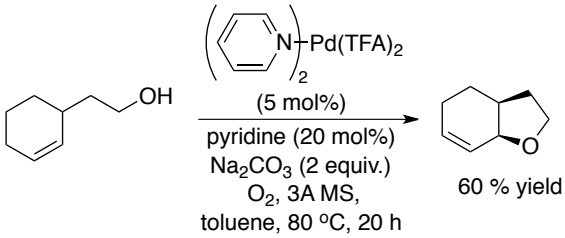
In 1995, Andersson and co-workers reported palladium-catalyzed oxidative alkoxylations of unsaturated alcohols using $O_2$ as the sole oxidant (Scheme 87).[39] In this case, the reactions are conducted in DMSO. The same conditions were used by Andersson and co-workers for the intramolecular oxidative aminations of unsaturated carbamates and tosylamides. These conditions are slightly different from those reported by Larock and co-workers for the oxidative lactonization of unsaturated carboxylic acids and the intramolecular oxidative aminations of unsaturated tosylamides.[39,63]




**Scheme 87: A palladium-catalyzed intramolecular oxidative alkoxylation of unsaturated alcohols using $Pd(OAc)_2$ as catalyst and $O_2$ as oxidant. Andersoon and co-workers reported the reaction in 1995.**

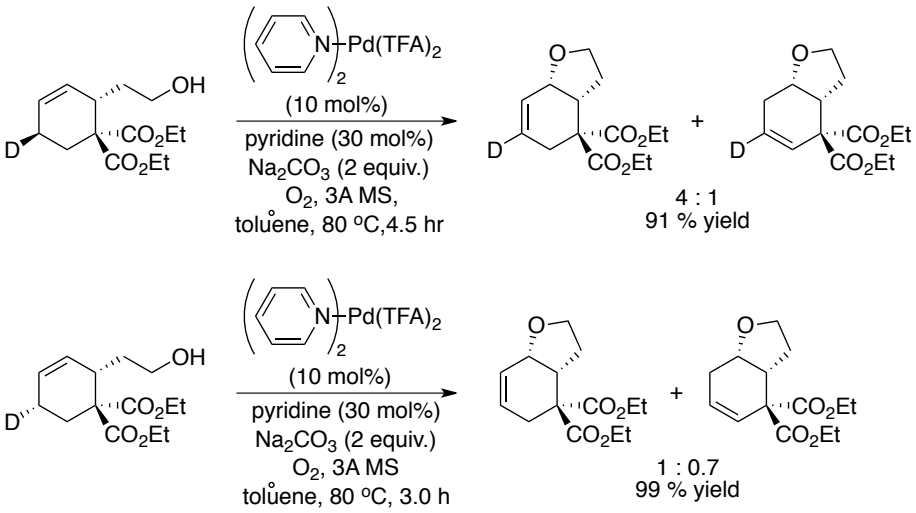
In this case, the additions of NaOAc and LiCl to the reactions inhibited the formations of furan products. More detailed studies on the rates and rate-dependences were not reported.

Stoltz and co-workers developed a separate set of conditions for the oxidative alkoxylations of 2-allyl phenols and γ,δ-unsaturated alcohols (Scheme 88).[61]




**Scheme 88: A palladium-catalyzed intramolecular oxidative alkoxylation of unsaturated alcohols using $Pd(pyridine)_2(TFA)_2$ as catalyst and $O_2$ as oxidant. Andersoon and co-workers reported the reaction in 2005.**

The mechanism for these reactions was investigated using enantiopure deuterated alcohols (Scheme 89).




**Scheme 89: The stereochemistry of the palladium-catalyzed oxidative alkoxylation of unsaturated alcohols developed by Stoltz and co-workers.**

The results suggest that alkoxypalladation occurs with syn selectivity. More detailed studies on the rates and rate-dependences were not reported.

## 1.6 Summary and Objectives

Despite the progress that has been made towards metal-catalyzed aminations and alkoxylations of alkenes, these processes remain challenging especially for unactivated alkenes. Rare earth metal complexes, such as those reported by Marks and co-workers, are incompatible with polar functional groups, and are difficult to synthesize. Group IV metal catalysts, such as those developed by the groups of Scott, Livinghouse, Schafer, and Hultzsch for the hydroaminations of amino alkenes exhibit greater tolerance for polar functional groups, but Group IV metal catalyzed hydroaminations are limited to aminoalkenes. Moreover, Group IV metal-catalyzed alkoxylations have not been reported. Late transition metal catalysts provide the greatest functional group compatibility and have been reported for both intra- and intermolecular aminations and alkoxylations, but these reactions are still confined to certain classes of substrates. Intermolecular hydroaminations, for example, are limited primarily to activated alkenes such as norbornene or acidic amines such as carboxamides, carbamates, and sulfonamides. Meanwhile the participation of metals in "metal-catalyzed" hydroalkoxylations of alkenes remains suspect. As a result of these limitations, the development of metal catalysts for the aminations and alkoxylations of alkenes remains an area of focus in organometallic chemistry.

This thesis summarizes research directed towards the development of new ligands (and consequently new catalysts) for the aminations and alkoxylations of alkenes. The research is divided into three sections. In the first section (Chapter 2), rhodium diphosphine amido and alkoxo complexes are developed for the purpose of studying the effects of alkene insertions into metal-amido and -alkoxo bonds. In the second section (Chapter 3) the effects of the ancillary ligand properties on the rates for alkene insertions into rhodium-alkoxo bonds are examined, and in the third section (Chapter 4), new ligands are developed and applied to the reactions of rhodium alkoxo alkene complexes. The research outlines a general approach to catalyst development in which one step of a catalytic cycle is examined so that ligands may be tailored to promote that step.

References


(1) (a) Muller, T. E.; Beller, M. *Chemical Reviews* **1998**, *98*, 675(b) Muller, T. E.; Hultzsch, K. C.; Yus, M.;

(2) (a) Gagne, M. R.; Marks, T. J. *Journal of the American Chemical Society* **1989**, *111*, 4108(b) Gagne, M. R.; Stern, C. L.; Marks, T. J. *Journal of the American Chemical Society* **1992**, *114*, 275(c) Giardello, M. A.; Conticello, V. P.; Brard, L.; Gagne, M. R.; Marks, T. J. *Journal of the American Chemical Society* **1994**, *116*, 10241(d) Li, Y. W.; Marks, T. J. *Organometallics* **1996**, *15*, 3770(e) Hong, S.; Marks, T. J. *Accounts of Chemical Research* **2004**, *37*, 673.

(3) The rate expressions for the intermolecular hydroaminations of alkenes show a first order dependence on catalyst concentration a first order dependence on alkene concentration and a zero-order dependence on amine concentration.

(4) Manna, K.; Kruse, M. L.; Sadow, A. D. *Acs Catalysis* **2011**, *1*, 1637.

(5) Crimmin, M. R.; Casely, I. J.; Hill, M. S. *Journal of the American Chemical Society* **2005**, *127*, 2042.

(6) Dunne, J. F.; Fulton, D. B.; Ellern, A.; Sadow, A. D. *Journal of the American Chemical Society* **2010**, *132*, 17680.

(7) Tobisch, S. *Chemistry-a European Journal* **2011**, *17*, 14974.

(8) (a) Walsh, P. J.; Baranger, A. M.; Bergman, R. G. *Journal of the American Chemical Society* **1992**, *114*, 1708(b) Baranger, A. M.; Walsh, P. J.; Bergman, R. G. *Journal of the American Chemical Society* **1993**, *115*, 2753.

(9) Kim, H.; Lee, P. H.; Livinghouse, T. *Chem Commun* **2005**, 5205.

(10) (a) Bexrud, J. A.; Beard, J. D.; Leitch, D. C.; Schafer, L. L. *Org Lett* **2005**, *7*, 1959(b) Thomson, R. K.; Bexrud, J. A.; Schafer, L. L. *Organometallics* **2006**, *25*, 4069.

(11) Allan, L. E. N.; Clarkson, G. J.; Fox, D. J.; Gott, A. L.; Scott, P. *Journal of the American Chemical Society* **2010**, *132*, 15308.

(12) Reznichenko, A. L.; Hultzsch, K. C. *Organometallics* **2009**, *29*, 24.

(13) Knight, P. D.; Munslow, I.; O'Shaughnessy, P. N.; Scott, P. *Chem Commun* **2004**, 894.

(14) Gribkov, D. V.; Hultzsch, K. C. *Angew Chem Int Edit* **2004**, *43*, 5542.

(15) Coulson, D. R. *Tetrahedron Letters* **1971**, 429.

(16) Casalnuovo, A. L.; Calabrese, J. C.; Milstein, D. *Journal of the American Chemical Society* **1988**, *110*, 6738.

(17) (a) Hesp, K. D.; Stradiotto, M. *Org Lett* **2009**, *11*, 1449(b) Hesp, K. D.; Tobisch, S.; Stradiotto, M. *Journal of the American Chemical Society* **2010**, *132*, 413.

(18) (a) Cochran, B. M.; Michael, F. E. *Journal of the American Chemical Society* **2008**, *130*, 2786(b) Michael, F. E.; Cochran, B. M. *Journal of the American Chemical Society* **2006**, *128*, 4246.

(19) Beller, M.; Eichberger, M.; Trauthwein, H. *Angewandte Chemie-International Edition in English* **1997**, *36*, 2225.

(20) (a) Takemiya, A.; Hartwig, J. F. *Journal of the American Chemical Society* **2006**, *128*, 6042(b) Utsunomiya, M.; Kuwano, R.; Kawatsura, M.; Hartwig, J. F. *Journal of the American Chemical Society* **2003**, *125*, 5608.

(21) Liu, Z.; Hartwig, J. F. *Journal of the American Chemical Society* **2008**, *130*, 1570.

(22) Liu, Z. J.; Yamamichi, H.; Madrahimov, S. T.; Hartwig, J. F. *Journal of the American Chemical Society* **2011**, *133*, 2772.

(23) Julian, L. D.; Hartwig, J. F. *Journal of the American Chemical Society* **2010**, *132*, 13813.

(24) Ambuehl, J.; Pregosin, P. S.; Venanzi, L. M.; Ughetto, G.; Zambonelli, L. *Journal of Organometallic Chemistry* **1978**, *160*, 329.

(25) (a) Palumbo, R.; Derenzi, A.; Panunzi, A.; Paiaro, G. *Journal of the American Chemical Society* **1969**, *91*, 3874(b) Panunzi, A.; Derenzi, A.; Paiaro, G. *Journal of the American Chemical Society* **1970**, *92*, 3488(c) Panunzi, A.; Derenzi, A.; Palumbo, R.; Paiaro, G. *Journal of the American Chemical Society* **1969**, *91*, 3879.

(26) (a) Brunet, J.-J.; Chu, N. C.; Diallo, O. *Organometallics* **2005**, *24*, 3104(b) Brunet, J. J.; Cadena, M.; Chu, N. C.; Diallo, O.; Jacob, K.; Mothes, E. *Organometallics* **2004**, *23*, 1264.

(27) (a) Karshtedt, D.; Bell, A. T.; Tilley, T. D. *Journal of the American Chemical Society* **2005**, *127*, 12640(b) Mcbee, J. L.; Bell, A. T.; Tilley, T. D. *Journal of the American Chemical Society* **2008**, *130*, 16562.

(28) Wang, X.; Widenhoefer, R. A. *Organometallics* **2004**, *23*, 1649.

(29) Bender, C. F.; Widenhoefer, R. A. *Journal of the American Chemical Society* **2005**, *127*, 1070.

(30) (a) Lober, O.; Kawatsura, M.; Hartwig, J. F. *Journal of the American Chemical Society* **2001**, *123*, 4366(b) Kawatsura, M.; Hartwig, J. F. *Journal of the American Chemical Society* **2000**, *122*, 9546(c) Utsunomiya, M.; Hartwig, J. F. *Journal of the American Chemical Society* **2003**, *125*, 14286(d) Johns, A. M.; Utsunomiya, M.; Incarvito, C. D.; Hartwig, J. F. *Journal of the American Chemical Society* **2006**, *128*, 1828(e) Minami, T.; Okamoto, H.; Ikeda, S.; Tanaka, R.; Ozawa, F.; Yoshifuji, M. *Angew Chem Int Edit* **2001**, *40*, 4501.

(31) Nettekoven, U.; Hartwig, J. F. *Journal of the American Chemical Society* **2002**, *124*, 1166.

(32) Pawlas, J.; Nakao, Y.; Kawatsura, M.; Hartwig, J. F. *Journal of the American Chemical Society* **2002**, *124*, 3669.

(33) (a) Zhang, J. L.; Yang, C. G.; He, C. *Journal of the American Chemical Society* **2006**, *128*, 1798(b) Kovacs, G.; Ujaque, G.; Lledos, A. *Journal of the American Chemical Society* **2008**, *130*, 853(c) Han, X. Q.; Widenhoefer, R. A. *Angew Chem Int Edit* **2006**, *45*, 1747.

(34) Rosenfeld, D. C.; Shekhar, S.; Takemiya, A.; Utsunomiya, M.; Hartwig, J. F. *Org Lett* **2006**, *8*, 4179.

(35) (a) Utsunomiya, M.; Hartwig, J. F. *Journal of the American Chemical Society* **2004**, *126*, 2702(b) Takaya, J.; Hartwig, J. F. *Journal of the American Chemical Society* **2005**, *127*, 5756.

(36) Hegedus, L. S.; Allen, G. F.; Waterman, E. L. *Journal of the American Chemical Society* **1976**, *98*, 2674.

(37) Hegedus, L. S.; Allen, G. F.; Bozell, J. J.; Waterman, E. L. *Journal of the American Chemical Society* **1978**, *100*, 5800.

(38) Hegedus, L. S.; McKearin, J. M. *Journal of the American Chemical Society* **1982**, *104*, 2444.

(39) Rönn, M.; Bäckvall, J.-E.; Andersson, P. G. *Tetrahedron Letters* **1995**, *36*, 7749.

(40) Larock, R. C.; Hightower, T. R.; Hasvold, L. A.; Peterson, K. P. *The Journal of Organic Chemistry* **1996**, *61*, 3584.

(41) (a) Brice, J. L.; Harang, J. E.; Timokhin, V. I.; Anastasi, N. R.; Stahl, S. S. *Journal of the American Chemical Society* **2005**, *127*, 2868(b) Kotov, V.; Scarborough, C. C.; Stahl, S. S. *Inorganic Chemistry* **2007**, *46*, 1910(c) Stahl, S. S. *Angewandte Chemie International Edition* **2004**, *43*, 3400.

(42) Liu, G. S.; Stahl, S. S. *Journal of the American Chemical Society* **2007**, *129*, 6328.

(43) Pugin, B.; Venanzi, L. M. *Journal of the American Chemical Society* **1983**, *105*, 6877.

(44) Bozell, J. J.; Hegedus, L. S. *The Journal of Organic Chemistry* **1981**, *46*, 2561.

(45) Hosokawa, T.; Takano, M.; Kuroki, Y.; Murahashi, S.-I. *Tetrahedron Letters* **1992**, *33*, 6643.

(46) Timokhin, V. I.; Anastasi, N. R.; Stahl, S. S. *Journal of the American Chemical Society* **2003**, *125*, 12996.

(47) Timokhin, V. I.; Stahl, S. S. *Journal of the American Chemical Society* **2005**, *127*, 17888.

(48) Brunet, J. J.; Commenges, G.; Neibecker, D.; Philippot, K.; Rosenberg, L. *Inorganic Chemistry* **1994**, *33*, 6373.

(49) Hintermann, L. *C-X Bond Formation* **2010**, *31*, 123.

(50) Dang, T. T.; Boeck, F.; Hintermann, L. *Journal of Organic Chemistry* **2011**, *76*, 9353.

(51) (a) Hori, K.; Kitagawa, H.; Miyoshi, A.; Ohta, T.; Furukawa, I. *Chemistry Letters* **1998**, 1083(b) Oe, Y.; Ohta, T.; Ito, Y. *Chem Commun* **2004**, 1620(c) Oe, Y.; Ohta, T.; Ito, Y. *Synlett* **2005**, 179.

(52) Komeyama, K.; Morimoto, T.; Nakayama, Y.; Takaki, K. *Tetrahedron Letters* **2007**, *48*, 3259.

(53) Qian, H.; Han, X. Q.; Widenhoefer, R. A. *Journal of the American Chemical Society* **2004**, *126*, 9536.

(54) Yang, C. G.; He, C. *Journal of the American Chemical Society* **2005**, *127*, 6966.

(55) Yang, C.-G.; Reich, N. W.; Shi, Z.; He, C. *Org Lett* **2005**, *7*, 4553.

(56) (a) Yu, X. H.; Seo, S.; Marks, T. J. *Journal of the American Chemical Society* **2007**, *129*, 7244(b) Dzudza, A.; Marks, T. J. *Org Lett* **2009**, *11*, 1523(c) Seo, S. Y.; Yu, X. H.; Marks, T. J. *Journal of the American Chemical Society* **2009**, *131*, 263(d) Dzudza, A.; Marks, T. J. *Chemistry-a European Journal* **2010**, *16*, 3403(e) Weiss, C. J.; Marks, T. J. *Dalton Transactions* **2010**, *39*, 6576.

(57) Hosokawa, T.; Maeda, K.; Koga, K.; Moritani, I. *Tetrahedron Letters* **1973**, *14*, 739.

(58) Hosokawa, T.; Ohkata, H.; Moritani, I. *Bulletin of the Chemical Society of Japan* **1975**, *48*, 1533.

(59) Hosokawa, T.; Miyagi, S.; Murahashi, S.; Sonoda, A. *The Journal of Organic Chemistry* **1978**, *43*, 2752.

(60) Hayashi, T.; Yamasaki, K.; Mimura, M.; Uozumi, Y. *Journal of the American Chemical Society* **2004**, *126*, 3036.

(61) Trend, R. M.; Ramtohul, Y. K.; Stoltz, B. M. *Journal of the American Chemical Society* **2005**, *127*, 17778.

(62) Hosokawa, T.; Hirata, M.; Murahashi, S.-I.; Sonoda, A. *Tetrahedron Letters* **1976**, *17*, 1821.

(63) Larock, R. C.; Hightower, T. R. *The Journal of Organic Chemistry* **1993**, *58*, 5298.

## CHAPTER 2: Alkene Insertions into Metal-Amido and -Alkoxo Bonds

### 2.1 Background

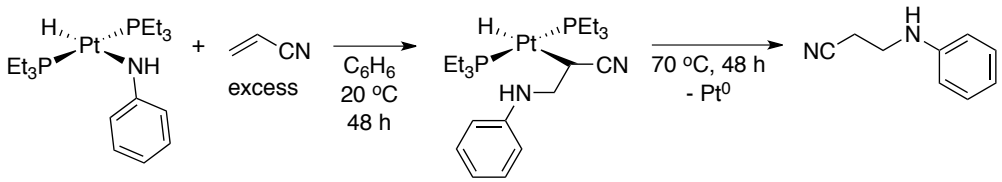
Alkene insertions into metal-ligand bonds are fundamental reactions in organometallic chemistry. Alkene insertions into metal-hydrogen bonds have been proposed for several metal-catalyzed reactions including alkene hydrogenations, hydroformylations, and hydrocyanations, while alkene insertions into metal-carbon bonds have been proposed for alkene polymerizations and the Mizoroki-Heck reaction. This chapter reviews those reactions in which alkene insertions into metal-amido or -alkoxo bonds are either proposed or observed, and summarizes original research directed towards the development of rhodium diphosphine amido and alkoxo alkene complexes for the direct observation of alkene insertions into rhodium-amido and -alkoxo bonds. While less common than alkene insertions into metal-hydrogen and metal-carbon bonds, alkene insertions into metal-amido and metal-alkoxo provided a potential route to alkene aminations and alkoxylations.[64] Moreover, the study of alkene insertions into metal-amido and -alkoxo bonds provides an opportunity to probe the differences between metal-amido and -alkoxo bonds and metal-hydrido, -alkyl, and -aryl bonds. The material is divided into three sections. The first section reviews alkene insertions into metal-amido bonds. The second section reviews alkene insertions into metal-alkoxo bonds, and the last section summarizes efforts to synthesize rhodium diphosphine amido and alkoxo complexes that react by insertion mechanisms. Reactions that result in difunctionalizations of alkenes are included in the first two sections, as are reactions that use stoichiometric amounts of metal complexes. Reactions covered in Chapter 1 are discussed briefly.

#### 2.1.1 Alkene Insertions into Metal-Amido Bonds

Alkene insertions into metal-amido bonds have been proposed for several metal-mediated reactions, including metal-catalyzed hydroaminations, oxidative aminations, aminoacetoxylations, aminoalkoxylations, aminochlorinations, and diaminations. In some cases, the insertion reaction is observed directly. In other cases, evidence for an insertion pathway comes primarily from the stereochemistry of the resulting products. The different products that can be formed by alkene insertions into metal-amido bonds result from the transformations of the metal alkyl complexes formed alkene insertion. Like the insertions of alkenes into metal-hydrogen and metal carbon bonds, the insertions of an alkenes into a metal-nitrogen bonds generate metal alkyl complexes. These complexes can undergo C-H bond-forming reactions to generate hydroamination products, β-hydrogen elimination to form oxidative amination products, or C-X bond forming reactions to generate difunctionalized products. This section examines those reactions in which alkene insertions into metal-amido bonds are either observed directly or inferred from circumstantial evidence. Reactions in which the insertion reaction is either observed directly or studied by a series of stoichiometric reactions are presented first. Reactions in which the occurrence of an insertion pathway is inferred from the stereochemistry of the products formed are presented second. Most of the examples presented in this section were reported within the last 20 years.

##### 2.1.1.1 Insertion of acrylonitrile into a platinum-anilido bonds

One of the earliest examples of an alkene insertion into a metal bond was reported by Trogler and Cowan in 1987.[65] In this case, insertion of acrylonitrile into the platinum-anilido bond of *trans*-$Pt(PEt_3)_2(H)(NHPh)$ is reported (Scheme 90).

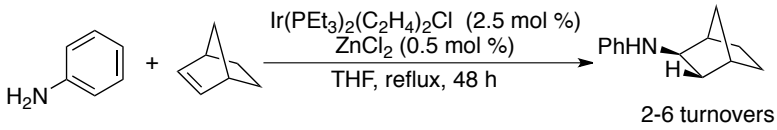



**Scheme 90: Insertion of acrylonitrile into the platinum-anilido bond of *trans*-Pt($PEt_3$)$_2$(H)(NHPh). The reaction was reported by Trogler and Cowan in 1987.**

The reaction produces a stable platinum(II) alkyl hydride, which upon heating to 70 C, eliminates 3-anilino-propionitrile. The platinum(II) anilido complex used in this reaction was synthesized by the reaction of sodium anilide with *trans*-Pt($PEt_3$)$_2$(H)($NO_3$). The platinum alkyl complex generated by insertion of acrylonitrile into the platinum-anilido bond of *trans*-Pt($PEt_3$)$_2$(H)(NHPh) was isolated at room temperature and characterized by x-ray crystallography. Insertion of methyl acrylate into the platinum-anilido bond of *trans*-Pt($PEt_3$)$_2$(H)(NHPh) was also reported. Additions of ethene and *cis*-stilbene to *trans*-Pt($PEt_3$)$_2$(H)(NHPh) resulted in the elimination of aniline, and the generation of platinum(0) complexes. Catalytic hydroaminations of acrylonitrile with aniline were not achieved.

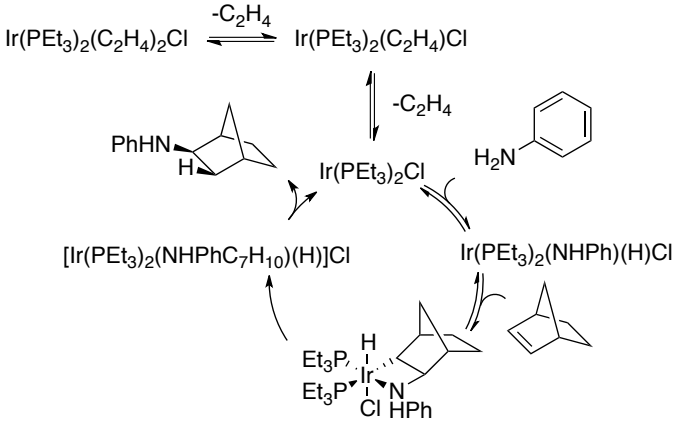
### 2.1.1.2 Insertion of norbornene into an iridium-anilido bonds

Insertion of norbornene into an iridium-anilido bond was proposed by Milstein and co-workers in 1988 (Scheme 91). [16]




**Scheme 91: An iridium-catalyzed hydroamination of norbornene with aniline. The mechanism for this reaction is thought to occur by norbornene insertion into an iridium-anilido bond.**

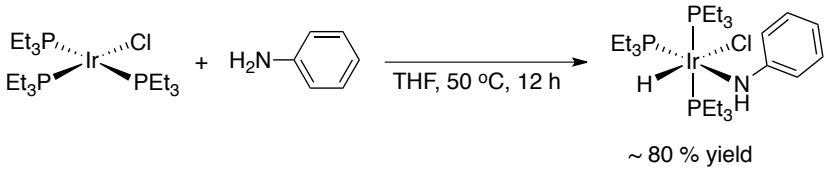
The reaction constitutes one step in an iridium-catalyzed hydroamination of norbornene with aniline (Scheme 92).




**Scheme 92: The mechanism proposed by Milstein and co-workers for the iridium-catalyzed hydroamination of norbornene with aniline. While the reaction is catalzyed by Ir($PEt_3$)$_2$($C_2H_4$)$_2$, but only a few turnovers are realized.**

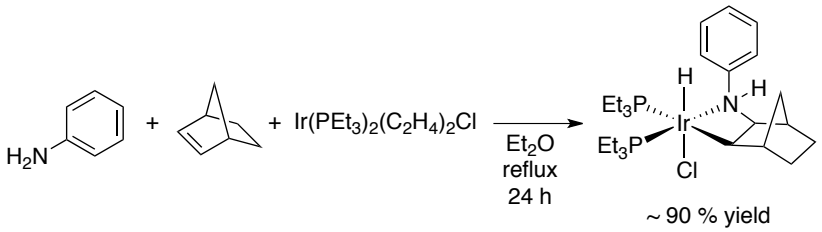
Each step of this catalytic cycle was demonstrated or investigated by a separate, stoichiometric reaction. Oxidative addition of an N-H bond of aniline to an iridium(I) triethylphosphine complex was demonstrated by the

reaction of $Ir(PEt_3)_3Cl$ with aniline, which results in the formation of a stable iridium(III) anilido hydrido complex (Scheme 93).



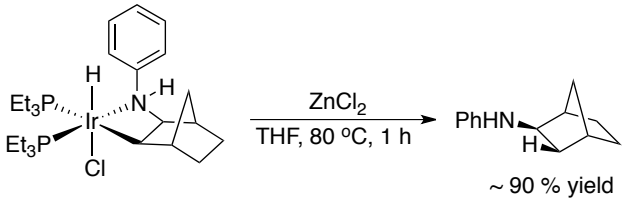

**Scheme 93: Oxidative addition of an N-H bond of aniline to $Ir(PEt_3)_3Cl$. A similar reaction is thought to occur between andiline and $Ir(PEt_3)_2$.**

Insertion of norbornene into the iridium(III)-anilido bond of $Ir(PEt_3)_2(H)(NHPh)Cl$, formed in situ by oxidative addition of aniline to $Ir(PEt_3)_2Cl$, was suggested by the stereochemistry of the resulting iridium(III) amino alkyl complex (Scheme 94).




**Scheme 94: The reaction of aniline, norbornene, and $Ir(PEt_3)_2(C_2H_4)_2$ in refluxing $Et_2O$. The reaction is thought to occur by N-H oxidative addition of aniline to iridium, followed by norbornene insertion into the iridium-anilido bond. The resulting iridium alkylamine complex was isolated in ~90 % yield.**

Reductive elimination of norbornyl aniline from $Ir(PEt_3)_2(H)(NHPhC_7H_{10})Cl$ was demonstrated by heating solutions of $Ir(PEt_3)_2(H)(NHPhC_7H_{10})Cl$ to 80 °C and by adding Lewis acids to $Ir(PEt_3)_2(H)(NHPhC_7H_{10})Cl$ at room temperature (Scheme 95).

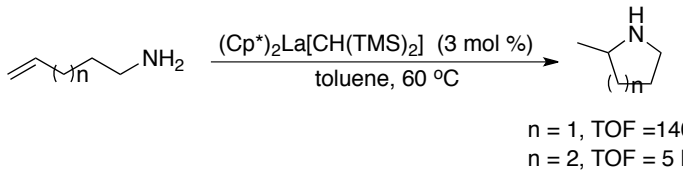



**Scheme 95: Reductive elimination of norbornyl aniline from the iridium alkylamine complex formed by the reaction of aniline, norbornene and $Ir(PEt_3)_2(C_2H_4)_2$. The reaction occurs at 80 °C in THF in the presence of added $ZnCl_2$.**

In this case, reductive elimination is thought to occur by chloride dissociation from $Ir(PEt_3)_2(H)(NHPhC_7H_{10})Cl$ to generate a cationic 16-electron iridium(III) complex, which then undergoes concerted C-H reductive elimination. The iridium(III) amino alkyl complex formed by insertion of norbornene into the iridium(III)-anilido bond of $Ir(PEt_3)_2(H)(NHPh)Cl$ was isolated at room temperature and characterized by x-ray crystallography. The formation of $Ir(PEt_3)_2(H)(NHPh)Cl$, prior to insertion of norbornene was not observed.

### 2.1.1.3 Insertions of unactivated alkenes into rare earth metal-amido bonds

Insertions of unactivated alkenes into rare earth metal-amido bonds were proposed by Marks and co-workers in 1989 for several rare earth metal-catalyzed hydroaminations of amino alkenes (Scheme 96).[2a-c,2e]

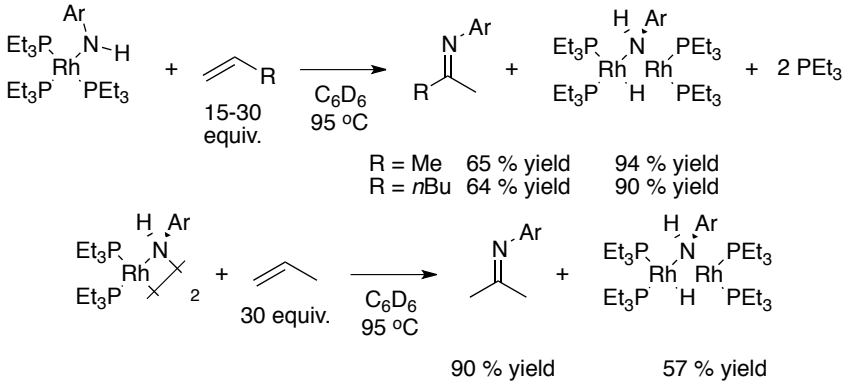



**Scheme 96: A rare earth metal-catalyzed intramolecular hydroamination of aminoalkenes. The reaction was originally reported by Marks and co-workers in 1989 and is thought to occur by alkene insertion into a metal-amido bond.**

The scope for this reaction was later expanded to encompass intermolecular reactions.[2d,66] The mechanisms for these reactions were studied by a series of kinetic and mechanistic experiments. The data from these experiments are consistent with a mechanism involving rapid deprotonation of a rare earth metal-alkyl bond by amine to form a rare earth metal-amido complex, followed by rate-limiting insertion of the alkene into the resulting rare earth metal-amido bond. The resting states of the catalysts were identified as rare earth metal amido and amido amine complexes. Similar mechanisms are proposed for alkaline earth metal-catalyzed hydroaminations and Group IV-metal catalyzed hydroaminations.

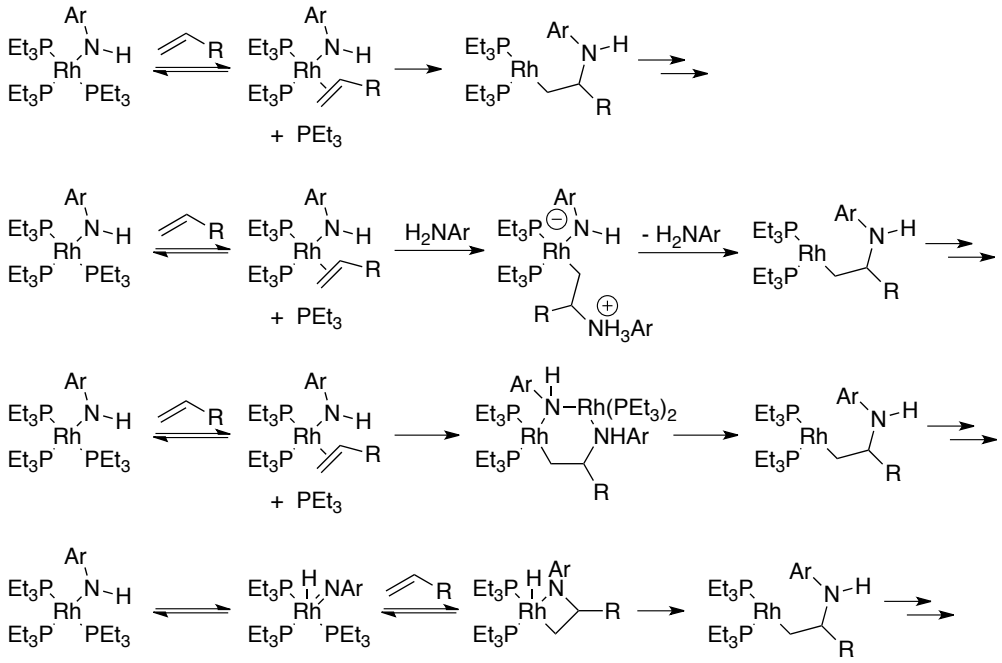
### 2.1.1.4 Insertions of unactivated alkenes into rhodium-anilido bonds

Insertions of unactivated alkenes into rhodium-anilido bonds were reported by Hartwig and co-workers in 2005 (Scheme 97).[67]




**Scheme 97: The reactions of unactivated alkenes with tris- and bis(triethylphosphine) rhodium anilido complexes. The reactions generate imines, presumably by a mechanism that involves alkene insertion into the rhodium-anilido bond of the starting complex and β-hydrogen elimination from the reulsting rhodium alkylamine complex. The reaction was reported by Hartwig and co-workers in 2005 and studied by a series of kinetic experiments.**

In this case, imines and enamines are formed by the additions of styrene, propene, and hexane to $[Rh(PEt_3)_3(\mu\text{-}NHAr)]_2$ and $Rh(PEt_3)_3(NHAr)$. The mechanism for these reactions was investigated by determining the rate expression for the reaction of for the reaction of $Rh(PEt_3)_3(NHAr)$ with styrene, which shows a first-order dependence on the concentration of styrene, a first-order dependence on the concentration of rhodium-anilido complex, an inverse first-order dependence on the concentration of $PEt_3$, and a zero-order dependence on the concentration of added aniline. The data are consistent with a mechanism involving substitution of a $PEt_3$ on $Rh(PEt_3)_3(NHAr)$ with styrene, and irreversible insertion of styrene into the rhodium-anilido bond of $Rh(PEt_3)_2(styrene)(NHAr)$. Other mechanisms considered for the formation imines and enamines in these reactions, include nucleophilic attacks by exogenous amines and rhodium amides onto coordinated alkenes and [2+2] cycloadditions (Scheme 98).

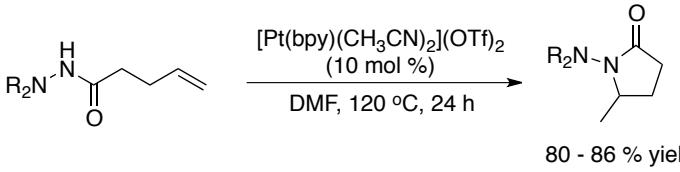


**Scheme 98: Four possible mechanisms for the reacitons of tris(triethylphosphine) rhodium anilido complexes with alkenes. The reactions generate imine products, presumably by a mechanism involving alkene insertion into a rhodium-anilido bond followed by β-hydrogen elimination from the resulting rhodium alkylamine complex.**

These mechanisms were systematically eliminated by the data. Reactions preformed with $d^8$-styrene and N-deutero anilide show negligible kinetic isotope effects. The data are inconsistent with mechanisms involving rate-limiting β-hydride elimination, and with mechanisms involving the reactions of rhodium imido complexes.

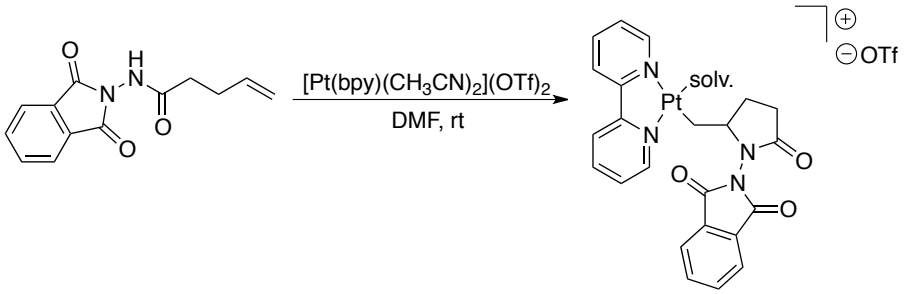
### 2.1.1.5 Insertions of tethered alkenes into platinum-hydrazido bonds

Insertions of tethered alkenes into platinum-hydrazido bonds were proposed by Michael and co-workers in 2010 for a platinum-catalyzed hydrohydrazination of alkenes (Scheme 99).[68]



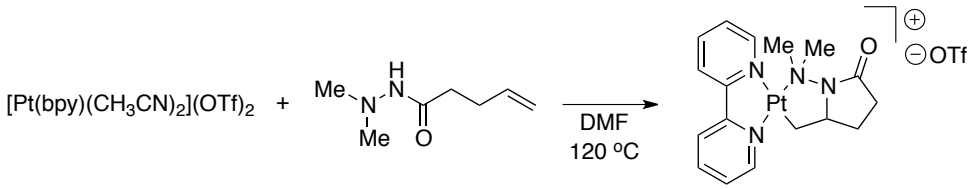
**Scheme 99: A platinum-catalyzed hydrohydrazination of unsaturated hydrazines. The reaction was reported by Michael and co-workers in 2010, and is thought to occur by alkene insertion into a platinum-hydrazido bond.**

Several different platinum complexes are formed by these reactions. The addition of pent-4-enoyl-N'-isoindole hydrazide to a solution of $[Pt(bpy)(CH_3CN)_2](OTf)$ at room temperature results in the formation of a cationic platinum(II) alkyl complex (Scheme 100). The complex was characterized in situ by NMR spectroscopy and mass spectrometry, and observed as the catalyst resting state for the platinum catalyzed hydrohydrazination of pent-4-enoyl-N'-isoindole hydrazide.



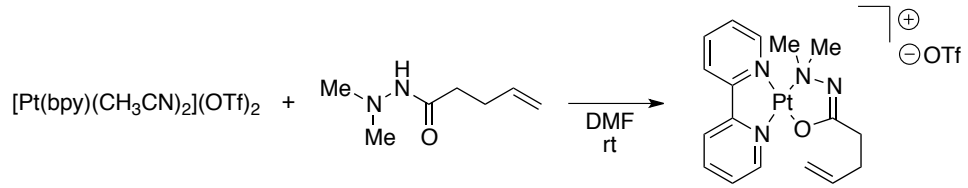

**Scheme 100: The addition of pent-4-enoyl-N'-isoindole hydrazide to a solution of [Pt(bpy)(CH$_3$CN)$_2$](OTf) in DMF. The reaction generates a cationic platinum(II) alkyl complex when performed at room temperature.**

The addition of pent-4-enoyl-*N'N'*-dimethyl hydrazide to a solution of [Pt(bpy)(CH$_3$CN)$_2$](OTf) at 120 °C results in the formation of a cationic platinum(II) amino alkyl complex (Scheme 101). This complex was characterized by NMR spectroscopy and mass spectrometry and observed as the catalyst resting state for the platinum catalyzed hydrohydrazination of pent-4-enoyl-*N'N'*-dimethyl hydrazide.



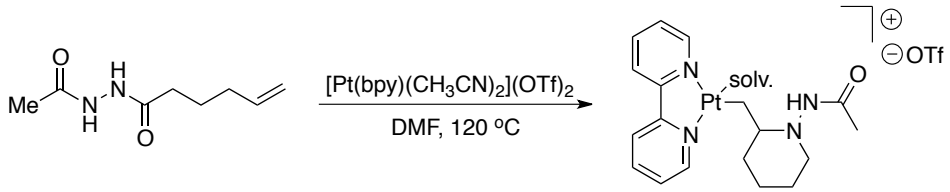

**Scheme 101: The addition of pent-4-enoyl-*N'N'*-dimethyl hydrazide to a solution of [Pt(bpy)(CH$_3$CN)$_2$](OTf). The reaction generates a cationic platinum(II) amino alkyl complex when performed at 120 °C.**

When the same reaction is performed at room temperature, a cationic platinum(II) amidate complex is formed by deprotonation of pent-4-enoyl-*N'N'*-dimethyl hydrazide (Scheme 102). This complex was isolated at room temperature and characterized by x-ray crystallography. Heating a solution of the cationic platinum(II) amidate complex to 120 °C generates the same cationic platinum(II) alkyl complex formed by the addition of pent-4-enoyl-*N'N'*-dimethyl hydrazide to [Pt(bpy)(CH$_3$CN)$_2$](OTf) at 120 °C.



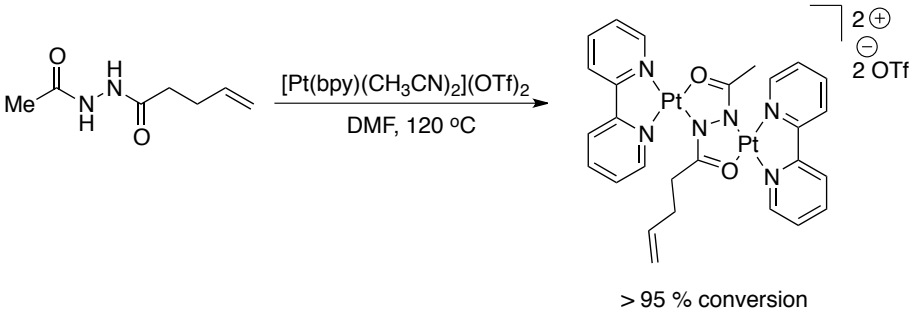

**Scheme 102: The addition of pent-4-enoyl-*N'N'*-dimethyl hydrazide to [Pt(bpy)(CH$_3$CN)$_2$](OTf). The reaction generates a cationic platinum(II) alkyl complex when performed at 120 °C.**

The addition of hex-5-enyl-*N'*-acetyl hydrazide to a solution of [Pt(bpy)(CH$_3$CN)$_2$](OTf) at 120 °C results in the formation of a cationic platinum(II) alkyl complex (Scheme 103). This complex was characterized by NMR spectroscopy and mass spectrometry and was observed as the catalyst resting state for the platinum catalyzed hydrohydrazination of hex-5-enyl-*N'*-acetyl hydrazide.

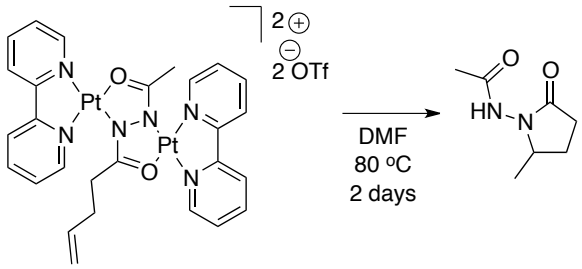



**Scheme 103: The addition of hex-5-enyl-*N*'-acetyl hydrazide to a solution of [Pt(bpy)(CH$_3$CN)$_2$](OTf). The reaction generates a cationic platinum(II) alkyl complex when performed at 120 °C.**

The addition of pent-4-enoyl-*N*'-acetyl hydrazide to a solution of [Pt(bpy)(CH$_3$CN)$_2$](OTf) results in the formation of a dinuclear dicationic platinum(II) amidate complex (Scheme 104). This complex was isolated at room temperature and characterized by NMR spectroscopy and mass spectrometry. Heating solutions of this dinuclear dicationic platinum(II) amidate complex to 80 °C for two days results in the formation of *N*-acetamido-2-methylpyrrolidin-5-one, without the observation of a platinum(II) alkyl intermediate (Scheme 105). Moreover the dinuclear dicationic platinum(II) amidate complex formed by the addition of pent-4-enoyl-*N*'-acetyl hydrazide to [Pt(bpy)(CH$_3$CN)$_2$](OTf) is observed as the catalyst resting state in the catalytic hydrohydrazination of pent-4-enoyl-*N*'-acetyl hydrazide with [Pt(bpy)(CH$_3$CN)$_2$](OTf).



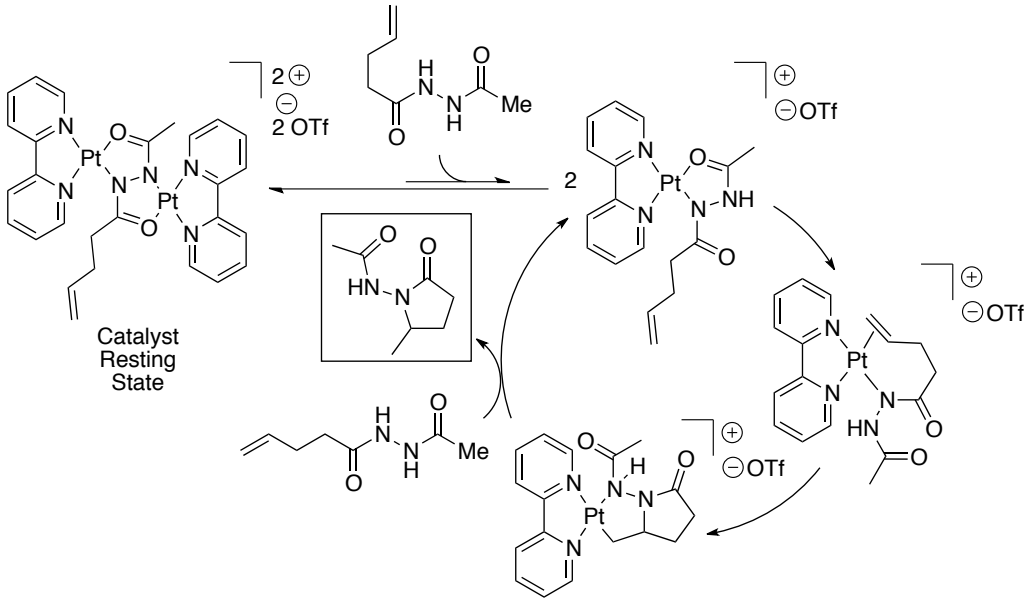

**Scheme 104: The addition of pent-4-enoyl-*N*'-acetyl hydrazide to a solution of [Pt(bpy)(CH$_3$CN)$_2$](OTf). The reaction generates a dinuclear dicationic platinum(II) amidate complex when performed at 120 °C.**




**Scheme 105: Decomposition of the dinuclear dicationic platinum(II) amidate complex formed by the addition of pent-4-enoyl-*N*'-acetyl hydrazide to a solution of [Pt(bpy)(CH$_3$CN)$_2$](OTf).The reaction occurs over the course of 2 days at 80 °C.**

To determine the effect of pH on the rate of alkene hydrohydrazination, catalytic reactions were performed in the presence of triflic acid (9 equivalents) and in the presence of 2,6-lutidine (2.5 equivalents). Both sets of conditions resulted in negligible differences in the rate of hydrohydrazination. Reactions performed in the presence of PhSiMe$_3$ also occurred with the same rate as those performed in the absence of PhSiMe$_3$. The data argue against a mechanism involving nucleophilic attack onto a coordinated alkene, which usually involve the formation of a zwitterionic intermediate and proton transfer from an ammonium group to the metal-alkyl bond. Reactions

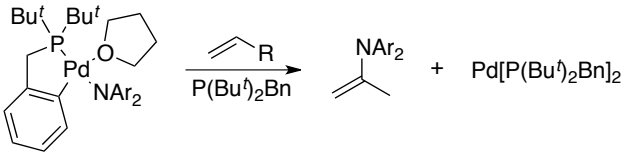
performed with the dinuclear dicationic platinum(II) amidate complex show a half-order dependence on the concentration of pent-4-enoyl-*N*'-acetyl hydrazide. The data are consistent with a mechanism in which protonation of the dinuclear dicationic platinum(II) amidate complex with pent-4-enoyl-*N*'-acetyl hydrazide precedes alkene insertion into the platinum-hydrazido bond and subsequent protonolysis of the platinum alkyl complex (Scheme 106).




**Scheme 106: The mechanism proposed by Michael and co-workers for the platinum-catalyzed hydrohydrazination of unsaturated hydrazines with [Pt(bpy)(CH$_3$CN)$_2$](OTf)$_2$.**

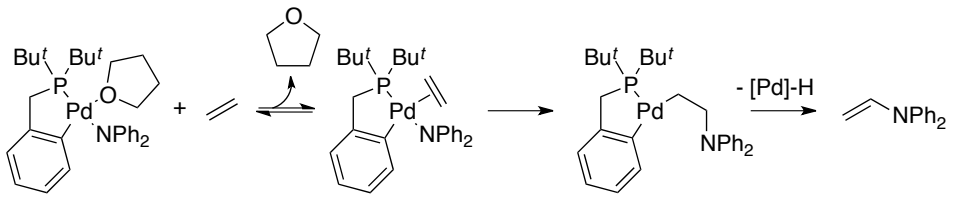
### 2.1.1.6 Insertions of unactivated alkenes into palladium-amido bonds

Insertions of unactivated alkene into palladium-diarylamido bonds were reported by Hartwig and co-workers in 2010 (Scheme 107).[69]



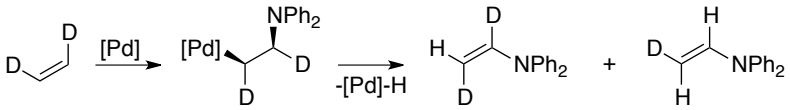

**Scheme 107: The addition of Pd[κ$^2$-P(bz)(tBu)$_2$] (NAr$_2$)(THF) to unactivated alkenes. The reaction was reported by Harwting and Hanley and 2010 and results in the formation of enamines, presumably by a mechanism involving alkene inseriton into a palladium-diarylamido bond.**

Reactions with ethene show a first-order dependence on catalyst concentration, a first order dependence on ethene concentration, and an inverse first-order dependence on THF concentration. The data are consistent with a mechanism in which substitution of THF with ethene precedes rate-limiting aminopalladation (Scheme 108).



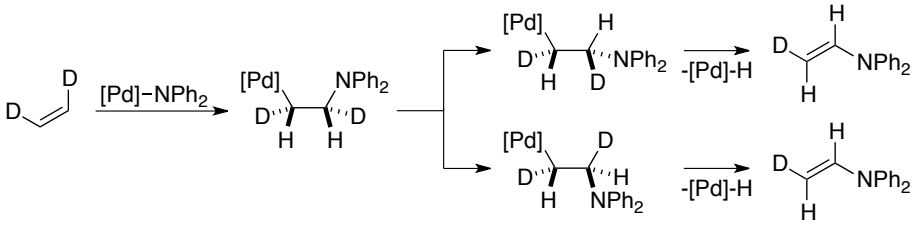
**Scheme 108: The mechanism proposed by Hartwig and Hanley for the additions of Pd[κ²-P(bz)(tBu)₂] (NAr₂)(THF) to unactivated alkenes. The reaction is thought to occur by a mechanism involving alkene inseriton into a palladium-diarylamido bond.**

To determine the mechanism for aminopalladation, reactions with *cis*-dideutero ethene were performed (Scheme 109).



**Scheme 109: The reaction between Pd[κ²-P(bz)(tBu)₂](NAr₂)(THF) and *cis*-dideuteroethene. The stereochemistries of the resulting enamines are consistent with a mechanism involving alkene insertion into the palladium-diarylamido bond of Pd[κ²-P(bz)(tBu)₂](NAr₂)(THF).**

The products from these reactions indicate that both palladium and the amino group add to the same face of the alkene (Scheme 110).



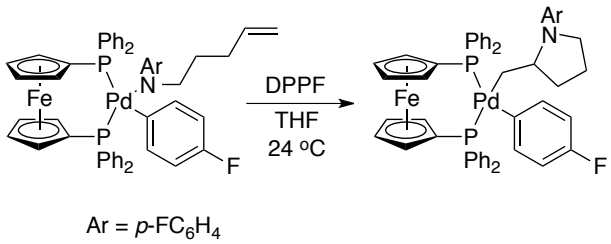
**Scheme 110: A mechanistic interpretatiion of the stereochemistries of the enamines formed by the reaction of Pd[κ²-P(bz)(tBu)₂](NAr₂)(THF) with *cis*-dideuteroethene. The stereochemistries of the resulting enamines are consistent with a mechanism involving alkene insertion into the palladium-diarylamido bond of Pd[κ²-P(bz)(tBu)₂](NAr₂)(THF).**

The outcome is consistent with an insertion mechanism.

To determine the effects of ligand properties on the rates for alkene insertion into palladium-amido bonds, reactions were performed with several different phosphines, amido groups and alkenes. The data indicate that reactions with more sterically-hindered phosphines are faster than reactions with less-sterically hindered phosphines. Moreover reactions with less electron-rich phosphines are faster than reactions with more electron-rich phosphines, and reactions with less electron-rich alkenes are faster than reactions with more electron-rich alkenes, and reactions with more electron-rich amido groups are faster than reactions with less electron-rich amido groups. The data are consistent with a mechanisms in which alkene insertion into the palladium-amido bond occurs by intramolecular nucleophilic attack of an amido ligand onto a coordinated alkene. Catalytic oxidative aminations are inhibited by rapid C-H reductive elimination of arene from the cyclometallated benzyl phosphine palladium hydride.

### 2.1.1.7 Insertions of tethered alkenes into palladium-amido bonds

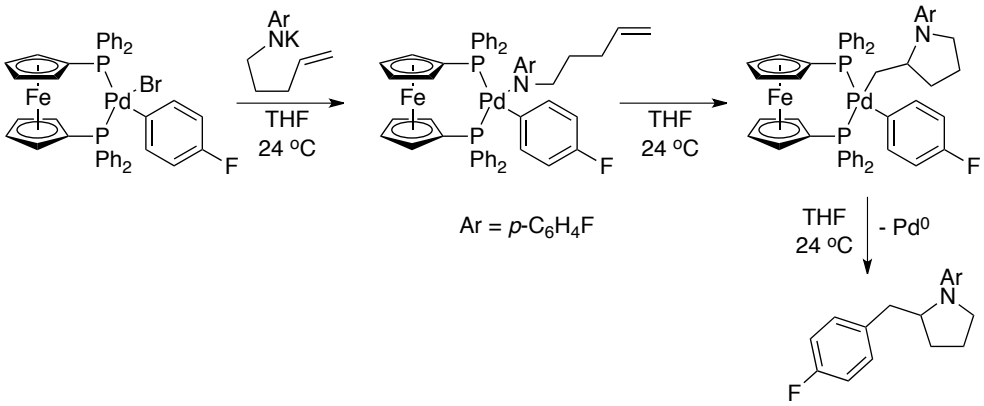
Insertions of tethered alkenes into palladium-amido bonds were reported by Wolfe 2010 (Scheme 111).[70]




**Scheme 111: The intramolecular additions of Pd-NAr bonds to tethered alkenes. The reactions were reported by Wolfe and co-workers in 2010 and are thought to occur by an insertion mechanism.**

The reactions constitute one step in a palladium-catalyzed carboamination of unsaturated amines with aryl halides. This latter reaction was reported in 2004, and was proposed to involve *syn*-aminopalladation or alkene insertions into palladium-amido bonds based on the identities of byproducts formed during the reactions (vide infra). The overall mechanism is thought to involve oxidative addition of an aryl halide to palladium(0), followed by base-assisted transmetallation of the amine to palladium(II), *syn*-aminopalladation, and $Csp^2$-$Csp^3$ reductive elimination of the substituted pyrrolidine product.

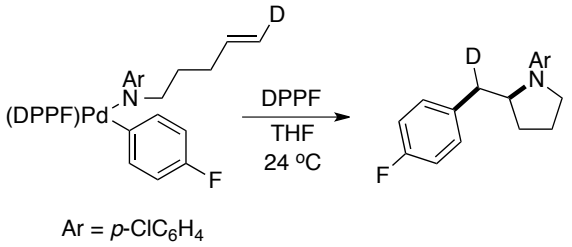
The aminopalladation step was eventually investigated by a series of stoichiometric reactions. Addition of potassium N-aryl-4-penten-1-amide to Pd(DPPF)(Br)(Ar) at room temperature generates a palladium(II) amido aryl complex, which undergoes intramolecular aminopalladation to form a palladium(II) aryl alkyl intermediate and eventually a substituted pyrrolidine by concerted $Csp^2$-$Csp^3$ reductive elimination (Scheme 112).



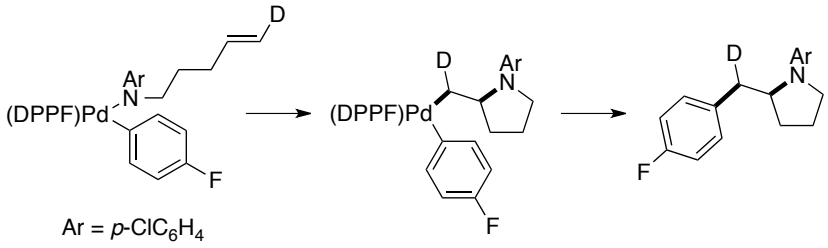

**Scheme 112: The addition of potassium N-aryl-4-penten-1-amide to Pd(DPPF)(Br)(Ar). The reaction generates a palladium(II) amido aryl complex, which undergoes intramolecular aminopalladation to form a palladium(II) aryl alkyl intermediate and eventually a substituted pyrrolidine by concerted $Csp^2$-$Csp^3$ reductive elimination.**

The palladium(II) aryl amido complex formed by the addition of potassium N-aryl-4-penten-1-amide to Pd(DPPF)(Br)(Ar) was characterized in situ by NMR spectroscopy. The palladium(II) aryl alkyl complex formed by aminopalladation was identified by $^{13}C$ NMR spectroscopy using a $^{13}C$-labeled amino alkene.

The mechanism for aminopalladation step was inferred from the reaction of a stereodefined deuterated amino alkene (Scheme 114).




**Scheme 113: Reactions performed with deuterated aminoalkenes to determine the stereochemistry of carboaminations. The stereochemistry of the pyrrolidine product is consistent with a mechanism involving alkene insertion into a palladium-amido bond..**



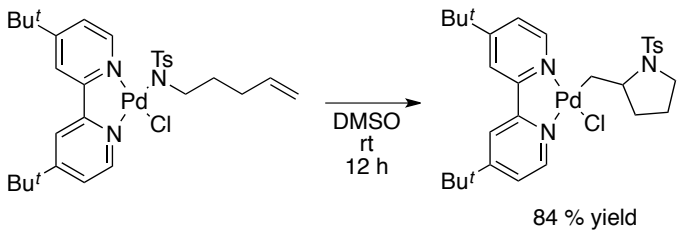

**Scheme 114: A possible mechanism for carboamination consistent with the stereochemistry of the resulting pyrollidine.**

The stereochemistry of the resulting pyrrolidine indicates that both the amino group and arene add to the same face of the alkene. Since carbon-carbon reductive elimination from palladium(II) occurs with retention of configuration at carbon, aminopalladation must occur by *syn*-aminopalladation or an insertion reaction.

To determine the effects of ligand properties on the rates for alkene insertion, reactions were performed with different diphosphines and amido groups on palladium. Reactions with more-electron-rich amido groups are faster than reactions with less-electron-rich amido groups. Reactions with less electron-rich diphosphines are faster than reactions with more electron-rich diphosphines, and reactions with diphosphine ligands having wider bite angles are faster than reactions with diphosphine ligands having smaller bite angles.

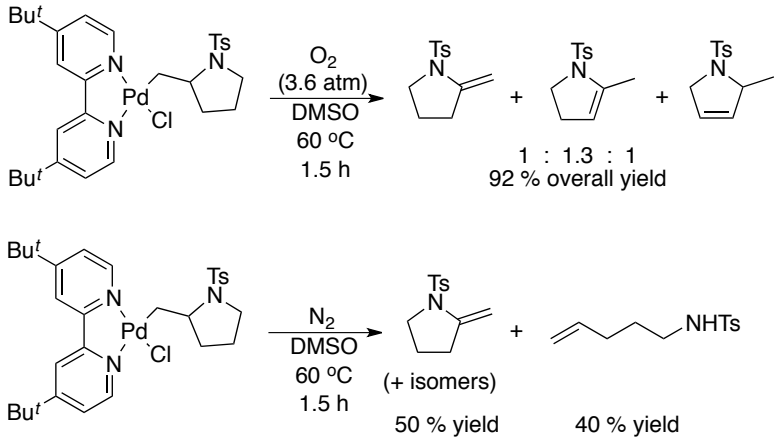
The data was interpreted in terms of a mechanism in which phosphine dissociation occurs to generate a four-coordinate palladium(II) aryl amido alkene complex. The faster rates observed with diphosphines having larger bite-angles and less electron-rich substituents were thought to arise from more facile dissociations of a phosphine group from palladium. It is not clear from the data, however, if phosphine dissociation from palladium actually occurs.

One year later, Stahl and co-workers reported the insertion of a tethered alkene into a palladium-tosylamido bond (Scheme 115).[71]



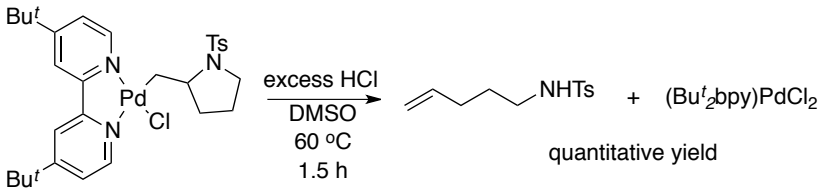

**Scheme 115: The intramolecular reaction of a palladium(II) bipyridyl amido chloride complex. The reaction was reported by Stahl and co-workers in 2011, and is thought to occur by alkene insertion into the palladium-amido bond of the starting complex.**

The reaction generates a stable palladium(II) alkyl chloride complex, which upon heating to 60 °C, in the presence of $O_2$, eliminates an unsaturated pyrrole. When the same reaction is performed in the absence of $O_2$, a significant amount of the unsaturated tosylamide is formed (Scheme 116).




**Scheme 116: The formation of unsaturated pyrollidines and tosylamides from the reactions of the palladium(II) bipyridyl alkyl chloride complexes reported by Stahl and co-workers. A signficant amoutn of the unsaturated tosylamide is formed when the reaction is performed in the absence of $O_2$.**

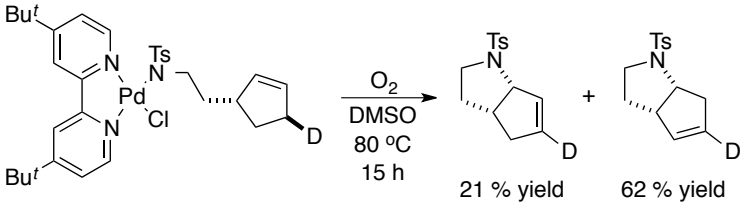
This change in product distribution was attributed to the formation of HCl in the reactions performed in the absence of $O_2$. The formation of HCl may occur by a mechanism involving aminopalladation of the alkene, followed by β-hydride elimination, and H-Cl reductive elimination from the resulting palladium hydrido chloride complex. Once formed, the generated HCl may react with the palladium alkyl chloride complex to form the unsaturated tosylamide. To test the possibility of this latter reaction, excess HCl was added to the palladium alkyl complex formed by aminopalladation (Scheme 117).




**Scheme 117: The addition of HCl to the palladium(II) bipyridyl alkyl chloride complexes reported by Stahl and co-workers. The reactions generate unsaturated tosylamides and palldium(II) dichlorides in quantitative yield.**

The reactions generated unsaturated tosylamide in quantitative yield. The results imply that aminopalladation is reversible. In this case elimination (or de-insertion) of an alkene from the palladium(II) alkyl chloride complex generates a palladium(II) amido chloride complex, which then reacts with acid to form the unsaturated amine. Protonation of the palladium-alkyl bond by added HCl is not observed.

To determine the mechanism for aminopalladation step, reactions were performed with enantiopure deuterated cyclopentenyl tosylamides (Scheme 118).




**Scheme 118: The reactions of palladium(II) bipyridyl amido chloride complexes performed with enantiopure deuterated cyclopentenyl tosylamides. The products formed by these reactions suggest that aminopalladation occurs by an insertion mechanism.**

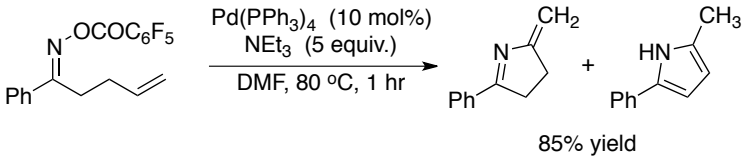
Similar experiments were performed by the groups of Hayashi, Stoltz, and Stahl to determine the mechanisms for alkoxo- and aminopalladations for separate oxidative alkoxylations and aminations. The products obtained from the reaction of are consistent with a mechanism involving alkene insertion into a palladium-amido bond.

The overall reaction is inhibited by added LiCl and promoted by polar solvents. The data are consistent with a mechanisms in which substitution of a chloride ion with alkene occurs prior to aminopalladation.

### 2.1.1.8 Additional reactions

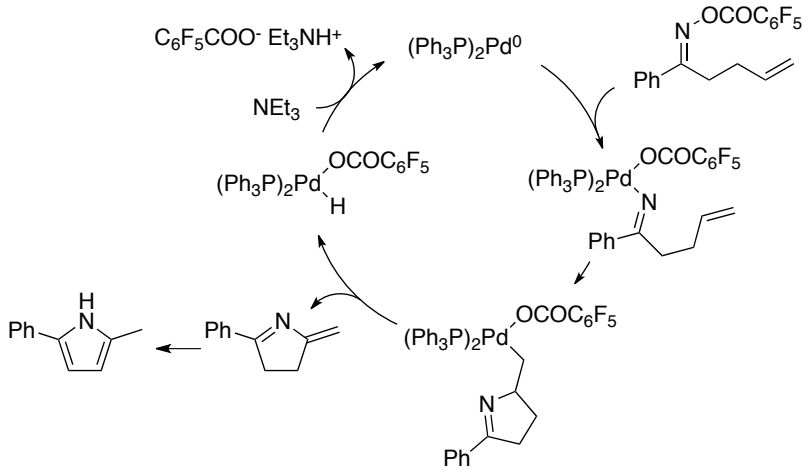
#### 2.1.1.8.1 Palladium-catalyzed hetero-Heck-type reactions and aminochlorinations of alkenes

Palladium-catalyzed hetero-Heck-type reactions of unsaturated *O*-pentafluorobenzoyloximes were reported by Tsutsui and Narasaka in 1999 (Scheme 119).[72]




**Scheme 119: A palladium-catalyzed hetero-Heck-type reactions of unsaturated *O*-pentafluorobenzoyloximes with Pd(PPh$_3$)$_4$. The reaction was reported by Tsutsui and Narasaka in 1999, and is thought to occur by N-O oxidative addition of the *O*-pentafluorobenzoyloximes substrate followed by alkene insertion into the resulting palladium-amido bond and β-hydrogen elimination.**

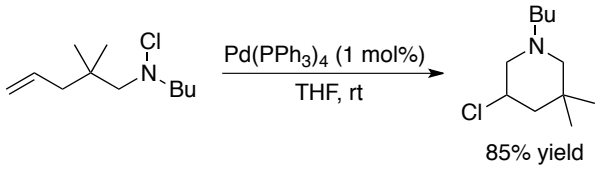
The reactions generate substituted pyrroles, presumably by a mechanism involving N-O oxidative addition of the *O*-pentafluorobenzoyloxime substrates at palladium(0), followed by alkene insertion into the resulting palladium-amido bond, and β-hydride elimination of a methylene dihydropyrrole, which subsequently rearranges to the substituted pyrrole (Scheme 120).




**Scheme 120: The mechanism proposed by by Tsutsui and Narasaka for the palladium-catalyzed formation of pyrroles from *O*-pentafluorobenzoyloximes.**

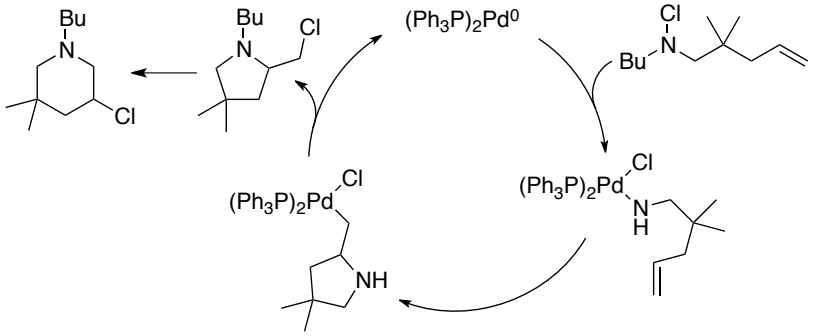
An insertion mechanism is proposed for these reactions based on the likelihood that N-O oxidative addition of the *O*-pentafluorobenzoyloximes occurs prior to alkene functionalization.

Similar palladium-catalyzed aminochlorinations of unsaturated *N*-chloroamines were reported by Helaja and Göttlich in 2002 (Scheme 121).[73]




**Scheme 121: A palladium-catalyzed amino chlorinations of unsaturated *N*-chloroamines. The reaction was reported by Helaja and Göttlich in 2002, and is thought to occur by N-Cl oxidative addition of the *N*-chloroamine, followed by alkene insertion into the resulting palladium-amido bond, C-Cl reductive elimination and rearrangement of the 2-chloromethylpyrrolidine product to a chloropiperidine.**

The reactions generate 3-chloropiperidines presumably by a mechanism involving oxidative addition of the N-Cl bond of the *N*-chloroamines at palladium(0), followed by alkene insertion into the resulting palladium(II)-amido bond, and C-Cl reductive elimination from palladium(II) (Scheme 122). The resulting 2-chloromethylpyrrolidines subsequently rearrange to 3-chloropiperidines.

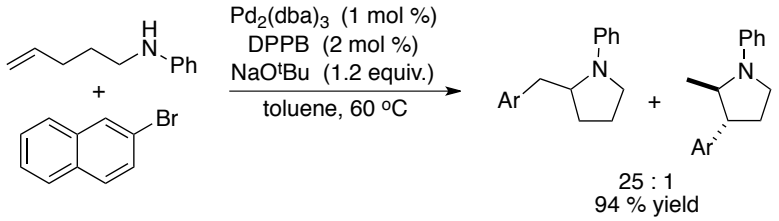



**Scheme 122: The mechanism proposed by Helaja and Göttlich for the palladium-catalyzed formation of chloropiperidines from *N*-chloroamines.**

An insertion mechanism is proposed for these reactions based on the likelihood that N-Cl oxidative addition occurs prior to alkene functionalization.

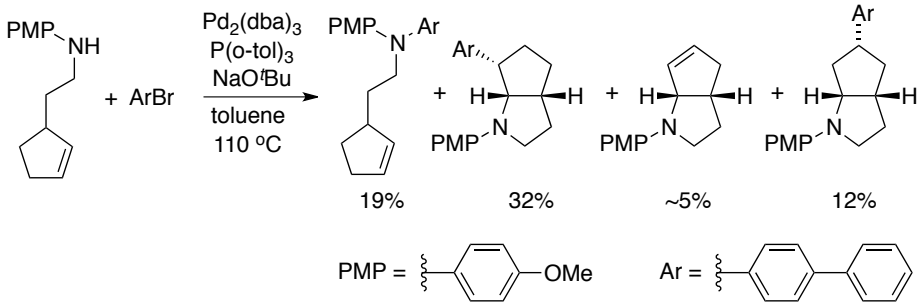
### 2.1.1.8.2 Palladium-catalyzed carboaminations

Palladium-catalyzed carboaminations of unsaturated alcohols were reported by Wolfe and co-workers in 2004 (Scheme 123).[74]



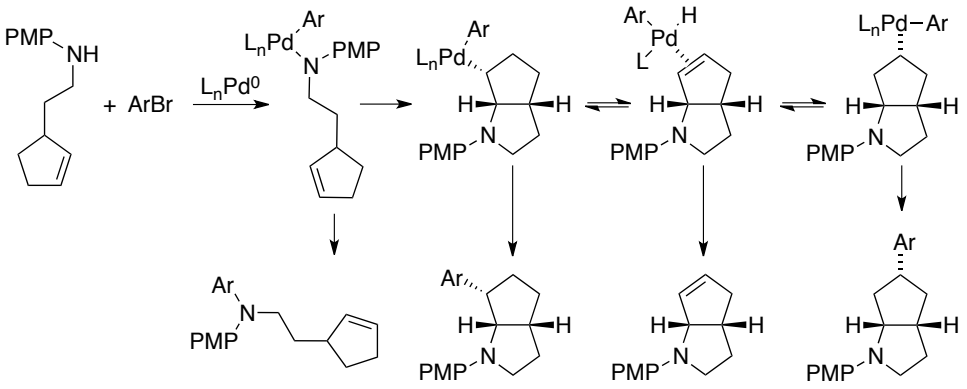

**Scheme 123: A palladium-catalyzed carboamination of unsaturated alcohols with aryl halides. The reaction was reported by Wolfe and co-workers in 2004, and is thought to occur by a mechanism involving oxidative addition of the aryl halide followed by base-assisted transmetallation of the amine to palladium(II), *syn*-aminopalladation, and $Csp^2$-$Csp^3$ reductive elimination of the substituted pyrrole product.**

The reactions are thought to occur by a mechanisms involving oxidative addition of an aryl halide to palladium(0), followed by base-assisted transmetallation of the amine to palladium(II), *syn*-aminopalladation, and $Csp^2$-$Csp^3$ reductive elimination of the substituted pyrrole product. Support for an insertion mechanism was initially provided by the reactions of cyclopentenylamines with aryl halides (Scheme 124).




**Scheme 124: The products formed by the reactions of $Pd_2(dba)_3$ with cyclopentenylamines and aryl bromides. The different products are thought to form from a common intermediate.**

The reactions of cyclopentenylamines under these conditions produce a mixture of aryl amine and bicyclic pyrrolidine products. The authors suggest that bicyclic pyrrolidines products arise from a common palladium(II) aryl alkyl intermediate formed by *syn*-aminopalladation of the alkene (Scheme 125).

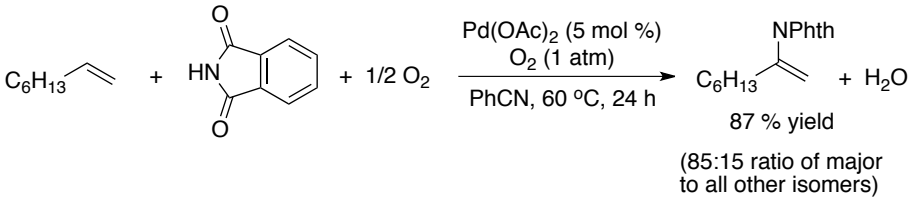


**Scheme 125: The mechanism proposed by Wolfe and co-workers to account for the products formed by the reactions of $Pd_2(dba)_3$ with cyclopentenylamines and aryl bromides**

This mechanism was later supported by the reactions of stereodefined deuterated alkenes (vide supra).

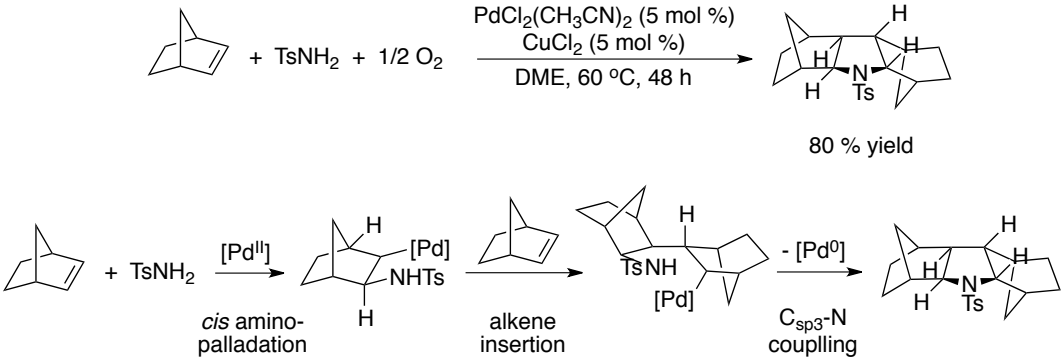
### 2.1.1.8.3 Palladium-catalyzed oxidative aminations

Palladium-catalyzed oxidative aminations of alkenes and unsaturated tosylamides were reported by Stahl and co-workers in 2005 and in 2007 (Scheme 126).[41a,42]



**Scheme 126: A palladium-catalyzed oxidative amination of simple alkenes with phthalimide. The reaction was reported by Stahl and co-workers in 2005 and 2007, and is thought to occur by a mechanism involving alkene insertion into a palladium-amido bond.**

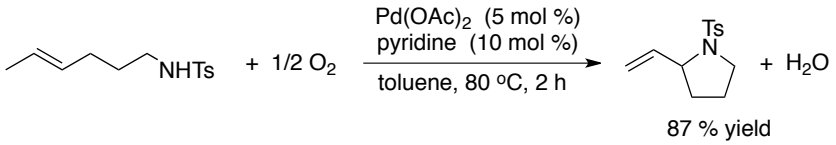
Although a mechanism was not proposed for the oxidative aminations of simple alkenes with phthalimides and tosylamides, the reactions of norbornene with tosylamides, $TsNH_2$, suggest a mechanism involving alkene insertion into a palladium-amido bond (Scheme 127).



**Scheme 127: A palladium-catalyzed oxidative amination of norbornene with tosylamides. The reaction was reported by Stahl and co-workers in 2005 and 2007, and is thought to occur by a mechanism involving alkene insertion into a palladium-amido bond.**

In this case, a substituted pyrrolidine is formed by successive insertions of norbornene into palladium-tosylamido and -alkyl bonds, and $Csp^3$-N reductive elimination.

An insertion mechanism for the palladium-catalyzed intramolecular oxidative amination of unsaturated tosylamides was later suggested by the reactions of stereodefined amino alkenes (Scheme 128).

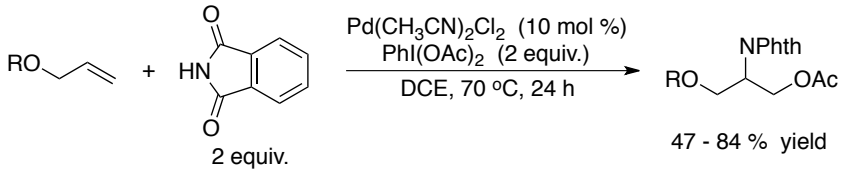



**Scheme 128: A palladium-catalyzed oxidative amination of unsaturated tosylamides. The reactions were reported by Stahl and co-workers in 2007, and are thought to occur by alkene insertion into a palladium-amido bond. Evidence supporting this mechanism is provided by the stereochemistries of the products formed from stereodefined deuterated alkenyl amines. These reactions are discussed in greater detail in Chapter 1.**

These reactions are discussed in Chapter 1.

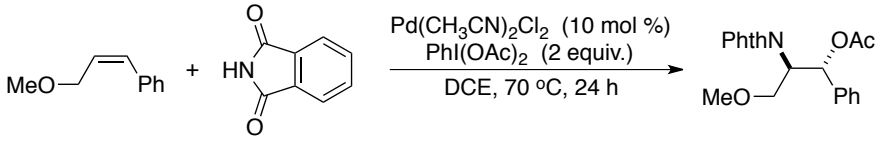
### 2.1.1.8.4 Palladium-catalyzed aminoacetoxylations

Palladium-catalyzed aminoacetoxylations of alkenes with phthalimide and $PhI(OAc)_2$ were reported by Stahl and co-workers in 2006 (Scheme 129).[75]



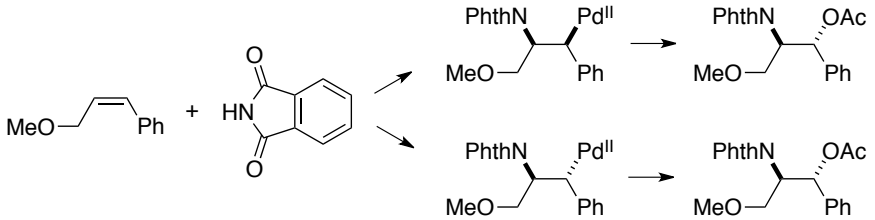

**Scheme 129: A palldium-catalyzed aminoalkoxylation of allylic ethers with phthalimide and $PhI(OAc)_2$. The reactions were reported by Stahl and co-workers in 2006, and are thought to occur by a mechanism involving alkene insertion into a palladium-amido bond. Evidence supporting this mechanism is provided by the diastereoselectivity of the reaction and by the stereochemistry of oxidative aminations performed under similar conditions.**

The reactions generate vicinal amino acetates from alkenes. Reactions performed with stereodefined internal alkenes show that phthalimide and acetate add to opposite faces of the alkene (Scheme 130).[75]



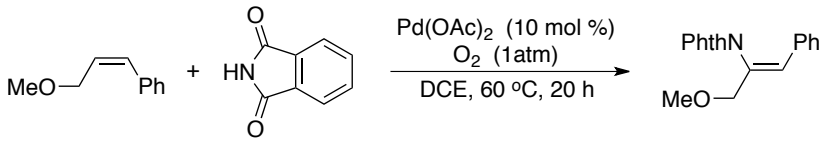

**Scheme 130: The reaction of a a stereodefined, Z-subsituted allylic ether with phthalimide and $PhI(OAc)_2$ in the presence of $Pd(CH_3CN)_2Cl_2$ (10 mol %). The reaction generates a vicinal amino aceetate whose relative stereochemistry is consistent with an insertion mechanism (vide infra).**

The diastereoselectivity of this reaction is consistent with two different mechanisms. In the first mechanism, *syn*-aminopalladation is followed by C-O reductive elimination with inversion of configuration at carbon. In the second mechanism, *anti*-aminopalladation is followed by C-O reductive elimination with retention of configuration at carbon (Scheme 131).




**Scheme 131: Two mechanistic pathways for the palladium-catalyzed formation of aminoacetates. The top pathway involves by *syn*-aminopalladation followed C-O bond formation with inversion of configuration, while the bottom pathway involves *anti*-aminopalladation followed by C-O bond formation with retention of configuration.**

To distinguish between these two mechanisms, oxidative aminations of allylic ethers were performed with phthalimide and $Pd(OAc)_2$ under similar conditions (Scheme 132).

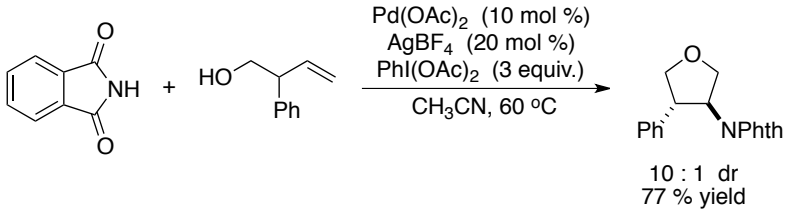



**Scheme 132: Oxidative amination of an allylic ether under similar conditions. The stereochemistry of the resulting enamine is consistent with a mechanistic pathway that involves *syn*-aminopalladation.**

The geometries of the resulting enamines are consistent with a mechanism in which palladium and phthalimide add to the same face of the alkene. Consequently, a mechanism involving *syn*-aminopalladation is proposed for the aminoacetoxylation reactions. To account for the overall *anti* diastereoselectivity of the aminoacetoxylation reaction, C-OAc bond formation must occur with inversion of configuration at carbon.

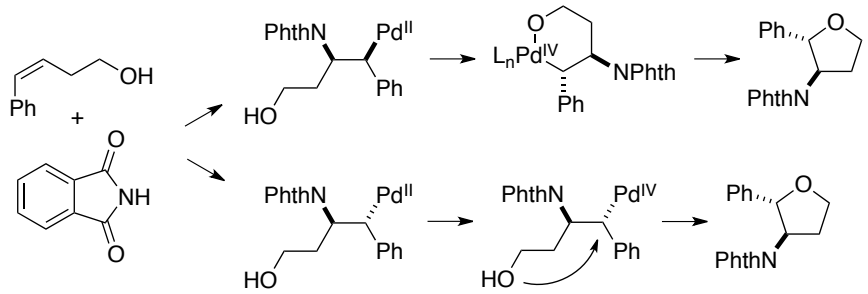
### 2.1.1.8.5 Palladium-catalyzed aminoalkoxylations

Palladium-catalyzed aminoalkoxylations of homoallylic alcohols with phthalimide and $PhI(OAc)_2$ were reported by Sanford and co-workers in 2007 (Scheme 133).[76]



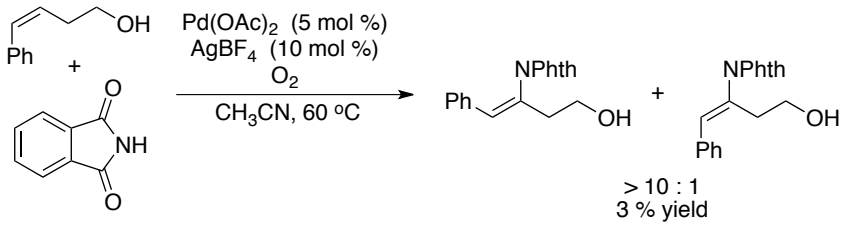

**Scheme 133: A palladium-catalyzed aminoalkoxylation of unsaturated alcohols with phthalimide and $PhI(OAc)_2$ as oxidant. The reaction was reported by Sanford and co-workers in 2007, and is thought to involve insertion of an alkene into a palladium-amido bond. Evidence supporting this mechanism is provided by the diastereoselectivity of the reaction and by the stereochemistry of oxidative aminations performed under similar conditions.**

The diastereoselectivity of this reaction is consistent with a mechanism in which *syn*-aminopalladation is followed by C-O reductive elimination with retention of configuration at carbon or with a mechanism in which *anti*-aminopalladation is followed by C-O reductive elimination with inversion of configuration at carbon (Scheme 134).




**Scheme 134: Two mechanistic pathways for the palladium-catalyzed formation of aminoacetates. The top pathway involves by *syn*-aminopalladation followed C-O bond formation with retention of configuration, while the bottom pathway involves *anti*-aminopalladation followed by C-O bond formation with inversion of configuration.**

Support for *syn*-aminopalladation pathway is provided by the oxidative amination of (Z)-4-phenyl-3-buten-1-ol under similar reaction conditions (Scheme 135).

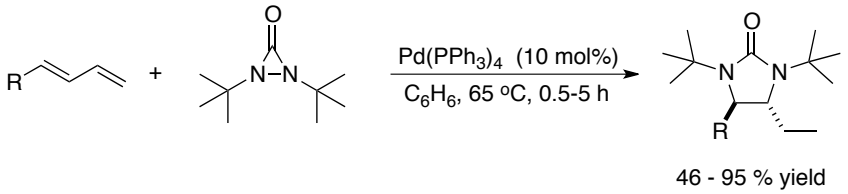



**Scheme 135: Oxidative amination of an unsaturated alcohol under similar conditions. The stereochemistry of the resulting enamine is consistent with a mechanistic pathway that involves *syn*-aminopalladation.**

The geometry of the resulting enamine supports a mechanism involving alkene insertion into a palladium(II)-amido bond. Consequently, alkene insertions into palladium-amido bonds are proposed for the palladium-catalyzed aminoalkoxylations of alkenes with phthalimide and $PhI(OAc)_2$. To account for the overall *syn* diastereoselectivity of the aminoalkoxylation reaction, C-OR bond formation must occur with retention of configuration at carbon

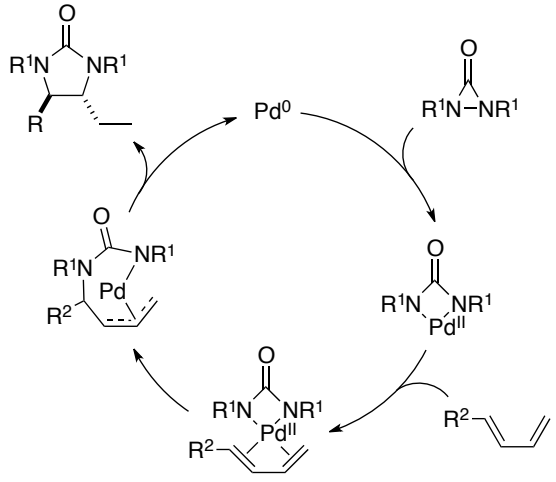
### 2.1.1.8.6 Palladium-catalyzed diaminations

Palladium-catalyzed diaminations of conjugated dienes with diaziridinones were reported by Shi and co-workers in 2007 (Scheme 136).[77]




**Scheme 136: A palladium-catalyzed diaminations of conjugated dienes with diaziridinones. The reactions were reported by Shi and co-workers in 2007, and are thought to occur by a mechanism involving alkene insertion into a palladium-amido bond.**

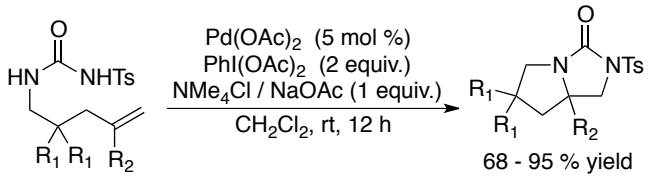
The reactions are proposed to occur by a mechanism involving N-N oxidative addition of the diaziridinone at palladium(0), followed by diene insertion into one of the palladium-amido bonds, and intramolecular nucleophilic attack onto the resulting $\eta^3$-allyl complex (Scheme 137).




**Scheme 137: The mechanism proposed by Shi and co-workers for the palladium-catalyzed diaminations of conjugated dienes with diaziridinones.**

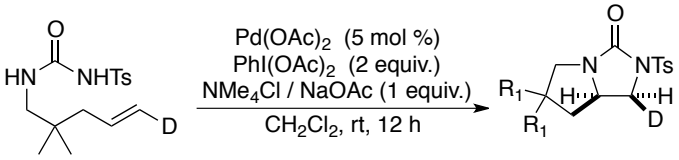
Support for an insertion mechanism comes primarily from the assumption that N-N oxidative addition of the diaziridinone occurs at palladium(0) to form two palladium-amido bonds prior to any transformation of the diene, and that the two amido groups do not dissociate from the metal.

Palladium-catalyzed diaminations of tethered alkenes with urea derivatives and sulfamides were reported by Muñiz and co-workers in 2008 (Scheme 138).[78]




**Scheme 138: A palladium-catalyzed intramolecular diamination of unsaturated urea derivatives. The reaction was first reported by Muñiz and co-workers in 2008, and is thought to occur by a mechanism involving alkene insertion into a palladium-amido bond followed by $C_{sp3}$-N bond formation with inversion of configuration (vide infra).**

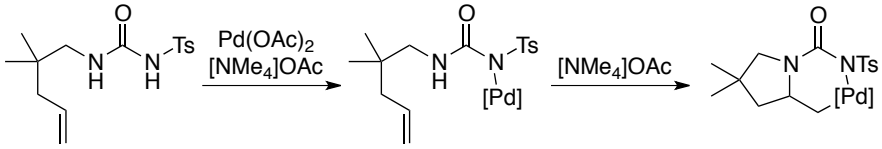
The reactions generate cyclic urea derivatives. When stereodefined deuterated alkenes are used, diastereopically pure cyclic ureas are formed (Scheme 139).




**Scheme 139: The stereochemistry for the palladium-catalyzed diamintion of unsaturated urea derivatives.**

The diastereoselectivity of this reaction indicates that the two amide groups add to opposite faces of the alkene. This diastereoselectivity is consistent with at least two different mechanisms. In the first mechanism, *syn*-aminopalladation is followed by C-O reductive elimination with inversion of configuration at carbon. In the second mechanism, *anti*-aminopalladation is followed by C-O reductive elimination with retention of configuration at carbon.

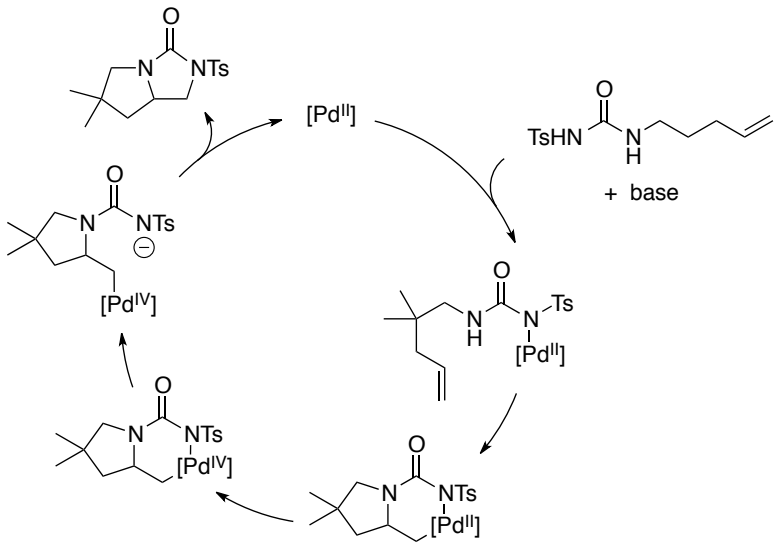
To determine the order of amine addition, mixtures of $Pd(OAc)_2$ and unsaturated urea were titrated with $[NMe_4]OAc$ (Scheme 140).




**Scheme 140: The addition of *N*-((2,2-dimethylpent-4-en-1-yl)carbamoyl)-4-methylbenzenesulfonamide to $Pd(OAc)_2$ / $[NMe_4]OAc$. In the presence of one equivalent of $[NMe_4]OAc$, palladium-amido complex is formed. In the presence of two equivalents of $[NMe_4]OAc$, palladium alkyl amido complex is formed, presumably by alkene insertion into the palladium-amido bond of the first complex formed.**

Upon the addition of one equivalent of $[NMe_4]OAc$, the tosylamide is completely and irreversibly deprotonated and a palladium amido complex forms. Upon addition of a second equivalent of $[NMe_4]OAc$, a palladium-alkyl complex or diazometallocyclohexane is formed.

Although the data is insufficient to determine which amido group adds by which mechanism, the authors propose that the non-tosyl amine adds to the alkene occurs by an insertion mechanism, while the tosyl amine adds to the resulting alkyl fragment by nucleophilic attack onto a palladium(IV) alkyl complex (Scheme 141).




**Scheme 141: The mechanism proposed by Muñiz and co-workers for the palladium-catalyzed intramolecular diaminations of unsaturated urea derivatives.**

#### 2.1.1.8.7 Copper-catalyzed aminooxygenations of alkenes

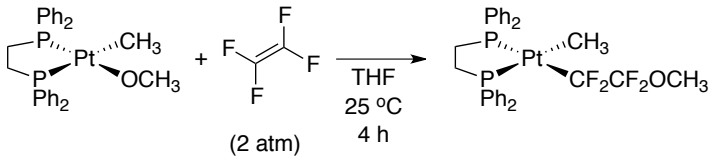
Alkene insertions into copper-amido bonds were proposed by Chemler and co-workers in 2007 for a copper-catalyzed aminoarylation of unsaturated tosylamides. Support for an insertion mechanism was initially provided by similarities between the diastereoselectivities of these reactions and the diastereoselectivities reported by Wolfe and co-workers for a palladium-catalyzed carboamination of amino alkenes (vide supra).

### 2.1.2 Alkene Insertions into Metal-Alkoxo Bonds

Alkene insertions into metal-alkoxo bonds have been reported for palladium-catalyzed oxidative alkoxylations and carboetherifications of alkenyl alcohols. Alkene insertions into metal-alkoxo bonds have also been proposed form the reactions of isolated platinum- and rhodium-alkoxo and -phenoxo complexes with activated and tethered alkenes. This section examines those reactions in which alkene insertions into metal-alkoxo bonds have either been observed directly or inferred from the stereochemistry of the resulting products. Examples of alkene insertions into metal-alkoxo bonds are less common than examples of alkene insertions into metal-amido bonds.

#### 2.1.2.1 Insertions of perfluoroalkenes into a platinum-methoxo bond

Insertion of tetrafluoroethene into the platinum-methoxo bond of Pt(DPPE)(Me)(OMe) was reported by Bryndza in 1984 (Scheme 142).[79]



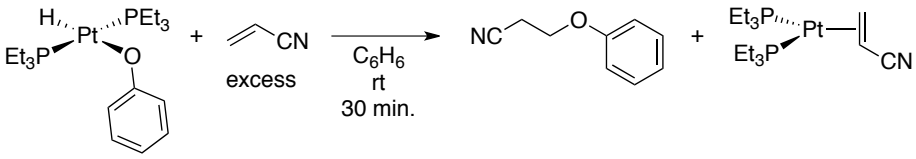

**Scheme 142: Insertion of tetrafluoroethene into the platinum-methoxide bond of Pt(DPPE)(Me)(OMe). The reaction was reported by Bryndza in 1984. Support for an inseriton mechanism was provided by a series of mechanistic and kinetic experiments.**

The reaction produces a stable platinum(II) alkyl complex, which can be isolated at room temperature. Other alkenes, such as ethene, 1-pentene, acrylonitrile, and methyl acrylate do not insert. In addition, only insertions

into the platinum-methoxide bond are observed; alkene insertions into the platinum-methyl bond are not reported. The rate-expression for the reaction shows a first-order dependence on platinum concentration and a first-order dependence on tetrafluoroethene concentration. The rates are too fast for the reaction to occur by methoxide dissociation. Moreover, less than 8% $OCD_3$ is incorporated in the final product when the reactions are performed in $d^4$-methanol. The data are consistent with a mechanism in which alkene coordination to platinum is followed by insertion into the platinum-methoxide bond. Additional support for an insertion mechanism is provided by the observation that at -80 °C, the $^{19}F$ chemical shift of tetrafluoroethene changes proportionally with the concentrations of $Pt(DPPE)(CH_3)(OCH_3)$ and tetrafluoroethene, suggesting the formation of a five-coordinate platinum methoxide alkene complex.

### 2.1.2.2 Insertion of acrylonitrile into a platinum-phenoxo bond

Insertion of acrylonitrile into the platinum-phenoxo bond of *trans*-$Pt(PEt_3)_2(H)(OPh)$ was reported by Cowan and Trogler in 1989 (Scheme 143).[65b]

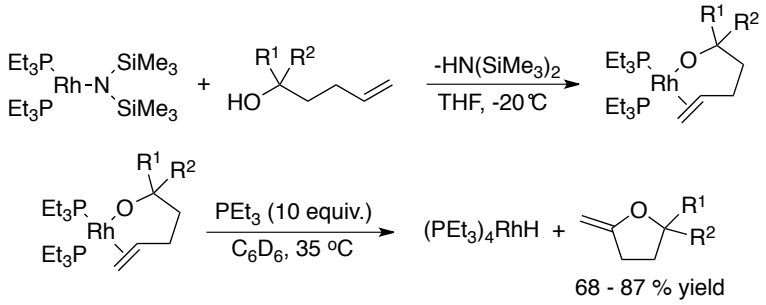



**Scheme 143: Insertion of acrylonitrile into the platinum-phenoxo bond of *trans*-$Pt(PEt_3)_2(H)(OPh)$. The reaction was reported by Cowan and Trogler in 1989.**

Similar reactions were reported with *trans*-$Pt(PEt_3)_2(H)(NHPh)$. The two reactions result in different products. Insertion of acrylonitrile into the platinum-phenoxo bond of *trans*-$Pt(PEt_3)_2(H)(OPh)$ results in the immediate formation of 3-phenoxy propionitrile. In contrast, insertion of acrylonitrile into the platinum-anilido bond of *trans*-$Pt(PEt_3)_2(H)(NHPh)$ results in the formation of a stable platinum(II) alkyl complex. Subsequent heating results in the formation of 3-aniline propionitrile. It is not immediately clear why the platinum(II) amino alkyl complex is relatively stable towards C-H reductive elimination and the analogous platinum(II) alkoxo alkyl complex is not.

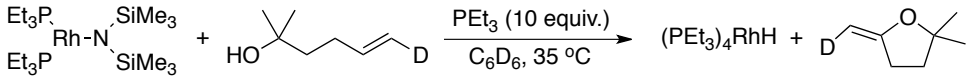
### 2.1.2.3 Insertions of tethered alkenes into rhodium-alkoxo bonds

Insertions of tethered alkenes into rhodium-alkoxo bonds were reported by Hartwig and co-workers in 2006 (Scheme 144).[80]



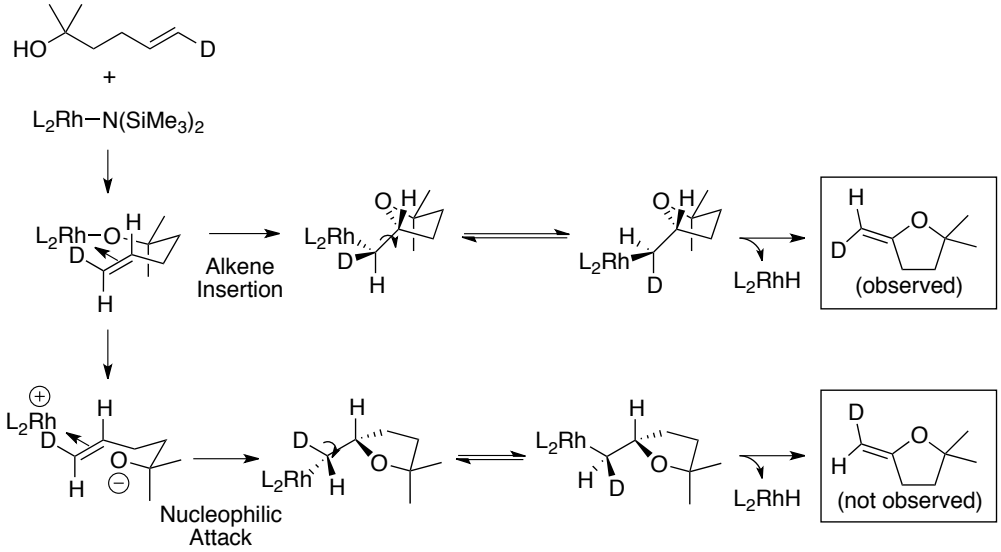

**Scheme 144: The insertions of tethered alkenes into the rhodium-alkoxo bonds of unsaturated rhodium alkoxide complexes. The reactions were reported by Hartwig and co-workers in 2006. Support for an insertion mechanism is provided by the stereochemistry of the unsaturated furan product forme by the addition of 6-deutero-2-methyl-5-hexen-1-ol to rhodium bis(triethylphosphine) hexamethyldisilylamide.**

The reactions result in the formation of substituted furans and rhodium-hydrido complexes. Characterization of the rhodium alkoxo alkene complexes formed prior to insertion was carried out at -20 °C. Support for an insertion mechanism was provided by the reactions of (*E*)-6-deutero-2-methyl-5-hexen-2-ol (Scheme 145).




**Scheme 145: The addition of 6-deutero-2-methyl-5-hexen-1-ol to rhodium bis(triethylphosphine) hexamethyldisilylamide. The reaction generates an unsaturated furan product, whose stereochemistry is consistent with a mechanism involving alkene insertion into a rhodium alkoxo bond.**

In this case, the geometry of the resulting 2,2-dimethyl-5-methylene furan is consistent with a mechanism involving alkene insertion into the rhodium-alkoxo bond of the corresponding alkoxo alkene complex (Scheme 146).



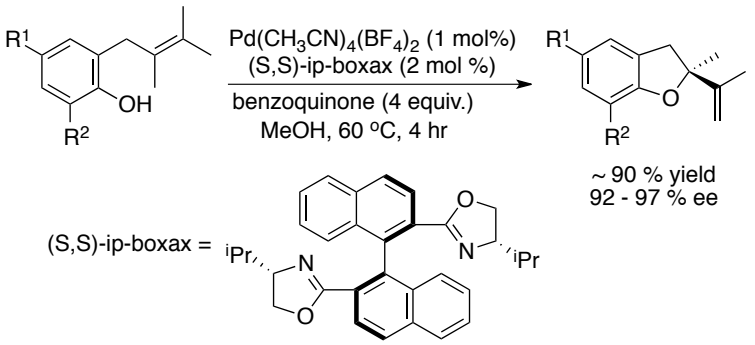

**Scheme 146: A mechanistic analysis of the products formed by the addition of 6-deutero-2-methyl-5-hexen-1-ol to rhodium bis(triethylphosphine) hexamethyldisilylamide.**

The reactions can be made catalytic by applying an appropriate hydrogen acceptor or oxidant.[81]

### 2.1.2.4 Additional reactions

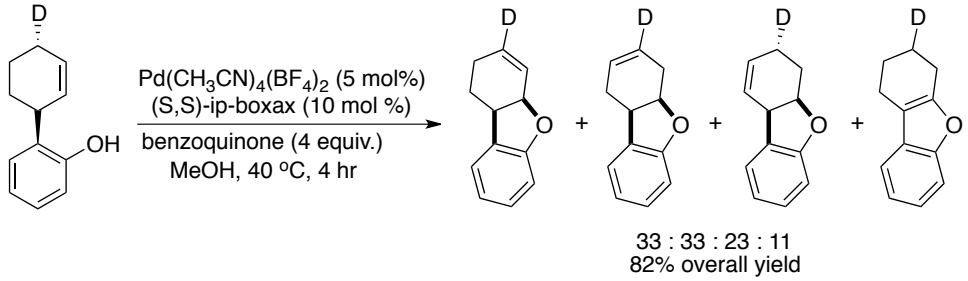
#### 2.1.2.4.1 Oxidative alkoxylations of 2-allyl phenols

Alkene insertions into palladium-alkoxo bonds, were reported by Hayashi and co-workers in 2004, for a palladium-catalyzed intramolecular oxidative alkoxylation of 2-allylphenols (Scheme 147).[60]



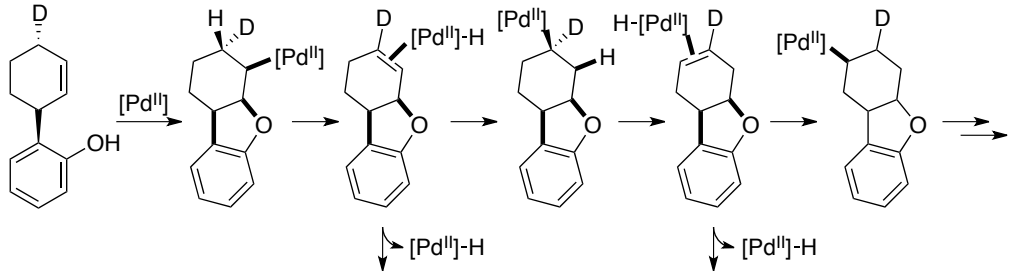

**Scheme 147: A palladium-catalyzed oxidative alkoxylation of 2-allylphenols. The reaction was reported by Hayashi and co-workers in 2004 and is thought to occur by a mechanism involving alkene insertion into a palladium-phenoxide bond.**

In this case, support for an insertion mechanism is provided by the reactions of enantiopure deuterated cyclohexenyl phenols (Scheme 148).




**Scheme 148: Products formd by the reaction of (1'*R*,4'*S*)-4'-deutero-1',2',3',4'-tetrahydro-[1,1'-biphenyl]-2-ol with $Pd(CH_3CN)_4(BF_4)_2$ (5 mol %), (S,S)-ip-boxax (10 mol %), and benzoquinone (4 equiv.). The identities of the products are consistent with a mechanism involving alkene insertion into a palladium-phenoxide bond (vide infra).**

The products from these reactions suggest that the phenoxo group and palladium add to the same face of the alkene. Additional products are formed by insertion of the enamide product into the resulting rhodium-hydrido bond with opposite regioselectivity and subsequent β-hydride elimination (Scheme 149).

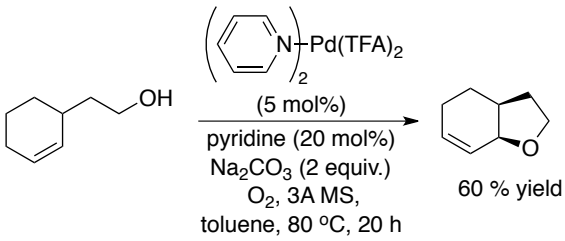



**Scheme 149: A mechanistic interpretation of the products formed by the reaction of (1'*R*,4'*S*)-4'-deutero-1',2',3',4'-tetrahydro-[1,1'-biphenyl]-2-ol with $Pd(CH_3CN)_4(BF_4)_2$ (5 mol %), (S,S)-ip-boxax (10 mol %), and benzoquinone (4 equiv.).**

These reactions are discussed in Chapter 1.

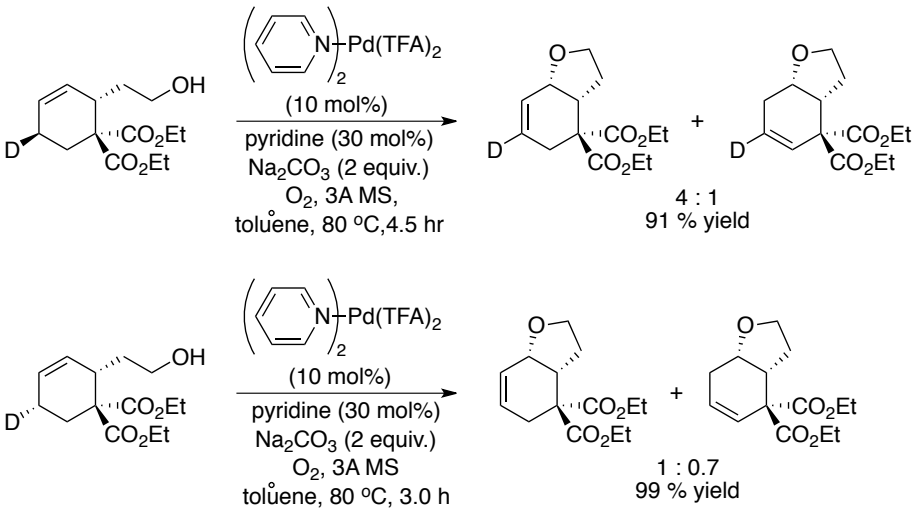
### 2.1.2.4.2 Oxidative alkoxylations of unsaturated alcohols

Similar reactions were performed by Stoltz and co-workers in 2005 to determine the mechanism for a palladium-catalyzed oxidative alkoxylation of unsaturated alcohols (Scheme 150). [61]




**Scheme 150: A palladium-catalyzed oxidative alkoxylation of unsaturated alcohols using $Pd(py)_2(TFA)_2$ (5 mol%) as catalyst and $O_2$ as oxidant. The reaction was reported by Stoltz and co-workers in 2005. The stereochemistry of the resulting furan products is consistent with a mechanism involving alkene insertion into a palladium alkoxo bond.**

In this case, the products formed by the oxidative alkoxylation of enantiopure deuterated cyclohexenyl alcohols are consistent with a mechanism involving syn-alkoxypalladation and β-hydride elimination with *syn* selectivity (Scheme 151).

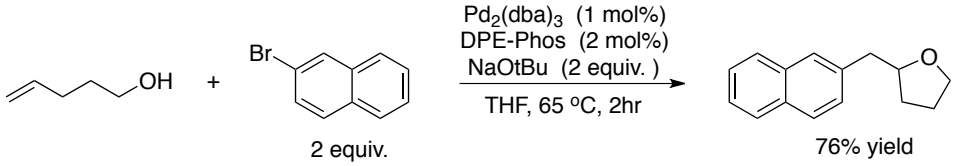



**Scheme 151: The reactions stereodefined, deuterated alkenyl alcohols. The stereochemistries of the resulting products are consistent with a mechanism involving alkene insertion into a palladium alkoxo bond.**

These reactions are also discussed in Chapter 1.

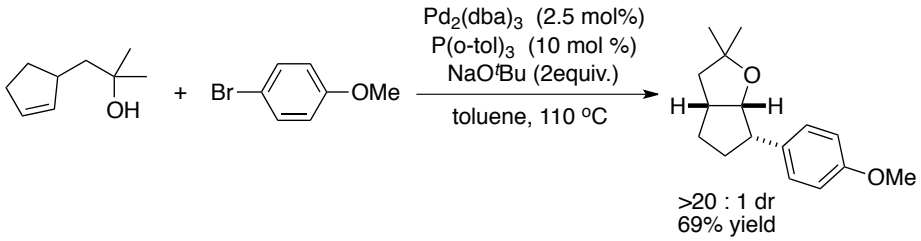
### 2.1.2.4.3 Palladium-catalyzed carboetherifications

Alkene insertions into palladium-alkoxo bonds were also proposed by Wolfe and co-workers for a palladium-catalyzed carboetherification of unsaturated alcohols with aryl halides (Scheme 152).[82]

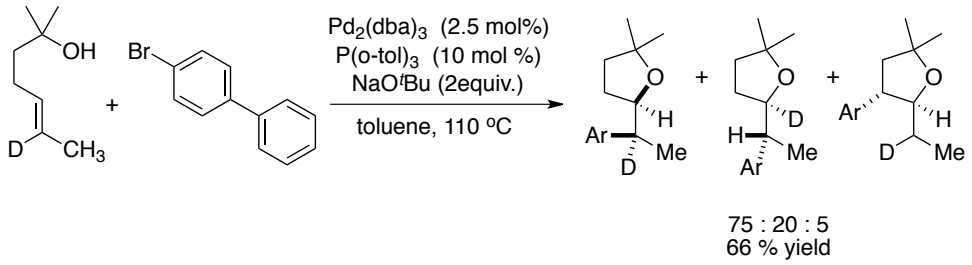



**Scheme 152: A palladium-catalyzed carboetherification of unsaturated alcohols with aryl halides. The reactions are thought to occur by a mechanism involving alkene insertion into a palladium-alkoxo bond.**

These reactions are similar to the palladium-catalyzed carboaminations of unsaturated amines discussed earlier. Support for an insertion mechanism is provided by the reactions of cyclopentenyl alcohols (Scheme 153) and stereodefined deuterated alkenyl alcohols (Scheme 154).

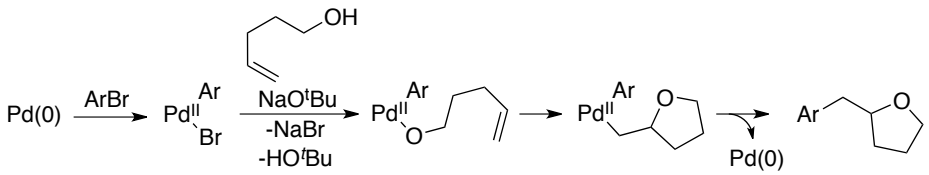



**Scheme 153: The palladium-catalyzed carboetherification of 1-(cyclopent-2-en-1-yl)-2-methylpropan-2-ol with 4-bromoanisole. The reaction occurs in the presence of 2 equivalents of NaO$^t$Bu and is catalyzed by a combination of $Pd_2(dba)_3$ (2.5 mol %) and P(*o*-Tol)$_3$ (10 mol %. The stereochemistry of the resulting aryl-substituted furan product supports a mechanism involving alkene insertion into a palladium-alkoxo bond.**




**Scheme 154: The palladium-catalyzed carboetherification of (*E*)-2-methylhept-5-en-2-ol with 4-bromo-1,1'-biphenyl. The reaction occurs in the presence of 2 equivalents of NaO$^t$Bu and is catalyzed by a combination of $Pd_2(dba)_3$ (2.5 mol %) and P(*o*-Tol)$_3$ (10 mol %. The stereochemistry of the resulting aryl-substituted furan product supports a mechanism involving alkene insertion into a palladium-alkoxo bond.**

In the former case, both the hydroxyl group and the arene from the aryl halide add to the same face of the alkene. The diastereoselectivity of this reaction is consistent with a mechanism in which oxidative addition of the aryl halide at palladium(0) is followed by alkene insertion into a palladium-alkoxo bond and $C_{sp2}$-$C_{sp3}$ reductive elimination with retention of configuration at carbon (Scheme 155).




**Scheme 155: The mechanism proposed by Wolfe and co-workers for the palladium catalzyed carboetherification of unsaturated alcohols with aryl haldies. The reaction occurs in the presence of 2 equivalents of NaO$^t$Bu and is catalyzed by a combination of $Pd_2(dba)_3$ (2.5 mol %) and P(*o*-Tol)$_3$ (10 mol %.**

In the latter case, the geometry of the resulting deutero methyl aryl furan is consistent with a mechanism in which alkene insertion into a palladium-alkoxo bond is followed by $C_{sp2}$-$C_{sp3}$ reductive elimination with retention of configuration. Since $C_{sp2}$-$C_{sp3}$ reductive elimination from palladium(II) is shown to occur with retention of configuration at carbon, both results suggest that alkoxopalladation occurs by insertion of an alkene into a palladium-alkoxo bond.

## 2.2 Present Research: The Reactions of Rhodium Diphosphine Amido and Alkoxo Alkene Complexes

Despite the number of reactions that have recently been proposed to occur by alkene insertions into late transition metal-amido and -alkoxo bonds, the reactions remain relatively rare and under-developed. By comparison, alkene insertions into metal-hydrogen and metal-carbon bonds and nucleophilic attacks onto coordinated alkenes are well-established reactions in organometallic chemistry. Alkene insertions into metal-

hydrogen bonds are proposed for metal-catalyzed hydrogenations, hydroformylations, and hydrocyanations. Alkene insertions into metal-carbon bonds are proposed for metal-catalyzed polymerizations and the Mizoroki-Heck reaction. Nucleophilic attacks onto coordinated alkenes were initially proposed for the Wacker reaction, and have been studied in this context since the 1970s.

The present section describes research directed towards the development of rhodium diphosphine amido and alkoxo complexes for the direct observation of alkene insertions into rhodium-amido and -alkoxo bonds. At the outset of this research, the only examples of unactivated alkene insertions into late transition metal-amido and -alkoxo bonds, were those reported by Hartwig and co-workers with rhodium bis(monophosphines) complexes.[67,80] To expand on these reports and to determine the effects of ancillary ligand properties on the rates for alkene insertions into metal-amido and -alkoxo bonds, a series of rhodium diphosphine amido and alkoxo complexes were sought, in which the properties of the diphosphine could be systematically varied. This section tracks the development of these systems from rhodium diphosphine anilido complexes analogous to those systems reported by Hartwig and co-workers for the insertions of unactivated alkenes into rhodium-anilido bonds to rhodium diphosphine alkoxo alkene complexes similar to those complexes reported by Hartwig and co-workers for the insertions of alkenes into rhodium-alkoxo bonds. Diphosphines were selected as the ancillary ligands because their properties could easily be modulated, and because many diphosphines are commercially available. Moreover, it was thought that diphosphines would be less likely to dissociate from the metal center than monophosphines, making the data obtained on the effects of ancillary ligand properties on the rates for alkene insertions into metal-amido bonds less ambiguous and easier to interpret. Preliminary studies focused on the syntheses of rhodium complexes of DPPF [1,1'-bis(diphenylphosphino)ferrocene], DPPP [1,3-bis(diphenylphosphino)propane], and BINAP [1,1'-bis(diphenylphosphino)binaphthyl], since these ligands provide a variety of ligand architectures. Initial studies targeted rhodium diphosphine anilido complexes analogous to the rhodium bis(monophosphine) anilido complexes reported by Hartwig and co-workers for the insertions of alkenes into rhodium anilido bonds

### 2.2.1 Results

#### 2.2.1.1 Synthesis and Reactivity of Rhodium Diphosphine Anilido Dimers, **3b**, **3g**, and **3i**.

Rhodium diphosphine anilido complexes **3b**, **3g**, and **3i** were synthesized in three steps from $[Rh(COE)_2(\mu\text{-}Cl)]_2$ and the appropriate diphosphine. The reactions were performed at room temperature in THF inside a nitrogen-filled glovebox. The complexes were characterized by NMR spectroscopy.

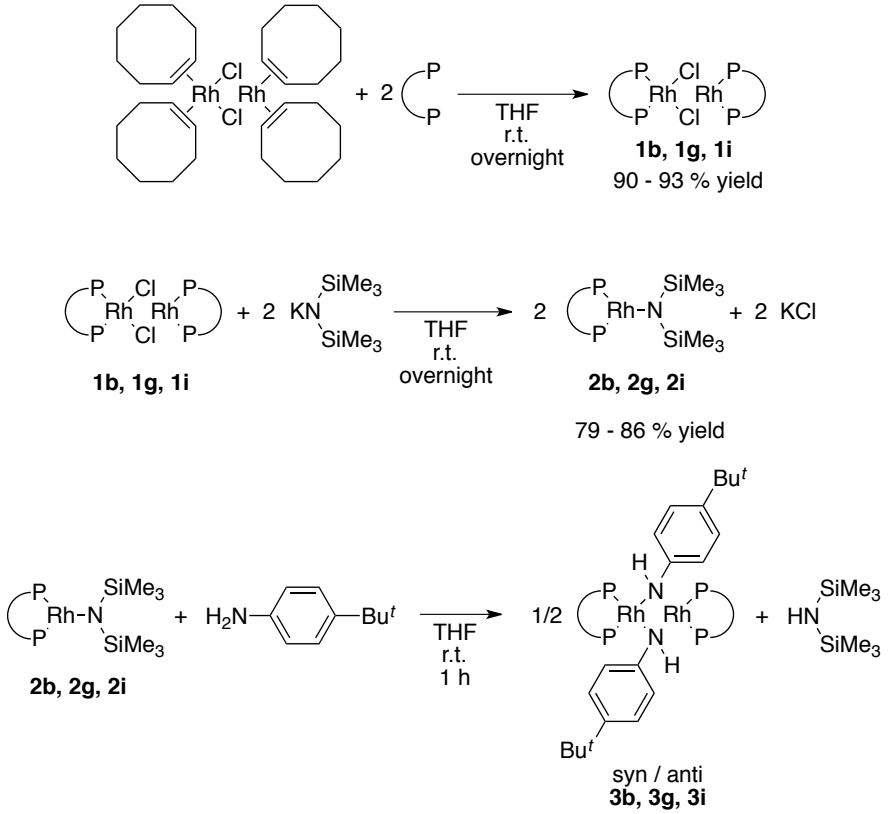
Rhodium diphosphine chloride complexes, **1b**, **1g**, and **1i** are largely insoluble in THF, pentane, $CH_2Cl_2$, benzene, toluene, and $Et_2O$, and were characterized primarily by $^{31}P$ NMR spectroscopy.

Rhodium diphosphine silylamido complexes **2b**, **2g**, and **2i** are soluble in THF, pentane, benzene, toluene, and $Et_2O$, and were characterized by $^{1}H$, $^{31}P$, and $^{13}C$ NMR spectroscopy.

Rhodium diphosphine anilido complexes **3b**, **3g**, and **3i** are soluble in THF, toluene, and benzene and were characterized by $^{1}H$ and $^{31}P$ NMR spectroscopy.

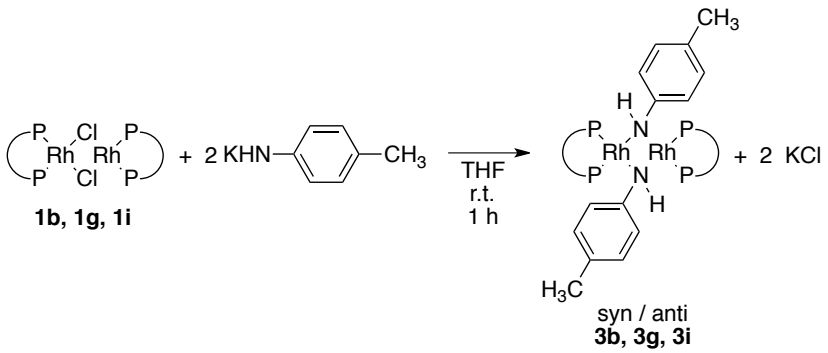
The $^{31}P$ NMR spectra of **1b**, **1g**, **1i, 2b**, **2g**, and **2i** show a doublet, consistent with a symmetrical rhodium diphosphine complex. The NMR spectra of **3b**, **3g**, and **3i** are consistent with a mixture of *syn* and *anti* isomers. The

$^{31}$P NMR spectra of **3b**, **3g**, and **3i** display two doublets, one for each isomer. The $^{1}$H NMR spectra of **3b**, **3g**, and **3i** also display two sets of signals.



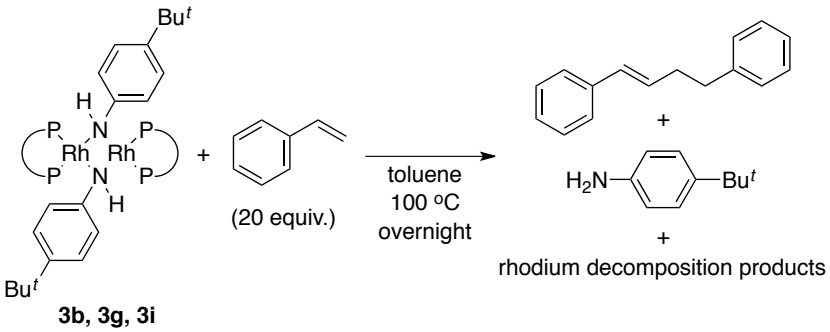

**Scheme 156: Syntheses of rhodium diphsophine anilido complexes 3b, 3g, and 3i.**

Rhodium diphosphine anilido complexes **3b**, **3g**, and **3i** could also be synthesized by the additions of potassium toluidide to rhodium diphosphine chloride complexes **1b**, **1g**, and **1i** (Scheme 157). The reactions, however, led to incomplete conversions of the rhodium diphosphine chloride complexes and often mixtures of products.




**Scheme 157: Syntheses of rhodium diphsophine anilido complexes 3b, 3g, and 3i by the additions of potassium toluidides to rhodium diphosphine chloride complexes 1b, 1g, and 1i. These reactions often lead to incomplete converstions or mixtures of products.**

To gauge the reactivities of **3b**, **3g**, and **3i** towards alkene aminations, preliminary reactions were preformed with solutions of **3b**, **3g**, and **3i** and excess styrene at room temperature and at 100 °C. Reactions with styrene were selected as model reactions because they give fewer products from alkene and imine isomerization, and because they were thought to be more likely to occur than reactions with 1-hexene and other alkyl alkenes. Reactions performed at room temperature resulted in no changes in the $^{31}$P NMR spectra of **3b**, **3g**, and **3i**. Reactions performed at 100 °C resulted in decomposition of the rhodium diphosphine anilido complexes along with the formation of aniline and styrene dimers.




**Scheme 158: The reactions of rhodium diphosphine anilido complexes 3b, 3g and 3i with excess styrene. The reactions result in a mixture of 4-tert-butylaniline and styrene dimers without the formation of alkene amination products.**

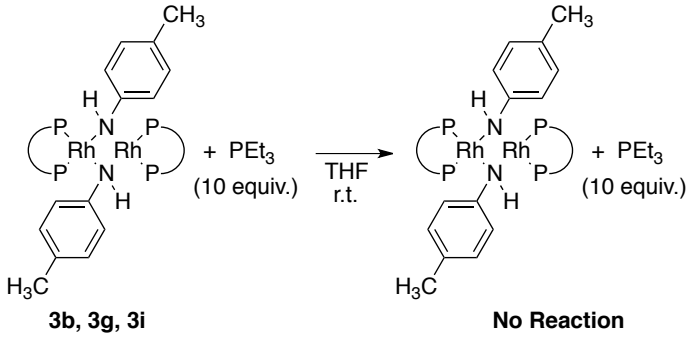
The results suggest that rhodium diphosphine anilido complexes **3b**, **3g**, and **3i** decompose before any reaction with styrene occurs. Similar $^{31}$P NMR spectra were obtained when complexes **3b**, **3g**, and **3i** were heated to 100 °C in the absence of styrene. Aniline was also observed in the product solutions. The results from these experiments contrast with the reactions of rhodium bis(monophosphine) anilido complexes, which generate imines through the aminations of simple alkenes.

The difference in reactivity can be attributed to the differences in ancillary ligands, although the exact properties of the ancillary ligands that are responsible for this contrasting reactivity are unclear. The formation of aniline may result from the presence of adventitious proton sources, such as water or from the reactions between two rhodium diphosphine anilido complexes. The source of the proton was not investigated. The formation of styrene dimers may result from the presence of rhodium hydrido complexes, formed by decomposition of **3b**, **3g**, and **3i** or by an unknown reaction.

The absence of alkene amination can be attributed to the stabilities of the rhodium diphosphine anilido complexes towards substitution or coordination (to the formation of anilido alkene complexes) or to the stabilities of the appropriate rhodium diphosphine anilido alkene complexes towards insertion reactions. The data are inconclusive. A rhodium diphosphine anilido alkene complex was not observe in any of the reactions of **3b**, **3g**, and **3i**.

In order to gauge the stabilities of rhodium diphosphine anilido complexes towards substitution and/or coordination reactions, solutions of **3b**, **3g**, and **3i** were allowed to react with excess $PEt_3$ at room temperature (Scheme 159). The $^{31}P$ NMR spectra of the resulting solutions show the presence of free $PEt_3$ and the persistence of the rhodium diphosphine anilido dimer; no other peaks are present in the $^{31}P$ NMR spectra.

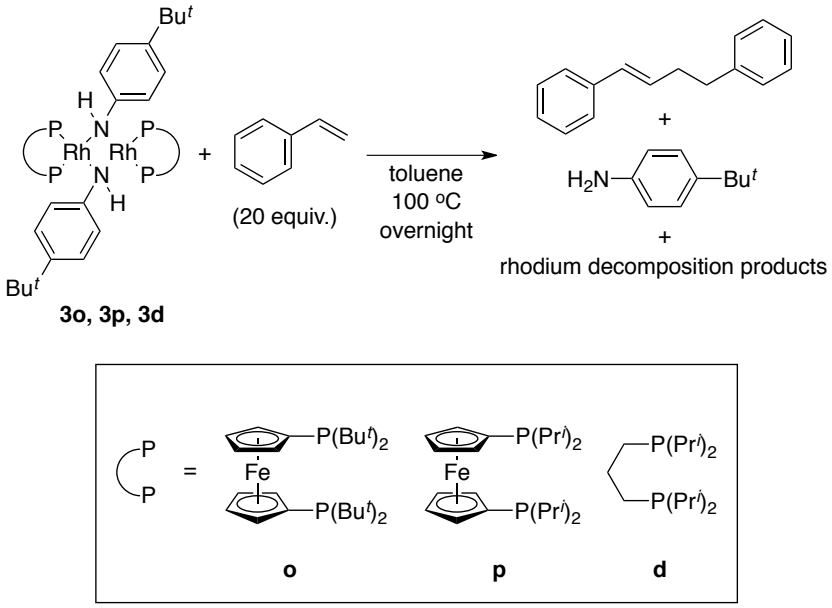
The data suggest that **3b**, **3g**, and **3i** are resistant to coordination and substitution by $PEt_3$ and imply through deductive reasoning, that substitution and/or coordination by less-donating alkenes is unfavorable as well. The reactions of rhodium diphosphine anilido complexes **3b**, **3g**, and **3i** were not investigated further. Instead, less stable rhodium diphosphine anilido complexes were sought.




**Scheme 159: The additions of $PEt_3$ to rhodium diphsophine anilido complexes 3b, 3g, and 3i. The reactions failed to produce adducts between $PEt_3$ and the rhodium diphosphine anilido complexes, and suggest that the rhodium anilido dimers of DPPF, DPPP, and BINAP are relatively resistant to dimer cleavage and/or substiuttion/coordination.**

### 2.2.1.2 Synthesis and Reactivity of Rhodium Diphosphine Anilido Dimers, **3o**, **3p**, and **3d**.

Rhodium diphosphine anilido complexes **3o**, **3p**, and **3d** were synthesized by the reactions of rhodium diphosphine silylamido complexes **2o**, **2p**, and **2d** with 4-*tert*-butylaniline. The expectation was that more bulky ancillary ligands may reduce the stability of rhodium diphosphine anilido dimers and promote their cleavage by alkenes. The reactions of **3o**, **3p**, and **3d** with excess styrene, however, resulted in the formation of aniline and styrene dimmers (Scheme 160).

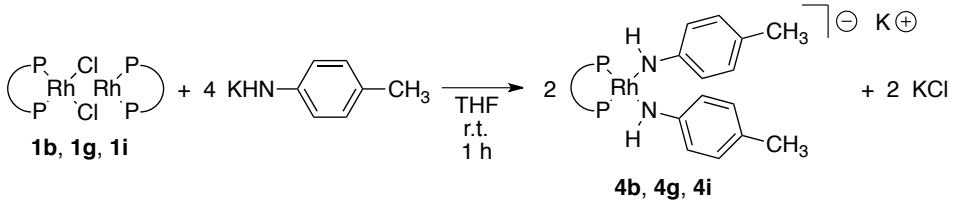


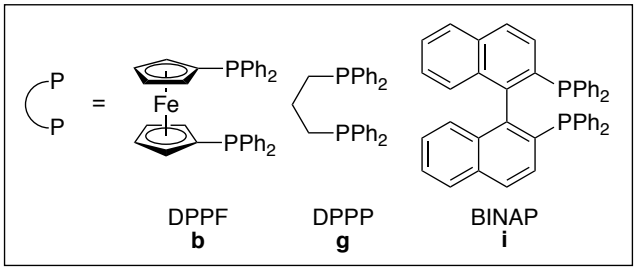

**Scheme 160: The reactions of rhodium diphosphine anilido complexes 3o, 3p and 3d with excess styrene. The reactions result in a mixture of 4-tert-butylaniline and styrene dimers without the formation of alkene amination products.**

Similar results were obtained for the reactions of rhodium diphosphine anilido complexes **3b**, **3g**, and **3i** with excess styrene (vide supra). As a result, the reactions of rhodium diphosphine anilido dimers, **3**, were abandoned, and the reactions of rhodium diphosphine dianilido were investigated.

### 2.2.1.3 Synthesis and Reactivity of Rhodium Diphosphine Dianilido Complexes, **4b**, **4g**, and **4i**.

Rhodium diphosphine dianilido complexes, **4b**, **4g**, and **4i** were prepared in situ by the reactions of 4 equivalents of sodium 4-*tert*-butylanilide to rhodium diphosphine chloride complexes **1b**, **1g**, and **1i**. (Scheme 161). The complexes were characterized by $^1$H and $^{31}$P NMR spectroscopy, but were not isolated. Attempts to isolate **4b**, **4g**, and **4i** resulted in the formation of rhodium diphosphine anilido dimers, **3b**, **3g**, and **3i**.

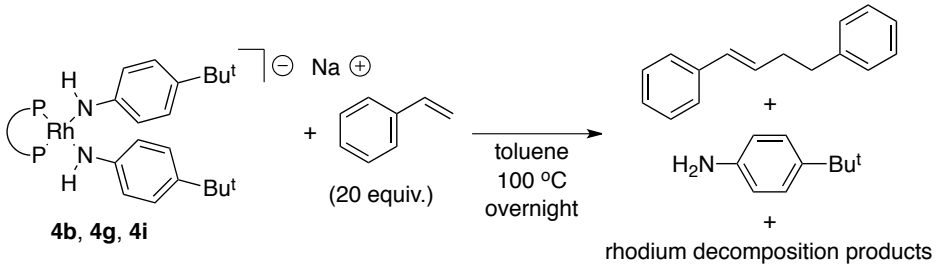



**Scheme 161: The syntheses of rhodium diphosphine dianilido complexes 4b, 4g, and 4i. The complexes were formed by the additions of 4 equivalents of potassium toluidide to rhodium diphosphine chloride complexes, 1b, 1g, and 1i and were unstable towards isolation.**

The NMR spectra of **4b**, **4g**, and **4i** are consistent with a monomeric complex. Only one doublet is observed in the $^{31}$P NMR spectra of **4b**, **4g**, and **4i**, and only one set of signals is observed in the $^{1}$H NMR spectra of **4b**, **4g**, and **4i**.

Heating solutions of **4b**, **4g**, and **4i** to 100 °C in the presence of 20 equivalents of styrene resulted in the formation of aniline, styrene dimers, and unidentified rhodium complexes (Scheme 162).

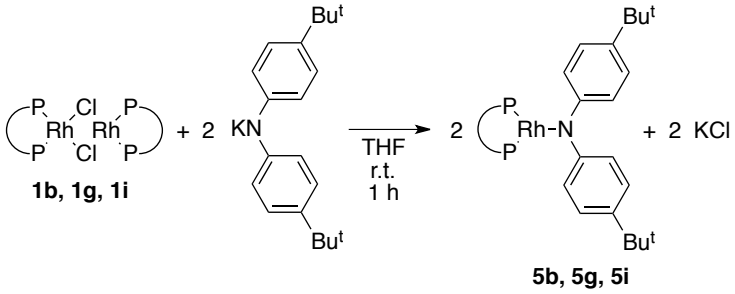


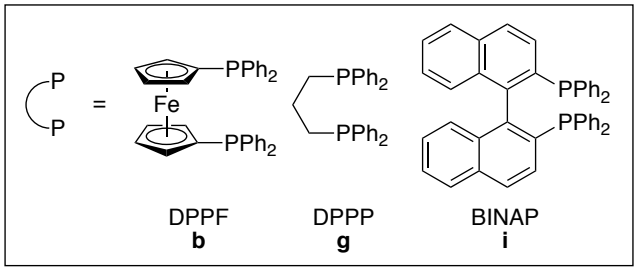

**Scheme 162: The reactions of rhodium diphosphine dianilido complexes 4b, 4g and 4i with excess styrene. The reactions result in a mixture of 4-tert-butylaniline and styrene dimers without the formation of alkene amination products.**

No products from alkene amination were observed. The causes for this outcome were not speculated, and the reactions of rhodium diphosphine dianilido complexes **4b**, **4g**, and **4i** were not investigated further. Instead, the reactions of rhodium diphosphine diarylamido complexes were examined.

### 2.2.1.4 Syntheses and Reactivities of Rhodium Diphosphine Diarylamido Complexes, **5b**, **5g**, and **5i.**

Rhodium diphosphine diarylamido complexes **5b**, **5g**, and **5i** were synthesized by the additions of sodium and potassium bis(4-*tert*-butylphenyl)amides to rhodium diphosphine chloride complexes **1b**, **1g**, and **1i** (Scheme 163). The complexes were characterized by $^{1}$H, $^{31}$P, and $^{13}$C NMR spectroscopy.

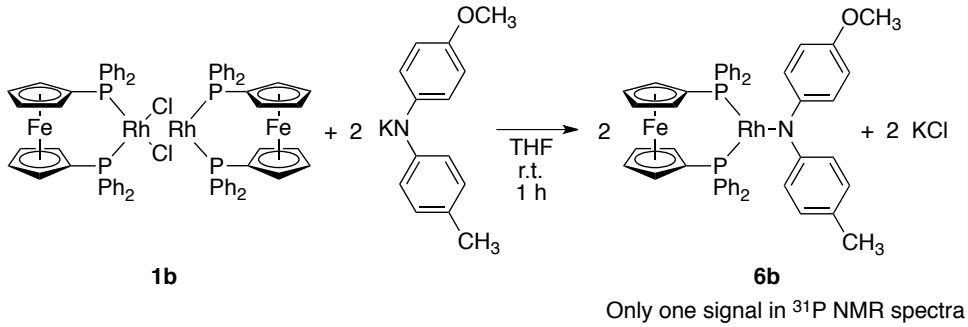



**Scheme 163: The syntheses of rhodium diphosphine diarylamdio complexes 5b, 5g, and 5i. The complexes were formed by the additions of potassium di(4-methylphenyl) amide to rhodium diphosphine chloride complexes, 1b, 1g, and 1i and isolated by trituration from THF solutions.**

The $^{31}$P NMR spectra of **5b**, **5g**, and **5i** show one doublet. The data are consistent with both monomeric and dimeric structures. To distinguish between these two possibilities, rhodium diphosphine diarylamido complex

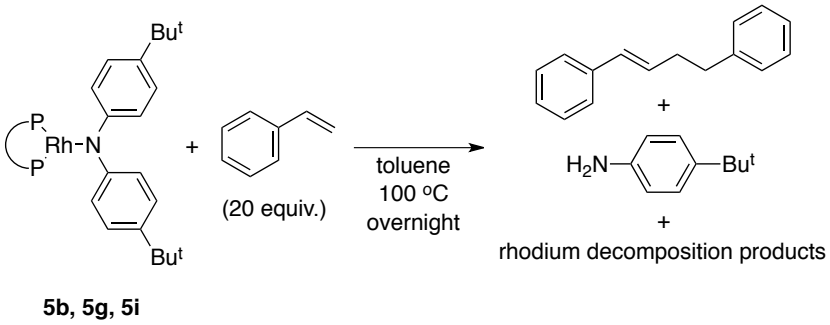
**6b** was synthesized by the addition of potassium *N*-(4-methoxyphenyl) toluidide to rhodium diphosphine chloride complex **1b** (Scheme 164).




**Scheme 164: The syntheses of rhodium diphosphine dianilido complex 6b. The complex was formed by the addition of potassium *N*-(4-methoxyphenyl) toluidide to rhodium diphosphine chloride complex 1b.**

The $^{31}$P NMR spectrum of **6b** also shows one doublet. The data are consistent with a monomeric species, but do not rule out the possibility that **6b** exists as a single isomer (syn or anti) of a dimeric complex. The structures of **5b**, **5g**, and **5i** were not investigated. The molecular weights of **5b**, **5g**, and **5i** were not measured.

Reactions of **5b**, **5g**, and **5i** with excess styrene were conducted at room temperature and at 100 °C. Reactions conducted at room temperature resulted in no changes in the $^{31}$P NMR spectra of **5b**, **5g**, and **5i**. Reactions conducted at 100 °C eventually resulted in the formation of diarylamine, styrene dimers, and a mixture of unidentified rhodium complexes (Scheme 165).



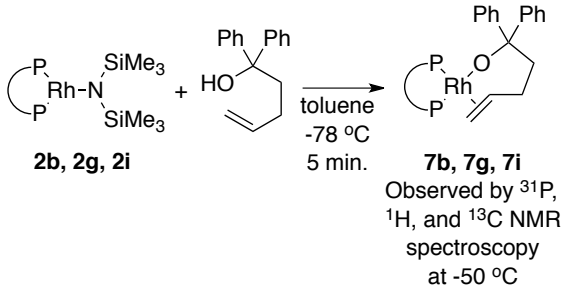

**Scheme 165: The reactions of rhodium diphosphine anilido complexes 5b, 5g and 5i with excess styrene. The reactions result in a mixture of 4-tert-butylaniline and styrene dimers without the formation of alkene amination products.**

In this case, the absence of alkene amination products in these reactions may result from the diarylamido complexes being too sterically hindered for alkene coordination to rhodium, but this hypothesis is only speculative. The reactions of **5b**, **5g**, and **5i** were not investigated further.

### 2.2.1.5 Syntheses and Reactivities of Rhodium Diphosphine Alkoxo Alkene Complexes, **7b**, **7g**, and **7i**.

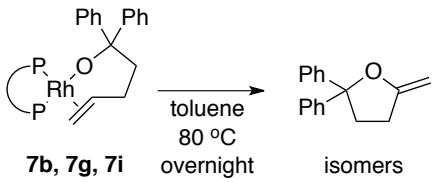
The absence of alkene amination products from the reactions of **4b**, **4g**, **4i, 5b**, **5g**, and **5i** prompted the investigations of rhodium alkoxo alkene complexes **7b**, **7g,** and **7i**. In this case, tethering the alkene to the alcohol is expected to favor coordination of the alkene to rhodium. A similar strategy was adopted by Hartwig, Zhao, and Incarvito for the syntheses of rhodium alkoxo alkene complexes of $PEt_3$.[80] In these examples, disubstitution at the α position of the alcohol is required to prevent the elimination of ketones and aldehydes from the alkoxo alkene complex.

Rhodium diphosphine alkoxo alkene complexes **7b**, **7g**, and **7i** were prepared in situ by the additions of 1,1-diphenyl-4-penten-1-ol to rhodium diphosphine silylamido complexes **2b**, **2g**, and **2i** (Scheme 166). The reactions were performed at -78 °C inside screw cap NMR tubes. The alkoxo alkene complexes were characterized by $^{1}H$, $^{31}P$, and $^{13}C$ NMR spectroscopy at -50 °C. The $^{31}P$ NMR spectra of **7b**, **7g**, and **7i** display two doublets of doublets, consistent with rhodium diphosphine complexes, in which the two phosphorus atoms exist in different chemical environments. The $^{1}H$ and $^{13}C$ NMR spectra of **7b**, **7g**, and **7i** are consistent with alkene coordination to rhodium (the alkenyl protons and carbon are both shifted upfield from their uncoordinated chemical shifts).




**Scheme 166: Syntheses of rhodium diphosphine alkoxo alkene complexes 7b, 7g, and 7i. The complexes were formed by the additions of 1,1-diphenyl-4-penten-1-ol to rhodium diphsophine silylamido complexes 2b, 2g, and 2i. Similar reactions were employed by Hartwign and co-workers for the syntheses of rhodium bis(triethylphosphine) alkoxo alkene complexes.**

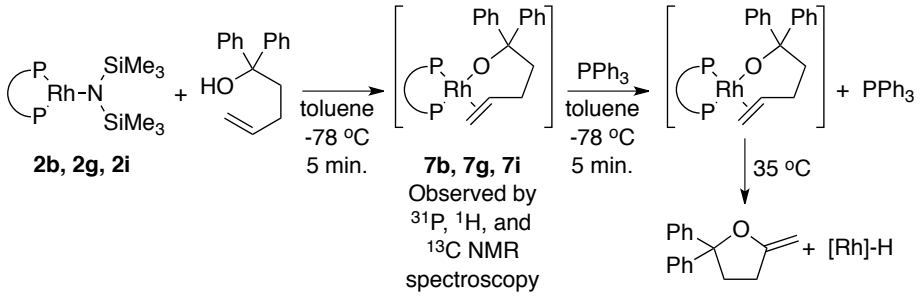
Preliminary reactions with rhodium diphosphine alkoxo alkene complexes, **7b**, **7g**, and **7i** were conducted at 80 °C (Scheme 167). The product solutions were analyzed by GC/MS. The data indicate the formation of 2,2-diphenyl-5-methylene tetrahydrofuran and isomers 2,2-diphenyl-5-methylene tetrahydrofuran. The results were confirmed by the independent syntheses of 2,2-diphenyl-5-methylene tetrahydrofuran and 2,2-diphenyl-5-methyl dihydrofuran. The furan products were formed in moderate to good yield.




**Scheme 167: The reactions of rhodium diphosphine alkoxo alkene complexes 7b, 7g, and 7i. Preliminary reactions were performed in toluene at 80 °C. The reactions generated a mixture of furan products, presumably via the insertion of the teterhed alkenes into the rhodium alkox bonds of 7b, 7g, and 7i.**

The formation of 2,2-diphenyl-5-methylene tetrahydrofuran was attributed to a sequence of reactions involving 1) C-O bond formation (either by nucleophilic attack onto a coordinated alkene or alkene insertion into the rhodium alkoxo bonds of **7b**, **7g**, and **7i**) and 2) β-hydride elimination from the resulting rhodium diphosphine furanyl alkyl complex. Similar reactions were reported by Hartwig and Zhao for the decompositions of rhodium bis(triethylphosphine) alkoxo alkene complexes. In those examples, the mechanism for C-O bond formation was determined by the reactions of stereodefined deuterated alkenes. The results from those investigations indicate that C-O bond formation occurs by an insertion mechanism. A similar mechanism is assumed here. The isomers of 2,2-diphenyl-5-methylene tetrahydrofuran were thought to arise from isomerization of the carbon-carbon double bond of 2,2-diphenyl-5-methylene tetrahydrofuran. These latter reactions were attributed to the presence of a rhodium hydrido complex formed by β-hydride elimination. The $^{1}H$ NMR spectra of

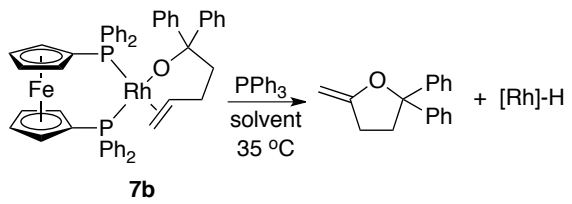
the product solutions formed by the reactions of **7b**, **7g**, and **7i** were complicated by the presence of multiple products.




**Scheme 168: The series of reactions involved in determining the rates for furan formation from rhodium diphsophine alkoxo alkene complexes 7b, 7g, and 7i. $PPh_3$ was added to solutions of 7b, 7g, and 7i to stabilize the rhodium diphosphine hydrido complexes formed by alkene insrtion and β-hydrogen elimination. The addition of $PPh_3$ to solutions of 7b, 7g, and 7i also prevents isomerization of the 5-methylene-2,2-diphenyl tetrahydrofuran and allows for the rates for furan formation to be determined. NMR spectra of 7b, 7g, and 7i were collected at -50 °C before and after the addition of $PPh_3$ to insure that PPh3 does not coordinate to the alkoxo alkene complexes prior to reaction.**

In order to suppress isomerization of 2,2-diphenyl-5-methylene tetrahydrofuran product, and generate less-complicated $^1$H NMR spectra of the product solutions, monophosphines were added to the alkoxo alkene complexes prior to furan formation. Monophosphines are expected to coordinate to the rhodium diphosphine hydrido complexes formed by β-hydride elimination and hinder isomerization of the carbon-carbon double bond. Several monophosphines were examined for their effect on alkene isomerization. Reactions between the added monophosphines and rhodium alkoxo alkene complexes **7b**, **7g**, and **7i** were performed at -78 °C. NMR spectra of the resulting solutions were collected at -50 °C. Of the monophosphines examine, $PPh_3$ provided the best results. Smaller, more electron-rich phosphines were shown to displace the alkene, in some cases. Moreover $PPh_3$ offered advantages by being easy to way (a solid), air stable, and relatively inexpensive. Subsequent reactions of **7b**, **7g**, and **7i** that were performed in the presence of excess $PPh_3$. The reactions clearly generated 2,2-diphenyl-5-methylene tetrahydrofuran without signs of product isomerization. The addition of excess $PPh_3$ enabled the generation of 2,2-diphenyl-5-methylene tetrahydrofuran to also be monitored by $^1$H NMR spectroscopy. The rates for furan formation and alkoxo alkene decomposition were subsequently determined by $^1$H NMR spectroscopy at 35 °C in the presence of 10 equivalents of $PPh_3$.

To determine the effect of added $PPh_3$ on the rates for rhodium diphosphine alkoxo alkene decompositions, reactions of rhodium alkoxo alkene complex **7b** were conducted in the presence and absence of added $PPh_3$ (Scheme 169).




**Scheme 169: The effect of added $PPh_3$ on the reactions of rhodium diphosphine alkoxo alkene complexes. The reactions were preformed with 0, 0.041, 0.41, and 0.82 M of added $PPh_3$. The corresponding rate constants for the decay of alkoxo alkene complex 7b, show only a slight variance, indicating that the effect of added $PPh_3$ is negligible.**

The reactions were monitored by $^1$H NMR spectroscopy. The rate constants for alkoxo alkene decomposition were determined by fitting exponential equations to plots of the integral values $^1$H NMR signals of the alkoxo alkene against time. The data indicate that in the absence of $PPh_3$ the rate constant for the decomposition of **7b** is 3.8 x $10^{-4}$ $s^{-1}$ ($t_{1/2}$ = 30 min.). Upon the addition of one equivalent of $PPh_3$ to a solution of **7b** in toluene-$d_8$ (2.45 x $10^{-5}$ mol, 600 μL total after addition of $PPh_3$, 0.041 M) the rate constant changes to 3.9 x $10^{-4}$ $s^{-1}$ ($t_{1/2}$ = 30 min.). Upon the addition of 10 equivalents of $PPh_3$ to a solution of **7b** in toluene-$d_8$ (2.45 x $10^{-4}$ mol, 600 μL total after addition of $PPh_3$, 0.41 M) the rate constant for decomposition changes to is 4.2 x $10^{-4}$ $s^{-1}$ ($t_{1/2}$ = 28 min.), and upon the addition of 20 equivalents of $PPh_3$ to (4.89 x $10^{-4}$ mol, 600 μL total after addition of $PPh_3$, 0.82 M), the rate constant for the decomposition of **7b** remains 4.2 x $10^{-4}$ $s^{-1}$ ($t_{1/2}$ = 28 min.). The data indicate that the effect of added $PPh_3$ is small for the reactions of **7b**. The effect of added $PPh_3$ on the reactions of **7g** and **7i** were not determined at this time.

To determine the effect of rhodium diphosphine alkoxo alkene concentration on the rates for complex decomposition and furan formation, the reaction of rhodium diphosphine alkoxo alkene complex **7b** was performed at 0.041 M and 0.155 M. Both reactions were performed in the absence of $PPh_3$. The reactions were monitored by $^1$H NMR spectroscopy. The rate for the decomposition of **7b** at 0.041 M was 1.61 x $10^{-5}$ M $s^{-1}$. The rate for the decomposition of **7b** at 0.155 M was 5.97 x $10^{-5}$ M $s^{-1}$. The data indicate that increasing the concentration of rhodium diphosphine alkoxo alkene complex **7b** by a factor of 3.78 increases the rate of decomposition by a factor of 3.71. The data are consistent with a first-order dependence of the rate on the concentration or rhodium alkoxo alkene complex, **7b**. The dependence of the rates of decomposition on the concentrations of rhodium diphosphine alkoxo alkene complexes **7g** and **7i** were not determined, but were assumed to be first-order as well.

To determine the effect of solvent identity on the rates for alkoxo alkene decomposition and furan formation, the reactions of rhodium diphosphine alkoxo alkene complex, **7b** were performed in toluene and in THF. Both reactions were performed at 35 °C in the presence of excess $PPh_3$. In toluene, the decomposition of **7b** occurs with a rate constant of 4.2 x $10^{-4}$ $s^{-1}$ ($t_{1/2}$ = 28 min.), as stated. In THF, the decomposition of 7b occurs with a rate constant of 3.5 x $10^{-4}$ $s^{-1}$ ($t_{1/2}$ = 33 min.). The data indicate that the reactions of rhodium diphosphine alkoxo alkene complex, **7b** is slightly (1.2 x) faster in toluene than in THF. The effect of solvent identity is small. A similar effect of solvent was observed for the reactions of rhodium bis(triethylphosphine) alkoxo alkene complexes.

The rate constants for the decompositions or rhodium diphosphine alkoxo alkene complexes **7g** and **7i** were also determined by $^1$H NMR spectroscopy. At 35 °C, in the presence of 10 equivalents of $PPh_3$, rhodium alkoxo alkene complex, **7g**, decomposes with a first-order rate constant of 8.4 x $10^{-4}$ $s^{-1}$ ($t_{1/2}$ = 14 min.). At 0 °C, in the presence of 10 equivalents of $PPh_3$, rhodium alkoxo alkene complex, **7i**, decomposes with a first-order rate constant of 4.5 x $10^{-4}$ $s^{-1}$ ($t_{1/2}$ = 26 min.). At 35 °C, in the presence of 10 equivalents of $PPh_3$, the reactions of rhodium alkoxo alkene complex, **7i**, are too fast to be determined accurately by

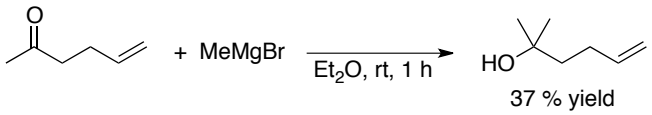
The results from these reactions point to a general system for studying the effects of ancillary ligand (diphosphine) properties on the rates for alkene insertions into late transition metal-alkoxo bonds. The effects of the electronic, steric, and bite angle properties of the ancillary ligand on the rates for alkene insertions into rhodium-alkoxo bonds are discussed in Chapter 3.

### 2.2.1.6 Syntheses of 2-methyl-5-hexen-2-ol, 1,1-diphenyl-4-penten-1-amine, 2-methyl-5-hexen-2-amine and 6-iodo-5,5-dimethyl-1-hexene.

Having established a system for studying the effects of ancillary ligand properties on the rates for alkene insertions into rhodium-alkoxo bonds, similar systems for studying the effects of ancillary ligand properties on the rates for alkene insertions into rhodium-amido and -alkyl bonds were pursued.

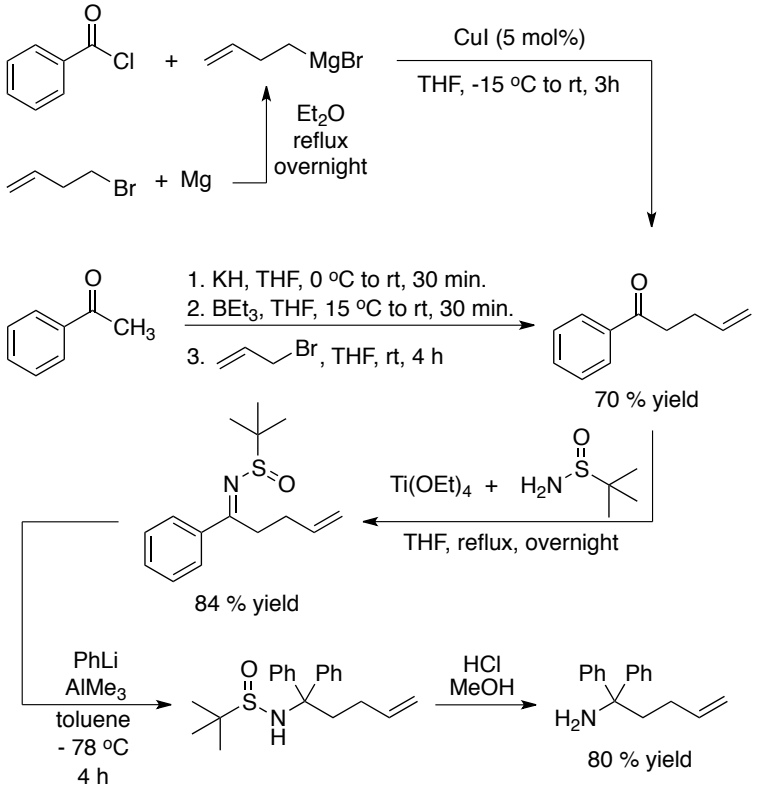
Attempts to synthesize rhodium diphosphine -amido and -alkyl alkene complexes similar to **7b**, **7g**, and **7i** led to the syntheses of 2-methyl-5-hexen-2-ol, 1,1-diphenyl-4-penten-1-amine, 2-methyl-5-hexen-2-amine and 6-iodo-5,5-dimethyl-1-hexene.

2-Methyl-5-hexen-1-ol was synthesized by the addition of methyl magnesium bromide to 5-hexen-2-one (Scheme 170).



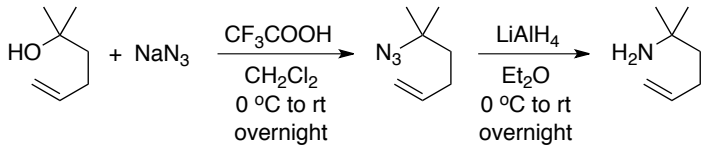

**Scheme 170: The synthesis of 2-methyl-5-hexen-1-ol from 5-hexen-2-one and methylmagnesium bromide.**

1,1-Diphenyl-4-penten-1-amine was synthesized by the addition of phenyllithium to phenyl 4-pentenyl *N*-*tert*-bultylsulfinyl imine (Scheme 171).

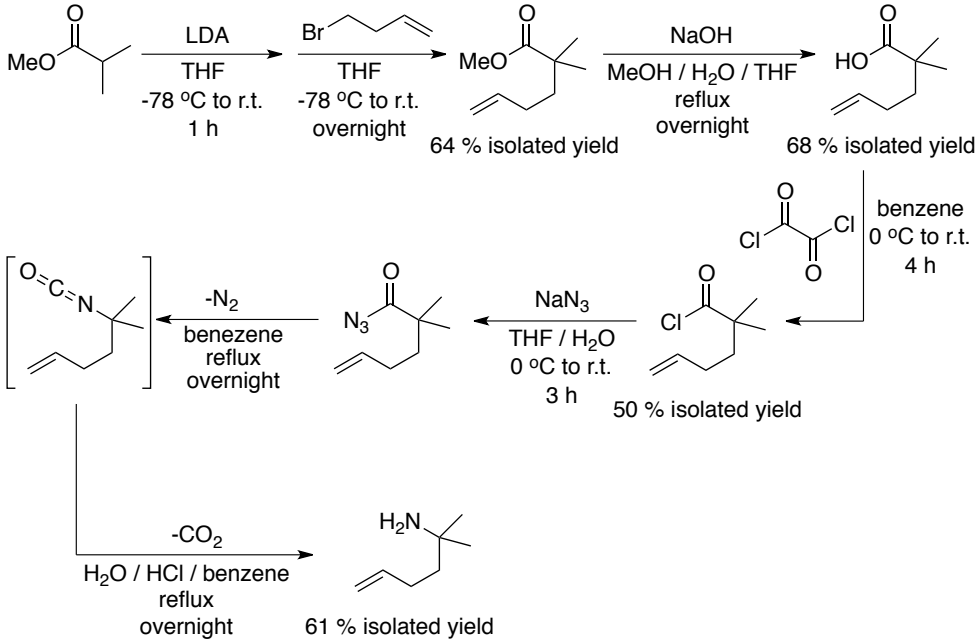



**Scheme 171: The synthesis of 1,1-diphenyl-4-penten-1-amine from benzoyl chloride, 4-bromo-1-butene, *tert*-butylsulfonamide, and phenyllithium and from acetophenone, allyl bromide *tert*-butylsulfonamide, and phenyllithium**

2-Methyl-5-hexen-2-amine was synthesized by lithium aluminum hydride reduction of 5-azido-5-methyl-1-hexene azide (Scheme 172) and by Curtius rearrangement of 2,2-dimethyl-5-hexenoyl azide (Scheme 173).

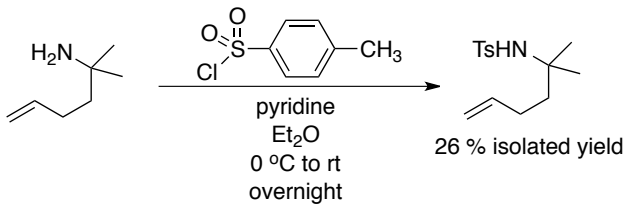



**Scheme 172: Synthesis of 2-methyl-5-hexen-2-amine from of 2-methyl-5-hexen-2-ol and sodium azide.**



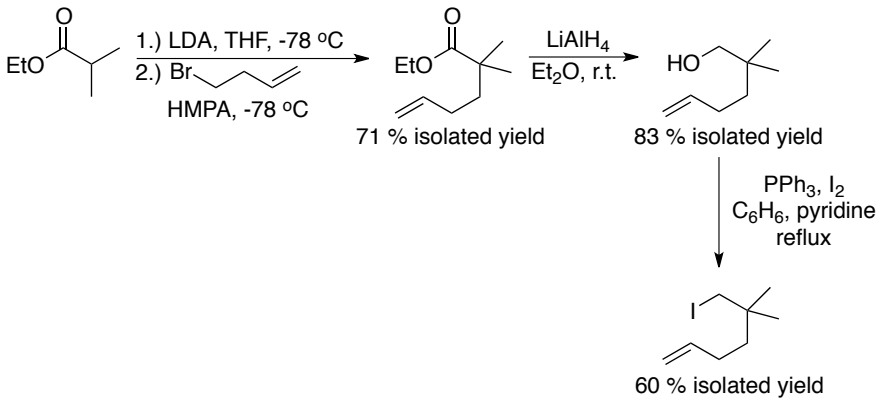

**Scheme 173: The synthesis of 2-methylhex-5-en-2-amine from methyl isobutyrate, 4-bromo-1-butene, oxalyl chloride, and sodium azide.**

*N*-Tosyl-2-methyl-5-hexen-1-amine was synthesized by tosylation of 2-methyl-5-hexen-1-amine with tosyl chloride (Scheme 174).



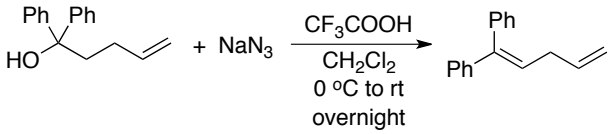

**Scheme 174: The synthesis of *N*-tosyl-2-methylhex-5-en-2-amine from 2-methylhex-5-en-2-amine.**

6-Iodo-5,5-dimethyl-1-hexene was synthesized in three steps from ethyl isobutyrate and 4-bromo-1-butene (Scheme 175).



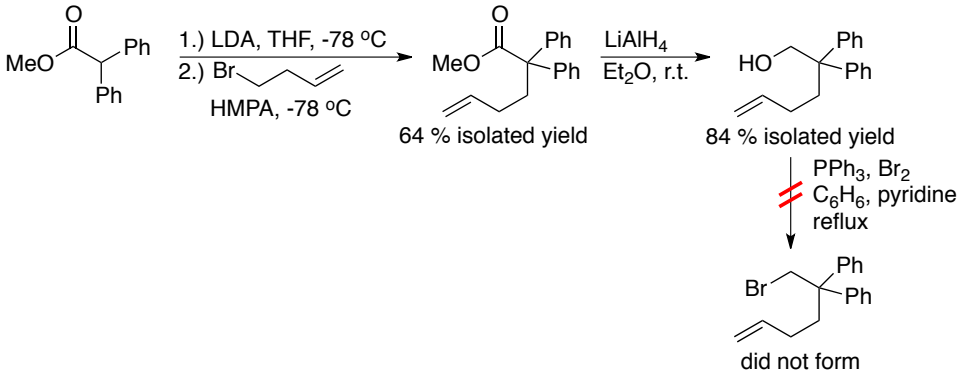

**Scheme 175: The synthesis of 6-iodo-5,5-dimethylhex-1-ene from ethyl isobutyrate, 4-bromo-1-butene, and iodine.**

Attempts to synthesize 1,1-diphenyl-4-penten-1-amine in two steps by the addition of hydrazoic acid to 1,1-diphenyl-4-penten-1-ol and reduction of the resulting azide were unsuccessful. The reaction of hydrazoic acid with 1,1-diphenyl-4-penten-1-ol resulted in the formation of dienes by acid-catalyzed dehydration (Scheme 176).




**Scheme 176: Attempt to synthesize 1,1-diphenyl-4-penten-1-amine from 1,1-diphenyl-4penten-1-ol.**

Attempts to synthesize 1-bromo-2,2-diphenyl-5-hexene from the appropriate alcohol by the addition bromine, $PPh_3$ and pyridine resulted in mixtures of products , but no alkyl bromides (Scheme 177).



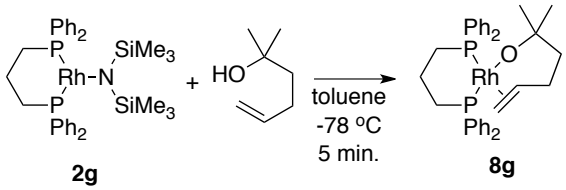

**Scheme 177: Attempt to synthesize (1-bromohex-5-ene-2,2-diyl)dibenzene from methyl isobutyrate, 4-bromo-1-butene, lithium aluminum hydride and bromine. The synthetic route was unsuccessful.**

The unsaturated alcohols, amines, and alkyl iodides were subsequently used for the syntheses of rhodium diphosphine alkoxo, amido, and alkyl complexes, **8g**, **9g**, **10g**, and **11g**.

### 2.2.1.7 Synthesis and Reactivity of Rhodium Diphosphine Alkoxo Alkene Complex, **8g**.

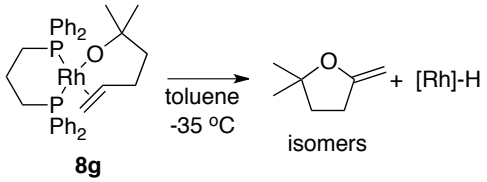
Rhodium diphosphine alkoxo alkene complex, **8g** was synthesized by the addition of 2-methyl-5-hexen-2-ol to rhodium diphosphine silylamido complex, **2g** (Scheme 178). The reaction was performed at -78 °C inside a screw cap NMR tube. NMR spectra of the **8g** were collected at -50 °C. The spectral data are consistent with a rhodium diphosphine alkoxo alkene complex. Two doublets of doublets appear in the $^{31}P$ NMR spectrum while

three broad signals appear between δ 5.38 (1H), 4.56 (1H), 4.15 (1H), 3.26 (1H), 2.67 (1H) and 1.28 (3H) ppm in the $^{1}$H NMR spectrum. Other peaks were hidden by overlapping signals.




**Scheme 178: The synthesis of rhodium diphosphine alkoxo alkene complex 8g. The complex was formed by the addition of 2-methyl-5-hexen-2-ol to rhodium diphosphine silylamido complex 2g.**

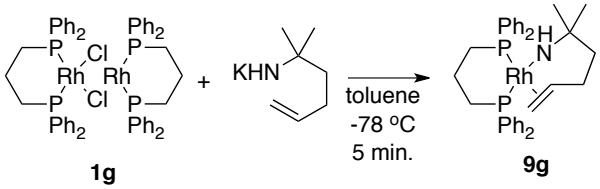
The decomposition of **8g** was monitored at -35 °C in the presence of $PPh_3$ and at 0 °C in the absence of $PPh_3$ (Scheme 179). The rate constant for the decomposition of **8g** in the presence of added $PPh_3$ was approximately 5.2 x $10^{-5}$ $s^{-1}$ ($t_{1/2}$ = 221 min.) at -35 °C, while the rate constant for the decomposition of **8g** in the absence of added $PPh_3$ was approximately 5.6 x $10^{-4}$ $s^{-1}$ ($t_{1/2}$ = 21 min.) at 0 °C.




**Scheme 179: The reaction of rhodium diphosphine alkoxo alkene complex 8g. Preliminary reactions were conducted in toluene at -35 °C. The reactions generated a mixture of furan isomers, presumably by alkene insertion, β-hydrogen elimination, and isomerization of 2,2-dimethyl-5-methylene tetrahydrofuran**

### 2.2.1.8 Synthesis and Reactivity of Rhodium Diphosphine Amido Alkene Complex, **9g**.

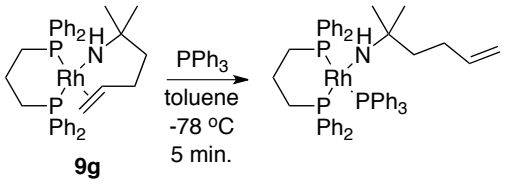
Deprotonation of 2-methyl-5-hexen-2-amine with potassium hydride and subsequent reaction with rhodium diphosphine chloride complex, **1g**, resulted in the appearance of two doublets of doublets in the $^{31}$P NMR spectrum, which were tentatively assigned to rhodium diphosphine amido alkene complex, **9g** (Scheme 180).




**Scheme 180: Synthesis of rhodium diphosphine amido alkene complex 9g from potassium 2-methyl-5-hexen-2-amide and rhodium diphosphine chloride complex 1g.**

The reactions were performed at room temperature and at -78 °C. The NMR spectra of the resulting complex were collected at -50 °C. The complex formed by the addition of potassium 2-methyl-5-hexenyl-2-amide to **1g** displays $^{1}$H NMR signals at δ 3.29 (1H), 3.15 (1H), 3.02 (1H), 2.58 (1H), 2.43 (1H), 0.081 (3H), and 0.06 (3H) ppm. The data are consistent with the presence of a rhodium diphosphine amido alkene complex. The listed signals were tentatively assigned to the amido alkene ligand. Two additional $^{1}$H signals were thought to occur between δ 2.1 and 1.5, but could not be identified due to overlapping signals from excess amino alkene and DPPP ligand. The $^{13}$C NMR spectrum of this complex shows two broad signals at δ 51.95 and δ 37.76 ppm, which were tentatively assigned to the alkenyl carbons of the amido alkene ligand.

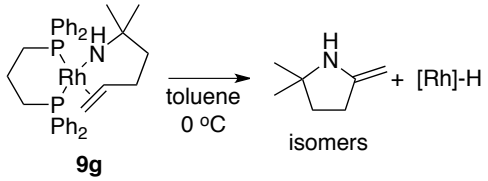
Addition of $PPh_3$ to the complex formed by the addition of potassium 2-methyl-5-hexenyl-2-amide to **1g** resulted in the disappearance of the $^1H$ signals assigned to the rhodium amido alkene complex and an increase in intensity of the uncoordinated alkene signals. The $^{31}P$ NMR spectra obtained the product solutions from these reactions show three doublets of doublets of doublets, consistent with the formation of a rhodium complex with three inequivalent phosphorus atoms. The spectral data are consistent with the displacement of the alkene group by $PPh_3$ (Scheme 181).




**Scheme 181: Addition of $PPh_3$ to rhodium diphosphine amido alkene complex 9g. The reaction leads to the displacement of the alkenyl ligand by $PPh_3$.**

All reactions were performed at -78 °C in a screw cap NMR tube. All NMR spectra were collected at -50 °C.

Reactions of rhodium diphosphine amido alkene complex, **9g**, were monitored by $^1H$ NMR spectroscopy at 0 °C (Scheme 182).




**Scheme 182: The reaction of rhodium diphosphine alkoxo alkene complex 9g. Preliminary reactions were conducted in toluene at 0 °C. The reactions generated a mixture of furan isomers, presumably by alkene insertion, β-hydrogen elimination, and isomerization of 2,2-dimethyl-5-methylene pyrrolidine.**

The reactions were performed in the absence of $PPh_3$. The amido alkene complex appears to decay a small amount before reaching an equilibrium or constant concentration. After 8 hours, roughly 85 % of the initial complex is still present. The data tentatively suggest that the reaction or rhodium diphosphine alkoxo alkene complex, **8g**, is faster than the reaction of rhodium diphosphine amido alkene complex **9g**. The shapes of the kinetic traces suggest that the decay of rhodium diphosphine complexes **8g** and **9g** may be more complicated than a simple first order reaction. The reactions were not investigated further.

The relative rates for the decompositions of **8g** and **9g** were also calculated by DFT. The energy barrier for the decomposition of **8g** was calculated to be 22.3 kcal/mol. The energy barrier for the decomposition of **9g** was calculated to be 23.6 kcal/mol. The calculations suggest that rhodium diphosphine alkoxo alkene complex **8g** will react faster than rhodium diphosphine amido alkene complex **9g**. The relative order of the calculated reaction rates appears to be consistent with the experimental findings. The shape of the kinetic traces for the decompositions of **8g** and **9g** cast some doubt on the rates that are actually being measured. While the formation of furans and pyrrolidines by the decompositions of **8g** and **9g** is assumed to occur by rate-limiting insertion or C-X (X = O, N) bond formation, it is also possible that the reactions occur by rate-limiting β-hydride elimination.

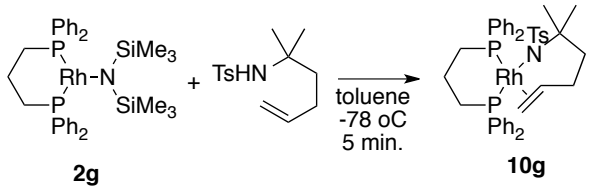
The results contrast with the barriers calculated for the insertions of ethene into rhodium-hydroxo and -amido bonds. In these examples, ethene insertion into the rhodium-amido bond of $(Me_3P)_2Rh(NH_2)(C_2H_4)$ occurs with a lower barrier than ethene insertion into the rhodium-hydroxo bond of $(Me_3P)_2Rh(OH)(C_2H_4)$.

This discrepancy may be due to the tether between the amido and alkoxo groups and the alkene. To test this hypothesis, DFT calculations were performed on the insertions of ethene into the rhodium amido and alkoxo bonds of (DPPP)Rh(NHBu$^t$)($C_2H_4$) and (DPPP)Rh(OBu$^t$)($C_2H_4$). The calculations suggest that insertion of ethene into the rhodium-amido bond of (DPPP)Rh(NHBu$^t$)($C_2H_4$) is faster than insertion of ethene into the rhodium-alkoxo bond of (DPPP)Rh(OBu$^t$)($C_2H_4$).

The results suggest that the tether between the amido and alkoxo ligands and the alkene may affect the rates for alkene insertion by either altering the orientations of the two reacting groups or by restricting their movements. These reactions were not investigated further.

### 2.2.1.9 Synthesis and Reactivity of Rhodium Diphosphine Tosylamido Alkene Complex, **10g**.

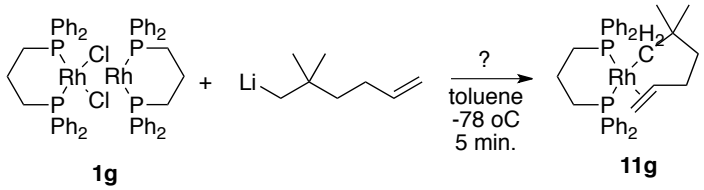
Rhodium diphosphine alkoxo alkene complex, **10g**, was synthesized by the addition of *N*-tosyl-2-methyl-5-hexen-2-amine to rhodium diphosphine silylamido complex, **2b** (Scheme 183). The reaction was conducted at -78 °C inside an NMR tube. The resulting rhodium diphosphine tosylamido alkene complex **10g** was characterized by $^1$H, $^{13}$C and $^{31}$P NMR spectroscopy. Decomposition of **10g** was monitored by $^1$H NMR spectroscopy at 0 °C. Ten equivalents of $PPh_3$ were added to the reactions to trap the rhodium hydride formed by β-hydride elimination. An accurate rate constant for the decomposition of **10g**, however was not obtained.




**Scheme 183: Synthesis of rhodium diphosphine tosylamido alkene complex 10g. The complex was formed by the addition of 4-methyl-*N*-(2-methylhex-5-en-2-yl)benzenesulfonamide to rhodium diphosphine silylamido complex 2g.**

### 2.2.1.10 Attempts to Synthesize Rhodium Diphosphine Alkyl Alkene Complex, **11g**.

Attempts to observe the rhodium diphosphine alkyl alkene complex **11g** began with attempts to synthesize 2,2-dimethyl-5-hexenyl lithium by lithium-halogen exchange of 6-iodo-5,5-dimethyl-1-hexene with *tert*-butyllithium (Scheme 184).



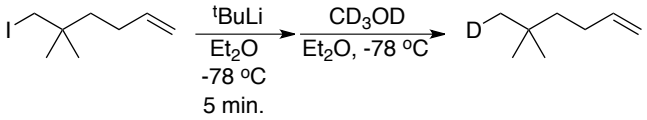

**Scheme 184: Tentative or proposed route for the synthesis of rhodium diphosphine alkyl alkene complex 11g.**

The reactions of 6-iodo-5,5-dimethyl-1-hexene with lithium diisopropylamide (LDA) were previously reported by Ashby and co-workers for the study of alkyl radicals, carbanions, and carbenes. The reactions generate a mixture of cyclic alkenes and alkanes, presumably by electron transfer from LDA to the alkyl iodide. The reactions were performed at 0 °C in THF.

The reactions of 6-iodo-1-hexenes with tert-butyllithium were also investigated by Bailey and co-workers. In this case, the reactions generate alkyl lithium reagents (by lithium-halogen exchange), which spontaneously cyclize at temperatures above -78 °C. Syntheses of the alkyl lithium reagents were performed at -78 °C in $Et_2O$-pentane solutions.

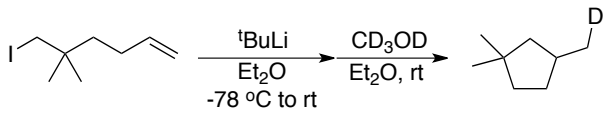
The reactions reported Ashby and Bailey support the possibility of generating 2,2-dimethyl-5-hexenyl lithium by the reaction of 6-iodo-5,5-dimethyl-1-hexene with *tert*-butyllithium. The formation 2,2-dimethyl-5-hexenyl lithium by lithium-halogen exchange suggested an entry point for the syntheses of rhodium diphosphine alkyl alkene complexes by a sequence of steps involving lithium- halogen exchange followed by salt metathesis with rhodium diphosphine alkoxo alkene complex **1g**.

To test this possibility, the reactions of 6-iodo-5,5-dimethyl-1-hexene with *tert*-butyllithium were performed in $Et_2O$-pentane at room temperature and at - 78 °C. The reactions were quenched with methanol-$d_4$ after 5 minutes. Reactions preformed at -78 °C resulted in the formation of 6-deutero-5,5-dimethyl-1-hexene and a small amount of 1,1-dimethyl-3-deuteromethyl-cyclopentane (Scheme 185).




**Scheme 185: Sequential addition of $^t$BuLi and $CD_3OD$ to 6-iodo-5,5-dimethyl-1-hexene. In this case, both reactions were performed at -78 °C. The addition of $^t$BuLi to 6-iodo-5,5-dimethyl-1-hexene is thought to generate 2,2-dimethyl-5-hexenyl lithium by lithium-halogen exchange, while the addition of $CD_3OD$ to 2,2-dimethyl-5-hexenyl lithium is thought to generate 6-deutero-5,5-dimethyl-1-hexene. Similar reactions were reported by Bailey and co-workers.**

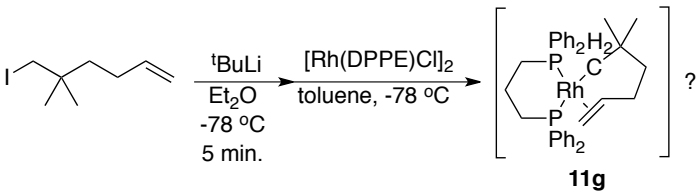
Reactions preformed at room temperature resulted in the formation of 1,1-dimethyl-3-deuteromethyl-cyclopentane (Scheme 186).




**Scheme 186: Sequential addition of $^t$BuLi and $CD_3OD$ to 6-iodo-5,5-dimethyl-1-hexene. In this case, the addition of $^t$BuLi to 6-iodo-5,5-dimethyl-1-hexene was performed at -78 °C, while the addition of $CD_3OD$ to 2,2-dimethyl-5-hexenyl lithium was performed at room temperature. The addition of $^t$BuLi to 6-iodo-5,5-dimethyl-1-hexene is thought to generate 2,2-dimethyl-5-hexenyl lithium, which spontaneously cyclizes to 5-(lithiomethyl)-2,2-dimethyl tetrahydrofuran at room temperature. Addition of $CD_3OD$ to generates 5-(deuteromethyl)-2,2-dimethyl tetrahydrofuran. Similar reactions were reported by Bailey and co-workers.**

Reactions conducted at -78 °C and warmed to room temperature also resulted in the formation of 1,1-dimethyl-3-deuteromethyl-cyclopentane. The products were analyzed by GC/MS. The data are consistent with the generation of 2,2-dimethyl-5-hexenyl lithium at -78 and spontaneous cyclization of the unsaturated alkyllithium reagent at temperatures above -78 °C. The results are consistent with the reports published by Bailey and co-workers.

To gauge the reactivity of the organolithium reagent generated by this sequence of reactions and to assess the ability of this route to generate rhodium(I) diphosphine alkyl alkene complexes, a toluene solution of **1g** was added to the alkyllithium reagent at -78 °C inside and NMR tube. The reaction resulted in the formation of a new complex, which was characterized by the appearance of two doublets of doublets in the $^{31}$P NMR spectrum (Scheme 187).



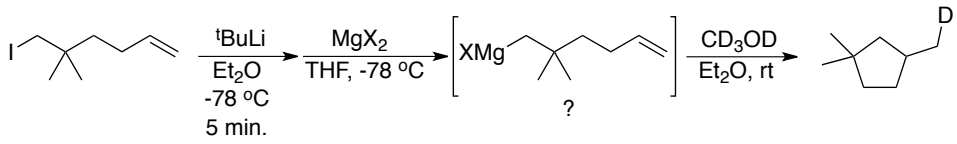

**Scheme 187: An attempt to synthesize rhodium diphosphine alkyl alkene complex 11g by the addition of 2,2-dimethyl-5-hexenyl lithium (formed in situ) to rhodium diphosphine chloride complex 1g. The reactions generated a new rhodium complex whose $^{31}$P NMR spectra displays two doublets of doublets, characteristic of a rhodium diphosphine complex in which the two phosphorus atoms occupy different chemical environments. It is not clear, however, if these spectra correspond to rhodium diphosphine alkyl alkene complex 11g or to another complex. The $^{1}$H NMR spectra of the product solution was complicated by pentane signals in the alkyl region.**

The $^{1}$H NMR spectrum of this solution is difficult to interpret. The presence of pentane from the *tert*-butyllithium solution complicates the alkyl region of the $^{1}$H NMR spectrum. The reactions were also complicated by the fact that **1g** is only slightly soluble in toluene at -78 °C. The reactions were difficult to reproduce.

In order to avoid some of the complications associated with using pentane solutions of *tert*-butyllithium to generate alkyllithium reagents in situ at -78 °C, alternative routes to rhodium(I) diphosphine alkyl alkene complex, **11g**, were examined.

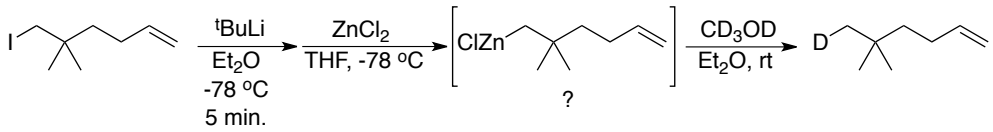
The additions of magnesium(0) and zinc(0) to solutions of 2,2-dimethyl-1-iodo-5-hexene and 1-bromo-2,2-dimethyl-5-hexene at room temperature did not generate the desired alkylmagnesium and alkylzinc reagents. Heating solutions of 2,2-dimethyl-1-iodo-5-hexene and 1-bromo-2,2-dimethyl-5-hexene in the presence of magnesium(0) and zinc(0) resulted in mixtures of both the linear and cyclized organometallic reagent.

Attempts to generate more stable alkyl organometallic reagents resulted in the additions of $MgBr_2$ and $ZnCl_2$ to solutions of 2,2-dimethyl-5-hexenyl lithium. The reactions were conducted at -78 °C. The addition of $MgBr_2$ to 2,2-dimethyl-5-hexenyl lithium resulted in an alkyl organometallic reagent which spontaneously cyclized upon warming to room temperature (Scheme 188).




**Scheme 188: The additions of $MgCl_2$ and $MgBr_2$ to 2,2-dimethyl-5-hexenyl lithium (formed in situ by the addition of tBuLi to ). The reactions were performed at -78 °C and then warmed to room temperature. The addition of $CD_3OD$ to the product solution resulted in the formation of 5-(deuteromethyl)-2,2-dimethyl tetrahydrofuran, suggesting that the alkyl magnesium bromide complex spontaneously cyclizes at room temperature.**

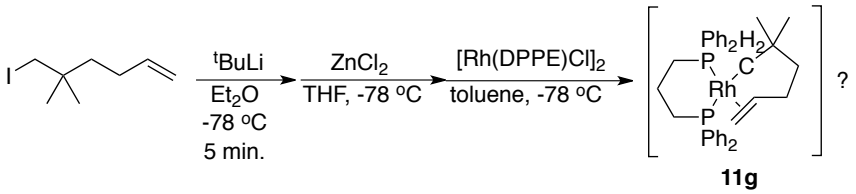
The addition of $ZnCl_2$ to 2,2-dimethyl-5-hexenyl lithium resulted in an alkyl organometallic reagent, which appeared to be stable at room temperature (Scheme 189).




**Scheme 189: The additions of $ZnCl_2$ to 2,2-dimethyl-5-hexenyl lithium. The reaction was performed at -78 °C and then warmed to room temperature. The addition of $CD_3OD$ to the product solution resulted in the formation of 5-(deuteromethyl)-2,2-dimethyl tetrahydrofuran, suggesting that the alkyl zinc reagent is stable at room temperature.**

Attempts to isolate this complex, however, were unsuccessful. In addition, the reaction was difficult to reproduce. The stability of the unsaturated alkyl zinc is unclear; intramolecular insertion of the alkenyl group into the carbon-zinc bond by a non-radical reaction has been proposed in at least one case.

Subsequent addition of rhodium diphosphine chloride complex, **1g**, to the organozinc reagent generated in situ from the addition of $ZnCl_2$ to (2,2-dimethylhex-5-en-1-yl)lithium resulted in a new rhodium diphosphine complex, which was characterized by two doublets of doublets in the $^{31}P$ NMR spectrum (Scheme 190).



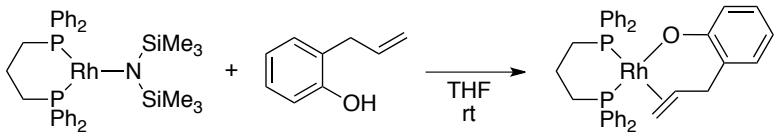

**11g**

**Scheme 190: The addition of the alkyl zinc reagent, formed by the sequential additions of $^{t}$BuLi and $ZnCl_2$ to 6-iodo-5,5-dimethyl-1-hexene, to rhodium diphosphine chloride complex 1g. The reactions generated a new rhodium complex. The reactions generated a new rhodium complex whose $^{31}P$ NMR spectra displays two doublets of doublets, characteristic of a rhodium diphosphine complex in which the two phosphorus atoms occupy different chemical environments. It is not clear, however, if these spectra correspond to rhodium diphosphine alkyl alkene complex 11g or to another complex. The $^{1}H$ NMR spectra of the product solution was complicated by pentane signals in the alkyl region.**

The chemical shifts of these doublets of doublets are inconsistent with the rhodium diphosphine complex formed by the addition of 2,2-dimethyl-5-hexenyl lithium to rhodium diphosphine chloride complex **1g**. The causes for this inconsistency are not understood. The $^{1}H$ signals of a rhodium diphosphine alkyl alkene complex could not be identified. Investigations of these complexes were eventually stopped.

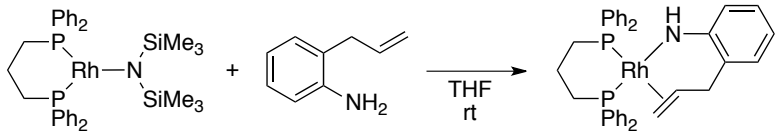
### 2.2.1.11 Syntheses and Reactivities of Rhodium Diphosphine Phenoxo and Anilido Alkene Complexes, **12g** and **13g**.

Finally, the reactions of rhodium diphosphine phenoxo and anilido alkene complexes, **12g** and **13g** were also investigated. Rhodium diphosphine phenoxo- and anilido- alkene complexes **12g** and **13g** were synthesized by the additions of 2-allylphenol and 2-allylaniline to rhodium diphosphine silylamido complex **2g** (Scheme 191 and Scheme 192).




**12g**

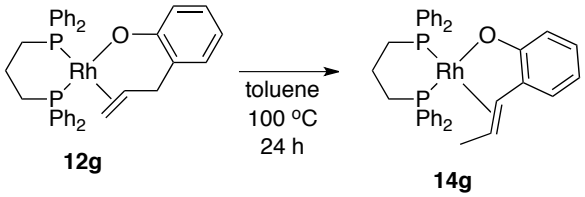
**Scheme 191: Synthesis of rhodium diphosphine phenoxo alkene complex 12g. The complex is formed by the addition of 2-allylphenol to rhodium diphosphine silylamido complex 2g and is stable at room temperature.**



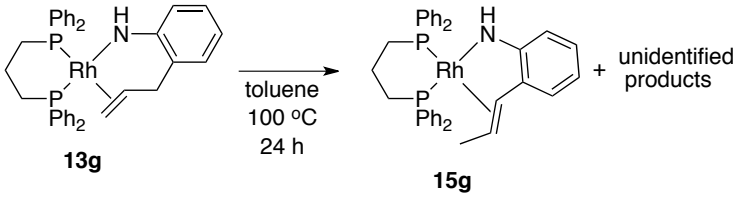

**13g**

**Scheme 192: Synthesis of rhodium diphosphine anilido alkene complex 13g. The complex is formed by the addition of 2-allylaniline to rhodium diphosphine silylamido complex 2g and is stable at room temperature.**

The complexes were stable at room temperature and were characterized by $^{1}H$ and $^{31}P$ NMR spectroscopy. Heating solutions of **12g** and **13g** to 100 °C resulted in the decomposition of these complexes to rhodium diphosphine complexes **14g** and **15g** (Scheme 193 and Scheme 194).




**Scheme 193: The reaction of rhodium diphosphine phenoxo alkene complex 12g at 100 °C. The reaction generates a rhodium diphosphine phenoxo alkene complex, 14g, which was isolated at room temperature and characertized by $^{1}H$ and $^{31}P$ NMR spectrscopy. The mechanism for this reaction is uncertain.**




**Scheme 194: The reaction of rhodium diphosphine anilido alkene complex 13g at 100 °C. The reaction generates a rhodium diphosphine anilido alkene complex, 15g, which was isolated at room temperature and characertized by $^{1}H$ and $^{31}P$ NMR spectrscopy. The mechanism for this reaction is uncertain. Other rhodium complexes were also observed from the reactions of 13g. These complexes were detected by $^{31}P$ NMR spectroscopy, but not identified.**

The mechanisms for these reactions were not investigated. Rhodium diphosphine phenoxo alkene complex, **14g**, was characterized by $^{1}H$ and $^{31}P$ NMR spectroscopy. Rhodium diphosphine anilido alkene complex **15g** precipitated from solution and was characterized by x-ray crystallography. The decomposition of **13g** resulted in the formation of other compounds, which were not characterized. GC/MS analysis of showed no signs of C-N bond formation.

### 2.2.2 Summary and Conclusions

The reactions of rhodium diphosphine silylamido complexes, **2b**, **2g**, and **2i** with 1,1-diphenyl-4-penten-1-ol and 2-methyl-5-hexen-2-ol at -78 °C point to a general route for the syntheses of rhodium diphosphine alkoxo alkene complexes. The fact that several rhodium silylamido complexes react is encouraging for further studies. The effects of ancillary ligand properties on the rates of alkene insertions into rhodium-alkoxo bonds are presented in Chapter 3.

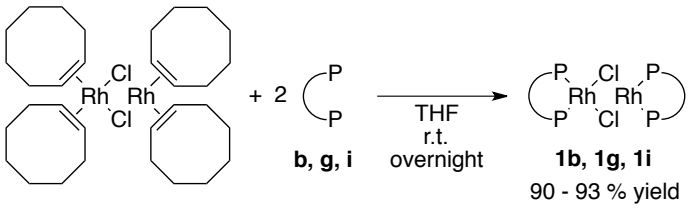
The reactions of rhodium diphosphine alkoxo and amido complexes, **8g**, **9g**, and **10g**, suggest that alkene insertions into rhodium-alkoxo bonds are faster than alkene insertions into rhodium-amido bonds. These results contrast with DFT calculations that suggest that alkene insertions into rhodium-amido bonds are faster than alkene insertions into rhodium-hydroxo bonds. In order to probe these discrepancies, DFT calculations were preformed on the reactions of **8g** and **9g**. The results from these latter calculations suggest that the reactions of rhodium diphosphine alkoxo alkene complex, **8g** should occur at a faster rate than the reactions of rhodium diphosphine amido alkene complex, **9g**. The relative order of reaction rates is consistent with the experimental findings. Consequently, DFT calculations were performed on rhodium *tert*-butoxide ethene complexes and rhodium *tert*-butylamide ethene complexes, to determine if the methylene linker or tether affects the relative order of calculated

reaction rates. The results from these latter calculations show that ethene insertions into rhodium(I)-*tert*-butylamide bonds are faster than ethene insertions into rhodium(I)-*tert*-butoxide bonds. Combined with the results for complexes **8g** and **9g**, the data suggest that the alkene tether plays an important role in determining the relative order or reaction rates. Although it is unclear how the tether affects the relative rates for alkene insertions into rhodium-amido and rhodium-alkoxo bonds, one hypothesis is that the tether affects the orientation of the amido and alkoxo groups and restricts the rotation of both groups.

The experimental data also show that the rate of reaction of **8g** is significantly faster than the rate of reaction **7g**. The difference between these two complexes is the identities of the two gem-disubstituted groups on the alkoxo alkene fragment. Rhodium alkoxo alkene complex **8g** has gem-dimethyl groups while rhodium alkoxo alkene complex **7g** has gem-diphenyl groups. Although it is speculative, the faster rates for the gem-dimethyl-substituted complex, **8g**, may result from greater congestion or more restricted motion of the alkoxo and alkene groups in **8g** (the gem-dimethyl substituted alkoxo alkene complex) relative to the congestion and range of motion of the alkoxo and alkene groups in **7g** (the gem-diphenyl substituted alkoxo alkene complex). This relative order of reaction rates is supported by DFT calculations performed on rhodium alkoxo alkene complexes of DMePP (1,3-bis(dimethylphosphino)propane).

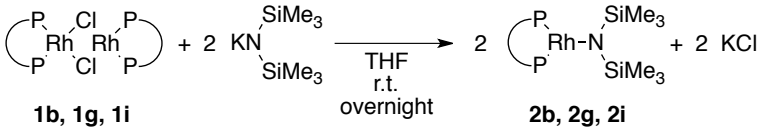
## 2.3 Experimental

### 2.3.1 Syntheses of Rhodium Diphosphine Chloride Complexes **1b**, **1g**, and **1i**.

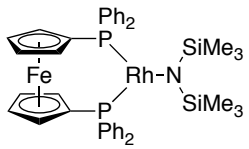



Rhodium diphosphine chloride complexes **1b**, **1g**, and **1i** were synthesized by the additions of diphosphines DPPF (**b**), DPPP (**e**), and BINAP (**g**) to $[Rh(COE)_2(\mu\text{-}Cl)]_2$. The reactions were performed at room temperature overnight in THF. A magnetic stir bar was used to stir the reaction. The solution was concentrated under vacuum and triturated with $Et_2O$. The precipitate solid was collected on a glass frit, washed with additional $Et_2O$, transferred to a tared vial and dried under vacuum. The solids were used without further purification. Recrystallizations from hot toluene were possible in some cases. The relatively poor solubility of these compounds at room temperature in THF, benzene, toluene, $CH_2Cl_2$ hinderexd their characterization.

### 2.3.2 Syntheses of Rhodium Diphosphine Silylamido Complexes **2b**, **2g**, and **2i**.




#### Synthesis of rhodium diphosphine silylamido complex, **2b**.




**2b**

Rhodium diphosphine chloride complex, **1b**, was weighed inside a glovebox in 20 ml vial (200 mg, 0.144 mmol, 1 equiv.). THF (2 ml) and a magnetic stir bar were added to the vial. A solution of KHMDS (57.6 mg, 0.289 mmol, 2 equiv.) in THF was prepared in a separate 20 ml vial and added to the rhodium diphosphine complex by pipet. The vial containing the two reagents was capped, and the resulting solution was stirred overnight inside the glovebox at room temperature. The solution became dark green and homogeneous. The solvent was removed under vacuum, and the resulting dark green residue was dissolved in pentane and filtered through celite. The filtrate was collected and the solvent removed under vacuum. A dark green solid was collected (221 mg, 0.270 mmol, 94 % yield).

$^1$H NMR: (499.4 MHz, $C_6D_6$) δ 7.99 (m, 8 H), 7.05 (t, J = 7.5 Hz, 8 H), 7.01 (q, J = 7.5 Hz, 4 H), 4.45 (s, broad, 4 H), 3.84 (s, broad, 4 H), 0.51 (s, 18 H) ppm.

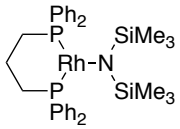
$^{13}C\{^{1}H\}$ NMR: (125.7 MHz, $C_6D_6$) δ 138.7 (t, $J^{C-P}$ = 23 Hz), 134.6 (t, $J^{C-P}$ = 6 Hz), 130.0, 128.7, 81.9, (t, $J^{C-P}$ = 30 Hz), 76.0 (t, unresolved), 72.4 (t, unresolved), 7.3 ppm.

$^{31}P\{^{1}H\}$ NMR: (202.2 MHz, $C_6D_6$) δ 64.1 (d, $J_{P-Rh}$ = 183 Hz) ppm.

Analysis Calculated For $C_{40}H_{46}FeNP_2RhSi_2$: C, 58.76; H, 5.67; N, 1.71.

Found: C, 58.80; H, 5.62; N, 1.38.

## Synthesis of rhodium diphosphine silylamido complex, **2g**.




**2g**

Rhodium diphosphine chloride complex, **1g**, was weighed inside a glovebox in 20 ml vial (200 mg, 0.182 mmol, 1 equiv.). THF (2 ml) and a magnetic stir bar were added to the vial. A solution of KHMDS (72.4 mg, 0.363 mmol, 2 equiv.) in THF (5 ml) was prepared in a 20 ml separate vial and added to the rhodium diphosphine complex by pipet. The vial containing the two reagents was capped, and the resulting solution was stirred overnight inside the glovebox at room temperature. The solution became dark blue and homogeneous (a yellow precipitate forms initially, but disappears over time). The THF solvent was removed under vacuum, and the resulting dark blue residue was dissolved in pentane and filtered through celite. The filtrate was collected and the solvent removed under vacuum to yield a dark blue solid (222 mg, 0.329 mmol, 91 % yield).

$^{1}H$ NMR: (499.92 MHz, THF-$d_8$) δ 7.70 (m, broad, 8H), 7.19 (m, broad, 12H), 2.39 (s, broad, 4H), 2.03 (m, broad, 4H), 0.12 (s, broad, 18H) ppm.

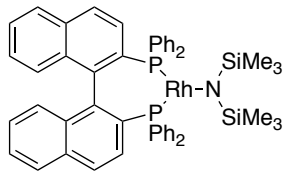
$^{13}C\{^{1}H\}$ NMR: (125.7 MHz, THF-$d_8$) δ 138.1 (t, $J^{C-P}$ = 23 Hz), 133.7 (t, J = 5.0 Hz), 130.2, 128.7 (t, J = 5.0 Hz), 26.6 (t, $J^{C-P}$ = 21.4 Hz), 21.3, 7.4 ppm.

$^{31}P\{^{1}H\}$ NMR: (202.2 MHz, $C_6D_6$) δ 40.5 (d, $J_{P-Rh}$ = 169 Hz) ppm.

Analysis Calculated For $C_{33}H_{44}NP_2RhSi_2$: C, 58.66; H, 6.56; N, 2.07.

Found: C, 58.92; H, 6.19; N, 1.87.

## Synthesis of rhodium diphosphine silylamido complex, **2i**.




**2i**

Rhodium diphosphine chloride complex, **1i**, was weighed inside a glovebox in 20 ml vial (200 mg, 0.131 mmol, 1 equiv.). THF (2 ml) and a magnetic stir bar were added to the vial. A THF (5 ml) solution of KHMDS (52.4 mg, 0.263 mmol, 2 equiv.) THF (5 ml) was prepared in a separate 20 ml vial and added to the rhodium diphosphine complex by pipet. The vial containing the two reagents was capped, and the resulting solution was stirred overnight inside the glovebox at room temperature. The solution became dark green and homogeneous. The solvent was removed under vacuum, and the resulting dark green residue was dissolved in pentane and filtered through celite. The filtrate was collected and the solvent removed under vacuum. A dark green solid was collected (222 mg, 0.250 mmol, 95 % yield).

$^{1}H$ NMR: (125.7 MHz, $C_6D_6$) δ 8.36 (quartet, $J^{H-H}$ = 5 Hz, 4H), 7.87 (s, broad, 4H), 7.55 (quintet, $J^{H-H}$ = 5 Hz, 2H), 7.25-7.15 (overlapping doublets of doublets, $J^{H-H}$ = 10 Hz, $J^{H-H}$ = 5 Hz, 8H), 7.02 (t, $J^{H-H}$ = 10 Hz, 2H), 6.98 (t, $J^{H-H}$

= 10 Hz, 2H), 6.85 (d, $J^{H-H}$ = 5 Hz, 2H), 6.72 (t, $J^{H-H}$ = 10 Hz, 2H), 6.35-6.25 (overlapping signals, 6H), 0.65 (s, 18H) ppm.

$^{1}$H NMR: (125.7 MHz, THF-$d_8$) δ 8.30 (s, broad, 4H), 7.87 (s, broad, 4H), 7.55 (d, broad, $J^{H-H}$ = 10 Hz, 2H), 7.50 (s, broad, 4H), 7.39 (s, broad, 6H), 7.30 (m, broad, 6H), 7.07 (m, broad, 2H), 6.95 (d, broad, $J^{H-H}$ = 10 Hz, 2H), 6.57 (m, broad, 2H), 6.48 (m, broad, 4H), 0.36 (s, 18H) ppm.

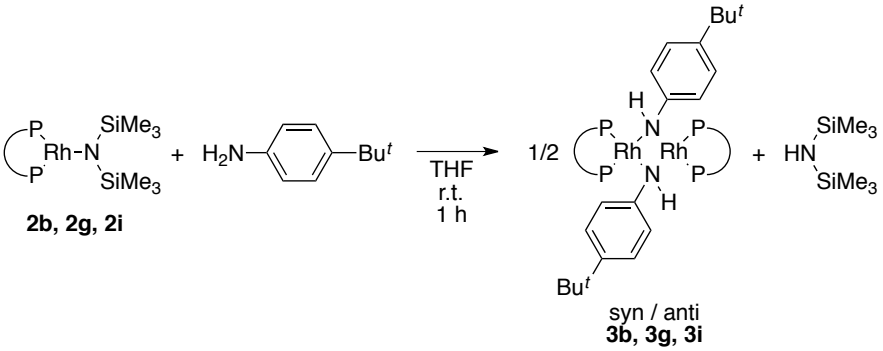
$^{13}$C{$^{1}$H} NMR: (125.7 MHz, THF- $d_8$) δ 138.8 (t, $J^{C-P}$ = 6 Hz), 136.0 (t, $J^{C-P}$ = 5 Hz), 135.5 (t, $J^{C-P}$ = 26 Hz), 135.3 ((t, $J^{C-P}$ = 24 Hz), 134.6, 134.2 (m, broad, overlapping), 134.1 (m, broad, overlapping), 133.5 (t, $J^{C-P}$ = 26 Hz), 130.7, 129.1, 128.9, 128.8, 128.7-128.4 (overlapping multiplets, 2C), 128.2, 127.1, 126.9 (t, $J^{C-P}$ = 5 Hz), 126.7, 7.8 ppm.

$^{31}$P{$^{1}$H} NMR: (202.2 MHz THF- $d_8$) δ 57.8 (d, $J^{P-Rh}$ = 174 Hz) ppm.

Analysis Calculated For $C_{50}H_{50}NP_2RhSi_2$: C, 67.78; H, 5.69; N, 1.58.

Found: C, 67.89; H, 5.56; N, 1.63.

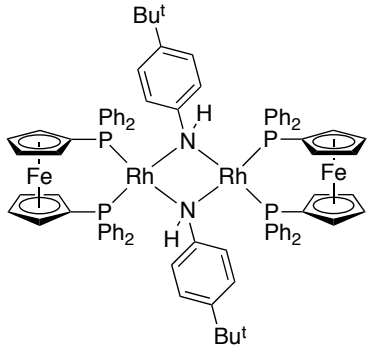
### 2.3.3 Syntheses of Rhodium Diphosphine Anilido Complexes **3b**, **3g**, and **3i**.




**2b, 2g, 2i**

**3b, 3g, 3i**

#### Synthesis of rhodium diphosphine anilido complex, **3b**.



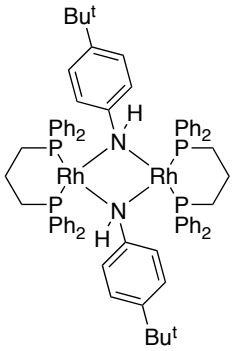

**3b**

Rhodium diphosphine silylamido complex, **2b**, (200 mg, 0.245 mmol, 1 equiv.) was weighed inside a glovebox in a 20 ml vial and dissolved in toluene (2 ml). A magnetic stir bar was added to the vial. A toluene (5 ml) solution of 4-*tert*-butylaniline (37 mg, 0.248 mmol, 1.01 equiv.) was prepared in a separate vial and added slowly to the rhodium diphosphine silylamido complex. The resulting solution became orange. The reagents were stirred at room temperature for 30 minutes. The toluene solution was concentrated under vacuum to approximately 1 ml total volume and triturated with pentane (15 ml). An orange solid precipitated. The solution was filtered through a glass frit. The solid was collected and washed with additional pentane. The collected solid was transferred to a 20 ml vial and dried under vacuum. An orange solid was obtained (57 mg, 0.035 mmol, 29 % yield) and used as collected.

$^{1}$H NMR: (399.95 MHz, THF-$d_8$) major isomer δ 8.05 (m, broad, 8H), 7.29 (m, 4H, overlapping signals), 7.20 (t, $J^{H-H}$ = 8 Hz, 8H), 7.08-7.01 (m, 12H, overlapping signals), 6.86 (d, $J^{H-H}$ = 8 Hz, 8H, overlapping signals), 3.89 (s, broad, 4H), 3.85 (s, broad, 4H), 3.74 (s, broad, 4H), 3.48 (s, broad, 4H), 1.36 (s, broad, 18H). minor isomer δ 7.97 (s, broad, 2.9H), 7.37 (s, broad, 2.9H), 7.26 (m, broad, 1.4H, overlapping signals) 7.08-7.01 (m, broad, 4.3H, overlapping signals), 6.84 (m, 2.9H, overlapping signals), 6.77 (s, broad, 2.9H), 4.21 (s, broad, 1.4H), 4.16 (s, broad, 1.4H), 4.07 (s, broad, 1.4H), 3.87 (s, broad, 1.4H, overlapping signals), 1.17 (s, broad, 6.4H) ppm.

$^{31}$P{$^{1}$H} NMR: (161.9 MHz, THF-$d_8$) major isomer δ 41.2 (d, $J^{P-Rh}$ = 183 Hz), minor isomer δ 44.0 (d, $J_{P-Rh}$ = 178 Hz) ppm. major-to-minor ratio = 1 : 0.36.

## Synthesis of rhodium diphosphine anilido complex, **3g**.



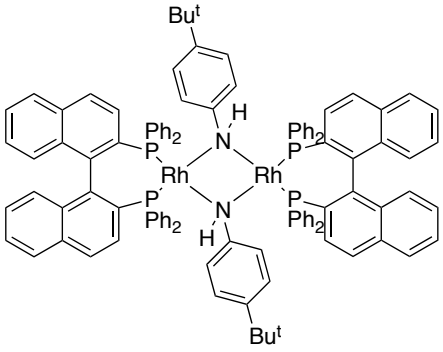

**3g**

Rhodium diphosphine silylamido complex, **2g**, (200 mg, 0.296 mmol, 1 equiv.) was weighed inside a glovebox in a 20 ml vial and dissolved in toluene (2 ml). A magnetic stir bar was added to the vial. A toluene (5 ml) solution of 4-*tert*-butylaniline (44 mg, 0.302 mmol, 1.02 equiv.) was prepared in a separate vial and added slowly to the rhodium diphosphine silylamido complex. The resulting solution became orange. The reagents were stirred at room temperature for 30 minutes. The toluene solution was concentrated under vacuum to approximately 1 ml total volume and triturated with pentane (15 ml). An orange solid precipitated. The solution was filtered through a glass frit. The solid was collected and washed with additional pentane. The collected solid was transferred to a 20 ml vial and dried under vacuum. An orange solid was obtained. (98.6 mg, 0.074 mmol, 50 % yield) and used as collected.

$^{1}$H NMR: (500.16 MHz, $C_6D_6$, 50 °C) major isomer δ 8.00 (s, broad, 8H), 7.31 (s, broad, 8H, overlapping signals), 7.13 (s, broad, 12H, overlapping signals) 7.09 (t, broad, $J^{H-H}$ = 5 Hz, 4H, overlapping signals), 6.85 (m, 8H, overlapping signals), 6.60 (s, broad, 8H), 1.99 (s, broad, 8H), 1.81 (d, broad, J = 30 Hz, 4H), 1.30 (s, broad, 18H). minor isomer δ 7.94 (s, broad, 4.8H), 7.35 (s, broad, 4.8H, overlapping signals), 7.09 (m, broad, 2.4H, overlapping signals) 6.99 (s, broad, 7.2H, overlapping signals), 6.88 (m, 4.8H, overlapping signals), 6.69 (s, broad, 4.8H), 1.58 (s, broad, 1.2H), 1.25 (m, broad, 4.8H, overlapping signals), 1.41 (s, broad, 10.8H, overlapping signals) 0.86 (t, $J^{H-H}$ = 5Hz, 1.2H) ppm.

$^{31}$P{$^{1}$H} NMR: (202.2 MHz, $C_6D_6$, 50 °C) major isomer δ 31.9 (d, $J^{P-Rh}$ = 166 Hz), minor isomer δ 30.8 (d, $J_{P-Rh}$ = 166 Hz) ppm. major-to-minor ratio = 1.0 : 0.6.

Synthesis of rhodium diphosphine anilido complex, **3i**.

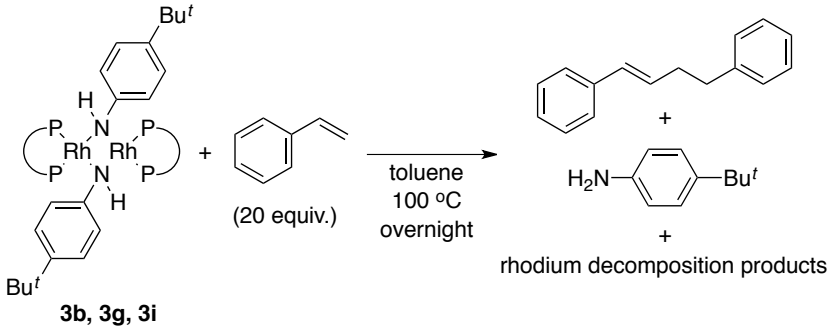



**3i**

Rhodium diphosphine silylamido complex, **2i**, (100 mg, 0.113 mmol, 1 equiv.) was weighed inside a glovebox in a 20 ml vial and dissolved in toluene (2 ml). A magnetic stir bar was added to the vial. A toluene (5 ml) solution of 4-*tert*-butylaniline (17 mg, 0.114 mmol, 1.01 equiv.) was prepared in a separate vial and added slowly to the rhodium diphosphine silylamido complex. The resulting solution became dark red. The reagents were stirred at room temperature for 30 minutes. The toluene solution was concentrated under vacuum to approximately 1 ml total volume and triturated with pentane (15 ml). An dark red solid precipitated. The solution was filtered through a glass frit. The solid was collected and washed with additional pentane. The collected solid was transferred to a 20 ml vial and dried under vacuum. An a dark red solid was obtained (55 mg, 0.031 mmol, 56 % yield) and used as collected.

$^{31}P\{^{1}H\}$ NMR: (202.2 MHz, $C_6D_6$, 50 °C) δ 48.84 (d, $J^{P\text{-}Rh}$ = 175 Hz), 45.72 (d, $J^{P\text{-}Rh}$ = 175 Hz) ppm.

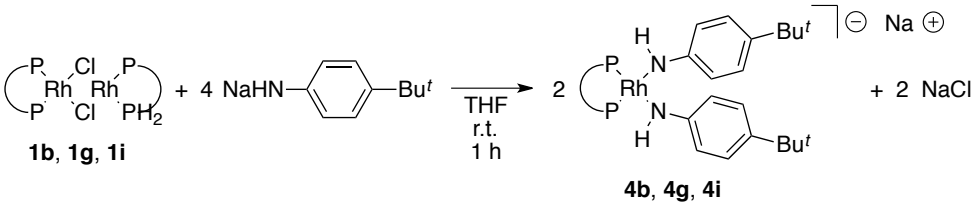
### 2.3.4 Syntheses of Rhodium Diphosphine Anilido Complexes **3b**, **3g**, and **3i**.




**3b, 3g, 3i**

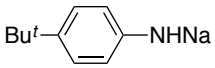
Rhodium anilido complexes **3b**, **3g**, and **3i** were weighed inside a glovebox in 3 ml vials (10 mg, 5.7 - 7.5 µmol, 1 equiv.). The complexes were dissolved in toluene (0.5 ml) and transferred to screw cap NMR tubes. Styrene (13.1 - 17.3 µL (0.906 g / ml), 0.114 - 0.151 mmol, 20 equiv.) was added by syringe. The tube was capped and removed from the glovebox. Phosphorous-31 NMR spectra were collected for each of the solutions. The NMR tubes were placed in a 100 °C oil bath, and the reaction was periodically monitored by $^{31}P$ NMR spectroscopy. After 24 hours, the $^{31}P$ NMR signals disappeared and the reactions were cooled to room temperature and analyzed by GC / MS. The mass spectra indicated the presence of 4-*tert*-butylaniline (M/z = 149), and styrene dimers (M/z = 208).

### 2.3.5 Syntheses of Anionic Rhodium Diphosphine Anilido Complexes **4b**, **4g**, and **4i**.




**1b**, **1g**, **1i** **4b**, **4g**, **4i**

Synthesis of sodium (4-(*tert*-butyl)phenyl)amide.

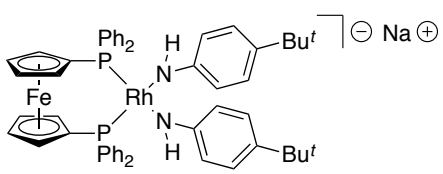



4-*tert*-butylaniline (1.0 g, 6.7 mmol, 1 equiv.) was weighed inside a glovebox in a 20 ml vial. Sodium hexamethyldisilylamide (NaHMDS; 1.35 g, 7.4 mmol, 1.1 equiv.) was weighed inside the glovebox in a separate 20 ml vial. The weighed NaHMDS was dissolved in 15 ml of toluene and transferred to the vial containing the weighed 4-*tert*-butylaniline. A magnetic stir bar was added to the vial. The vial was capped and the contents of the vial stirred overnight at room temperature inside the glovebox. A yellow-white precipitate formed. The solution was filtered through a glass frit inside the glovebox. The collected solid was washed with additional pentane, transferred to a tared 20 ml vial and dried under vacuum. The resulting solid was used as collected 1.1 g, 6.4 mmol, 96 % yield).

$^{1}$H NMR: (400 MHz, THF-$d_8$) δ 6.67 (d, $J^{H-H}$ = 8 Hz, 2H), 6.12 (d, JH-H = 8 Hz, 2H), 2.31 (s, 1H), 1.16 (s, 18H) ppm.

$^{13}$C{$^{1}$H} NMR: (125.7 MHz, THF-$d_8$) δ 164.6, 128.2, 126.2, 114.9, 33.8, 32.6 ppm.

Synthesis of rhodium diphosphine dianilido complex, **4b**.



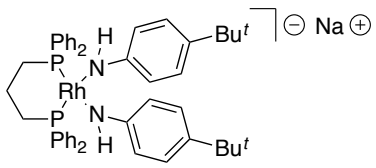

**4b**

Rhodium diphosphine chloride complex, **1b**, was weighed inside a glovebox in a 20 ml vial (80 mg, 0.058 mmol, 1 equiv.). THF (3 ml) was added to the vial along with a magnetic stir bar. A solution of sodium 4-*tert*-butylanilide (40 mg, 0.234 mmol, 4.05 equiv.) in THF (3 ml) was prepared in a separate 3 ml vial and added to the rhodium diphosphine chloride complex by pipet. The vial was capped, and the reaction was stirred at room temperature overnight. An orange solution formed. The solvent was removed under vacuum. The resulting residue was dissolved in benzene and filtered through celite. The filtrate was collected and frozen. The frozen benzene was removed under vacuum to yield an orange solid (21 mg, 0.036 mmol, 31 % yield; used as collected). The product was only slightly soluble in THF.

$^{1}$H NMR: (499.92 MHz, THF-$d_8$) δ 7.79 (s, broad, 8H), 7.10 (s, broad, 16H), 6.60 (s, broad, 4H), 4.07 (s, broad, 8H), 1.19 (s, broad, 18H) ppm.

$^{31}$P{$^{1}$H} NMR: (202.5 MHz, THF-$d_6$ δ 44.3 (d, $J^{P-Rh}$ = 177 Hz) ppm.

Synthesis of rhodium diphosphine dianilido complex, **4g**.



**4g**

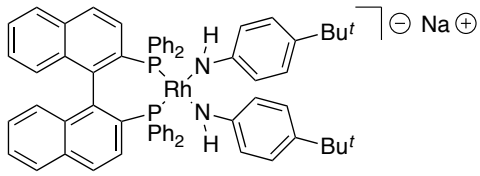
Rhodium diphosphine chloride complex, **1b**, was weighed inside a glovebox in a 20 ml vial (80 mg, 0.073 mmol, 1 equiv.). THF (3 ml) was added to the vial along with a magnetic stir bar. A solution of sodium 4-*tert*-butylanilide (50 mg, 0.292 mmol, 4.02 equiv.) in THF (3 ml) was prepared in a separate 3 ml vial and added to the rhodium diphosphine chloride complex by pipet. The vial was capped, and the reaction was stirred at room temperature overnight. An orange solution formed. The solvent was removed under vacuum. The resulting residue was dissolved in benzene and filtered through celite. The filtrate was collected and frozen. The frozen benzene was removed under vacuum to yield an orange solid (59 mg, 0.143 mmol, 99 % yield; used as collected).

$^{1}$H NMR: (499.92 MHz, THF-$d_8$) δ 7.62 (s, broad, 8H), 7.17-7.01 (overlapping signals, 12H), 6.55 (dd, $J^{H-H}$ = 8 Hz, 4H), 6.28 (s, 4H), 2.31 (s, 1H), 2.18 (2, broad, 4H), 1.55 (s, broad, 4H), 1.18 (s, 18H) ppm.

$^{13}$C{$^{1}$H} NMR: (125.7 MHz, THF-$d_8$) δ 160.6, 138.3 (m, broad), 133.3, 130.5, 127.5, 126.8, 124.4, 115.9, 33.0, 31.6, 29.8 (t, $J^{C-P}$ = 17 Hz), 19.7 ppm.

$^{31}$P{$^{1}$H} NMR: (202.5 MHz, THF-$d_6$ δ 32.7 (d, $J^{P-Rh}$ = 162 Hz) ppm.

Synthesis of rhodium diphosphine dianilido complex, **4i**.



**4i**

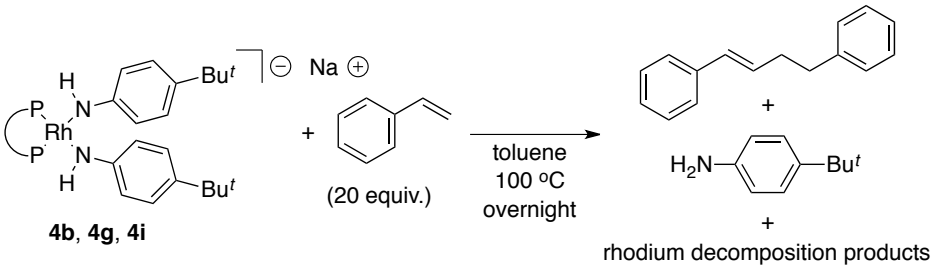
Rhodium diphosphine chloride complex, **1b**, was weighed inside a glovebox in a 20 ml vial (80 mg, 0.053 mmol, 1 equiv.). THF (3 ml) was added to the vial along with a magnetic stir bar. A solution of sodium 4-*tert*-butylanilide (36 mg, 0.210 mmol, 4 equiv.) in THF (3 ml) was prepared in a separate 3 ml vial and added to the rhodium diphosphine chloride complex by pipet. The vial containing was capped, and the reaction was stirred at room temperature overnight. An orange solution formed. The solvent was removed under vacuum. The resulting residue was dissolved in benzene and filtered through celite. The filtrate was collected and frozen. The frozen benzene was removed under vacuum to yield an orange solid (34 mg, 0.055 mmol, 52 % yield; used as collected).

$^{1}$H NMR: (499.92 MHz, THF-$d_8$) δ 7.92 (s, broad, 4H), 7.57 (s, broad, 2H), 7.48-7.34 (overlapping signals, m, 12H), 7.06 (m, 2H), 6.98 (d, $J^{H-H}$ = 8 Hz, 2H), 6.73 (t, $J^{H-H}$ = 8 Hz, 2H), 6.57 (d, $J^{H-H}$ = 8 Hz, 4H), 6.40 (dd, J = 16 Hz, J = 8 Hz, 4H), 6.53-6.24 (overlapping signals, 6H), 6.20 (s, broad, 2H), 2.31 (s, 1H), 1.13 (s, 18H) ppm.

$^{13}$C{$^{1}$H} NMR: (125.7 MHz, THF-$d_8$) δ 162.6, 140.0 (t, $J^{C-P}$ = 25 Hz), 137.8, 137.6 (t, $J^{C-P}$ = 17 Hz), 135.9 (broad), 134.4, 133.7, 132.1, 131.6 (t, $J^{C-P}$ = 16 Hz), 128.6, 128.2, 127.8, 127.7, 127.4, 126.7 (broad), 125.8, 125.4, 125.1, 117.3, 34.0, 32.5 ppm.

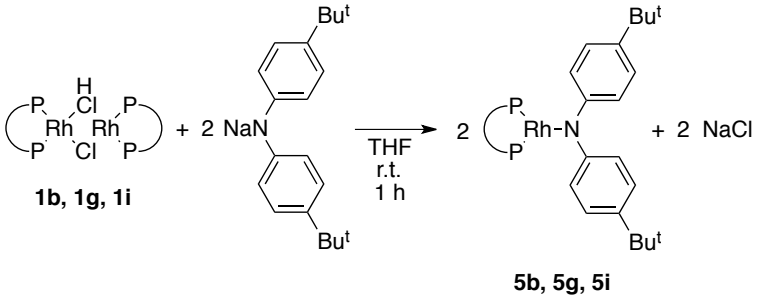
$^{31}$P{$^{1}$H} NMR: (202.5 MHz, THF-$d_6$ δ 47.1 (d, $J^{P-Rh}$ = 173 Hz) ppm.

### 2.3.6 Reactions of Anionic Rhodium Diphosphine Diarylamido Complexes, **4b**, **4g**, and **4i** with Styrene.

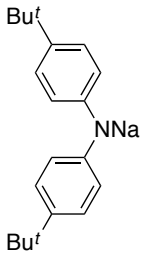



Rhodium anilido complexes **4b**, **4g**, and **4i** were weighed inside a glovebox in 3 ml vials (10 mg, 9.6 - 12.0 µmol, 1 equiv.). The complexes were dissolved in toluene (0.5 ml) and transferred to screw cap NMR tubes. Styrene (22 - 23 µL (0.906 g / ml), 0.191 - 0.200 mmol, 20 equiv.) was added by syringe. The tube was capped and removed from the glovebox. Phosphorous-31 NMR spectra were collected for each of the solutions. The NMR tubes were placed in a 100 °C oil bath, and the reaction was periodically monitored by $^{31}$P NMR spectroscopy. After 24 hours, the $^{31}$P NMR signals disappeared and the reactions were cooled to room temperature and analyzed by GC / MS. The mass spectra indicated the presence of 4-*tert*-butylaniline (M/z = 149), and styrene dimers (M/z = 208).

### 2.3.7 Syntheses of Rhodium Diphosphine Anilido Complexes **5b**, **5g**, and **5i**.



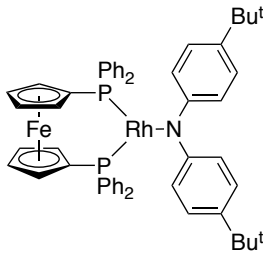

#### Synthesis of sodium bis(4-(*tert*-butyl)phenyl)amide.




N,N-(4-*tert*-butylphenyl)amine (1.0 g, 3.6 mmol, 1 equiv.) was weighed inside a glovebox in a 20 ml vial. Sodium hexamethyldisilylamide (NaHMDS; 0.72 g, 3.9 mmol, 1.1 equiv.) was weighed inside the glovebox in a separate 20 ml vial. The weighed NaHMDS was dissolved in 15 ml of toluene and transferred to the vial containing the weighed 4-*tert*-butylaniline. A magnetic stir bar was added to the vial. The vial was capped and the contents of the vial stirred overnight at room temperature inside the glovebox. A yellow-white precipitate formed. The solution was filtered through a glass frit inside the glovebox. The collected solid was washed with additional pentane, transferred to a tared 20 ml vial and dried under vacuum. The resulting solid was used as collected (1.04 g, 3.4 mmol, 96 % yield). $^1$H NMR: (500.2 MHz,THF-$d_8$) δ 6.41 (d, $J^{H-H}$ = 5 Hz, 4H), 6.31 (d, $J^{H-H}$ = 5 Hz, 4H), 0.69 (s, 18H) ppm.

$^{13}C\{^{1}H\}$ NMR: (125.7 MHz,THF-$d_8$) δ 156.76, 135.41, 126.29, 118.50 ppm.

## Synthesis of rhodium diphosphine diarylamido complex, **5b**.




**5b**

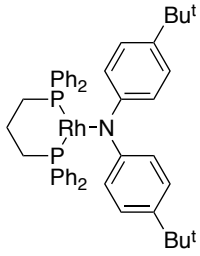
Rhodium diphosphine chloride complex, **1b**, was weighed inside a glovebox in a 20 ml vial (120 mg, 0.087 mmol, 1 equiv.). THF (3 ml) was added to the vial along with a magnetic stir bar. A solution of sodium N,N-(4-*tert*-butylphenyl)amide (56 mg, 0.175 mmol, 2.0 equiv.) in THF (3 ml) was prepared in a separate 3 ml vial and added to the rhodium diphosphine chloride complex by pipet. The vial was capped, and the reaction was stirred at room temperature overnight. An orange solution formed. The solvent was removed under vacuum. The resulting residue was dissolved in benzene and filtered through celite. The filtrate was collected and frozen. The frozen benzene was removed under vacuum to yield an orange solid (148 mg, 0.158 mmol, 91 % yield).

$^{1}H$ NMR: (499.7 MHz, THF-$d^8$) δ 7.56 (quartet, $J^{H-H}$ = 5 Hz, 8H), 7.24 (t, $J^{H-H}$ = , 4H), 7.15 (t, $J^{H-H}$ = , 8H), 6.70 (overlapping signals, 8H), 4.17 (s, 8HH), 1.08 (s, 18H) ppm.

$^{13}C\{^{1}H\}$ NMR: (125.7 MHz, THF-$d^8$) δ 148.2, 141.9, 138.9 (t, $J^{C-P}$ = 21 Hz), 135.0, 129.5, 128.1, 128.0, 116.0, 83.6 (t, $J^{C-P}$ = 32 Hz), 75.9, 72.1, 34.6, 31.9 ppm.

$^{31}P\{^{1}H\}$ NMR: (202.3 MHz, THF-$d^8$) δ 46.1 (d, $J^{P-Rh}$ = 224 Hz) ppm.

## Synthesis of rhodium diphosphine diarylamido complex, **5g**.




**5g**

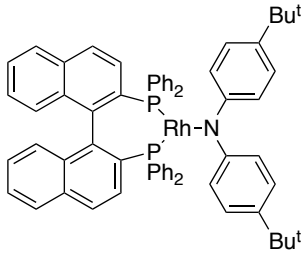
Rhodium diphosphine chloride complex, **1g**, was weighed inside a glovebox in a 20 ml vial (120 mg, 0.109 mmol, 1 equiv.). THF (3 ml) was added to the vial along with a magnetic stir bar. A solution of sodium N,N-(4-*tert*-butylphenyl)amide (73 mg, 0.229 mmol, 2.1 equiv.) in THF (3 ml) was prepared in a separate 3 ml vial and added to the rhodium diphosphine chloride complex by pipet. The vial was capped, and the reaction was stirred at room temperature overnight. An orange solution formed. The solvent was removed under vacuum. The resulting residue was dissolved in benzene and filtered through celite. The filtrate was collected and frozen. The frozen benzene was removed under vacuum to yield an orange solid (162 mg, 0.204 mmol, 93 % yield).

$^{1}H$ NMR: (499.92 MHz, THF-$d^8$) δ 7.53 (s, broad, 8H), 7.13 (s, broad, 12H), 6.75 (d, broad, J = 20 Hz, 8H), 2.13 (s, broad, 4H), 1.59 (s, broad, 2H), 1.14 (s, 18H) ppm.

$^{13}C\{^{1}H\}$ NMR: (125.7 MHz, THF-$d^8$) δ 147.5, 140.9, 138.4 (t, $J^{C-P}$ = 18 Hz),133.9, 129.5, 128.3, 128.0, 115.2, 34.5, 32.0, 30.7 (t, $J^{C-P}$ = 18 Hz), 20.8 ppm.

$^{31}P\{^{1}H\}$ NMR: (202.5 MHz, $C_6D_6$) δ 30.8 ($J^{P-Rh}$ = 203 Hz) ppm.

Synthesis of rhodium diphosphine diarylamido complex, **5i**.




**5i**

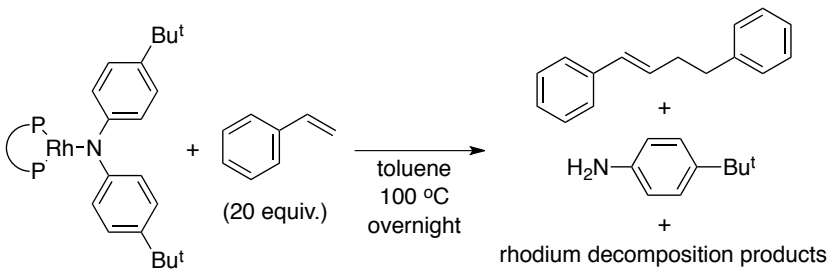
Rhodium diphosphine chloride complex, **1b**, was weighed inside a glovebox in a 20 ml vial (120 mg, 0.079 mmol, 1 equiv.). THF (3 ml) was added to the vial along with a magnetic stir bar. A solution of sodium N,N-(4-*tert*-butylphenyl)amide (53 mg, 0.166 mmol, 2.1 equiv.) in THF (3 ml) was prepared in a separate 3 ml vial and added to the rhodium diphosphine chloride complex by pipet. The vial was capped, and the reaction was stirred at room temperature overnight. An purple solution formed. The solvent was removed under vacuum. The resulting residue was dissolved in benzene and filtered through celite. The filtrate was collected and frozen. The frozen benzene was removed under vacuum to yield an purple solid (149 mg, 0.148 mmol, 94 % yield).

$^1$H NMR: (499.7 MHz, THF-$d^8$) δ 7.74 (m, broad, 4H), 7.47 (d, $J^{H-H}$ = 8 Hz, 2H), 7.46 (m, broad, 4H), 7.36 (d, $J^{H-H}$ = 8 Hz, 2H), 7.24 (m, 2H), 7.21 (overlapping signals, 8H), 6.95 (triplet of doublets, $J^{H-H}$ = 8 Hz, $J^{H-H}$ = 3 Hz, 2H), 6.61 (t, $J^{H-H}$ = 8 Hz, 8H), 6.52 (t, $J^{H-H}$ = 8 Hz, 4H), 6.46 (d, $J^{H-H}$ = 8 Hz, 4H), 1.26 (s, 18H) ppm.

$^{13}$C{$^1$H} NMR: (125.7 MHz, THF-$d^8$) δ 142.8,141.1, 138.0 (t, $J^{C-P}$ = 6 Hz), 137.5 (t, $J^{C-P}$ = 24 Hz), 136.3 (t, $J^{C-P}$ = 19 Hz), 135.7 (t, broad), 135.1 (t, broad),134.1 (t, broad), 134.1 (overlapping),131.5 ((t, $J^{C-P}$ = 21 Hz), 129.9, 129.0, 128.6, 128.6, 128.4, 128.3-128.2 (2 overlapping signals), 128.0 (t, broad), 126.6, 126.2, 113.9, 34.5, 31.8 ppm.

$^{31}$P{$^1$H} NMR: (202.2 MHz, THF-$d_8$) δ 49.3 (d, $J^{P-Rh}$ = 218 Hz) ppm.

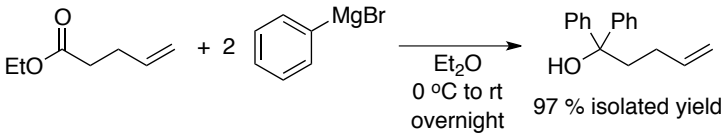
### 2.3.8 Reactions of Rhodium Diphosphine Diarylamido Complexes, **5b**, **5g**, and **5i** with Styrene.




**5b, 5g, 5i**

Rhodium anilido complexes **5b**, **5g**, and **5i** were weighed inside a glovebox in 3 ml vials (10 mg, 9.9 - 12.5 µmol, 1 equiv.). The complexes were dissolved in toluene (0.5 ml) and transferred to screw cap NMR tubes. Styrene (23 - 29 µL (0.906 g / ml), 0.199 - 0.251 mmol, 20 equiv.) was added by syringe. The tube was capped and removed from the glovebox. Phosphorous-31 NMR spectra were collected for each of the solutions. The NMR tubes were placed in a 100 °C oil bath, and the reaction was periodically monitored by $^{31}$P NMR spectroscopy. After 24 hours, the $^{31}$P NMR signals disappeared and the reactions were cooled to room temperature and analyzed by GC / MS. The mass spectra indicated the presence of 4-*tert*-butylaniline (M/z = 149), and styrene dimers (M/z = 208).

### 2.3.9 Synthesis of 1,1-diphenyl-4-penten-1-ol.[83]

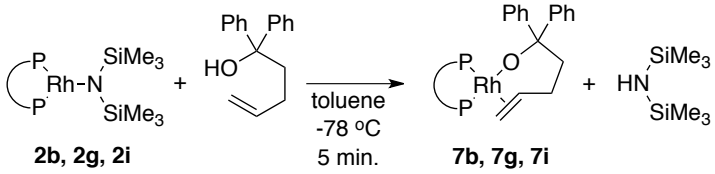



A 250 ml Schlenk flask, equipped with a magnetic stir bar, was connected to a Schlenk manifold by a rubber hose and purged of $O_2$ and moisture by successively applying vacuum and $N_2$. The flask was placed under an $N_2$ atmosphere and charged with 75 ml of dry $Et_2O$. Ethyl 4-pentenoate (11.2 ml, 10 g, 78 mmol, 1 equiv.) was added to the flask by syringe. The flask was placed in an ice bath, and a solution of phenylmagnesium bromide in $Et_2O$ (3 M, 57 ml, 172 mmol, 2.2 equiv.) was added slowly to the reaction flask by syringe. The reaction was stirred overnight. The ice bath was allowed to warm to room temperature. A saturated solution of sodium sulfate (35 ml) was added to the flask. The aqueous and organic phases were separated and the organic phase was washed with brine (3 x 75 ml). The organic phase was dried over anhydrous $MgSO_4$. The diethyl ether solvent was removed under a gentle vacuum (300 Torr). The colorless oil that was obtained was slowly solidified to a white solid (18 g, 76 mmol, 97 % yield). The product used without further purification. The $^1H$ NMR spectrum of the product showed no signs of byproducts.

$^1H$ NMR: (500.16 MHz, toluene-$d_8$) δ7.31 (d, $J^{H-H}$ = 7 Hz, 4H), 7.09 (t, $J^{H-H}$ = 7 Hz, 4H, overlaps with solvent), 7.00 (t, $J^{H-H}$ = 7 Hz, 4H, overlaps with solvent), 5.74 (ddt, $J^{H-H}$ = 17 Hz, $J^{H-H}$ = 10 Hz, $J^{H-H}$ = 7 Hz, 1H), 4.95 (m, 2H), 4.92 (m, 2H), 2.11 (m, 2H, overlaps with solvent), 1.99 (dd, $J^{H-H}$ =15 Hz, $J^{H-H}$ = 7 Hz, 2H) 1.42 (s, 1H) ppm.

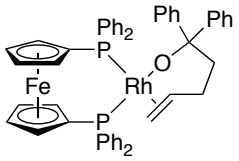
$^{13}C\{^1H\}$ NMR: (150.9 MHz, toluene-$d_8$) δ 147.3, 139.0, 128.1, 126.7, 126.3, 114.5, 77.4, 40.8, 28.4 ppm.

### 2.3.10 Syntheses of Rhodium Diphosphine Alkoxo Alkene Complexes **7b**, **7g**, and **7i**.




**2b, 2g, 2i** **7b, 7g, 7i**

#### Synthesis of rhodium diphosphine alkoxo alkene complex, **7b**.




**7b**

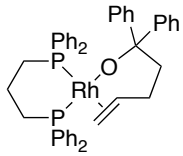
Rhodium diphosphine silylamido complex, **2b**, (14.8 mg, 0.018 mmol, 1 equiv.) was weighed inside a glovebox in a 3 ml vial. The weighed complex was dissolved in $d^8$-toluene (0.5 ml) and transferred to a screw cap NMR tube. 1,3,5-trimethoxybenzene (1.2 mg) was added to the NMR tube as an internal standard. The screw cap NMR tube was capped with a septum-bearing cap. 1,1-Diphenyl-4-penten-1-ol (4.3 mg, 0.018 mmol, 1

equiv.) was weighed inside the glovebox in a 3 ml vial and dissolved in 0.1 ml of $d^8$-toluene. The 1,1-diphenyl-4-penten-1-ol solution was loaded into a 250 µL syringe. The syringe was stoppered and both the syringe and the screw cap NMR tube were removed from the glovebox. The screw cap NMR tube was placed in a dry ice / acetone bath. An NMR probe was cooled to -50 °C. Initial $^1$H and $^{31}$P NMR spectra of the silylamido complex, **2b**, were collected at -50 °C. The NMR tube was ejected and placed in the dry ice / acetone bath. The 1,1-diphenyl-4-penten-1-ol solution was syringed into the NMR tube. The NMR tube was kept in the dry ice / acetone bath for 5 minutes and then shaken vigorously for 10 seconds before returning the sample to the dry ice acetone bath. This was repeated two more times. The dark green silylamido solution became bright orange. NMR spectra of orange solution were collected at -50 °C.

$^1$H NMR: (499.7 MHz, toludene-$d_8$) δ 8.23 (s, broad, 2H), 8.05-7.85 (overlapping signals, broad, 4H), 7.47-6.78 (overlapping signals, broad, 24H), 5.16 (s, broad, 1H), 4.55 (d, broad, J = 13 Hz, 1H), 4.24 (s, broad, 1H), 4.21 (s, broad, 1H), 3.96 (s, broad, overlapping signals, 2H), 3.74 (s, broad, 1H), 3.71 (s, broad, 1H), 3.60 (s, broad, 1H), 3.49 (s, broad, 1H), 3.31 (s, broad, 1H), 2.69 (m, broad, 2H), 2.25 (s, broad, 1H), 1.68 (s, broad, 1H) ppm.

$^{31}$P{$^1$H} NMR: (202.2 MHz, toluene-$d_8$) δ 51.43 (dd, $J^{P\text{-}Rh}$ = 151 Hz, $J^{P\text{-}P}$ = 47 Hz), 14.33 (dd, $J^{P\text{-}Rh}$ = 166 Hz, $J^{P\text{-}P}$ = 47 Hz) ppm.

### Synthesis of rhodium diphosphine alkoxo alkene complex, **7g**.



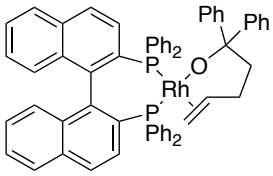

**7g**

Rhodium diphosphine silylamido complex, **2g**, (12.2 mg, 0.018 mmol, 1 equiv.) was weighed inside a glovebox in a 3 ml vial. The weighed complex was dissolved in $d^8$-toluene (0.5 ml) and transferred to a screw cap NMR tube. 1,3,5-trimethoxybenzene (1.2 mg) was added to the NMR tube as an internal standard. The screw cap NMR tube was capped with a septum-bearing cap. 1,1-Diphenyl-4-penten-1-ol (4.3 mg, 0.018 mmol, 1 equiv.) was weighed inside the glovebox in a 3 ml vial and dissolved in 0.1 ml of $d^8$-toluene. The 1,1-diphenyl-4-penten-1-ol solution was loaded into a 250 µL syringe. The syringe was stoppered and both the syringe and the screw cap NMR tube were removed from the glovebox. The screw cap NMR tube was placed in a dry ice / acetone bath. An NMR probe was cooled to -50 °C. Initial $^1$H and $^{31}$P NMR spectra of the silylamido complex, **2g**, were collected at -50 °C. The NMR tube was ejected and placed in the dry ice / acetone bath. The 1,1-diphenyl-4-penten-1-ol solution was syringed into the NMR tube. The NMR tube was kept in the dry ice / acetone bath for 5 minutes and then shaken vigorously for 10 seconds before returning the sample to the dry ice acetone bath. This was repeated two more times. The dark blue silylamido solution became bright orange. NMR spectra of orange solution were collected at -50 °C.

$^1$H NMR: (500.16 MHz, toluene-$d_8$) δ 7.87 (s, broad, 2H), 7.65 (s, broad, 2H), 7.34-6.72 (overlapping signals, broad, 26H), 4.81 (s, broad, 1H), 4.10 (s, broad, 1H), 3.54 (s, broad, 1H), 2.75 (s, broad, 2H), 2.53 (s, broad, 1H), 1.98 (s, broad, 2H), 1.85 (s, broad, 1H), 1.77 (s, broad, 1H), 1.54 (s, broad, 1H), 1.23 (s, broad, 2H) ppm.

$^{31}$P{$^1$H} NMR: (202.2 MHz, toluene-$d_8$) δ 34.94 (dd, $J^{P\text{-}Rh}$ = 140 Hz, $J^{P\text{-}P}$ = 61 Hz), 0.18 (dd, $J^{P\text{-}Rh}$ = 161 Hz, $J^{P\text{-}P}$ = 61 Hz) ppm.

Synthesis of rhodium diphosphine alkoxo alkene complex, **7i**.



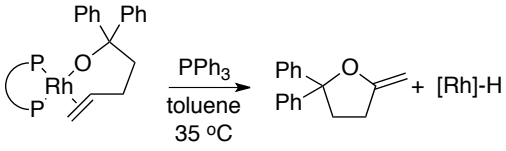

**7i**

Rhodium diphosphine silylamido complex, **2i**, (16.1 mg, 18.2 mmol, 1 equiv.) was weighed inside a glovebox in a 3 ml vial. The weighed complex was dissolved in $d^8$-toluene (0.5 ml) and transferred to a screw cap NMR tube. 1,3,5-trimethoxybenzene (1.2 mg) was added to the NMR tube as an internal standard. The screw cap NMR tube was capped with a septum-bearing cap. 1,1-Diphenyl-4-penten-1-ol (4.3 mg, 0.018 mmol, 1 equiv.) was weighed inside the glovebox in a 3 ml vial and dissolved in 0.1 ml of $d^8$-toluene. The 1,1-diphenyl-4-penten-1-ol solution was loaded into a 250 µL syringe. The syringe was stoppered and both the syringe and the screw cap NMR tube were removed from the glovebox. The screw cap NMR tube was placed in a dry ice / acetone bath. An NMR probe was cooled to -50 °C. Initial $^1$H and $^{31}$P NMR spectra of the silylamido complex, **2i**, were collected at -50 °C. The NMR tube was ejected and placed in the dry ice / acetone bath. The 1,1-diphenyl-4-penten-1-ol solution was syringed into the NMR tube. The NMR tube was kept in the dry ice / acetone bath for 5 minutes and then shaken vigorously for 10 seconds before returning the sample to the dry ice acetone bath. This was repeated two more times. The dark green silylamido solution became bright orange. NMR spectra of orange solution were collected at -50 °C.

$^1$H NMR: (499.4 MHz, THF-$d_8$) δ 8.00 (s, broad, 1H), 7.79 (s, broad, 2H), 7.73 (s, broad, 1H), 7.62-6.78 (overlapping signals, broad, 30H), 6.46 (s, broad, overlapping signals, 4H), 6.37 (s, broad, overlapping signals, 4H)4.37 (d, J =12 Hz, 1H), 4.14 (s, broad, 1H), 3.08 (s, broad, 1H), 2.94 (s, broad, 1H), 2.74 (s, broad, 1H), 1.91 (s, broad, 1H), 1.42 (s, broad, 1H) ppm.

$^{31}$P{$^1$H} NMR: (202.2 MHz, THF-$d_8$) δ 54.73 (dd, $J^{P\text{-}Rh}$ = 138 Hz, $J^{P\text{-}P}$ = 60 Hz), 22.12 (dd, $J^{P\text{-}Rh}$ = 165 Hz, $J^{P\text{-}P}$ = 60 Hz) ppm.

### 2.3.11 Reactions of Rhodium Diphosphine Alkoxo Alkene Complexes **7b**, **7g**, and **7i**.

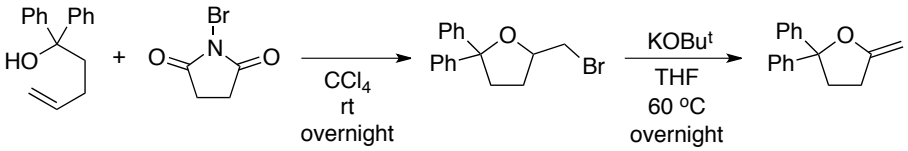


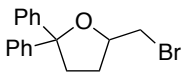

**7b, 7g, 7i**

Rhodium alkoxo alkene complexes **7b**, **7g**, and **7i**, were synthesized according to the procedures described above. The complexes were kept cold, inside screw cap NMR tubes placed in a dry ice / acetone bath. $PPh_3$ (10 equiv.) was weighed inside a glovebox in a 3 ml vial, dissolved in $d^8$-toluene (150 µL) and loaded into a 250 µL syringe. The syringe was stoppered and removed from the glovebox. The $PPh_3$ solution was added to the rhodium alkoxo alkene complex at -78 °C. The reagents were allowed to mix at -78 °C for 5 min., and then shaken vigorously for 10 seconds and returned to the dry ice / acetone bath. This was repeated two more times. The NMR probe was cooled to -50 °C. NMR spectra were collected at -50 °C. The spectra show no signs that $PPh_3$ coordinates to the metal.

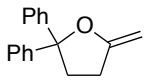
The NMR tube was ejected from the probe and returned to the dry ice / acetone bath. The NMR probe was warmed to 35 °C. The NMR tube was returned to the NMR probe, and a series of $^{1}$H NMR spectra were collected every two minutes for the next 8 hours or until the rhodium alkoxo alkene complex was completely consumed. The rates for alkene insertion were too fast at 35 °C for rhodium alkoxo alkene complex, **7i**, and rates were consequently measured at 0°C.

### 2.3.12 Independent Syntheses of 2.2-diphenyl-5-methylene-tetrahydrofuran.




2,2-Diphenyl-5-methylene-tetrahydrofuan was synthesized according to the procedures reported by Hartwig and co-workers.[80] A 20 ml vial, equipped with a magnetic stir bar, was charged with 1,1-diphenyl-4-penten-1-ol, $CCl_4$, and *N*-bromosuccinimide. The vial was capped and the resulting solution was stirred overnight at room temperature. Pentane was added to the product solution and the solution was filtered through celite. The filtrate was collected. NaOAc was added to the filtrate and the solvent was removed under vacuum. The resulting 2,2-diphenyl-5-bromomethyltetrahydrofuan was used without further purification.

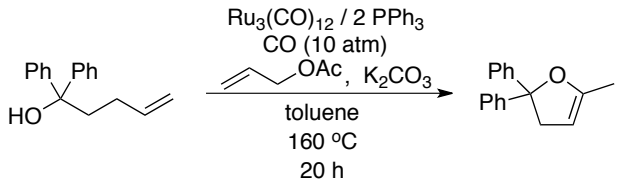



The crude 2,2-diphenyl-5-bromomethyltetrahydrofuan was transferred to a 20 ml vial inside a glovebox. The vial was equipped with a magnetic stir bar and then charged with dry THF and KO$^{t}$Bu. The vial was capped and removed from the glovebox. The reaction was heated to 60 °C overnight. The product solution was cooled to room temperature and concentrated under vacuum. The residual solid was extracted with pentane and filtered through celite. The filtrate was collected and concentrated under vacuum. The crude product was purified by column chromatography. A white solid was obtained. The product slowly decomposed at room temperature over the course of a year.

$^{1}$H NMR: (499.7 MHz, $C_6D_5$) δ 7.40 (d, $J^{H-H}$ = 7 Hz, 4H), 7.08 (t, $J^{H-H}$ = 7 Hz, 4H), 6.99 (d, $J^{H-H}$ = 7 Hz, 2H), 4.72 (s, 1H), 3.98 (s, 1H), 2.23 (s, 4H) ppm.

$^{13}$C{$^{1}$H} NMR: (125.6 MHz, $CDCl_3$) δ 162.13, 144.89, 128.44, 127.35, 125.97, 90.83, 80.25, 38.00, 29.10 ppm.

### 2.3.13 Independent Syntheses of 5-methyl-2,2-diphenyl-2,3-dihydrofuran.

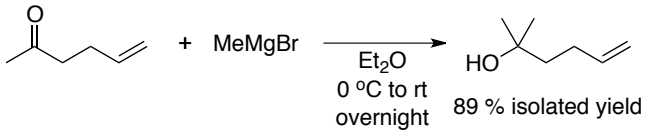



5-Methyl-2,2-diphenyl-2,3-dihydrofuran was synthesized according to the procedures reported by Mitsudo and co-workers.[84] A steel Parr bomb, equipped with a magnetic stir bar, was charged with $Ru_3(CO)_{12}$, $PPh_3$, allyl acetate, $K_2CO_3$, 1,1-diphenyl-4-penten-1-ol, and toluene inside a nitrogen-filled glovebox. The bomb was sealed and removed from the box. The bomb was then charged with CO and heated to 160 °C for 20 hours. The bomb was opened and the product solution washed with brine and purified by column chromatography.

$^1$H NMR: (499.7 MHz, $CDCl_3$) δ 7.52 (d, $J^{H-H}$ = 8 Hz, 4H), 7.39 (t, $J^{H-H}$ = 8 Hz, 4H), 7.31 (d, $J^{H-H}$ = 8 Hz, 2H), 4.66 (s, 1H), 3.41 (s, 2H), 2.02 (s, 3H) ppm.

$^{13}$C{$^1$H} NMR: (125.6 MHz, $CDCl_3$) δ 153.37, 146.54,128.08, 126.95, 125.75, 93.92, 90.66, 45.00, 13.76 ppm.

### 2.3.14 Synthesis of 2-methyl-5-hexen-2-ol. [83b,85]

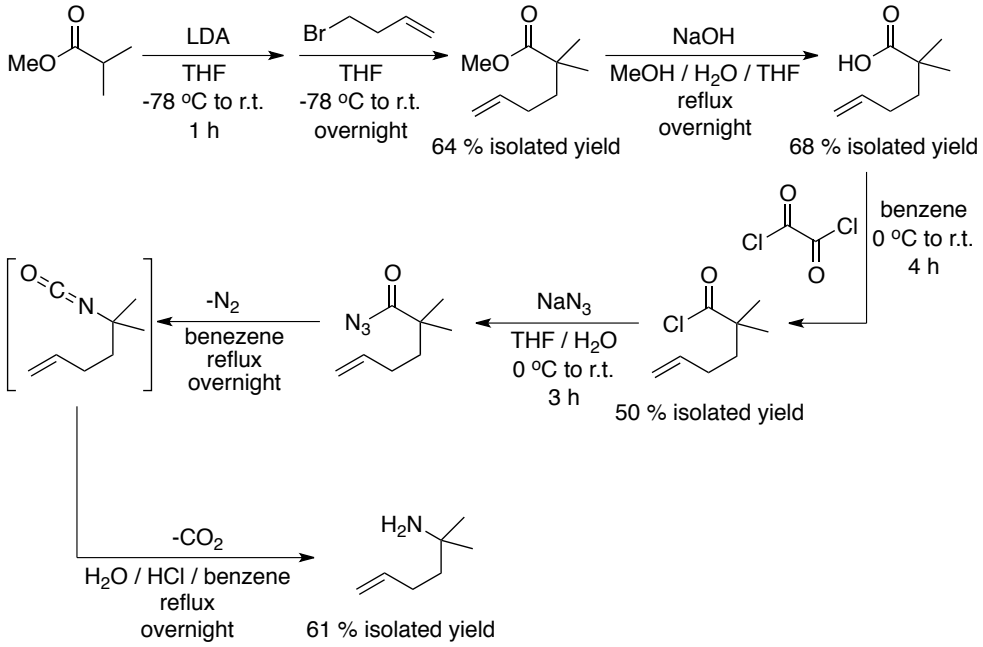



A 250 ml Schlenk flask, equipped with a magnetic stir bar, was connected to a Schlenk manifold by a rubber hose and purged of $O_2$ and moisture by successively applying vacuum and $N_2$. The flask was placed under an $N_2$ atmosphere and charged with 75 ml of dry $Et_2O$. 5-Hexen-2-one (30 ml, 25 g, 255 mmol, 1 equiv.) was added to the flask by syringe. The flask was placed in an ice bath, and a solution of methylmagnesium bromide in $Et_2O$ (3 M, 93 ml, 280 mmol, 1.1 equiv.) was added slowly to the reaction flask by syringe. The reaction was stirred overnight. The ice bath was allowed to warm to room temperature. A saturated solution of sodium sulfate (35 ml) was added to the flask. The aqueous and organic phases were separated and the organic phase was washed with brine (3 x 75 ml). The organic phase was dried over anhydrous $MgSO_4$. The diethyl ether solvent was removed under a gentle vacuum (300 Torr). The colorless oil that was obtained was used without further purification (26 g, 228 mmol, 89 % yield). The $^1$H NMR spectrum of the product showed no signs of byproducts.

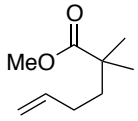
$^1$H NMR: (499.7 MHz, $CDCl_3$) δ 5.78 (ddt, $J^{H-H}$ = 17 Hz, $J^{H-H}$ = 10 Hz, $J^{H-H}$ = 7 Hz, 1H), 4.97 (ddd, $J^{H-H}$ = 17 Hz, $J^{H-H}$ = 4 Hz, $J^{H-H}$ = 2 Hz, 1H), 4.88 (ddt, $J^{H-H}$ = 10 Hz, $J^{H-H}$ = 2 Hz, $J^{H-H}$ = 1 Hz, 1H), 2.07 (m, 2H), 1.95 (s, 1H), 1.50 (m, 2H), 1.15 (s, 6H) ppm.

$^{13}$C{$^1$H} NMR: (125.7 MHz, $CDCl_3$) δ 139.22, 114.48, 71.01, 42.98, 29.39, 28.97 ppm.

### 2.3.15 Synthesis of 2-methyl-5-hexen-1-amine



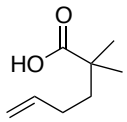

### Synthesis of methyl 2,2-dimethyl-5-hexenoate.[86]



A 1 L three-neck round bottom flask was equipped with a magnetic stir bar, two rubber septa, and a ground glass joint-to-barb flow control adaptor (has a glass stopcock). The flask was connected to a Schlenk manifold through a rubber hose and purged with dry $N_2$. Dry THF (50 ml) and diisopropylamine (62.8 ml, 45 g, 0.444 mol, 1.2 equiv.) were charged to the flask. The flask was placed in a dry ice / acetone bath, and a solution of *n*-BuLi in hexanes (1.6 M, 255 ml, 0.408 mol, 1.1 equiv.) was added slowly to the solution of diisopropylamine in THF. The ensuing reaction was stirred at -78 °C for 1 hour and then at 0 °C for 1 hour. The flask was then cooled to -78 °C and a solution of methyl isobutyrate (50.9 ml, 45.3 g, 0.444 mol, 1.2 equiv.) in dry $Et_2O$ (50 ml) was added. The following reaction was stirred at -78 °C for 20 minutes. A solution of 4-bromo-1-butene (50 g, 0.370 mol, 1 equiv.) in HMPA (100 ml) was added to the reaction by cannula transfer. The ensuing reaction was stirred overnight, during which time the dry ice acetone bath was allowed to warm to room temperature. The product mixture was cooled to 0 °C in an ice bath. An aqueous solution of HCl (1 N, 240 ml) was added to product mixture at 0 °C. The mixture was extracted with $Et_2O$ (3 x 300 ml). The organic extracts were combined, washed with water and aqueous $NaHCO_3$ (2 x 160 ml), dried over anhydrous $MgSO_4$, and concentrated by rotary evaporation. The crude product was distilled under vacuum to afford methyl 2,2-dimethyl-5-hexenoate, as a colorless oil (37.0 g, 0.237 mol, 64 % yield).

$^1$H NMR: (399.9 MHz, $CDCl_3$) δ 5.67 (ddt, $J^{H-H}$ = 17 Hz, $J^{H-H}$ = 10 Hz, $J^{H-H}$ = 7 Hz, 1H), 5.02 (d, broad, $J^{H-H}$ = 17 Hz, 1H), 4.89 (ddd, $J^{H-H}$ = 17 Hz, $J^{H-H}$ = 3 Hz, $J^{H-H}$ = 2 Hz, 1H), 4.82 (m = 2 Hz, 1H), 3.55 (s, 3H), 1.88 (m, 2H), 1.52 (m, 2H), 1.08 (s, 6H) ppm.

### Synthesis of 2,2-Dimethyl-5-hexenoic acid.[86]

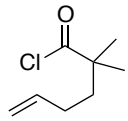


A 1 L Erlenmeyer flask was charged with methyl 2,2-dimethyl-5-hexenoate (37.0 g, 0.237 mol, 1 equiv.), THF (100 ml), water (150 ml), methanol (250 ml), and KOH (132 g, 2.37 mol, 10 equiv.). The resulting solution was stirred overnight at room temperature. The product mixture was treated with ice and concentrated HCl (150 ml). The acidified solution was extracted with $Et_2O$ (4 x 300 ml). The organic extracts were combined, washed with brine (240 ml), dried over anhydrous $MgSO_4$ and concentrated by rotary evaporation. The crude product was distilled under vacuum to afford 2,2-dimethyl-5-hexenoic acid as a colorless oil (23.0 g, 0.162 mol, 68 % yield).

$^1$H NMR: (499.4 MHz, $CDCl_3$) δ 5.79 (m, 1H), 5.02 (d, broad, $J^{H-H}$ = 17 Hz, 1H), 4.94 (d, broad, $J^{H-H}$ = 10 Hz, 1H), 2.05 (dd, $J^{H-H}$ = 16 Hz, $J^{H-H}$ = 7 Hz, 2H), 1.64 (dd, $J^{H-H}$ = 10 Hz, $J^{H-H}$ = 7 Hz, 2H), 1.21 (s, 6H) ppm.

$^{13}$C{$^1$H} NMR: (125.7 MHz, $CDCl_3$) δ 184.90, 138.27, 114.57, 41.96, 39.50, 29.21, 24.89 ppm.

### Synthesis of 2,2-dimethyl-5-hexenoyl chloride.[87]

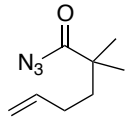


A 250 ml Schlenk flask, equipped with a magnetic stir bar, was charged with 2,2-dimethyl-5-hexenoic acid (23.0 g, 0.162 mol, 1 equiv.), and dry benzene (60 ml). The flask was connected to a $N_2$ line, and subsequently placed in an ice bath. Oxalyl chloride (41.1 g, 0.324 mol, 2 equiv.) was added drop-wise to the reaction solution at 0 °C. The resulting mixture was then warmed to room temperature and stirred for an additional 3 hours. Evaporation of the solvent under vacuum yielded a colorless oil (12.9 g, 0.080 mol, 50 % yield). The product was used without further purification.

$^1$H NMR: (399.7 MHz, toluene-$d_8$) δ 5.58 (ddt, $J^{H-H}$ = 17 Hz, $J^{H-H}$ = 10 Hz, $J^{H-H}$ = 7 Hz, 1H), 4.93 (m, 1H), 4.89 (m, 1H), 1.79 (ddd, $J^{H-H}$ = 9 Hz, $J^{H-H}$ = 8 Hz, $J^{H-H}$ = 7 Hz, 1H), 1.42 (m, 2H), 0.92 (s, 6H) ppm.

$^{13}$C{$^1$H} NMR: (125.7 MHz, toluene-$d_8$) δ 179.64, 138.03, 115.55, 52.94, 39.88, 29.56, 25.22 ppm.

### Synthesis of 2,2-Dimethyl-5-hexenoyl azide.[88]

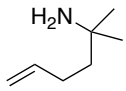


A 250 ml round bottom flask was charged with sodium azide (52.2 g, 0.803 mol, 12.4 equiv.) and water (100 ml). The flask was cooled to 0 °C, and a solution of 2,2-dimethyl-5-hexenoyl chloride (12.9 g, 0.080 mol, 1 equiv.) in dry THF was added drop-wise the reaction mixture. The resulting solution was stirred at 0 °C for 1 hour. The reaction was then diluted with ice water and extracted with $Et_2O$. The organic extracts were combined, dried over $MgSO_4$, and concentrated by rotary evaporation to a colorless oil. The product was carried on without further purification.

$^1$H NMR: (399.7 MHz, $CDCl_3$) δ 5.69 (m, 1H), 4.90 (m, 1H), 4.83 (m, 1H), 1.89 (m, 2H), 1.52 (m, 2H), 1.08 (s, 6H) ppm.

$^{13}$C{$^1$H} NMR: (125.6 MHz, $CDCl_3$) δ 177.90, 138.31, 114.29, 60.12, 39.70, 29.24, 24.99 ppm.

Synthesis of 2-Methyl-5-hexen-2-amine.[89]

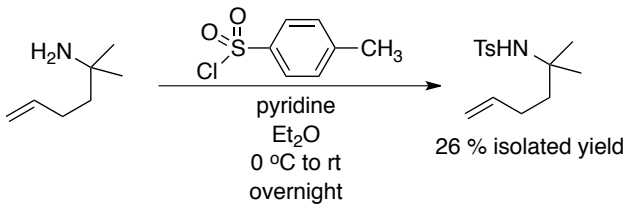


A 250 ml round bottom flask, equipped with a magnetic stir bar and a reflux condenser, was charged with dimethyl-5-hexenoic acid azide and benzene (100) ml. The solution was refluxed for 24 hours. Dilute HCl (10 % 50 ml) was added to the reaction and the mixture was refluxed again for 24 hours. The reaction mixture was cooled to room temperature. The solution was poured into a separatory funnel. The aqueous layer was removed from the organic layer. The organic layer was extracted with dilute HCl (5 %, 3 x 100 ml). The acidic extracts were combined and basified with $K_2CO_3$. The basic solution was extracted with $CH_2Cl_2$. The organic extracts were combined, dried over $MgSO_4$, and concentrated. The resulting product was distilled under vacuum to yield 2-methyl-5-hexen-2-amine (5.6 g, 0.049 mol, 62 % yield).

$^1$H NMR: (499.4 MHz, $CDCl_3$) δ 5.74 (ddt, $J^{H-H}$ = 17 Hz, $J^{H-H}$ = 10 Hz, $J^{H-H}$ = 7 Hz, 1H), 4.93 (d, broad, $J^{H-H}$ = 17 Hz, 1H), 4.84 (d, broad, $J^{H-H}$ = 10 Hz, 1H), 4.70 (s, 2H), 1.99 (dd, $J^{H-H}$ = 17 Hz, $J^{H-H}$ = 16 Hz, $J^{H-H}$ = 7 Hz, 2H), 1.52, 2H), 1.35 (m, 2H), 1.01 (s, 6H) ppm.

$^{13}$C{$^1$H} NMR: (125.6 MHz, $CDCl_3$) δ 139.25, 114.30, 49.55, 44.23, 30.42, 29.16 ppm.

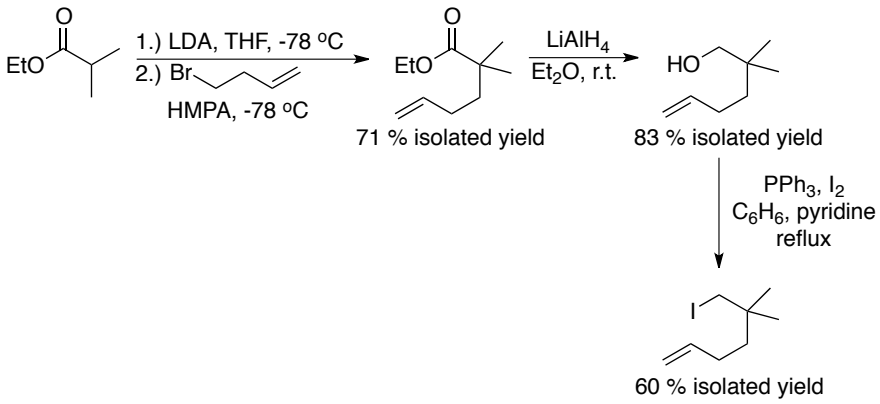
### 2.3.16 Synthesis of *N*-tosyl-2-methyl-5-hexen-1-amine.



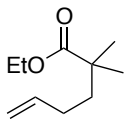

A 250 ml Schlenk flask, equipped with a magnetic stir bar, was charged with 2-methyl-5-hexen-1-amine (5.6 g, 0.049 mol, 1 equiv.) and pyridine (80 ml). The Schlenk flask was stoppered with a rubber septum and then connected to an $N_2$ line. The flask was placed in an ice bath. *p*-Toluenesulfonlyl chloride (18.9 g, 0.099 mol, 2 equiv.) was added slowly to the reaction. The reaction was stirred overnight at 0 °C. The reaction mixture was then poured into a 500 ml Erlenmeyer flask containing ice water (100 ml). The mixture was extracted with $CH_2Cl_2$ (3 x 100 ml). The organic extracts were combined, dried over $MgSO_4$, and concentrated under vacuum to yield a white solid (3.5 g, 0.013 mol, 26 % yield).

$^1$H NMR: (500 MHz, $CDCl_3$) δ 7.76 (d, J = 8 Hz, 2H), 7.27 (d, J = 8 Hz, 2H), 5.72 (ddt, J = 16.8 Hz, J = 10.2 Hz, J = 6.5 Hz, 1H), 4.97 (m, 1H), 4.93 (m, 1H), 4.46 (s, 1H), 2.42 (s, 3H), 2.03 (dddd, J = 9 Hz, J = 5 Hz, J = 3 Hz, J = 1 Hz, 2H), 1.57 (m, 2H) ppm.

### 2.3.17 Synthesis of 2,2-dimethyl-1-iodo-5-hexene.

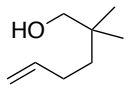



#### Synthesis of ethyl 2,2-dimethyl-5-hexenoate.[90]



A 250 ml Schlenk flask was equipped with a magnetic stir bar and a rubber septum. The flask was connected to a Schlenk manifold through a rubber hose and purged with dry $N_2$. Dry THF (30 ml) and diisopropylamine (14.1 ml, 10.1 g, 0.100 mol, 1 equiv.) were charged to the flask. The flask was placed in a dry ice / acetone bath, and a solution of *n*-BuLi in hexanes (1.6 M, 62.5 ml, 0.1.00 mol, 1 equiv.) was added slowly to the diisopropylamine solution by syringe. The ensuing reaction was stirred at -78 °C for 1 hour, and then at 0 °C for 1 hour. The flask was cooled to -78 °C and a solution of ethyl isobutyrate (13.4 ml, 11.6 g, 0.100 mol, 1 equiv.) in dry $Et_2O$ (30 ml) was added. The following reaction was stirred at -78 °C for 20 minutes. A solution of 4-bromo-1-butene (10.3 ml, 13.5 g, 0.100 mol, 1 equiv.) in HMPA (25 ml) was added to the reaction by cannula transfer. The ensuing reaction was stirred overnight, during which time the dry ice acetone bath was allowed to warm to room temperature. The product mixture was cooled to 0 °C in an ice bath. An aqueous solution of HCl (2 N, 100 ml) was added to product mixture at 0 °C. The mixture was extracted with $Et_2O$ (3 x 300 ml). The organic extracts were combined, washed with water and aqueous $NaHCO_3$ (2 x 160 ml), dried over anhydrous $MgSO_4$, and concentrated by rotary evaporation. The crude product was distilled under vacuum to afford ethyl 2,2-dimethyl-5-hexenoate, as a colorless oil (12.1 g, 0.071 mol, 71 % yield).

#### Synthesis of 2,2-dimethyl-5-hexen-1-ol.[90b,c]

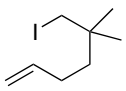


Lithium aluminum hydride ($LiAlH_4$, 8.1 g, 0.213 mol, 3 equiv.) was weighed inside a nitrogen-filled glovebox and transferred, as a solid, to a 500 ml three-neck round bottom flask, equipped with a magnetic stir bar. Dry $Et_2O$ (100 ml) was added to the flask, and the flask was fitted with two rubber septa and a ground glass joint-to-barb flow control adaptor (has a glass stopcock). The three-neck flask was then removed from the glovebox and connected to a Schlenk manifold by a rubber hose. The hose was purged three times by successively applying vacuum and $N_2$, and then the flow control adaptor on the three-neck flask was opened to the $N_2$. The flask was placed in a dry ice /acetone bath. A solution of ethyl 2,2-dimethyl-5-hexenoate (12.1 g, 0.071 mol, 1 equiv.) in dry $Et_2O$ (20 ml) was added slowly to the $LiAlH_4$ solution at -78 °C. The ensuing

reaction was allowed to stir overnight. The dry ice / acetone was allowed to warm to room temperature. The flask was then placed in an ice bath. The reaction was quenched slowly by the sequential additions of water (8.1 ml), aqueous NaOH (3 N, 8.1 ml), and water (8.1 ml). The resulting mixture was stirred at room temperature for another 2 hours until the solid in the flask was completely white. The product solution was filtered through Whatman paper on a Buchner funnel, and the collected white solid was washed with additional $Et_2O$ (3 x 100 ml). The organic extracts were dried over $MgSO_4$ and concentrated by rotary evaporation. The crude product was distilled under vacuum to yield a colorless oil, 2,2-dimethyl-5-hexen-1-ol (7.6 g, 0.059 mol, 83 % yield).

$^1$H NMR: (499.7 MHz, $CDCl_3$) δ 5.81 (ddt, $J^{H-H}$ = 17 Hz, $J^{H-H}$ = 10 Hz, $J^{H-H}$ = 7 Hz, 1H), 5.00 (d, broad, $J^{H-H}$ = 17 Hz, 1H), 4.91 (d, broad, $J^{H-H}$ = 10 Hz, 1H), 3.30 (s, 2H), 2.00 (m, 2H), 1.95 (s, 1H), 1.87 (s, broad, 1H), 1.31 (m, 2H), 0.86 (s, 6H) ppm.

### Synthesis of 2,2-dimethyl-6-iodo-5-hexene.[90b,c,91]

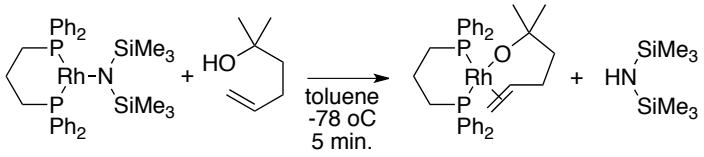


A 250 ml three neck round bottom flask, equipped with a magnetic stir bar, a reflux condenser, a ground glass joint-to-barb flow control adaptor (has a glass stopcock) and two rubber septa, was placed under a $N_2$ atmosphere. The flask was then charged with $PPh_3$ (2.2 g, 8.39 mmol, 1), dry benzene (125 ml), $I_2$ (1.8 g, 7.09 mmol, 1.01 equiv.), and dry pyridine (7 ml). The resulting mixture was stirred at room temperature for 1 hour. An orange solid precipitated. The flask was charged with a solution of 2,2-dimethyl-5-hexen-1-ol (0.9 g, 7.02 mmol, 1 equiv.) in benzene (25 ml), and the resulting mixture was heated to reflux overnight. The progress of the reaction was monitored by GC/MS. Upon completion, the reaction was cooled to room temperature and treated with a saturated sodium thiosulfate solution (100 ml). The aqueous and organic layers were separated, and the aqueous fraction was extracted with $Et_2O$ (3 x 100 ml). The combined organic solutions were dried over anhydrous $MgSO_4$ and concentrated by rotary evaporation. The crude product was distilled. 2,2-Dimethyl-1-iodo-5-hexene was obtained as a colorless oil (1.0 g, 4.20 mmol, 60 % yield).

$^1$H NMR: (499.7 MHz, $CDCl_3$) δ 5.81 (ddtd, $J^{H-H}$ = 10 Hz, $J^{H-H}$ = 8 Hz, $J^{H-H}$ = 7 Hz, $J^{H-H}$ = 1 Hz, 1H), 5.02 (ddd, $J^{H-H}$ = 3 Hz, $J^{H-H}$ = 2 Hz, $J^{H-H}$ = 7 Hz, 1H), 4.94 (ddd, $J^{H-H}$ = 10 Hz, $J^{H-H}$ = 2 Hz, $J^{H-H}$ = 1 Hz, 1H), 3.15, (s, 2H), 1.99 (m, 2H), 1.42 (m, 2H), 1.03 (s, 6H) ppm.

$^{13}$C{$^1$H} NMR: (125.6 MHz, $CDCl_3$) δ 138.75, 114.56, 40.23, 33.51, 28.86, 26.83, 24.18 ppm.

### 2.3.18 Synthesis of Rhodium Diphosphine Alkoxo Alkene Complex **8g**.



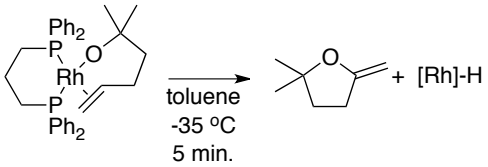

**2g** **8g**

Rhodium diphosphine silylamido complex, **2g**, (12.2 mg, 0.018 mmol, 1 equiv.) was weighed inside a glovebox in a 3 ml vial. The weighed complex was dissolved in $d^8$-toluene (0.5 ml) and transferred to a screw cap NMR tube. 1,3,5-trimethoxybenzene (1.2 mg) was added to the NMR tube as an internal standard. The screw cap NMR tube was capped with a septum-bearing cap. 2-methyl-5-hexen-2-ol (2.1 mg, 18.4 mmol, 1 equiv.) was weighed inside

the glovebox in a 3 ml vial and dissolved in 0.1 ml of $d^8$-toluene. The 1,1-diphenyl-4-penten-1-ol solution was loaded into a 250 µL syringe. The syringe was stoppered and both the syringe and the screw cap NMR tube were removed from the glovebox. The screw cap NMR tube was placed in a dry ice / acetone bath. An NMR probe was cooled to -50 °C. NMR spectra ($^1$H and $^{31}$P) of the silylamido complex, **2g**, were collected at -50 °C. The NMR tube was ejected and placed in the dry ice / acetone bath. The 2-methyl-5-hexen-2-ol solution was syringed into the NMR tube. The NMR tube was kept in the dry ice / acetone bath for 5 minutes and then shaken vigorously for 10 seconds before returning the sample to the dry ice acetone bath. This was repeated two more times. The dark green silylamido solution became bright orange. NMR spectra of orange solution were collected at -50 °C.

$^{31}$P{$^1$H} NMR: (202.2 MHz, toluene-$d_8$) δ 35.9 (dd, $J^{P\text{-}Rh}$ = 140 Hz, $J^{P\text{-}P}$ = 56 Hz), 1.0 (dd, $J^{P\text{-}Rh}$ = 163 Hz, $J^{P\text{-}P}$ = 56 Hz) ppm.

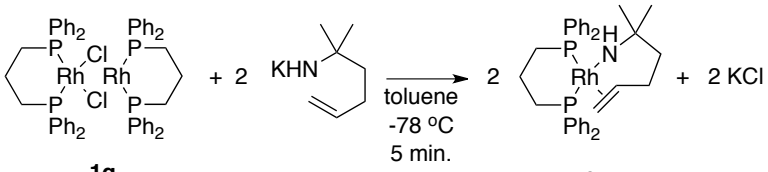
### 2.3.19 Reactions of Rhodium Diphosphine Alkoxo Alkene Complex, **8g**.




**8g**

Rhodium alkoxo alkene complexes **8g**, was synthesized according to the procedures described above and allowed to react at -35 °C in the absence of $PPh_3$. The reaction was monitored by $^1$H NMR spectroscopy.

### 2.3.20 Synthesis of Rhodium Diphosphine Amido Alkene Complex **9g**.



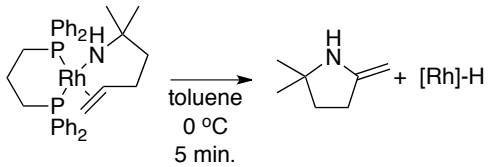

**1g** **9g**

Rhodium diphosphine chloride complex, **1g**, was weighed inside a glovebox in a 3 ml vial (10 mg, 9.1 mmol, 1 equiv.). The weighed complex was dissolved in $d^8$-toluene (0.5 ml) and transferred to a screw-cap NMR tube. 1,3,5-trimethoxybenzene (1.2 mg) was added to the NMR tube as an internal standard. The NMR tube was capped with a septum-bearing cap. 2-Methyl-5-hexene-2-amine (1 mg, 8.8 mol, 1 equiv.) was weighed inside the box in a 3 ml vial and dissolved in 0.1 ml of $d^8$-toluene. The solution was transferred to a 3 ml vial containing 0.4 mg of KH (1.0 mmol, 1.1 equiv.) The reagents were mixed with a 250 µL syringe and then loaded into the syringe. The syringe was stoppered. Both the syringe and the NMR tube were removed from the glovebox. The NMR tube was placed in a dry ice / acetone bath. An NMR probe was cooled to -50 °C. NMR spectra of the rhodium diphosphine chloride solution were collected at -50 °C. The sample was ejected and returned to the dry ice / acetone bath. The potassium 2-methyl-5-hexen-2-amide solution was syringed into the NMR tube through the septum. The reagents were allowed to mix at -78 °C for 5 min. The NMR tube was then shaken vigorously for 10 seconds to mix the

reagents further. This sequence of steps was repeated two more times. The NMR tube was returned to the NMR probe. A second set of NMR spectra were collected at -50 °C.

$^{31}P\{^{1}H\}$ NMR: (202.2 MHz, toluene-$d_8$) δ 38.9 (dd, $J^{P\text{-}Rh}$ = 136 Hz, $J^{P\text{-}P}$ = 50 Hz), 1.0 (dd, $J^{P\text{-}Rh}$ = 127 Hz, $J^{P\text{-}P}$ = 50 Hz) ppm.

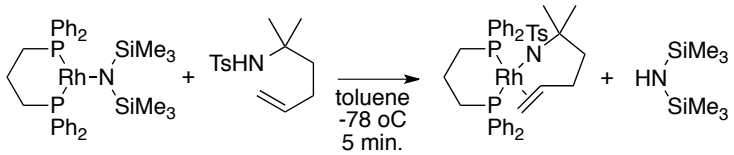
### 2.3.21 Reactions of Rhodium Diphosphine Alkoxo Alkene Complex, **9g**.




**9g**

Rhodium amido alkene complexes **9g**, was prepared in situ by the addition of potassium 2-methyl-5-hexenyl-2-amide to rhodium diphosphine chloride complex, **1g**. The resulting complex was allowed to react at 0 °C in the absence of $PPh_3$. The reaction was monitored by $^{1}H$ NMR spectroscopy.

### 2.3.22 Synthesis of Rhodium Diphosphine Tosylamido Alkene Complex, **10g**.

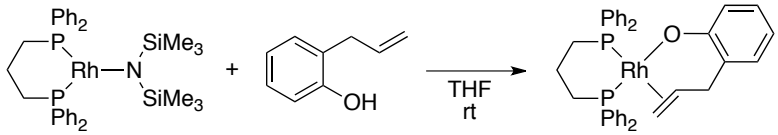



**2g** **10g**

Rhodium diphosphine tosylamido alkene complex, **10g**, was synthesized by the addition of *N*-tosyl-2-methyl-5-hexen-2-amine to rhodium diphosphine silylamido complex, **2g**. The reaction was performed at -78 °C inside a screw cap NMR tube.

$^{31}P\{^{1}H\}$ NMR: (162 MHz, toluene-$d_8$) δ 37.9 (d, broad, $J^{P\text{-}Rh}$ = 144 Hz), 3.5 (d, $J^{P\text{-}Rh}$ = 149 Hz) ppm.

### 2.3.23 Synthesis of Rhodium Diphosphine Phenoxo Alkene Complex, **11g**.




**2g** **11g**

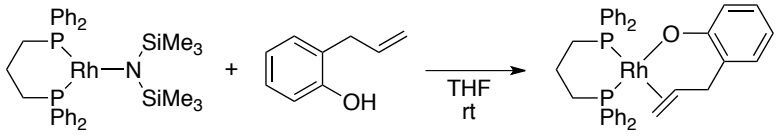
Rhodium diphosphine silylamido complex, **2g**, (80 mg, 0.118 mmol, 1 equiv.) was weighed inside a glovebox in a 20 ml vial. 2-Allylphenol (16 mg, 0.119 mmol, 1 equiv.) weighed inside a glovebox in a 3 ml vial. The weighed silylamido complex was dissolved in 3 ml of THF. The weighed 2-allylphenol was dissolved in 2 ml of THF. The THF solution of 2-allylphenol was transferred to the vial containing the silylamido complex. The reagents were mixed together with a pipette. The dark blue solution became yellow. A magnetic stir bar was added to the vial. The solvent was removed under vacuum. The residual solid was dissolved in a small amount of THF (~ 1ml) and pentane was added to the concentrated solution to precipitate the 2-allyl phenoxo complex as a yellow solid. The

product solution was filtered through a glass frit. The yellow solid was collected, transferred to a tared 20 ml vial, and dried under vacuum (60 mg, 0.093 mmol, 78 % yield).

$^{1}$H NMR: (500.16 MHz, toluene-$d_8$) δ 7.97 (m, 2H), 7.81 (m, 2H), 7.42 (m, 2H), 7.35 (m, 2H), 7.21 (m, 1H), 7.18-6.909 (overlapping signals, m, 13H), 6.83 (dd, J = 8Hz, J = 1 Hz, 1H), 6.64 (triplet of doublets, J = 7 Hz, J = 1 Hz, ), 4.42 (s, broad, 1H), 4.05 (d. J = 18 Hz, 1H), 3.51 (d, J = 14 Hz, 1H), 3.31 (s, broad, 1H), 2.94 (d, J = 18 Hz, 1H), 1.91 (m, broad, 4H), 1.50 (s, broad, 2H).

$^{31}$P{$^{1}$H} NMR: (162 MHz, toluene-$d_8$) δ 40.06 (dd, $J^{P\text{-}Rh}$ = 153 Hz, $J^{P\text{-}P}$ = 59 Hz), 4.37 (dd, $J^{P\text{-}Rh}$ = 161 Hz, $J^{P\text{-}P}$ = 60 Hz)

### 2.3.24 Synthesis of Rhodium Diphosphine Phenoxo Alkene Complex, **11g**.



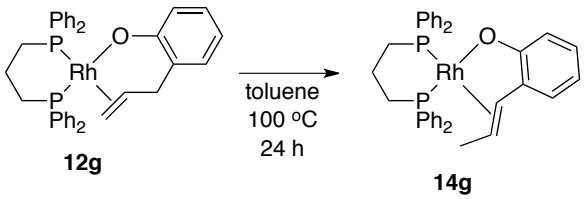

**12g**

Rhodium diphosphine silylamido complex, **2g**, (80 mg, 0.118 mmol, 1 equiv.) was weighed inside a glovebox in a 20 ml vial. 2-Allylphenol (16 mg, 0.119 mmol, 1 equiv.) weighed inside a glovebox in a 3 ml vial. The weighed silylamido complex was dissolved in 3 ml of THF. The weighed 2-allylphenol was dissolved in 2 ml of THF. The THF solution of 2-allylphenol was transferred to the vial containing the silylamido complex. The reagents were mixed together with a pipette. The dark blue solution became yellow. A magnetic stir bar was added to the vial. The solvent was removed under vacuum. The residual solid was dissolved in a small amount of THF (~ 1ml) and pentane was added to the concentrated solution to precipitate the 2-allyl phenoxo complex as a yellow solid. The product solution was filtered through a glass frit. The yellow solid was collected, transferred to a tared 20 ml vial, and dried under vacuum (60 mg, 0.093 mmol, 78 % yield).

$^{1}$H NMR: (500.16 MHz, toluene-$d_8$) δ 7.97 (m, 2H), 7.81 (m, 2H), 7.42 (m, 2H), 7.35 (m, 2H), 7.21 (m, 1H), 7.18-6.909 (overlapping signals, m, 13H), 6.83 (dd, J = 8Hz, J = 1 Hz, 1H), 6.64 (triplet of doublets, J = 7 Hz, J = 1 Hz, ), 4.42 (s, broad, 1H), 4.05 (d. J = 18 Hz, 1H), 3.51 (d, J = 14 Hz, 1H), 3.31 (s, broad, 1H), 2.94 (d, J = 18 Hz, 1H), 1.91 (m, broad, 4H), 1.50 (s, broad, 2H) ppm.

$^{31}$P{$^{1}$H} NMR: (162 MHz, toluene-$d_8$) δ 40.06 (dd, $J^{P\text{-}Rh}$ = 153 Hz, $J^{P\text{-}P}$ = 59 Hz), 4.37 (dd, $J^{P\text{-}Rh}$ = 161 Hz, $J^{P\text{-}P}$ = 60 Hz) ppm.

### 2.3.25 Decomposition of Rhodium Diphosphine Phenoxo Alkene Complex, **11g**.



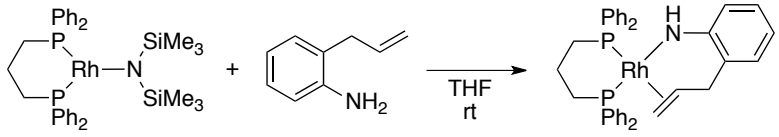

**12g** **14g**

Rhodium diphosphine phenoxo alkene complex, **11g**, (10 mg, 0.015 mmol, 1 equiv.) was weighed inside a glovebox in a 20 ml vial. The complex was dissolved in 0.5 ml of toluene-$d_8$ and transferred to a screw cap NMR tube. The NMR tube was capped and removed from the glovebox. The NMR tube was placed in a 100 °C oil bath and left overnight. NMR spectra were collected at room temperature. No attempts were made to isolate the rhodium diphosphine phenoxo alkene product.

$^1$H NMR: (500.16 MHz, toluene-$d_8$) δ 7.92 (m, 2H), 7.84 (m, 2H), 7.78 (m, broad, 1H), 7.48 (t, J = 8 Hz, 2H), 7.36 (t, J = 8 Hz, 2H), 7.20-6.94 (overlapping signals, m, 12H), 6.84 (dd, J = 7Hz, J = 1 Hz, 1H), 6.68 (d, J = 8 Hz, 1H), 6.50 (triplet of doublets, J = 7 Hz, J = 1 Hz, 1H), 5.01 (dd, J = 8 Hz, J = 4 Hz, 1H), 4.42 (d. J = 14 Hz, 6 Hz, 1H), 2.25 (d, J = 6 Hz, 3H), 3.31 (s, broad, 1H), 2.94 (d, J = 18 Hz, 1H), 2.06-1.73 (overlapping signals, 6H) ppm.

$^{31}$P{$^1$H} NMR: (162 MHz, toluene-$d_8$) δ 38.68 (dd, $J^{P\text{-}Rh}$ = 146 Hz, $J^{P\text{-}P}$ = 59 Hz), 5.94 (dd, $J^{P\text{-}Rh}$ = 161 Hz, $J^{P\text{-}P}$ = 59 Hz) ppm.

### 2.3.26 Synthesis of Rhodium Diphosphine Anilido Alkene Complex, **12g**.

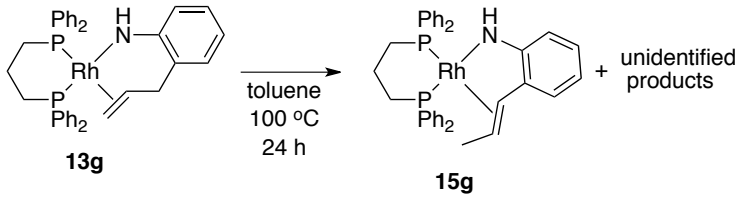



**13g**

Rhodium diphosphine silylamido complex, **2g**, (80 mg, 0.118 mmol, 1 equiv.) was weighed inside a glovebox in a 20 ml vial. 2-Allylaniline (16 mg, 0.120 mmol, 1 equiv.) weighed inside a glovebox in a 3 ml vial. The weighed silylamido complex was dissolved in 3 ml of THF. The weighed 2-allylphenol was dissolved in 2 ml of THF. The THF solution of 2-allylphenol was transferred to the vial containing the silylamido complex. The reagents were mixed together with a pipette. The dark blue solution became yellow. A magnetic stir bar was added to the vial. The solvent was removed under vacuum. The residual solid was dissolved in a small amount of THF (~ 1ml) and pentane was added to the concentrated solution to precipitate the 2-allyl phenoxo complex as a red solid. The product solution was filtered through a glass frit. The red solid was collected, transferred to a tared 20 ml vial, and dried under vacuum (55 mg, 0.085 mmol, 72 % yield).

$^{1}$H NMR: (500.16 MHz, toluene-$d_8$) δ 7.89 (m, 2H), 7.69 (m, 2H), 7.53 (m, 2H), 7.17 (m, 2H), 7.12-6.90 (overlapping signals, m, 14H), 6.49 (t, J = 7 Hz, 2H), 6.26 (d, J = 8 Hz, 1H), 4.18 (s, broad, 1H), 4.03 (d, J = 18 Hz, 1H), 3.67 (d, J = 10 Hz, 1), 3.45 (d, J =14 Hz, 1H), 3.19 (d, J = 18 Hz, 1H), 2.10 (m, 4H), 1.95 (m, 2H) ppm.
$^{31}$P{$^{1}$H} NMR: (162 MHz, toluene-$d_8$) δ 31.89 (dd, $J^{P\text{-}Rh}$ = 131 Hz, $J^{P\text{-}P}$ = 55 Hz), 5.94 (dd, $J^{P\text{-}Rh}$ = 164 Hz, $J^{P\text{-}P}$ = 55 Hz) ppm.

### 2.3.27 Decomposition of Rhodium Diphosphine Anilido Alkene Complex, **12g**.




**13g** **15g**

Rhodium diphosphine phenoxo alkene complex, **12g**, (10 mg, 0.015 mmol, 1 equiv.) was weighed inside a glovebox in a 20 ml vial. The complex was dissolved in 0.5 ml of toluene-$d_8$ and transferred to a screw cap NMR tube. The NMR tube was capped and removed from the glovebox. The NMR tube was placed in a 100 °C oil bath and left overnight. NMR spectra were collected at room temperature. Rhodium diphosphine anilido alkene product, **14g**, precipitated from solution and was characterized by x-ray crystallography

References


(1) Note: Other mechanisms for metal-catalyzed aminations and alkoxylations of alkenes include nucleophilic

(2) (a) Cowan, R. L.; Trogler, W. C. *Organometallics* **1987**, *6*, 2451(b) Cowan, R. L.; Trogler, W. C. *Journal of the American Chemical Society* **1989**, *111*, 4750.

(3) Casalnuovo, A. L.; Calabrese, J. C.; Milstein, D. *Journal of the American Chemical Society* **1988**, *110*, 6738.

(4) (a) Gagne, M. R.; Marks, T. J. *Journal of the American Chemical Society* **1989**, *111*, 4108(b) Gagne, M. R.; Stern, C. L.; Marks, T. J. *Journal of the American Chemical Society* **1992**, *114*, 275(c) Giardello, M. A.; Conticello, V. P.; Brard, L.; Gagne, M. R.; Marks, T. J. *Journal of the American Chemical Society* **1994**, *116*, 10241(d) Hong, S.; Marks, T. J. *Accounts of Chemical Research* **2004**, *37*, 673.

(5) (a) Li, Y. W.; Marks, T. J. *Organometallics* **1996**, *15*, 3770(b) Ryu, J. S.; Li, G. Y.; Marks, T. J. *Journal of the American Chemical Society* **2003**, *125*, 12584.

(6) Zhao, P. J.; Krug, C.; Hartwig, J. F. *Journal of the American Chemical Society* **2005**, *127*, 12066.

(7) Hoover, J. M.; DiPasquale, A.; Mayer, J. M.; Michael, F. E. *Journal of the American Chemical Society* **2010**, *132*, 5043.

(8) (a) Hanley, P. S.; Markovic, D.; Hartwig, J. F. *Journal of the American Chemical Society* **2010**, *132*, 6302(b) Hanley, P. S.; Hartwig, J. F. *Journal of the American Chemical Society* **2011**, *133*, 15661.

(9) (a) Neukom, J. D.; Perch, N. S.; Wolfe, J. P. *Journal of the American Chemical Society* **2010**, *132*, 6276(b) Neukom, J. D.; Perch, N. S.; Wolfe, J. P. *Organometallics* **2011**, *30*, 1269.

(10) White, P. B.; Stahl, S. S. *Journal of the American Chemical Society* **2011**, *133*, 18594.

(11) Tsutsui, H.; Narasaka, K. *Chemistry Letters* **1999**, 45.

(12) Helaja, J.; Gottlich, R. *Chem Commun* **2002**, 720.

(13) (a) Ney, J. E.; Wolfe, J. P. *Angew Chem Int Edit* **2004**, *43*, 3605(b) Lira, R.; Wolfe, J. P. *Journal of the American Chemical Society* **2004**, *126*, 13906(c) Ney, J. E.; Wolfe, J. P. *Journal of the American Chemical Society* **2005**, *127*, 8644(d) Yang, Q. F.; Ney, J. E.; Wolfe, J. P. *Org Lett* **2005**, *7*, 2575(e) Bertrand, M. B.; Neukom, J. D.; Wolfe, J. P. *Journal of Organic Chemistry* **2008**, *73*, 8851.

(14) (a) Brice, J. L.; Harang, J. E.; Timokhin, V. I.; Anastasi, N. R.; Stahl, S. S. *Journal of the American Chemical Society* **2005**, *127*, 2868(b) Liu, G. S.; Stahl, S. S. *Journal of the American Chemical Society* **2007**, *129*, 6328.

(15) Liu, G. S.; Stahl, S. S. *Journal of the American Chemical Society* **2006**, *128*, 7179.

(16) Desai, L. V.; Sanford, M. S. *Angew Chem Int Edit* **2007**, *46*, 5737.

(17) (a) Du, H. F.; Yuan, W. C.; Zhao, B. G.; Shi, Y. *Journal of the American Chemical Society* **2007**, *129*, 7496(b) Du, H. F.; Yuan, W. C.; Zhao, B. G.; Shi, Y. A. *Journal of the American Chemical Society* **2007**, *129*, 11688(c) Du, H. F.; Zhao, B. G.; Shi, Y. *Journal of the American Chemical Society* **2007**, *129*, 762(d) Zhao, B. G.; Du, H. F.; Cui, S. L.; Shi, Y. A. *Journal of the American Chemical Society* **2010**, *132*, 3523.

(18) Muniz, K.; Hovelmann, C. H.; Streuff, J. *Journal of the American Chemical Society* **2008**, *130*, 763.

(19) (a) Bryndza, H. E.; Calabrese, J. C.; Wreford, S. S. *Organometallics* **1984**, *3*, 1603(b) Bryndza, H. E. *Organometallics* **1985**, *4*, 406.

(20) Zhao, P. J.; Incarvito, C. D.; Hartwig, J. F. *Journal of the American Chemical Society* **2006**, *128*, 9642.

(21) unpublished results.

(22) Hayashi, T.; Yamasaki, K.; Mimura, M.; Uozumi, Y. *Journal of the American Chemical Society* **2004**, *126*, 3036.

(23) Trend, R. M.; Ramtohul, Y. K.; Stoltz, B. M. *Journal of the American Chemical Society* **2005**, *127*, 17778.

(24) (a) Wolfe, J. P.; Rossi, M. A. *Journal of the American Chemical Society* **2004**, *126*, 1620(b) Hay, M. B.; Hardin, A. R.; Wolfe, J. P. *Journal of Organic Chemistry* **2005**, *70*, 3099(c) Hay, M. B.; Wolfe, J. P. *Journal of the American Chemical Society* **2005**, *127*, 16468.

(25) (a) Brunet, J. J.; Commenges, G.; Neibecker, D.; Philippot, K.; Rosenberg, L. *Inorganic Chemistry* **1994**, *33*, 6373(b) Brunet, J. J.; Daran, J. C.; Neibecker, D.; Rosenberg, L. *Journal of Organometallic Chemistry* **1997**, *538*, 251.

## CHAPTER 3: The Effects of Ancillary Ligand Properties on Metal-Mediated Reactions

### 3.1 Background

The identities of the ancillary ligands on a metal complex can have a tremendous impact on the outcome of a reaction. Small changes in the ancillary ligands can have a large impact on the yield, rate, or selectivity of a metal-mediated process. Changing the ancillary ligand from P($^t$Bu)$_2$Et to P($^t$Bu)$_2$Me, for example, can change the yields of palladium-catalyzed Suzuki reactions from 2-4 % to 78-85 %, and lower the barrier for oxidative additions of alkylbromides from 25.4 kcal/mol to 19.5 kcal/mol.[92] Understanding how specific ligand properties affect both the rates and yields of metal-mediated reactions can lead to a better understanding of the reaction mechanism and to the development new ligands and catalysts. This chapter examines the effects of ancillary ligand steric, electronic, and bite angle properties on the rates and yields of metal-mediated reactions. This chapter also summarizes original research on the effects of ancillary ligand properties on the rates for alkene insertions into rhodium-alkoxo bonds. The chapter is divided into six sections. The first three sections examine how the electronic, steric, and bite angle properties of the ancillary ligand can affect the rates and yields of various metal-mediated reactions. The last three sections present research on the effects of various ligand properties on the rates for alkene insertions into rhodium-alkoxo bonds.

#### 3.1.1 The Effects of Ancillary Ligand Electronic Properties on the Rates and Yields of Metal-Mediated Reactions

The electronic properties of a ligand generally refer to the contributions a particular ligand makes to the overall electron density of a metal complex. The electron properties of a ligand can be gauged by several different methods. Common methods include measuring the carbonyl stretching frequencies, $\nu_{CO}$, of the appropriate or corresponding metal carbonyl complexes. Other methods include examining the acidity of its conjugate acid (most ligands are Lewis bases). Plots of the ligand parameters $\nu_{CO}$ and $\sigma$ versus a particular feature of a reaction, such as yield, selectivity or rate can reveal correlations between the electronic properties of the ligand and those properties or features of the reaction. In general, more electron-rich ligands favor oxidative additions, while less electron-rich ligands favor reductive eliminations and insertions. Other correlations between the electronic properties of the ancillary ligand and the rates, yields, and selectivities of the metal-mediated reaction are less established or are complicated by seemingly conflicting results. In some cases, the trends are supported by a series of individual reports on different metal-mediated reactions (deductive reasoning), and in other cases, systematic studies have been performed to elucidate the roles of specific ligand properties on the rates and yields of a particular metal-mediated reaction (inductive reasoning). This section examines primarily systematic studies that reveal how the electronic properties of the ancillary ligand can affect the outcome of a metal-mediated reaction.

##### 3.1.1.1 Ligand Substitution Reactions

Ligand substitutions are the replacement of one ligand on a metal complex with another ligand. Extensive studies on how the electronic properties of the ancillary ligands affect the rate and equilibria of ligand substitutions have been performed. Two different mechanisms have been proposed. Associative substitutions occur when bond formation or partial bond formation between the metal and the incoming ligand occurs prior to bond dissociation or partial bond dissociation between the metal and the outgoing ligand. Dissociative substitutions occur when bond

dissociation or partial bond dissociation occurs prior to any bond formation or partial bond formation between the metal and the incoming ligand. The different mechanisms can be distinguished by their rate expressions. Associative mechanisms show a first-order dependence on the concentration of incoming ligand while dissociative mechanisms show a zero-order dependence on the concentration of incoming ligand. Intermediate mechanisms have also been proposed.

The effects of the electronic properties of the ancillary ligand on the rates and equilibria of ligand substitutions depend on the mechanism that is involved. Strong σ-donors and π-acceptors, for example, have been shown to increase the rates of ligand substitutions at coordinatively unsaturated square planar $d^8$ metal complexes. In this case, the ligands trans to the strong σ-donors and π-acceptors are substituted preferentially. The effects of these ligands on the rates for ligand substitutions are collectively referred to as trans effects, and have been observed with several metal complexes. The origin of trans effects can be traced to two factors. Strong σ donors facilitate the loss of non-π-accepting ligands by weakening the bonds trans to them through electron-electron repulsions. Strong π-acceptors facilitate ligand substitutions by stabilizing the transition states for associative mechanisms by accepting the added electron density that occurs upon ligand association of the incoming ligand. Similar, to the trans effect, the trans influence refers to changes that occur in the ground state properties of metal complexes as a consequence of the ligands bound to the metal. In many cases, the trans influence specifically refers to the weakening of metal-ligands bonds trans to strong σ-donors and π-acceptors.

The extent to which a ligand affects the strength of the metal-ligand bond trans to it depends on the identities of both ligands. The presence of a π-accepting ligand trans to a σ-donating ligand is expected to strengthen both metal-ligand bonds. The presence of a strong σ-donor ligand trans to a weak σ-donor ligand is expected to weaken the metal-ligand bond of the weak σ-donor. A general order of ligands according to their trans effect or trans influence is $R_3Si^- > H^- \approx CH_3^- \approx CN^- \approx$ alkenes $\approx CO > PR_3 \approx NO_2^- \approx I^- \approx SCN^- > Br^- > Cl^- > RNH_2 \approx NH_3 > OH^- > NO_3^- \approx H_2O$.[93] The magnitudes of the trans effects can span as many as 4 orders of magnitude or more.

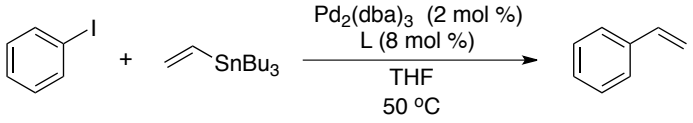
In contrast, to associative ligand substitutions, dissociative ligand substitutions are generally accelerated by the presence of weak σ-donor ligands and weak π-accepting ligands. Most dissociative mechanisms occur with coordinatively saturated 18-electron complexes. In this case, weak σ-donor ligands and weak π-accepting ligands have a tendency to labilize the ligands located cis to them. This trend is especially prevalent for substitutions at 18-electron $d^6$ octahedral complexes. The origin of this cis effect has been traced back to an electronic preference of $d^6$-square pyramid complexes to have weak σ-donors and π-acceptors in the basal plane, but may be more complicated than that. A general order of ligands according their cis effects is $NO_3^- > OAc^- > HCO_2^- > NHR \approx SH^- > OR^- > Cl^- > Br^- > I^-$ > carbene > $PPh_3 > H^- > CO$. The strong cis effects observed with $NO_3^-$, $OAc^-$, and $HCO_2^-$ ligands has been attributed to their ability to adopt $\kappa^2$ coordination modes upon the loss of a ligand from the metal complex.

#### 3.1.1.2 Transmetallations

Transmetallations are the transfer of covalent ligands (usually alkyl, aryl, alkoxides, and amides), from one metal to another metal. Common examples of transmetallations include the transfer of aryl and alkyl groups from magnesium, aluminum, boron, tin, and zinc to transition metal halide complexes to form transition metal-aryl and

alkyl complexes and magnesium, aluminum, boron, tin, and zinc halides or hydroxides. The reactions occur in several catalytic cycles including the majority of cross-coupling reactions. In many cases, the exact details of the transmetallation step and the effects of the ancillary ligand properties on the rates and yields of the reaction are unclear. In only a few examples are transmetallations thought to be the rate-limiting step. Stille reactions provide one example in which transmetallation is thought to be rate-limiting.

The effects of the electronic properties of the ancillary ligand on the rates for palladium-catalyzed couplings of aryl iodides with organotin reagents (the Stille reaction) were investigated by Farina and Krishnan at Bristol Meyer Squibb (Scheme 195).[94]




L = $PPh_3$, $PMePh_2$, $P(CH_2CH_2CN)_3$, $P(4\text{-}MeO\text{-}C_6H_4)_3$, $P[2,4,6\text{-}(MeO)\text{-}C_6H_2]_3$, $P(4\text{-}F\text{-}C_6H_4)_3$, $P(4\text{-}Cl\text{-}C_6H_4)_3$, $P(2\text{-}Me\text{-}C_6H_4)_3$, $P(2\text{-furyl})_3$, $P(2\text{-tienyl})_3$, $PPh_2(C_6F_5)$, $P(C_6F_5)_3$, $P(OPh)_3$, $P(O^iPr)_3$, $AsPh_3$, $SbPh_3$

**Scheme 195: The effects of ancillary ligand electronic properties on transmetallations of vinyl tri-butyl tin to palladium(II) iodo phenyl complexes.**

The reactions were performed with iodobenzene and vinyltributyltin at 50 °C in THF. Palladium dibenzylideneacetone, $Pd_2(dba)_3$, was used as a catalyst precursor. The reactions show a first-order dependence on catalysts concentration, a first-order dependence on organotin concentration, and a zero-order dependence or aryl iodide concentration. The data from these reactions are consistent with a mechanism involving rate-limiting transmetallation of the organotin reagent to the palladium(II) aryl iodide. To investigate the effects of the ancillary ligand properties on the rates and yields for these reactions, several monophosphines and monophosphites were applied to the reactions of iodobenzene, and vinyltributyltin. The results suggest that less electron-rich ancillary ligands promote faster rates and higher yields for the coupling of aryl iodides with organotin reagents, than more electron-rich ancillary ligands. The data from these reactions, however, are inconsistent. The correlation between the electronic properties of the ancillary ligands and the rates and yields of the reaction is rough at best. The absence of a clear trend between the electronic properties of the ancillary ligand the rates and yields of the coupling reaction is attributed to the fact that several individual steps or reactions are involved in the couplings of aryl halides and organotin reagents. Transmetallation is thought to be favored by less electron-rich ancillary ligands, while oxidative addition is thought to be favored by more electron-rich ancillary ligands. Complicating matters further, is the effect of ligand coordination on the rates of oxidative addition, transmetallation, and reductive elimination. The authors suggest that dissociation of a phosphine ligand from $Pd(PAr_3)_2(Ph)(I)$ accelerates the rate of transmetallation. This hypothesis is supported by the effects of added copper and by detailed kinetic studies on the reactions of $Pd(AsPh_3)_2(Ph)(I)$.[95] Because ligand dissociation may play an important role in transmetallation reactions, ligand properties that favor the dissociation of a phosphine from $Pd(PAr_3)_2(Ph)(I)$ may also increase the rate of transmetallations.

More recently, fast rates for a palladium-catalyzed coupling of iodobenzene with vinyltributyltin were observed with tris[2,6-bis(trifluoromethyl)-4-pyridyl]phosphine as the ancillary ligand.[96] DFT calculations

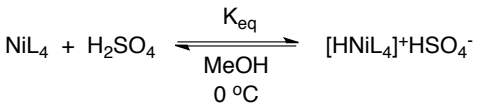
performed on this reaction suggest that the accelerating effect of less electron-rich phosphines is due to faster rates for transmetallation of the organotin reagent to palladium(II).

#### 3.1.1.3 Oxidative Additions

Oxidative additions are the formal insertions of metals and metal complexes into the covalent bonds of various compounds and molecules to form two metal-ligand covalent bonds. The reactions are accompanied by an increase in the formal in the oxidation state of the metal or metals, depending on the mechanism of the reaction and an increase in the coordination number of the metal complex. Examples of oxidative additions include the additions of aryl halides to palladium(0) complexes to form palladium(II) aryl halide complexes, the addition of $H_2$ to rhodium(I) and iridium(I) complexes to form rhodium(III) and iridium(III) dihydrido complexes, and the additions of benzyl halides to cobalt(II) complexes through radical-mediated reactions to form cobalt(III) halide and benzyl complexes. The reactions play an important role in several metal-catalyzed reactions, especially cross-couplings and hydrogenations, in which oxidative addition is either the rate-limiting step or the enantioselective step. The effects of the ancillary ligand properties on the rates for oxidative addition have been systematically studied in a few cases. Generalizations on the effects of ancillary ligand properties on the rates for various oxidative additions appear to come from these studies and from a broad analysis of the chemical literature. This subsection focuses on systematic studies of the effects of the electronic properties on the rates and yields of oxidative additions.

##### 3.1.1.3.1 Protonations of Nickel(0) Complexes

Tolman studied the effects of the ancillary ligand electronic properties on the equilibrium constants for the protonation of nickel(0) complexes, $NiL_4$ (Scheme 196).[97] The ligands on nickel were varied from $P(OCH_2CCl_3)_3$ to $P(OCH_2CH_2Cl)_3$ to $P(OMe)_3$ to $P(OEt)_3$ to $PPh(OEt)_2$. The reactions were performed in methanol at 0 °C using $H_2SO_4$ as the proton source. Equilibrium constants were determined spectrophotometrically.



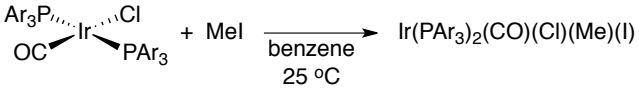

$L = PPh(OEt)_2, P(OEt)_3, P(OMe)_3, P(OCH_2CH_2Cl)_3, P(OCH_2CCl_3)_3$

**Scheme 196: The effects of ancillary ligand electronic properties on the protonations of nickel(0) complexes**

The equilibrium constant for the reaction of $Ni[P(OCH_2CCl_3)_3]_4$ with $H_2SO_4$ to form $HNi[P(OCH_2CCl_3)_3]_4$ is less than 0.1 $M^{-1}$. The equilibrium constants for the protonations of $Ni[P(OCH_2CH_2Cl)_3]_4$, $Ni[P(OMe)_3]_4$ , $HNi[P(OEt)_3]_4$, and $Ni[PPh(OEt)_2]_4$ with $H_2SO_4$ are 1.2 $M^{-1}$, 35 $M^{-1}$, 33 $M^{-1}$, and 107 $M^{-1}$. The values span 4 orders of magnitudes. To gauge how the ancillary ligands effect the electron density at the metal center, the $\nu_{CO}(A_1)$ stretching frequencies of the corresponding nickel(0) tris(carbonyl) complexes, $Ni(CO)_3L$ were measured. The $\nu_{CO}(A_1)$ stretching frequency for $Ni(CO)_3[P(OCH_2CCl_3)_3]$ is 2091 $cm^{-1}$. The $\nu_{CO}(A_1)$ stretching frequencies for $Ni(CO)_3[P(OCH_2CH_2Cl)_3]$, $Ni(CO)_3[P(OMe)_3]$, $Ni(CO)_3[P(OEt)_3]$, and $Ni(CO)_3[PPh(OEt)_2]$ are 2084 $cm^{-1}$, 2079 $cm^{-1}$, 2076 $cm^{-1}$, and 2094 $cm^{-1}$, respectively. The data from these reactions indicate that more electron-rich phosphines (lower $\nu_{CO}(A_1)$ values) result in greater equilibrium constants for the protonation of $NiL_4$ with $H_2SO_4$ than less electron-rich phosphines. The data from these reactions are consistent with the general trend that more electron-rich phosphines stabilize metals in higher oxidation states better than less electron-rich metals.

### 3.1.1.3.2 Oxidative Additions of MeI and $H_2$ to Iridium(I) Complexes

Oxidative additions of MeI and $H_2$ to iridium(I) have been studied by the groups of Vaska, Shaw, Halpern, Ugo, Thompson, and Hall. Ugo and co-workers studied the effects of the electronic properties of the ancillary ligands on the rates for MeI oxidative addition by changing the aryl groups on the phosphine ligands (Scheme 197).

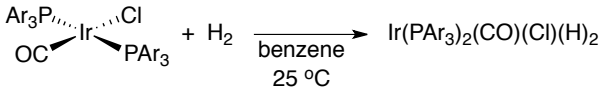


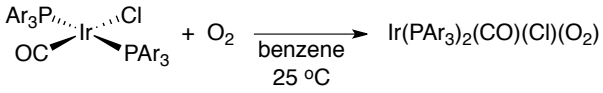

$PAr_3$ = $P(4\text{-Cl-}C_6H_4)_3$, $P(4\text{-F-}C_6H_4)_3$, $PPh_3$, $P(4\text{-Me-}C_6H_4)_3$, $P(4\text{-MeO-}C_6H_4)_3$,

**Scheme 197: The effects of ancillary ligand electronic properties on the oxidative additions of methyl iodide to bis(triarylphosphine) iridium(I) chloride carbonyl complexes.**

The reactions were performed in benzene at 25 °C. Rate constants were determined by monitoring the reactions by UV-Vis spectroscopy. The rate constant for the oxidative addition of MeI to $Ir(PAr_3)_2(CO)Cl$ (Ar = *p*-Cl-$C_6H_4$) is 3.7 x $10^{-5}$ $M^{-1}$ $s^{-1}$. The rate constants for the oxidative addition of MeI to $Ir(PAr_3)_2(CO)Cl$ (Ar = *p*-F-$C_6H_4$), $Ir(PPh_3)_2(CO)Cl$, $Ir(PAr_3)_2(CO)Cl$ (Ar = *p*-$CH_3$-$C_6H_4$), and $Ir(PAr_3)_2(CO)Cl$ (Ar = *p*-MeO-$C_6H_4$) are 1.5 x $10^{-4}$ $M^{-1}$ $s^{-1}$, 3.3 x $10^{-3}$ $M^{-1}$ $s^{-1}$, 1.5 x $10^{-2}$ $M^{-1}$ $s^{-1}$, and 3.5 x $10^{-2}$ $M^{-1}$ $s^{-1}$. The data from these reactions show that the rate of the reaction increases as the aryl groups become more electron-rich. The origin of this effect is related to the ability of electron-rich ligands to stabilize metals in high oxidation states.

Ugo and co-workers also reported the oxidative additions of $H_2$ and $O_2$ to Iridium(I) complexes (Scheme 198).




$PAr_3$ = $P(4\text{-Cl-}C_6H_4)_3$, $P(4\text{-F-}C_6H_4)_3$, $PPh_3$, $P(4\text{-Me-}C_6H_4)_3$, $P(4\text{-MeO-}C_6H_4)_3$,

**Scheme 198: Reactions used to study the effects of ancillary ligand electronic properties on the oxidative additions of $H_2$ and $O_2$ to x bis(triarylphosphine) iridium(I) chloride complexes.**

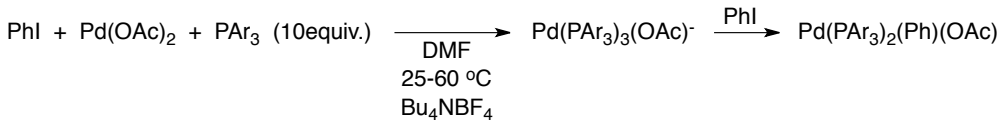
In both cases, a similar effect is observed. Rates for the oxidative additions of $H_2$ and $O_2$ increase as the ligands on the metal become more basic. The magnitudes of these effects, however, are smaller. The rate constant for the oxidative addition of $H_2$ to $Ir(PAr_3)_2(CO)Cl$ (Ar = *p*-Cl-$C_6H_4$) is 2.1 x $10^{-1}$ $M^{-1}$ $s^{-1}$. The rate constants for the oxidative addition of $H_2$ to $Ir(PAr_3)_2(CO)Cl$ (Ar = *p*-F-$C_6H_4$), $Ir(PPh_3)_2(CO)Cl$, $Ir(PAr_3)_2(CO)Cl$ (Ar = *p*-$CH_3$-$C_6H_4$), and $Ir(PAr_3)_2(CO)Cl$ (Ar = *p*-MeO-$C_6H_4$), are 2.2 x $10^{-1}$ $M^{-1}$ $s^{-1}$, 6.7 x $10^{-1}$ $M^{-1}$ $s^{-1}$, 4.8 x $10^{-1}$ $M^{-1}$ $s^{-1}$, and 5.6 x $10^{-2}$ $M^{-1}$ $s^{-1}$, respectively. It is not clear why the reaction of $Ir(PPh_3)_2(CO)Cl$, is the fastest.

The effects of ancillary ligand electronic properties on the oxidative addition of MeI to $Ir(PAr_3)_2(CO)Cl$ was also studied by Thompson and Sears.[98] The rate constants for these reactions are slightly different. The rate constant for the oxidative addition of MeI to $Ir(PAr_3)_2(CO)Cl$ (Ar = *p*-F-$C_6H_4$) is 8.54 x $10^{-5}$ $M^{-1}$ $s^{-1}$. The rate constant for the oxidative addition of MeI to $Ir(PPh_3)_2(CO)Cl$ is 2.67 x $10^{-3}$ $M^{-1}$ $s^{-1}$. The rate constant for the

oxidative addition of MeI to $Ir(PAr_3)_2(CO)Cl$ (Ar = *p*-$CH_3$-$C_6H_4$) is 1.32 x $10^{-2}$ $M^{-1}$ $s^{-1}$, and the rate constant for the oxidative addition of MeI to $Ir(PAr_3)_2(CO)Cl$ (Ar = *p*-MeO-$C_6H_4$) is 2.53 x $10^{-2}$ $M^{-1}$ $s^{-1}$. The data from these reactions show that the rate increases as the aryl groups become more electron-rich. The rate constants span three orders of magnitude. The origin of this effect is related to the ability of electron-rich ligands to stabilize metals in high oxidation states.

#### 3.1.1.3.3 Oxidative Additions of PhI to Palladium(0) Complexes

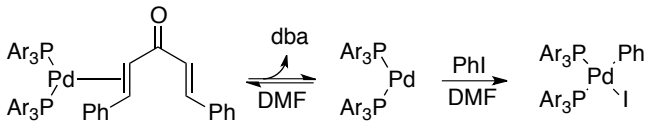
Oxidative additions of aryl halides to palladium(0) complexes were studied by the group of Amatore and Jutand (Scheme 199).[99]




**Scheme 199: Reactions used to study the effects of ancillary ligand electronic properties on the oxidative additions of iodobenzene to anionic palladium(0) complexes.**

The effects of the electronic properties of the ancillary ligands on the rates of the reactions were probed by applying different triarylphosphines to the reaction of phenyl iodide with $Pd(OAc)_2$. In this case, a palladium(0) complex is formed in situ from the reaction of $Pd(OAc)_2$ with phosphine. The combined reactions ($Pd(OAc)_2$ reduction and ArX oxidative addition) were monitored by cyclic voltammetry. The rates for $Pd(OAc)_2$ reduction were shown to vary with the basicity of the phosphine. Less electron-rich phosphines provided faster rates for $Pd(OAc)_2$ reduction than more electron-rich phosphines. The mechanism for these reactions is thought to involve the formation of $Pd(OAc)_2(PR_3)_2$ through coordination of the added phosphine to $Pd(OAc)_2$ and an inner-sphere nucleophilic attack of one of the acetate ligands onto one of the coordinated phosphines. When the reactions are performed in excess phosphine, an anionic palladium(0) trisphosphine acetate complex, $Pd(PR_3)_3(OAc)^-$, is formed. The reduction of $Pd(OAc)_2$ to palladium(0) in the presence of added phosphines shows a first-order dependence on palladium(II) concentration and a zero-order dependence on phosphine concentration. The rates for the oxidative addition of phenyl iodide to $Pd(PAr_3)_3(OAc)^-$ were also determined by cyclic voltammetry. These data show that the rates for oxidative addition increase as the phosphines on palladium become more electron-rich. This is in agreement with other studies on the effects of ancillary ligand properties on the rates of oxidative additions.

Oxidative additions of aryl halides to palladium(0) complexes were also studied using $Pd(dba)_2$ as the palladium(0) source (Scheme 200).[100]




**Scheme 200: The effects of ancillary ligand electronic properties on the oxidative additions of iodobenzene to neutral palladium(0) complexes.**

In this case, the rates of reaction show a "bell-shaped" dependence on the electronic properties of the ancillary ligands. This "bell-shaped" dependence was attributed to two conflicting effects of the ancillary ligand

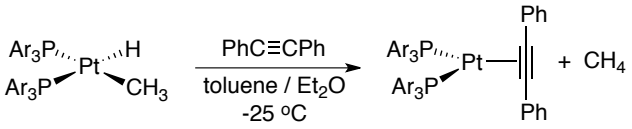
electronic properties. In this case, more electron-rich phosphines are thought to increase the rate of oxidative addition while decreasing the rate of alkene (dba) dissociation from the palladium(0). Since alkene dissociation from palladium(0) is required for oxidative addition, the overall effect of the electronic properties of the ancillary ligand on the rate of oxidative addition is non-linear. Maximum rates are achieved when hydrogen is in the *para* position of the triarylphosphine.

#### 3.1.1.4 Reductive Eliminations

Reductive eliminations are the reverse of oxidative additions. Reductive eliminations result in the elimination of compounds from metal complexes, a decrease in the formal oxidation state of the metal complex, and a decrease in the overall coordination number of the metal. The reactions are generally favored by less electron-rich and sterically bulky ligands, which can stabilize the lower oxidation state of the resulting metal complex. Examples of reductive eliminations include the eliminations of biaryls, aryl amines, and aryl ethers from palladium(II) complexes. Like oxidative additions, the reductive eliminations play an important role in several metal-catalyzed reactions including metal-catalyzed cross-couplings and alkene hydrocyanations. This subsection focuses on systematic studies that reveal the effects of the electronic properties of the ancillary ligand on the rates and yields of metal-mediated reactions.

##### 3.1.1.4.1 Carbon-Hydrogen Bond-Forming Reductive Eliminations from Platinum(II)

Reductive eliminations of methane from *cis*-platinum(II) hydrido methyl complexes were reported by Halpern and co-workers (Scheme 201).[101]



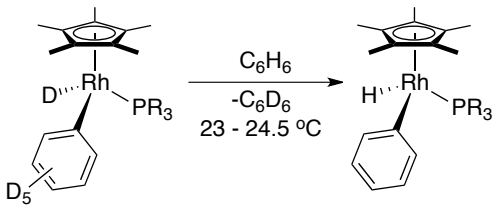

$PAr_3$ = $P(4\text{-Cl-}C_6H_4)_3$, $PPh_3$, $P(4\text{-}CH_3\text{-}C_6H_4)_3$, $P(4\text{-MeO-}C_6H_4)_3$

**Scheme 201: Reactions used to study the effects of ancillary ligand electronic properties on the reductive eliminaiton of methane from bis(triarylphosphine) platiunm(II) methyl hydrido complexes.**

The platinum(II) complexes were formed in situ by the reactions of *trans*-platinum(II) bis(monophosphines) hydrido halides and methyl magnesium bromide. The reactions used to synthesize these complexes were preformed at -78 °C in toluene / ether mixtures. The complexes are stable at -50 °C and characterized by $^1H$ and $^{31}P$ NMR spectroscopy. Elimination of methane from $Pt(PR_3)_2(H)(Me)$ occurred at -25 °C. The effects of the electronic properties of the ancillary ligands on the rates for methane reductive elimination were determined by varying the aryl groups on phosphorus. Reactions preformed with $P(p\text{-Cl-}C_6H_4)_3$, $PPh_3$, $P(p\text{-}CH_3\text{-}C_6H_4)_3$, and $P(p\text{-MeO-}C_6H_4)_3$. The rate constants for these reactions were 9.2 x 10-4 $s^{-1}$, 4.5 x 10-4 $s^{-1}$, 1.4 x 10-4 $s^{-1}$, and 0.47 x 10-4 $s^{-1}$, respectively. The data from these reactions indicate that less electron-rich phosphines promote faster rates for reductive elimination than more electron-rich phosphines. The rates show a first order dependence on the concentration of platinum and a zero-order dependence on the concentration of excess ligand. A kinetic isotope effect of $K_H/K_D = 3.3 \pm 0.3$ was measured for the reactions of *cis*-$Pt(PPh_3)_2(CH_3)(D)$. No cross-over products were observed when the reactions of *cis*-$Pt(PPh_3)_2(CH_3)(D)$ and *cis*-$Pt(PPh_3)_2(CD_3)(H)$ and from the

reactions of *cis*-Pt($PPh_3$)$_2$($CD_3$)(D) and *cis*-Pt($PPh_3$)$_2$($CH_3$)(H). The data from these reactions point to a concerted mechanism for methane elimination.

Reductive eliminations of $C_6D_6$ from rhodium(III) cyclopentadienyl phosphine complexes were studied by Jones and co-workers (Scheme 202).[102]



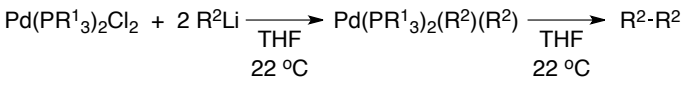

$PR_3$ = $PMe_3$, $PMe_2Ph$, $PMePh_2$, $PPh_3$, $PMe_2(^tBu)$, $PMe_2(^nBu)$, $P(^nBu)_3$

**Scheme 202: Reactions used to study the effects of ancillary ligand electronic properties on the reductive eliminations of $C_6D_6$ from rhodium(III) pentadeuteriophenyl deuteride complexes.**

The reactions were performed at temperatures between 23 and 24.5 °C in benzene solvent with $PMe_3$, $PMe_2Ph$, $PMePh_2$, $PPh_3$, $PMe_2(^tBu)$, $PMe_2(^nBu)$, and $P(^nBu)_3$ on rhodium. The rates for D-$C_5D_5$ reductive elimination were measured by monitoring the rate of ligand exchange with benzene solvent. The rhodium(III) pentadeuterophenyl deuterido complexes were prepared by irradiation of the corresponding rhodium(III) dihydrido complexes in $C_6D_6$. A comparison of the rates for the reductive elimination of $C_6D_6$ from the rhodium(III) complexes of $PMe_2Ph$ ($\theta$ = 122 °; $k_{obs}$ = 1.08 x $10^{-6}$ $s^{-1}$) and $PMe_3$ ($\theta$ = 118 °; $k_{obs}$ = 3.35 x $10^{-7}$ $s^{-1}$) suggests that less electron-rich phosphines promote faster rates for C-D reductive elimination than more electron-rich phosphines. This trend, however, is inconsistent with the rate for the reductive elimination of $C_6D_6$ from the rhodium(III) complex of $PMe_2(^nBu)$ ($\theta$ = 123 °; $k_{obs}$ = 1.25 x $10^{-5}$ $s^{-1}$). The rate constants for the reductive elimination of $C_6D_6$ from the rhodium(III) complexes of $PMePh_2$ ($\theta$ = 136 °; $k_{obs}$ = 1.11 x $10^{-5}$ $s^{-1}$), $P(^nBu)_3$ ($\theta$ = 132 °; $k_{obs}$ = 2.4 x $10^{-6}$ $s^{-1}$) and $PMe_2(^tBu)$ ($\theta$ = 139 °; $k_{obs}$ = 6.6 x $10^{-6}$ $s^{-1}$) also suggests that less electron-rich phosphines promote faster rates for C-D reductive elimination than more electron-rich phosphines. The discrepancies in these data were not accounted for.

### 3.1.1.4.2 Carbon-Carbon Bond Forming Reductive Eliminations from Palladium(II)

Negishi and co-workers examined the rates for carbon-carbon reductive eliminations from palladium(II) bis(monophosphine) complexes (Scheme 203).[103]




$PR^1_3$ = $PEt_3$, $PPhMe_2$, $PPh_2Me$, $PPh_3$

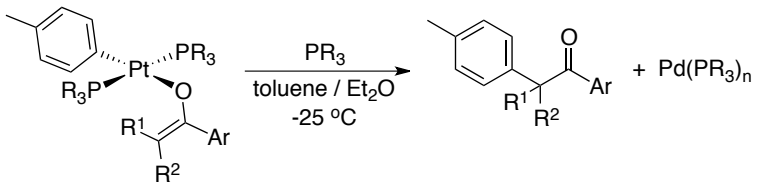
**Scheme 203: Reactions used to study the effects of ancillary ligand electronic properties on the reductive eliminations of carbon-carbon bonds from bis(monophosphine) palladium(II) complexes.**

In this case, the effects of the ancillary ligand properties on the rates for carbon-carbon reductive elimination were probed by varying the phosphines on palladium. The reactions were performed with $PEt_3$ to $PPhMe_2$ to $PPh_2Me$ to $PPh_3$ on palladium.

The data from these reactions indicate that the yields of coupled products decrease as the basicity of the phosphine increases. Reactions performed with $PEt_3$ as the ancillary ligand generated the lowest yields of organic products while reactions performed with $PPh_3$ as the ancillary ligand generated the highest yields of organic products. The effects of the steric properties of the ancillary ligands on the rates for carbon-carbon reductive elimination were not considered. Moreover, the results were not placed within the context of a particular mechanism.

Yates and Ariafard studied carbon-carbon reductive eliminations from palladium(II) complexes by DFT.[104] Model calculations were performed on $Pd(L)_2(R)_2$, where L = $PMe_3$, $PCl_3$, $PH_3$, $PPh_3$, $PPh_2Me$, and $PPhMe_2$ and R = Me, $CHCH_2$. The results from these calculations suggest that the basicity of the phosphine plays an important role in determining the barriers for carbon-carbon reductive elimination from four coordinate palladium(II) complexes, $Pd(L)_2(R)_2$. The effects of the electronic properties of the ancillary ligand on the rates for reductive elimination from three coordinated palladium(II) complexes, $Pd(L)(R)_2$ is less pronounced. For the reactions of four coordinate palladium(II) complexes greater phosphine basicity results in greater destabilization of the transition state for reductive elimination with respect to the ground state, increasing the barrier for reductive elimination. For the reactions of three coordinate palladium(II) complexes, phosphine dissociation from $Pd(L)_2(R)_2$ determines the relative rates. More basic phosphines result in stronger metal-phosphine bonds and slower rates for phosphine dissociation.

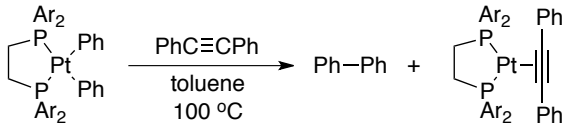
The effects of the electronic properties of the ancillary ligands on the rates for carbon-carbon reductive eliminations of aryl ketones from palladium(II) bis(monophosphine) aryl enolate complexes reported by Hartwig and Culkin (Scheme 204).[105]




**Scheme 204: Reactions used to study the effects of ancillary ligand electronic properties on carbon-carbon reductive eliminaitons from bis(monophosphine) palladium(II) enolate compexes.**

In this case, palladium(II) aryl enolate complexes ligated by $PPh_3$ react below room temperature, while palladium complexes ligated by $PEtPh_2$ are stable at room temperature and react at 110 °C. Meanwhile, palladium(II) aryl enolate complexes ligated by $PMePh_2$ do not undergo reductive eliminations of α-aryl ketones. The data from these reactions suggest that less electron-rich phosphines promote reductive eliminations to a greater extent than more electron-rich phosphines. The differences in the stabilities of these complexes are attributed to the differences in the basicities of the phosphine ligands. Complexes ligated by less basic phosphines are more likely to undergo reductive eliminations than complexes ligated by more basic phosphines.

The effects of the electronic properties of the ancillary ligands on the rates for carbon-carbon reductive eliminations of biphenyls from platinum(II) diphosphine complexes were studied by Sakai and co-workers (Scheme 205).[106]




Ar = Ph, 4-F-$C_6H_4$, 3,5-$F_2$-$C_6H_3$, 2,6-$F_2$-$C_6H_3$, 3,4,5-$F_3$-$C_6H_2$, 2,4,6-$F_3$-$C_6H_2$, 2,3,5,6-$F_4$-$C_6H$, $C_6F_5$, 4-$CF_3$-$C_6F_4$

**Scheme 205: Reactions used to study the effects of ancillary ligand electronic properties on the reductive eliminations of biphenyl from 1,2-bis(diarylphosphino)ethane palladium(II) diphenyl complexes.**

Model reactions were performed in toluene at 100 °C. The platinum(II) diphosphine complexes reported in this study were synthesized by the additions of diphosphines to $Pt(COD)Cl_2$ followed by treatment of the resulting complex with 2 equivalents of PhMgBr. Diphenyl ethyne was added to the reactions to trap the platinum(0) complexes formed by reductive elimination. Only derivatives of DPPE (1,2-bis(diphenylphosphino)ethane) are reported.

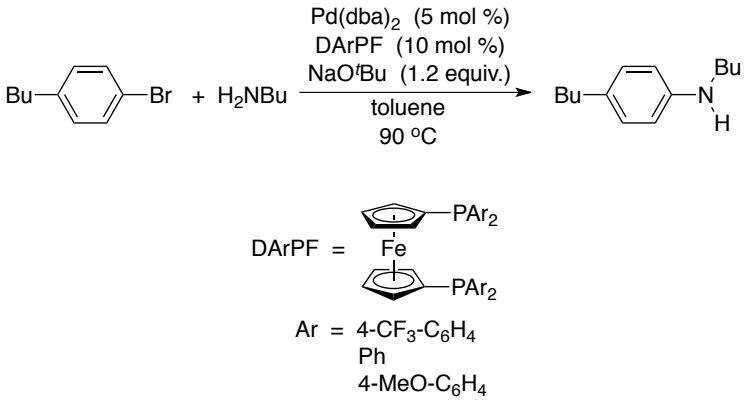
The electronic properties of the ligands were varied by changing substituents on the aryl rings of the diphosphines. Reductive elimination of biphenyl from the platinum(II) complex of 1,2-bis[bis(4-heptafluorotolyl)phosphino]ethane occurred at room temperature. The rate constant for this reaction was not reported. Reductive eliminations of biphenyl from the remaining platinum(II) complexes occurred at 100 °C.

The pseudo first order rate constant for the reductive elimination of biphenyl from the platinum(II) complex of 1,2-bis[bis(pentafluorophenyl)phosphino]ethane is $2.23 \times 10^{-4}$ $s^{-1}$. This complex reacted the fastest out of those reported. The pseudo first order rate constant for the reductive elimination of biphenyl from the platinum(II) complex of DPPE is $1.80 \times 10^{-7}$ $s^{-1}$. This complex reacted the slowest out of those reported. The difference in rate constants for the reductive elimination of biphenyl from the platinum(II) complexes of 1,2-bis[bis(pentafluorophenyl)phosphino]ethane and DPPE spans 3 orders of magnitude. Platinum(II) complexes of diphosphines having intermediate Taft σ* values display rate constants that are intermediate of $2.23 \times 10^{-4}$ $s^{-}{}_1$ and $1.80 \times 10^{-7}$ $s^{-}1$.

The data from these reactions show a positive correlation between the Taft σ* value of the ligand and rate constant for the reaction. A plot of the Taft σ* values of the ligands against rate constants for the reaction reveals two classes of ligands: DPPE derivatives with fluorine atoms at the 2 and 6 positions of the aryl rings bound to phosphorus and DPPE derivatives with hydrogen atoms at the 2 and 6 positions of the aryl rings bound to phosphorus. Complexes of ligands having fluorine atoms at the 2 and 6 positions of the aryl rings on phosphorus react slightly faster than complexes of ligands having similar Taft σ* values, but without fluorine atoms at the 2 and 6 positions. The difference in rate constants is attributed to the steric differences between hydrogen and fluorine. The diphosphine ligands having fluorine atoms at the 2 and 6 positions are slightly larger than the diphosphine ligands having hydrogen atoms at the 2 and 6 positions. This increase in steric bulky results in slightly faster rates for reductive elimination of biphenyl from platinum(II).

#### 3.1.1.4.3 Carbon-Nitrogen Bond Forming Reductive Eliminations from Palladium(II)

Hartwig and Hamman studied the effects of the electronic properties of the ancillary ligand on the yields of aryl amine products generated by palladium-catalyzed arylation of amines with aryl bromides (Scheme 206).[107]




**Scheme 206: Reactions used to study the effects of ancillary ligand electronic properties on the yields for carbon-nigtrogen bond forming reductive eliminations from palladium(II) aryl anilido complexes.**

Model reactions were performed in toluene at 90 °C using 5 mol % $Pd(dba)_2$, 10 mol % ligand ,1.2 equivalents of $NaO^tBu$, and *n*-butylamine as the amine source. The effect of the electronic properties of the ancillary ligands on the yields of aryl amine products was investigated by applying a series of electronically modified DPPF derivatives to the reactions. Reactions performed with 1,1'-bis[bis(4-methoxyphenyl)phosphino]ferrocene (*p*-MeO-DPPF) as the ancillary ligand resulted in a 4.0 % yield of arene (from protodehalogenation), a 55 % yield of monoarylamine, and a 21 % yield of diarylamine, while reactions performed with DPPF as the ancillary ligand resulted in a 4.4 % yield of arene (from protodehalogenation), a 52 % yield of monoarylamine, and a 22 % yield of diarylamine. Reactions performed with 1,1'-bis[bis(4-(trifluoromethyl)phenyl)phosphino]ferrocene (*p*-$CF_3$-DPPF) as the ancillary ligand resulted in a 5.5 % yield of arene (from protodehalogenation), a 53 % yield of monoarylamine, and a 18 % yield of diarylamine.

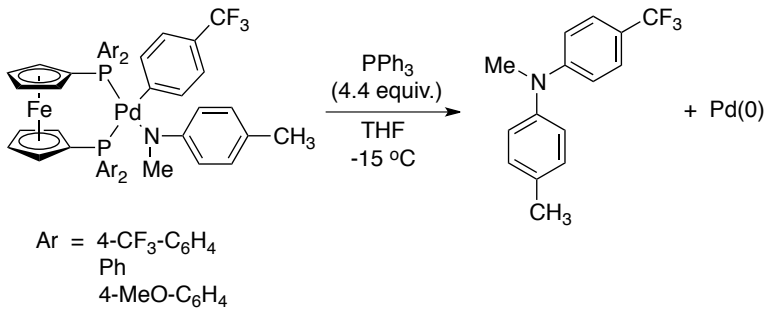
The data from these reactions show that less electron-rich DPPF derivatives give slightly lower yields of arylamine products and slightly higher yields of protodehalogenated products than reactions with more electron-rich DPPF derivatives. The effects were slightly more pronounced with isobutylamine than with *n*-butylamine. The ratios of monoaryl to diaryl amines were not affected.

To determine the effects of the electronic properties of the ancillary ligand on the electron density at the metal, the carbonyl stretching frequencies for the nickel(0) dicarbonyl complexes of DPPF and *p*-MeO-DPPF were measured. The data from these reactions suggest that changing the para substituent on the aryl rings of DPPF from H to MeO affords only a small change in the electron density at the metal center. The data from these reactions may explain the lack of a significant electronic effect on the yields of amine products.

Trends in the data are not well-defined. The relatively small effects observed in arene and amine yields observed upon changing the substituents on phosphorus can be explained by a weak transmission of electronic information from phosphorus to palladium. This hypothesis is supported by the $\nu_{CO}$ stretching frequencies observed with $Ni(diphosphine)(CO)_2$. The increase in the amount of arene formed by decreasing the basicity of the diphosphine is not well-understood. The mechanism for this reaction was investigated by performing the reactions with deuterated amines. The results from these experiments suggest that proton involved in the protodehalogenation

of the aryl halide does not originate from the amine through β-hydride elimination of an imine from a palladium(II) amido complex.

The effect of the electronic properties of the ancillary ligands on the rates for C-N reductive eliminations from palladium(II) complexes were also reported by Hartwig and co-workers. In this case, a series of palladium(II) aryl anilido complexes ligated by electronically modified DPPF derivatives were generated in situ at -78 °C by the reactions of palladium(II) diphosphine aryl iodides with *N*-methyl potassium anilides and characterized by NMR spectroscopy (Scheme 207).

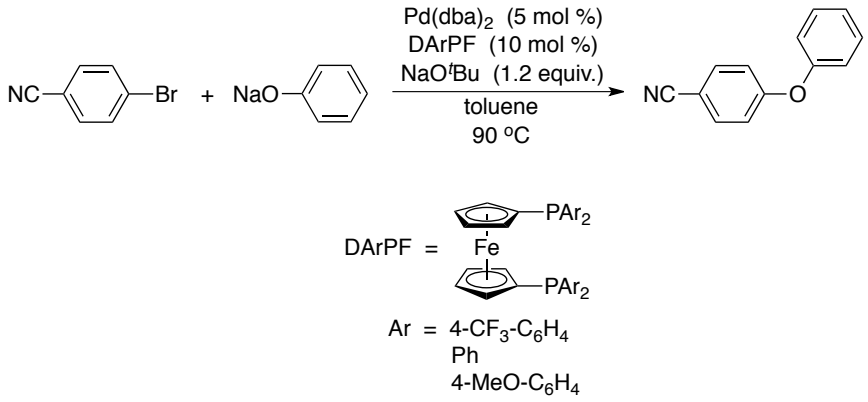



**Scheme 207: Reactions used to study the effects of ancillary ligand electronic properties on the rates for carbon-nigtrogen bond forming reductive eliminations from palladium(II) aryl anilido complexes.**

Reductive eliminations of *N*-methyl diaryl amines from these complexes were observed at -15 °C. The reactions were monitored by $^{19}F$ NMR spectroscopy. Rate constants were determined by plotting the integrations of the $^{19}F$ NMR signals these complexes over time, and fitting equations for exponential decay to the data from these reactions. The data from these reactions indicate that C-N reductive eliminations from less electron-rich palladium(II) complexes are faster than that C-N reductive eliminations from more electron-rich palladium(II) complexes. The rate constants span roughly one order of magnitude. Reductive elimination of diaryl amine from the palladium(II) aryl anilido complex of MeO-DPPF occurs with a rate constant of 4.6 x 10-$^{4}$ s$^{-1}$, while reductive elimination of diaryl amine from the palladium(II) aryl anilido complex of DPPF occurs with a rate constant of 12.8 x 10-$^{4}$ s$^{-1}$. Reductive elimination of diaryl amine from the palladium(II) aryl anilido complex of $CF_3$-DPPF occurs with a rate constant of 27.0 x 10-$^{4}$ s$^{-1}$. The data from these reactions suggest that less electron-rich phosphines accelerate the rate for C-N reductive eliminations from palladium(II) aryl amido complexes relative to more electron-rich phosphines.

#### 3.1.1.4.4 Carbon-Oxygen Bond Forming Reductive Eliminations from Palladium(II)

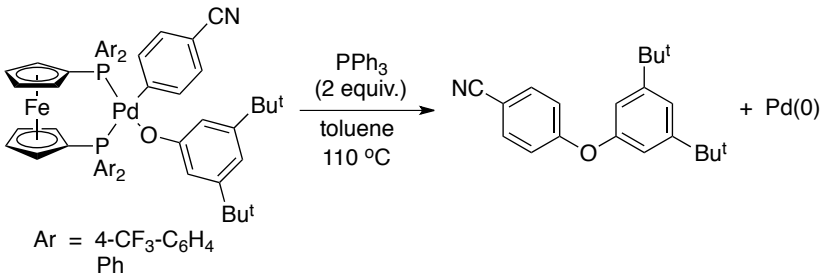
The effect of the electronic properties of the ancillary ligands on the yields of diaryl ethers formed by a palladium-catalyzed coupling of aryl bromides with sodium phenoxides were reported by Hartwig and Mann (Scheme 208).[108]




**Scheme 208: Reactions used to study the effects of ancillary ligand electronic properties on the yields for carbon-oxygen bond forming reductive eliminations from palladium(II) aryl phenoxo complexes.**

Model reactions were performed using 5-10 mol % $Pd(dba)_2$ and 6-11 mol % diphosphine in mixtures of toluene and THF at 100-120 °C. The effect of the electronic properties of the ancillary ligands on the yields of diaryl ether products were investigated using a series of electronically modified DPPF derivatives. The reaction of 4-bromobenzontirile with sodium phenoxide. $Pd(dba)_2$ and a para methoxo derivative of DPPF, yielded corresponding diaryl ether in 8.5 % yield, as determined by gas chromatography. The reaction of 4-bromobenzontirile with sodium phenoxide. $Pd(dba)_2$ and DPPF yielded the corresponding diaryl ether in 51 % yield, as determined by gas chromatography. The reaction of 4-bromobenzontirile with sodium phenoxide. $Pd(dba)_2$ and a para trifluoromethyl derivative of DPPF, yielded the corresponding diaryl ether in 74 % yield, as determined by gas chromatography. The data from these reactions show that the yields of diaryl ethers increase as the electron-donating properties of the ancillary ligand decreases. The effect of the electronic properties of the ancillary ligand on the yield of diaryl ether product was attributed to an increased rate for C-O reductive elimination.

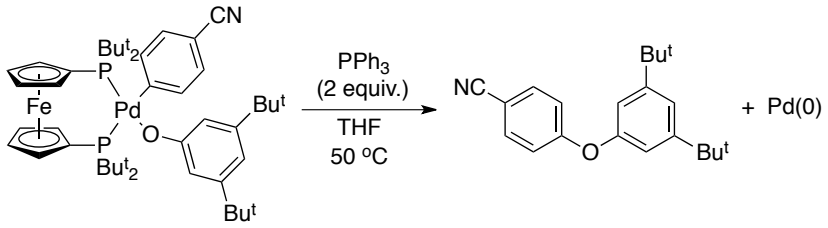
The reactions of isolated palladium(II) diphosphine aryl phenoxide complexes have also been reported. In this case, the rates for C-O reductive elimination from palladium(II) were measured directly.[109]




**Scheme 209: Reactions used to study the effects of ancillary ligand electronic properties on the rates for carbon-oxygen bond forming reductive eliminations from palladium(II) aryl phenoxo complexes.**

The reactions of $Pd(DPPF)(Ar^1)(OAr^2)$ and $Pd(p\text{-}CF_3\text{-}DPPF)(Ar^1)(OAr^2)$ ($Ar^1$ = $p$-CN-$C_6H_4$; $Ar^2$ = 3,5-($^t$Bu)$_2$-$C_6H_3$) reveal a small electronic effect for the reductive elimination of diaryl ether from palladium(II). The less electron-rich complex, $Pd(p\text{-}CF_3\text{-}DPPF)(Ar^1)(OAr^2)$, reacts 2x faster than the parent palladium(II) complex, $Pd(DPPF)(Ar^1)(OAr^2)$.[110] In contrast, the more sterically hindered complex, $Pd(D^tBuPF)(Ar^1)(OAr^2)$ ($Ar^1$ = $p$-CN-

$C_6H_4$; $Ar^2$ = 3,5-($^t$Bu)$_2$-$C_6H_3$; D$^t$BuPF = 1,1'-bis(di-*tert*-butylphosphino)ferrocene), reacts 100x faster than the parent palladium(II) complex, Pd(DPPF)($Ar^1$)($OAr^2$) (Scheme 210) .

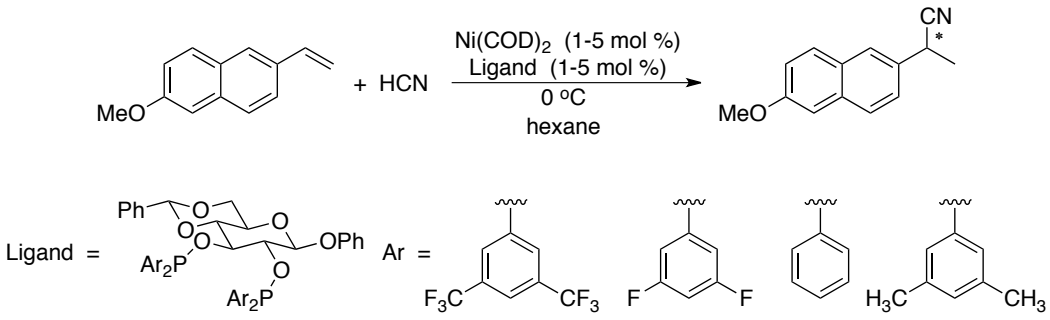



**Scheme 210: Reactions used to study the effects of ancillary ligand steric properties on the yields for carbon-oxygen bond forming reductive eliminations from palladium(II) aryl phenoxo complexes.**

The data from these reactions clearly show that the steric properties of the diphosphines have a greater effect on the rates for diaryl ether eliminations from palladium(II) than the electronic properties of the diphosphines.

### 3.1.1.5 Asymmetric Hydrocyanations of Vinyl Arenes

The groups of Casalnuovo and RajanBabu investigated the effects of the electronic properties of the ancillary ligands on the enantioselectivities of nickel-catalyzed asymmetric hydrocyanations of vinyl arenes (Scheme 211).[111]




**Scheme 211: Reactions used to study the effects of ancillary ligand electronic properties on the enantioselectivities of nickel-catalzyed asymmetric hydrocyanations of vinyl arenes.**

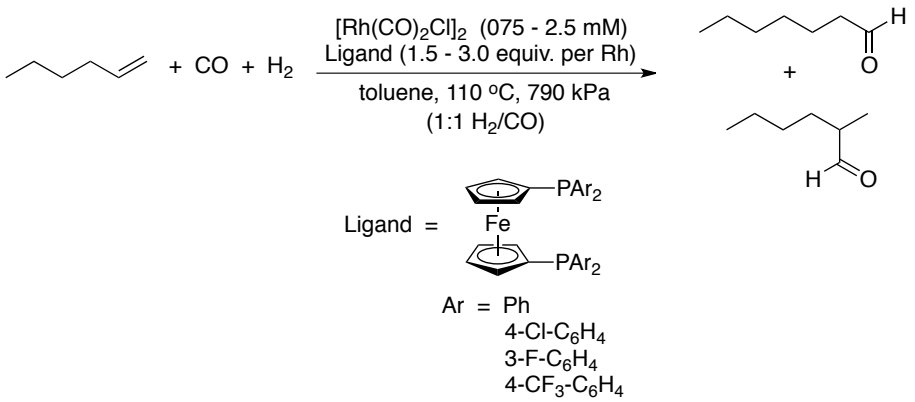
In this case, the ligands on nickel were glucose-derived diphosphinites. The active catalysts were formed in situ by the addition of 1 equivalent of the appropriate diphosphinite to $Ni(COD)_2$. The reactions were performed at room temperature (25 °C) in benzene, toluene, or hexane. The enantiomeric excesses were determined by HPLC analysis of the product mixtures. Only branched nitriles were detected. The electronic properties of the ancillary ligands were varied by varying the substituents on the aryl rings of the phosphinite. The data from these reactions show that catalysts formed from less electron-rich diphosphinites generate higher ee's of the branched nitrile product. The mechanism for these reactions was studied by a series of stoichiometric reactions, low temperature NMR and kinetic experiments, and reactions with deuterium-labeled substrates. The results from these studies suggest a mechanism in which the formation of a nickel(II) hydrido cyano alkene complex is followed by reversible alkene insertion into the nickel-hydrido bond and irreversible C-CN reductive elimination. The effect of the electronic properties of the phosphinite on the enantiomeric excess of the reaction is attributed to a disproportionate increase in the rate of C-CN reductive elimination. The data from these reactions cannot distinguish whether alkene insertion into the nickel-hydrido bond or C-CN reductive elimination is the rate-limiting step. In one scenario,

reversible alkene insertion is followed by rate-limiting C-CN reductive elimination. The enantioselectivity of the reaction is determined by a disproportionate increase in the rate of reductive elimination of one enantiomer of the alkyl nitrile product. In the other scenario, the barrier to C-CN reductive elimination is lowered to the point that alkene insertion into the metal-hydrido bond becomes rate-limiting, and the overall enantioselectivity of the reaction is then determined by alkene insertion. It is possible that decreasing the electron-donating properties of the diphosphinite changes the rate-limiting step from C-CN reductive elimination to alkene insertion. The amount of deuterium scrambling observed with deuterated alkenes decreases as the diphosphinites become less electron-rich.

An enhanced activity of nickel catalysts for the hydrocyanation of alkene with less electron-rich ancillary ligands was later confirmed by van Leeuwen and co-workers using electronically-modified Thixantphos-type ligands.[112]

### 3.1.1.6 Rhodium-Catalyzed Hydroformylation Reactions

The effects of the electronic properties of the ancillary ligands on the rates and selectivities of rhodium diphosphine catalyzed hydroformylations were studied by Unruh and Christenson (Scheme 212).[113]

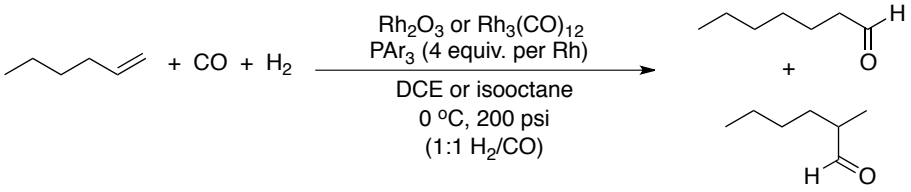



**Scheme 212: Reactions used to study the effects of the electronic properties of the ancillary ligands on the rates and selectivities of rhodium diphosphine catalyzed hydroformylations.**

In this case, both the rate and the linear-to-branched selectivity decreased with more electron-rich diphosphines on the metal. The reactions were performed with electronically modified DPPF derivatives. The data from these reactions were interpreted in terms of two mechanisms. In the first mechanism, linear aldehydes are formed by alkene insertion into a rhodium-hydrido bond, alkyl migration to a coordinated carbon monoxide (CO insertion) and hydrogenolysis of the resulting rhodium(I) acyl complex. The rate-limiting step varies with the $H_2$/CO pressure. At low $H_2$/CO pressures, hydrogenolysis is the rate-limiting step. At high $H_2$/CO pressures, alkyl migration or CO insertion becomes the rate-limiting step. In the second mechanism, branched aldehydes are formed by essentially the same sequence of steps. The rate-limiting step, however, is alkene insertion into the rhodium-hydrido bond. Alkene insertion is also the step that determines the regioselectivity of the reaction. The data from these reactions suggest that alkene insertion is the rate-limiting step at both high and low $H_2$/CO pressures. Support for both mechanisms is provided by the dependencies of the reactions on the $H_2$/CO pressure. Maximum rates were achieved at a rhodium-to-diphosphine ration of 1:2. From this observation, the authors argue that the three phosphorus atoms are bonded to the rhodium atom of the active catalyst; two of the phosphorus atoms originate from one diphosphine while the third phosphorus atom is part of a diphosphine that bridges to rhodium atoms

together. An explanation is not given for the observed effects of the ancillary ligand electronic properties on the rates and selectivities for the rhodium-catalyzed hydroformylation of 1-alkenes.

The effects of ancillary ligand electronic properties on the rates and yields of rhodium-catalyzed hydroformylations were also examined by Moser and co-workers using in situ IR spectroscopy (Scheme 213).[114]




$PAr_3$ = $P[4\text{-}(NMe_2)\text{-}C_6H_4]_3$, $P(4\text{-}MeO\text{-}C_6H_4)_3$, $PPh_3$, $P(4\text{-}F\text{-}C_6H_4)_3$, $P(4\text{-}Cl\text{-}C_6H_4)_3$, $P[4\text{-}(CF_3)\text{-}C_6H_4)]_3$

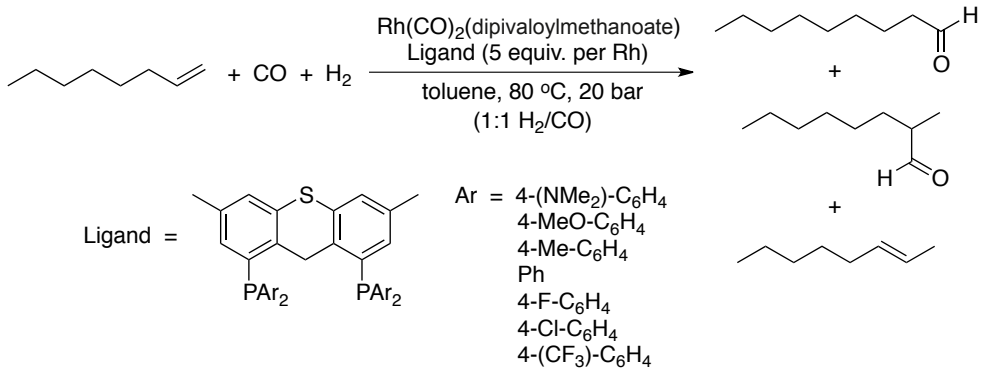
**Scheme 213: Reactions used to study the effects of the electronic properties of the ancillary ligands on the rates and selectivities of rhodium catalyzed hydroformylations with monophosphines.**

In this case, the active catalysts were generated by the reactions of either $Rh_2O_3$ or $Rh_4(CO)_{12}$ with 4 equivalents of $PAr_3$ per rhodium atom in ethane at room temperature and 160 psi (1:1 $H_2$/CO). Catalytic reactions were performed at 200 psi (1:1 $H_2$/CO) and 70 °C. The catalyst resting states were identified as the trigonal bipyramid complexes, $Rh(PAr_3)_2(CO)_2H$. The effects of the electronic properties of the ancillary ligands on the rates for alkene hydroformylation were probed by varying the aryl groups on phosphorus.

To determine the effects of the electronic properties of the ancillary ligands on the electron density at the metal center, the $\nu_{CO}$ stretching frequencies of the $Rh(PAr_3)_2(CO)_2H$ complexes were measured in situ by IR spectroscopy. A linear correlation between the $\nu_{CO}$ stretching frequencies of the rhodium(I) bis(monophosphine) dicarbonyl hydrido complexes and the Hammet σ parameters of the para substituents on the aryl rings of the phosphines was established. Moreover, the data from these reactions indicate that both the linear-to-branched regioselectivity and the catalyst activity increase with decreasing electron-richness of the added triarylphosphines. The data from these reactions are consistent with the observations reported by Unruh and Christenson on the effects of ancillary ligand electronic properties on the rates and selectivities of rhodium-catalyzed hydroformylations using electronically modified DPPF derivatives as ancillary ligands.

The authors note that as the phosphines become less electron-rich, the catalyst resting state shifts from the rhodium(I) bis(monophosphine) dicarbonyl hydrido complexes formed by the reactions of $Rh_4(CO)_{12}$ with $PAr_3$ to rhodium(I) bis(monophosphine) dicarbonyl alkyl complexes formed by alkene insertions into the rhodium-hydrido bonds of $Rh(PAr_3)_2(CO)_2H$. The observations suggest that the rate-limiting step for the hydroformylation of alkenes changes with the electron-richness of the ancillary ligands. These changes, also suggest that the energy barriers for the separate steps of the catalytic cycle are similar. Unruh and Christenson reached a similar conclusion. An explanation for the changes in the linear-to-branched ratios with decreasing electron-richness was not provided.

The effects of ancillary ligand properties on the rates and selectivities of rhodium-catalyzed hydroformylations have also been investigated by van Leeuwen and co-workers (Scheme 214).[115]




**Scheme 214: Reactions used to study the effects of ancillary ligand properties on the rates and selectivities of rhodium-catalyzed hydroformylations.**

In this case, the effects of the electronic properties of the ancillary ligands on the rates and selectivities of rhodium-catalyzed hydroformylations were investigated by performing the reactions with a series of electronically modified Thixantphos ligands. NMR spectra of the corresponding trigonal bipyramid rhodium(I) diphosphine dicarbonyl hydrido complexes suggest that more electron-rich diphosphines prefer an equatorial-axial arrangement of the phosphorus atoms around rhodium. In comparison, less electron-rich diphosphines seem to prefer and equatorial-equatorial arrangement. The two configurations are in dynamic equilibrium. IR spectra collected during the catalytic reactions of these complexes suggest that the two configurations of Rh(diphosphine)$(CO)_2$(H) are the only observable rhodium complexes in solution. The data from these reactions suggest that the rate-limiting step for rhodium-catalyzed hydroformylation is either CO dissociation from Rh(diphosphine)$(CO)_2$(H) or alkene coordination. Evidence supporting rate-limiting alkene coordination is provided by an inverse dependence of rate on CO pressure, a direct dependence of rate on alkene concentration, and an inverse dependence or rate on phosphine basicity.

Hydroformylation reactions with electronically modified Thixantphos-type ligands and 1-octene were conducted at 80 °C and 20 bar with a 1:1 $CO/H_2$ ratio. The catalysts were prepared in situ from the reactions of Rh(dipivaloylmethanoate)$(CO)_2$ and 5 equivalents of ligand. The production of octene isomers (from alkene isomerization), nonanal, and 2-methyloctanal were monitored by gas chromatography. Turnover frequencies were determined at 20 % conversion. The data from these reactions indicate that the rates for the rhodium-catalyzed hydroformylation of 1-octene increase as the basicity of the phosphine decreases. Two exceptions to this trend are the ligands formed with *para*-fluorophenyl and *para*-chlorophenyl groups on phosphorus. Possible explanations for this deviant behavior displayed by the reactions of these diphosphines include incomplete catalyst formation and catalyst deactivation through reactions of the aryl halide groups.

The inverse dependency of the reaction rate on the basicity of the diphosphine may be attributed to an increased rate for CO dissociation from rhodium(I) and an increased rate of alkene association associated with less basic phosphines. A weakening of the rhodium-carbonyl bond in rhodium diphosphine dicarbonyl hydrido complexes with less basic diphosphines is evidenced by an increase in the carbonyl stretching frequencies of these complexes.

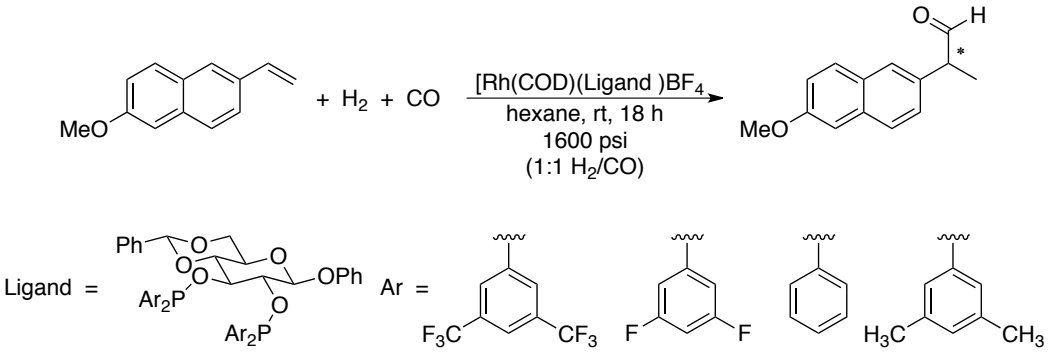
Decreasing the basicity of the phosphine also results in an increase in the linear-to-branched ratio of aldehydes formed by these reactions and an increase in the amount of 2-octene formed by alkene isomerization. The overall amount of linear aldehyde (relative to the amounts of 2-methyl octanal and 2-octene) remains relatively constant. The data from these reactions suggest that the formation of internal alkenes is favored over the formation of branched aldehydes, but that the ratio of linear aldehydes to other products remains constant.

Similar increases in the linear-to-branched selectivities for aldehydes were observed with styrene. In this case, the formation of internal alkenes through alkene isomerization is not possible and consequently the overall selectivity for linear aldehydes relative to all other products also increases.

Increased activities for rhodium-catalyzed hydroformylations with less basic phosphinites were also reported by Bakos and co-workers. [116]

### 3.1.1.7 Asymmetric Hydroformylation Reactions

The effects of the electronic properties of the ancillary ligands on the enantioselectivities of rhodium-catalyzed hydroformylations were investigated by RajanBabu and co-workers (Scheme 215).[117]



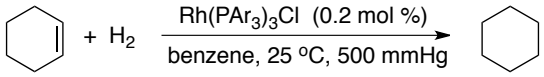

**Scheme 215: Reactions used to study the effects of the electronic properties of the ancillary ligands on the enantioselectivities of rhodium-catalyzed hydroformylations.**

In this case, model reactions were performed in benzene at 60 °C with 2-vinylnaphthalene as the alkene, diphosphinites as the ligands, and $[Rh(COD)_2]BF_4$ as the rhodium source. The effect of the electronic properties of the diphosphinites on the enantioselectivity of the reactions was probed by changing the aryl groups on phosphorus. Reactions performed with phenyl groups on phosphorus resulted in 20 % conversion, 95:5 branched-to-linear selectivity and 10 % ee. Reactions performed with 3,5-bis(trifluoromethyl)phenyl groups on phosphorus, resulted in 43 % conversion, 97:3 branched-to-linear selectivity and 38 % ee. The data from these reactions suggest that less electron-rich ligands promote higher enantioselectivities.

The reactions also show a pronounced solvent effect. Reactions performed in THF, benzene, and hexane under otherwise identical conditions resulted in ee's of 12 %, 38 %, and 51 %. In addition, the enantioselectivities of the reaction are dependent on the $H_2$/CO pressure. An explanation for these trends was not provided. Although the changes in ee's are modest, the data from these reactions suggest that higher ee's are obtained with less basic phosphinites.

### 3.1.1.8 Rhodium-Catalyzed Hydrogenations of Alkenes

The effects of the electronic properties of the ancillary ligand on the rates for rhodium-catalyzed alkene hydrogenations were studied by Wilkinson and co-workers. In this case, rhodium(I) tris(triarylphosphine) complexes were used as catalyst precursors and cyclohexene was used as a model substrate (Scheme 216).[118]




$PAr_3$ = $P(4\text{-MeO-}C_6H_4)_3$, $PPh_3$, $P(4\text{-F-}C_6H_4)_3$

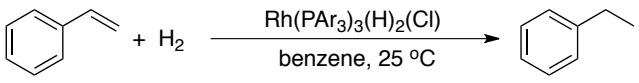
**Scheme 216: Reactions used to study the effects of the electronic properties of the ancillary ligand on the rates for rhodium-catalyzed alkene hydrogenations.**

The reactions were preformed in benzene at 25 °C and 500 Torr of $H_2$. Reactions were monitored by $H_2$ uptake. The mechanism for these reactions was studied previously. The data from these reactions from these studies suggest that the rate-limiting step is substitution of a solvent molecule of on $Rh(PAr_3)_2(H)_2(Cl)$ with alkene to generate $Rh(PAr_3)_2(H)_2(Cl)$(alkene). The identity of the ligand was shown to affect the rates for $H_2$ oxidative addition, ligand dissociation, and alkene coordination. The effects of the electronic properties of the ancillary ligands on the rates for alkene hydrogenation were investigated by applying electronically modified $PPh_3$ ligands to the reaction. The data from these reactions show that changing the aryl groups on the phosphorus ligand from 4-MeO-$C_6H_4$ to $C_6H_5$ to 4-F-$C_6H_4$ changes the observed rate constants from 0.34 $M^{-1}$ $s^{-1}$ to 0.25 $M^{-1}$ $s^{-1}$ to 0.02 $M^{-1}$ $s^{-1}$. The results suggest that more electron-rich aryl phosphines result in faster rates for alkene hydrogenation. The faster rates observed with more electron-rich phosphines were attributed to faster rates for alkene coordination, and faster rates for $H_2$ oxidative addition.

This trend does not extend to aryl alkyl phosphines. Replacement of a phenyl group on $PPh_3$ with and ethyl group resulted in a less active catalyst. In fact, catalyst activity decreases from $PPh_3$ to $PPh_2Et$ to $PPhEt_2$ to $PEt_3$. This decrease in catalyst activity was attributed to greater stabilization of the rhodium(III) dihydrido complex with more electron-rich phosphines and to slower rates for alkene insertion and reductive eliminations. The rate-limiting step in these reactions is thought to involve transfer of the hydrido ligands from $Rh(PAr_3)_2(H)_2(Cl)$ to the alkene. It is not clear from these data whether alkene insertion into the rhodium hydrido bonds is the rate--limiting step in these reactions or whether reductive elimination of the alkane from the hydrido alkyl intermediate is rate-limiting.

### 3.1.1.9 Alkene Insertions into Rhodium-Hydrido Bonds

Halpern and Okamoto studied the effects of ancillary ligand electronic properties on the rates for alkene insertions into rhodium-hydrido bonds (Scheme 217).[119]



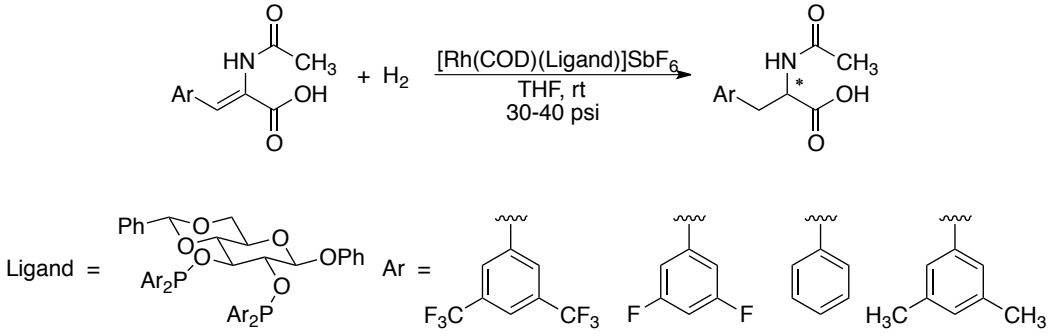

$PAr_3$ = $P(4\text{ClO-}C_6H_4)_3$, $P(4\text{-F-}C_6H_4)_3$, $PPh_3$, $P(4\text{-Me-}C_6H_4)_3$, $P(4\text{-MeO-}C_6H_4)_3$,

**Scheme 217: Reactions used to study the effects of ancillary ligand electronic properties on the rates for alkene insertions into rhodium-hydrido bonds.**

In this case, rhodium(III) hydrido complexes of mono-, tri-arylphosphines are reported. The reactions generate alkanes and rhodium(I) tris(triarylphosphine) chloride complexes. The mechanism for this reaction is thought to involve 1) loss of a phosphine ligand from $Rh(PR_3)_3(H)_2(Cl)$ by a dissociative mechanism and alkene coordination to rhodium 2) alkene insertion into the rhodium-hydrido bond adjacent to the coordinated alkene (*cis* insertion), 3) C-H reductive elimination of alkane from $Rh(PR_3)_2(H)(alkyl)(Cl)$, and 4) coordination of phosphine to the resulting rhodium(I) chloride complex. The reactions were performed under pseudo-first-order conditions in the presence of excess alkene and phosphine. Rate constants for alkene insertion into the rhodium hydrido bonds of $Rh(PR_3)_2(alkene)(H)_2(Cl)$ were determined by plotting the observed rate constants against the phosphine-to-alkene ratio. The electronic properties of the monophosphines were varied by changing the para substituents on the aryl rings. The rates for alkene hydrogenation were measured for the rhodium complexes of P(*p*-Cl-$C_6H_4)_3$, P(*p*-F-$C_6H_4)_3$, $PPh_3$, P(*p*-Me-$C_6H_4)_3$, and P(*p*-MeO-$C_6H_4)_3$. The data from these reactions indicate that the equilibrium constants for phosphine dissociation and alkene coordination reaches a maximum value with $PPh_3$ and decreases as the phosphines become more or less basic. The rates for alkene insertions into the rhodium-hydrido bonds of $Rh(PR_3)_2(alkene)(H)_2(Cl)$ decrease steadily as the monophosphines on rhodium become less basic. The authors suggest that increasing the electron-donating abilities of the phosphine may help stabilize the product of alkene insertion, but do not elaborate on this point. The effect of the electronic properties of the ancillary ligands on the rates for alkene insertions into rhodium-hydrido bonds reported here seem anomalous when compared to the effects of ligand electronic properties on other insertion reactions (vide infra).

### 3.1.1.10 Asymmetric Hydrogenations

The effects of ancillary ligand electronic properties on the rates and enantioselectivities of rhodium catalyzed hydrogenations of amino acid derivatives have been reported by the groups of RajanBabu, and Bakos.[120] In this case, more electron-rich phosphines and phosphinites provide greater enantiomeric excesses and higher catalyst activities than less electron-rich phosphines and phosphinites. A particularly large effect was observed by RajanBabu and co-workers for the hydrogenations of amino acids with glucose derived phosphinites (Scheme 218).[121]



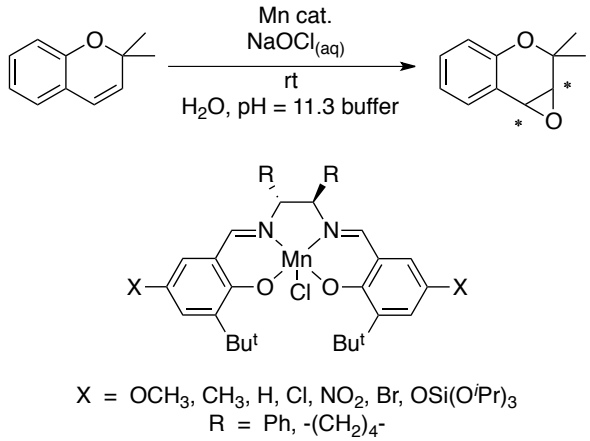

**Scheme 218: Reactions used to study the effects of ancillary ligand electronic properties on the rates and enantioselectivities of rhodium catalyzed hydrogenations of amino acid derivatives.**

The enantiomeric excess of the resulting alkane changed by a factor of 19.4 or from 5 % to 97 % ee upon changing the substitution on the aryl rings of the phosphinite from 3,5-$CF_3$ to 3,5-Me. The origin of this effect was attributed to a disproportionate increase in the rate of $H_2$ oxidative addition to the one of the diastereomers of the

rhodium(I) alkene complexes. This effect was later investigated by Spencer and co-workers, who suggested that the increased enantioselectivities observed with more electron-rich phosphines and phosphinites was due to changes in the regioselectivities of the hydrometallation or insertion step.

### 3.1.1.11 Asymmetric Epoxidations

The electronic properties of the ancillary ligand have also been shown to affect the enantioselectivity of manganese(III)-salen-catalyzed alkene epoxidations (Scheme 219).[122]




**Scheme 219: Reactions used to study the effects of ancillary ligand electronic properties on the enantioselectivities of manganese(III)-salen-catalyzed alkene epoxidations.**

In this case, more electron-rich salen ligands provide higher ee's for the corresponding epoxides than less electron-rich salen ligands. The extent to which the electronic properties of the ligand control the enantioselectivity of the reaction depends on the identity of alkene. In the case of 2,2-dimethylchromene, the enantiomeric excess obtained with a nitro-substituted salen derivative was 22 %, while enantiomeric excess obtained with a methoxy-substituted salen derivative was 96 % ee. A possible explanation for this trend was provided. The greater ee's observed with the more electron-rich salen ligands was attributed to the generation of a less reactive Mn(V)-oxo complex. The lower activity of this complex allows for a later transition state and consequently greater interactions between the alkene substrate and the ligand on the metal catalyst. These interactions between the alkene and metal catalyst ultimately determine the enantioselectivity of the reaction; the greater the interactions, the greater the enantioselectivity.

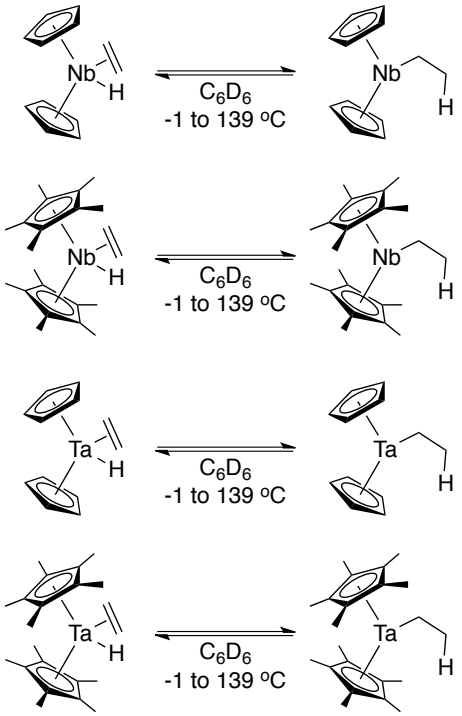
This hypothesis was later investigated through the reactions of *cis*-β-deuteriostyrene.[123] The magnitude of the resulting kinetic isotope effect, due to rehybridization of the carbon-hydrogen bonds from $sp^2$ to $sp^3$, should reflect the position of the transition state along the reaction coordinate. Smaller KIEs correspond to later transition states, while larger KIEs correspond to earlier transition states. Remarkably, the KIEs observed with different salen complexes correlate with both the electron-richness of the salen ligand and the enantioselectivity of the epoxidation reaction. The data from these reactions suggest that more electron-rich salen complexes result in later transition states and higher enantiomeric excesses.

An additional effect of the ligand electronic properties on the epoxidations of alkenes by manganese(III)-salen complexes was observed by the cis/trans ratio of products obtained from the epoxidations of *cis*-β-deuteriostyrene. In this case, smaller cis/trans ratios are thought to arise from longer-lived radical intermediates and

greater cis/trans isomerization. A comparison of the cis/trans ratios obtained with different salen complexes suggests that less-electron-rich complexes result in greater cis/trans ratios and by extension, shorter-lived radical intermediates. The results suggest that both carbon-oxygen bond-forming reactions are accelerated by less electron-rich salen ligands.

### 3.1.1.12 Alkene Insertions into Group V Metal-Hydrido Bonds

An electronic effect on the rates for alkene insertions into Group V metal-hydrido bonds were reported by Bercaw and co-workers for the reactions of Group V metal hydrido alkene complexes.[124] The reactions were performed with niobium and tantalum cyclopentadienyl complexes of styrene, propene, or ethene at temperatures between -1 and 139 °C in benzene-d (Scheme 220).




**Scheme 220: Reactions used to study the effects of ancillary ligand electronic properties on the rates for alkene insertions into Group V metal-hydrido bonds**

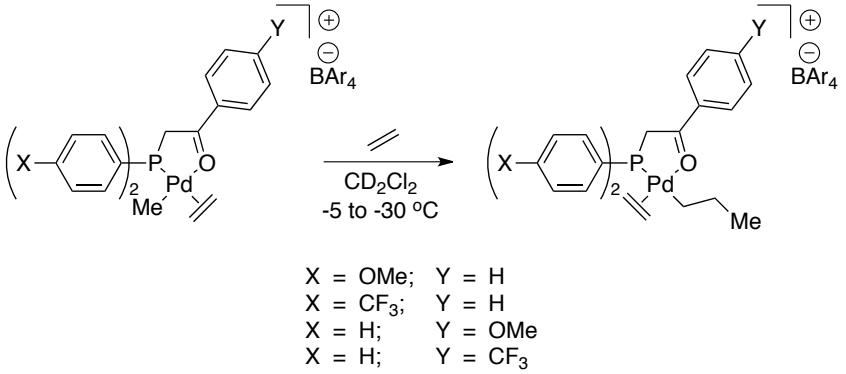
The reactions (alkene insertion) were shown to be reversible. Rates were measured by coalescence and spin magnetization transfer techniques. A comparison of the energy barriers for the insertion of ethene into the niobium(III) and tantalum(III)-hydrido bonds of $Nb(C_5H_5)_2(H)(CH_2CH_2)$, $Nb(C_5Me_5)_2(H)(CH_2CH_2)$, $Ta(C_5H_5)_2(H)(CH_2CH_2)$, and $Ta(C_5Me_5)_2(H)(CH_2CH_2)$ shows that $Nb(C_5H_5)_2(H)(CH_2CH_2)$ has the lowest barrier ($\Delta G^{\ddagger}$ = 17.3 kcal/mol), followed by $Nb(C_5Me_5)_2(H)(CH_2CH_2)$ ($\Delta G^{\ddagger}$ = 18.3 kcal/mol), $Ta(C_5H_5)_2(H)(CH_2CH_2)$ ($\Delta G^{\ddagger}$ = 20.4 kcal/mol), and $Ta(C_5Me_5)_2(H)(CH_2CH_2)$ ($\Delta G^{\ddagger}$ = 21.3 kcal/mol). The data from these reactions suggest that less electron-rich complexes (Nb and $C_5H_5$) react faster than more electron-rich complexes. The authors attribute this trend to greater π-interactions between the metals and the alkenes for more electron-rich complexes. These π-interactions stabilize the ground state of the hydrido alkene complex by strengthening the metal-alkene bonds raise the barrier for alkene insertion. As a result the barriers for alkene insertions into the metal-hydrido bonds of more

electron-rich metal complexes are higher than the barriers for alkene insertions into the metal-hydrido bonds of less electron-rich metal complexes.

Changing the alkene from ethene to propene changes the observed trend in energy barriers. In this case, *endo*-Nb($C_5Me_5$)$_2$(H)($CH_2CHCH_3$) has the lowest energy barrier ($\Delta G^{\ddagger}$ = 14.1 kcal/mol) followed by *endo*-Nb($C_5H_5$)$_2$(H)($CH_2CHCH_3$) ($\Delta G^{\ddagger}$ = 16.5 kcal/mol), *exo*-Nb($C_5H_5$)$_2$(H)($CH_2CHCH_3$) ($\Delta G^{\ddagger}$ = 17.7 - 19.1 kcal/mol), *endo*-Ta($C_5Me_5$)$_2$(H)($CH_2CHCH_3$) ($\Delta G^{\ddagger}$ = 18.1 kcal/mol), *endo*-Ta($C_5H_5$)$_2$(H)($CH_2CHCH_3$) ($\Delta G^{\ddagger}$ = 19.6 kcal/mol), and *exo*-Ta($C_5H_5$)$_2$(H)($CH_2CHCH_3$) ($\Delta G^{\ddagger}$ = 22.8 kcal/mol). The data from these reactions suggest that the steric properties of the pentamethyl cyclopentadienyl ligand relative to the steric properties of the cyclopentadienyl ligand outweigh the electronic differences between these two ligands. The increased steric hindrance of the pentamethyl cyclopentadienyl ligand relative to the cyclopentadienyl ligand is thought to destabilize the ground states of the corresponding hydrido alkene complexes and reduce the barrier for insertion.

### 3.1.1.13 Alkene Insertions into Palladium-Carbon Bonds

Brookhart and Malinoski reported an electronic effect for the insertion of ethene into the palladium-methyl and nickel-methyl bonds of cationic palladium(II) and nickel(II) methyl complexes.[125] In this case the complexes were ligated by electronically modified phenacyldiarylphosphines. The reaction were performed at temperatures between -30 and -5 °C in $CD_2Cl_2$ (Scheme 221).



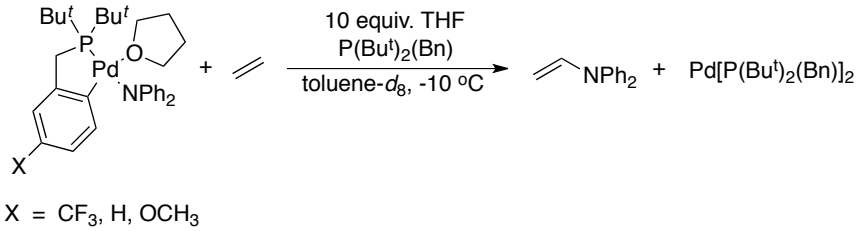

**Scheme 221: Reactions used to study the effects of ancillary ligand electronic properties on the rates for ethene insertions into palladium(II)-methyl bonds.**

The cationic palladium(II) methyl ethene complexes were formed in situ by the addition of ethene to the corresponding cationic palladium(II) methyl ether adducts at -78 °C. The cationic palladium(II) methyl ether adducts, in turn, were synthesized by the addition of NaBAr'$_4$ (Ar' = 3,5-($CF_3$)$_2$-$C_6H_3$)to the appropriate palladium(II) methyl halide complex in $Et_2O$. The rates for ethene insertion were determined by monitoring the loss of the $^1$H NMR signal of the methyl groups on palladium. The effects of the electronic properties of the phenacyldiarylphosphine ligands on the rates for ethene insertion were determined by changing the para substituents on both the phenacyl group and on the aryl rings of the phosphine. Changing the para substituents on the phenacyl group from -OMe to -H to -$CF_3$, changes the barrier for ethene insertion from 20.2 kcal/mol to 19.2 kcal/mol to 18.7 kcal/mol. Changing the aryl groups on phosphorus from 4-MeO-$C_6H_4$ to $C_6H_5$ to 4-$CF_3$-$C_6H_4$, changes the barrier for insertion from 20.3 kcal/mol to 19.2 kcal/mol to 18.2 kcal/mol. The data from these reactions indicate that less electron-rich ancillary ligands promote faster rates for alkene insertions than more electron-rich ancillary ligands.

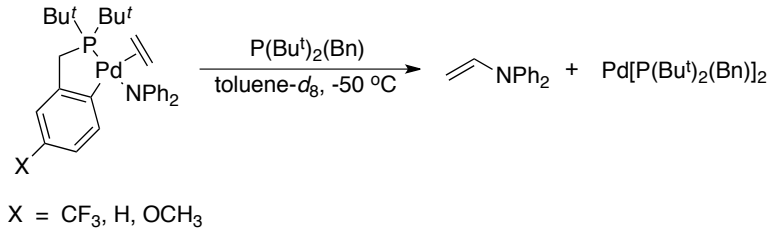
The results are consistent with the general trend that increasing the electrophilicity of the metal decreases the barrier for insertion.

### 3.1.1.14 Alkene Insertions into Palladium-Nitrogen Bonds

Hartwig and Hanley investigated the effects of ancillary ligand electronic properties on the rates for ethene insertions into palladium-amido bonds. The reactions were performed at -50 °C in toluene and followed by $^{31}P$ NMR spectroscopy (Scheme 223).[126]




**Scheme 222: Reactions used to study the effects of ancillary ligand electronic properties on the rates for ethene insertions into palladium(II)-diarylamido bonds.**




**Scheme 223: Reactions used to study the effects of ancillary ligand electronic properties on the rates for ethene insertions into palladium(II)-diarylamido bonds.**

The ligands on palladium were varied from (3-methoxybenzyl) di-*tert*-butyl phosphine to benzyl di-*tert*-butyl phosphine, to [3-(trifluoromethyl)benzyl] di-*tert*-butyl phosphine. The rate constants for these reactions were 3.8 x $10^{-4}$ $s^{-1}$, 8.7 x $10^{-4}$ $s^{-1}$, and 2.6 x $10^{-3}$ $s^{-1}$, respectively. The data from these reactions suggest that the insertion of ethene into the palladium-amido bonds of complexes with less electron-rich ancillary ligands are faster than the insertions of ethene into the palladium-amido bonds of complexes with more electron-rich ancillary ligands. Similar trends have been observed for alkene insertions into metal-carbon bonds.

## 3.1.2 The Effects of Ancillary Ligand Steric Properties on the Rates and Yields of Metal-Mediated Reactions

The steric properties of an ancillary ligand are often gauged or defined by the ligand cone angle, θ. The cone angle was defined by Tolman as the angle of the cone, centered at a point 2.28 Å away from the bonding atoms of the ligand that just encompasses the van der Waals radii of the outermost atoms of the ligand. The cone angle was originally developed to explain deviations between rates and equilibria of ligand substitutions and dissociations and the electronic properties of the ligand. The ligand parameter was originally applied to phosphorus ligands. The idea that the steric properties of the ancillary ligand can affect the outcome of a metal-mediate reaction, however, has generally been accepted for most ligands. Like the effect of the electronic properties of the ancillary ligand on the rates and yields of metal-mediated reactions, the effects of the steric properties of the ancillary ligand on metal-mediated reactions depend largely on the mechanisms of the reactions. Reactions that occur by an associative mechanism are generally favored by smaller ancillary ligands, while reactions that occur by

a dissociative oxidative mechanism are usually favored by larger ancillary ligands. Associative and dissociative mechanisms have been reported for ligand substitutions, oxidative additions, and reductive eliminations. This section examines the effects of the steric properties of the ancillary ligands on various metal-mediate reactions. In general, ligand dissociations, reactions that occur by dissociative mechanisms, reductive eliminations and insertions are favored by larger ancillary ligands, while reactions that occur by an associative mechanism are generally favored by smaller ancillary ligands.

### 3.1.2.1 Ligand Substitution Reactions

Tolman studied the effects of the steric properties of the ancillary ligand on the relative binding affinities of phosphines, phosphinites, phosphonites, and phosphites to nickel(0) complexes (Scheme 224).[127]

$$NiL^1_4 + 4\,L^2 \rightleftharpoons NIL^1_3L^2 + NiL^1_2L^2_2 + NiL^1L^2_3 + NiL^2_4 + L^1$$

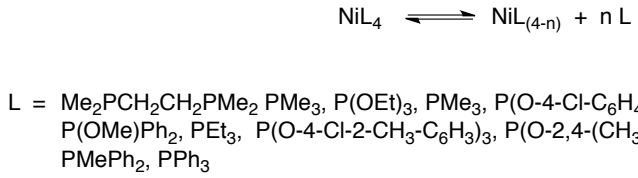
L = $P(Bu^t)_3$, $P(Pr^i)_3$, $PBu_4$, $PEt_3$, $(CH_3)_2PCH_2CH_2P(CH_3)_2$ $PMe_3$, $P(2\text{-}Me\text{-}C_6H_4)_3$, $PPh_2Et$, $PPh_3$, $PPh_2(OEt)$, $PPh(OEt)_2$, $P(OEt)_3$, $P(OMe)_3$, $PMe_2(CF_3)$, $P(OCH_2CH_2Cl)_3$, $P(O\text{-}4\text{-}C_6H_4OMe)_3$, $P(O\text{-}4\text{-}C_6H_4Me)_3$, $P(O\text{-}2\text{-}C_6H_4Me)_3$, $P(OPh)_3$, $P(OCH_2)_3CEt$, $P(OCH_2)_3CMe$, $P(C_6F_5)_3$, $P(OCH_2CCl_3)_3$, $P(O\text{-}4\text{-}C_6H_4CN)_3$

**Scheme 224: Reactions used to study the effects of ancillary ligand steric properties on the rates for ligand dissociation and exchange at nickel(0).**

The reactions were preformed at ambient temperature or at 100 °C with four equivalents each of two different phosphines, phosphinites, phosphinites, or phosphites. The extent to which any ligand replaced another ligand on nickel was determined by $^{31}P$ NMR spectroscopy. The size of the different phosphines, phosphinites, phosphonites, and phosphites were determined by measuring the cone, centered at a point 2.28 Å away from the phosphorus atom that just encompasses the van der Waals radii of the outermost atoms of the ligand. The electronic properties of the ligands were determined by measuring the $\nu_{CO}(A_1)$ stretching frequencies of the nickel(0) tris(carbonyl) complexes, $Ni(CO)_3L$, formed by each ligand. A plot of the relative binding affinities of the ligands as determined by the $^{31}P$ NMR spectra of the reactions, against the $\nu_{CO}(A_1)$ stretching frequencies of the corresponding nickel(0) tris(carbonyl) complexes shows no clear correlation between the electronic properties of the phosphines, phosphinites, phosphonites, and phosphites and their relative binding affinities to nickel(0). In contrast, a plot of the relative binding affinities against the cone angles, θ, of the various ligands shows a much better correlation between the steric properties of the phosphines, phosphinites, phosphonites, and phosphites and their relative binding affinities to nickel(0). The data from these reactions indicate that larger ligands are displaced in preference to smaller ligands. The data from these reactions also suggest that the steric properties of the ligands play a much greater role in determining the binding affinities of the various ligands to nickel(0) than the electronic properties of the ligands. The mechanisms for ligand substitution at tetra-coordinate nickel(0) complexes are expected to be dissociative (based on the 18-electron rule).

### 3.1.2.2 Ligand Dissociations

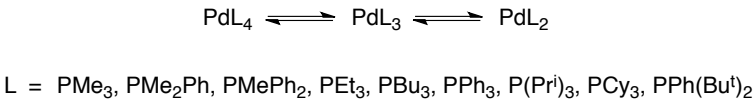
Tolman and co-workers also studied the effect of the steric properties of the ancillary ligand on the rates and equilibria for ligand dissociations from 18-electron nickel(0) complexes (Scheme 225).[128]




**Scheme 225: Reactions used to study the effects of ancillary ligand steric properties on the equilibria for ligand dissociation from nickel(0) complexes.**

In this case, the equilibrium constants for ligand dissociation were greater with more bulky phosphines than with less bulky phosphines. This effect was attributed to the relief of steric strain from the tetra-coordinated nickel(0) complex upon ligand dissociation. The equilibrium constants for these reactions differ by as many as 8 orders of magnitude. The rates for ligand dissociation also increase with increasing steric properties of the ligands.

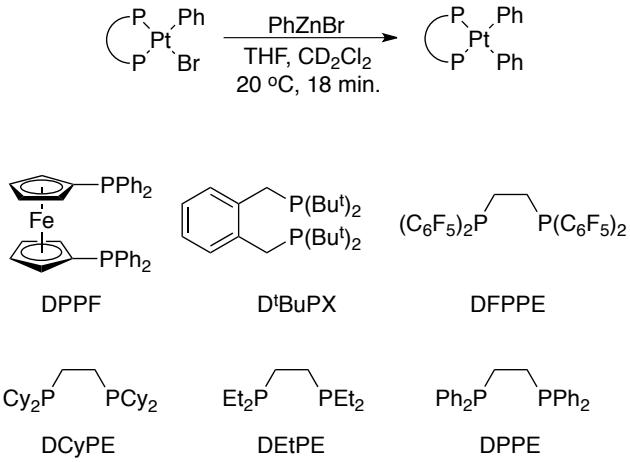
A similar effect was observed by Musco and co-workers for the dissociations of phosphines from tetra-coordinate palladium(0) complexes (Scheme 226).[129]




**Scheme 226: Reactions used to study the effects of ancillary ligand steric properties on the equilibria for ligand dissociation from palladium(0) complexes.**

### 3.1.2.3 Transmetallations

The effects of the steric properties of the ancillary ligands on the yields of platinum(II) diphenyl complexes formed by transmetallation of a phenyl group from PhZnBr to a platinum(II) diphosphine phenyl bromide complex, Pt(diphosphine)(Ph)(Br), was studied by Clarke and Heydt (Scheme 227).[130]




**Scheme 227: Reactions used to study the effects of ancillary ligand steric properties on transmetallations of phenyl zinc bromide to palladium(II) diphosphine phenyl bromide complexes.**

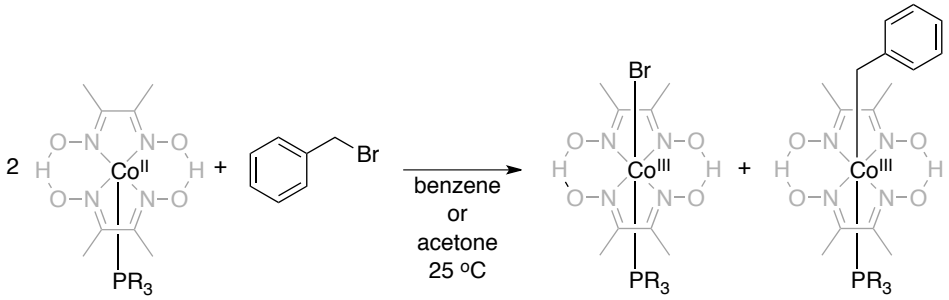
The reactions were performed at room temperature in $CD_2Cl_2$ / THF mixtures using 13 equivalents of PhZnBr per platinum. Platinum complexes were selected because the rate for carbon-carbon reductive elimination is slow and the immediate products from transmetallation, Pt(diphosphine)$(Ph)_2$ could be observed directly. The diphosphines on platinum were varied from DPPE to DEtPE to DCyPE to D(4-F-$C_6H_4$)PE, DPPF, and D$^t$BuPX (D$^t$BuPX = 1,2-bis(di-*tert*-butylphosphino)xylene). Reactions performed with DPPE, DEtPE, D(4-F-$C_6H_4$)PE, and

DPPF as the ancillary ligand resulted in quantitative yields of the corresponding platinum(II) diphenyl complexes in 18 minutes. Reactions performed with DCyPE as the ancillary ligand resulted in 62 % conversion after 18 minutes. Reactions performed with D$^t$BuPX as the ancillary ligand resulted in 0 % conversion after 18 minutes. The data from these reactions suggest that more sterically-hindered diphosphines may slow down or even inhibit transmetallation by preventing interactions between the organometallic reagent and the transition metal complex. In this case, dissociation of a phosphine ligand, which has been proposed as a key step in other transmetallation reactions, is most likely inhibited by chelation. In the absence of chelation, more sterically hindered phosphines are expected to promote phosphine dissociation and consequently enhance the rate of transmetallation. The reactions of platinum(II) phenyl bromide complexes with monophosphine ligands were not reported.

### 3.1.2.4 Oxidative Additions

#### 3.1.2.4.1 Oxidative Additions of Benzyl Halides to Cobalt(II) Complexes

A steric effect for the oxidative addition of benzyl halides to cobalt(II) bis(dioximato) phosphine complexes was reported by Halpern and Phelan (Scheme 228).[131]

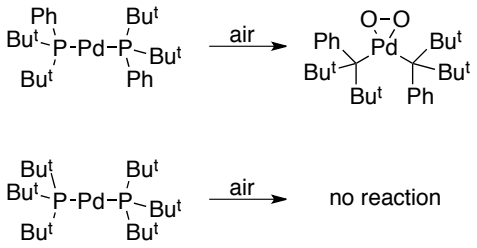



**Scheme 228: Reactions used to study the effects of ancillary ligand steric properties on the oxidative additions of benzyl halides to cobalt(II) bis(dioximato) phosphine complexes.**

In this case, the reactions are thought to occur by a mechanism involving electron transfer from cobalt(II) to the organic halide. The reaction generates a cobalt(III) bis(dioximato) phosphine halide complex and an organic radical, which reacts with a second cobalt(II) bis(dioximato) phosphine complex to generate a cobalt(III) bis(dioximato) phosphine benzyl complex. The reactions were performed at 25 °C in either acetone or benzene with $PMe_3$, $P(^nBu)_3$, $PEt_3$, $PPh_3$, and $PCy_3$ as the ancillary ligands. The rates of the reaction were determined by UV spectroscopy. The rates show a direct correlation to the basicity of the phosphine on cobalt. Specifically, complexes with more basic (or more electron-rich) phosphines react faster than complexes with less basic (or less electron-rich) phosphines. The rates, however deviate from the expected value for more sterically bulky phosphines. The authors attribute this deviation to the steric properties of the ligands. To determine if a correlation exists between the steric properties of the ancillary ligands and the rates for R-X oxidative addition, the authors plotted the log of the rate constants versus the Tolman cone angle, θ, of the phosphine. The plot shows a good correlation between the reaction rate and the cone angle of the ancillary phosphine. The data from these reactions suggest that the complexes of more sterically hindered phosphines react slower than the complexes of less sterically hindered phosphines. The slower rates observed with more sterically hindered phosphines may result from a "lower effective basicity" of the phosphine or from reduced interactions between the cobalt(II) center and the benzyl halide.

### 3.1.2.4.2 Oxidative Additions to Palladium(0) Complexes

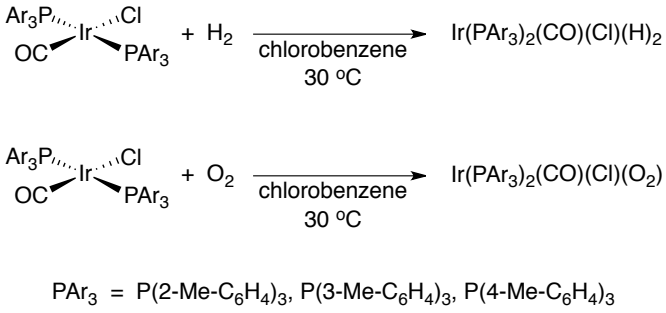
Oxidative addition of $O_2$ to palladium(0) bis(monophosphine) complexes were investigated by Otsuka and co-workers (Scheme 229).[132]




**Scheme 229: Reactions used to study the effects of ancillary ligand steric properties on the oxidative additions of $O_2$ to palladium(0) bis(monophosphine) complexes.**

The reaction of $Pd[P(Ph)(^tBu)_2]_2$ with $O_2$ generates $PdO_2[P(Ph)(^tBu)_2]_2$, while the reaction of $Pd[P(^tBu)_3]_2$ with $O_2$ does not appear to form oxidized products. The stability of $Pd[P(^tBu)_3]_2$ towards oxidation was attributed to the steric properties of $P(^tBu)_3$ relative to $P(Ph)(^tBu)_2$. It is not clear if the added steric bulk of $P(^tBu)_3$ prevents $O_2$ from interacting with the palladium(0) center or simply raises the barrier for oxidative addition by stabilizing the palladium(0) complex.

An effect of the steric properties of the ancillary ligands on the rates and equilibria for $H_2$, $O_2$ additions to iridium(I) bis(monophosphine) carbonyl chloride complexes, was also reported by Vaska and co-workers (Scheme 230).[133]



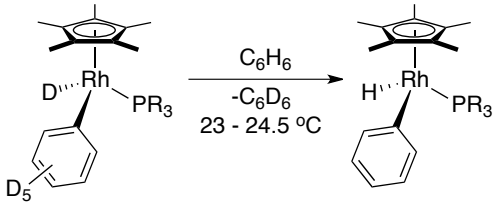

**Scheme 230: Reactions used to study the effects of ancillary ligand steric properties on the oxidative additions of $H_2$ and $O_2$ to iridium(I) bis(monophosphine) chloride carbonyl complexes.**

In this case, the more hindered iridium(I) complex, *trans*-$Ir[P(o\text{-}CH_3\text{-}C_6H_4)_3]_2(Cl)(CO)$ is inert to $H_2$ and $O_2$ while the less hindered iridium(I) complexes, *trans*-$Ir[P(p\text{-}CH_3\text{-}C_6H_4)_3]_2(Cl)(CO)$ and *trans*-$Ir[P(m\text{-}CH_3\text{-}C_6H_4)_3]_2(Cl)(CO)$ react with $H_2$ and $O_2$ to form the corresponding iridium(III) complexes, $Ir[P(p\text{-}CH_3\text{-}C_6H_4)_3]_2(Cl)(CO)(O_2)$ and $Ir[P(m\text{-Tol})_3]_2(Cl)(CO)(H)_2$. the measurements were performed in chlorobenzene at 30 °C. It is unclear whether tris(*ortho*-tolyl)phosphine, $P(o\text{-}CH_3\text{-}C_6H_4)_3$, restricts interactions between the iridium(I) center and $H_2$ and $O_2$ or whether the bulkier ligands destabilize the resulting product and/or transition state of $H_2$ and $O_2$ oxidative addition relative to the ground state of *trans*-$Ir[P(o\text{-}CH_3\text{-}C_6H_4)_3]_2(Cl)(CO)$. Reaction rates were determined by spectrophotometry.

### 3.1.2.5 Reductive Eliminations

#### 3.1.2.5.1 Carbon-Hydrogen Bond Forming Reductive Eliminations From Rhodium(III)

A steric effect for the reductive elimination of $C_6D_6$ from rhodium(III) complexes was reported by Jones and co-workers for the reactions of $Rh(C_5H_5)(PMe_3)(D)(C_6D_5)$, $Rh(C_5H_5)(P^tBuMe_2)(D)(C_6D_5)$, and $Rh(C_5H_5)(P^tBu_2Me)(D)(C_6D_5)$ (Scheme 231).[102]



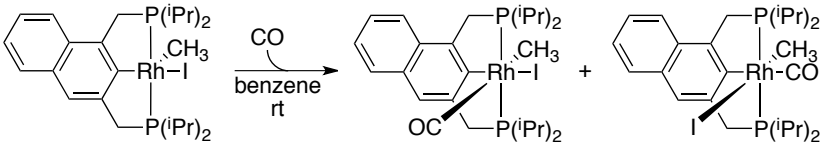

$PR_3$ = $PMe_3$, $PMe_2Ph$, $PMePh_2$, $PPh_3$, $PMe_2(^tBu)$, $PMe_2(^nBu)$, $P(^nBu)_3$

**Scheme 231: Reactions used to study the effects of ancillary ligand steric properties on the reductive eliminations of C6D6 from iridium(III) pentadeuteriophenyl deuteride complexes.**

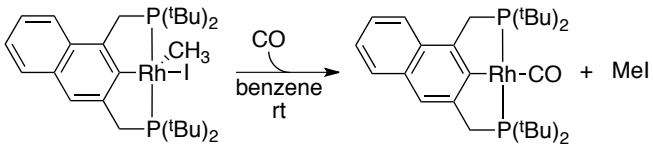
The reactions were performed at temperatures between 23 and 24.5 °C in benzene. The rates for D-$C_5D_5$ reductive elimination were measured by monitoring the rate of ligand exchange with benzene solvent. The rate constants for the reductive elimination of $C_6D_6$ from $Rh(C_5H_5)(PMe_3)(D)(C_6D_5)$ ($\theta_{PMe3}$ = 118 °), $Rh(C_5H_5)(P^tBu_3)(D)(C_6D_5)$ ($\theta_{PMe3}$ = 132 °), and $Rh(C_5H_5)(P^tBuMe_2)(D)(C_6D_5)$ ($\theta_{PMe3}$ = 139 °) are 3.35 x $10^{-7}$ $s^{-1}$, 2.4 x $10^{-6}$ $s^{-1}$, and 6.6 x $10^{-6}$ $s^{-1}$. The data from these reactions suggest that more sterically hindered phosphines promote faster rates for C-D reductive elimination than less sterically hindered phosphines. Inconsistent with this trend, however, is the rate constant for the reductive elimination of $C_6D_6$ from $Rh(C_5H_5)(P^tBu_2Me)(D)(C_6D_5)$ ($\theta_{PMe3}$ = 123 °), which is $k_{obs}$ = 1.25 x $10^{-5}$ $s^{-1}$. It is not clear why the rate constant for this complex does not conform to the general trend. Despite this unexpected result, the authors argue that the rates for C-D reductive elimination increase with increasing steric bulk of the ancillary phosphines.

#### 3.1.2.5.2 Reductive Eliminations of Methyl Iodide from Rhodium(III) PCP Complexes

The reductive elimination of methyl iodide from the rhodium(III) PCP complex, $Rh[C_{10}H_5(CH_2P^tBu_2)_2](Me)(I)$ was reported by Milstein and Frech (Scheme 232 and Scheme 233).[134]




**Scheme 232: Reactions used to study the effects of ancillary ligand steric properties on the reductive eliminations of methyl iodide from rhodium(III) PCP pincer complexes.**

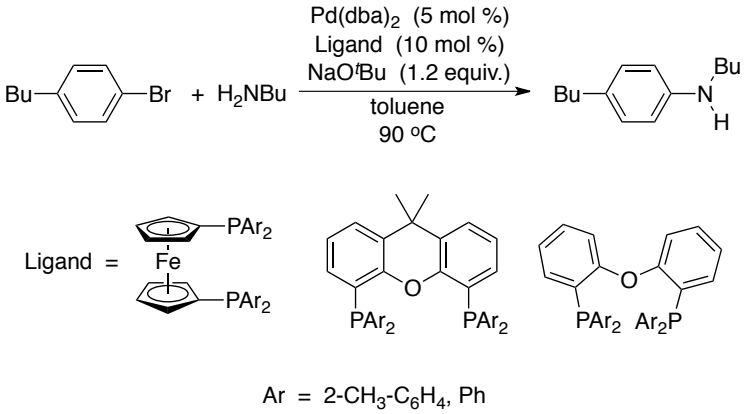



**Scheme 233: Reactions used to study the effects of ancillary ligand steric properties on the reductive eliminations of methyl iodide from rhodium(III) PCP pincer complexes.**

The reaction occurs at room temperature in the presence of 100 equivalents of CO. Reactions between $Rh[C_{10}H_5(CH_2PtBu_2)_2](Me)(I)$ and $CD_3I$ in the absence of CO resulted suggest that MeI reductive elimination is reversible. The addition of CO to the reaction traps the resulting rhodium(I) complex. Significantly, when 100 equivalents of CO were added to the rhodium(III) PCP complex, $Rh[C_{10}H_5(CH_2P^iPr_2)_2](Me)(I)$, CO adducts $Rh[C_{10}H_5(CH_2P^iPr_2)_2](Me)(I)(CO)$ were formed with no signs of MeI reductive elimination. The data from these reactions suggest that the reductive elimination of MeI from rhodium(III) is favored by larger ligands. The rates are unaffected by presence of MeI or $Bu_4NI$ (50 equivalents). Moreover the formation of an $\eta^2$ C-C agostic complex, was shown to be unproductive towards Me-I reductive elimination. The data from these reactions argue against mechanisms involving iodide dissociation and the formation of an $\eta^2$ C-C agostic intermediates. Consequently a mechanism involving concerted reductive elimination of MeI was proposed. Although an explanation of the steric effect was not provided, it is assumed that the formation of a CO adduct of $Rh[C_{10}H_5(CH_2P^tBu_2)_2](Me)(I)$ is unfavorable due to the steric properties of the *tert*-butyl groups on phosphorus. Oxidative addition of MeI to $Rh[C_{10}H_5(CH_2P^tBu_2)_2](CO)$ formed initially by MeI reductive elimination does not occur. In contrast, oxidative addition of MeI to $Rh[C_{10}H_5(CH_2P^iPr_2)_2](CO)$ was demonstrated.

### 3.1.2.5.3 Carbon-Nitrogen Bond Forming Reductive Eliminations from Palladium(II)

The effects of ancillary ligand properties on the yields of amines and arenes generated by a palladium diphosphine catalyzed coupling of amines with aryl halides were investigated by Hartwig and Hamann.[107] Model reactions were performed in toluene at 90 °C using 5 mol % $Pd(dba)_2$, 10 mol % ligand and 1.2 equivalents of $NaO^tBu$. The effects of the steric properties of the ancillary ligands on the yields of aryl amine products were investigated using a series of sterically modified DPPF, Xantphos and DPEphos derivatives (Scheme 234).




**Scheme 234: Reactions used to study the effects of ancillary ligand steric properties on the yields of C-N bond forming reductive eliminations of aryl amines from palladium(II) aryl amido complexes.**

Reactions performed with 1,1'-bis[bis(2-methylphenyl)phosphino]ferrocene (*o*-Tol-DPPF) as the ancillary ligand resulted in a 34 % yield of arene (from protodehalogenation), a 36 % yield of monoarylamine, and a 5.8 % yield of diarylamine. In contrast, reactions performed with DPPF as the ancillary ligand resulted in a 4.4 % yield of arene (from protodehalogenation), a 52 % yield of monoarylamine, and a 22 % yield of diarylamine. The data from these reactions show that changing the aryl groups on DPPF from phenyl to 2-methylphenyl results in a 7.7 -

fold increase in the amount of protodehalogenated products formed and a 1.4 -fold decrease in the amount of monoarylamine formed, and a 3.8 x decrease in the amount of diarylamine formed.

Reactions performed with bis[2-[bis(2-methylphenyl)phosphino]phenyl] ether (*o*-Tol-DPEphos) as the ancillary ligand resulted in a 46 % yield of arene (from protodehalogenation), a 25 % yield of monoaryl amine, and a 2.0 % yield of diaryl amine. Reactions performed with DPEphos as the ancillary ligand resulted in a 40 % yield of arene (from protodehalogenation), a 11 % yield of monoaryl amine, and a 3.6 % yield of diaryl amine. In this case changing the phenyl substituents on DPEphos to *ortho*-tolyl groups resulted in a 1.2x increase in the amount of protodehalogenated products formed, a 2.3x increase in the amount of monoarylamine formed, and a 1.8x decrease in the amount of diarylamine formed.

Reactions performed with 9,9-dimethyl-4,5-bis[bis(2-methylphenyl)phosphine]xanthene (*o*-Tol-Xantphos) as the ancillary ligand resulted in a 22 % yield of arene (from protodehalogenation), a35 % yield of monoaryl amine, and a 7.6 % yield of diaryl amine. Reactions performed with DPEphos as the ancillary ligand resulted in a 24 % yield of arene (from protodehalogenation), a 47 % yield of monoaryl amine, and a 7.0 % yield of diaryl amine. In this case changing the phenyl substituents on Xantphos to *ortho*-tolyl groups resulted in a 1.1x decrease in the amount of protodehalogenated products formed, a 1.3x increase in the amount of monoarylamine formed, and a 1.1x increase in the amount of diarylamine formed.

#### 3.1.2.5.4 Carbon-Oxygen Bond Forming Reductive Eliminations from Palladium(II)

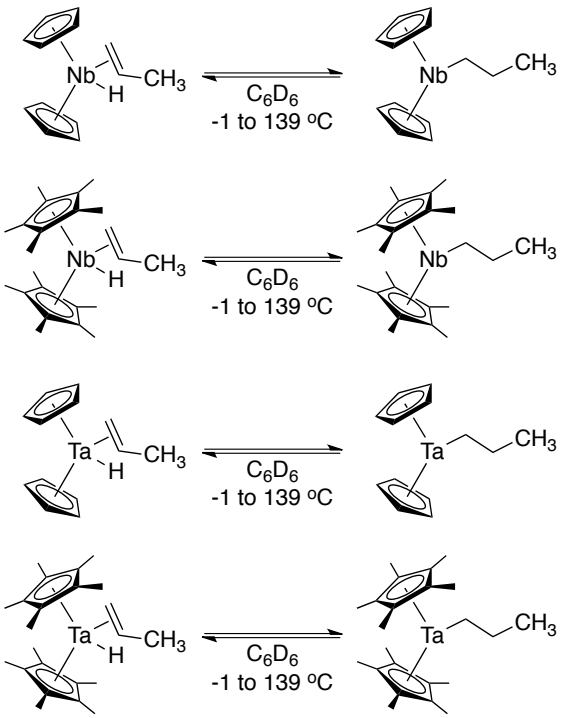
The effects of ancillary ligand properties on the rates for C-O reductive elimination from palladium(II) diphosphine aryl phenoxide complexes were also investigated by Hartwig and co-workers.[109] In this case, the rates for C-O bond formation were measured directly from the reactions isolated palladium(II) diphosphine aryl phenoxide complexes (Scheme 209 and Scheme 210). The half-lives for the reductive eliminations of 4-(3,5-di-*tert*-butylphenoxy)-benzonitrile from Pd(DPPF)($Ar^1$)($OAr^2$) and Pd(D$^t$BuPF)($Ar^1$)($OAr^2$) ($Ar^1$ = *p*-CN-$C_6H_4$; $Ar^2$ = 3,5-($^t$Bu)$_2$-$C_6H_3$; D$^t$BuPF = 1,1'-bis(di-*tert*-butylphosphino)ferrocene) at 50 °C are 2.4 x $10^5$ s and 2.4 x $10^3$ s. The data from these reactions indicate that the rates for C-O reductive elimination from palladium(II) is significantly affected by the steric properties of the ancillary ligand. In comparison, the effect of the electronic properties of the ancillary ligand on the rates for C-O reductive elimination are relatively small.

#### 3.1.2.5.5 Carbon-Sulfur Bond Forming Reductive Eliminations from Palladium(II)

A steric effect was also reported for the reductive eliminations of thioethers from palladium(II) aryl and alkyl sulfide complexes. In this case, however, the steric properties of the reacting ligands were varied. The results show that sterically more encumbered aryl groups on palladium result in faster rates for carbon-sulfur reductive elimination than sterically less encumbered aryl groups. The data from these reactions fit the general trend that reductive eliminations are favored by larger ligands.

### 3.1.2.6 Alkene Insertions into Group V Metal-Hydrido Bonds

Bercaw and co-workers reported a steric effect for insertions of propene into Group V metal-hydrido bonds (Scheme 235).[124]

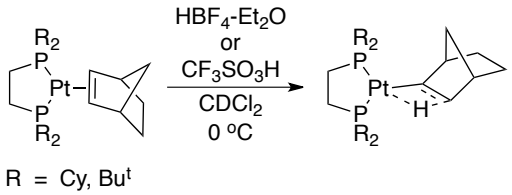



**Scheme 235: Reactions used to study the effects of ancillary ligand steric properties on the insertions of propene into Group V metal-hydrido bonds.**

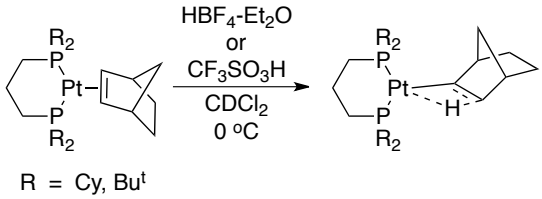
These reactions were discussed in Section 3.1.1.12. The activation barrier for the insertion of propene into the niobium-hydrido bond of $Nb(Cp^*)_2(CH_2CHCH_3)(H)$ is 14.1 kcal/mol. In contrast, he activation barrier for the insertion of propene into the niobium-hydrido bond of $Nb(Cp)_2(CH_2CHCH_3)(H)$ is 16.5 kcal/mol. The data from these reactions suggest alkene insertions into Group V metal-hydrido bonds are faster with more sterically hindered ancillary ligands on the metal than with less sterically hindered ancillary ligands. Similar results were observed for the insertions of propene into the tantalum-hydrido bonds of $Ta(Cp^*)_2(CH_2CHCH_3)(H)$ ($\Delta G^{\ddagger}$ = 18.1 kcal/mol) and $Ta(Cp)_2(CH_2CHCH_3)(H)$ ($\Delta G^{\ddagger}$ = 19.6 kcal/mol). An opposite effect is observed for the insertions of ethene into the niobium- and tantalum-hydrido bonds of $Nb(Cp^*)_2(CH_2CH_2)(H)$ ($\Delta G^{\ddagger}$ = 18.3 kcal/mol), $Nb(Cp)_2(CH_2CH_2)(H)$ ($\Delta G^{\ddagger}$ = 17.3 kcal/mol), $Ta(Cp^*)_2(CH_2CH_2)(H)$ ($\Delta G^{\ddagger}$ = 21.3 kcal/mol) and $Ta(Cp)_2(CH_2CH_2)(H)$ ($\Delta G^{\ddagger}$ = 20.4 kcal/mol). In this case, less bulky ligands promote faster rates for alkene insertion than more bulky ligands. The data from these reactions suggest that the steric effect is sensitive to the identity of the alkene, and that small changes in structure can lead to significant changes in the observed trends.

### 3.1.2.7 Alkene Insertions into Platinum-Hydrido Bonds

A steric effect on the insertions of alkenes into platinum-hydrido bonds was proposed by the groups of Orpen and Spencer for a series of cationic platinum(II) diphosphine complexes.[135] The complexes were generated by the reactions for $HBF_4 \bullet OEt_2$ and $CF_3SO_3H$ with platinum(0) diphosphine norbornene complexes (Scheme 236 and Scheme 237).




**Scheme 236: Reactions used to study the effects of ancillary ligand steric properties on the insertions of on the insertions of alkenes into platinum(II)-hydrido bonds.**

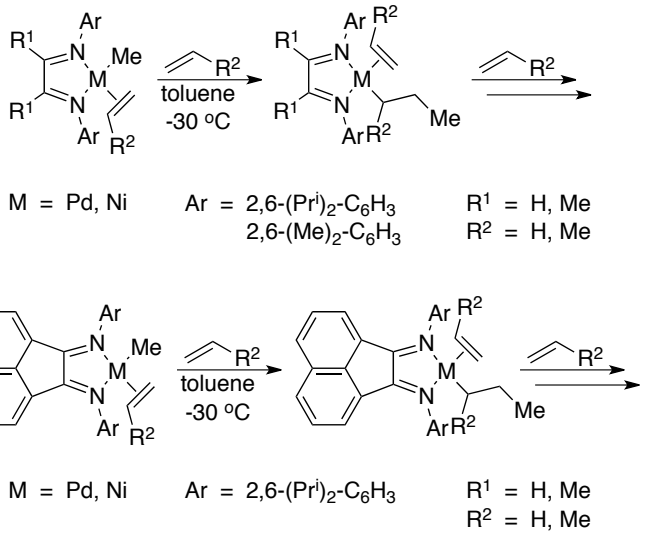



**Scheme 237: Reactions used to study the effects of ancillary ligand steric properties on the insertions of on the insertions of alkenes into platinum(II)-hydrido bonds.**

The $J^{Pt-H}$, $J^{Pt-P}$, and $J^{P-H}$ coupling constants of the resulting platinum(II) diphosphine alkyl complexes suggest a β-agostic interaction and gradual change in the platinum alkyl character towards a hydrido alkene complex. The steric properties of the diphosphines were varied by changing the alkyl groups on phosphorus from cyclohexyl to *tert*-butyl. Changing the R groups on $R_2PCH_2CH_2PR_2$ from cyclohexyl to *tert*-butyl changes the $J^{Pt-H}$ and $J^{Pt-P}$ coupling constants from 324 Hz to 136 Hz and from 3866 Hz to 4909 Hz. Changing the R groups on $R_2PCH_2CH_2CH_2PR_2$ from cyclohexyl to *tert*-butyl changes the $J^{Pt-H}$ and $J^{Pt-P}$ coupling constants from 102 Hz to 85 Hz and from4852 Hz to 5067 Hz. The data from these reactions suggest that the platinum(II) complexes with cyclohexyl groups on phosphorus have greater hydridic character (greater $J^{Pt-H}$ coupling constants and smaller $J^{Pt-P}$ coupling constants) than the platinum(II) complexes with *tert*-butyl groups on phosphorus. By extension of these observations, the authors suggest that the barriers for alkene insertions into the platinum-hydrido bonds of complexes having less bulky ancillary ligands are higher than the barriers for alkene insertions into the platinum-hydrido bonds of complexes having more bulky ancillary ligands. A bite angle effect is also observed from this data and is discussed in Section 2.1.13.1.3.14.

### 3.1.2.8 Late Transition Metal-Catalyzed Alkene Polymerizations

Brookhart and co-workers reported a steric effect for palladium- and nickel-catalyzed polymerizations of alkenes (Scheme 238).[136]



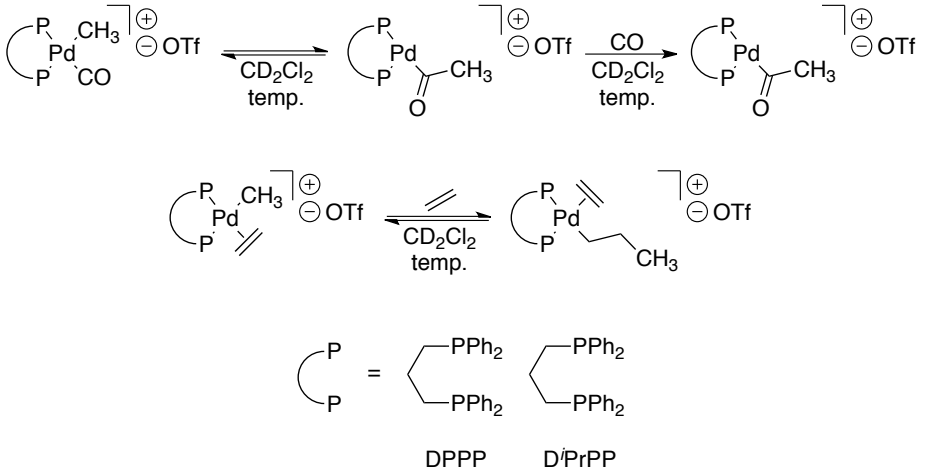

**Scheme 238: Reactions used to study the effects of ancillary ligand steric properties on palladium- and nickel-catalyzed polymerizations reactions.**

The catalysts in these reactions were generated by the reactions of the nickel- and palladium(II) N-aryl diimine dimethyl complexes with $HBF_4$•$OEt_2$ or by treatment of the nickel(II) N-aryl diimine dimethyl dibromide complex with 1000 equivalents of methyl aluminoxane (MAO). The complexes were formed at -78 °C. Polymerizations were monitored at -30 °C. The catalysts are some of the most active late transition metal catalysts for the polymerizations of alkenes.

The effects of the steric properties of the ancillary ligands on the properties of the resulting polymers were investigated by varying the *ortho* substituents on the aryl rings of the *N*-aryl diimines. The data from these reactions show that changing the *ortho* substituents from methyl groups to isopropyl groups increases the molecular weight of the resulting polymer from 11 x $10^4$ g/mol to 39 x $10^4$ g/mol, and changes the number of branches per 1000 carbons from 1.2 to 74. The trends were interpreted in terms of a mechanism in which β-hydride elimination from a metal(II) alkyl intermediate results in a metal(II) hydrido alkene complex which can either re-insert the alkene with opposite regiochemistry to form a branched point or undergo associative substitution with an alkene monomer to terminate propagation and start a new polymer chain (this series of reactions is often termed chain transfer). The presence of bulky substituents on the aryl rings of the diimine ligands is thought to restrict associative substitution of the long chain alkene with incoming monomer, and as a result, promote the formation of higher molecular weight polymers with a higher degree of branching.

These systems were later investigated by DFT and molecular mechanics studies.[137] The results from these calculations support the hypothesis proposed by Brookhart and suggest that bulky ligands on nickel also promote faster rates for alkene insertions into nickel-carbon bonds by destabilizing the nickel(II) alkyl alkene complexes.

A steric effect was also reported by reported by Brookhart and co-workers for ethene and CO insertions into palladium-methyl bonds (Scheme 239).[138]




**Scheme 239: Reactions used to study the effects of ancillary ligand steric properties on the insertions of ethene into palladium(II)-acyl and palladium(II)-methyl bonds.**

In this case, the effects of the steric properties of the ancillary ligands on the rates for CO insertion were determined by varying the substituents on phosphorus atoms of the diphosphine on palladium. Reactions performed with DPPP as the ancillary ligand displayed a 14.8 kcal/mol barrier for CO insertion, while reactions performed with D$^{i}$PrPP as the ancillary ligand displayed a 14.1 kcal/mol barrier for CO insertion. The data from these reactions suggest that more bulky ligand promote lower barriers and faster rates for CO insertion than less bulky ligands. The effects of the electronic properties on the rates for CO insertions into palladium-carbon bonds suggest that the more electron-rich ligand, D$^{i}$PrPP, should react slower than the less electron-rich ligand, DPPP. Consequently, the faster rates for CO insertion into the palladium-methyl bonds of [Pd(D$^{i}$PrPP)(Me)(OEt$_2$)]BF$_4$ relative to [Pd(DPPP)(Me)(OEt$_2$)]BF$_4$ suggests that the steric properties of the diphosphine play a bigger role in determining the rate of the reaction than the electronic properties of the diphosphine, in this instance. The rates for CO insertion measured at - 82 °C in $CD_2Cl_2$. The lower barriers for CO insertion.

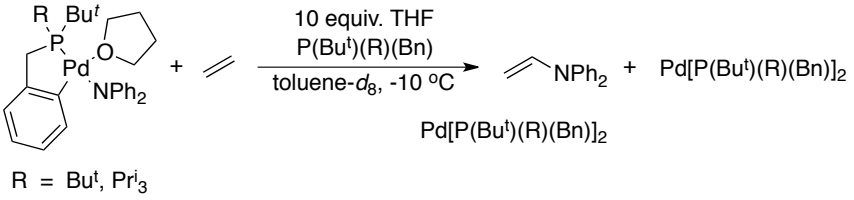
The effect of the steric properties of the ancillary ligands on the rates for ethene insertions into palladium-methyl bonds was also reported by Brookhart and co-workers. In this case, the energy barrier for ethene insertion into the palladium-methyl bond of [Pd(DPPP)(Me)($C_2H_4$)]BF$_4$ is 16.6 kcal/mol, while the barrier for ethene insertion into the palladium-methyl bond of [Pd(D$^{i}$PrPP)(Me)($C_2H_4$)]BF$_4$ is 16.5 kcal/mol. The relatively small change in the energy barrier upon changing the ancillary ligand from DPPP to D$^{i}$PrPP was attributed to a slight relief of steric strain or energy upon ethene insertion. The smaller steric effect observed for insertion so ethene into palladium-methyl bonds versus insertions of CO into palladium-methyl bonds was attributed to the size of the ethene molecule and its relative orientation in the transition state for insertion. For alkene insertions into metal-ligand bonds, the alkene has to rotate into the square plane of the palladium(II) complex. The transition state for alkene insertion consequently resembles a metallocyclobutane complex. In contrast, the transition state for CO insertion resembles a metallocyclopropane complex. The differences in the sizes of these two transition state structures suggests that greater steric relief occurs upon CO insertion since the metallocyclopropane structure is smaller than the metallocyclobutane structure. Consequently, the effects of the steric properties of the ancillary ligands on the rates

for CO insertions into palladium-methyl bonds are greater than the effects of the steric properties of the ancillary ligands on the rates for ethene insertions into palladium-methyl bonds.

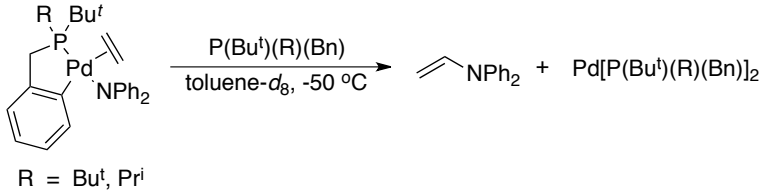
Changing the steric properties of the ancillary ligand also changed the resting state for alkene polymerization. The catalyst resting state for ethene polymerization by $[Pd(DPPP)(Me)(OEt_2)]BF_4$ is a cationic palladium(II) alkyl alkene complex. The catalyst resting state for the polymerization of ethene with $[Pd(D^iPrPP)(Me)(OEt_2)]BF_4$ is a cationic a palladium(II) β-agostic alkyl complex. In this case, the larger steric properties of the DiPrPP ligand relative to the DPPP ligand stabilize the β-agostic alkyl complex relative to the palladium(II) alkyl alkene complex or destabilizes the palladium(II) alkyl alkene relative to the β-agostic alkyl complex. In either case, alkene coordination to the palladium(II) alkyl complex of $D^iPrPP$ is not observed, suggesting that the rate-limiting step has changed from alkene insertion to alkene coordination.

### 3.1.2.9 Alkene Insertions into Palladium-Amido Bonds

The effects of the steric properties of the ancillary ligand steric properties on the rates for ethene insertions into palladium-amido bonds were reported by Hartwig and Hanley (Scheme 240 and Scheme 241).[126]




**Scheme 240: Reactions used to study the effects of ancillary ligand steric properties on the insertions of ethene into palladium(II)-diarylamido bonds.**




**Scheme 241: Reactions used to study the effects of ancillary ligand steric properties on the insertions of ethene into palladium(II)-diarylamido bonds.**

The reactions were conducted at -50 °C in toluene at high ethene concentrations. The high concentrations of ethene were required to ensure that most of the palladium in the solution existed as the palladium(II) ethene amido complex and not as other complexes in equilibrium with the palladium(II) ethene amido complex. The ligands on palladium were cyclometallated benzyl di-*tert*-butylphosphine and cyclometallated benzyl *tert*-butyl isopropyl phosphine. The rate constants for the reactions of these two complexes at -50 °C were 8.7 x $10^{-4}$ $s^{-1}$ and 0.97 x $10^{-4}$ $s^{-1}$, respectively. The results suggest that more sterically hindered phosphines promote faster rates for alkene insertions into palladium-amido bonds than less sterically hindered phosphines. DFT calculations performed on these same reactions support this trend.

Reactions performed with THF-ligated palladium(II) amido complexes of benzyl di-*tert*-butylphosphine and benzyl *tert*-butyl isopropyl phosphine resulted in similar rate constants (4.6 x 10-4 $s^{-1}$ and 5.3 x 10-4 $s^{-1}$). The reactions were conducted at -10 °C. Equilibrium constants for the binding of THF and ethene to the palladium(II) complexes of benzyl di-*tert*-butylphosphine and benzyl *tert*-butyl isopropyl phosphine were measured at 22 °C and -

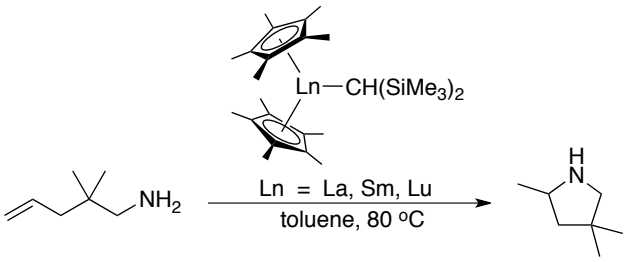
65 °C, respectively. The equilibrium constant for the binding of THF to the palladium(II) complex of benzyl di-*tert*-butylphosphine at 22 °C is 6.8 $M^{-1}$. The equilibrium constant for the binding of THF to the palladium(II) complex of benzyl *tert*-butyl isopropyl phosphine at 22 °C is 14 $M^{-1}$. The equilibrium constant for the binding of ethene to the palladium(II) complex of benzyl di-*tert*-butylphosphine at -65 °C is 11 $M^{-1}$. The equilibrium constant for the binding of THF to the palladium(II) complex of benzyl *tert*-butyl isopropyl phosphine at -65 °C is 149 $M^{-1}$. The data from these reactions suggest that while the more hindered phosphine promotes faster rates for alkene insertion into palladium-amido bonds, it also hinders the formation of the palladium(II) ethene amido complex to a greater extent than the less sterically hindered phosphine. The combined effects explain the similar rate constants observed for the reactions of the THF-ligated palladium(II) amido complexes.

The data from these reactions also demonstrate a steric effect on the equilibrium constants for THF substitution with ethene. In this case, ethene coordination to palladium and THF substation are favored by less sterically hindered phosphines. The data from these reactions are consistent with an associative mechanism for substitution.

### 3.1.2.10 Rare Earth Metal-Catalyzed Hydroaminations

An effect of the ancillary ligand steric properties on the rates for rare earth metal-catalyzed hydroaminations was reported by Marks and co-workers (Scheme 242 and Scheme 243).[2b] Rare earth metal complexes with larger ionic radii and less sterically demanding ancillary ligands provided higher turnover frequencies than rare earth metal complexes with smaller ionic radii and more sterically demanding ancillary ligands.

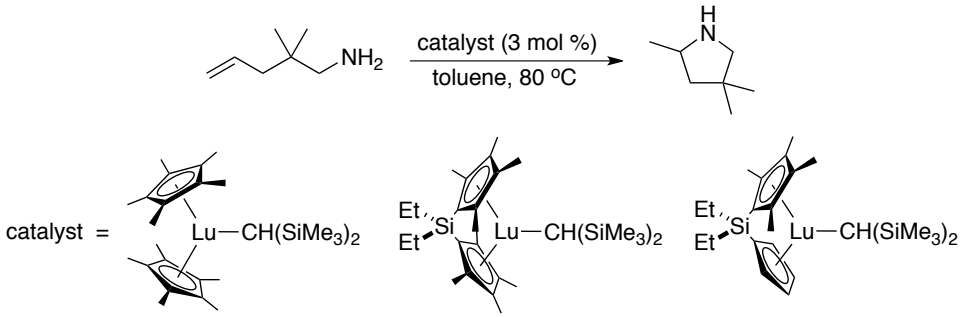
Cyclization of 2,2-dimethyl-aminopent-4-ene occurs at 25 °C with a bis(pentamethylcyclopentadienyl) lanthanum(III) catalyst at a rate of 95 turnovers per hour. The ionic radius of the lanthanum(III) is 1.106 Å. Cyclization of 2,2-dimethyl-aminopent-4-ene with a bis(pentamethylcyclopentadienyl) samarium(III) catalyst occurs at 60 °C, with a turnover rate of 48 turnovers per hour. The ionic radius of samarium(III) is 1.079 Å. Cyclization of 2,2-dimethyl-aminopent-4-ene with a bis(pentamethylcyclopentadienyl) lutetium(III) catalyst occurs at 60 °C, with a turnover rate of 48 turnovers per hour. The ionic radius of lutetium(III) is 0.977 Å. Reactions were performed in toluene-$d_8$.




**Scheme 242: Rare earth metal-catalyzed hydroaminations.**

The turnover frequencies span for the different metal complexes span three orders of magnitude. The metal complexes with larger ionic radii are thought to be less sterically congested and consequently more compliant with sterically demanding transition states. It is unclear how the steric properties of the ancillary ligand affect the rates for alkene hydroamination.

Larger ancillary ligands have also been shown to decrease the turnover frequencies for rare earth metal-catalyzed hydroaminations of amino alkenes (Scheme 243).




**Scheme 243: Reactions used to study the effects of ancillary ligand steric properties on the turnover frequencies for rare earth metal-catalyzed hydroaminations.**

The turnover frequency for the cyclization of 2,2-dimethyl-aminopent-4-ene with a bis(pentamethylcyclopentadienyl) lutetium(III) catalyst is less than 1 turnover per hour at 80 °C. The turnover frequency for the cyclization of 2,2-dimethyl-aminopent-4-ene with a diethyl silyl-linked *ansa*-bis(pentamethylcyclopentadienyl) lutetium(III) catalyst is 75 turnovers per hour (at 80 °C), and the turnover frequency for the cyclization of 2,2-dimethyl-aminopent-4-ene with a diethyl silyl-linked *ansa*-cyclopentadienyl, pentamethylcyclopentadienyl lutetium(III) catalyst is 200 turnovers per hour at 80 °C. The origin of this effect is uncertain, but is most likely related to the effect of the ionic size on the turnover frequencies. Larger ancillary ligands result in more congested metal centers and restrict sterically demanding transition states. An opposite effect is observed for the cyclization of amino alkynes. Rare earth metal complexes with smaller ionic radii promote higher turnover frequencies than rare earth metal complexes with larger ionic radii.

### 3.1.3 The Effects of Ligand Bite Angles on the Rates and Yields of Metal-Mediated Reactions

Ligand bite angles are a third parameter used to describe ligand properties. Bite angles are defined as the angle subtended by the two donor atom-metal bonds of a bidentate ligand. Bite angles are a geometric property. For any give ligand, the observed bite angle can vary for different metal complexes of the same bidentate ligand. This variation results from the flexibility of the ligand backbone and is often caused by variations in the identity or oxidation state of the metal and/or the presence of different groups coordinated to the metal center.

In order to separate the "preferred" bite angle of a ligand from the actual bite angle of a ligand observed in a metal complex, Casey and Whiteker developed the concept of the "natural bite angle." The natural bite is the geometry adopted by a bidentate ligand in the absence of steric and electronic influences. Natural bite angles are calculated by molecular mechanics. Since then, good correlations between the natural bite angle and the reactivities of metal complexes have been observed. Ligand bite angles, for example, have been linked to linear-to-branched selectivities in rhodium-catalyzed hydroformylations and in palladium-catalyzed allylic substitutions, and to faster rates and higher yields in nickel catalyzed hydrocyanations. Ligand bite angles have also been linked to the rates of simple organometallic reactions such as reductive eliminations and carbon monoxide insertions, and to the acid and base properties of metal hydrides.

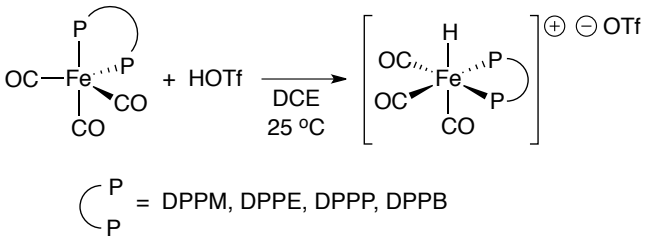
To explain these effects, van Leeuwen and co-workers developed the concepts of "steric bite angle effects" and "electronic bite angle effects." The steric bite angle effect is thought to arise from an increase in the effective bulk of a bidentate ligand (as suggested by the larger effective cone angle) that occurs increasing bite angle. Larger bite angles result in greater "embracement" of the metal center, which, in turn, decrease the space available for other ligands to coordinate. This decrease in space can result in increased ligand-ligand and ligand-substrate interactions, which can cause the reaction to change course. A steric bite angle effect is thought to account for the increased selectivities for linear aldehydes observed with ligands having larger bite angles in rhodium-diphosphine catalyzed hydroformylation of alkenes. In this case, greater steric constraints placed on the metal by diphosphines with larger bite angles result in destabilization of the branched rhodium alkyl intermediates in favor of linear ones. Steric bite angle effects may also contribute to the selectivities of palladium catalyzed CO/ethene copolymerizations and allylic alkylations.

By comparison, the electronic bite angle effect is attributed to differences between the electronically preferred geometry of a metal complex or transition state and the geometry imposed on it by the bite angle of the bidentate ligand coordinated to the metal. These differences can either stabilize or destabilize an intermediate or transition state. For complexes formed strictly from monodentate ligands, the angles between the metal-ligand bonds (and hence the geometry of the complex) are determined by the identity of the metal, its oxidation state, and the steric and electronic properties of the ligands surrounding it. For metal complexes formed with at least one bidentate ligand, the angles between the metal-ligand bonds are still determined by the identity of the metal, its oxidation state, and the ligands surrounding, but are also influenced by the size and geometry of the metal chelate and the ability of the chelate to adapt to differing steric or electronic demands (its flexibility). The electronically preferred geometry of a metal complex is usually inferred from the geometry adopted by the metal when only monodentate ligands are present on the metal and the donor atoms of the ligands are the same. When this geometry differs from the geometry of the metal complex imparted by bidentate ligands, an electronic bite angle effect is inferred. The effects of ligand bite angles on the rates for carbon-carbon reductive eliminations and the hydricities of palladium(II) hydrides are both considered to be electronic bite angle effects.

The present section examines a few of the reactions in which bite angle effects are observed. More comprehensive reviews have also been written.[139]

#### 3.1.3.1 Metal Basicities

The effects of ligand bite angles on the basicities of iron(0) diphosphine carbonyl complexes was investigated by Angelici and co-workers (Scheme 244).[140] The reactions were performed in 1,2-dichloroethane at 25 °C using $CF_3SO_3H$ as the protonating agent. The basicities of the metal complexes were determined by measuring the heats of protonation through calorimetry. The effect of the ligand bite angle on the heats of protonation was determined by varying the diphosphine on iron from DPPM to DPPE to DPPP to DPPB.




**Scheme 244: Reactions used to study the effects of ancillary ligand bite angle on the basicities of iron tris(carbonyl) diphosphine complexes.**

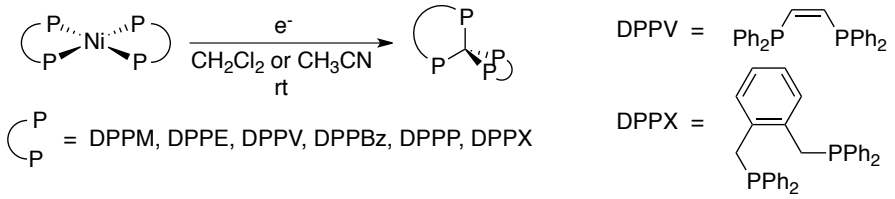
The data from these reactions indicate that diphosphines with smaller bite angles generate more basic metal centers than diphosphines with larger bite angles. The heat of protonation for $Ir(DPPM)(CO)_3$ is -24.0 kcal/mol. The heat of protonation for $Ir(DPPB)(CO)_3$ is -20.1 kcal/mol. The differences span 4 kcal/mol. The protonated metal complexes were characterized by IR and NMR spectroscopy. A fac geometry was assigned to the resulting iron complexes based on their IR spectra. In each case, $^1H$ NMR spectra revealed only one hydride resonance consistent with only one isomer being present. The protonated metal complexes were not isolated.

The trend in the heats of protonation of the metal complexes, does not follow the trend for $\Delta H_{HP}$ the heats of protonation of the free phosphines; the most basic phosphine is DPPB generates the least basic metal complex and vice versa. With monodentate phosphines, the basicity of the phosphine is usually reflected by the basicity of the metal (see Tolman, Section 3.1.1.3.1). The differences in the trend observed in the present system with diphosphines and the trends generally observed with monophosphines was attributed to distortions of the metal complex away from an electronically preferred geometry through chelation of the diphosphine. For monodentate phosphines, the preferred geometry is trigonal bipyramid for $Fe(CO)_3(PR_3)_2$ and octahedral for $FeH(CO)_3(PR_3)_2$. In both cases, the two phosphines occupy positions trans to each other. With DPPM, DPPE, DPPP, and DPPB as the ligands on iron, the two phosphorus atoms occupy positions cis to each other. The authors suggest that chelation forces the metal complex to occupy a less stable geometry. The heat of protonation for *trans*-$Fe(CO)_3[Ph_2P(CH_2)_nPPh_2]$ is -17.6 kcal/mol, lower than any value obtained with DPPM, DPPE, DPPP, and DPPB as the ancillary ligand.

X-ray structures of several $Fe(DPPM)(CO)_3$ and $Fe(DPPE)(CO)_3$ reveal substantial differences in the P-Fe-P bite angle. The P-Fe-P bite angle observed with DPPM as the diphosphine is 73.5°. The bite angle P-Fe-P bite angle observed with DPPE as the diphosphine is 84.1° Extended Hückel MO calculations for $d^8$ $ML_5$ systems support the hypothesis that the basicity varies with the geometry of the metal complex. The hypothesis that the basicity varies with the geometry of the metal complex conclusion is also supported by thermochemical data, which shows that the heat of formation for $Mo(CO)_4[Ph_2P(CH_2)PPh_2]$ is ~ 6 kcal/mol higher than the heat of formation for *cis*-$Mo(CO)_4(Ph_2PMe)_2$; this destabilization was attributed to ring strain in the chelate complex.

### 3.1.3.2 Nickel(II)/(I) Redox Potentials

DuBois and co-workers investigated the effects of ligand bite angles on the Ni(II)/Ni(I) redox potentials of nickel(I) bis(diphosphine) complexes, $[Ni(diphosphine)_2](BF_4)_2$ (Scheme 245).[141]

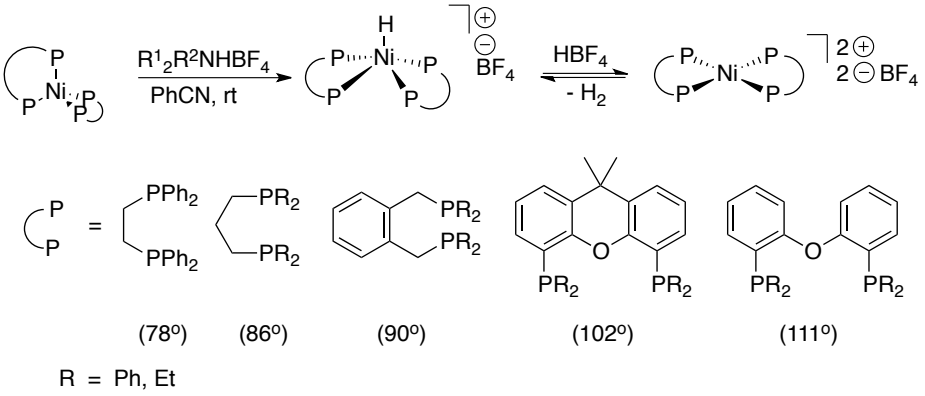



**Scheme 245: Reactions used to study the effects of ancillary ligand bite angle on the redox potentials of nickel(I) bis(diphosphine) complexes.**

Reactions were performed in $CH_2Cl_2$ and $CH_3CN$ at room temperature using in an electrochemical cell. Diphosphines with large bite angles favor less negative reduction potentials, than diphosphines with small bite angles. The trend is associated with tetrahedral distortions among the nickel(II) diphosphine complexes. Diphosphines with larger bite angles create larger tetrahedral distortions and less negative reduction potentials than diphosphines with smaller bite angles. The tetrahedral distortions are thought to reduce the energy barrier for nickel(II) to nickel(I) reduction by either destabilizing the square planar nickel(II) complexes or stabilizing the transition state to the tetrahedral nickel(I) product. The changes in reduction potentials reflect changes in the orbital energies that accompany changes in the geometry of the metal complex. Thus, the effect of bite angle on the redox potentials of nickel(II) complexes is an electronic bite angle effect. The data from these reactions collected from these studies on nickel(II)/nickel(I) complexes were used to generate stable palladium(I) complexes.

### 3.1.3.3 Metal Hydricities

DuBois and co-workers have also shown that the bite angles of the diphosphine ligands on palladium, platinum, and nickel hydrido complexes can affect the reactions of these complexes with acids (Scheme 246).[142]




**Scheme 246: Reactions used to study the effects of ancillary ligand bite angle on the hydricities of nickel(I) bis(diphosphine) complexes.**

In this case, complexes that have diphosphines with smaller bite angles are more hydridic complexes than complexes that have diphosphines with larger bite angles. The trend in metal-hydricities was linked to the tetrahedral distortions that occur by varying the bite angle of the diphosphine. Diphosphines with larger bite angles result in greater tetrahedral distortions than diphosphines with smaller bite angles. These greater tetrahedral distortions, in turn, result in lower LUMO energy levels for the corresponding palladium(II) bis(diphosphine) complexes. As a result of these lower LUMO energy levels, palladium(II) bis(diphosphine) complexes with larger bite angles are better hydride acceptors and worse hydride donors than palladium(II) bis(diphosphine) complexes with small bite angles. The hydricities of these complexes are inversely related to the (II/I) reduction potentials.

Complexes that are easier to reduce are worse hydride donors than complexes that are harder to reduce. The $Pd(diphosphine)_2H^+$ complexes reported in these studies were synthesized the by reactions of $HBF_4$ with $Pd(diphosphine)_2$. Palladium diphosphine complexes $Pd(diphosphine)_2$ were synthesized by the reductions of $[Pd(diphosphine)_2][BF_4]_2$ with hydrazine. The changes in hydricities for the $Pd(diphosphine)_2H^+$ reported in this study span a range of 27 kcal/mol.

#### 3.1.3.4 Rhodium-Catalyzed Hydroformylations

Casey and co-workers reported a bite angle effect for the linear-to-branched selectivities of rhodium-catalyzed hydroformylation reactions. In this case, diphosphines with bite angles larger bite angles promote higher linear-to-branched selectivities than diphosphines with smaller bite angles. The mechanism for the reaction is thought to involve CO dissociation from an 18-electron penta-coordinate rhodium(I) diphosphine dicarbonyl hydrido complex to form a 16-electron tetra-coordinate rhodium(I) diphosphine carbonyl hydrido complex, alkene coordination and insertion, CO coordination and insertion, and hydrogenolysis of the resulting rhodium(I) diphosphine acyl complex. The resting state of the catalyst was identified as the rhodium(I) or diphosphine dicarbonyl hydrido complex. The linear-to-branched selectivities for these reactions were originally linked to the positions of the two phosphorus atoms in the trigonal bipyramid rhodium or diphosphine hydrido carbonyl alkene complex formed prior to insertion. These complexes, however, were not observed. The geometries of the rhodium diphosphine hydrido carbonyl alkene complex were inferred from geometries of the rhodium diphosphine dicarbonyl hydrido complexes. Linear aldehydes were thought to arise when the two phosphorus atoms of the diphosphine occupy equatorial positions in the trigonal bipyramid complex. Branched aldehydes were thought to form when one of the phosphorus atoms of the diphosphine occupies an equatorial position and the other phosphorus atom occupies an axial position. Diphosphines with larger bite angles were thought to favor an equatorial-equatorial arrangement of the two phosphorus atoms and consequently linear aldehydes, while diphosphines with smaller bite angles were thought to favor an equatorial-axial arrangement of the two phosphorus atoms and consequently branched aldehydes.

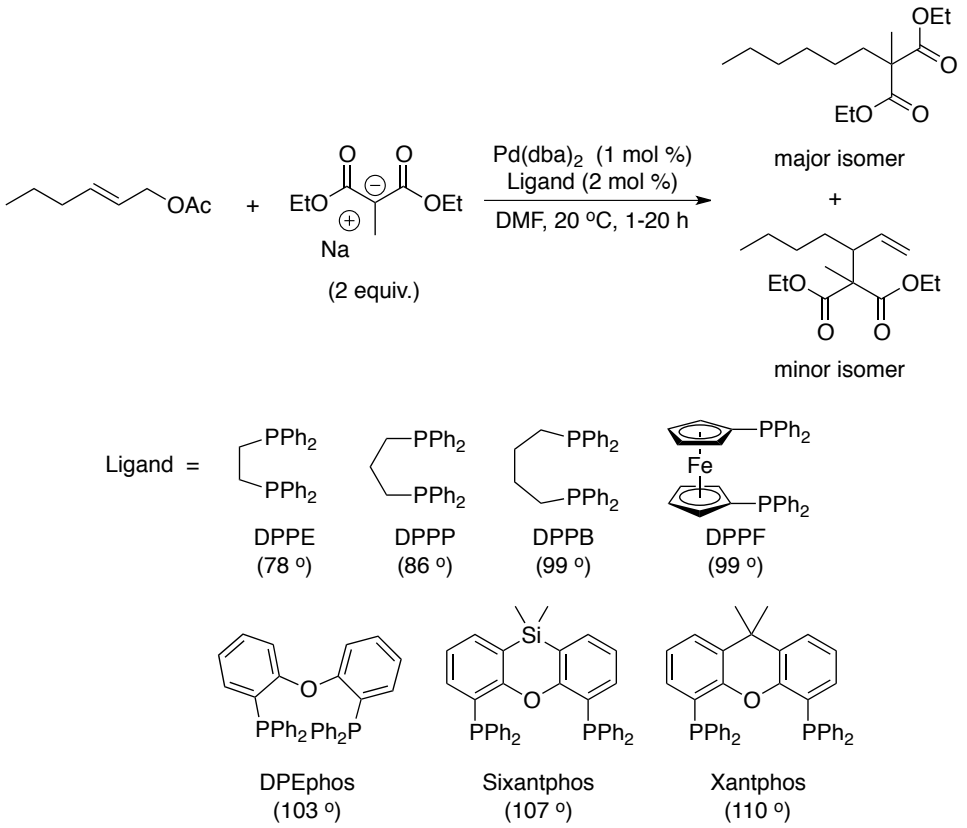
Careful studies by van Leeuwen and co-workers have shown that the linear-to-branched selectivity actually arises from a steric bite angle effect and not from differences in the conformations of the trigonal bipyramid isomers of the rhodium(I) bis(monophosphine) or diphosphine hydrido carbonyl alkene complex. In this case, diphosphines with wider bite angles increase the steric congestion around the metal and destabilize the transition state for the formation of branched products relative to the transition state for the formation of linear products.

van Leeuwen and co-workers also noticed an increase in the rates for alkene hydroformylations when diphosphines with wider bite angles were employed.[143] In this case, the faster rates for alkene hydroformylation were attributed to faster rates for CO dissociation from the rhodium(I) diphosphine dicarbonyl hydrido complexes that lead to alkene coordination and eventually insertion (compare with the electronic effect observed for rhodium-catalyzed hydroformylations of alkenes: Section 3.1.1.6).

Model reactions were conducted at 120 °C and 10 bar of $H_2$/CO (1:1) using 0.5 mM solutions of rhodium precatalyst and 10 equivalents of diphosphine per rhodium atom.

### 3.1.3.5 Palladium-Catalyzed Allylic Alkylations.

A steric bite angle effect has also been proposed for palladium-catalyzed allylic alkylations of allyl acetates (Scheme 247). [143]

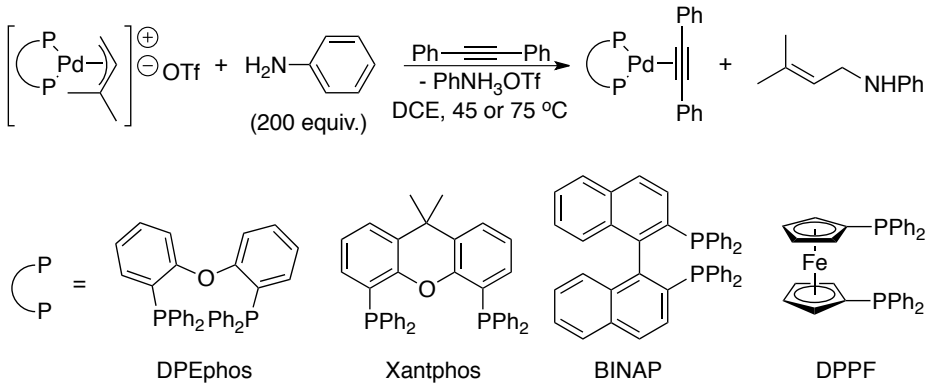



**Scheme 247: Reactions used to study the effects of ancillary ligand bite angle on palladium-catalyzed allylic alkylations of allyl acetates.**

In this case, diphosphines with wider bite angles promote higher linear-to-branched selectivities than diphosphines with smaller bite angles. The effect is not well-understood. Larger bite angles support faster rates of reaction and as a result may promote the formation of kinetic products over thermodynamic products, but this possibility was not investigated.

### 3.1.3.6 Amine Additions to Palladium $\eta^3$-Benzyl and $\eta^3$-Allyl Complexes.

A bite angle effect on the rates of amine additions to palladium(II) allyl and benzyl complexes was reported by Hartwig and co-workers (Scheme 248).[30d]

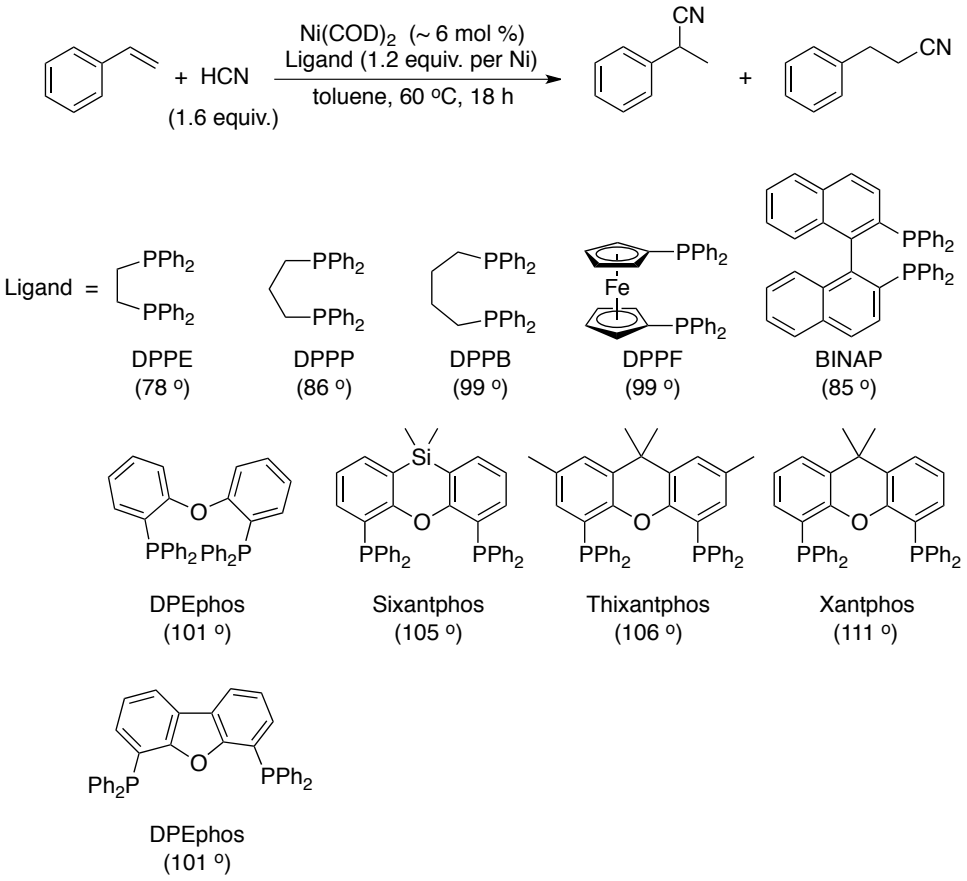



**Scheme 248: Reactions used to study the effects of ancillary ligand bite angle on the additions of arylamines to palladium(II) allyl complexes.**

In this case, faster rates for nucleophilic attack onto $\eta^3$-benzyl complexes and unsymmetrical $\eta^3$-allyl complexes were observed with diphosphines having larger bite angles. No effect of ligand bite angle on the rates of amine additions to symmetric $\eta^3$-allyl complexes was observed. Nevertheless, the stabilities of these symmetric $\eta^3$-allyl complexes appeared to vary with ligand bite angle. Reactions performed with diphosphines having smaller bite angles resulted in lower concentrations of the $\eta^3$-allyl complex and higher concentrations of catalytically inactive Pd(diphosphine)$Cl_2$. The origin of this catalyst instability is unclear. Faster rates for nucleophilic attacks onto $\eta^3$-benzyl complexes and unsymmetrical $\eta^3$-allyl complexes having diphosphine ligands with larger bite angles was attributed to a lengthening of one of the palladium-carbon bond of the benzyl or allyl fragment. The result of this lengthening is a weaker and more-reactive palladium-carbon bond. It is not clear if a similar explanation is applicable to the allylic alkylations of allyl acetates reported by van Leeuwen and co-workers.

### 3.1.3.7 Nickel-Catalyzed Hydrocyanations

The effect of ligand bite angles on the yields of nickel-catalyzed hydrocyanations of alkenes was also studied by van Leeuwen and co-workers. using Xantphos-type ligands (Scheme 249).[144]




**Scheme 249: Reactions used to study the effects of ancillary ligand bite angle on the yields of nickel-catalyzed hydrocyanations of vinyl alkenes.**

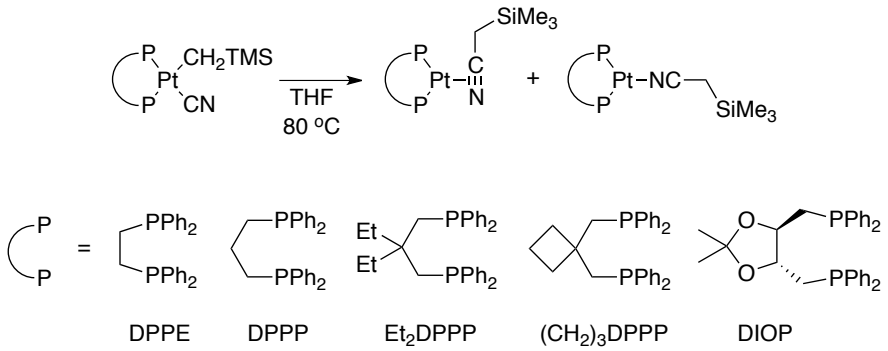
In this case, the yields of alkyl nitriles increased as the bite angle approached 105°. Reactions performed with DPEphos ($\beta_n$ = 101°) resulted in a 35-41% yield of alkyl nitrile product. Reactions performed with Sixantphos ($\beta_n$ = 105°), Thixantphos ($\beta_n$ = 106°), Xantphos ($\beta_n$ = 109°), and DPFphos ($\beta_n$ = 131°) resulted in yields of 94-95%, 69-91% , 27-75%, and 0.7 %. Reactions performed with DPPE, DPPP, DPPB, and BINAP also resulted in low yields of alkyl nitrile products. The sharp dependence of product yield on the bite angle of the diphosphine was attributed to two effects: 1) faster rates for C-CN reductive elimination from nickel(II) diphosphine alkyl cyano complexes with diphosphines having larger bite angles, and 2) slower rates for the formation of catalytically inactive nickel(II) diphosphine dicyano complexes, which prefer square planar geometries. Both effects are considered to be electronic in origin. The faster rates for C-CN reductive elimination observed with diphosphines having bite angles close to 109° were attributed to a greater stabilization of the nickel(0) tetrahedral geometry relative to the nickel(II) square planar geometry. The slower rates for the formation of nickel(II) diphosphine dicyano complexes was linked to a similar stabilization of nickel(0) tetrahedral geometries relative to the nickel(II) square planar geometries of nickel(II) diphosphine dicyano complexes.

The rates and yields of these complexes is remarkable when compared to the reactions of other nickel(II) diphosphine complexes. The linear-to-branched selectivity for the hydrocyanation reactions was also shown to

increase as the bite angle of the diphosphine approaches 105°. This effect was also attributed to faster rates for C-CN reductive elimination, the rate-limiting step.

### 3.1.3.8 Carbon-Nitrile Bond Forming Reductive Eliminations from Palladium(II) Complexes.

An effect of the bite angle of the ancillary ligand on the rates C-CN reductive elimination from palladium(II) diphosphine complexes, Pd(diphosphine)($CH_2TMS$)(CN) was reported by Moloy and co-workers in 1998 (Scheme 250).[145]



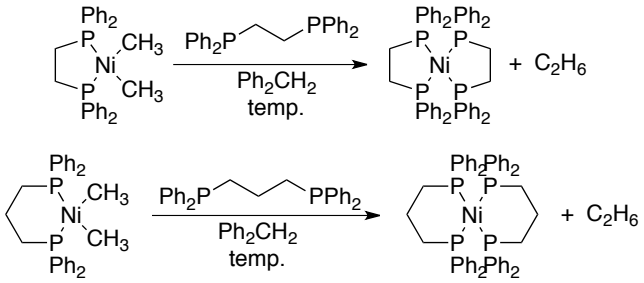

**Scheme 250: Reactions used to study the effects of ancillary ligand bite angle on the reductive eliminations of alkyl nitriles from platinum(II) diphosphine cyano alkyl complexes.**

The palladium complexes used in this study were synthesized by protonation of Pd(diphosphine)($CH_2TMS$) with one equivalent of $CF_3CO_2H$ and treatment with $Bu_4NCN$ or by the addition of one equivalent of HCN to Pd(diphosphine)($CH_2TMS$). The complexes are stable at room temperature. Heating solutions of Pd(diphosphine)($CH_2TMS$)(CN) to temperatures between 35 °C and 120 °C in the presence of 1.5 equivalents of diphosphine resulted in the formation of $TMSCH_2CN$ and palladium(0) bis(diphosphine) complexes. The rates for these reactions were monitored at different temperatures and the energies of activation determined by Erying analysis. The data from these reactions show a $10^4$ increase in the rate of C-CN reductive elimination upon changing the diphosphine from DPPE (bite angle ≈ 85 °) to DIOP (bite angle ≈ 100 °). Reactions performed with DPPP (bite angle ≈ 90 °) as the ancillary ligand show an intermediate rate. The data from these reactions suggest that ligands with wider bite angles promote faster rates for C-CN reductive eliminations from palladium(II). The faster rates for C-CN reductive elimination may result from greater compression of the C-Pd-C bond angles and consequently destabilization of the ground state of the palladium(II) complex or from greater stabilization of the palladium(0) complex formed by C-CN reductive elimination.

DFT calculations performed on the reductive eliminations of organic molecules from palladium(II) diphosphine complexes, Pd(diphosphine)$R^1R^2$ (diphosphine = DPPM, DPPE, DPPP, DPPB; $R^1 = CH_3$, $R^2 = OCH_3$, CN), suggest that larger bite angles promote faster rates for reductive elimination and the origin of this effect is mostly electronic in nature (i.e. larger bite angles stabilize the lower oxidation state of the metal or destabilize the higher oxidation state of the metal complex).[146]

### 3.1.3.9 Carbon-Carbon Bond Forming Reductive Eliminations from Nickel(II) Complexes.

Reductive eliminations of ethane from nickel diphosphine dimethyl complexes, Ni(DPPE)$(Me)_2$ and Ni(DPPP)$(Me)_2$ were reported by Yamamoto and co-workers (Scheme 251).[147] The reactions were monitored by $^{31}P$ NMR spectroscopy at various temperatures.

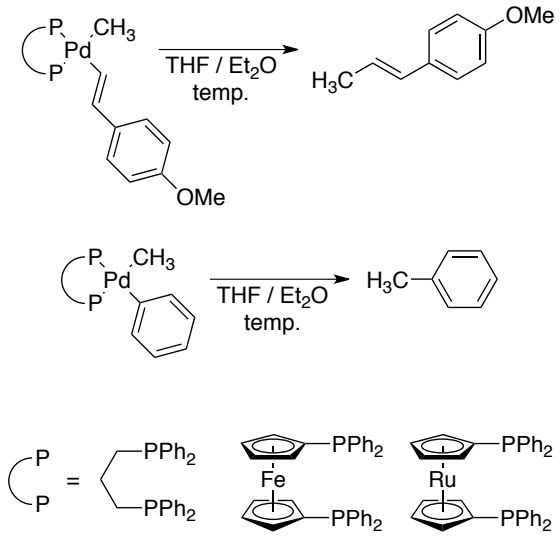


**Scheme 251: Reactions used to study the effects of ancillary ligand bite angle on the reductive eliminations of ethane from nickel(II) diphosphine dimethyl complexes.**

At 64.3 °C, the elimination of ethane from Ni(DPPP)$(Me)_2$ is 46 times faster than the elimination of ethane from Ni(DPPE)$(Me)_2$. The authors suggest several possible explanations for this observation. Reductive elimination from Ni(DPPP)$(Me)_2$ may be faster than reductive elimination from Ni(DPPE)$(Me)_2$ because Ni(DPPP)$(Me)_2$ is less stable than Ni(DPPE)$(Me)_2$ or because the nickel(0) complex of DPPP is more stable than the nickel(0) complex of DPPE. Reductive elimination from Ni(DPPP)$(Me)_2$ may also be faster than reductive elimination from Ni(DPPE)$(Me)_2$ because reductive elimination occurs from a three-coordinate complex and a phosphorus atom on DPPP can more easily dissociate from the metal than a phosphorus atom on DPPE. The mechanism for reductive elimination of ethane from Ni(DPPE)$(Me)_2$ and Ni(DPPP)$(Me)_2$ was not investigated.

### 3.1.3.10 Carbon-Carbon Bond Forming Reductive Eliminations from Palladium(II) Complexes.

Brown and Guiry reported bite angle effects for the reductive eliminations of alkenes and arenes from palladium(II) diphosphine aryl methyl and vinyl methyl complexes (Scheme 252).[148]



**Scheme 252: Reactions used to study the effects of ancillary ligand bite angle on the reductive eliminations of alkenes and arenes from palladium(II) diphosphine aryl methyl and vinyl methyl complexes**

The complexes were synthesized in situ by a sequence of steps preformed inside NMR tubes at low temperatures. In the first step, palladium(II) diphosphine dichloride complexes are reduced to palladium(0) diphosphine complexes by treatment with dilithium cyclooctatetraenide. In the second step, oxidative addition of an aryl- or vinyl-halide at palladium(0) is effected by the additions of aryl and vinyl halides to the in situ formed

palladium(0) complexes. In the final step, MeMgBr is added to the palladium(II) aryl and vinyl halides generated at low temperatures by oxidative additions of aryl and vinyl halides to palladium(0). Each step was followed by NMR spectroscopy. Upon completion of the last step, the temperature of the probe was adjusted until decomposition of the palladium(II) aryl methyl or vinyl methyl complex was observed. The temperature at which decomposition is observed varies with the diphosphine on the metal complex. DPPE, DPPF, and DPPR (1,1'-bis(diphenylphosphino)ruthenocene) were applied to the above reactions. The results provide a qualitative comparison of the effect of the diphosphine (P-P) on the rate of reductive elimination.

Decomposition of Pd(DPPP)(Me)(CH=CHAr) (Ar = p-$MeOC_6H_4$; $\beta_n$ = 89°) occurred at 25 °C, but with a slow rate of reaction. Decomposition of Pd(DPPP)(Me)(CH=CHAr) (Ar = p-$MeOC_6H_4$; $\beta_n$ = 97°) occurred at -30 °C with a half-life of approximately 20 minutes. The reaction is considerably faster than the reactions of Pd(DPPP)(Me)(CH=CHAr). Decomposition of Pd(DPPR)(Me)(CH=CHAr) (Ar = p-$MeOC_6H_4$; $\beta_n$ = > 97°) was observed at -70 °C, but did not occur with a significant rate until the temperature was raised to -40 to -35 °C.

A direct comparison of the decompositions of Pd(DPPF)(Me)(CH=CHAr) and Pd(DPPR)(Me)(CH=CHAr) was conducted at -35 °C. The DPPR complex appeared to react slightly faster than the DPPF complex, but the difference in rates was not significant. Rates for the reductive eliminations of toluene from palladium(II) diphosphine phenyl methyl complexes show similar trends. Complexes of DPPP react at slower rates than complexes of DPPF and DPPR. The data from these reactions suggest that diphosphines with larger bite angles favor faster rates for carbon-carbon reductive eliminations from palladium(II) complexes than diphosphines with smaller bite angles. Similar results were obtained for the reductive eliminations of toluene from palladium(II) diphosphine methyl phenyl complexes.

These trends are supported by extended Hückel calculations performed on similar systems.[149]

#### 3.1.3.11 Palladium-Catalyzed Kumada Reactions

van Leeuwen and co-workers investigated the effects of ligand bite angles on a palladium diphosphine-catalyzed Kumada reaction.[150] In this case, the selectivity for 2-phenylbutane increased upon changing the diphosphine from DPPE to DPPP to DPPB to DPPF and decreased upon changing the diphosphine from DPEphos to Sixantphos to Thixantphos to Xantphos. The data from these reactions suggest an optimal bite angle of approximately 99-103 °. The author suggest that increasing the bite angle of the diphosphine from 78 ° (DPPE) to 99 ° (DPPF) decreases the distances between the two coupling partners on palladium and destabilizes the ground state of this complex relative to the transition state. Increasing the bite angle even further (from 103 ° for DPEphos to 111 ° for Xantphos) may result in structural distortions that disfavor aryl alkyl reductive elimination. The authors suggest that ligands that favor the formation of trigonal bipyramid structures may also favor β-hydride elimination from the palladium(II) aryl alkyl complex and the formation biaryl products. These hypotheses, however, were not investigated further.

#### 3.1.3.12 Palladium-Catalyzed C-N Cross-Coupling Reactions

Hartwig and co-workers studied the effects of ligand bite angles on palladium-catalyzed arylations of amines and anilines with aryl halides.[107] In this case, diphosphines with smaller bite angles give higher yields and better selectivities for monoarylated amines than diphosphines having larger bite angles. The effect of ligand bite

angle on the yields of arylamine products is not fully understood. Larger bite angles may favor dissociation of one of the phosphorus atoms from palladium. The formation of a three-coordinate palladium(II) aryl amido complex may, in turn, lead to β-hydride elimination from the amine and the formation of arenes by subsequent C-H reductive elimination.

#### 3.1.3.13 Carbon-Sulfur Bond Forming Reductive Eliminations from Palladium(II)

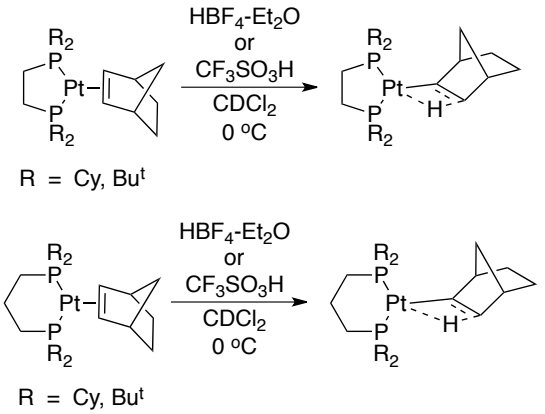
Hartwig and co-workers also studied the effects of ligand bite angles on the reductive eliminations of thioethers from palladium(II) diphosphine methyl thiolato complexes.[150] In this case, diphosphines with wider bite angles resulted in faster rates for reductive elimination than diphosphines with smaller bite angles. Reductive elimination of methyl *tert*-butyl thioether from Pd(DPPE)(Me)(S$^t$Bu) occurred with a half-life of 10 hours. Reductive elimination of methyl *tert*-butyl thioether from Pd(DPPBz)(Me)(S$^t$Bu) occurred with a half-life of 9 hours. Reductive elimination of methyl *tert*-butyl thioether from Pd(DPPP)(Me)(S$^t$Bu) occurred with a half-life of 5 hours. Reductive elimination of methyl *tert*-butyl thioether from Pd(DPPF (Me)(S$^t$Bu) occurred with a half-life of 0.5 hours. The reactions were conducted in $C_6D_6$ at 95 °C. Rates for reductive elimination were measured by NMR spectroscopy.

Bite angle effects have also been reported for the reductive eliminations of aryl cyano alkyls and N-aryl amidates from palladium(II). [105,151] The data from these reactions are limited to the of only a few palladium(II) diphosphine complexes. Nevertheless, the results show that diphosphines with wider bite angles promote faster rates for reductive elimination than diphosphines with smaller bite angles. The data from these reactions support a general trend that reductive eliminations are supported by ligands having wide bite angles.

#### 3.1.3.14 Alkene Insertions into Platinum-Hydrido Bonds

Extended Hückel calculations on the insertion of alkenes into platinum-hydrido bond of $[Pt(PH_3)_2(C_2H_4)(H)]^+$ were performed by Hoffmann and Thorn. The data from these reactions suggest that the P-Pt-P angle increases from 95°, in the ground state of the platinum hydrido alkene complex, $Pt(PH_3)_2(C_2H_4)(H)^+$, to 110° in the transition state for alkene insertion into the platinum-hydrido bond. From this data, the authors proposed that diphosphine ligands having bite angles close to 110° will promote faster rates for alkene insertions into the platinum hydrido bonds than diphosphine ligands with bite angles close to 95°.

A bite angle effect for the insertions of alkenes into platinum-hydrido bonds was reported by the groups of Spencer and Orpen (Scheme 253).[135,152]

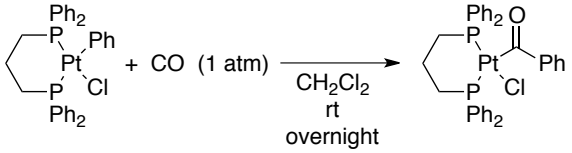



**Scheme 253: Reactions used to study the effects of ancillary ligand bite angle on the insertions of alkenes into palladium-hydrido bonds.**

In this case, a series of platinum(II) diphosphine alkyl complexes were synthesized by the additions of $HBF_4$•$OEt_2$ and $CF_3SO_3H$ to Pt(diphosphine)(norbornene). Analysis of the Pt-P, Pt-H, and P-H coupling constants for the resulting platinum(II) diphosphine alkyl complexes reveal a β-agostic interaction between the hydrogen atom transferred to the alkene and platinum. The strengths of these interactions vary with the diphosphine on platinum and are reflected by the magnitudes of the Pt-P, Pt-H, and P-H coupling constants. Smaller Pt-H coupling constants along with larger Pt-P coupling constants suggest less hydridic (alkene) character than larger Pt-H coupling constants and smaller Pt-P coupling constants. A comparison of the bite angle of the ancillary ligand with the Pt-H and Pt-P coupling constants of the corresponding platinum(II) diphosphine alkyl complexes suggest that diphosphines with larger bite angles result in greater platinum(II) alkyl character than diphosphines having smaller bite angles. The data from these reactions were interpreted in terms of alkene insertions into platinum-hydrido bonds and the extent to which these insertions occur. Diphosphines having large bite angles are thought to promote alkene insertions into platinum(II) bonds to a greater extent than diphosphines having small bite angles. The data from these reactions are consistent with the hypothesis of Hoffmann and Thorn (vide supra). Similar conclusions were reached with palladium(II) complexes and with ethene as the alkene.[135,153]

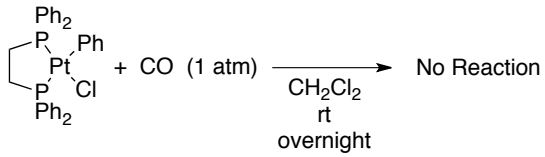
### 3.1.3.15 Alkene and Carbon Monoxide Insertions into Platinum- and Palladium-Aryl and -Alkyl Bonds

Insertion of carbon monoxide into platinum-aryl bond of Pt(DPPP)(Ph)(Cl) was reported by Anderson and co-workers in 1985 (Scheme 254).[154] The reaction generates a platinum acyl chloride complex, Pt(DPPP)(COPh)(Cl).




**Scheme 254: Reactions used to study the effects of ancillary ligand bite angle on the insertions of carbon monoxide into platinum(II)-phenyl bonds.**

In contrast, the reaction of Pt(DPPE)(Ph)(Cl) with CO does not generate a platinum(II) acyl complex (Scheme 255).

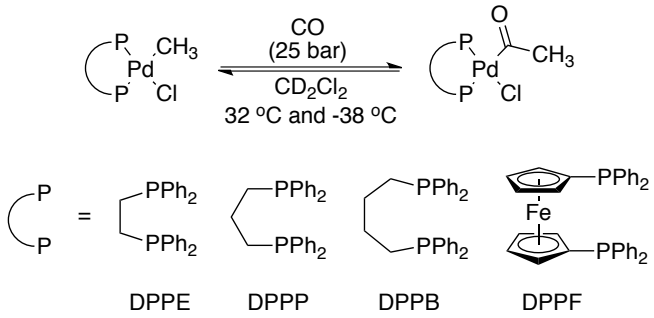



**Scheme 255: Reactions used to study the effects of ancillary ligand bite angle on the insertions of carbon monoxide into platinum(II)-phenyl bonds.**

The difference between the reactivities of these two complexes was attributed to the greater flexibility of the metal chelate formed by DPPP. According to this hypothesis, Pt(DPPP)(Ph)(Cl) inserts CO because the chelate formed by DPPP can accommodate changes in the metal geometry required for CO insertion; Pt(DPPE)(Ph)(Cl) does not insert CO because the chelate formed by DPPE cannot accommodate these changes. Although, the explanation seems reasonable, the data from these reactions are limited, and the hypothesis difficult to test. Consequently, it is unclear if this is the actual reason Pt(DPPP)(Ph)(Cl) inserts CO and Pt(DPPE)(Ph)(Cl) does not. Nevertheless, these data hint that CO insertions into platinum-carbon bonds are favored by diphosphines with larger bite angles.

Insertions of CO into the palladium-methyl bonds of Pd(DPPE)(Me)(Cl), Pd(DPPP)(Me)(Cl), Pd(DPPB)(Me)(Cl), and Pd(DPPF)(Me)(Cl) were reported by van Leeuwen and co-workers in 1992.[139,155] The reactions represent one step in a palladium-catalyzed copolymerization of ethene and CO. The effect of ligand bite angle on the catalytic copolymerization of ethene with CO is dramatic. Changing the diphosphine from DPPM ($\beta_n$ = 72 °) to DPPP ($\beta_n$ = 91 °) results in a 6000-fold increase in catalysts activity. Changing the diphosphine from DPPP to DPPB decreases the catalytic activity by a factor of 2.6.

To investigate the effects of ligand bite angle on the rates for CO insertions into palladium-methyl bonds, isolated palladium(II) methyl chloride complexes to were allowed react with CO (Scheme 256).

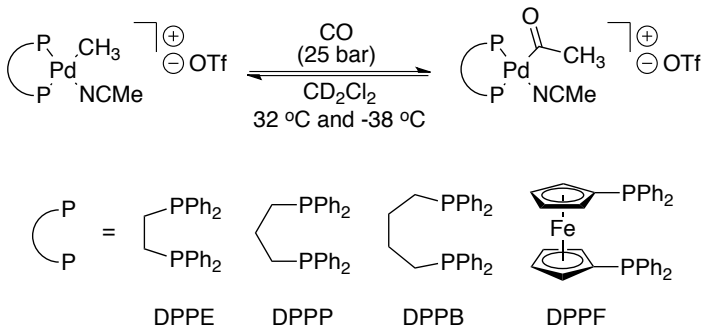



**Scheme 256: Reactions used to study the effects of ancillary ligand bite angle on the insertions of carbon monoxide into the pladium(II)-methyl bonds of neural palladium(II) diphosphine methyl complexes.**

The reactions generate metal-acyl complexes, which eliminate CO upon lowering the pressure of CO to 1 atm. The palladium diphosphine methyl chloride complexes used in these reactions were synthesized by the additions of DPPE, DPPP, DPPB, and DPPF to Pd(COD)(Me)(Cl). These complexes were isolated at room temperature and characterized by a combination of NMR spectroscopy and elemental analysis. The reactions between CO and Pd(DPPE)(Me)(Cl), Pd(DPPP)(Me)(Cl), Pd(DPPB)(Me)(Cl), and Pd(DPPF)(Me)(Cl) were monitored by NMR spectroscopy. The palladium acyl complexes generated by CO insertion were characterized in situ by a combination of NMR spectroscopy and IR spectroscopy.

Insertion of CO into the palladium-methyl bond of Pd(DPPE)(Me)(Cl) occurs at 32 °C and 25 bar. The half-life of this reaction is 170 ± 5 min. Insertions of CO into the palladium-methyl bonds of Pd(DPPP)(Me)(Cl), Pd(DPPB)(Me)(Cl), and Pd(DPPF)(Me)(Cl) occur at -38 °C and 25 bar. The half-lives of these reactions are 26 ± 3 min., 18 ± 3 min., and 36 ± min. The data from these reactions indicate that the rates for CO insertions into palladium-methyl bonds of Pd(DPPE)(Me)(Cl), Pd(DPPP)(Me)(Cl), Pd(DPPB)(Me)(Cl), and Pd(DPPF)(Me)(Cl) decrease according to Pd(DPPB)(Me)(Cl) > Pd(DPPP)(Me)(Cl) > Pd(DPPF)(Me)(Cl) >> Pd(DPPE)(Me)(Cl). A comparison of the rates for CO insertion into the palladium-methyl bonds of Pd(DPPE)(Me)(Cl), Pd(DPPP)(Me)(Cl), and Pd(DPPB)(Me)(Cl) suggest that CO insertion is faster with diphosphines having wider bite angles than diphosphines having smaller bite angles. These data, however, should be interpreted with caution. The reaction of Pd(DPPF)(Me)(Cl) with CO does not follow the trend of increasing rates with increasing bite angles. Moreover, the authors point out that the reactions of palladium(II) diphosphine methyl complexes with CO involve other steps, including CO coordination, and possible ligand dissociation, substitution and isomerization. The effects of ligand bite angles on these other reactions were not investigated.

Insertions of carbon monoxide into the palladium-methyl bonds of cationic palladium(II) diphosphine methyl complexes were also reported by van Leeuwen and co-workers (Scheme 257).[155]

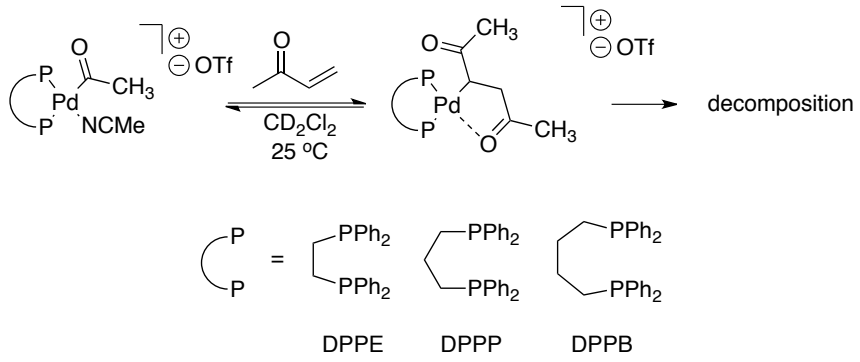



**Scheme 257: Reactions used to study the effects of ancillary ligand bite angle on the insertions of carbon monoxide into the pladium(II)-methyl bonds of cationic palladium(II) diphosphine methyl complexes.**

The reactions of these cationic complexes are significantly faster than the reactions of Pd(DPPE)(Me)(Cl), Pd(DPPP)(Me)(Cl), Pd(DPPB)(Me)(Cl), and Pd(DPPF)(Me)(Cl) under similar conditions. Insertion of CO into the palladium-methyl bond of [Pd(DPPE)(Me)][$SO_3CF_3$] occurs at -38 °C and 25 bar, with a half-life of this reaction is 2.5 ± 0.5 min. Insertions of CO into the palladium-methyl bonds of [Pd(DPPP)(Me)][$SO_3CF_3$], [Pd(DPPB)(Me)][$SO_3CF_3$], and [Pd(DPPF)(Me)][$SO_3CF_3$] occur at -38 °C and 25 bar with half-lives that are less than 1.5 ± 3 min.. Additional reactions were not performed to determine the order of reactivity of these latter complexes at lower temperatures. The data from these reactions indicate that the reactions of Pd(DPPP)(Me)][$SO_3CF_3$], [Pd(DPPB)(Me)][$SO_3CF_3$], and [Pd(DPPF)(Me)][$SO_3CF_3$] are faster than the reactions of Pd(DPPE)(Me)][$SO_3CF_3$], but do not offer a possible explanation for this trend in rates. The authors suggest that the flexibility of the diphosphine plays an important role in determining the rates for CO insertions into palladium(II)-methyl bonds; more flexible diphosphines result in faster rates than less flexible ligands. The data from these reactions are supported by calculations, which suggest that the P-Pd-P bond angle increases upon CO insertion. The slower than expected rates observed with [Pd(DPPF)(Me)][$SO_3CF_3$] may be attributed to other factors, such as the

ferrocenyl backbone. It is unclear why these reactions are slower than the reactions of Pd(DPPP)(Me)][$SO_3CF_3$] and [Pd(DPPB)(Me)][$SO_3CF_3$] with CO. The faster rates observed with the cationic palladium(II) complexes suggest that ligand dissociation from palladium(II) is critical to the overall rate of reaction. The effect of ligand bite angle on the rates for ligand dissociations from palladium(II) complexes was not investigated in this report.

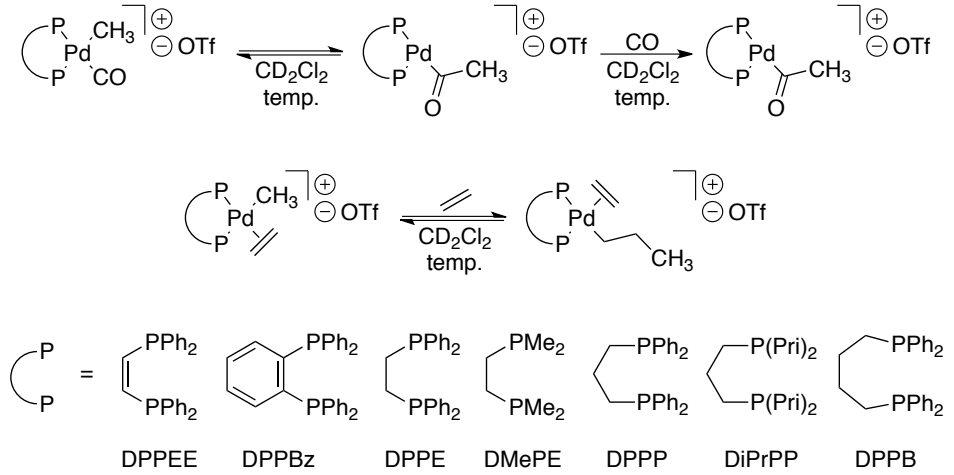
Insertions of alkenes into palladium-acyl bonds were also studied by van Leeuwen and co-workers (Scheme 258).[156]




**Scheme 258: Reactions used to study the effects of ancillary ligand bite angle on the insertions of activated alkenes into the pladium(II)-acyl bonds of cationic palladium(II) diphosphine acyl complexes.**

In this case a variety of alkenes and palladium complexes are reported. Insertion of methyl vinyl ketone into the palladium-acetyl bonds of [Pd(DPPE)(COMe)($CH_3CN$)][$SO_3CF_3$] and [Pd(DPPP)(COMe)($CH_3CN$)][$SO_3CF_3$] suggest that alkene insertions into palladium(II)-acetyl bonds are faster when the diphosphine on the metal has a larger bite angle than when the diphosphine on the metal has a smaller bite angle, but the data from these reactions are limited. The reactions of [Pd(DPPB)(COMe)($CH_3CN$)][$SO_3CF_3$] with alkenes are anomalous and the authors attribute this behavior to the formation of oligomeric metal complexes of DPPB. Additional data supporting a bite angle effect on the rates for alkene insertions into metal-acetyl bonds are not provided. Moreover, it is not clear if the observed rates of reaction are caused by rate-limiting insertions of alkenes or by other processes, such as ligand dissociation.

Insertions of carbon monoxide and ethene into the palladium-methyl bonds of cationic palladium(II) diphosphine complexes were reported by Brookhart and co-workers in 2001 (Scheme 259).[138]



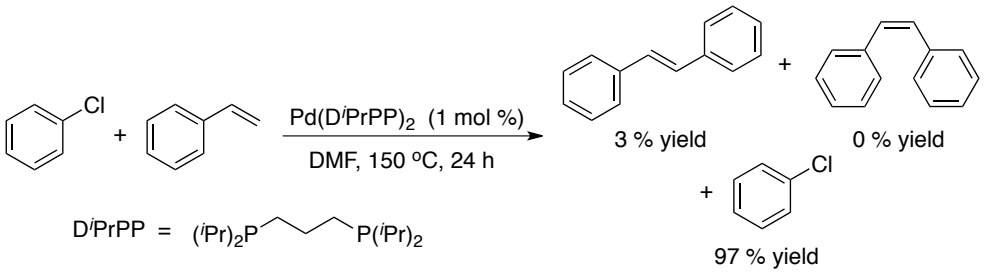

**Scheme 259: Reactions used to study the effects of ancillary ligand bite angle on the insertions of carbon monoxide and ethene into the palladium-methyl bonds of cationic palladium(II) diphosphine complexes**

The diphosphines used in this study include DPPEE, DPPBz, DPPE, DMPE, DPPP, D$^{i}$PrPP, and DPPB. The cationic palladium(II) methyl carbonyl and methyl ethene complexes that undergo CO and ethene insertions were formed in situ from the reactions of [Pd(diphosphine)(Me)(OEt$_2$)]BAr$_4$ (Ar = 3,5-(CF$_3$)$_2$C$_6$H$_3$) with CO and ethene. The complexes were characterized by $^{1}$H, $^{13}$C, and $^{31}$P NMR spectroscopy. Rates for CO insertion into the palladium-methyl bonds of the cationic palladium diphosphine methyl CO complexes were measured between -35 °C and -85 °C. The free energy barriers for CO and ethene insertion, $\Delta G^{\ddagger}$, were calculated with different diphosphines on palladium. The data from these reactions show that diphosphines with larger bite angles promote faster rates for CO insertion than diphosphines with smaller bite angles. A smaller, but similar effect is observed for ethene insertions into the palladium-methyl bonds of the cationic palladium diphosphine methyl ethene complexes. In both cases, larger bite angles are thought to destabilize the ground states of the methyl complexes by compressing the C-Pd-C bond angles or forcing the two reacting ligands closer together. Insertion is expected to relieve some of the steric strain placed on the reacting system by the larger bite angles. The faster rates for CO insertion relative to ethene insertion were attributed to the fact that ethene insertions involve four atoms in the transition state (metallocyclobutane) whereas CO insertions involve three atoms (metallocyclopropane). The larger number of atoms involved in the transition state for ethene insertions is expected to decrease the amount of strain energy that is relieved in the transition state. In other words, the effect of ligand bite angle on the rates for ethene insertions into metal-carbon bonds is smaller than the effect of ligand bite angle on the rates for CO insertions into metal-carbon bonds, because the transition state for ethene insertion is larger than the transition state for CO insertion, and the decrease in the space occupied by the two reacting ligands is not as great. These concepts are reflected in the changes in the P-Pd-C bonds that occur upon CO and ethene insertions; CO insertions result in a 27° decrease in the P-Pd-C bond angle; ethene insertions result in a 12° decrease in the P-Pd-C bond angle.

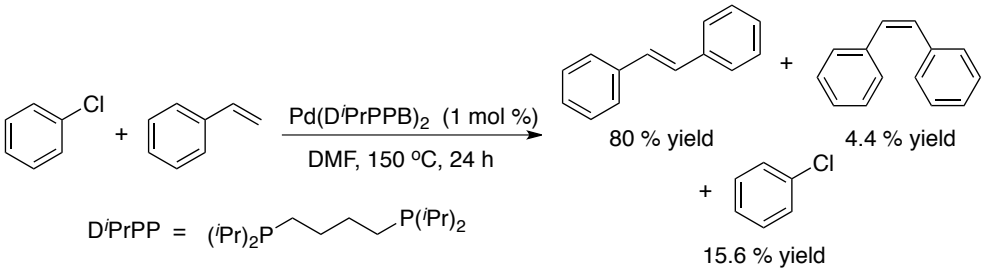
### 3.1.3.16 Palladium-Catalyzed Mizoroki-Heck Reactions

Milstein and co-workers reported a bite angle effect for a palladium-catalyzed Heck reaction of styrene with aryl chlorides (Scheme 260 and Scheme 261). In this case, Pd(D$^{i}$PrPP)$_2$ and Pd(D$^{i}$PrPB)$_2$ were used as

catalysts. Reactions performed with Pd(D$^i$PrPP)$_2$ resulted in low yields of stilbene under a variety of conditions. Reactions performed with Pd(D$^i$PrPB)$_2$ resulted in high yields of stilbene.

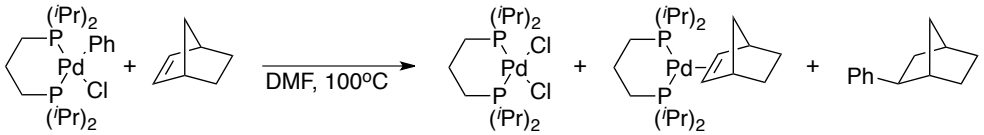



**Scheme 260: Reactions used to study the effects of ancillary ligand bite angle on the Mizoroki-Heck reactions of styrene with aryl chlrordies.**

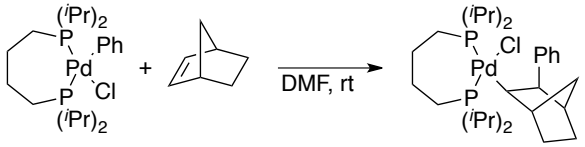



**Scheme 261: Reactions used to study the effects of ancillary ligand bite angle on the Mizoroki-Heck reactions of styrene with aryl chlrordies.**

Each step of the catalytic cycle was subsequently investigated. Oxidative additions of aryl chlorides to Pd(D$^i$PrPP)$_2$ and Pd(D$^i$PrPB)$_2$ resulted in the formation of two different palladium complexes. Oxidative addition of ArCl to Pd(D$^i$PrPP)$_2$ resulted in the formation of Pd(D$^i$PrPP)(Ar)(Cl). Oxidative addition of ArCl to Pd(D$^i$PrPB)$_2$ resulted in the formation of *trans*-Pd($\kappa^1$-D$^i$PrPB)$_2$(Ar)(Cl). Addition of norbornene to Pd(D$^i$PrPP)(Ar)(Cl) resulted in the formation of a palladium(II) diphosphine dichloride complex and a palladium(0) diphosphine alkene complex. A third complex was also observed in the reactions of norbornene with Pd(D$^i$PrPP)(Ar)(Cl) and assigned as the product from alkene insertion. The reaction is faster in DMF than in dioxane. The reactions are also faster when Pd(DiPrPP)(Ar)(Br) is used instead of Pd(DiPrPP)(Ar)(Cl).




**Scheme 262: Insertion of norborene into the palladium(II)-phenyl bond of DiPrPP-ligated palladium(II) phenyl chloride complexes.**

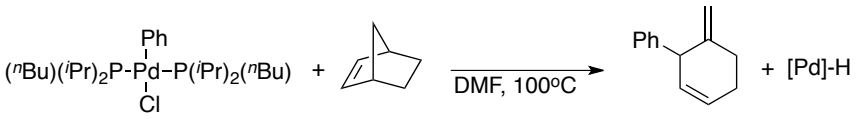



**Scheme 263: Insertion of norborene into the palladium(II)-phenyl bond of DiPrPB-ligated palladium(II) phenyl chloride complexes.**

To determine the effect of the bite angle on the rate for norbornene insertion, the reactions of Pd(D$^i$PrPE)(Ar)(Cl) and Pd(D$^i$PrPE)(Ar)(Cl) with norbornene were compared. The reaction of Pd(D$^i$PrPE)(Ar)(Cl)

with norbornene is orders of magnitude faster than the reaction of Pd(DiPrPP)(Ar)(Cl) with norbornene. The data from these reactions point to a pronounced bite angle effect, but do not explain the differences in the catalytic reactions of Pd(D$^i$PrPP)$_2$ and Pd(D$^i$PrPB)$_2$.

To investigate the mechanisms further, reactions were performed with monodentate phosphines (Scheme 264).




**Scheme 264: Insertion of norborene into the palladium(II)-phenyl bond of D($^t$Bu)($^i$Pr)$_2$-ligated palladium(II) phenyl chloride complexes.**

Additions of norbornene to *trans*-($^i$Pr$_2$$^n$BuP)$_2$Pd(Ph)Cl and *trans*-($^i$Pr$_2$$^n$BuP)$_2$Pd(Ph)Br resulted in unsaturated phenyl substituted methylene cyclohexenes, presumably by a sequence of reactions involving norbornene insertion into the palladium-aryl bonds of *trans*-($^i$Pr$_2$$^n$BuP)$_2$Pd(Ph)Cl and *trans*-($^i$Pr$_2$$^n$BuP)$_2$Pd(Ph)Br, β-alkyl elimination and β-hydride elimination.

When an extra equivalent of $^i$Pr$_2$$^n$BuP is added to the reactions of *trans*-($^i$Pr$_2$$^n$BuP)$_2$Pd(Ph)Cl and *trans*-($^i$Pr$_2$$^n$BuP)$_2$Pd(Ph)Br the rate of reaction decreases by a factor of 12.7 When 2 equivalents of $^i$Pr$_2$$^n$BuP are added to the reactions of *trans*-($^i$Pr$_2$$^n$BuP)$_2$Pd(Ph)Cl and *trans*-($^i$Pr$_2$$^n$BuP)$_2$Pd(Ph)Br the reaction is practically stopped. In comparison, the addition of 1 equivalent of $^i$Pr$_2$$^n$BuP to the reaction of Pd(D$^i$PrPP)(Ph)Cl with norbornene has no effect on the reaction rate.

When 1 equivalent of LiCl is added to the reactions of Pd(D$^i$PrPP)(Ph)Cl with norbornene, the rate decreases by a factor of 5.4. When LiCl is added to the reactions of *trans*-($^i$Pr$_2$$^n$BuP)$_2$Pd(Ph)Cl, no effect is observed.

The data from these reactions suggest two different mechanisms for the reactions of monophosphine and diphosphine complexes. The authors propose that monophosphine complexes, *trans*-($^i$Pr$_2$$^n$BuP)$_2$Pd(Ph)Cl and *trans*-($^i$Pr$_2$$^n$BuP)$_2$Pd(Ph)Br, react by initial substitution of a phosphine ligand with alkene to generate a neutral four-coordinate palladium phosphine aryl alkene complex. Alkene insertion subsequently generates a three-coordinate palladium(II) alkyl complex, which rapidly decomposes. In contrast, the reactions of Pd(D$^i$PrPP)(Ph)Cl and Pd(D$^i$PrPE)(Ph)Cl are thought to occur by substitution of the halide ligand with alkene, followed by alkene insertion into the palladium-aryl bond and decomposition of the resulting palladium(II) alkyl complex.

The mechanisms for catalytic reactions of Pd(D$^i$PrPB)$_2$ are thought to be intermediate of the monophosphine and diphosphine mechanisms proposed above. Reactions performed in DMF are only 2.3 times faster than reactions performed in 1,4-dioxane. Reactions performed in the presence of 1 equivalent of $^i$Pr$_2$$^n$BuP, the reaction rate decreases by a factor of 1.6. When 1 equivalent of LiCl is added to the reactions of Pd(D$^i$PrPB)$_2$ with aryl chlorides and norbornene, the rate decreases by a factor of 1.7. These observations are in agreement with an intermediate mechanism.

The low catalytic activity associated with Pd(D$^i$PrPP)$_2$ was attributed to the formation of Pd(D$^i$PrPP)(Cl)$_2$ at the end of each catalytic cycle. The addition of Zn powder to these reactions eliminated the build-up of Pd(D$^i$PrPP)(Cl)$_2$ and improved catalytic activity.

The faster rates for alkene insertions into the palladium-aryl bond of Pd($D^{i}$PrPE)(Ar)(Cl) was attributed to a greater equilibrium constant for chloride dissociation for Pd($D^{i}$PrPE)(Ar)(Cl) relative to Pd($D^{i}$PrPP)(Ar)(Cl). This hypothesis was not investigated. The authors assumed that alkene insertions into palladium-carbon bonds are favored by diphosphines having large bite angles. Support for this assumption is provided by the works of others.

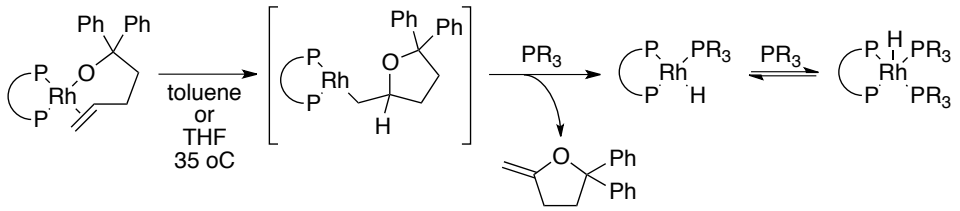
## 3.2 Present Research: The Effects of Ancillary Ligand Properties on the Reactions of Rhodium Diphosphine Alkoxo Alkene Complexes

The present research focuses on the effects of ancillary ligand properties (electronic, steric and bite angle properties) on the rates for alkene insertions into rhodium-alkoxo bonds. Prior to this research, the only examples of alkene insertions into late transition metal-alkoxo bonds were the insertion of tetrafluoroethene into the palladium(II)-methoxo bond of Pt(DPPE)(OMe)(Me), DPPE = 1,2-bis(diphenylphosphino)ethane,[79] the insertion of acrylonitrile into the platinum(II)-phenoxo bond of *trans*-Pt($PEt_3$)$_2$(OPh)(H) and the insertions of tethered alkenes into the rhodium(I)-alkoxo bonds of rhodium bis(triethylphosphine) alkoxo alkene complexes. This last reaction was reported by Hartwig and co-workers in 2006.

In order to determine the effects of the ancillary ligand on the rates for alkene insertion into late transition metal-alkoxo bonds, the reactions of rhodium diphosphine alkoxo alkene complexes were examined. Diphosphines were selected as the ancillary ligands because their properties are easily modulated, because many diphosphines are commercially available, and because it was thought that diphosphines would be less likely to dissociate from the metal center than monophosphines, making the data obtained on the effects of ancillary ligand properties on the rates for alkene insertions into metal-amido bonds less ambiguous and easier to interpret.

Preliminary studies focused on the syntheses of rhodium complexes of DPPF [1,1'-bis(diphenylphosphino)ferrocene], DPPP [1,3-bis(diphenylphosphino)propane], and BINAP [1,1'-bis(diphenylphosphino)binaphthyl], since these ligands provide a variety of ligand architectures. Rhodium(I) diphosphine alkoxo alkene complexes, **7b**, **7g**, and **7i** were synthesized by the addition of 1,1-diphenyl-4-penten-1-ol to the appropriate rhodium silylamido complex (**2b**, **2g**, or **2i)**. The complexes were synthesized at -78 °C in either toluene or THF, and characterized in situ by NMR spectroscopy at -50 °C. The $^{31}$P NMR spectra of **7a-m** display two doublets of doublet resonances or two broad doublet resonances, which are characteristic of a rhodium diphosphine complex in which the two phosphorus atoms of the diphosphines occupy different chemical environments. The $^{1}$H NMR spectra of **7b**, **7g**, and **7i** display seven signals between δ 6 and 0.5 ppm for the alkyl and alkene portion of the alkoxo alkene ligand. The presence of diastereotopic methylene hydrogen atoms is consistent with the generation of a stereocenter by coordination of the alkene to rhodium.

To determine the reactivity of rhodium diphosphine alkoxo alkene complexes, alkoxo alkene complexes towards alkene insertion or furan formation, solutions of **7b**, **7g**, and **7i** were warmed to room temperature and to 80 °C. The products from these reactions were then analyzed by GC and GC/MS. GC and GC/MS spectra of the product solutions indicate the formation of furan products presumably by a sequence of steps involving 1) alkene insertion into the rhodium-alkoxo bonds of **7b**, **7g**, and **7i** and 2) β-hydride elimination (the reactions of the rhodium bis(triethylphosphine) alkoxo alkene complexes were shown to occur by a combination of migratory insertion of the alkene into the rhodium-alkoxo bond, followed by β-hydrogen elimination).




**Scheme 265: Previous studies on alkene insertions into rhodium-alkoxo bonds of bis(triethylphosphine) rhodium alkoxo alkene complexes.**

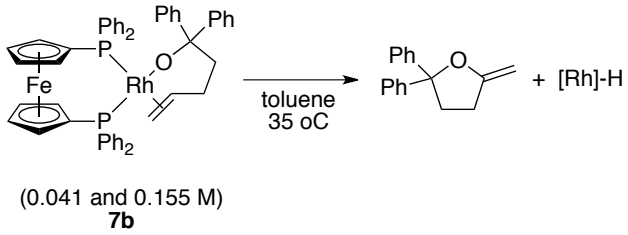
Isomerization of 5-methylene-2,2-diphenyln tetrahydrofuran was attributed to the formation of rhodium hydrido complexes by β-hydrogen elimination.

To stabilize the rhodium diphosphine hydrido complex formed by β-hydrogen elimination and suppress isomerization of the 5-methylene-2,2-diphenyl tetrahydrofuran product, excess $PPh_3$, was added to the reactions. In the presence of excess $PPh_3$, only 5-methylene-2,2-diphenyl tetrahydrofuran is observed, and isomerization is suppressed.

To determine the rates alkoxo alkene decomposition and furan formation, the reactions of **7b**, **7g**, and **7i** were monitored by $^1$H NMR spectroscopy. All reactions were performed in the presence of excess $PPh_3$. The rate constant for the decomposition of **7b** was 4.2 x $10^{-4}$ $s^{-1}$ ($t_{1/2}$ = 28 min). The rate constant for the decomposition of **7g** was 8.4 x $10^{-4}$ $s^{-1}$ ($t_{1/2}$ = 14 min). The reaction of rhodium diphosphine alkoxo alkene complex **7i** was too fast to be measured by $^1$H NMR spectroscopy at 35 °C. Consequently, the reaction of **7i** was measured at 0 °C. The rate constant for the reaction of **7i** at 0 °C (in the presence of excess $PPh_3$) was 4.5 x $10^{-4}$ $s^{-1}$ ($t_{1/2}$ = 26 min). The yields of furan products varied from 51 to 61 percent.

### 3.2.1 The Effects of Rhodium Diphosphine Alkoxo Alkene Complex Concentration on the Rates for Furan Formation and Alkoxo Alkene Decomposition.

To determine the effect of the concentration of the rhodium diphosphine alkoxo alkene complex on the rates for formation of the methylene tetrahydrofuran, the reactions off DPPF-ligated rhodium diphosphine alkoxo alkene complex **7b** was performed at 0.041 M and 0.155 M concentrations of **7b** (Scheme 266).



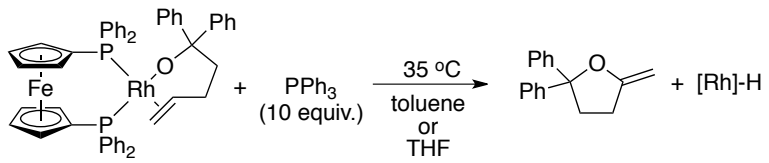

**Scheme 266: Determining the effect of the concentration of 3b on the rate constant for the reaction of 3b.**

At 0.041 M, the rate constant for the reaction of **7b** is 3.2 x $10^{-4}$ $s^{-1}$. At 0.155 M, the rate constant for the reaction of **7b** 3.1 x $10^{-4}$ $s^{-1}$. Both reactions were performed in the absence of $PPh_3$, and monitored by $^1$H NMR spectroscopy. The data from these reactions indicate that increasing the concentration of rhodium diphosphine alkoxo alkene complex **7b** by a factor of 3.78 does not change the observed rate constant for the decay of rhodium diphosphine alkoxo alkene complex **7b**. The data from these reactions are consistent with a first-order dependence of the rate on

the concentration or rhodium alkoxo alkene complex, **7b**. The reactions of other alkoxo alkene complexes were assumed to also have a first-order dependence on the concentration of alkoxo alkene complex.

### 3.2.2 The Effects of Rhodium Solvent Identity on the Rates for Furan Formation and Alkoxo Alkene Decomposition.

To determine the effect of solvent on the reactions of rhodium diphosphine alkoxo alkene complexes, the reactions of DPPF-ligated alkoxo alkene complex **3b** were performed in toluene and in THF (Scheme 267). Both reactions were performed at 35 °C in the presence of excess $PPh_3$.



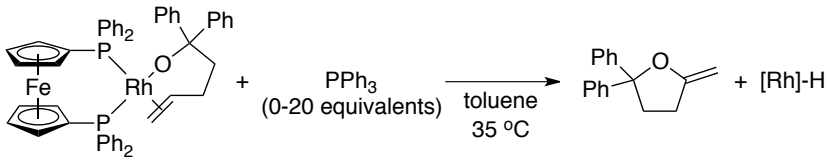

**7b**

**Scheme 267: Determining the effect of solvent identity on the rate constant for the reaction of 3b.**

In toluene at 35 °C, the reaction of **7b** occurs with a rate constant of 4.2 x $10^{-4}$ $s^{-1}$ ($t_{1/2}$ = 28 min), as stated above. In THF at 35 °C, the reaction of **7b** occurred with a rate constant of 3.5 x $10^{-4}$ $s^{-1}$ ($t_{1/2}$ = 33 min). The data from these reactions show that the reaction of **7b** is slightly (1.2 x) faster in toluene than in THF. A similar effect of solvent is observed for the reactions of rhodium bis(triethylphosphine) alkoxo alkene complexes, and, therefore, is expected for the reactions of other rhodium diphosphine alkoxo alkene complexes.

### 3.2.3 The Effects of Added $PPh_3$ Concentration on the Rates for Furan Formation and Alkoxo Alkene Decomposition.

To determine the effect of added $PPh_3$ on the reactions of **7a-m**, the reactions of DPPF-ligated alkoxo alkene complex **7b** were performed in the presence and in the absence of added $PPh_3$ (Scheme 268).




**7b**

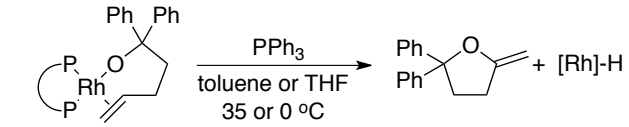
**Scheme 268: Determining the effect of $PPh_3$ concentration on the rate constant for the reaction of 3b.**

In the absence of $PPh_3$, the rate constant for the reaction of DPPF-ligated complex **7b** is 3.8 x $10^{-4}$ $s^{-1}$ ($t_{1/2}$ = 30 min). In the presence of 0.041 M $PPh_3$ (1 equivalent of $PPh_3$ per rhodium), the rate constant for the reaction of DPPF-ligated complex **7b** is 3.9 x $10^{-4}$ $s^{-1}$ ($t_{1/2}$ = 30 min). In the presence of 0.41 M $PPh_3$ (10 equivalents of $PPh_3$ per rhodium) the rate constant for the reaction of DPPF-ligated complex **7b** is 4.2 x $10^{-4}$ $s^{-1}$ ($t_{1/2}$ = 28 min), and in the presence of 0.82 M $PPh_3$, (20 equivalents of $PPh_3$ per rhodium), the rate constant for the reaction of DPPF-ligated complex **7b** is 4.2 x $10^{-4}$ $s^{-1}$ ($t_{1/2}$ = 28 min). The data from these reactions indicate that the reaction of the alkoxo alkene complex is zero order in added $PPh_3$. A similar effect of added $PPh_3$ on the reactions of rhodium diphosphine alkoxo alkene complexes **7a**, **7b-m** is assumed.

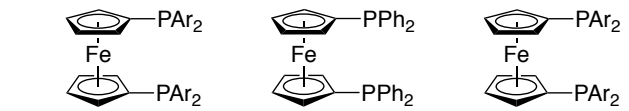
### 3.2.4 The Effects of the Electronic Properties of the Ancillary Ligands on the Rates for Alkene Insertions into Rhodium-Alkoxo Bonds.

To determine the effects of the electronic properties of the ancillary ligand on the rates for reaction of the rhodium alkoxo alkene complexes, the rate constants for reactions of rhodium alkoxo alkene complexes, **7a**, **7b**, and **7c** were compared (Table 1). Rhodium alkoxo alkene complex **7a** contains 1,1'-bis[bis(4-methoxyphenyl)phosphino]ferrocene as the ancillary ligand. Rhodium alkoxo alkene complex **7b** contains 1,1'-bis(diphenylphosphino)ferrocene (DPPF) as the ancillary ligand, and rhodium alkoxo alkene complex **7c** contains 1,1'-bis[bis(4-trifluoromethylphenyl)phosphino]ferrocene as the ancillary ligand. Each complex was prepared in situ at -78 °C by the additions of 1,1-diphenyl-4-penten-1-ol to rhodium diphosphine silylamido complexes **7a-c**. The complexes were characterized by $^{1}H$ and $^{31}P$ NMR spectroscopy at -50 °C, and allowed to react at 35 °C in the presence of excess $PPh_3$ (5-20 equivalents). The reactions of alkoxo alkene complexes **7a-c** resulted in the formation of 5-methylene-2,2-diphenyl tetrahydrofuran in 48-70 % yield. Rates for the decompositions of alkoxo alkene complexes 7a-c and the formations of 5-methylene-2,2-diphenyl tetrahydrofuran were determined by $^{1}H$ NMR spectroscopy at 35 °C.

The $^{31}P$ NMR spectra of alkoxo alkene complexes **7a-c** display two doublets of doublet resonances, which are characteristic of a rhodium diphosphine complex in which the two phosphorus atoms of the diphosphines occupy different chemical environments. The $^{1}H$ NMR spectra of **7a-c** display seven signals between δ 6 and 0.5 ppm for the alkyl and alkene portion of the alkoxo alkene ligand. The presence of diastereotopic methylene hydrogen atoms is consistent with the generation of a stereocenter by coordination of the alkene to rhodium.




**7a-c**







**a** **b** **c**

| Ar | Complex | Solvent | $k_{obs}$ ($s^{-1}$) | $t_{1/2}$ | Yield (%) |
|---|---|---|---|---|---|
| *p*-$MeOC_6H_4$ | **7a** | Toluene | 2.8 x $10^{-4}$ | 41 min | 70 |
| Ph | **7b** | Toluene | 4.2 x $10^{-4}$ | 28 min | 61 |
| Ph | **7b** | THF | 3.5 x $10^{-4}$ | 33 min | 60 |
| *p*-$CF_3C_6H_4$ | **7c** | THF | 5.6 x $10^{-4}$ | 21 min | 48 |

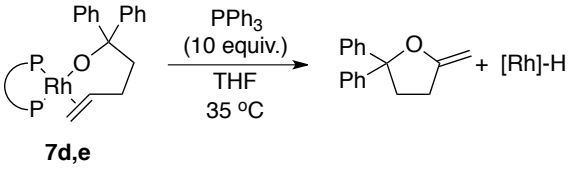
**Table 1: The effect of diphosphine electronic properties on the decay of rhodium diphosphine alkoxo alkene complexes (7a-c).**

Kinetic data from the reactions of **7a-c** indicate that less electron-rich alkoxo alkene complexes react faster than more electron-rich alkoxo alkene complexes. Rhodium diphosphine alkoxo alkene complex **3a** reacts with a rate constant of 2.8 x $10^{-4}$ $s^{-1}$ ($t_{1/2}$ = 41 min) in toluene at 35 °C. Rhodium diphosphine alkoxo alkene complex **3b**

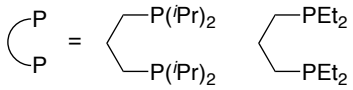
reacts with a rate constant of 4.2 x $10^{-4}$ $s^{-1}$ ($t_{1/2}$ = 28 min) in toluene at 35 °C and with a rate constant of 3.5 x $10^{-4}$ $s^{-1}$ ($t_{1/2}$ = 33 min) in THF at 35 °C. Rhodium diphosphine alkoxo alkene complex, **3c** reacts with a rate constant of 5.6 x $10^{-4}$ $s^{-1}$ ($t_{1/2}$ = 21 min) in THF at 35 °C. The rate constant for the reaction of **3c** is greater than that for reaction of **3b** under analogous conditions. Likewise the rate constant for the reaction of **3b** is greater than the rate constant for the reaction of **3a** under similar conditions. The reactions were conducted in two solvents because the initial rate data collected for the decay of rhodium alkoxo alkene complex **3c** in toluene was complicated by the decay of rhodium diphosphine silylamido alkene complex **2c** prior to the addition of 1,1-diphenyl-4-penten-1-ol. In general, the silylamido complexes of 1,1'-bis[bis(4-trifluoromethylphenyl)phosphino] ferrocene and 1,1'-bis[bis(4-methoxyphenyl)phosphino] ferrocene were the least stable of the silylamido complexes isolated.

### 3.2.5 The Effects of the Steric Properties of the Ancillary Ligands on the Rates for Alkene Insertions into Rhodium-Alkoxo Bonds.

To determine the effects of the steric properties of the ancillary ligand on the rates for furan formation from rhodium diphosphine alkoxo alkene complexes, the reactions of **7d** and **7e** were compared (Table 2).




**7d,e**




DiPrPP **d** DEtPP **e**

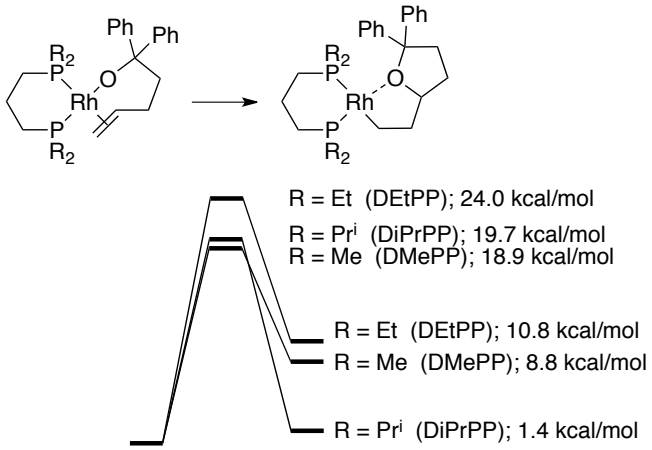
| R | Complex | $k_{obs}$ ($s^{-1}$) | $t_{1/2}$ | Yield (%) |
|---|---|---|---|---|
| iPr | **7d** | 2.2 x $10^{-4}$ | 53 min. | 88 |
| Et | **7e** | 7.5 x $10^{-4}$ | 15 min. | 96 |

**Table 2: Reactions used to study the effects of diphosphine steric properties on the decay of rhodium diphosphine alkoxo alkene complexes (7e and 7d).**

Rhodium diphosphine alkoxo alkene complex **7d** (DiPrPP) decomposes with a rate constant of 2.2 x $10^{-4}$ $s^{-1}$ ($t_{1/2}$ = 53 min.), while rhodium diphosphine alkoxo alkene complex **7e** (DEtPP) decomposes with a rate constant of 7.5 x $10^{-4}$ $s^{-1}$ ($t_{1/2}$ = 15 min.). Both reactions were performed in the presence of excess $PPh_3$ (10 equivalents relative to rhodium) in toluene at 35 °C.

The rate constants from these two reactions indicate that the complex containing the less bulky ligand decomposes faster than the complex containing the more bulky ancillary ligand. The results appear to conflict with the effects of ancillary ligand steric properties on the rates for alkene insertions into Group V metal-hydrido bonds and palladium(II)-methyl and -amido bonds.[124,126,138] In these latter examples, the complexes containing larger ancillary ligands undergo insertion faster than the complexes containing smaller ancillary ligands. In these cases, the data are consistent with a greater destabilization of the ground state of the alkene complex relative to the transition state for insertion.

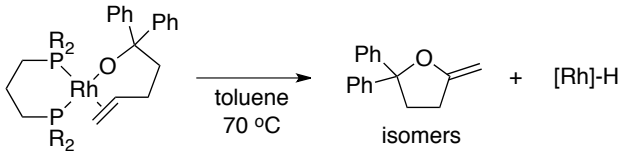
To understand how smaller ancillary ligands could promote faster rates for alkene insertions in to rhodium-alkoxo bonds, DFT calculations were performed on the rhodium(I) alkoxo alkene complexes of DMePP, DEtPP, and D$^{i}$PrPP (Scheme 269).




**Scheme 269: Calculated energy barriers and reaction energies for the insertions of tethered alkenes into the rhodium alkoxo bonds of DiPrPP-, DEtPP-, and DMePP-ligated complexes.**

All calculations were performed in the Gaussian 09 program package using the B3LYP functional and a GENECP (5d, 7f) basis set. The calculated energy barriers for alkene insertion were 18.9, 24.0, and 19.7 kcal/mol, respectively. The calculated changes in free energy were 8.8, 10.8, and 1.4 kcal/mol, respectively. These calculations suggest that the more bulky ligand, DiPrPP promotes faster rates for alkene than the less bulky ligand, DEtPP. The results from these calculations parallel the effects of ancillary ligand properties on the rates for alkene insertions into palladium(II)-methyl and -amido bonds and for alkene insertions into Group V metal-hydrido bonds, but conflict with the experimental data obtained for the reactions of **3d** and **3e**.

To investigate the discrepancies between the experimental results and the results obtained from DFT calculations, the reactions of **7d** and **7e** were conducted in the absence of added $PPh_3$ (to mirror the calculated reactions more closely). Surprisingly, the rates for furan formation and alkoxo alkene decomposition were too slow to be measured at 35 °C. As a result, the complexes were heated to 70 °C and monitored by $^{1}$H NMR spectroscopy at 70 °C. At 70 °C, in the absence of added $PPh_3$, rhodium diphosphine alkoxo alkene complex **7d** decomposes with a rate constant of 8.8 x $10^{-3}$ $s^{-1}$ ($t_{1/2}$ = 1.3 min.), while rhodium diphosphine alkoxo alkene complex 7e decomposes with rate constant of 3.0 x $10^{-4}$ $s^{-1}$ ($t_{1/2}$ = 39 min.) (Table 3). The yields for these reactions were approximately 40%.




**7d,e**

| R | Complex | $k_{obs}$ ($s^{-1}$) | $t_{1/2}$ |
|---|---|---|---|
| $^{i}$Pr | **7d** | 8.8 x $10^{-4}$ | 1.3 min. |
| Et | **7e** | 3.0 x $10^{-4}$ | 39 min. |

**Table 3: The decompositions of rhodium diphosphine alkoxo alkene complexes in the absence of added $PPh_3$.**

The data from these reactions suggest that the decompositions of rhodium alkoxo alkene complexes **7d** and **7e** are at least an order of magnitude faster in the presence of $PPh_3$ than in the absence of $PPh_3$. The data from these reactions also indicate that the relative rates for alkene insertions into the rhodium alkoxo bonds of **7d** and **7e** reverses upon adding or removing $PPh_3$. In the absence of added $PPh_3$, rhodium(I) alkoxo alkene complex **7d** reacts significantly faster than rhodium(I) alkoxo alkene complex **7e**. In the presence of added $PPh_3$, rhodium(I) alkoxo alkene complex **7e** reacts faster than the rhodium(I) alkoxo alkene complex **7d**. The cause of this effect is unclear. The faster rates observed with the less bulky diphosphine in the presence of added $PPh_3$ may reflect more facile coordination of $PPh_3$ to the rhodium complex and consequently a faster rate of decomposition, but how coordination of $PPh_3$ to rhodium increases the rate of decomposition is uncertain.

Attempts to measure a steric effect with the rhodium diphosphine alkoxo alkene complexes of 1,1'-bis[bis(2-methylphenyl)phosphino] ferrocene and 1,3-bis[bis(2-methylphenyl)phosphino] propane were unsuccessful. The additions of KHMDS and potassium 1,1-diphenyl-4-peten-1-alkoxide to the rhodium chloride complexes of 1,1'-bis[bis(2-methylphenyl)phosphino] ferrocene and 1,3-bis[bis(2-methylphenyl)phosphino] propane generated mixtures of unidentified products without the formation of furans.

### 3.2.6 The Effects of Ligand Bite Angle on the Rates for Alkene Insertions into Rhodium-Alkoxo Bonds.

**To determine the effects of ligand bite angle on the rates for alkene insertions into rhodium-alkoxo bonds, the reactions of 7g-n were compared (**

| Ligand | Complex | Bite Angle | Solvent | Temp. | $k_{obs}$ ($s^{-1}$) | $t_{1/2}$ | Yield (%) |
|---|---|---|---|---|---|---|---|
| DPPP | **7g** | 91 ° | Toluene | 35 °C | $8.4 \times 10^{-4}$ | 14 min. | 51 |
| DPPB | **7h** | 94 ° | Toluene | 35 °C | $1.4 \times 10^{-3}$ | 8 min. | 57 |
| BINAP | **7i** | 93 ° | Toluene | 0 °C | $4.5 \times 10^{-4}$ | 26 min. | 57 |
| BIPHEP | **7j** | | THF | 0 °C | $2.1 \times 10^{-4}$ | 57 min. | 87 |
| Homoxantphos | **7k** | 102 ° | Toluene | 35 °C | $3.2 \times 10^{-4}$ | 36 min. | 37 |
| DPEphos | **7l** | 104 ° | Toluene | 35 °C | $2.2 \times 10^{-4}$ | 52 min. | 70 |
| Sixantphos | **7m** | 108.5 ° | Toluene | 35 °C | $7.2 \times 10^{-4}$ | 16 min. | 61 |
| Xantphos | **7n** | 111 ° | Toluene | 35 °C | $1.8 \times 10^{-3}$ | 6 min. | 48 |

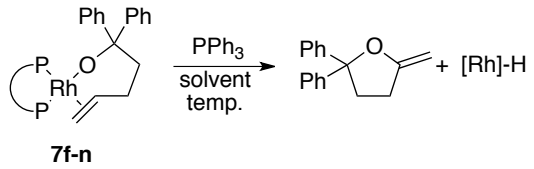
Table 4). Rhodium alkoxo alkene complexes **7g-k** were prepared in situ by the addition of 1,1-diphenyl-4-penten-1-ol to rhodium diphosphine silylamido complexes **2g-k** and characterized in situ by a combination of $^{1}H$, $^{31}P$, and $^{13}C$ NMR spectroscopy at -50 °C. Rhodium alkoxo alkene complexes **7l-n** were prepared in situ by the addition of 1,1-diphenyl-4-penten-1-ol to rhodium diphosphine silylamido complexes **2l-n** and characterized in situ by a combination of $^{1}H$ and $^{31}P$ NMR spectroscopy at -50 °C (at low temperatures and high concentrations, and low temperatures, complexes **7l-n** precipitate from solution, preventing characterization by $^{13}C$ NMR spectroscopy). All reactions were preformed at -78 °C in either toluene or THF.

**The 31P NMR spectra of 7g-n display two doublets of doublet resonances, which are characteristic of a rhodium diphosphine complex in which the two phosphorus atoms of the diphosphines occupy different chemical environments. The 1H NMR spectra of 7g-n display seven signals between δ 6 and 0.5 ppm for the alkyl and alkene portion of the alkoxo alkene ligand. The presence of diastereotopic methylene hydrogen atoms is consistent with the generation of a stereocenter by coordination of the alkene to rhodium. Following characterization by NMR spectroscopy, PPh3 was added to the alkoxo alkene complexes, and the complexes were allowed to react at 35 or 0 °C. The reactions were followed by 1H NMR spectroscopy and rate constants for the decompositions 7g-h and 7i-n and for the**

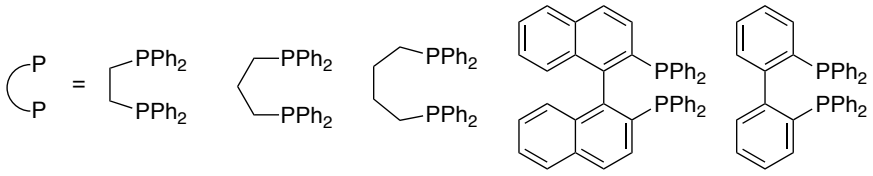
formation of 1,1-diphenyl-5-methylene tetrahydrofuran were determined by fitting exponential equations to plots of the integral values of the 1H NMR signals of 7g-h, 7i-n, and 1,1-diphenyl-5-methylene tetrahydrofuran against time. The rate data are presented in

| Ligand | Complex | Bite Angle | Solvent | Temp. | $k_{obs}$ ($s^{-1}$) | $t_{1/2}$ | Yield (%) |
|---|---|---|---|---|---|---|---|
| DPPP | **7g** | 91 ° | Toluene | 35 °C | $8.4 \times 10^{-4}$ | 14 min. | 51 |
| DPPB | **7h** | 94 ° | Toluene | 35 °C | $1.4 \times 10^{-3}$ | 8 min. | 57 |
| BINAP | **7i** | 93 ° | Toluene | 0 °C | $4.5 \times 10^{-4}$ | 26 min. | 57 |
| BIPHEP | **7j** | | THF | 0 °C | $2.1 \times 10^{-4}$ | 57 min. | 87 |
| Homoxantphos | **7k** | 102 ° | Toluene | 35 °C | $3.2 \times 10^{-4}$ | 36 min. | 37 |
| DPEphos | **7l** | 104 ° | Toluene | 35 °C | $2.2 \times 10^{-4}$ | 52 min. | 70 |
| Sixantphos | **7m** | 108.5 ° | Toluene | 35 °C | $7.2 \times 10^{-4}$ | 16 min. | 61 |
| Xantphos | **7n** | 111 ° | Toluene | 35 °C | $1.8 \times 10^{-3}$ | 6 min. | 48 |

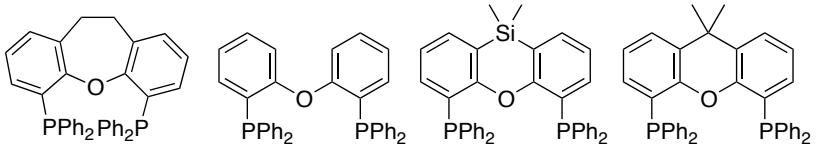
Table 4.




**7f-n**




DPPE **f** | DPPP **g** | DPPB **h** | BINAP **i** | BIPHEP **j**



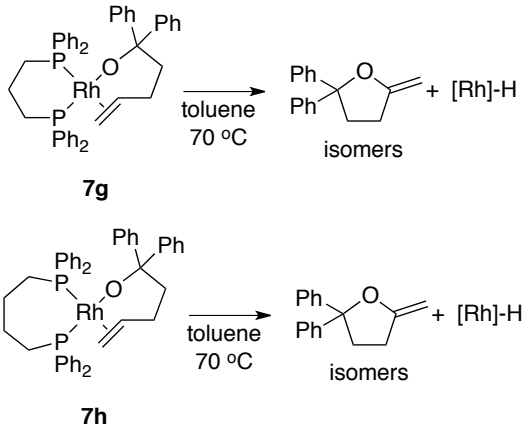

Homoxantphos **k** | DPEphos **l** | Sixantphos **m** | Xantphos **n**

| Ligand | Complex | Bite Angle | Solvent | Temp. | $k_{obs}$ ($s^{-1}$) | $t_{1/2}$ | Yield (%) |
|---|---|---|---|---|---|---|---|
| DPPP | **7g** | 91 ° | Toluene | 35 °C | $8.4 \times 10^{-4}$ | 14 min. | 51 |
| DPPB | **7h** | 94 ° | Toluene | 35 °C | $1.4 \times 10^{-3}$ | 8 min. | 57 |
| BINAP | **7i** | 93 ° | Toluene | 0 °C | $4.5 \times 10^{-4}$ | 26 min. | 57 |
| BIPHEP | **7j** | | THF | 0 °C | $2.1 \times 10^{-4}$ | 57 min. | 87 |
| Homoxantphos | **7k** | 102 ° | Toluene | 35 °C | $3.2 \times 10^{-4}$ | 36 min. | 37 |
| DPEphos | **7l** | 104 ° | Toluene | 35 °C | $2.2 \times 10^{-4}$ | 52 min. | 70 |
| Sixantphos | **7m** | 108.5 ° | Toluene | 35 °C | $7.2 \times 10^{-4}$ | 16 min. | 61 |
| Xantphos | **7n** | 111 ° | Toluene | 35 °C | $1.8 \times 10^{-3}$ | 6 min. | 48 |

**Table 4: Reactions used to study the effects of diphosphine bite angle on the decay of rhodium diphosphine alkoxo alkene complexes (7g-n).**

The rate constants for the reactions or rhodium alkoxo alkene complexes **7g** and **7h** indicate that rhodium diphosphine alkoxo alkene complex **7h** (ancillary ligand = DPPB, $k_{obs} = 1.4 \times 10^{-3}$ $s^{-1}$, $t_{1/2} = 8$ min.) reacts faster than rhodium diphosphine alkoxo alkene complex **7g** (ancillary ligand = DPPP, $k_{obs} = 8.4 \times 10^{-4}$ $s^{-1}$, $t_{1/2} = 14$ min.). The data from these reactions suggest that diphosphines with wider bite angles promote faster rates for furan formation and alkoxo alkene decomposition than diphosphines with smaller bite angles. The results are consistent with the effects of ligand bite angles on the rates for ethene insertions into palladium(II) methyl bonds. In these latter examples, wider bite angles are thought to increase the steric congestion around the alkene complex relative to the transition states for alkene insertion.

To determine the effect of added $PPh_3$ on the reactions of **7g** and **7h**, the reactions of **7g** and **7h** were also performed in the absence of $PPh_3$ (Scheme 270).




**Scheme 270: The reactions of rhodium diphosphine alkoxo alkene complexes 7g and 7h in the absence of added $PPh_3$**

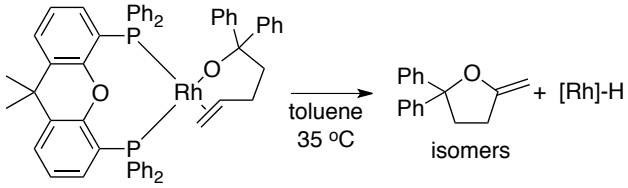
In the absence of $PPh_3$, **7g** and **7h** are significantly slower than in the presence of one or more equivalents of $PPh_3$. As a result, the decompositions of **7g** and **7h** were monitored at 70 °C in the absence of $PPh_3$. At 70 °C, in the absence of $PPh_3$, rhodium diphosphine alkoxo alkene complex, **7g** decomposes with a rate constant of $1.1 \times 10^{-3}$ $s^{-1}$ ($t_{1/2} = 11$ min.), and rhodium diphosphine alkoxo alkene complex, **7g** decomposes with a rate constant of $5.3 \times 10^{-3}$

$s^{-1}$ ($t_{1/2}$ = 2 min.). The data from these reactions also suggest that diphosphines with wider bite angles promote faster rates for furan formation than diphosphines with smaller bite angles.

Additional evidence for the effect of ligand bite angle on the rates of furan formation from rhodium diphosphine alkoxo alkene complexes is supplied by the reactions of rhodium diphosphine alkoxo alkene complexes **7k-n**. The reactions of rhodium diphosphine alkoxo alkene complexes **7k-n** were monitored by $^1$H NMR spectroscopy. All of the reactions were performed at 35 °C in toluene, in the presence of excess $PPh_3$. Under these conditions, Homoxantphos-ligated rhodium diphosphine alkoxo alkene complex **7k** decomposes with a rate constant of 3.2 x $10^{-4}$ $s^{-1}$ ($t_{1/2}$ = 36 min.), while DPEphos-, Sixantphos-, and Xantphos-ligated alkoxo alkene complexes **7l-n** decompose with rate constants of 2.2 x $10^{-4}$ $s^{-1}$ ($t_{1/2}$ = 52 min.), 7.2 x $10^{-4}$ $s^{-1}$ ($t_{1/2}$ = 16 min.), and 8.0 x $10^{-4}$ $s^{-1}$ ($t_{1/2}$ = 57 min.), respectively.

The kinetic data from these reactions support the general trend that the rhodium alkoxo alkene complexes of diphosphines with wider bite angles decompose more rapidly than the rhodium alkoxo alkene complexes of diphosphines with smaller bite angles, while also suggesting that trend is not linear. The rate constant for the decomposition of **7k** (ancillary ligand = Homoxantphos, $\beta_n$ = 102 °) is larger than the rate constant for the decomposition of **7l** (ancillary ligand = DPEphos, $\beta_n$ = 104 °). In contrast, the rate constants for the decompositions of **7m** (ancillary ligand = Sixantphos, $\beta_n$ = 109 °) and **7n** (ancillary ligand = Xantphos, $\beta_n$ = 111 °) are greater than the rate constants for the decompositions of **7k** (ancillary ligand = Homoxantphos, $\beta_n$ = 102 °) and **7l** (ancillary ligand = DPEphos, $\beta_n$ = 104 °). It is not clear why the rate constant for the decomposition of **7k** (ancillary ligand = Homoxantphos, $\beta_n$ = 102 °) is larger than the rate constant for the decomposition of **7l** (ancillary ligand = DPEphos, $\beta_n$ = 104 °), and this result was not investigated further.

To determine the effect of added $PPh_3$ on the reactions of rhodium diphosphine alkoxo alkene complexes, **7k-n**, the reaction of **7n** was performed in the absence of $PPh_3$ (Scheme 271).




**7n**

**Scheme 271: The reaction of rhodium diphosphine alkoxo alkene complexes 7n in the absence of added $PPh_3$**

At 35 °C, in the absence of added $PPh_3$, Xantphos ligated rhodium alkoxo alkene complex **7n** decomposes with a rate constant of 2.5 x $10^{-3}$ $s^{-1}$ ($t_{1/2}$ = 5 min.). By comparison, the rate constant for the decomposition of Xantphos-ligated **7n** in the presence of $PPh_3$ (10 equivalents) is 1.8 x $10^{-3}$ $s^{-1}$. The data from these reactions suggest that the reactions of **7n**, and presumably **7k-m**, are unaffected by the presence of $PPh_3$.

When compared to the effects of added $PPh_3$ on the reactions of DPPP- and DPPB-ligated alkoxo alkene complexes, **7g** and **7h**, the absence of an effect of added $PPh_3$ on the reactions of DPPF-ligated complex **7b** and Xantphos-ligated complex **7n** suggest that the decompositions of rhodium diphosphine alkoxo alkene complexes with bite angles, $\beta_n$, greater than 99 ° are unaffected by the presence of added $PPh_3$, while the decompositions of

rhodium diphosphine alkoxo alkene complexes with bite angles, $\beta_n$, less than 99 ° are affected by the presence of added $PPh_3$. The lack of an observable effect of added $PPh_3$ on the reactions of rhodium alkoxo alkene complexes **7b** and **7n** may be attributed to an increase in the steric congestion around the metal center, which prevents $PPh_3$ coordination prior to the rate-limiting step. The absence of a $PPh_3$ effect in the reactions of DPPF-ligated **7b** and Xantphos-ligated **7n** may also indicate that the reactions of these complexes occur by a different mechanism and/or rate-limiting step than the reactions of D$^i$PrPP-, DEtPP-, DPPP-, and DPPB-ligated **7d,e,g,h**. The accelerating effects of added $PPh_3$ on the reactions of **7g** and **7h** are not well- understood and require further investigations.

In contrast to the reactions of DPPP- and DPPB-ligated **7g,h** and Homoxantphos-, DPEphos-, Sixantphos-, and Xantphos-ligated **7k-n**, the reactions of BINAP- and BIPHEP-ligated diphosphine alkoxo alkene complexes, **7i** and **7j** are too fast to be measured accurately at 35 °C. Consequently, the reactions of **7i** and **7j** were monitored at 0 °C. The rate constant for the decomposition of **7i** at 0 °C and in the presence of excess $PPh_3$ is 4.5 x $10^{-4}$ $s^{-1}$ ($t_{1/2}$ = 26 min.). The rate constant for the decomposition of **7j** under the same conditions is 2.1 x $10^{-4}$ $s^{-1}$ ($t_{1/2}$ = 57 min.). Both reactions were conducted in the presence of excess $PPh_3$. In the absence of added $PPh_3$, rhodium diphosphine alkoxo alkene complex, **7i**, decomposes with rate constant of 6.5 x $10^{-5}$ $s^{-1}$ ($t_{1/2}$ = 180 min.). The rate constant for the decomposition of rhodium complex, **7j**, was not measured in the absence of $PPh_3$.

The data from these reactions imply a significant effect of added $PPh_3$. Moreover, these data suggest that complexes of diphosphines containing biphenyl linkages between the two phosphorus atoms (BINAP and BIPHEP) form the furan faster than complexes of diphosphines lacking biphenyl linkages. It is not clear why the alkoxo alkene complexes ligated by diphosphines with biphenyl linkages between the two phosphorus atoms react significantly faster than those containing diphosphines lacking biphenyl linkages.

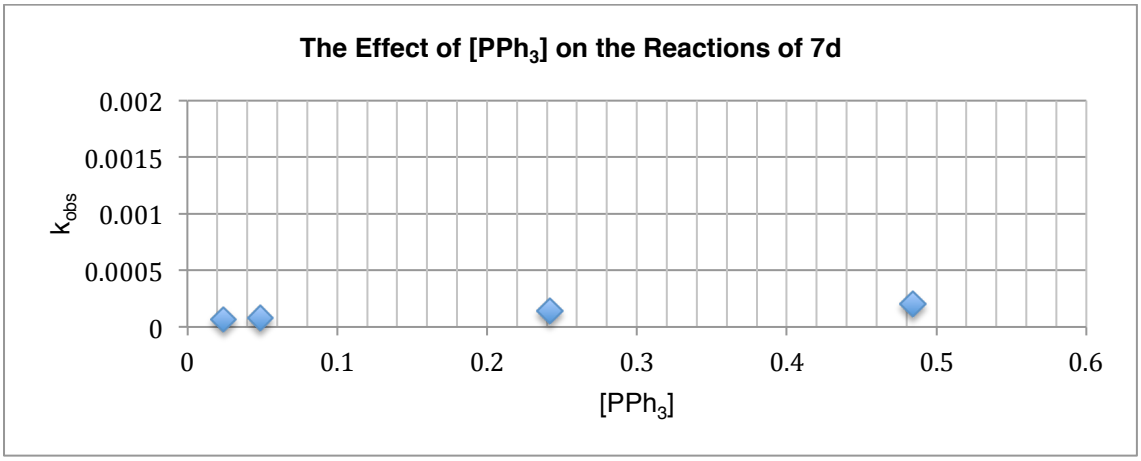
Attempts to observe a bite angle effect with other rhodium diphosphine alkoxo alkene complexes were unsuccessful. The additions of KHMDS and potassium 1,1-diphenyl-4-peten-1-alkoxide to the rhodium diphosphine chloride complexes of Benzylnixantphos, Isopropoxantphos, Benzoxantphos, and DBFphos generated mixtures of unidentified products with no signs of furan formation in the latter case. By comparison, the additions of potassium 1,1-diphenyl-4-peten-1-alkoxide to the rhodium diphosphine chloride complexes of DPPBz and DPPN generated furan products when performed at room temperature, but the rhodium alkoxo alkene complexes of these ligands could not be observed when the reactions were performed at lower temperatures due to the insolubility of the rhodium diphosphine chloride complexes. Attempts to synthesize the rhodium diphosphine silylamido complexes of DPPBz and DPPN resulted in the formation of multiple decomposition products. Addition of $PPh_3$ to the rhodium alkoxo alkene complex of DPPE resulted in displacement of the alkenyl ligand by $PPh_3$. The reactions of this complex were not investigated further.

### 3.2.7 The Effects of added $PPh_3$ on the Rates for Alkene Insertions into Rhodium-Alkoxo Bonds.

To understand the effects of added $PPh_3$ on the reactions of rhodium alkoxo alkene complexes **7d**,**e**,**g**,**h**, the reactions of **7d**, **7g**, and **7h** were performed with varying amounts of added $PPh_3$ (0.0242, 0.0484, 0.121, and 0.484 M; 1, 2, 5, 10 and 20 equivalents relative to Rh). The rate constants for the reactions of DiPrPP-ligated rhodium alkoxo alkene complex **7d** were 6.5 x $10^{-5}$ $s^{-1}$, 7.4 x $10^{-5}$ $s^{-1}$, 1.4 x $10^{-4}$ $s^{-1}$, and 2.0 x $10^{-4}$ $s^{-1}$ at 0.0242, 0.0484, and 0.484 M $PPh_3$, respectively. The rate constants for the reactions of DPPP-ligated rhodium alkoxo alkene complex

**7g** were 1.0 x $10^{-3}$ $s^{-1}$, 8.6 x $10^{-4}$ $s^{-1}$, 1.5 x $10^{-3}$ $s^{-1}$, 7.7 x $10^{-4}$ $s^{-1}$, and 8.0 x $10^{-4}$ $s^{-1}$ at 0.0242, 0.0484, 0.121, 0.242, and 0.484 M $PPh_3$, respectively. The rate constants for the reactions of DPPP-ligated rhodium alkoxo alkene complex **7h** were 1.4 x $10^{-3}$ $s^{-1}$, 1.2 x $10^{-3}$ $s^{-1}$, 1.2 x $10^{-3}$ $s^{-1}$, 1.4 x $10^{-3}$ $s^{-1}$, and 1.3 x $10^{-3}$ $s^{-1}$ at 0.0242, 0.0484, 0.121, 0.242, and 0.484 M $PPh_3$, respectively.

The data from these reactions indicate that the reaction is much faster in the presence of added $PPh_3$ than in the absence of $PPh_3$, but that the order in the concentration of added $PPh_3$ above 1 equivalent of added $PPh_3$ is zero (All reactions were performed with at least one equivalent of $PPh_3$ per rhodium).



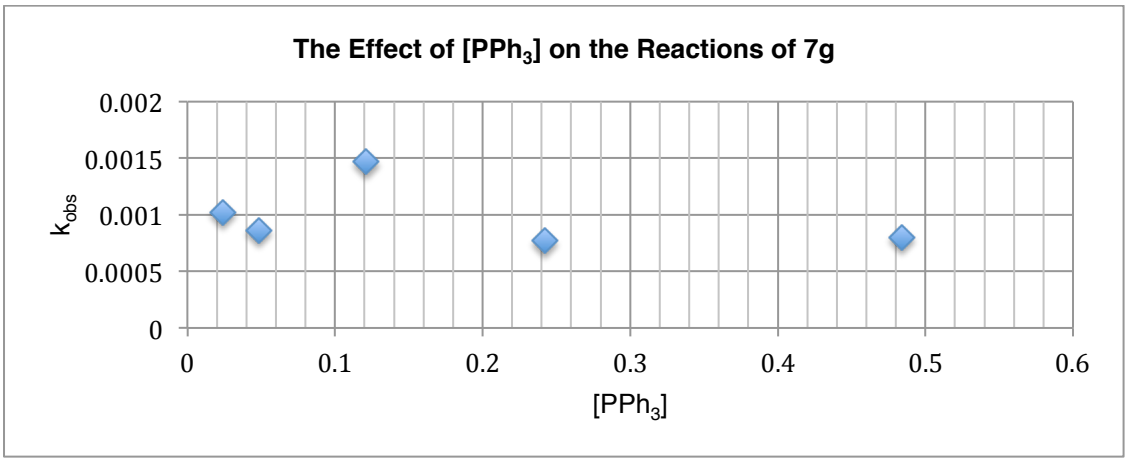




**Figure 1: The effects of added PPh3 on the reactions of 7d, 7g, and 7h. Figure 1 continues on page 184.**

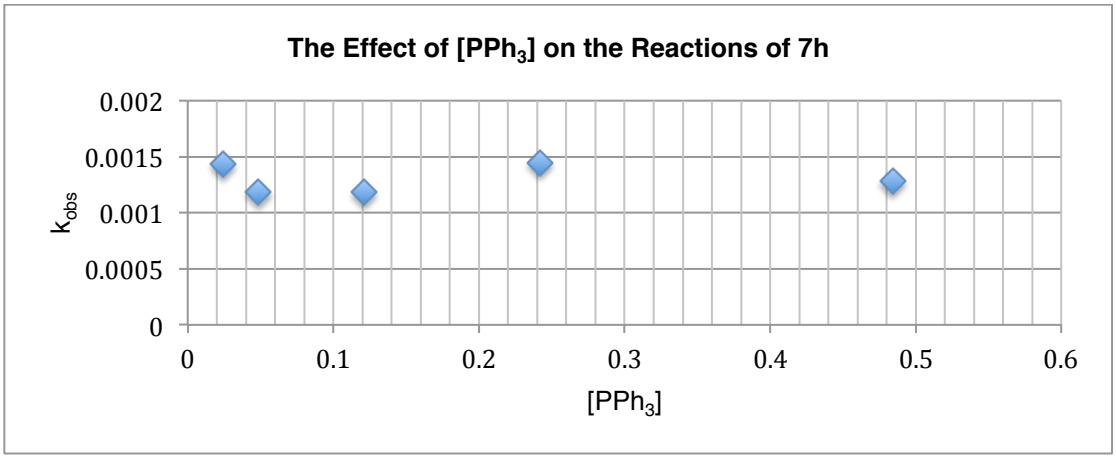


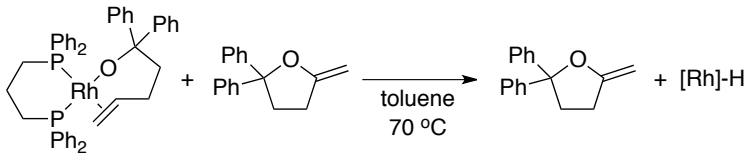

**Figure 1 (continued): The effects of added PPh3 on the reactions of 7d, 7g, and 7h, continued.**

The data from these reactions are consistent with the formation of adducts between $PPh_3$ and the rhodium complexes involved in the series of reactions. Adducts between $PPh_3$ and the rhodium diphosphine alkoxo alkene complexes **7d**, **7e**, **7g**, **7h**, and **7i** however, were not observed by $^{31}P$ and $^{1}H$ NMR spectroscopy, suggesting that coordination of $PPh_3$ to rhodium may occur after alkene insertion. Moreover, attempts to calculated the structure and stability of an adduct that could form between $PPh_3$ and complex **7g** (DPPP-ligated) simply led to dissociation of $PPh_3$.

It is possible, that C-O bond formation is reversible in the reactions of **7d**, **7e**, **7g**, **7h**, and **7i** and that $PPh_3$ coordination to the furanyl alkyl intermediate generated by alkene insertion or nucleophilic attack favors the reaction by stabilizing the product. It is also possible that furan formation occurs by rate-limiting β-hydrogen elimination, and that coordination of $PPh_3$ to the furanyl alkyl intermediate accelerates β-hydrogen elimination. The accelerating effects of added $PPh_3$ on the reactions of **7d**, **7e**, **7g**, **7h**, and **7i** are not well-understood and require further investigations.

### 3.2.8 Addition of 5-Methylene-2,2-diphenyl Tetrahydrofuran to the Reaction of Rhodium Diphosphine Alkoxo Alkene Complex, **7g**.

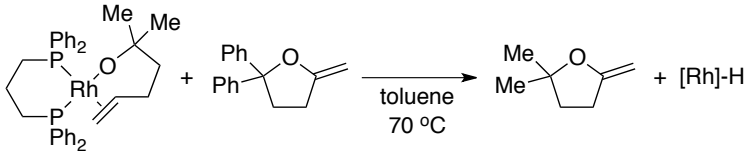
To assess the potential reversibility of furan formation in the reactions of **7d**, **7e**, **7g**, **7h**, and **7i**, the reaction of DPPP-ligated complex **7g** was performed in the presence of added 5-methylene-2,2-diphenyl tetrahydrofuran (Scheme 272). The reaction was performed at 70 °C in the absence of added $PPh_3$. The rate constant for the decomposition of rhodium alkoxo alkene complex **7g**, in the presence of added 5-methylene-2,2-diphenyl tetrahydrofuran was $1.3 \times 10^{-3}$ $s^{-1}$ ($t_{1/2}$ = 9 min). By comparison, the rate constant for the decomposition of rhodium alkoxo alkene complex **7g** in the absence of added 5-methylene-2,2-diphenyl tetrahydrofuran was $1.1 \times 10^{-3}$ $s^{-1}$ ($t_{1/2}$ = 11 min.) (vide supra). The yields of furan products from both of these reactions were approximately 40 %, as determined by gas chromatography. The data from these reactions show that the decay of **7g** is unaffected by the presence of 5-methylene-2,2-diphenyl tetrahydrofuran and that furan formation is irreversible.




**3f**

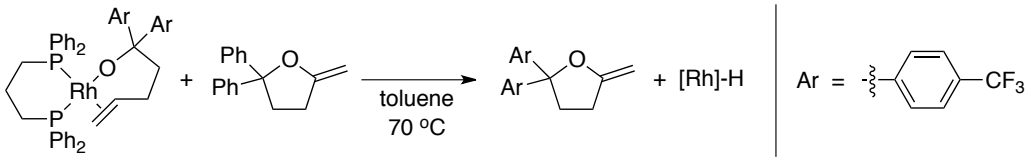
**Scheme 272: Decay or rhodium diphopshine alkoxo alkene complex 3f in the presence of added 5-methylene-2,2-diphenyl tetrahydrofuran. The rate was unaffected by the presence of furan product.**

Further support for the irreversibility of furan formation is provided by the reactions of the rhodium diphosphine alkoxo alkene complexes **16g** and **17g** in the presence of 5-methylene-2,2-diphenyl tetrahydrofuran (Scheme 273 and Scheme 274). Rhodium diphosphine alkoxo alkene complex **16g** is generated by the addition of 2-methyl-5-hexen-2-ol to rhodium diphosphine silylamido complex, **2g**, while rhodium diphosphine alkoxo alkene complex **17g** is generated by the addition of 1,1-bis(4-trifluoromethylphenyl)-4-penten-1-ol to rhodium diphosphine silylamido complex, **2g**. In both cases, the added furan is different from the one that would be formed from the rhodium complex. Therefore, the presence of **7g** in either reaction solution would suggest reversible β-hydride elimination and alkene insertion. No evidence for the accumulation of alkoxo alkene complex **7g**, however, was obtained by $^{1}$H and $^{31}$P NMR spectroscopy and no signs of 1,1-diphenyl-4-penten-1-ol were obtained by gas chromatography after the reactions were quenched with water.




**4f**

**Scheme 273: Decay or rhodium diphopshine alkoxo alkene complex 4f in the presence of added 5-methylene-2,2-diphenyl tetrahydrofuran. There was no evidence for the formation of rhodium diphosphine alkoxo alkene complex 3f or for the formation of 1,1-diphenyl-4-penten-1-ol upon quenching the reqction with water.**




**5f**

**Scheme 274: Decay or rhodium diphopshine alkoxo alkene complex 5f in the presence of added 5-methylene-2,2-diphenyl tetrahydrofuran. There was no evidence for the formation of rhodium diphosphine alkoxo alkene complex 3f or for the formation of 1,1-diphenyl-4-penten-1-ol upon quenching the reqction with water.**

### 3.2.9 Decay of Rhodium Diphosphine Alkoxo Alkene Complex **7g**, in the Absence of $PPh_3$.

Further investigations into the effect of added PPh3 on the reactions of rhodium diphosphine alkoxo alkene complexes **7d**, **7e**, **7g**, **7h**, and **7i** prompted us to monitor the reaction of DPPP-ligated complex **7g** at 35 °C in the absence of $PPh_3$. When the reaction of rhodium diphosphine alkoxo alkene complex **7g** is performed in the absence of $PPh_3$ at 35 °C, a first-order decay was observed for the first 110 min (approximately 33 % reaction) and an approximately linear decay was observed for the next 600 min (). After 710 minutes approximately 36 % of the original material is still present.

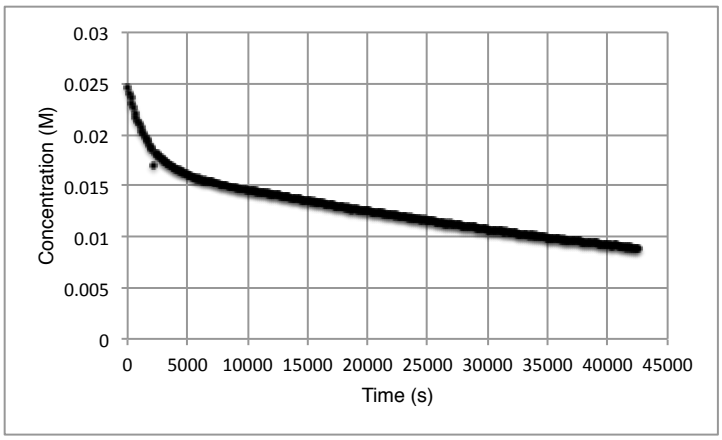



**Figure 2: Decay of DPPP-ligated rhodium alkoxo alkene complex, 3f, in the absence of $PPh_3$ at 35 °C.**

The cause of this unusual decay profile is not clear. The data, however, are consistent with a mechanism in which the initial alkoxo alkene complex **7g** decays to an equilibrium concentration before undergoing a slow irreversible decay.

DFT calculations performed on the decomposition of **7g** to a rhodium diphosphine furanyl alkyl complex, suggest that the formation of a rhodium diphosphine furanyl alkyl intermediate by alkene insertion (or nucleophilic attack) is endothermic by 4-5 kcal/mol.

### 3.2.10 The Observation of a Second Rhodium Complex

Further examinations of the $^1H$ NMR spectra of the reactions of **7d**, **7e**, **7g**, **7h**, and **7i** in the presence of 1-5 equivalents of $PPh_3$ reveal the formation and decay of a second rhodium complex. These rhodium complexes are tentatively assigned as a second rhodium alkoxo alkene complex. The $^1H$ NMR spectrum of the complex exhibits three $^1H$ signals in a 1:1:1 ratio slightly downfield of the alkenyl signals of the starting alkoxo alkene complex and a fourth signal slightly upfield of the alkyl signals of the starting alkoxo alkene complex. In addition, two new doublets of doublets appear in the $^{31}P$ NMR spectrum of the reaction after 30 min at 35 °C. These doublets of doublets are only resolved at temperatures between 0 and 10 °C. At temperatures below 0 °C and above 10 °C, the doublets of doublets appear as broad signals in the $^{31}P$ NMR spectrum of the reaction or are hidden by broad overlapping signals. Reactions run with successively increased concentrations of $PPh_3$ (0.024, 0.048, 0.121, 0.242, and 0.484 M; 1, 2, 5, 10, and 20 equivalents of $PPh_3$ relative to rhodium alkoxo alkene complex) generate successively lower concentrations of this intermediate. At 0.242 M $PPh_3$ (10 equivalents of $PPh_3$ relative to rhodium alkoxo alkene complex), the formation of this second complex can barely be detected. Decay of this second complex at 35 °C results in the slow formation of 5-methylene-2,2-diphenyl tetrahydrofuran.

Kinetic traces of these reactions show that this new species forms and decays by a standard A → B → C sequence in which the rate constants for the formation of B is significantly greater than the rate constant for the decay of B (Figure 3). Upon the disappearance of the starting alkoxo alkene complex, the concentration of the second rhodium complex reaches a maximum and then decays to furan product at a rate that appears to be an order of magnitude slower than the decay of the starting alkoxo alkene complex.

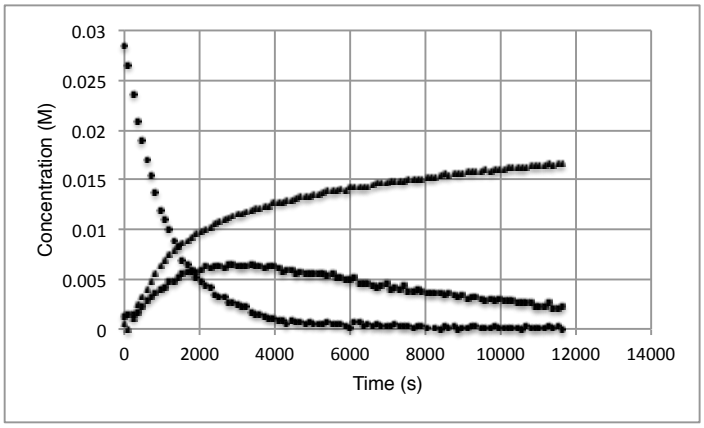



**Figure 3: The decay of alkoxo alkene complex, 7g in the presence of 2 equivalents of added $PPh_3$ in toluene at 35 °C. The circles correspond to rhodium alkoxo alkene complex, 7g. The triangles correspond to the furan product. The squares correspond to the second rhodium complex.**

The identity of this second complex is uncertain. An effect of added $PPh_3$ was not observed for the reactions of rhodium diphosphine alkoxo alkene complexes, **3b** and **3m**. An effect of added $PEt_3$ was not observed for the reactions of rhodium bis(triethylphosphine) alkoxo alkene complexes.

It is possible that $PPh_3$ coordination occurs after alkene insertion into the rhodium-alkoxo bond in which case the addition of $PPh_3$ may favor decomposition of the alkoxo alkene complexes by stabilizing the resulting furanyl alkyl or hydrido complexes. In this scenario, alkene insertion and possibly β-hydride elimination are reversible. It is also possible that β-hydride elimination is the rate-limiting step, and that $PPh_3$ coordination occurs prior to β-hydride elimination. In this case, coordination of $PPh_3$ to the rhodium diphosphine furanyl alkyl complex increases the rate of β-hydride elimination. The formation of a rhodium diphosphine triphenylphosphine furanyl alkyl complex prior to furan formation could not be established due to the number of overlapping signals in the alkyl region of the $^1H$ NMR spectra. Phosphorus-31 NMR spectra collected during the course of the reaction reveal multiple broad peaks, indicative of a dynamic process or processes. Lowering the temperature of the reaction below 10 °C did not reveal a rhodium diphosphine $PPh_3$ complex..

The decreasing intensity of the $^1H$ NMR signals of the second rhodium complex upon increasing the concentration of $PPh_3$ suggests that the second rhodium complex may form by dissociation of $PPh_3$ from an adduct between $PPh_3$ and a rhodium diphosphine complex involved in the series of reactions. The identity of this adduct, however, cannot be established from the current set of data. Further investigations are required.

### 3.2.11 Summary and Conclusions

Overall, the data from these reactions suggest that less electron-rich diphosphines with larger steric properties and larger bite angles promote faster rates for rhodium alkoxo alkene decomposition and furan formation than more electron-rich diphosphines with smaller steric properties and smaller bite angles. The results are consistent with the effects of ligand bite angles on the rates for alkene insertions into palladium-methyl and –amido bonds, but do not imply that alkene insertions into the rhodium alkoxo bonds of **7g-n** are the rate-limiting step. The mechanism for alkoxo alkene decomposition / furan formation is uncertain. It is possible that β-hydride elimination is the rate-limiting step. It is also possible that the mechanism and/or rate-limiting step changes with the identity of the ancillary ligand. An effect of added $PPh_3$ is observed with rhodium alkoxo alkene complexes **7d,e,g,h,I**, but not

with rhodium alkoxo alkene complexes **7b** and **7n**. These data suggest that rhodium diphosphine alkoxo alkene complexes with bite angles greater than 100 ° are unaffected by the presence of $PPh_3$, while rhodium diphosphine alkoxo alkene complexes with bite angles less than 100 ° react faster in the presence of $PPh_3$ than in the absence of $PPh_3$. The effect of added $PPh_3$ on these latter reactions is not completely understood. An effect of added $PEt_3$ is not observed for the reactions of rhodium bis(triethylphosphine) alkoxo alkene complexes.

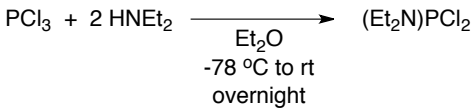
It is not clear how $PPh_3$ increases the rate for alkene insertion for the rhodium diphosphine alkoxo alkene complexes of **7d**, **7e**, **7g**, **7h**, and **7i**. It is also unclear why rhodium alkoxo alkene complexes, **7h** and **7i** are significantly faster than the rhodium alkoxo alkene complexes of diphosphines with similar bite angles. Coordination of $PPh_3$ may increase the steric strain associated with either the rhodium diphosphine alkoxo alkene complex formed prior to insertion or the rhodium diphosphine furanyl alkyl complex formed prior to β-hydride elimination. Coordination of $PPh_3$ to the rhodium diphosphine furanyl alkyl complex formed by alkene insertion into the rhodium-alkoxo bonds of **7d**, **7e**, **7g**, **7h**, and **7i** elimination may also stabilize these complexes and favor their formation. Rate data obtained for the decompositions of **7d**, **7g**, and **7h** in the presence of added $PPh_3$ support the formation of a $PPh_3$ adduct prior to the rate-limiting step.

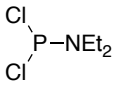
The magnitudes of the changes that occur upon changing the electronic, steric, or bite angle properties of the ancillary ligand vary. The effects of changing the electronic properties of the ancillary ligand on the rates for furan formation appear to be relatively small, whereas the effects of changing the steric properties of the ancillary ligand on the rates of furan formation appear to be relatively large. The effects of changing the bite angle of the ancillary ligand on the rates for furan formation appear to be more complicated. Within certain classes of ligands, such as diphosphines with alkyl backbones (DPPP and DPPB) or Xantphos-type ligands, the effects of ligand bite angle appear to be relatively small. Moreover, comparing the reactions of the alkoxo alkene complexes of the two classes of ligands in the presence of added $PPh_3$ does not reveal any dramatic effect. However, comparing the reactions of DPPP-ligated **7g** and DPPB-ligated **7h** with the reactions of Xantphos-ligated **7n** in the absence of $PPh_3$ suggests that the bite angle of the diphosphine can have a large effect on the rates for furan formation. The differences in rate constants reflect the magnitudes of the effects of added $PPh_3$ on the reactions of **7d**, **7e**, **7g**, **7h**, and **7i**. Again, the origin of this effect is unclear. Further studies are needed to probe the mechanism for furan formation and alkoxo alkene decomposition and to probe the effect of added $PPh_3$.

## 3.3 Experimental

### 3.3.1 Syntheses of Diphosphine Ligands

#### 3.3.1.1 Synthesis of N,N-diethylphosphoramidous dichloride, $(Et_2N)PCl_2$.



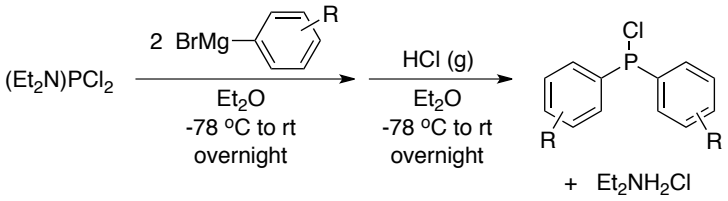

Diethylphosphoramidous dichloride, $(Et_2N)PCl_2$, was synthesized according to literature procedures. A solution of $PCl_3$ (50 ml, 79 g, 570 mmol, 1 equiv.) in $Et_2O$ (dry, 200 ml) was prepared in a 500 ml three neck flack equipped with a magnetic stir bar, two rubber septa and a 24/40-to-barb flow control adapter attached to a Schlenk manifold by a rubber hose. The flask was placed in a dry ice / acetone bath. Diethyl amine (distilled from sodium, 118 ml, 84 g, 1.15 mol, 2 equiv.) was added drop-wise to the solution of $PCl_3$ at -78 °C. Additional $Et_2O$ (dry, 100 ml) was added to the flask to ensure stirring, the flask was slowly warmed to room temperature, and the resulting solution was stirred overnight. A white precipitate formed. The heterogeneous solution was filtered through a glass frit into a second 500 ml three neck flask equipped with a magnetic stir bar, a septum and a 24/40-to-barb flow control adapter (the flask was purged of air and moisture and placed under an $N_2$ atmosphere). The collected solid was washed with additional $Et_2O$ (100 ml total), and the collected filtrate concentrated under vacuum to yield a colorless oil. The crude product was distilled under vacuum (50 ml, 60 g, 340 mmol, 60 yield).

$^1$H NMR: (499.9 MHz, toluene- $d_8$) δ 2.91 (doublet of quartets, $J^{H-P}$ = 14 Hz, $J^{H-H}$ = 7 Hz, 4H), 0.84 (t, broad, $J^{H-H}$ = 7 Hz, 6H) ppm.

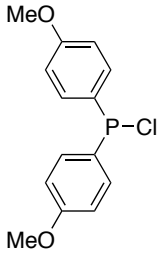
$^{13}$C{$^1$H} NMR: (125.7 MHz, toluene- $d_8$) δ 41.6 (d, $J^{C-P}$ = 23 Hz), 13.9 (d, $J^{C-P}$ = 5 Hz) ppm.

$^{31}$P{$^1$H} NMR: (202.4 MHz, toluene- $d_8$) δ 162.3 ppm.

#### 3.3.1.2 Synthesis of Diarylchlorophosphines.



#### 3.3.1.2.1 Synthesis of Bis(4-methoxyphenyl)chlorophosphine, (4-MeO-$C_6H_4$)$_2$PCl. [111,157]

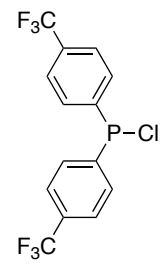



A 500 ml three-neck round bottom flask, equipped with a magnetic stir bar, a 24/40-to-barb flow control adapter, a reflux condenser, and two rubber septa, was charged with 3.17 g of magnesium turnings (3.17 g, 132 mmol, 2.4 equiv.). The flask was connected to a Schlenk manifold through a rubber hose and purged of $O_2$ and moisture by successively applying vacuum and $N_2$ (3x). The three-neck flask was then placed under an $N_2$ atmosphere and charged with 250 ml of dry $Et_2O$. Iodine crystals (1-2) were added to the flask to activate the magnesium. The resulting solution was stirred at room temperature until the orange color disappeared. 4-bromoanisole (15.2 ml, 22.7 g, 121 mmol, 2.2 equiv.) was then added to the flask over the course of 45 minutes. The $Et_2O$ solution began to reflux (caution: the reaction of 4-bromoanisole with magnesium is exothermic, autocatalytic). The solution was stirred overnight at room temperature, and then cooled to -78 °C. N,N-Diethylphosphoramidous dichloride, $(Et_2N)PCl_2$ (8.0 ml, 9.6 g, 55 mmol, 1 equiv.), was weighed inside a glovebox and then dissolved in dry $Et_2O$ (30 ml). The N,N-diethylphosphoramidous dichloride solution was loaded into a 50 ml syringe, removed from the glovebox (the syringe was stoppered), and slowly added to the Grignard reagent (4-methoxyphenyl magnesium bromide) at -78 °C. The resulting solution was warmed to room temperature and stirred overnight. The flask was then placed in a dry ice / acetone bath, and anhydrous HCl(g) was bubbled through the solution over the course of 4 hours. The bubbling was stopped, and the resulting solution was warmed to room temperature and stirred overnight. A white precipitate formed. The heterogeneous solution was filtered through celite. into a second 500 ml three-neck flask, equipped with a filter stick, a magnetic stir bar, a 24/40-to-barb flow control adapter, and a rubber septum. The collected solid was washed with addition $Et_2O$ (3 x 30 ml), and the filter stick was removed under a high $N_2$ pressure and replaced with a second rubber septum. The solvent was removed under vacuum to yield a yellow oil (3.4 g, 12 mmol, 22 % yield).

$^1$H NMR: (499.9 MHz, THF- $d_8$) δ 7.50 (t, J = 8 Hz, 4H), 6.96 (d, J = 8 Hz, 4H), 3.80 (s, 6H) ppm.

$^{31}$P{$^1$H} NMR: (202.3 MHz, THF- $d_8$) δ 85.8 ppm.

#### 3.3.1.2.2 Synthesis of Bis(4-trifluoromethylphenyl)chlorophosphine, (4-$CF_3$-$C_6H_4$)$_2$PCl.[113,158]



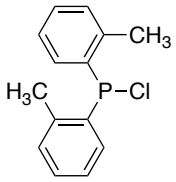

A 500 ml three-neck round bottom flask, equipped with a magnetic stir bar, a 24/40-to-barb flow control adapter, a reflux condenser, and a rubber septum, was charged with 3.17 g of magnesium turnings (3.17 g, 132 mmol, 2.4 equiv.). The flask was connected to a Schlenk manifold through a rubber hose and purged of $O_2$ and moisture by successively applying vacuum and $N_2$ (3x). The three-neck flask was then placed under an $N_2$ atmosphere and charged with 250 ml of dry $Et_2O$. Iodine crystals (1-2) were added to the flask to activate the magnesium. The resulting solution was stirred at room temperature until the orange color disappeared. 4-bromo-benzotrifluoride (16.9 ml, 27.2 g, 121 mmol, 2.2 equiv.) was then added to the flask over the course of 45 minutes. The $Et_2O$ solution began to reflux (caution: the reaction of 4-bromoanisole with magnesium is exothermic, autocatalytic). The solution was stirred overnight at room temperature, and then cooled to -78 °C. N,N-Diethylphosphoramidous dichloride, $(Et_2N)_2PCl$ (8.0 ml, 9.6 g, 55 mmol, 1 equiv.) was weighed inside a glovebox and then dissolved in dry $Et_2O$ (30 ml). The N,N-

diethylphosphoramidous dichloride solution was loaded into a 50 ml syringe, removed from the glovebox (the syringe was stoppered), and slowly added to the Grignard reagent (4-trifluoromethylphenyl magnesium bromide) at -78 °C. The resulting solution was warmed to room temperature and stirred overnight. The flask was then placed in a dry ice / acetone bath, and anhydrous HCl(g) was bubbled through the solution over the course of 4 hours. The bubbling was stopped, and the resulting solution was warmed to room temperature and stirred overnight. A white precipitate formed. The heterogeneous solution was filtered through celite into a second 500 ml three-neck flask, equipped with a filter stick, a magnetic stir bar, a 24/40-to-barb flow control adapter, and a rubber septum. The collected solid was washed with addition $Et_2O$ (3 x 30 ml), and the filter stick was removed under a high $N_2$ pressure and replaced with a second rubber septum. The solvent was removed under vacuum to yield a yellow oil. The crude product was distilled under vacuum to give a colorless oil (7.6 g, 21 mmol, 39 % yield).

$^1$H NMR: (499.9 MHz, THF- $d_8$) δ 7.84 (t, J = 8 Hz, 4H), 7.78 (d, J = 8 Hz, 4H) ppm.

$^{31}P\{^1H\}$ NMR: (202.3 MHz, THF- $d_8$) δ 77.0 ppm.

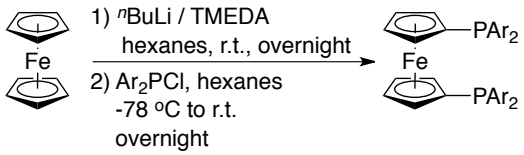
#### 3.3.1.2.3 Synthesis of Bis(2-methylphenyl)chlorophosphine, $(2\text{-Me-}C_6H_4)_2PCl$.[159]



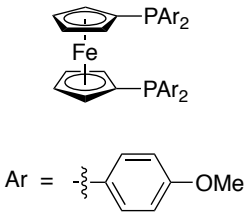

A 500 ml three-neck round bottom flask, equipped with a magnetic stir bar, a 24/40-to-barb flow control adapter, a reflux condenser, and two rubber septa, was charged with 3.17 g of magnesium turnings (3.17 g, 132 mmol, 2.4 equiv.). The flask was connected to a Schlenk manifold through a rubber hose and purged of $O_2$ and moisture by successively applying vacuum and $N_2$ (3x). The three-neck flask was then placed under an $N_2$ atmosphere and charged with 250 ml of dry $Et_2O$. Iodine crystals (1-2) were added to the flask to activate the magnesium. The resulting solution was stirred at room temperature until the orange color disappeared. 2-bromotoluene (14.6 ml, 20.7 g, 121 mmol, 2.2 equiv.) was then added to the flask over the course of 45 minutes. The $Et_2O$ solution began to reflux (caution: the reaction of 4-bromoanisole with magnesium is exothermic, autocatalytic). The solution was stirred overnight at room temperature, and then cooled to -78 °C. N,N-Diethylphosphoramidous dichloride, $(Et_2N)_2PCl$ (8.0 ml, 9.6 g, 55 mmol, 1 equiv.) was weighed inside a glovebox and then dissolved in dry $Et_2O$ (30 ml). The N,N-diethylphosphoramidous dichloride solution was loaded into a 50 ml syringe, removed from the glovebox (the syringe was stoppered), and slowly added to the Grignard reagent (2-methylphenyl magnesium bromide) at -78 °C. The resulting solution was warmed to room temperature and stirred overnight. The flask was then placed in a dry ice / acetone bath, and anhydrous HCl(g) was bubbled through the solution over the course of 4 hours. The bubbling was stopped, and the resulting solution was warmed to room temperature and stirred overnight. A white precipitate formed. The heterogeneous solution was filtered through celite into a second 500 ml three-neck flask, equipped with a filter stick, a magnetic stir bar, a 24/40-to-barb flow control adapter, and a rubber septum. The collected solid was washed with addition $Et_2O$ (3 x 30 ml), and the filter stick was removed under a high $N_2$ pressure and replaced with a second rubber septum. The solvent was removed under vacuum to yield a yellow oil. The crude product was distilled under vacuum to give a colorless oil (4.2 g, 17 mmol, 31 % yield).

$^{31}P\{^1H\}$ NMR: (202.3 MHz, THF- $d_8$) δ 90.2 ppm.

### 3.3.1.2.4 Synthesis of DPPF derivatives.




### 3.3.1.2.5 Synthesis of 1,1'-Bis[bis(4-methoxyphenyl)phosphino]ferrocene, **a**.[157]



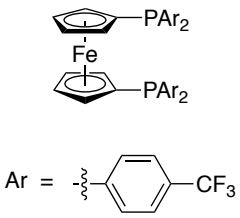

Ferrocene (1.0 g, 5.4 mmol, 1 equiv.) was weighed in a 20 ml vial and transferred to a 100 ml Schlenk flask. The Schlenk flask was equipped with a magnetic stir bar, sealed with a septum, and connected to a Schlenk manifold (by a rubber hose). The flask was purged of air by successively applying vacuum and dry $N_2$ (3x), and then placed under an $N_2$ atmosphere. Dry pentane (30 ml) was added to the Schlenk flask via syringe. The resulting solution was stirred at room temperature. A solution of $^n$BuLi in hexanes (7.4 ml, 1.6 M, 11.8 mmol, 2.2 equiv.) was added slowly to the ferrocene solution. A solution of TMEDA (distilled from sodium, 1.8 ml, 1.4 g, 12 mmol, 2.2 equiv.) in pentane (30 ml) was added slowly to the mixture of ferrocene and $^n$BuLi. The resulting solution was stirred overnight at room temperature under an $N_2$ atmosphere. An orange solid precipitated. The solution was placed in a dry ice / acetone bath and cooled to -78 °C. Bis(4-methoxyphenyl)chlorophosphine, (4-MeO-$C_6H_4$)$_2$PCl (3.4 g, 12.1 mmol, 2.2 equiv.), was weighed inside a glovebox in a 20 ml vial. The compound was dissolved in approximately 20 ml of dry THF and loaded into a 50 ml syringe. A rubber septum was placed on the needle of the syringe and the syringe was removed from the glovebox. The solution of (4-MeO-$C_6H_4$)$_2$PCl in THF was added slowly to the solution of 1,1'-dilithioferrocene / 2 TMEDA at -78 °C. The dry ice / acetone bath was removed and the reaction was allowed to stir at room temperature overnight. The resulting solution was filtered through celite into a second 250 ml Schlenk flask equipped with a magnetic stir bar and a filter stick. The filter stick was removed from the Schlenk flask under a high $N_2$ pressure and replaced with a rubber septum. The solvent was removed from the filtrate under vacuum. The residue was washed with pentane. A yellow solid was obtained (2 g, 3 mmol, 60 % yield).

$^1$H NMR: (400 MHz, $CD_2Cl_2$) δ 7.25 (s, broad, 8H), 6.85 (d, J = 7 Hz, 8H), 4.27 (s, broad, 4H), 3.79 (s, broad, 4H) ppm.

$^{13}$C{$^1$H} NMR: (101 MHz, $CD_2Cl_2$) δ 160.69, 135.19 (d, J = 21 Hz), 130.77 (d, J = 8 Hz), 114.22 (d, J = 8 Hz), 78.50 (d, J = 8 Hz), 74.00 (d, J = 15 Hz), 72.77, 55.65 ppm.

$^{31}$P{$^1$H} NMR: (162.0 MHz, $CD_2Cl_2$) δ -20.05 ppm.

### 3.3.1.2.6 Synthesis of 1,1'-Bis[bis(4 trifluoromethylphenyl)phosphino]ferrocene, **c**.[107,113,160]




Ferrocene (1.8 g, 9.6 mmol, 1 equiv.) was weighed in a 20 ml vial and transferred to a 100 ml Schlenk flask. The Schlenk flask was equipped with a magnetic stir bar, sealed with a septum, and connected to a Schlenk manifold (by a rubber hose). The flask was purged of air by successively applying vacuum and dry $N_2$ (3x), and then placed under an $N_2$ atmosphere. Dry pentane (30 ml) was added to the Schlenk flask via syringe. The resulting solution was stirred at room temperature. A solution of $^n$BuLi in hexanes (13.2 ml, 1.6 M, 21.1 mmol, 2.2 equiv.) was added slowly to the ferrocene solution. A solution of TMEDA (distilled from sodium, 3.2 ml, 2.5 g, 21.4 mmol, 2.2 equiv.) in pentane (30 ml) was added slowly to the mixture of ferrocene and $^n$BuLi. The resulting solution was stirred overnight at room temperature under an $N_2$ atmosphere. An orange solid precipitated. The solution was placed in a dry ice / acetone bath and cooled to -78 °C. Bis(4-trifluoromethylphenyl)chlorophosphine, $(4\text{-}CF_3\text{-}C_6H_4)_2PCl$ (7.6 g, 21.3 mmol, 2.2 equiv.), was weighed inside a glovebox in a 20 ml vial. The compound was dissolved in approximately 20 ml of dry THF and loaded into a 50 ml syringe. A rubber septum was placed on the needle of the syringe and the syringe was removed from the glovebox. The solution of $(4\text{-}CF_3\text{-}C_6H_4)_2PCl$ in THF was added slowly to the solution of 1,1'-dilithioferrocene / 2 TMEDA at -78 °C. The dry ice / acetone bath was removed and the reaction was allowed to stir at room temperature overnight. The resulting solution was filtered through celite into a second 250 ml Schlenk flask equipped with a magnetic stir bar and a filter stick. The filter stick was removed from the Schlenk flask under a high $N_2$ pressure and replaced with a rubber septum. The solvent was removed from the filtrate under vacuum. The residue was washed with pentane. A yellow solid was obtained (2 g, 2 mmol, 30 % yield).

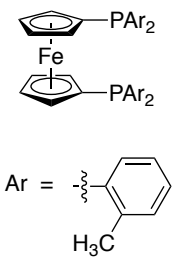
$^1$H NMR: (400 MHz, $CD_2Cl_2$) δ 7.57 (d, J = 8 Hz, 8H), 7.41 (t, J = 7 Hz, 8H), 4.35 (m, 4H), 4.01 (d J = 4 Hz, J = 2 Hz, 4H) ppm.

$^{13}$C{$^1$H} NMR: (101 MHz, $CD_2Cl_2$) δ 143.90 (d, J = 14 Hz), 134.27 (d, J = 20 Hz), 131.16 (d, J = 33 Hz), 125.53 (dt, J = 8 Hz, J = 4 Hz), 75.36 (d, J = 8 Hz), 74.48 (d, J = 15 Hz), 73.36 (d, J = 4Hz).

$^{31}$P{$^1$H} NMR: (162.0 MHz, $CD_2Cl_2$) δ -20.05 ppm.

$^{19}$F{$^1$H} NMR: (376.5 MHz, $CD_2Cl_2$) δ -62.95 ppm.

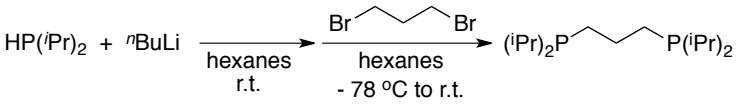
### 3.3.1.2.7 Synthesis of 1,1'-Bis[bis(2-methylphenyl)phosphino]ferrocene.[161]




Ferrocene (1.4 g, 7.6 mmol, 1 equiv.) was weighed in a 20 ml vial and transferred to a 100 ml Schlenk flask. The Schlenk flask was equipped with a magnetic stir bar, sealed with a septum, and connected to a Schlenk manifold (by a rubber hose). The flask was purged of air by successively applying vacuum and dry $N_2$ (3x), and then placed under an $N_2$ atmosphere. Dry pentane (30 ml) was added to the Schlenk flask via syringe. The resulting solution was stirred at room temperature. A solution of $^n$BuLi in hexanes (10.4 ml, 1.6 M, 16.6 mmol, 2.2 equiv.) was added slowly to the ferrocene solution. A solution of TMEDA (distilled from sodium, 2.5 ml, 2.0 g, 16.8 mmol, 2.2 equiv.) in pentane (30 ml) was added slowly to the mixture of ferrocene and $^n$BuLi. The resulting solution was stirred overnight at room temperature under an $N_2$ atmosphere. An orange solid precipitated. The

solution was placed in a dry ice / acetone bath and cooled to -78 °C. Bis(2-methylphenyl)chlorophosphine, $(2\text{-}CH_3\text{-}C_6H_4)_2PCl$ (4.2 g, 16.9 mmol, 2.2 equiv.), was weighed inside a glovebox in a 20 ml vial. The compound was dissolved in approximately 20 ml of dry THF and loaded into a 50 ml syringe. A rubber septum was placed on the needle of the syringe and the syringe was removed from the glovebox. The solution of $(2\text{-}CH_3\text{-}C_6H_4)_2PCl$ in THF was added slowly to the solution of 1,1'-dilithioferrocene / 2 TMEDA at -78 °C. The dry ice / acetone bath was removed and the reaction was allowed to stir at room temperature overnight. The resulting solution was filtered through celite into a second 250 ml Schlenk flask equipped with a magnetic stir bar and a filter stick. The filter stick was removed from the Schlenk flask under a high $N_2$ pressure and replaced with a rubber septum. The solvent was removed from the filtrate under vacuum. The residue was washed with pentane. A yellow solid was obtained (2 g, 3 mmol, 40 % yield).

### 3.3.1.3 Synthesis of 1,3-Bis(diisopropylphosphino)propane, D$^i$PrPP (**d**).[162]



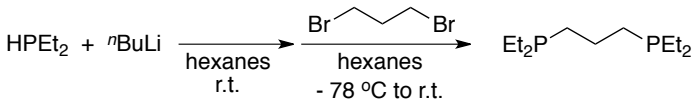

Diisopropylphosphine, $^iPr_2PH$ (10 g of 10 % wt in hexanes, 1.0 g, 8.5 mmol, 2 equiv. was weighed inside a glovebox in a 3 ml vial. The compound was dissolved in 2 ml of pentane and transferred to a 50 ml Schlenk flask. Additional pentane (10 ml) was added tot the flake. The flask was equipped with a magnetic stir bar. A solution of $^n$BuLi in hexanes (1.6 M, 5.8 ml, 9.3 mmol, 1.1 equiv.) was added to the solution of $^iPr_2PH$ at room temperature. The flask was stoppered and sealed from the box atmosphere. The resulting solution was stirred overnight at room temperature. A white solid precipitated. The Schlenk flask was removed from the glovebox and connected to a Schlenk manifold by a rubber hose. The hose and neck of the Schlenk flask were purged of air by applying vacuum and $N_2$ successively 3 times. The Schlenk flask was then opened to an $N_2$ atmosphere and placed in a dry ice / acetone bath. 1,3-Dibromopropane (0.430 ml, 0.86 g, 4.2 mmol, 1 equiv.) was loaded into a syringe and slowly added to the diethyllithium phosphide solution at -78 °C. The reaction was slowly warmed to room temperature and stirred overnight. The product solution was filtered through celite into a second 50 ml Schlenk flask, equipped with a magnetic stir bar and fitted with a filter stick. The solid was washed with additional pentane (3 x 10 ml). The filter stick was removed from the second Schlenk flask under a high $N_2$ pressure and replaced with a rubber septum. The pentane was removed from the filtrate under vacuum. A yellow oil was obtained. The crude product was distilled under vacuum to give a colorless oil (0.55 g, 2.0 mmol, 47 % yield).

Lithium diisopropylphosphide could also be prepared by the addition of chlorodiisopropylphosphine to lithium metal. Lithium metal (4.09 g, 589 mmol, 6 equiv.) was weighed inside an argon-filled glovebox and loaded into a 250 ml Schlenk flask equipped with a magnetic stir bar. The flask was stoppered with a septum, sealed from the box atmosphere and removed from the glovebox. The Schlenk flask was connected to a Schlenk manifold by a rubber hose that was purged of air by applying vacuum and argon successively 3 times. The Schlenk flask was opened to

an argon atmosphere, charged with dry THF (100 ml), and placed in an ice bath. Chlorodiisopropylphosphine (15 g, 98 mmol, 1 equiv.) was added slowly to the solution of lithium metal (the reaction is exothermic). The reaction was stirred overnight. The ice bath was allowed to warm to room temperature. The colorless solution became green. ($^{31}P\{^{1}H\}$ NMR: δ -4.75 ppm.). The heterogeneous solution was cannulated into a glass filter stick connected a second 250 ml Schlenk flask that had been purged of air and moisture. The filter stick was replaced with a rubber septum under a high argon pressure, and the Schlenk flask was subsequently placed in a dry ice / acetone bath. 1,3-Dibromopropane (4.5 ml, 9.0 g, 44 mmol, 0.45 equiv.) in dry THF (20 ml) was slowly added to the solution of lithium diisopropylphosphide at -78 °C. The resulting solution was stirred overnight. The dry ice / acetone bath was allowed to warm to room temperature. The crude product was concentrated under vacuum and transferred to a two neck round bottom flask, fitted with a short-path distillation apparatus and purged of air and moisture. The crude product was distilled under vacuum to yield a colorless, pyrophoric oil (11 g, 41 mmol, 83 % yield).

$^{31}P\{1H\}$ NMR: (162 MHz, THF) δ 2.37 ppm.

### 3.3.1.4 Synthesis of 1,3-Bis(diethylphosphino)propane, DEtPP (**d**).[142a]



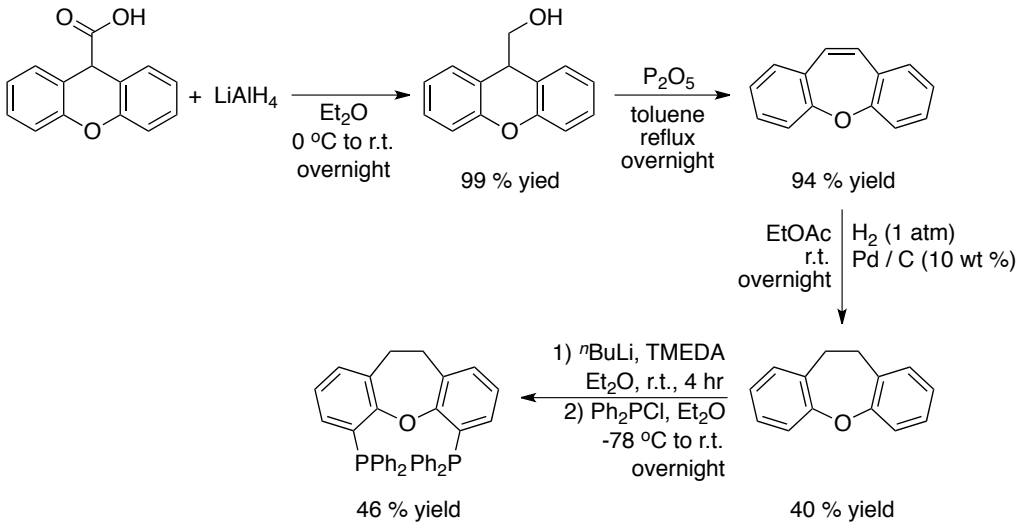

Diethylphosphine, $Et_2PH$ (1.0 g, 11 mmol, 2 equiv. was weighed inside a glovebox in a 3 ml vial. The compound was dissolved in 2 ml of pentane and transferred to a 50 ml Schlenk flask. Additional pentane (10 ml) was added tot the flake. The flask was equipped with a magnetic stir bar. A solution of $^{n}$BuLi in hexanes (1.6 M, 6.9 ml, 11 mmol, 2 equiv.) was added to the solution of $Et_2PH$ at room temperature. The flask was stoppered and sealed from the box atmosphere. The resulting solution was stirred overnight at room temperature. A white solid precipitated. The Schlenk flask was removed from the glovebox and connected to a Schlenk manifold by a rubber hose. The hose and neck of the Schlenk flask were purged of air by applying vacuum and $N_2$ successively 3 times. The Schlenk flask was then opened to an $N_2$ atmosphere and placed in a dry ice / acetone bath. 1,3-Dibromopropane (0.57 ml, 1.12 g, 5.5 mmol, 1 equiv.) was loaded into a syringe and slowly added to the diethyllithium phosphide solution at -78 °C. The reaction was slowly warmed to room temperature and stirred overnight. The product solution was filtered through celite into a second 50 ml Schlenk flask, equipped with a magnetic stir bar and fitted with a filter stick. The solid was washed with additional pentane (3 x 10 ml). The filter stick was removed from the second Schlenk flask under a high $N_2$ pressure and replaced with a rubber septum. The pentane was removed from the filtrate under vacuum. A yellow oil was obtained. The crude product was distilled under vacuum to give a colorless oil (0.78 g, 3.5 mmol, 64 % yield).

$^{1}H$ NMR: (400 MHz, $C_6D_6$) δ 1.57 (m, 2H), 1.37 (m, 4H), 1.24 (m, 8H), 0.98 (m, 12H) ppm.

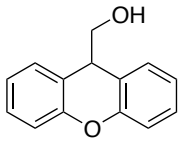
$^{13}C\{^{1}H\}$ NMR: (101 MHz, $C_6D_6$) δ 28.94 (dd, $J^{C-P}$ = 15 Hz, $J^{C-P}$ = 10 Hz), 23.03 (t, $J^{C-P}$ = 15 Hz), 19.47 (d, $J^{C-P}$ = 13 Hz), 9.90 (d, $J^{C-P}$ = 13 Hz) ppm.

$^{31}P\{^{1}H\}$ NMR: (162 MHz, $C_6D_6$) δ -23.96 ppm.

### 3.3.1.5 Synthesis of Homoxantphos.




#### 3.3.1.5.1 Synthesis of 9-Xanthylmethanol.[163]

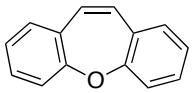


Lithium aluminum hydride, $LiAlH_4$ (3.8 g, 100 mmol, 3 equiv.) was weighed inside a glovebox in a 20 ml vial, and transferred, as a solid, to a 500 ml three-neck round bottom flask. The flask was equipped with a magnetic stir bar, charged with 200 ml of dry $Et_2O$, and fitted with a 24/40-to-barb flow control adapter and two rubber septa. The three-neck flask was then removed from the glovebox and connected to a Schlenk manifold. The hose connecting the flask to the manifold was purged of air by successively applying vacuum and $N_2$ (3x), and the flask was opened to an $N_2$ atmosphere, which was continuously bled through a bubbler. The reaction vessel was placed in an ice bath. Xanthene-9-carboxyilic acid (7.5 g, 33 mmol, 1 equiv.) was weighed inside the glovebox in a 20 ml vial. The compound was dissolved in 30 ml of dry $Et_2O$ and loaded into a 50 ml syringe. The syringe was stoppered with a rubber septum and removed from the glovebox. The solution of xanthene-9-carboxylic acid was slowly added to the solution of $LiAlH_4$ at 0 °C (caution: the reaction is vigorous and expels $H_2$ gas). The reaction was warmed to room temperature and then stirred overnight. The reaction was quenched by sequential addition of 10 ml $H_2O$, 10 ml 3 N NaOH(aq), and 10 ml $H_2O$, and then filtered after all of the gray solid to become white. The filtered solid was washed with additional $Et_2O$ (3 x 60 ml). The combined filtrates and washings were concentrated under vacuum to yield a white solid, which was recrystallized from cold pentane (5.9 g, 28 mmol, 84 % yield).

$^{1}H$ NMR: (400 MHz, $CDCl_3$) δ 7.29 (triplet of doublets, overlapping signals, J = 8 Hz, J = 1 Hz, 2H), 7.27 (d, overlapping signals, J = 8 Hz, 2H), 7.17 (d, J = 8 Hz, 4H), 7.12 (triplet of doublets, J = 8 Hz, J = 1 Hz), 3.99 (t, J = 6 Hz, 1H), 3.61 (d, J = 5 Hz, 2H), 2.52 (s, 1H) ppm.

$^{13}C\{^{1}H\}$ NMR: (100.6 MHz, $CDCl_3$) δ 152.18, 129.15, 128.13, 123.16, 122.12, 116.45, 68.79, 41.99 ppm.

#### 3.3.1.5.2 Synthesis of Dibenz[*b*,*f*]oxepine.[163-164]

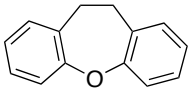


$P_2O_5$ (26.8 g, 189 mmol, 4 equiv.) was weighed inside a glovebox in a 20 ml vial and transferred as a solid to a 500 ml three-neck round bottom flask, equipped with a magnetic stir bar, a 24/40-to-barb flow control adapter, and a reflux condenser. Dry toluene (250 ml) was added to the flask, the flask was stoppered with two rubber septa and sealed from the box atmosphere. The three-neck flask was then removed from the glovebox and connected to a Schlenk manifold by a rubber hose. The hose was purged of $O_2$ by successively applying vacuum and $N_2$, and the flask was then opened to an $N_2$ atmosphere. 9-Xanthylmethanol (10. g, 47 mmol, 1 equiv.) was weighed inside the glovebox in a 20 ml vial, dissolved in toluene (30 ml), and loaded into a 50 ml syringe. The syringe was stoppered with a rubber septum and removed from the glovebox. The solution of 9-xanthylmethanol was added to the solution of $P_2O_5$ at room temperature. The reaction was then heated to reflux and stirred overnight. The reaction was cooled to 0 °C and water (100 ml) was added to the reaction vessel. The reagents were mixed thoroughly. The aqueous phase was separated from the organic phase and extracted with $Et_2O$ (3 x 100 ml). The organic fractions were combined and concentrated under vacuum. The product crystallized from a small amount of MeOH as a white solid (8.6 g, 44 mmol, 94 % yield).

$^1$H NMR: (600 MHz, $CDCl_3$) δ 7.26 (triplet of doublets, J = 8 Hz, J = 2 Hz, 2H), 7.14 (m, overlapping signals, 4H), 7.06 (triplet of doublets, J = 8 Hz, J = 2 Hz, 2H), 6.66 (s, 2H ppm.

$^{13}$C{$^1$H} NMR: (150.9 MHz, $CDCl_3$) δ 157.36, 130.59, 130.09, 129.94, 139.39, 124.99, 121.38 ppm.

#### 3.3.1.5.3 Synthesis of 10,11-dihydrodibenzo[*b*,*f*]oxepine.[164]

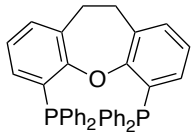


A 100 ml Schlenk flask, equipped with a magnetic stir bar, was charged with dibenz[*b*,*f*]oxepine (4.43 g, 22.8 mmol, 1 equiv.). Palladium on carbon (10 % wt, 1.6 g) was added to the flask as a solid. The flask was stoppered and connected to a Schlenk manifold by a rubber hose. The flask was then purged of $O_2$ by applying vacuum and $N_2$ successively 3 times, and then opened to $N_2$. The flask was charged with 50 ml of dry THF. A bubbler was connected to the Schlenk flask by a hose and needle, and the flask was then closed to $N_2$. A balloon filled with hydrogen and fitted with a syringe and 12 inch needle was connected to the flask. The tip of the needle was placed in the solution of dibenz[*b*,*f*]oxepine so that the solution could be sparged with $H_2$. This was repeated two more times. The bubbler was disconnected. A fourth balloon filled with hydrogen and connected to the Schlenk flask through a needle. The reaction was stirred overnight at room temperature under an atmosphere of $H_2$. The balloon was removed. The reaction was diluted with EtOAc and filtered through celite using a glass frit. The filtrate was collected and the solvent removed. The crude product was purified by column chromatography (eluent = 100 % hexanes) to yield a colorless oil (1.8 g, 9.2 mmol. 40 % yield).

$^1$H NMR: (400 MHz, THF-$d_8$) δ 7.14-7.03 (overlapping signals, m, 6H), 6.94 (ddd, J = 8 Hz, J = 6 Hz, J = 2 Hz, 4H), 3.04 (s, 4H) ppm.

$^{13}$C{$^1$H} NMR: (150.9 MHz, $CDCl_3$) δ 158.03, 132.72, 131.09, 127.99, 124.54, 121.63, 31.96 ppm.

### 3.3.1.5.4 Synthesis of 10,11-dihydro-4,5-bis(diphenylphosphino)dibenzo[*b*,*f*]oxepine, Homoxantphos (**k**).[165]

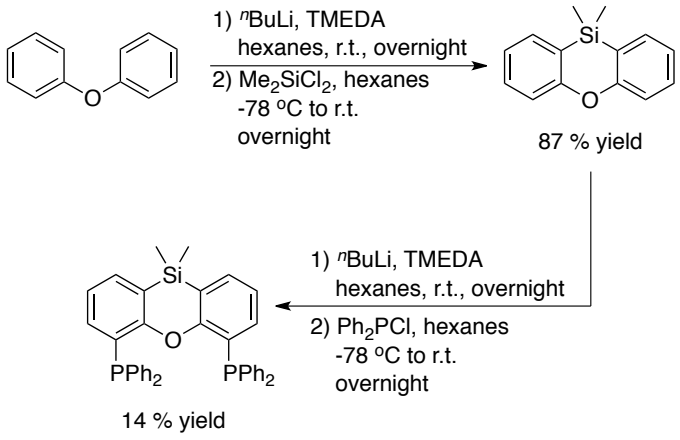



10,11-dihydrodibenzo[*b*,*f*]oxepine (2.02 g, 10.3 mmol, 1 equiv.) was weighed in a 20 ml vial and transferred as a solid to a 250 ml Schlenk flask. The Schlenk flask was equipped with a magnetic stir bar and then connected to a Schlenk manifold by a rubber hose. The flask was purged of $O_2$ by successively applying vacuum and $N_2$, and placed under an $N_2$ atmosphere. Dry $Et_2O$ (80 ml) and TMEDA (distilled from sodium, 3.37 ml, 2.63 g, 22.6 mmol, 2.2 equiv.) were added to the flask by syringe. The flask was placed in a dry ice / acetone bath and a solution of $^n$BuLi in hexanes (1.6 M, 14.2 ml, 22.7 mmol, 2.2 equiv.) was slowly added to the solution of 10,11-dihydrodibenzo[*b*,*f*]oxepine and TMEDA by syringe. The reaction was warmed to room temperature and stirred overnight. The flask was then placed in a dry ice acetone / bath and $Ph_2PCl$ (4.1 ml, 5.04 g, 22.8 mmol, 2.2 equiv.) was added to the reaction flask by syringe. The reaction was warmed to room temperature and stirred overnight. The solvent was removed under vacuum, and the resulting residue was dissolved in $CH_2Cl_2$. The $CH_2Cl_2$ solution was filtered through celite into a second 250 ml Schlenk flask equipped with a magnetic stir bar. The collected solid was washed with additional $CH_2Cl_2$ (3 x 20 ml). The filter stick was removed from the second Schlenk flask under a high $N_2$ pressure and replaced with a rubber septum. The $CH_2Cl_2$ was removed under vacuum. The crude product was washed with pentane (2 x 30 ml) and dried under vacuum. A white solid was obtained (2.70 g, 4.78 mmol, 46 % yield).

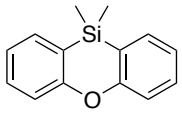
$^1$H NMR: (400 MHz, THF-$d_8$) δ 7.28-7.16 (overlapping signals, m, 12H), 7.15-7.10 (overlapping signals, m, 8H), 7.08 (dd, J = 8 Hz, J = 1 Hz, 2H), 6.82 (t, J = 8 Hz, 2H), 6.48 (dd, J = 8 Hz, J = 1 Hz, 2H), 3.07 (s, 4H) ppm.

$^{31}$P{$^1$H} NMR: (161.9 MHz, THF-$d_8$) δ -16.39 ppm.

### 3.3.1.6 Synthesis of Sixantphos.



#### 3.3.1.6.1 Synthesis of 10,10-Dimethylphenoxasilin.[166]

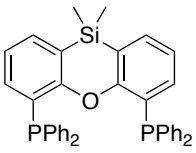


A 500 ml three-neck round bottom flask was equipped with a magnetic stir bar, a 24/40-to-barb flow control adapter, and two rubber septa.. The flask was connected to a Schlenk manifold by a rubber hose and purged of $O_2$ and water by successively applying vacuum and $N_2$. The flask was then placed under an $N_2$ atmosphere and charged with dry pentane (300 ml), diphenyl ether (18.6 ml, 20.0 g, 0.118 mol, 1 equiv.) and TMEDA (38.5 ml, 30.0 g, 0.258 mol, 2.2 equiv.). A dry ice / acetone bath was prepared and the flask was cooled to -78 °C. A solution of $^n$BuLi in hexanes (1.6 M, 162 ml, 0.259 mol, 2.2 equiv.) was added to the solution of diphenyl ether and TMEDA at -78 °C. The resulting reaction was warmed to room temperature and stirred overnight. A dark red solution formed. The reaction was cooled to -78 °C, and dichlorodimethylsilane (31.5 ml, 33.4 g, 0.259 mol, 2.2 equiv.) was added. The reaction was warmed to room temperature and stirred overnight. Water (100 ml) was added to the reaction and the organic and aqueous layers were separated. The aqueous phase was washed with $Et_2O$ (3 x 100 ml). The organic fractions were combined and concentrated under vacuum. A dark red oil was obtained. The crude product was purified by column chromatography (eluent = 100 % hexanes) to yield a white solid (23.1 g, 0.102 mol, 87 % yield).

$^1$H NMR: (500 MHz, $CDCl_3$) δ 7.76 (dd, J = 7 Hz, J = 2 Hz, 2H), 7.64 (m, 2H), 7.46 (d, J = 8 Hz, 2H), 7.36 (td, J = 7 Hz, J = 1 Hz, 2H), 0.72 (s, 6H) ppm.

$^{13}$C{$^1$H} NMR: (125.8 MHz, $CDCl_3$) δ 159.77, 134.05, 131.28, 122.74, 119.20, 118.15, -0.21 ppm.

#### 3.3.1.6.2 Synthesis of Sixantphos (**m**).[165,166c]

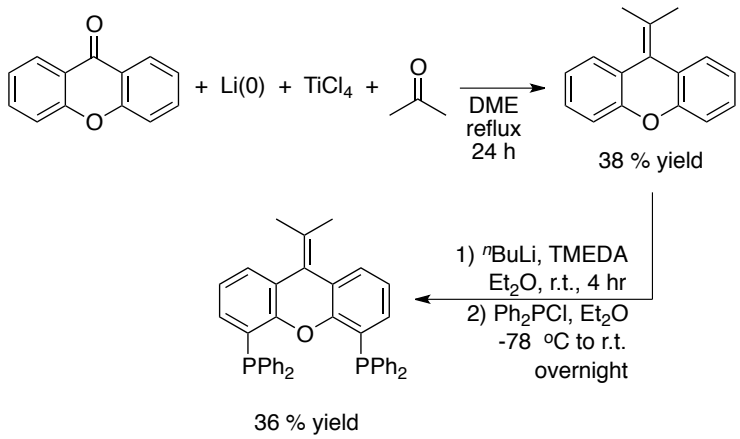


10,10-Dimethylphenoxasilin (3.56 g, 15.7 mmol, 1 equiv.) was weighed in a 20 ml vial and transferred as a solid to a 250 ml Schlenk flask. The Schlenk flask was equipped with a magnetic stir bar and then connected to a Schlenk manifold by a rubber hose. The flask was purged of $O_2$ by successively applying vacuum and $N_2$, and placed under an $N_2$ atmosphere. Dry $Et_2O$ (80 ml) and TMEDA (distilled from sodium, 5.15 ml, 4.02 g, 34.6 mmol, 2.2 equiv.) were added to the flask by syringe. The flask was placed in a dry ice / acetone bath and a solution of $^n$BuLi in hexanes (1.6 M, 21.6 ml, 34.6 mmol, 2.2 equiv.) was slowly added to the solution of 10,10-dimethylphenoxasilin and TMEDA by syringe. The reaction was warmed to room temperature and stirred overnight. The flask was then placed in a dry ice acetone / bath and $Ph_2PCl$ (7.1 ml, 8.68 g, 39.3 mmol, 2.5 equiv.) was added to the reaction flask by syringe. The reaction was warmed to room temperature and stirred overnight. The solvent was removed under vacuum, and the resulting residue was dissolved in $CH_2Cl_2$. The $CH_2Cl_2$ solution was filtered through celite into a second 250 ml Schlenk flask equipped with a magnetic stir bar. The collected solid was washed with additional $CH_2Cl_2$ (3 x 20 ml). The filter stick was removed from the second Schlenk flask under a high $N_2$ pressure and replaced with a rubber septum. The $CH_2Cl_2$ was removed under vacuum. The residue was dissolved in benzene and passed through a plug of silica gel. Crystallization from isopropanol afforded a white solid (1.32 g, 2.2 mmol, 14 % yield).

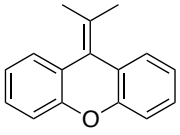
$^1$H NMR: (400 MHz, $CDCl_3$) δ 7.52 (d, J = 7 Hz, 2H), 7.29 (overlapping signals, m, 12H), 7.22 (s, 8H), 7.03 (t, J = 7 Hz, 2H), 6.82 (d, J = 7 Hz, 2H), 0.57 (s, 6H) ppm.

$^{31}$P{$^1$H} NMR: (202.2 MHz, $CDCl_3$) δ -17.62 ppm.

### 3.3.1.7 Synthesis of Isopropoxantphos




#### 3.3.1.7.1 Synthesis of 10-Isopropylidenexanthene.[167]

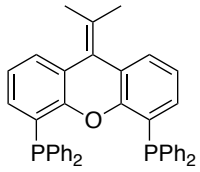


Lithium metal (9.9 g, 1.43 mol, 28 equiv.) was weighed inside an argon-filled glovebox in a 20 ml vial. The lithium was then transferred to a 500 ml three-neck round bottom flask. The flask was charged with 300 ml of anhydrous DME, equipped with a magnetic stir bar, a 24/40-to-barb flow control adapter, and a reflux condenser and then stoppered with two rubber septa. The flask was sealed from the box atmosphere and removed from the glovebox. A rubber hose was fitted to the 24/40-to-barb flow control adapter and connected to a Schlenk manifold. The hose was purged of air by successively applying vacuum and $N_2$ (3x). The three-neck flask was then opened to an $N_2$ atmosphere. $TiCl_4$ (39.3 ml, 67.8 g, 0.358 mol, 7 equiv.) was carefully loaded into a syringe under a stream of $N_2$ atmosphere (caution: $TiCl_4$ fumes). The $TiCl_4$ was then added to the solution of lithium metal in DME. A yellow solution formed. The yellow solution was heated to reflux for 1 hour. The reaction was then cooled to room temperature, and xanthone (10 g, 0.051 mol, 1 equiv.) and acetone (dried of molecular sieves, 3.74 ml, 2.96 g, 0.051 mol, 1 equiv.) were added to the flask (note: xanthone is insoluble in DME and was added to the three-neck flask as a solid under a high $N_2$ pressure). The resulting solution was heated to reflux and stirred for 24 hours. The solution was cooled to room temperature, and diluted with light petroleum ether (250 ml). The product solution was filtered through celite and then concentrated under vacuum. The crude product was purified by column chromatography (eluent = 100 % hexanes). A yellow solid was obtained (4.28 g, 0.019 mol, 38 % yield).

$^1$H NMR: (600 MHz, $CDCl_3$) δ 7.45 (d, J = 7 Hz, 2H), 7.26 (t, J = 7 Hz, 2H), 7.22 (d, J = 7 Hz, 2H), 7.16 (t, J = 7 Hz, 2H), 2.16 (6H) ppm.

$^{13}$C{$^1$H} NMR: (150.9 MHz, $CDCl_3$) δ 154.40, 130.88, 128.59, 127.30, 127.05, 122.83, 122.55, 116.37, 23.38 ppm.

#### 3.3.1.7.2 Synthesis of Isopropoxantphos.[165,168]

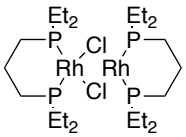



10-Isopropylidenexanthene (2.1 g, 9.4 mmol, 1 equiv.) was weighed in a 20 ml vial and transferred as a solid to a 250 ml Schlenk flask. The Schlenk flask was equipped with a magnetic stir bar and then connected to a Schlenk manifold by a rubber hose. The flask was purged of $O_2$ by successively applying vacuum and $N_2$, and placed under an $N_2$ atmosphere. Dry $Et_2O$ (80 ml) and TMEDA (distilled from sodium, 3.2 ml, 2.5 g, 21 mmol, 2.3 equiv.) were added to the flask by syringe. The flask was placed in a dry ice / acetone bath and a solution of $^{n}$BuLi in hexanes (1.6 M, 13.1 ml, 21 mmol, 2.2 equiv.) was slowly added to the solution of 10-isopropylidenexanthene and TMEDA by syringe. The reaction was warmed to room temperature and stirred overnight. The flask was then placed in a dry ice acetone / bath and $Ph_2PCl$ (4.2 ml, 5.2 g, 23 mmol, 2.5 equiv.) was added to the reaction flask by syringe. The reaction was warmed to room temperature and stirred overnight. The solvent was removed under vacuum, and the resulting residue was dissolved in $CH_2Cl_2$. The $CH_2Cl_2$ solution was filtered through celite into a second 250 ml Schlenk flask equipped with a magnetic stir bar. The collected solid was washed with additional $CH_2Cl_2$ (3 x 20 ml). The filter stick was removed from the second Schlenk flask under a high $N_2$ pressure and replaced with a rubber septum. The $CH_2Cl_2$ was removed under vacuum. The crude product was washed with pentane (2 x 30 ml) and dried under vacuum. A white solid was obtained (2.0 g, 3.4 mmol, 36 % yield).

$^{1}$H NMR: (400 MHz, THF-$d_8$) δ 7.40 (dd, J = 8 Hz, J = 1 Hz, 2H), 7.30-7.13 (overlapping signals, m, 20H), 7.00 (t, J = 8 Hz, 2H), 6.59 (dd, J = 8 Hz, J = 2 Hz, 2H), 2.10 (s, 6H) ppm.

$^{31}$P{$^{1}$H} NMR: (161.9 MHz, THF-$d_8$) δ -17.63 ppm.

### 3.3.1.8 Synthesis of rhodium diphosphine chloride complex, **1e**.




**1e**

$[Rh(COE)_2(\mu\text{-}Cl)]_2$ (100. mg, 0.139 mmol, 1 equiv.) was weighed inside a glovebox in a 20 ml vial. DEtPP (63.4 mg, 0.288 mmol, 2.1 equiv.) was weighed inside the same glovebox in a 20 ml vial. The weighed DEtPP was dissolved in 6 ml of dry pentane and transferred to the vial containing the weighed $[Rh(COE)_2(\mu\text{-}Cl)]_2$. A magnetic stir bar was added to the vial. The vial was capped, and the reaction was stirred overnight at room temperature. The solution was concentrated under vacuum to a volume of approximately 1 ml, and placed in the freezer. The precipitated solid was collected on a glass frit and transferred to a tared 20 ml vial. The solid was dried under vacuum and used as obtained (44 mg, 0.06 mmol, 44 % yield).

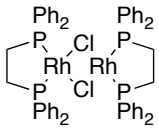
$^{1}$H NMR: (499.7 MHz, toluene- $d_8$) δ 1.89 (m, broad, 4H), 1.53 (m, broad, 2H), 1.32 (m, overlapping signals, 16H), 0.92 (s, 4H) ppm.

$^{31}$P{$^{1}$H} NMR: (202.3 MHz, toluene- $d_8$) δ 35.3 (d, $J^{P\text{-}Rh}$ = 185 Hz) ppm.

Analysis Calculated For $C_{22}H_{52}Cl_2P_4Rh_2$: C, 36.84; H, 7.31; N, 0.00.

Found: C, 36.83; H, 7.43; N, 0.26.

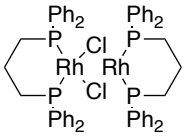
### 3.3.1.9 Synthesis of rhodium diphosphine chloride complex, **1f**.



**1f**

$[Rh(COE)_2(\mu\text{-}Cl)]_2$ (100. mg, 0.139 mmol, 1 equiv.) was weighed inside a glovebox in a 20 ml vial. DPPE (111 mg, 0.279 mmol, 2 equiv.) was weighed inside the same glovebox in a 20 ml vial. The weighed DPPE was dissolved in 6 ml of dry THF and transferred to the vial containing the weighed $[Rh(COE)_2(\mu\text{-}Cl)]_2$. A magnetic stir bar was added to the vial. The vial was capped, and the reaction was stirred overnight at room temperature. The solution was concentrated under vacuum to a volume of approximately 1 ml, and diluted with $Et_2O$ (~15 ml). The precipitated solid was collected on a glass frit and transferred to a tared 20 ml vial. The solid was dried under vacuum and used as obtained (124 mg, 0.116 mmol, 83 % yield).

### 3.3.1.10 Synthesis of rhodium diphosphine chloride complex, **1g**.



**1g**

$[Rh(COE)_2(\mu\text{-}Cl)]_2$ (200. mg, 0.279 mmol, 1 equiv.) was weighed inside a glovebox in a 20 ml vial. DPPP (230 mg, 0.279 mmol, 2 equiv.) was weighed inside the same glovebox in a 20 ml vial. The weighed DPPP was dissolved in 6 ml of dry THF and transferred to the vial containing the weighed $[Rh(COE)_2(\mu\text{-}Cl)]_2$. A magnetic stir bar was added to the vial. The vial was capped, and the reaction was stirred overnight at room temperature. The solution was concentrated under vacuum to a volume of approximately 1 ml, and diluted with $Et_2O$ (~15 ml). The precipitated solid was collected on a glass frit and transferred to a tared 20 ml vial. The solid was dried under vacuum and used as obtained (272 mg, 0.247 mmol, 89 % yield).

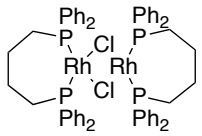
$^1$H NMR: (499.92 MHz, THF-$d_8$) δ 7.66 (s, broad, 8H), 7.17 (t, $J^{H\text{-}H}$ = 7 Hz, 4H), 7.05 (t, $J^{H\text{-}H}$ = 7 Hz, 8H), 2.19 (s, broad, 4H), 1.67 (s, broad, 2H) ppm.

$^{31}$P{$^1$H} NMR: (202.2 MHz, THF-$d_8$) δ 32.23 (d, $J^{P\text{-}Rh}$ = 183 Hz) ppm.

Analysis Calculated For $C_{56}H_{56}Cl_2P_4Rh_2$: C, 58.88; H, 4.76; N, 0.00.

Found: C, 58.68; H, 4.84; N, 0.33.

### 3.3.1.11 Synthesis of rhodium diphosphine chloride complex, **1h**.



**1h**

$[Rh(COE)_2(\mu\text{-}Cl)]_2$ (100. mg, 0.139 mmol, 1 equiv.) was weighed inside a glovebox in a 20 ml vial. DPPB (119 mg, 0.279 mmol, 2 equiv.) was weighed inside the same glovebox in a 20 ml vial. The weighed DPPB was dissolved in 6 ml of dry THF and transferred to the vial containing the weighed $[Rh(COE)_2(\mu\text{-}Cl)]_2$. A magnetic stir bar was added to the vial. The vial was capped, and the reaction was stirred overnight at room temperature. The solution was concentrated under vacuum to a volume of approximately 1 ml, and diluted with $Et_2O$ (~15 ml). The precipitated solid was collected on a glass frit and transferred to a tared 20 ml vial. The solid was dried under vacuum and used as obtained (150. mg, 0.133 mmol, 95 % yield).

$^1$H NMR: (499.92 MHz, $C_6D_6$) δ 7.73 (m, broad, 4H), 7.05 (m, broad, 8H), 1.92 (s, broad, 4H), 1.64 (s, broad, 4H) ppm.

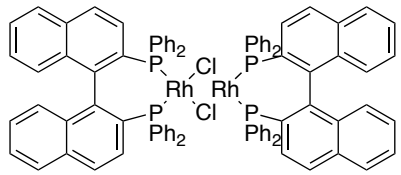
$^{13}C\{^{1}H\}$ NMR: (100.6 MHz, THF- $d_8$) δ 128.45 (t, $J^{C-P}$ = 21 Hz), 133.87, 128.85, 127.49, 29.43 (t, $J^{C-P}$ = 17 Hz), 24.14 ppm.

$^{31}P\{^{1}H\}$ NMR: (161.9 MHz, $C_6D_6$) δ 45.5 (d, $J^{P-Rh}$ = 190 Hz) ppm.

Analysis Calculated For $C_{56}H_{56}Cl_2P_4Rh_2$: C, 59.54; H, 5.00; N, 0.00.

Found: C, 59.71; H, 5.10; N, 0.27.

### 3.3.1.12 Synthesis of rhodium diphosphine chloride complex, **1i**.




**1i**

$[Rh(COE)_2(\mu\text{-}Cl)]_2$ (100. mg, 0.139 mmol, 1 equiv.) was weighed inside a glovebox in a 20 ml vial. BINAP (174 mg, 0.279 mmol, 2 equiv.) was weighed inside the same glovebox in a 20 ml vial. The weighed BINAP was dissolved in 6 ml of dry THF and transferred to the vial containing the weighed $[Rh(COE)_2(\mu\text{-}Cl)]_2$. A magnetic stir bar was added to the vial. The vial was capped, and the reaction was stirred overnight at room temperature. The solution was concentrated under vacuum to a volume of approximately 1 ml, and diluted with $Et_2O$ (~15 ml). The precipitated solid was collected on a glass frit and transferred to a tared 20 ml vial. The solid was dried under vacuum and used as obtained (194 mg, 0.127 mmol, 91 % yield).

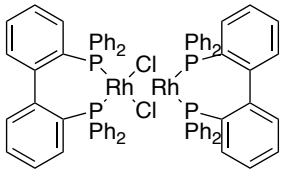
$^{1}H$ NMR: (600 MHz, $CD_2Cl_2$) δ 7.87 (s, broad, 4H, overlapping signal), 7.79 (s, broad, 4H, overlapping signal), 7.51 (d, J = 8Hz, 2H), 7.42 (d, J = 9Hz, 2H), 7.32-7.23 (overlapping signals, m, 4H), 7.09 (t, J = 7 Hz, 2H), 7.03-6.93 (overlapping signals, m, 6H), 6.72 (t, J = 7Hz, 2H), 6.64 (s, broad, 4H, overlapping signal), 6.61 (d, J = 9 Hz, 2H) ppm.

$^{31}P\{^{1}H\}$ NMR: (202.2 MHz, $CD_2Cl_2$) δ 49.9 (d, $J^{P-Rh}$ = 196 Hz) ppm.

Analysis Calculated For $C_{88}H_{64}Cl_2P_4Rh_2$: C, 69.44; H, 4.24; N, 0.00.

Found: C, 69.37; H, 4.53; N, 0.01.

### 3.3.1.13 Synthesis of rhodium diphosphine chloride complex, **1j.**

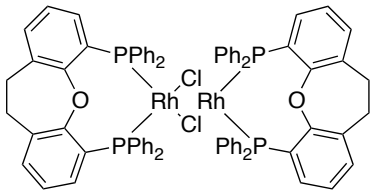



**1j**

$[Rh(COE)_2(\mu\text{-}Cl)]_2$ (100. mg, 0.139 mmol, 1 equiv.) was weighed inside a glovebox in a 20 ml vial. BIPHEP (146 mg, 0.279 mmol, 2 equiv.) was weighed inside the same glovebox in a 20 ml vial. The weighed BIPHEP was dissolved in 6 ml of dry THF and transferred to the vial containing the weighed $[Rh(COE)_2(\mu\text{-}Cl)]_2$. A magnetic stir bar was added to the vial. The vial was capped, and the reaction was stirred overnight at room temperature. The solution was concentrated under vacuum to a volume of approximately 1 ml, and diluted with $Et_2O$ (~15 ml). The precipitated solid was collected on a glass frit and transferred to a tared 20 ml vial. The solid was dried under vacuum and used as obtained (174 mg, 0.132 mmol, 94 % yield).

$^{31}P\{^{1}H\}$ NMR: (202.2 MHz, THF) δ 46.8 (d, $J^{P-Rh}$ = 192 Hz) ppm.

### 3.3.1.14 Synthesis of rhodium diphosphine chloride complex, **1k**.



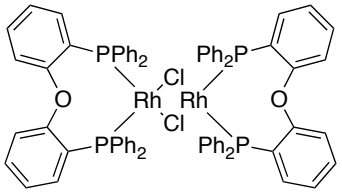

**1k**

$[Rh(COE)_2(\mu\text{-}Cl)]_2$ (100. mg, 0.139 mmol, 1 equiv.) was weighed inside a glovebox in a 20 ml vial. Homoxantphos (157 mg, 0.278 mmol, 2 equiv.) was weighed inside the same glovebox in a 20 ml vial. The weighed Homoxantphos was dissolved in 6 ml of dry THF and transferred to the vial containing the weighed $[Rh(COE)_2(\mu\text{-}Cl)]_2$. A magnetic stir bar was added to the vial. The vial was capped, and the reaction was stirred overnight at room temperature. The solution was concentrated under vacuum to a volume of approximately 1 ml, and diluted with $Et_2O$ (~15 ml). The precipitated solid was collected on a glass frit and transferred to a tared 20 ml vial. The solid was dried under vacuum and used as obtained (178 mg, 0.127 mmol, 91 % yield).

$^1H$ NMR: (499.7 MHz, $CD_2Cl_2$) δ 7.55 (s, broad, 8H), 7.10 (t, $J^{H\text{-}H}$ = 8 Hz, 4H), 7.06 (d, $J^{H\text{-}H}$ = 8 Hz, 2H), 6.97 (t, $J^{H\text{-}H}$ = 8 Hz, 8H), 6.68 (t, $J^{H\text{-}H}$ = 8 Hz, 2H), 6.29 (m, 2H), 2.89 (s, 4H) ppm.

$^{31}P\{^1H\}$ NMR: (161.9 MHz, $CD_2Cl_2$) δ 37.4 (d, $J^{P\text{-}Rh}$ = 204 Hz) ppm.

### 3.3.1.15 Synthesis of rhodium diphosphine chloride complex, **1l**.

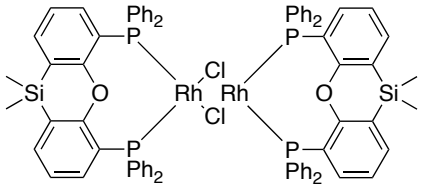



**1l**

$[Rh(COE)_2(\mu\text{-}Cl)]_2$ (100. mg, 0.139 mmol, 1 equiv.) was weighed inside a glovebox in a 20 ml vial. DPEphos (150 mg, 0.279 mmol, 2 equiv.) was weighed inside the same glovebox in a 20 ml vial. The weighed DPEphos was dissolved in 6 ml of dry THF and transferred to the vial containing the weighed $[Rh(COE)_2(\mu\text{-}Cl)]_2$. A magnetic stir bar was added to the vial. The vial was capped, and the reaction was stirred overnight at room temperature. The solution was concentrated under vacuum to a volume of approximately 1 ml, and diluted with $Et_2O$ (~15 ml). The precipitated solid was collected on a glass frit and transferred to a tared 20 ml vial. The solid was dried under vacuum and used as obtained (200 mg, 0.143 mmol, 97 % yield).

$^{31}P\{^1H\}$ NMR: (202 MHz, $CD_2Cl_2$) δ 18.13 (d, $J^{P\text{-}Rh}$ = 107 Hz) ppm.

### 3.3.1.16 Synthesis of rhodium diphosphine chloride complex, **1m**.



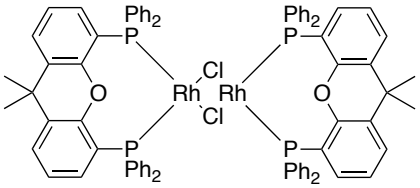

**1m**

$[Rh(COE)_2(\mu\text{-}Cl)]_2$ (100. mg, 0.139 mmol, 1 equiv.) was weighed inside a glovebox in a 20 ml vial. Sixantphos (166 mg, 0.279 mmol, 2 equiv.) was weighed inside the same glovebox in a 20 ml vial. The weighed Sixantphos was dissolved in 6 ml of dry THF and transferred to the vial containing the weighed $[Rh(COE)_2(\mu\text{-}Cl)]_2$. A magnetic stir bar was added to the vial. The vial was capped, and the reaction was stirred overnight at room temperature. The solution was concentrated under vacuum to a volume of approximately 1 ml, and diluted with $Et_2O$ (~15 ml). The precipitated solid was collected on a glass frit and transferred to a tared 20 ml vial. The solid was dried under vacuum and used as obtained (180 mg, 0.123 mmol, 88 % yield).

$^{31}P\{^1H\}$ NMR: (161.9 MHz,$CD_2Cl_2$) δ 42.38 (d, $J^{P\text{-}Rh}$ = 193 Hz) ppm.

Analysis Calculated For $C_{76}H_{64}Cl_2O_2P_4Rh_2Si_2$: C, 62.26 H, 4.40; N, 0.00.
Found: C, 61.93 H, 4.75; N, 0.39.

### 3.3.1.17 Synthesis of rhodium diphosphine chloride complex, **1n**.



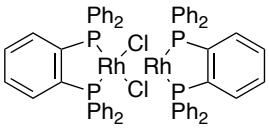

**1n**

$[Rh(COE)_2(\mu\text{-}Cl)]_2$ (100. mg, 0.139 mmol, 1 equiv.) was weighed inside a glovebox in a 20 ml vial. Xantphos (161 mg, 0.278 mmol, 2 equiv.) was weighed inside the same glovebox in a 20 ml vial. The weighed Xantphos was dissolved in 6 ml of dry THF and transferred to the vial containing the weighed $[Rh(COE)_2(\mu\text{-}Cl)]_2$. A magnetic stir bar was added to the vial. The vial was capped, and the reaction was stirred overnight at room temperature. The solution was concentrated under vacuum to a volume of approximately 1 ml, and diluted with $Et_2O$ (~15 ml). The precipitated solid was collected on a glass frit and transferred to a tared 20 ml vial. The solid was dried under vacuum and used as obtained (184 mg, 0.128 mmol, 92 % yield).

$^{31}P\{^1H\}$ NMR: (161.9 MHz, $CD_2Cl_2$) δ 32.8 (d, $J^{P\text{-}Rh}$ = 122 Hz) ppm.

Analysis Calculated For $C_{78}H_{64}Cl_2O_2P_4Rh_2$: C, 65.33; H, 4.50; N, 0.00.
Found: C, 65.47; H, 4.98; N, 0.24.

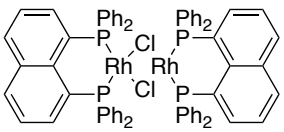
### 3.3.1.18 Synthesis of 1,2-bis(diphenylphosphino)benzene rhodium chloride.




$[Rh(COE)_2(\mu\text{-}Cl)]_2$ (100. mg, 0.139 mmol, 1 equiv.) was weighed inside a glovebox in a 20 ml vial. DPPBz (125 mg, 0.280 mmol, 2 equiv.) was weighed inside the same glovebox in a 20 ml vial. The weighed DPPBz was dissolved in 6 ml of dry THF and transferred to the vial containing the weighed $[Rh(COE)_2(\mu\text{-}Cl)]_2$. A magnetic stir bar was added to the vial. The vial was capped, and the reaction was stirred overnight at room temperature. The solution was concentrated under vacuum to a volume of approximately 1 ml, and diluted with $Et_2O$ (~15 ml). The precipitated solid was collected on a glass frit and transferred to a tared 20 ml vial. The solid was dried under vacuum and used as obtained (153 mg, 0.131 mmol, 94 % yield).

$^{31}P\{^1H\}$ NMR: (161.9 MHz, $CD_2Cl_2$) δ 62.9 (d, $J^{P\text{-}Rh}$ = 134 Hz) ppm.

### 3.3.1.19 Synthesis of 1,8-bis(diphenylphosphino)naphthyl rhodium chloride.



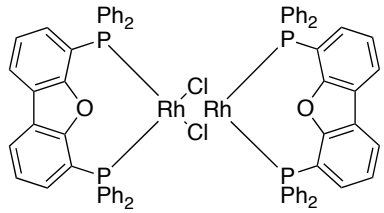

$[Rh(COE)_2(\mu\text{-}Cl)]_2$ (100. mg, 0.139 mmol, 1 equiv.) was weighed inside a glovebox in a 20 ml vial. DPPN (139 mg, 0.280 mmol, 2 equiv.) was weighed inside the same glovebox in a 20 ml vial. The weighed DPPN was dissolved in 6 ml of dry THF and transferred to the vial containing the weighed $[Rh(COE)_2(\mu\text{-}Cl)]_2$. A magnetic stir bar was added to the vial. The vial was capped, and the reaction was stirred overnight at room temperature. The solution was concentrated under vacuum to a volume of approximately 1 ml, and diluted with $Et_2O$ (~15 ml). The precipitated solid was collected on a glass frit and transferred to a tared 20 ml vial. The solid was dried under vacuum and used as obtained (125 mg, 0.098 mmol, 71 % yield).

$^{31}P\{^{1}H\}$ NMR: (161.9 MHz, toluene) δ 47.2 (d, broad, $J^{P\text{-}Rh}$ = 188 Hz) ppm.

Analysis Calculated For $C_{68}H_{52}Cl_2P_4Rh_2$: C, 64.32; H, 4.13; N, 0.00.

Found: C, 64.09; H, 4.49; N, 0.00.

### 3.3.1.20 Synthesis of DBFphos rhodium chloride.



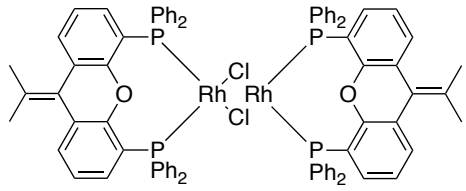

$[Rh(COE)_2(\mu\text{-}Cl)]_2$ (100. mg, 0.139 mmol, 1 equiv.) was weighed inside a glovebox in a 20 ml vial. DBFphos (150 mg, 0.280 mmol, 2 equiv.) was weighed inside the same glovebox in a 20 ml vial. The weighed DBFphos was dissolved in 6 ml of dry THF and transferred to the vial containing the weighed $[Rh(COE)_2(\mu\text{-}Cl)]_2$. A magnetic stir bar was added to the vial. The vial was capped, and the reaction was stirred overnight at room temperature. The solution was concentrated under vacuum to a volume of approximately 1 ml, and diluted with $Et_2O$ (~15 ml). The precipitated solid was collected on a glass frit and transferred to a tared 20 ml vial. The solid was dried under vacuum and used as obtained (179 mg, 0.133 mmol, 95 % yield).

### 3.3.1.21 Synthesis of Benzoxantphos rhodium chloride.

$[Rh(COE)_2(\mu\text{-}Cl)]_2$ (100. mg, 0.139 mmol, 1 equiv.) was weighed inside a glovebox in a 20 ml vial. Benzoxantphos (164 mg, 0.280 mmol, 2 equiv.) was weighed inside the same glovebox in a 20 ml vial. The weighed Benzoxantphos was dissolved in 6 ml of dry THF and transferred to the vial containing the weighed $[Rh(COE)_2(\mu\text{-}Cl)]_2$. A magnetic stir bar was added to the vial. The vial was capped, and the reaction was stirred overnight at room temperature. The solution was concentrated under vacuum to a volume of approximately 1 ml, and diluted with $Et_2O$ (~15 ml). The precipitated solid was collected on a glass frit and transferred to a tared 20 ml vial. The solid was dried under vacuum and used as obtained (200. mg, 0.138 mmol, 99 % yield).

$^{31}P\{^{1}H\}$ NMR: (161.9 MHz, toluene) δ 19.2 (d, $J^{P\text{-}Rh}$ =149 Hz), 18.9 (d, $J^{P\text{-}Rh}$ = 148 Hz) ppm.

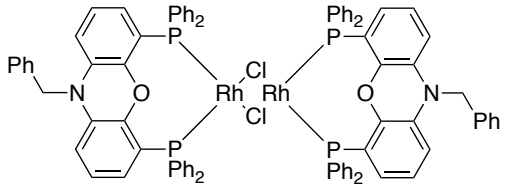
### 3.3.1.22 Synthesis of Isopropoxantphos rhodium chloride.




$[Rh(COE)_2(\mu\text{-}Cl)]_2$ (100. mg, 0.139 mmol, 1 equiv.) was weighed inside a glovebox in a 20 ml vial. Isopropoxantphos (165 mg, 0.279 mmol, 2 equiv.) was weighed inside the same glovebox in a 20 ml vial. The weighed Isopropoxantphos was dissolved in 6 ml of dry THF and transferred to the vial containing the weighed $[Rh(COE)_2(\mu\text{-}Cl)]_2$. A magnetic stir bar was added to the vial. The vial was capped, and the reaction was stirred overnight at room temperature. The solution was concentrated under vacuum to a volume of approximately 1 ml, and diluted with $Et_2O$ (~15 ml). The precipitated solid was collected on a glass frit and transferred to a tared 20 ml vial. The solid was dried under vacuum and used as obtained (184 mg, 0.126 mmol, 91 % yield).

$^{31}P\{^{1}H\}$ NMR: (161.9 MHz, toluene) δ 47.2 (d, broad, $J^{P\text{-}Rh}$ = 188 Hz) ppm.

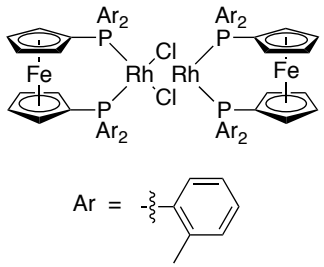
### 3.3.1.23 Synthesis of Benzylnixantphos rhodium chloride.




$[Rh(COE)_2(\mu\text{-}Cl)]_2$ (100. mg, 0.139 mmol, 1 equiv.) was weighed inside a glovebox in a 20 ml vial. Benzylnixantphos (179 mg, 0.279 mmol, 2 equiv.) was weighed inside the same glovebox in a 20 ml vial. The weighed Benzylnixantphos was dissolved in 6 ml of dry THF and transferred to the vial containing the weighed $[Rh(COE)_2(\mu\text{-}Cl)]_2$. A magnetic stir bar was added to the vial. The vial was capped, and the reaction was stirred overnight at room temperature. The solution was concentrated under vacuum to a volume of approximately 1 ml, and diluted with $Et_2O$ (~15 ml). The precipitated solid was collected on a glass frit and transferred to a tared 20 ml vial. The solid was dried under vacuum and used as obtained (171 mg, 0.110 mmol, 79 % yield).

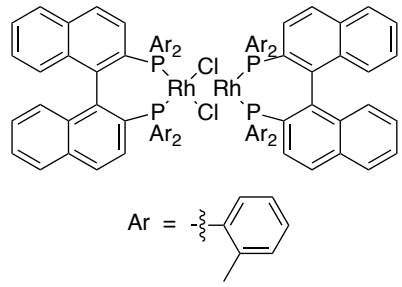
$^{31}P\{^1H\}$ NMR: (202.2 MHz, THF) δ 26.4 (d, broad, $J^{P\text{-}Rh}$ = 203 Hz) ppm.

### 3.3.1.24 Synthesis of 1,1'-bis(di-*o*-tolylphosphino)ferrocene rhodium chloride.




$[Rh(COE)_2(\mu\text{-}Cl)]_2$ (100. mg, 0.139 mmol, 1 equiv.) was weighed inside a glovebox in a 20 ml vial. DArPF (Ar = 2-$CH_3$-$C_6H_4$) (170 mg, 0.278 mmol, 2 equiv.) was weighed inside the same glovebox in a 20 ml vial. The weighed DArPF was dissolved in 6 ml of dry THF and transferred to the vial containing the weighed $[Rh(COE)_2(\mu\text{-}Cl)]_2$. A magnetic stir bar was added to the vial. The vial was capped, and the reaction was stirred overnight at room temperature. The solution was concentrated under vacuum to a volume of approximately 1 ml, and diluted with $Et_2O$ (~15 ml). The precipitated solid was collected on a glass frit and transferred to a tared 20 ml vial. The solid was dried under vacuum and used as obtained (189 mg, 0.126 mmol, 91 % yield).

### 3.3.1.25 Synthesis of 2,2-bis(di-*o*-tolylphosphino)-1,1-binaphthyl rhodium chloride.



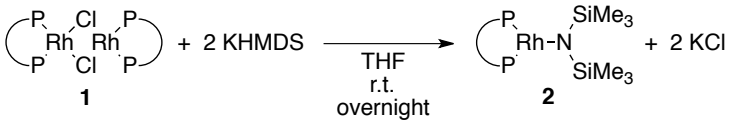

$[Rh(COE)_2(\mu\text{-}Cl)]_2$ (100. mg, 0.139 mmol, 1 equiv.) was weighed inside a glovebox in a 20 ml vial. 2,2-bis(di-*o*-tolylphosphino)-1,1-binaphthyl (189 mg, 0.278 mmol, 2 equiv.) was weighed inside the same glovebox in a 20 ml vial. The weighed DArPF was dissolved in 6 ml of dry THF and transferred to the vial containing the weighed $[Rh(COE)_2(\mu\text{-}Cl)]_2$. A magnetic stir bar was added to the vial. The vial was capped, and the reaction was stirred overnight at room temperature. The solution was concentrated under vacuum to a volume of approximately 1 ml, and diluted with $Et_2O$ (~15 ml). The precipitated solid was collected on a glass frit and transferred to a tared 20 ml vial. The solid was dried under vacuum and used as obtained (189 mg, 0.116 mmol, 83 % yield).

$^1H$ NMR: (500 MHz, THF-$d_8$) δ 7.83 (d, J = 8 Hz, 4H), 7.70 (d, J = 8 Hz, 4H), 7.43 (d, J = 8 Hz, 4H), 7.25-7.15 (overlapping signals, m, 8H), 7.10 (m, 4H), 7.06-7.01 (m, 4H), 7.00 (t, J = 7 Hz, 4H), 6.96-6.87 (overlapping

signals, m, 8H), 6.6.76 (s, broad, 4H), 6.55 (s, broad, 4H), 6.46 (m, 1H), 6.13 (dd, J = 8 Hz, J = 3 Hz, 1H), 1.73 (s, 12H), 1.59 (s, 12H).

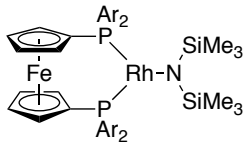
$^{31}P\{^{1}H\}$ NMR: (202 MHz, THF-$d_8$) δ 47.34 (d, J = 195 Hz) ppm.

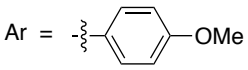
### 3.3.2 Syntheses of Rhodium Diphosphine Silylamido Complexes.




**1** **2**

#### 3.3.2.1 Synthesis of Rhodium Diphosphine Silylamido Complex, **2a**.




**2a**

Rhodium diphosphine chloride complex, **1a**, was weighed inside a glovebox in 20 ml vial (208 mg, 0.128 mmol, 1 equiv.). THF (2 ml) and a magnetic stir bar were added to the vial. A solution of KHMDS (51.1 mg, 0.256 mmol, 2 equiv.) in THF (5 ml) was prepared in a 20 ml separate vial and added to the rhodium diphosphine complex by pipet. The vial containing the two reagents was capped. The resulting solution was stirred overnight inside the glovebox at room temperature. The solution became dark green, homogeneous. The THF solvent was removed under vacuum. The green residue was dissolved in pentane and filtered through celite. The filtrate was collected and the solvent removed under vacuum to yield a dark blue solid (144 mg, 0.154 mmol, 60 % yield).

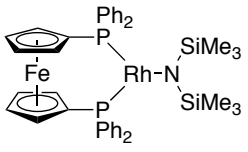
$^{1}H$ NMR: (499.92 MHz, toluene- $d_8$) δ 7.97 (s, broad, 8H), 6.71 (d, $J^{H-H}$ = 8 Hz, 8H), 4.59 (s, 4H), 3.95 (s, 4H), 3.15 (s, 12H), 0.65 (s, 18H) ppm.

$^{13}C\{^{1}H\}$ NMR: (125.7 MHz, THF- $d_8$) δ 161.6 (t, $J^{C-P}$ = 25.1 Hz), 136.0, 130.11, 111.4, 83.5 (t, $J^{C-P}$ = 28.9Hz), 75.9, 72.2, 55.4, 7.1 ppm.

$^{31}P\{^{1}H\}$ NMR: (202.2 MHz, toluene- $d_8$) δ 62.5 (d, $J^{P-Rh}$ = 182 Hz) ppm.

Analysis Calculated For $C_{44}H_{54}FeNO_4P_2RhSi_2$: C, 56.35; H, 5.80; N, 1.49.

#### 3.3.2.2 Synthesis of Rhodium Diphosphine Silylamido Complex, **2b**.




**2b**

Rhodium diphosphine chloride complex, **1b**, was weighed inside a glovebox in 20 ml vial (200. mg, 0.144 mmol, 1 equiv.). THF (2 ml) and a magnetic stir bar were added to the vial. A solution of KHMDS (57.6 mg, 0.289 mmol, 2 equiv.) in THF was prepared in a separate 20 ml vial and added to the rhodium diphosphine complex by pipet. The vial containing the two reagents was capped. The resulting solution was stirred overnight inside the glovebox at room temperature. The solution became dark green, homogeneous. The solvent was removed under vacuum. The dark green residue was dissolved in pentane and filtered through celite. The filtrate was collected and the solvent removed under vacuum. A dark green solid was collected (221 mg, 0.270 mmol, 94 % yield).

$^{1}$H NMR: (499.4 MHz, $C_6D_6$) δ 7.99 (m, 8 H), 7.05 (t, J = 7.5 Hz, 8 H), 7.01 (q, J = 7.5 Hz, 4 H), 4.45 (s, broad, 4 H), 3.84 (s, broad, 4 H), 0.51 (s, 18 H) ppm.

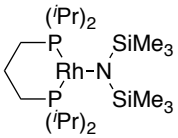
$^{13}$C{$^{1}$H} NMR: (125.7 MHz, $C_6D_6$) δ 138.7 (t, $J^{C-P}$ = 23 Hz), 134.6 (t, $J^{C-P}$ = 6 Hz), 130.0, 128.7, 81.9, (t, $J^{C-P}$ = 30 Hz), 76.0 (t, unresolved), 72.4 (t, unresolved), 7.3 ppm.

$^{31}$P{$^{1}$H} NMR: (202.2 MHz, $C_6D_6$) δ 64.1 (d, $J_{P-Rh}$ = 183 Hz) ppm.

Analysis Calculated For $C_{40}H_{46}FeNP_2RhSi_2$: C, 58.76; H, 5.67; N, 1.71.

Found: C, 58.80; H, 5.62; N, 1.38.

### 3.3.2.3 Synthesis of Rhodium Diphosphine Silylamido Complex, **2d**.




**2d**

Rhodium diphosphine chloride complex, **1d**, was weighed inside a glovebox in 20 ml vial (200. mg, 0.144 mmol, 1 equiv.). THF (2 ml) and a magnetic stir bar were added to the vial. A solution of KHMDS (57.6 mg, 0.289 mmol, 2 equiv.) in THF was prepared in a separate 20 ml vial and added to the rhodium diphosphine complex by pipet. The vial containing the two reagents was capped. The resulting solution was stirred overnight inside the glovebox at room temperature. The solution became purple. The solvent was removed under vacuum. The purple residue was dissolved in pentane and filtered through celite. The filtrate was collected and the solvent removed under vacuum. A purple solid was collected (221 mg, 0.270 mmol, 94 % yield).

$^{1}$H NMR: (500 MHz, toluene-$d_8$) δ 1.67 (s, broad, 4H), 1.40 (s, broad, 2H), 1.13 (s, broad, 12H), 1.05 (s, broad, 12H), 0.74 (s, broad, 4H), 0.51 (s, broad, 18H) ppm.

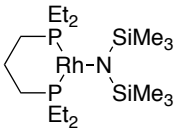
$^{13}$C{$^{1}$H} NMR: (125.7 MHz, toluene-$d_8$) δ 27.58 (t, J = 12.8 Hz), 22.45, 19.55, 19.20, 19.17 (t, J = 17 Hz), 7.86 ppm.

$^{31}$P{$^{1}$H} NMR: (202.2 MHz, toluene-$d_8$) δ 63.3 (d, $J^{P-Rh}$ = 164 Hz) ppm.

Analysis Calculated For $C_{21}H_{52}NP_2RhSi_2$: C, 46.74; H, 9.71; N, 2.60.

Found: C, 46.94; H, 9.58; N, 2.28.

### 3.3.2.4 Synthesis of Rhodium Diphosphine Silylamido Complex, **2e**.




**2e**

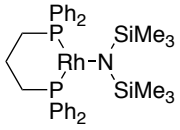
Rhodium diphosphine chloride complex, **1e**, was weighed inside a glovebox in 20 ml vial (200. mg, 0.279 mmol, 1 equiv.). THF (2 ml) and a magnetic stir bar were added to the vial. A solution of KHMDS (111 mg, 0.558 mmol, 2 equiv.) in THF was prepared in a separate 20 ml vial and added to the rhodium diphosphine complex by pipet. The vial containing the two reagents was capped. The resulting solution was stirred overnight inside the glovebox at room temperature. The solution became purple. The THF solvent was removed under vacuum. The purple residue was dissolved in pentane and filtered through celite. The filtrate was collected and the solvent removed under vacuum. A purple solid was collected (255 mg, 0.527 mmol, 95 % yield).

$^{1}$H NMR: (500.2 MHz, toluene-$d_8$) δ 1.45-1.25 (overlapping multiplets, 10H), 1.03 (quintet, $J^{H-H}$ = $J^{H-P}$ = 8 Hz, 12H), 0.97 (s, broad, 4H), 0.48 (s, 18H) ppm.

$^{13}$C{$^{1}$H} NMR: (125.7 MHz, toluene- $d_8$) δ 24.0 (t, 20 Hz), 22.7 (t, $J^{C-P}$ = 13 Hz), 20.1, 9.1, 7.7 ppm.

$^{31}P\{^{1}H\}$ NMR: (202.2 MHz, toluene- $d_8$) δ 39.1 (d, $J^{P\text{-}Rh}$ = 157 Hz) ppm.

### 3.3.2.5 Synthesis of Rhodium Diphosphine Silylamido Complex, **2g**.




**2g**

Rhodium diphosphine chloride complex, **1g**, was weighed inside a glovebox in 20 ml vial (200. mg, 0.182 mmol, 1 equiv.). THF (2 ml) and a magnetic stir bar were added to the vial. A solution of KHMDS (72.4 mg, 0.363 mmol, 2 equiv.) in THF (5 ml) was prepared in a 20 ml separate vial and added to the rhodium diphosphine complex by pipet. The vial containing the two reagents was capped. The resulting solution was stirred overnight inside the glovebox at room temperature. The solution became dark blue and homogeneous (a yellow precipitate forms initially, but disappears over time). The THF solvent was removed under vacuum. The dark blue residue was dissolved in pentane and filtered through celite. The filtrate was collected and the solvent removed under vacuum to yield a dark blue solid (222 mg, 0.329 mmol, 91 % yield).

$^{1}H$ NMR: (499.92 MHz, THF-$d_8$) δ 7.70 (m, broad, 8H), 7.19 (m, broad, 12H), 2.39 (s, broad, 4H), 2.03 (m, broad, 4H), 0.12 (s, broad, 18H) ppm.

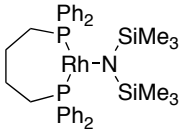
$^{13}C\{^{1}H\}$ NMR: (125.7 MHz, THF-$d_8$) δ 138.1 (t, $J^{C\text{-}P}$ = 23 Hz), 133.7 (t, J = 5.0 Hz), 130.2, 128.7 (t, J = 5.0 Hz), 26.6 (t, $J^{C\text{-}P}$ = 21.4 Hz), 21.3, 7.4 ppm.

$^{31}P\{^{1}H\}$ NMR: (202.2 MHz, $C_6D_6$) δ 40.5 (d, $J_{P\text{-}Rh}$ = 169 Hz) ppm.

Analysis Calculated For $C_{33}H_{44}NP_2RhSi_2$: C, 58.66; H, 6.56; N, 2.07.

Found: C, 58.92; H, 6.19; N, 1.87.

### 3.3.2.6 Synthesis of Rhodium Diphosphine Silylamido Complex, **2h**.




**2h**

Rhodium diphosphine chloride complex, **1h**, was weighed inside a glovebox in 20 ml vial (80. mg, 0.07 mmol, 1 equiv.). THF (2 ml) and a magnetic stir bar were added to the vial. A solution of KHMDS (28.3 mg, 0.142 mmol, 2 equiv.) in THF was prepared in a separate 20 ml vial and added to the rhodium diphosphine complex by pipet. The vial containing the two reagents was capped. The resulting solution was stirred overnight inside the glovebox at room temperature. The solution became dark blue, homogenous. The solvent was removed under vacuum. The dark blue residue was dissolved in pentane and filtered through celite. The filtrate was collected and the solvent removed under vacuum. A dark blue solid was collected (57 mg, 0.080 mmol, 58 % yield).

$^{1}H$ NMR: (399.7 MHz, THF-$d_8$) δ 7.70 (m, 8H), 7.34(q, $J^{H\text{-}H}$ = 7 Hz, 4H), 7.30 (q, $J^{H\text{-}H}$ = 7 Hz, 8H), 2.41 (s, broad, 4H), 1.87 (m, broad, 4H), 0.02 (s, 18H) ppm.

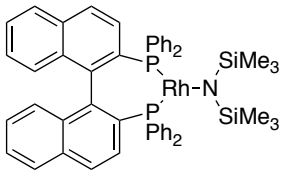
$^{13}C\{^{1}H\}$ NMR: (125.7 MHz, THF- $d_8$) δ 138.8 (t, $J^{C\text{-}P}$ = 21.4 Hz), 133.5, 129.9, 128.65, 29.5 (t, $J^{C\text{-}P}$ = 17.6 Hz), 24.8, 6.8 ppm.

$^{31}P\{^{1}H\}$ NMR: (202.3 MHz, THF-$d_8$) δ 59.7 (d, $J^{P\text{-}Rh}$ = 171 Hz) ppm.

Analysis Calculated For $C_{34}H_{46}NP_2RhSi_2$: C, 59.20; H, 6.72; N, 2.03.

Found: C, 59.24; H, 6.69; N, 2.30.

### 3.3.2.7 Synthesis of Rhodium Diphosphine Silylamido Complex, **2i**.




**2i**

Rhodium diphosphine chloride complex, **1i**, was weighed inside a glovebox in 20 ml vial (200. mg, 0.131 mmol, 1 equiv.). THF (2 ml) and a magnetic stir bar were added to the vial. A THF (5 ml) solution of KHMDS (52.4 mg, 0.263 mmol, 2 equiv.) THF (5 ml) was prepared in a separate 20 ml vial and added to the rhodium diphosphine complex by pipet. The vial containing the two reagents was capped. The resulting solution was stirred overnight inside the glovebox at room temperature. The solution became dark green and homogeneous. The solvent was removed under vacuum. The dark green residue was dissolved in pentane and filtered through celite. The filtrate was collected and the solvent removed under vacuum. A dark green solid was collected (222 mg, 0.250 mmol, 95 % yield).

$^{1}$H NMR: (125.7 MHz, $C_6D_6$) δ 8.36 (quartet, $J^{H-H}$ = 5 Hz, 4H), 7.87 (s, broad, 4H), 7.55 (quintet, $J^{H-H}$ = 5 Hz, 2H), 7.25-7.15 (overlapping doublets of doublets, $J^{H-H}$ = 10 Hz, $J^{H-H}$ = 5 Hz, 8H), 7.02 (t, $J^{H-H}$ = 10 Hz, 2H), 6.98 (t, $J^{H-H}$ = 10 Hz, 2H), 6.85 (d, $J^{H-H}$ = 5 Hz, 2H), 6.72 (t, $J^{H-H}$ = 10 Hz, 2H), 6.35-6.25 (overlapping signals, 6H), 0.65 (s, 18H) ppm.

$^{1}$H NMR: (125.7 MHz, THF-$d_8$) δ 8.30 (s, broad, 4H), 7.87 (s, broad, 4H), 7.55 (d, broad, $J^{H-H}$ = 10 Hz, 2H), 7.50 (s, broad, 4H), 7.39 (s, broad, 6H), 7.30 (m, broad, 6H), 7.07 (m, broad, 2H), 6.95 (d, broad, $J^{H-H}$ = 10 Hz, 2H), 6.57 (m, broad, 2H), 6.48 (m, broad, 4H), 0.36 (s, 18H) ppm.

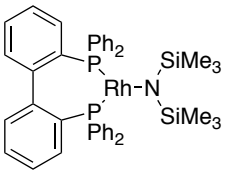
$^{13}$C{$^{1}$H} NMR: (125.7 MHz, THF- $d_8$) δ 138.8 (t, $J^{C-P}$ = 6 Hz), 136.0 (t, $J^{C-P}$ = 5 Hz), 135.5 (t, $J^{C-P}$ = 26 Hz), 135.3 ((t, $J^{C-P}$ = 24 Hz), 134.6, 134.2 (m, broad, overlapping), 134.1 (m, broad, overlapping), 133.5 (t, $J^{C-P}$ = 26 Hz), 130.7, 129.1, 128.9, 128.8, 128.7-128.4 (overlapping multiplets, 2C), 128.2, 127.1, 126.9 (t, $J^{C-P}$ = 5 Hz), 126.7, 7.8 ppm.

$^{31}$P{$^{1}$H} NMR: (202.2 MHz THF- $d_8$) δ 57.8 (d, $J^{P-Rh}$ = 174 Hz) ppm.

Analysis Calculated For $C_{50}H_{50}NP_2RhSi_2$: C, 67.78; H, 5.69; N, 1.58.

Found: C, 67.89; H, 5.56; N, 1.63.

### 3.3.2.8 Synthesis of Rhodium Diphosphine Silylamido Complex, **2j**.




**2j**

Rhodium diphosphine chloride complex, **1j**, was weighed inside a glovebox in 20 ml vial (80. mg, 0.06 mmol, 1 equiv.). THF (2 ml) and a magnetic stir bar were added to the vial. A solution of KHMDS (24.1 mg, 0.121 mmol, 2 equiv.) in THF was prepared in a separate 20 ml vial and added to the rhodium diphosphine complex by pipet. The vial containing the two reagents was capped. The resulting solution was stirred overnight inside the glovebox at room temperature. The solution became dark green and homogeneous. The solvent was removed under vacuum. The dark green residue was dissolved in pentane and filtered through celite. The filtrate was collected and the solvent removed under vacuum. A dark green solid was collected (45 mg, 0.06 mmol, 47 % yield).

$^{1}$H NMR: (500.1 MHz, toluene- $d_8$) δ 8.18 (quartet, $J^{H-H}$ = 5 Hz, 4H), 7.98 (s, broad, 4H), 7.12 (t, $J^{H-H}$ = 5 Hz, 4H), 7.08 (quartet, $J^{H-H}$ = 5 Hz, 2H), 7.01 (t, $J^{H-H}$ = 5 Hz, 2H), 6.84 (overlapping signals, 6H), 6.73 (t, $J^{H-H}$ = 5 Hz, 2H), 6.54 (t, $J^{H-H}$ = 5 Hz, 2H), 6.45 (d, $J^{H-H}$ = 5 Hz, 2H), 0.65 (s, 18H) ppm.

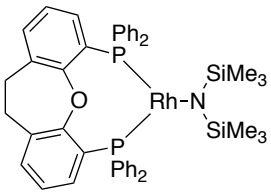
$^{13}C\{^{1}H\}$ NMR: (125.7 MHz, THF- $d_8$) δ 144.6, 135.8, 135.4, 135.0, 133.6, 131.4, 130.6, 130.53, 130.0, 129.7, 128.9, 128.6, 127.8, 127.4, 126.5, 7.6 ppm.

$^{31}P\{^{1}H\}$ NMR: (202.2 MHz, THF- $d_8$) δ 57.8 (d, $J^{P\text{-}Rh}$ = 174 Hz) ppm.

Analysis Calculated For $C_{42}H_{46}NP_2RhSi_2$: C, 64.19; H, 5.90; N, 1.78.

Found: C, 64.12; H, 6.17; N, 1.55.

### 3.3.2.9 Synthesis of Rhodium Diphosphine Silylamido Complex, **2k**.




**2k**

Rhodium diphosphine chloride complex, **1k**, was weighed inside a glovebox in 20 ml vial (200. mg, 0.142 mmol, 1 equiv.). THF (2 ml) and a magnetic stir bar were added to the vial. A solution of KHMDS (56.8 mg, 0.285 mmol, 2 equiv.) in THF was prepared in a separate 20 ml vial and added to the rhodium diphosphine complex by pipet. The vial containing the two reagents was capped. The resulting solution was stirred overnight inside the glovebox at room temperature. The solution became dark green and homogeneous. The solvent was removed under vacuum. The dark green residue was dissolved in pentane and filtered through celite. The filtrate was collected and the solvent removed under vacuum. A dark green solid was collected (232 mg, 0.280 mmol, 98 % yield).

$^{1}H$ NMR: (500.2 MHz, THF-$d_8$) δ 7.40 (s, broad, 8H), 7.25 (d, $J^{H\text{-}H}$ = 5 Hz, 2H), 7.21 (t, $J^{H\text{-}H}$ = 5 Hz, 4H), 7.08 (t, $J^{H\text{-}H}$ = 5 Hz, 8H), 6.83 (t, $J^{H\text{-}H}$ = 5 Hz, 2H), 6.26 (s, broad, 2H), 3.25 (s, 4H), 0.15 (s, 18H) ppm.

$^{1}H$ NMR: (500.1 MHz, toluene-$d_8$) δ 7.55 (s, broad, 8H), 6.98-6.87 (overlapping signals, 12H), 6.80 (d, $J^{H\text{-}H}$ = 5 Hz, 2H), 6.54 (t, $J^{H\text{-}H}$ = 5 Hz, 2H), 6.44 (m, broad, 2H), 2.79 (s, broad, 4H), 0.47 (s, broad, 18H). ppm.

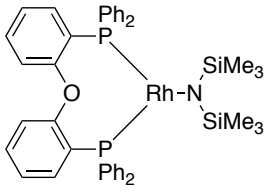
$^{13}C\{^{1}H\}$ NMR: (125.7 MHz, THF-$d_8$) δ 158.6, 135.1 (overlapping signals, 2C, one carbon signal is a triplet, $J^{ury\text{-}P}$ = 25 Hz), 133.4, 133.3, 131.5, 129.9, 128.4 (t, $J^{Rh\text{-}P}$ = 5 Hz), 127.9 (t, $J^{Rh\text{-}P}$ = 23 Hz), 125.1, 31.6, 6.7 ppm.

$^{31}P\{^{1}H\}$ NMR: (202.2 MHz, THF-$d_8$) δ 57.4 (d, $J^{P\text{-}Rh}$ = 180 Hz) ppm.

Analysis Calculated For $C_{44}H_{48}NOP_2RhSi_2$: C, 63.83; H, 5.84; N, 1.69.

Found: C, 64.23; H, 6.13; N, 1.38.

### 3.3.2.10 Synthesis of Rhodium Diphosphine Silylamido Complex, **2l**.




**2l**

Rhodium diphosphine chloride complex, **1l**, was weighed inside a glovebox in 20 ml vial (100. mg, 0.074 mmol, 1 equiv.). THF (2 ml) and a magnetic stir bar were added to the vial. A solution of KHMDS (29.5 mg, 0.148 mmol, 2 equiv.) in THF was prepared in a separate 20 ml vial and added to the rhodium diphosphine complex by pipet. The vial containing the two reagents was capped. The resulting solution was stirred overnight inside the glovebox at room temperature. The solution became dark green and homogeneous. The solvent was removed under vacuum. The green residue was dissolved in pentane and filtered through celite. The filtrate was collected and the solvent removed under vacuum. A dark green solid was collected (77.1 mg, 0.096 mmol, 65 % yield).

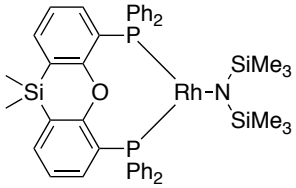
$^{1}$H NMR: (499.4 MHz, THF-$d_8$) δ 7.52 (s, broad, 8H), 7.32 (s, broad, 6H), 7.23 (s, broad, 8H), 6.71 (s, broad, 2H), 6.34 (s, broad, 2H), 0.002 (s, 18H) ppm.

$^{1}$H NMR: (499.4 MHz, toluene-$d_8$) δ 7.74 (s, broad, 8H), 6.97 (overlapping signals, broad, 12H), 6.78 (s, broad, 2H), 6.74 (s, broad, 2H), 6.47 (s, broad, 2H), 6.25 (s, broad, 2H), 0.50 (s, broad, 18H) ppm.

$^{13}$C{$^{1}$H} NMR: (125.8 MHz, THF-$d_8$) δ 160.5, 136.7 (t, $J^{C-P}$ = 25 Hz), 134.0, 133.6, 131.4, 129.4, 129.1, 127.8, 127.3 (t, $J^{C-P}$ = 24 Hz), 124.1, 122.6, 5.9 ppm.

$^{31}$P{$^{1}$H} NMR: (202.2 MHz, THF-$d_8$) δ 56.3 (d, $J^{P-Rh}$ = 181 Hz) ppm.

### 3.3.2.11 Synthesis of Rhodium Diphosphine Silylamido Complex, **2m**.




**2m**

Rhodium diphosphine chloride complex, **1m**, was weighed inside a glovebox in 20 ml vial (87 mg, 0.059 mmol, 1 equiv.). THF (2 ml) and a magnetic stir bar were added to the vial. A solution of KHMDS (24 mg, 120 mmol, 2 equiv.) in THF was prepared in a separate 20 ml vial and added to the rhodium diphosphine complex by pipet. The vial containing the two reagents was capped. The resulting solution was stirred overnight inside the glovebox at room temperature. The solution became dark green and homogeneous. The solvent was removed under vacuum. The dark green residue was dissolved in pentane and filtered through celite. The filtrate was collected and the solvent removed under vacuum. A dark green solid was collected (84 mg, 0.10 mmol, 82 % yield).

$^{1}$H NMR: (499.4 MHz, toluene-$d_8$) δ 8.02-7.03 (overlapping signals, broad, 26H), 1.06 (s, broad, 3H), 0.87 (s, broad, 3H), 0.20 (s, broad, 18H) ppm.

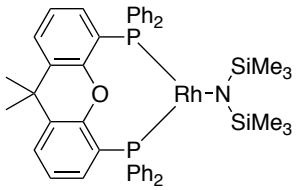
$^{13}$C{$^{1}$H} NMR: (126 MHz, THF-$d_8$) δ 164.13, 136.58 (broad), 135.95, 133. 74, 133.59 (broad), 130.41 (broad), 129.59 (broad), 126.35, 125.82 (t, J = 23 Hz), 125.06 ppm.

$^{31}$P{$^{1}$H} NMR: (202.2 MHz, toluene-$d_8$) δ 52.98 (d, $J^{P-Rh}$ = 183 Hz) ppm.

Analysis Calculated For $C_{44}H_{50}NOP_2RhSi_3$: C, 61.59; H, 5.87; N, 1.63.

Found: C, 61.61; H, 6.12; N, 1.44.

### 3.3.2.12 Synthesis of Rhodium Diphosphine Silylamido Complex, **2n**.




**2n**

Rhodium diphosphine chloride complex, **1n**, was weighed inside a glovebox in 20 ml vial (100. mg, 0.070 mmol, 1 equiv.). THF (2 ml) and a magnetic stir bar were added to the vial. A solution of KHMDS (27.8 mg, 0.139 mmol, 2 equiv.) in THF was prepared in a separate 20 ml vial and added to the rhodium diphosphine complex by pipet. The vial containing the two reagents was capped. The resulting solution was stirred overnight inside the glovebox at room temperature. The solution became dark green and homogeneous. The solvent was removed under vacuum. The dark green residue was dissolved in pentane and filtered through celite. The filtrate was collected and the solvent removed under vacuum. A dark green solid was collected (76 mg, 0.09 mmol, 65 % yield).

$^{1}$H NMR: (499.4 MHz, $C_6D_6$) δ 7.33 (s, broad, 4H), 7.08 (m, broad, 2H), 7.00 (d, broad, $J^{H-H}$ = 7Hz, 2H), 6.80 (t, $J^{H-H}$ = 7Hz, 2H), 6.69-6.57 (overlapping signals, m, 6H), 6.40 (s, broad, 2H), 1.50 (s, broad, 3H), 1.41 (s, broad, 3H), 0.67 (s, broad, 9H), 0.23 (s, broad, 9H) ppm.

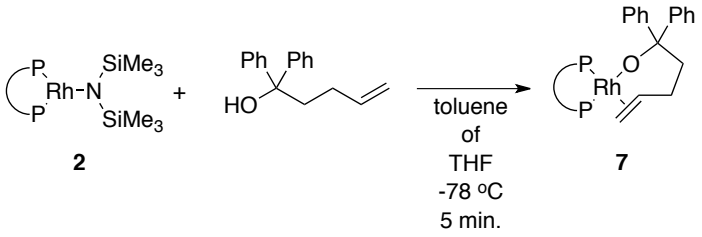
$^{13}$C{$^{1}$H} NMR: (125.7 MHz, THF-$d_8$) δ 156.9, 137.4, 136.6 (broad), 133.5 (broad), 130.5 (broad), 129.6, 128.6 (broad), 126.4, 125.6 (t, $J^{C-P}$ = 21 Hz), 125.1 (m), 38.0, 30.3, 22.8, 6.42, 2.8 ppm.

$^{31}$P{$^{1}$H} NMR: (202.2 MHz, $C_6D_6$) δ 49.6 (d, $J^{P-Rh}$ = 187 Hz) ppm.

Analysis Calculated For $C_{45}H_{50}NOP_2RhSi_2$: C, 64.20; H, 5.99; N, 1.66.

Found: C, 63.91; H, 5.89; N, 1.84.

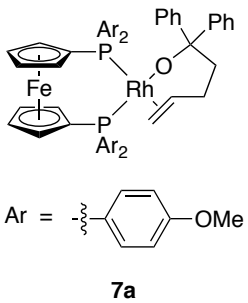
### 3.3.3 Syntheses of Rhodium Diphosphine Alkoxo Alkene Complexes, **7**.




**2** **7**

Rhodium diphosphine alkoxo alkene complexes, **7a-e** and **7g-n** were prepared in situ by the reactions of 1,1-diphenyl-4-penten-1-ol to rhodium diphosphine silylamido complexes **2a-e** and **2g-n**. The reactions were conducted in screw cap NMR tubes in either toluene-$d_8$ or THF-$d_8$ at -78 °C. NMR spectra were collected at -50 °C.

#### 3.3.3.1 Synthesis of Rhodium Diphosphine Silylamido Complex, **7a**.



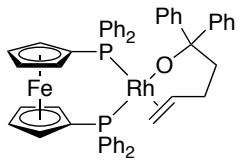

**7a**

Rhodium diphosphine silylamido complex, **2a**, (17.0 mg, 0.018 mmol, 1 equiv.) was weighed inside a glovebox in a 3 ml vial. The weighed complex was dissolved in d$^8$-toluene (0.5 ml) and transferred to a screw cap NMR tube. 1,3,5-trimethoxybenzene (1.2 mg) was added to the NMR tube as an internal standard. The screw cap NMR tube was capped with a septum-bearing cap. 1,1-Diphenyl-4-penten-1-ol was weighed inside the glovebox in a 3 ml vial and dissolved in 0.1 ml of d$^8$-toluene. The 1,1-diphenyl-4-penten-1-ol (4.3 mg, 0.02 mmol, 1 equiv.) solution was loaded into a 250 µL syringe. The syringe was stoppered and both the syringe and the screw cap NMR tube were removed from the glovebox. The screw cap NMR tube was placed in a dry ice / acetone bath. An NMR probe was cooled to -50 °C. Initial $^{1}$H and $^{31}$P NMR spectra of the silylamido complex, **2a**, were collected at -50 °C. The NMR tube was ejected and placed in the dry ice / acetone bath. The 1,1-diphenyl-4-penten-1-ol solution was syringed into the NMR tube. The NMR tube was kept in the dry ice / acetone bath for 5 minutes and then shaken vigorously for 10 seconds before returning the sample to the dry ice acetone bath. This was repeated two more times. The dark green silylamido solution became dark red. NMR spectra of the red solution were collected at -50 °C.

$^{1}$H NMR: (499.4 MHz, toludene-$d_8$) δ 8.28 (s, broad, 2H), 8.00 (t, J =9 Hz, 2H), 7.91 (s, broad, 1H), 7.53 (d, J = 7 Hz, 2H), 7.34 (d, overlapping signals, J = 8 Hz, 2H), 7.32 (m, overlapping signals, 1H), 7.12-7.05 (overlapping signals, 4H), 7.02 (m, overlapping signals, 1H), 6.97 (m 1H), 6.88 (d, J = 8 Hz, 2H), 6.62 (m, overlapping signals, 4H), 6.54 (t, overlapping signals, J = 8 Hz, 4H), ( 5.14 (s, 1H), 4.63 (d, J = 13 Hz, 1H), 4.43 (s, 1H), 4.27 (s, 1H), 4.08 (s, 1H), 4.04 (m, broad, 1H), 3.89 (s, 1H), 3.84 (s, 1H), 3.77 (s, 1H), 3.72 (s, 1H), 3.40 (m, broad, 1H), 3.33 (s, 3H), 3.25 (s, 3H), 3.11 (s, 3H), 3.09 (s, 3H), 2.76 (m, overlapping signals, 2H), 2.38 (m, broad, 1H), 1.36 (m, broad, 1H) ppm.

$^{31}$P{$^{1}$H} NMR: (202.2 MHz, toluene-$d_8$) δ 48.6 (dd, $J^{P\text{-}Rh}$ = 153 Hz, $J^{P\text{-}P}$ = 49 Hz), 10.4 (dd, $J^{P\text{-}Rh}$ = 165 Hz, $J^{P\text{-}P}$ = 49 Hz) ppm.

### 3.3.3.2 Synthesis of Rhodium Diphosphine Silylamido Complex, **7b**.



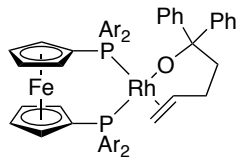

**7b**

Rhodium diphosphine silylamido complex, **2b**, (14.8 mg, 0.018 mmol, 1 equiv.) was weighed inside a glovebox in a 3 ml vial. The weighed complex was dissolved in d$^{8}$-toluene (0.5 ml) and transferred to a screw cap NMR tube. 1,3,5-trimethoxybenzene (1.2 mg) was added to the NMR tube as an internal standard. The screw cap NMR tube was capped with a septum-bearing cap. 1,1-Diphenyl-4-penten-1-ol was weighed inside the glovebox in a 3 ml vial and dissolved in 0.1 ml of d$^{8}$-toluene. The 1,1-diphenyl-4-penten-1-ol (4.3 mg, 0.02 mmol, 1 equiv.) solution was loaded into a 250 µL syringe. The syringe was stoppered and both the syringe and the screw cap NMR tube were removed from the glovebox. The screw cap NMR tube was placed in a dry ice / acetone bath. An NMR probe was cooled to -50 °C. Initial $^{1}$H and $^{31}$P NMR spectra of the silylamido complex, **2b**, were collected at -50 °C. The NMR tube was ejected and placed in the dry ice / acetone bath. The 1,1-diphenyl-4-penten-1-ol solution was syringed into the NMR tube. The NMR tube was kept in the dry ice / acetone bath for 5 minutes and then shaken vigorously for 10 seconds before returning the sample to the dry ice acetone bath. This was repeated two more times. The dark green silylamido solution became dark red. NMR spectra of the red solution were collected at -50 °C.

$^{1}$H NMR: (499.7 MHz, toludene-$d_8$) δ 8.23 (s, broad, 2H), 8.05-7.85 (overlapping signals, broad, 4H), 7.47-6.78 (overlapping signals, broad, 24H), 5.16 (s, broad, 1H), 4.55 (d, broad, J = 13 Hz, 1H), 4.24 (s, broad, 1H), 4.21 (s, broad, 1H), 3.96 (s, broad, overlapping signals, 2H), 3.74 (s, broad, 1H), 3.71 (s, broad, 1H), 3.60 (s, broad, 1H), 3.49 (s, broad, 1H), 3.31 (s, broad, 1H), 2.69 (m, broad, 2H), 2.25 (s, broad, 1H), 1.68 (s, broad, 1H) ppm.

$^{31}$P{$^{1}$H} NMR: (202.2 MHz, toluene-$d_8$) δ 51.43 (dd, $J^{P\text{-}Rh}$ = 151 Hz, $J^{P\text{-}P}$ = 47 Hz), 14.33 (dd, $J^{P\text{-}Rh}$ = 166 Hz, $J^{P\text{-}P}$ = 47 Hz) ppm.

### 3.3.3.3 Synthesis of Rhodium Diphosphine Silylamido Complex, **7b**.



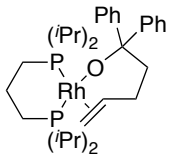

**7c**

Rhodium diphosphine silylamido complex, **2c**, (19.8 mg, 0.018 mmol, 1 equiv.) was weighed inside a glovebox in a 3 ml vial. The weighed complex was dissolved in $d^8$-toluene (0.5 ml) and transferred to a screw cap NMR tube. 1,3,5-trimethoxybenzene (1.2 mg) was added to the NMR tube as an internal standard. The screw cap NMR tube was capped with a septum-bearing cap. 1,1-Diphenyl-4-penten-1-ol was weighed inside the glovebox in a 3 ml vial and dissolved in 0.1 ml of $d^8$-toluene. The 1,1-diphenyl-4-penten-1-ol (4.3 mg, 0.02 mmol, 1 equiv.) solution was loaded into a 250 µL syringe. The syringe was stoppered and both the syringe and the screw cap NMR tube were removed from the glovebox. The screw cap NMR tube was placed in a dry ice / acetone bath. An NMR probe was cooled to -50 °C. Initial $^1$H and $^{31}$P NMR spectra of the silylamido complex, **2c**, were collected at -50 °C. The NMR tube was ejected and placed in the dry ice / acetone bath. The 1,1-diphenyl-4-penten-1-ol solution was syringed into the NMR tube. The NMR tube was kept in the dry ice / acetone bath for 5 minutes and then shaken vigorously for 10 seconds before returning the sample to the dry ice acetone bath. This was repeated two more times. The dark green silylamido solution became dark red. NMR spectra of the red solution were collected at -50 °C.

$^1$H NMR: (499.7 MHz, THF-$d_8$) δ 8.25 (m, broad, 1H), 8.13 (s, broad, 1H), 7.93 (s, broad, 1H), 7.83 (m, 2H), 7.77 (d, J= 8 Hz, 2H), 7.63 (t, overlapping signals, J = 7.3 Hz, 3H), 7.47 (d, J = 7 Hz, 4H) 7.24 (dd, overlapping signals, J = 15 Hz, J = 8 Hz, 4H), 7.13 (m, 1H), 7.05 (d, J = 6 Hz, 2H), 6.92 (d, J = 7Hz, 2H), 6.83 (s, broad, 2H), 6.75 (s, broad, 2H), 5.23 (s, 1H), 4.76 (s, 1H), 4.54 (s, 1H), 4.51 (s, 1H), 4.33 (d, J = 13 Hz, 1H), 4.28 (s, 1H), 4.24 (s, 1H), 3.79 (s, broad, overlapping signal, 1H), 3.76 (s, 1H), 3.48 (s, 1H), 3.15 (s, broad, 1H), 2.48 (m, broad, 1H), 2.33 (m, 1H), 2.00 (s, broad, 1H), 1.43 (s, broad, 1H) ppm.

$^{31}$P{$^1$H} NMR: (202.3 MHz, THF-$d_8$) δ 51.8 (dd, $J^{P\text{-}Rh}$ = 154 Hz, $J^{P\text{-}P}$ = 48 Hz), 14.5 (dd, $J^{P\text{-}Rh}$ = 168 Hz, $J^{P\text{-}P}$ = 48 Hz) ppm.

### 3.3.3.4 Synthesis of Rhodium Diphosphine Silylamido Complex, **7d**.




**7d**

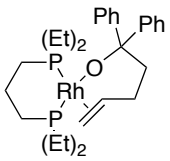
Rhodium diphosphine silylamido complex, **2d**, (9.8 mg, 0.018 mmol, 1 equiv.) was weighed inside a glovebox in a 3 ml vial. The weighed complex was dissolved in $d^8$-toluene (0.5 ml) and transferred to a screw cap NMR tube. 1,3,5-trimethoxybenzene (1.2 mg) was added to the NMR tube as an internal standard. The screw cap NMR tube was capped with a septum-bearing cap. 1,1-Diphenyl-4-penten-1-ol was weighed inside the glovebox in a 3 ml vial and dissolved in 0.1 ml of $d^8$-toluene. The 1,1-diphenyl-4-penten-1-ol (4.3 mg, 0.02 mmol, 1 equiv.) solution was loaded into a 250 µL syringe. The syringe was stoppered and both the syringe and the screw cap NMR tube were removed from the glovebox. The screw cap NMR tube was placed in a dry ice / acetone bath. An NMR probe was cooled to -50 °C. Initial $^1$H and $^{31}$P NMR spectra of the silylamido complex, **2d**, were collected at -50 °C. The NMR tube was ejected and placed in the dry ice / acetone bath. The 1,1-diphenyl-4-penten-1-ol solution was syringed into the NMR tube. The NMR tube was kept in the dry ice / acetone bath for 5 minutes and then shaken vigorously for 10 seconds

before returning the sample to the dry ice acetone bath. This was repeated two more times. The dark blue silylamido solution became orange. NMR spectra of the orange solution were collected at -50 °C.

$^{1}$H NMR: (499.4 MHz, toluene-$d_8$) δ 7.51 (s, broad, 2H), 7.44 (s, broad, 2H), 7.11 (s, broad, 4H), 6.98 (s, broad, 2H), 4.21 (s, broad, 1H), 4.09, (s, broad, overlapping signals, 2H), 3.61 (s, broad, 1H), 2.63 (s, broad, 1H), 2.41(s, broad, 1H), 2.22 (s, broad, 1H), 2.12 (s, broad, 1H) 2.06-0.80 (overlapping signals, broad, 33H) ppm.

$^{31}$P{$^{1}$H} NMR: (202.2 MHz, toluene-$d_8$) δ 27.50 (dd, $J^{P\text{-}Rh}$ = 144 Hz, $J^{P\text{-}P}$ = 57 Hz), 7.76 (dd, $J^{P\text{-}Rh}$ = 162 Hz, $J^{P\text{-}P}$ = 56 Hz) ppm.

### 3.3.3.5 Synthesis of Rhodium Diphosphine Silylamido Complex, **7e**.



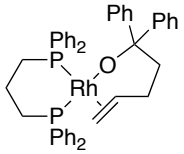

**7e**

Rhodium diphosphine silylamido complex, **2e**, (8.8 mg, 0.02 mmol, 1 equiv.) was weighed inside a glovebox in a 3 ml vial. The weighed complex was dissolved in d$^{8}$-toluene (0.5 ml) and transferred to a screw cap NMR tube. 1,3,5-trimethoxybenzene (1.2 mg) was added to the NMR tube as an internal standard. The screw cap NMR tube was capped with a septum-bearing cap. 1,1-Diphenyl-4-penten-1-ol was weighed inside the glovebox in a 3 ml vial and dissolved in 0.1 ml of d$^{8}$-toluene. The 1,1-diphenyl-4-penten-1-ol (4.3 mg, 0.02 mmol, 1 equiv.) solution was loaded into a 250 µL syringe. The syringe was stoppered and both the syringe and the screw cap NMR tube were removed from the glovebox. The screw cap NMR tube was placed in a dry ice / acetone bath. An NMR probe was cooled to -50 °C. Initial $^{1}$H and $^{31}$P NMR spectra of the silylamido complex, **2e**, were collected at -50 °C. The NMR tube was ejected and placed in the dry ice / acetone bath. The 1,1-diphenyl-4-penten-1-ol solution was syringed into the NMR tube. The NMR tube was kept in the dry ice / acetone bath for 5 minutes and then shaken vigorously for 10 seconds before returning the sample to the dry ice acetone bath. This was repeated two more times. The dark blue silylamido solution became orange. NMR spectra of the orange solution were collected at -50 °C.

$^{1}$H NMR: (500.16 MHz, toluene-$d_8$) δ 7.90 (m, broad, 2H), 7.75 (d, broad, J = 7 Hz, 2H), 7.44-7.30 (overlapping signals, 3H), 7.24 (m, 2H), 7.17 (m, broad, 1H), 4.68 (d, broad, J = 13 Hz, 1H), 4.14 (s, broad, 1H), 4.02 (s, broad, 1H), 2.80 (t, J = 8Hz, 1H), 2.70 (t, J=11 Hz, 1H), 2.33 (m, 2H), 2.12 (s, broad, 1H), 1.64-0.56 (overlapping signals, 25H) ppm.

$^{31}$P{$^{1}$H} NMR: (202.2 MHz, toluene-$d_8$) δ 27.13 (dd, $J^{P\text{-}Rh}$ = 145 Hz, $J^{P\text{-}P}$ = 58 Hz), 7.70 (dd, $J^{P\text{-}Rh}$ = 161 Hz, $J^{P\text{-}P}$ = 59 Hz) ppm.

### 3.3.3.6 Synthesis of Rhodium Diphosphine Silylamido Complex, **7g**.




**7g**

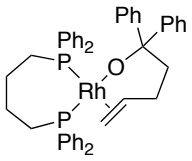
Rhodium diphosphine silylamido complex, **2g**, (12.2 mg, 0.018 mmol, 1 equiv.) was weighed inside a glovebox in a 3 ml vial. The weighed complex was dissolved in d$^{8}$-toluene (0.5 ml) and transferred to a screw cap NMR tube. 1,3,5-trimethoxybenzene (1.2 mg) was added to the NMR tube as an internal standard. The screw cap NMR tube was capped with a septum-bearing cap. 1,1-Diphenyl-4-penten-1-ol was weighed inside the glovebox in a 3 ml vial and dissolved in 0.1 ml of d$^{8}$-toluene. The 1,1-diphenyl-4-penten-1-ol (4.3 mg, 0.02 mmol, 1 equiv.) solution was loaded into a 250 µL syringe. The syringe was stoppered and both the syringe and the screw cap NMR tube were removed from the

glovebox. The screw cap NMR tube was placed in a dry ice / acetone bath. An NMR probe was cooled to -50 °C. Initial $^{1}$H and $^{31}$P NMR spectra of the silylamido complex, **2g**, were collected at -50 °C. The NMR tube was ejected and placed in the dry ice / acetone bath. The 1,1-diphenyl-4-penten-1-ol solution was syringed into the NMR tube. The NMR tube was kept in the dry ice / acetone bath for 5 minutes and then shaken vigorously for 10 seconds before returning the sample to the dry ice acetone bath. This was repeated two more times. The dark blue silylamido solution became bright orange. NMR spectra of the orange solution were collected at -50 °C.

$^{1}$H NMR: (500.16 MHz, toluene-$d_8$) δ 7.87 (s, broad, 2H), 7.65 (s, broad, 2H), 7.34-6.72 (overlapping signals, broad, 26H), 4.81 (s, broad, 1H), 4.10 (s, broad, 1H), 3.54 (s, broad, 1H), 2.75 (s, broad, 2H), 2.53 (s, broad, 1H), 1.98 (s, broad, 2H), 1.85 (s, broad, 1H), 1.77 (s, broad, 1H), 1.54 (s, broad, 1H), 1.23 (s, broad, 2H) ppm.

$^{31}$P{$^{1}$H} NMR: (202.2 MHz, toluene-$d_8$) δ 34.94 (dd, $J^{P\text{-}Rh}$ = 140 Hz, $J^{P\text{-}P}$ = 61 Hz), 0.18 (dd, $J^{P\text{-}Rh}$ = 161 Hz, $J^{P\text{-}P}$ = 61 Hz) ppm.

### 3.3.3.7 Synthesis of Rhodium Diphosphine Silylamido Complex, **7h**.



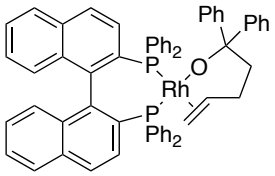

**7h**

Rhodium diphosphine silylamido complex, **2h**, (12.5 mg, 0.018 mmol, 1 equiv.) was weighed inside a glovebox in a 3 ml vial. The weighed complex was dissolved in d$^{8}$-toluene (0.5 ml) and transferred to a screw cap NMR tube. 1,3,5-trimethoxybenzene (1.2 mg) was added to the NMR tube as an internal standard. The screw cap NMR tube was capped with a septum-bearing cap. 1,1-Diphenyl-4-penten-1-ol was weighed inside the glovebox in a 3 ml vial and dissolved in 0.1 ml of d$^{8}$-toluene. The 1,1-diphenyl-4-penten-1-ol (4.3 mg, 0.02 mmol, 1 equiv.) solution was loaded into a 250 µL syringe. The syringe was stoppered and both the syringe and the screw cap NMR tube were removed from the glovebox. The screw cap NMR tube was placed in a dry ice / acetone bath. An NMR probe was cooled to -50 °C. Initial $^{1}$H and $^{31}$P NMR spectra of the silylamido complex, **2h**, were collected at -50 °C. The NMR tube was ejected and placed in the dry ice / acetone bath. The 1,1-diphenyl-4-penten-1-ol solution was syringed into the NMR tube. The NMR tube was kept in the dry ice / acetone bath for 5 minutes and then shaken vigorously for 10 seconds before returning the sample to the dry ice acetone bath. This was repeated two more times. The dark blue silylamido solution became bright orange. NMR spectra of the orange solution were collected at -50 °C.

$^{1}$H NMR: (500.2 MHz, toluene-$d_8$) δ 7.98 (s, broad, 2H), 7.60 (s, broad, 1H), 7.42 (s, broad, overlapping signals, 6H), 7.26-6.76 overlapping signals, broad, 20H), 4.64 (s, broad, 1H), 3.65 (s, broad, 1H), 3.04 (s, broad, 1H), 2.60 (m, broad, 2H), 2.43 (s, broad, 1H), 2.10 k(overlapping signals, broad, 1H), 1.97 (s, broad, 2H), 1.90-1.62 (overlapping signals, broad, 4H), 1.33 (s, broad, 1H) ppm.

$^{31}$P{$^{1}$H} NMR: (202.2 MHz, toluene-$d_8$) δ 52.28 (s, broad), 1.98 (s, broad) ppm.

### 3.3.3.8 Synthesis of Rhodium Diphosphine Silylamido Complex, **7i**.



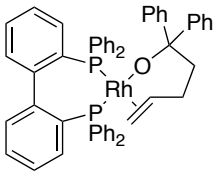

**7i**

Rhodium diphosphine silylamido complex, **2i**, (16.1 mg, 0.018 mmol, 1 equiv.) was weighed inside a glovebox in a 3 ml vial. The weighed complex was dissolved in $d^8$-toluene (0.5 ml) and transferred to a screw cap NMR tube. 1,3,5-trimethoxybenzene (1.2 mg) was added to the NMR tube as an internal standard. The screw cap NMR tube was capped with a septum-bearing cap. 1,1-Diphenyl-4-penten-1-ol was weighed inside the glovebox in a 3 ml vial and dissolved in 0.1 ml of $d^8$-toluene. The 1,1-diphenyl-4-penten-1-ol (4.3 mg, 0.02 mmol, 1 equiv.) solution was loaded into a 250 µL syringe. The syringe was stoppered and both the syringe and the screw cap NMR tube were removed from the glovebox. The screw cap NMR tube was placed in a dry ice / acetone bath. An NMR probe was cooled to -50 °C. Initial $^1$H and $^{31}$P NMR spectra of the silylamido complex, **2i**, were collected at -50 °C. The NMR tube was ejected and placed in the dry ice / acetone bath. The 1,1-diphenyl-4-penten-1-ol solution was syringed into the NMR tube. The NMR tube was kept in the dry ice / acetone bath for 5 minutes and then shaken vigorously for 10 seconds before returning the sample to the dry ice acetone bath. This was repeated two more times. The dark green silylamido solution became dark red. NMR spectra of the red solution were collected at -50 °C.

$^1$H NMR: (499.4 MHz, THF-$d_8$) δ 8.00 (s, broad, 1H), 7.79 (s, broad, 2H), 7.73 (s, broad, 1H), 7.62-6.78 (overlapping signals, broad, 30H), 6.46 (s, broad, overlapping signals, 4H), 6.37 (s, broad, overlapping signals, 4H)4.37 (d, J =12 Hz, 1H), 4.14 (s, broad, 1H), 3.08 (s, broad, 1H), 2.94 (s, broad, 1H), 2.74 (s, broad, 1H), 1.91 (s, broad, 1H), 1.42 (s, broad, 1H) ppm.

$^{31}$P{$^1$H} NMR: (202.2 MHz, THF-$d_8$) δ 54.73 (dd, $J^{P\text{-}Rh}$ = 138 Hz, $J^{P\text{-}P}$ = 60 Hz), 22.12 (dd, $J^{P\text{-}Rh}$ = 165 Hz, $J^{P\text{-}P}$ = 60 Hz) ppm.

### 3.3.3.9 Synthesis of Rhodium Diphosphine Silylamido Complex, **7j**.

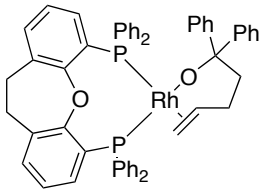



**7j**

Rhodium diphosphine silylamido complex, **2j**, (14.3 mg, 0.018 mmol, 1 equiv.) was weighed inside a glovebox in a 3 ml vial. The weighed complex was dissolved in $d^8$-toluene (0.5 ml) and transferred to a screw cap NMR tube. 1,3,5-trimethoxybenzene (1.2 mg) was added to the NMR tube as an internal standard. The screw cap NMR tube was capped with a septum-bearing cap. 1,1-Diphenyl-4-penten-1-ol was weighed inside the glovebox in a 3 ml vial and dissolved in 0.1 ml of $d^8$-toluene. The 1,1-diphenyl-4-penten-1-ol (4.3 mg, 0.02 mmol, 1 equiv.) solution was loaded into a 250 µL syringe. The syringe was stoppered and both the syringe and the screw cap NMR tube were removed from the glovebox. The screw cap NMR tube was placed in a dry ice / acetone bath. An NMR probe was cooled to -50 °C. Initial $^1$H and $^{31}$P NMR spectra of the silylamido complex, **2j**, were collected at -50 °C. The NMR tube was ejected and placed in the dry ice / acetone bath. The 1,1-diphenyl-4-penten-1-ol solution was syringed into the NMR tube. The NMR tube was kept in the dry ice / acetone bath for 5 minutes and then shaken vigorously for 10 seconds before returning the sample to the dry ice acetone bath. This was repeated two more times. The dark green silylamido solution became dark red. NMR spectra of the red solution were collected at -50 °C.

$^{1}$H NMR: (499.4 MHz, THF-$d_8$) δ 7.83-6.63 (overlapping signals, 48H), 4.14 (d, J = 13 Hz, 1H), 3.97 (s, 1H), 2.76 (m, 1H), 2.52 (s, 1H), 2.38 (t, J = 11 Hz, 1H), 1.73 (s, 1H), 1.59 (s, 1H), 1.22 (s, 1H) ppm.
$^{31}$P{$^{1}$H} NMR: (202.2 MHz, THF-$d_8$) δ 50.4 (dd, $J^{P\text{-}Rh}$ = 138 Hz, $J^{P\text{-}P}$ = 61 Hz), 16.46 (dd, $J^{P\text{-}Rh}$ = 162 Hz, $J^{P\text{-}P}$ = 61 Hz) ppm.

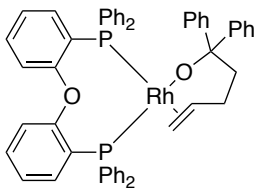
### 3.3.3.10 Synthesis of Rhodium Diphosphine Silylamido Complex, **7k**.




**2k**

Rhodium diphosphine silylamido complex, **2k**, (15.0 mg, 0.018 mmol, 1 equiv.) was weighed inside a glovebox in a 3 ml vial. The weighed complex was dissolved in d$^{8}$-toluene (0.5 ml) and transferred to a screw cap NMR tube. 1,3,5-trimethoxybenzene (1.2 mg) was added to the NMR tube as an internal standard. The screw cap NMR tube was capped with a septum-bearing cap. 1,1-Diphenyl-4-penten-1-ol was weighed inside the glovebox in a 3 ml vial and dissolved in 0.1 ml of d$^{8}$-toluene. The 1,1-diphenyl-4-penten-1-ol (4.3 mg, 0.02 mmol, 1 equiv.) solution was loaded into a 250 µL syringe. The syringe was stoppered and both the syringe and the screw cap NMR tube were removed from the glovebox. The screw cap NMR tube was placed in a dry ice / acetone bath. An NMR probe was cooled to -50 °C. Initial $^{1}$H and $^{31}$P NMR spectra of the silylamido complex, **2k**, were collected at -50 °C. The NMR tube was ejected and placed in the dry ice / acetone bath. The 1,1-diphenyl-4-penten-1-ol solution was syringed into the NMR tube. The NMR tube was kept in the dry ice / acetone bath for 5 minutes and then shaken vigorously for 10 seconds before returning the sample to the dry ice acetone bath. This was repeated two more times. The dark green silylamido solution became dark red. NMR spectra of the red solution were collected at -50 °C.
$^{1}$H NMR: (499.4 MHz, toluene-$d_8$) δ 8.28 (s, broad, 2H), 8.17 (d, J = 7 Hz, 2H), 7.69 (d, J = 8 Hz, 2H), 7.45 (m, 2H), 7.37 (d, J = 8 Hz, 2H), 7.25-6.75 (overlapping signals, m, 22H), 6.68 (m, 1H), 6.49 (d, J = 8 Hz, 2H), 6.30 (t, J = 8 Hz, 1H),5.16 (d, J = 13 Hz, 1H), 3.68 (s, 1H), 3.19 (t, J = 12 Hz, 1H), 3.01 (s, broad, 1H), 2.79 (s, broad, overlapping signal, 2H), 2.75 (s, broad, overlapping signal, 1H), 2.64-2.40 (s, broad, overlapping signal, 1H), 2.47 (m, overlapping signal, 1H), 2.40-2.21 (overlapping signals, m, 2H) ppm.
$^{31}$P{$^{1}$H} NMR: (202.2 MHz, toluene-$d_8$) δ 37.0 (dd, $J^{P\text{-}Rh}$ = 155 Hz, $J^{P\text{-}P}$ = 31 Hz), -7.59 (d, broad, $J^{P\text{-}Rh}$ = 155 Hz) ppm.

### 3.3.3.11 Synthesis of Rhodium Diphosphine Silylamido Complex, **7l**.




**7l**

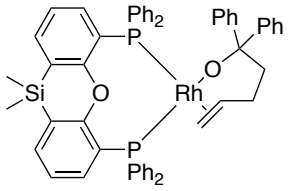
Rhodium diphosphine silylamido complex, **2l**, (14.6 mg, 0.018 mmol, 1 equiv.) was weighed inside a glovebox in a 3 ml vial. The weighed complex was dissolved in d$^{8}$-toluene (0.5 ml) and transferred to a screw cap NMR tube. 1,3,5-trimethoxybenzene (1.2 mg) was added to the NMR tube as an internal standard. The screw cap NMR tube was capped with a septum-bearing cap. 1,1-Diphenyl-4-penten-1-ol was weighed inside the glovebox in a 3 ml vial and dissolved in 0.1 ml of d$^{8}$-toluene. The 1,1-diphenyl-4-penten-1-ol (4.3 mg, 0.02 mmol, 1 equiv.) solution was loaded into a 250 µL syringe. The syringe was stoppered and both the syringe and the screw cap NMR tube were removed from the glovebox. The screw cap NMR tube was placed in

a dry ice / acetone bath. An NMR probe was cooled to -50 °C. Initial $^{1}$H and $^{31}$P NMR spectra of the silylamido complex, **2l**, were collected at -50 °C. The NMR tube was ejected and placed in the dry ice / acetone bath. The 1,1-diphenyl-4-penten-1-ol solution was syringed into the NMR tube. The NMR tube was kept in the dry ice / acetone bath for 5 minutes and then shaken vigorously for 10 seconds before returning the sample to the dry ice acetone bath. This was repeated two more times. The dark green silylamido solution became dark red. NMR spectra of the red solution were collected at -50 °C.

$^{1}$H NMR: (499.4 MHz, toluene-$d_8$) δ 8.03 (s, broad, 2H), 7.86 (s, broad, 2H), 7.59 (s, broad, 2H), 7.52 (s, broad, 2H), 7.32 (s, broad, 2H), 7.28-6.83 (overlapping signals, broad, 20H), 6.70 (s, broad, 2H), 6.57 (s, broad, 4H), 6.32 (s broad, 1H), 6.17 (s, broad, 1H), 5.12 (s, broad, 1H), 3.66 (s, broad, 1H), 3.03 (s, broad, 1H), 2.68 (overlapping signals, broad, 3H), 2.24 (s, broad, 1H) ppm.

$^{31}$P{$^{1}$H} NMR: (202.2 MHz, toluene-$d_8$) δ 35.87 (dd, $J^{P\text{-}Rh}$ = 148 Hz, $J^{P\text{-}P}$ = 32 Hz), -2.76 (dd, $J^{P\text{-}Rh}$ = 162 Hz, $J^{P\text{-}P}$ = 32 Hz) ppm.

### 3.3.3.12 Synthesis of Rhodium Diphosphine Silylamido Complex, **7m**.



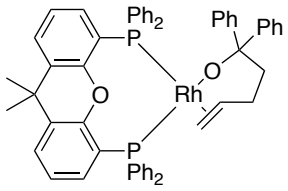

**7m**

Rhodium diphosphine silylamido complex, **2m**, (15.6 mg, 0.018 mmol, 1 equiv.) was weighed inside a glovebox in a 3 ml vial. The weighed complex was dissolved in d$^{8}$-toluene (0.5 ml) and transferred to a screw cap NMR tube. 1,3,5-trimethoxybenzene (1.2 mg) was added to the NMR tube as an internal standard. The screw cap NMR tube was capped with a septum-bearing cap. 1,1-Diphenyl-4-penten-1-ol was weighed inside the glovebox in a 3 ml vial and dissolved in 0.1 ml of d$^{8}$-toluene. The 1,1-diphenyl-4-penten-1-ol (4.3 mg, 0.02 mmol, 1 equiv.) solution was loaded into a 250 µL syringe. The syringe was stoppered and both the syringe and the screw cap NMR tube were removed from the glovebox. The screw cap NMR tube was placed in a dry ice / acetone bath. An NMR probe was cooled to -50 °C. Initial $^{1}$H and $^{31}$P NMR spectra of the silylamido complex, **2m**, were collected at -50 °C. The NMR tube was ejected and placed in the dry ice / acetone bath. The 1,1-diphenyl-4-penten-1-ol solution was syringed into the NMR tube. The NMR tube was kept in the dry ice / acetone bath for 5 minutes and then shaken vigorously for 10 seconds before returning the sample to the dry ice acetone bath. This was repeated two more times. The dark green silylamido solution became dark red. NMR spectra of the red solution were collected at -50 °C.

$^{1}$H NMR: (499.4 MHz, toluene-$d_8$) δ 8.33 (s, broad, 2H), 7.50-6.27 (broad, overlapping signals, 34H), 4.16 (d, J = 12 Hz, 1H), 2.89 (d, broad, overlapping signal, J = 13 Hz, 2H), 2.84 (s, broad, overlapping signal, 1H), 2.57 (m, broad, overlapping signal, 1H), 2.51 (s, broad, overlapping signal, 1H), 2.21 (t J = 17 Hz, 1H), 0.38 (s, broad, 3H), 0.31 (s, broad, 3H) ppm.

$^{31}$P{$^{1}$H} NMR: (202.2 MHz, toluene-$d_8$) δ 39.2 (s, broad), 8.21 (s, broad) ppm.

### 3.3.3.13 Synthesis of Rhodium Diphosphine Silylamido Complex, **7n**.




**7n**

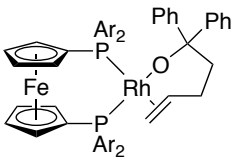
Rhodium diphosphine silylamido complex, **2n**, (15.3 mg, 0.018 mmol, 1 equiv.) was weighed inside a glovebox in a 3 ml vial. The weighed complex was dissolved in $d^8$-toluene (0.5 ml) and transferred to a screw cap NMR tube. 1,3,5-trimethoxybenzene (1.2 mg) was added to the NMR tube as an internal standard. The screw cap NMR tube was capped with a septum-bearing cap. 1,1-Diphenyl-4-penten-1-ol was weighed inside the glovebox in a 3 ml vial and dissolved in 0.1 ml of $d^8$-toluene. The 1,1-diphenyl-4-penten-1-ol (4.3 mg, 0.02 mmol, 1 equiv.) solution was loaded into a 250 µL syringe. The syringe was stoppered and both the syringe and the screw cap NMR tube were removed from the glovebox. The screw cap NMR tube was placed in a dry ice / acetone bath. An NMR probe was cooled to -50 °C. Initial $^1$H and $^{31}$P NMR spectra of the silylamido complex, **2n**, were collected at -50 °C. The NMR tube was ejected and placed in the dry ice / acetone bath. The 1,1-diphenyl-4-penten-1-ol solution was syringed into the NMR tube. The NMR tube was kept in the dry ice / acetone bath for 5 minutes and then shaken vigorously for 10 seconds before returning the sample to the dry ice acetone bath. This was repeated two more times. The dark green silylamido solution became dark red. NMR spectra of the red solution were collected at -50 °C.

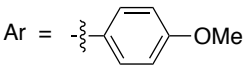
$^1$H NMR: (499.4 MHz, toluene-$d_8$) δ 8.46 (s, broad, 2H), 8.19 (s, broad, 2H), 7.48 (s, broad, 4H), 7.44 (s, broad, 4H), 7.31-6.42 (overlapping signals, 24H), 3.83 (d, broad, J=10 Hz, 1H), 2.80 (overlapping signals, broad, 2H), 1.06 (s, broad, 1H), 2.37 (s, broad, 1H), 2.25-2.00 (overlapping signals, broad, 2H), 1.46 (s, broad, 3H), 1.42 (s, broad, 3H) ppm.

$^{31}$P{$^1$H} NMR: (202.3 MHz, toluene-$d_8$) δ 55.4 (dd, $J^{P\text{-}Rh}$ = 135 Hz, $J^{P\text{-}P}$ = 55 Hz), 22.9 (dd, broad, $J^{P\text{-}Rh}$ = 158 Hz, $J^{P\text{-}P}$ = 57 Hz) ppm.

### 3.3.4 Procedures for obtaining $^{13}$C NMR spectra of **7a-e,g-k**.

#### 3.3.4.1 Rhodium diphosphine alkoxo alkene complex, **7a**.



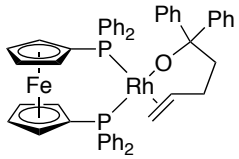

**7a**

Rhodium diphosphine silylamido complex, **2a**, was prepared in situ by the reaction of rhodium diphosphine chloride complex **1a** (200 mg, 0.123 mmol, 1 equiv.) with KHMDS (49.1 mg, 0.246 mmol, 2 equiv.). The reaction was performed in THF-$d_8$ (0.5 ml) inside a glovebox at room temperature. The reaction was allowed to stir overnight. The resulting solution was transferred to a screw cap NMR tube. The NMR tube was capped with a septum-bearing cap. 1,1-Diphenyl-4-penten-1-ol (58.6 mg, 0.246 mmol, 2 equiv.) was weighed inside the glovebox in a 3 ml vial and dissolved in 0.1 ml of THF-$d_8$. The 1,1-diphenyl-4-penten-1-ol solution was loaded into a 250 µL syringe. The syringe was stoppered with a rubber septum, and both the syringe and the screw cap NMR tube were removed from the glovebox. The screw cap NMR tube was placed in a dry ice / acetone bath. An NMR probe was cooled to -50 °C. Initial $^1$H and $^{31}$P NMR spectra of the silylamido complex, **2g**, were collected at -50 °C. The NMR tube was ejected and placed in the dry ice / acetone bath. The 1,1-diphenyl-4-penten-1-ol solution was syringed into the NMR tube. The NMR tube was kept in the dry ice / acetone bath for 5 minutes and then shaken vigorously for 10 seconds

before returning the sample to the dry ice acetone bath. This was repeated two more times. The dark green silylamido solution became red-orange. NMR spectra of the orange solution were collected at -50 °C.

$^{13}C\{^{1}H\}$ NMR (alkenyl carbons): (126 MHz, THF-$d_8$) δ 78.47 (m), 63.55 (m) ppm.

### 3.3.4.2 Rhodium diphosphine alkoxo alkene complex, **7b**.

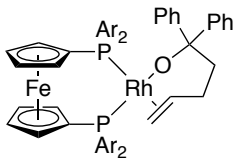


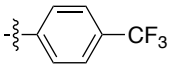

**7b**

Rhodium diphosphine silylamido complex, **2b**, was weighed inside a glovebox in a 3 ml vial. The complex was dissolved in THF-$d_8$ (0.5 ml) and transferred to a screw cap NMR tube. The NMR tube was capped with a septum-bearing cap. 1,1-Diphenyl-4-penten-1-ol was weighed inside the glovebox in a 3 ml vial and dissolved in 0.1 ml of THF-$d_8$. The 1,1-diphenyl-4-penten-1-ol solution was loaded into a 250 µL syringe, and the syringe was stoppered with a rubber septum. Both the stoppered syringe and the screw cap NMR tube were removed from the glovebox. The screw cap NMR tube was placed in a dry ice / acetone bath. An NMR probe was cooled to -50 °C. Initial $^{1}H$ and $^{31}P$ NMR spectra of the silylamido complex, **2b**, were collected at -50 °C. The NMR tube was ejected and placed in the dry ice / acetone bath. The 1,1-diphenyl-4-penten-1-ol solution was syringed into the NMR tube. The NMR tube was kept in the dry ice / acetone bath for 5 minutes and then shaken vigorously for 10 seconds before returning the sample to the dry ice acetone bath. This was repeated two more times. The dark green silylamido solution became red-orange. NMR spectra of the orange solution were collected at -50 °C.

$^{13}C\{^{1}H\}$ NMR (alkenyl carbons): (126 MHz, toluene-$d_8$) δ 72.67 (m), 64.26 (m) ppm.

### 3.3.4.3 Rhodium diphosphine alkoxo alkene complex, **7c**.

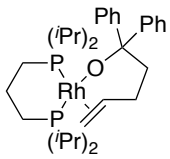



Ar = 


**7c**

Rhodium diphosphine silylamido complex, **2c**, was prepared in situ by the reaction of rhodium diphosphine chloride complex **1c** (150 mg, 0.078 mmol, 1 equiv.) with KHMDS (31.0 mg, 0.155 mmol, 2 equiv.). The reaction was performed in THF-$d_8$ (0.5 ml) inside a glovebox at room temperature. The reaction was allowed to stir overnight. The resulting solution was transferred to a screw cap NMR tube. The NMR tube was capped with a septum-bearing cap. 1,1-Diphenyl-4-penten-1-ol (37.1 mg, 0.156 mmol, 2 equiv.) was weighed inside the glovebox in a 3 ml vial and dissolved in 0.1 ml of THF-$d_8$. The 1,1-diphenyl-4-penten-1-ol solution was loaded into a 250 µL syringe. The syringe was stoppered with a rubber septum, and both the syringe and the screw cap NMR tube were removed from the glovebox. The screw cap NMR tube was placed in a dry ice / acetone bath. An NMR probe was cooled to -50 °C. Initial $^{1}H$ and $^{31}P$ NMR spectra of the silylamido complex, **2c**, were collected at -50 °C. The NMR tube was ejected and placed in the dry ice / acetone bath. The 1,1-diphenyl-4-penten-1-ol solution was syringed into the NMR tube. The NMR tube was kept in the dry ice / acetone bath for 5 minutes and then shaken vigorously for 10 seconds before returning the sample to the dry ice acetone bath. This was repeated two more times. The dark green silylamido solution became red-orange. NMR spectra of the orange solution were collected at -50 °C.

### 3.3.4.4 Rhodium diphosphine alkoxo alkene complex, **7d**.

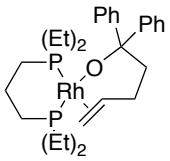



**7d**

Rhodium diphosphine silylamido complex, **2d**, was prepared in situ by the reaction of rhodium diphosphine chloride complex **1c** (72 mg, 0.087 mmol, 1 equiv.) with KHMDS (34.6 mg, 0.174 mmol, 2 equiv.). The reaction was performed in THF-$d_8$ (0.5 ml) inside a glovebox at room temperature. The reaction was allowed to stir overnight. The resulting solution was transferred to a screw cap NMR tube. The NMR tube was capped with a septum-bearing cap. 1,1-Diphenyl-4-penten-1-ol (41.4 mg, 0.174 mmol, 2 equiv.) was weighed inside the glovebox in a 3 ml vial and dissolved in 0.1 ml of THF-$d_8$. The 1,1-diphenyl-4-penten-1-ol solution was loaded into a 250 µL syringe. The syringe was stoppered with a rubber septum, and both the syringe and the screw cap NMR tube were removed from the glovebox. NMR spectra ($^1$H and $^{31}$P) of the silylamido complex, **2d**, were collected at room temperature. The NMR tube was ejected. The 1,1-diphenyl-4-penten-1-ol solution was syringed into the NMR tube. The dark blue solution became bright orange. NMR spectra of the orange solution were collected at room temperature.

$^{13}$C{$^1$H} NMR (alkenyl carbons): (126 MHz, toluene-$d_8$) δ 71.83 (m), 66.04 (m) ppm.

### 3.3.4.5 Rhodium diphosphine alkoxo alkene complex, **7e.**

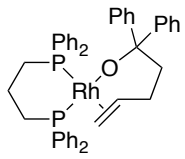



**7e**

Rhodium diphosphine silylamido complex **2e** (123 mg, 0.254 mmol, 1 equiv.) was weighed inside a glovebox in a 3 ml vial. 1,1-Diphenyl-4-penten-1-ol (61 mg, 0.256 mmol, 1 equiv.) was weighed inside a glovebox in a 3 ml vial. The weighed silylamido complex was dissolved in toluene-$d_8$ (0.4 ml) and transferred to a screw cap NMR tube. The NMR tube was capped with a septum-bearing cap. The weighed 1,1-diphenyl-4-penten-1-ol was dissolved in approximately 0.2 ml toluene-$d_8$ and loaded into a 500 µL syringe. The syringe was stoppered with a rubber septum. The syringe and screw cap NMR tube were removed from the glovebox. NMR spectra ($^1$H, $^{31}$P, and $^{13}$C) of the rhodium diphosphine silylamido solution were collected at room temperature. The NMR tube was ejected. The solution of 1,1-diphenyl-4-penten-1-ol was syringed into the NMR tube at room temperature. The NMR tube was shaken to mix the two reagents. The dark blue solution became orange NMR spectra ($^1$H, $^{31}$P, and $^{13}$C) of the resulting rhodium diphosphine alkoxo alkene complex, **7e**, were collected at room temperature.

$^{13}$C{$^1$H} NMR (alkenyl carbons): (126 MHz, toluene-$d_8$) δ 81.02 (m), 68.84 (m) ppm.

### 3.3.4.6 Rhodium diphosphine alkoxo alkene complex, **7g**.




**7g**

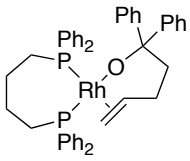
Rhodium diphosphine silylamido complex, **2g**, was prepared in situ by the reaction of rhodium diphosphine chloride complex **1g** (100 mg, 0.091 mmol, 1 equiv.) with KHMDS (36.2 mg, 0.181 mmol, 2 equiv.). The reaction was performed in THF-$d_8$ (0.5 ml) inside a glovebox at room temperature. The reaction was allowed to stir overnight. The resulting solution was transferred to a screw cap NMR tube. The NMR tube was capped with a septum-bearing cap. 1,1-Diphenyl-4-penten-1-ol (43.3 mg, 0.182 mmol, 2 equiv.) was weighed inside the glovebox in a 3 ml vial and dissolved in 0.1 ml of THF-$d_8$. The 1,1-diphenyl-4-penten-1-ol solution was loaded into a 250 µL syringe. The syringe was stoppered with a rubber septum, and both the syringe and the screw cap NMR tube were removed from

the glovebox. The screw cap NMR tube was placed in a dry ice / acetone bath. An NMR probe was cooled to -50 °C. Initial $^{1}H$ and $^{31}P$ NMR spectra of the silylamido complex, **2g**, were collected at -50 °C. The NMR tube was ejected and placed in the dry ice / acetone bath. The 1,1-diphenyl-4-penten-1-ol solution was syringed into the NMR tube. The NMR tube was kept in the dry ice / acetone bath for 5 minutes and then shaken vigorously for 10 seconds before returning the sample to the dry ice acetone bath. This was repeated two more times. The dark blue silylamido solution became bright orange. NMR spectra of the orange solution were collected at -50 °C.

$^{13}C\{^{1}H\}$

NMR (alkenyl carbons): (126 MHz, THF-$d_8$) δ 83.06 (m), 70.06 (m) ppm.

### 3.3.4.7 Rhodium diphosphine alkoxo alkene complex, **7h**.

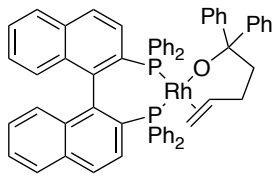



**7h**

Rhodium diphosphine silylamido complex, **2h**, was prepared in situ by the reaction of rhodium diphosphine chloride complex **1h** (100 mg, 0.085 mmol, 1 equiv.) with KHMDS (35.3 mg, 0.177 mmol, 2 equiv.). The reaction was performed in THF-$d_8$ (0.5 ml) inside a glovebox at room temperature. The reaction was allowed to stir overnight. The resulting solution was transferred to a screw cap NMR tube. The NMR tube was capped with a septum-bearing cap. 1,1-Diphenyl-4-penten-1-ol (42.2 mg, 0.177 mmol, 2 equiv.) was weighed inside the glovebox in a 3 ml vial and dissolved in 0.1 ml of THF-$d_8$. The 1,1-diphenyl-4-penten-1-ol solution was loaded into a 250 µL syringe. The syringe was stoppered with a rubber septum, and both the syringe and the screw cap NMR tube were removed from the glovebox. The screw cap NMR tube was placed in a dry ice / acetone bath. An NMR probe was cooled to -50 °C. Initial $^{1}H$ and $^{31}P$ NMR spectra of the silylamido complex, **2h**, were collected at -50 °C. The NMR tube was ejected and placed in the dry ice / acetone bath. The 1,1-diphenyl-4-penten-1-ol solution was syringed into the NMR tube. The NMR tube was kept in the dry ice / acetone bath for 5 minutes and then shaken vigorously for 10 seconds before returning the sample to the dry ice acetone bath. This was repeated two more times. The dark blue silylamido solution became bright orange. NMR spectra of the orange solution were collected at -50 °C.

$^{13}C\{^{1}H\}$ NMR (alkenyl carbons): (126 MHz, THF-$d_8$) δ 73.79 (m), 63.54 (m) ppm.

### 3.3.4.8 Rhodium diphosphine alkoxo alkene complex, **7i**.



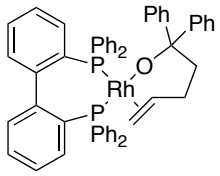

**7i**

Rhodium diphosphine silylamido complex, **2i**, was prepared in situ by the reaction of rhodium diphosphine chloride complex **1i** (200 mg, 0.131 mmol, 1 equiv.) with KHMDS (52.4 mg, 0.263 mmol, 2 equiv.). The reaction was performed in THF-$d_8$ (0.5 ml) inside a glovebox at room temperature. The reaction was allowed to stir overnight. The resulting solution was transferred to a screw cap NMR tube. The NMR tube was capped with a septum-bearing cap. 1,1-Diphenyl-4-penten-1-ol (62.6 mg, 0.263 mmol, 2 equiv.) was weighed inside the glovebox in a 3 ml vial and dissolved in 0.1 ml of THF-$d_8$. The 1,1-diphenyl-4-penten-1-ol solution was loaded into a 250 µL syringe. The syringe was stoppered with a rubber septum, and both the syringe and the screw cap NMR tube were removed from the glovebox. The screw cap NMR tube was placed in

a dry ice / acetone bath. An NMR probe was cooled to -50 °C. Initial $^{1}H$ and $^{31}P$ NMR spectra of the silylamido complex, **2i**, were collected at -50 °C. The NMR tube was ejected and placed in the dry ice / acetone bath. The 1,1-diphenyl-4-penten-1-ol solution was syringed into the NMR tube. The NMR tube was kept in the dry ice / acetone bath for 5 minutes and then shaken vigorously for 10 seconds before returning the sample to the dry ice acetone bath. This was repeated two more times. The dark green silylamido solution became red. NMR spectra of the red solution were collected at -50 °C. A dark red precipitate slowly crashed out of solution.

$^{13}C\{^{1}H\}$ NMR (alkenyl carbons): (126 MHz, THF-$d_8$) δ 82.34 (m), 2$^{nd}$ signal overlaps with THF-$d_8$ ppm.

### 3.3.4.9 Rhodium diphosphine alkoxo alkene complex, **7j**.

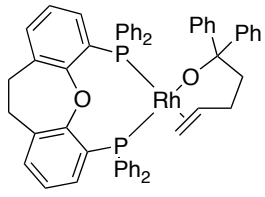



**7j**

Rhodium diphosphine silylamido complex, **2j**, was prepared in situ by the reaction of rhodium diphosphine chloride complex **1j** (150 mg, 0.113 mmol, 1 equiv.) with KHMDS (45.3 mg, 0.227 mmol, 2 equiv.). The reaction was performed in THF-$d_8$ (0.5 ml) inside a glovebox at room temperature. The reaction was allowed to stir overnight. The resulting solution was transferred to a screw cap NMR tube. The NMR tube was capped with a septum-bearing cap. 1,1-Diphenyl-4-penten-1-ol (54.1 mg, 0.227 mmol, 2 equiv.) was weighed inside the glovebox in a 3 ml vial and dissolved in 0.1 ml of THF-$d_8$. The 1,1-diphenyl-4-penten-1-ol solution was loaded into a 250 µL syringe. The syringe was stoppered with a rubber septum, and both the syringe and the screw cap NMR tube were removed from the glovebox. The screw cap NMR tube was placed in a dry ice / acetone bath. An NMR probe was cooled to -50 °C. Initial $^{1}H$ and $^{31}P$ NMR spectra of the silylamido complex, **2j**, were collected at -50 °C. The NMR tube was ejected and placed in the dry ice / acetone bath. The 1,1-diphenyl-4-penten-1-ol solution was syringed into the NMR tube. The NMR tube was kept in the dry ice / acetone bath for 5 minutes and then shaken vigorously for 10 seconds before returning the sample to the dry ice acetone bath. This was repeated two more times. The dark green silylamido solution became red. NMR spectra of the red solution were collected at -50 °C. A brown precipitate slowly crashed out of solution. A dark red precipitate slowly crashed out of solution.

$^{13}C\{^{1}H\}$ NMR (alkenyl carbons): (126 MHz, THF-$d_8$) δ 80.71 (m), 65.28 (m) ppm.

### 3.3.4.10 Rhodium diphosphine alkoxo alkene complex, **7k**.



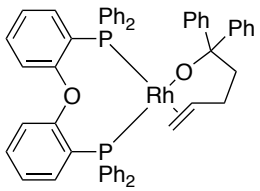

**2k**

Rhodium diphosphine silylamido complex, **2g**, was prepared in situ by the reaction of rhodium diphosphine chloride complex **1g** (100 mg, 0.071 mmol, 1 equiv.) with KHMDS (28.4 mg, 0.142 mmol, 2 equiv.). The reaction was performed in THF-$d_8$ (0.5 ml) inside a glovebox at room temperature. The reaction was allowed to stir overnight. The resulting solution was transferred to a screw cap NMR tube. The NMR tube was capped with a septum-bearing cap. 1,1-Diphenyl-4-penten-1-ol (33.9 mg, 0.142 mmol, 2 equiv.) was weighed inside the glovebox in a 3 ml vial and dissolved in 0.1 ml of THF-$d_8$. The 1,1-diphenyl-4-penten-1-ol solution was loaded into a 250 µL syringe. The syringe was stoppered with a rubber septum, and both the syringe and the screw cap NMR tube were removed from the glovebox. The screw cap NMR tube was placed in a dry ice /

acetone bath. An NMR probe was cooled to -50 °C. Initial $^{1}$H and $^{31}$P NMR spectra of the silylamido complex, **2g**, were collected at -50 °C. The NMR tube was ejected and placed in the dry ice / acetone bath. The 1,1-diphenyl-4-penten-1-ol solution was syringed into the NMR tube. The NMR tube was kept in the dry ice / acetone bath for 5 minutes and then shaken vigorously for 10 seconds before returning the sample to the dry ice acetone bath. This was repeated two more times. The dark green silylamido solution became red-orange. NMR spectra of the red solution were collected at -50 °C.

$^{13}$C{$^{1}$H} NMR (alkenyl carbons): (126 MHz, THF-$d_8$) δ 60.67 (m), 59.98 (m) ppm.

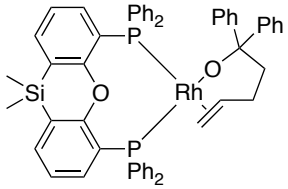
### 3.3.4.11 Rhodium diphosphine alkoxo alkene complex, **7l**.




**7l**

Complex **7l** precipitated from solution. Consequently, a $^{13}$C NMR spectrum was not obtained.

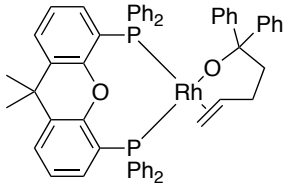
### 3.3.4.12 Rhodium diphosphine alkoxo alkene complex, **7m**.




**7m**

Complex **7m** precipitated from solution. Consequently, a $^{13}$C NMR spectrum was not obtained.

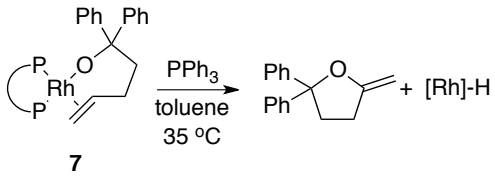
### 3.3.4.13 Rhodium diphosphine alkoxo alkene complex, **7n**.




**7n**

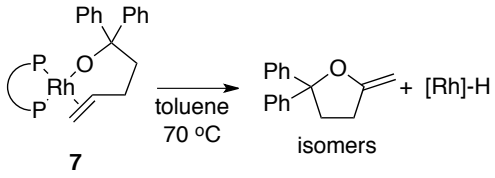
Complex **7n** precipitated from solution. Consequently, a $^{13}$C NMR spectrum was not obtained.

### 3.3.5 Reactions of Rhodium Diphosphine Alkoxo Alkene Complexes **7a-e** and **7g-n** in the presence of $PPh_3$

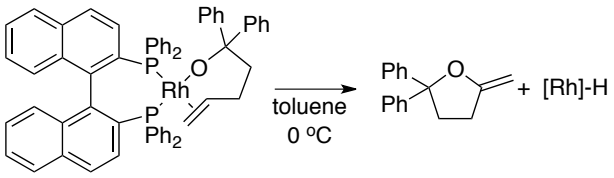



Rhodium alkoxo alkene complexes **7a-e** and **7g-n** were prepared in situ by the additions of 1,1-diphenyl-4-penten-1-ol to rhodium diphosphine silylamido complexes, **2a-e** and **2g-n**. The complexes were kept cold, inside screw cap NMR tubes placed in a dry ice / acetone bath. $PPh_3$ (10 equiv.) was weighed inside a glovebox in a 3 ml vial, dissolved in $d^8$-toluene (150 µL) and loaded into a 250 µL syringe. The syringe was stoppered and removed from the glovebox. The $PPh_3$ solution was added to the rhodium alkoxo alkene complex at -78 °C. The reagents were allowed to mix at -78 °C for 5 min., and then shaken vigorously for 10 seconds and returned to the dry ice / acetone bath. This was repeated two more times. The NMR probe was cooled to -50 °C. NMR spectra were collected at -50 °C. The spectra show no signs that $PPh_3$ coordinates to the metal. The NMR tube was ejected from the probe and returned to the dry ice / acetone bath. The NMR probe was warmed to 35 °C. The NMR tube was returned to the NMR probe, and a series of $^1H$ NMR spectra were collected every two minutes for the next 8 hours or until the rhodium alkoxo alkene complex was completely consumed. The rates for alkene insertion were too fast at 35 °C for rhodium alkoxo alkene complex, **7i**, and rates were consequently measured at 0°C.

### 3.3.6 Reactions of Rhodium Diphosphine Alkoxo Alkene Complexes **7d,e,g,h** in the absence of $PPh_3$ at 70 °C




Rhodium alkoxo alkene complexes **7d,e,g,h** were prepared in situ by the additions of 1,1-diphenyl-4-penten-1-ol to rhodium diphosphine silylamido complexes, **7d,e,g,h**. The reactions were performed at room temperature inside NMR tubes. The resulting complexes were characterized by $^1H$ and $^{31}P$ NMR spectroscopy at room temperature. The sample was ejected. The NMR probe was warmed to 70 °C. The NMR tube was returned to the NMR probe, and a series of $^1H$ NMR spectra were collected every two minutes for the next 8 hours or until the rhodium alkoxo alkene complex was completely consumed.




**7g**

The decomposition of rhodium diphosphine alkoxo alkene complex, **7i**, was also measured at 0°C in the absence of $PPh_3$. The complex was prepared in situ by the addition of 1,1-diphenyl-4-penten-1-ol to rhodium diphosphine silylamido complex, **2i**.

References


(1) (a) Kirchhoff, J. H.; Netherton, M. R.; Hills, I. D.; Fu, G. C. *J Am Chem Soc* **2002**, *124*, 13662(b) Netherton, M. R.; Fu, G. C. *Angewandte Chemie International Edition* **2002**, *41*, 3910(c) Hills, I. D.; Netherton, M. R.; Fu, G. C. *Angewandte Chemie International Edition* **2003**, *42*, 5749.

(2) Hartwig, J. F. *Organotransition Metal Chemistry; From Bonding to Catalysis*; 1 ed.; University Science Books: Sausalito, CA, 2010.

(3) Farina, V.; Krishnan, B. *J Am Chem Soc* **1991**, *113*, 9585.

(4) (a) Farina, V.; Kapadia, S.; Krishnan, B.; Wang, C.; Liebeskind, L. S. *The Journal of Organic Chemistry* **1994**, *59*, 5905(b) Amatore, C.; Bahsoun, A. A.; Jutand, A.; Meyer, G.; Ndedi, N.; Ricard, L. *J Am Chem Soc* **2003**, *125*, 4212.

(5) Korenaga, T.; Ko, A.; Uotani, K.; Tanaka, Y.; Sakai, T. *Angewandte Chemie International Edition* **2011**, *50*, 10703.

(6) Tolman, C. A. *Inorg Chem* **1972**, *11*, 3128.

(7) Thompson, W. H.; Sears, C. T. *Inorg Chem* **1977**, *16*, 769.

(8) Amatore, C.; Carre, E.; Jutand, A.; M'Barki, M. A. *Organometallics* **1995**, *14*, 1818.

(9) Amatore, C.; Jutand, A.; Meyer, G. *Inorganica Chimica Acta* **1998**, *273*, 76.

(10) (a) Abis, L.; Sen, A.; Halpern, J. *J Am Chem Soc* **1978**, *100*, 2915(b) Halpern, J. *Accounts Chem Res* **1982**, *15*, 332.

(11) Jones, W. D.; Kuykendall, V. L. *Inorg Chem* **1991**, *30*, 2615.

(12) Negishi, E.-i.; Takahashi, T.; Akiyoshi, K. *Journal of Organometallic Chemistry* **1987**, *334*, 181.

(13) Ariafard, A.; Yates, B. F. *Journal of Organometallic Chemistry* **2009**, *694*, 2075.

(14) Culkin, D. A.; Hartwig, J. F. *Organometallics* **2004**, *23*, 3398.

(15) Korenaga, T.; Abe, K.; Ko, A.; Maenishi, R.; Sakai, T. *Organometallics* **2010**, *29*, 4025.

(16) Hamann, B. C.; Hartwig, J. F. *J Am Chem Soc* **1998**, *120*, 3694.

(17) Mann, G.; Hartwig, J. F. *Tetrahedron Lett* **1997**, *38*, 8005.

(18) Mann, G.; Shelby, Q.; Roy, A. H.; Hartwig, J. F. *Organometallics* **2003**, *22*, 2775.

(19) The rate constant for the reductive elimination of 4-(3,5-di-tert-butylphenoxy)-benzonitrile from Pd(DPPF)(Ar1)(OAr2) (Ar1 = p-CN-C6H4; Ar2 = 3,5-(tBu)2-C6H3) at 105 °C is 1.0 x 10-4 s-1. The rate constant for the reductive elimination of 4-(3,5-di-tert-butylphenoxy)-benzonitrile from Pd(p-CF3-DPPF)(Ar1)(OAr2) (Ar1 = p-CN-C6H4; Ar2 = 3,5-(tBu)2-C6H3) at 105 °C is 2.0 x 10-4 s-1.

(20) Casalnuovo, A. L.; RajanBabu, T. V.; Ayers, T. A.; Warren, T. H. *J Am Chem Soc* **1994**, *116*, 9869.

(21) Goertz, W.; Keim, W.; Vogt, D.; Englert, U.; D. K. Boele, M.; A. van der Veen, L.; C. J. Kamer, P.; W. N. M. van Leeuwen, P. *Journal of the Chemical Society, Dalton Transactions* **1998**, 2981.

(22) Unruh, J. D.; Christenson, J. R. *Journal of Molecular Catalysis* **1982**, *14*, 19.

(23) Moser, W. R.; Papile, C. J.; Brannon, D. A.; Duwell, R. A.; Weininger, S. J. *Journal of Molecular Catalysis* **1987**, *41*, 271.

(24) van der Veen, L. A.; Boele, M. D. K.; Bregman, F. R.; Kamer, P. C. J.; van Leeuwen, P. W. N. M.; Goubitz, K.; Fraanje, J.; Schenk, H.; Bo, C. *J Am Chem Soc* **1998**, *120*, 11616.

(25) Hegedüs, C.; Madarász, J.; Gergely, I.; Szöllo˝sy, Á.; Monsees, A.; Riermeier, T.; Bakos, J. *Tetrahedron: Asymmetry* **2004**, *15*, 2507.

(26) RajanBabu, T. V.; Ayers, T. A. *Tetrahedron Lett* **1994**, *35*, 4295.

(27) Montelatici, S.; van der Ent, A.; Osborn, J. A.; Wilkinson, G. *Journal of the Chemical Society A: Inorganic, Physical, Theoretical* **1968**, 1054.

(28) Halpern, J.; Okamoto, T. *Inorganica Chimica Acta* **1984**, *89*, L53.

(29) (a) RajanBabu, T. V.; Ayers, T. A.; Casalnuovo, A. L. *J Am Chem Soc* **1994**, *116*, 4101(b) Gergely, I.; Hegedüs, C.; Szöllősy, Á.; Monsees, A.; Riermeier, T.; Bakos, J. *Tetrahedron Lett* **2003**, *44*, 9025(c) Herseczki, Z.; Gergely, I.; Hegedüs, C.; Szöllősy, Á.; Bakos, J. *Tetrahedron: Asymmetry* **2004**, *15*, 1673.

(30) Wu, H.-C.; Hamid, S. A.; Yu, J.-Q.; Spencer, J. B. *J Am Chem Soc* **2009**, *131*, 9604.

(31) Jacobsen, E. N.; Zhang, W.; Guler, M. L. *J Am Chem Soc* **1991**, *113*, 6703.

(32) Palucki, M.; Finney, N. S.; Pospisil, P. J.; Güler, M. L.; Ishida, T.; Jacobsen, E. N. *J Am Chem Soc* **1998**, *120*, 948.

(33) Burger, B. J.; Santarsiero, B. D.; Trimmer, M. S.; Bercaw, J. E. *J Am Chem Soc* **1988**, *110*, 3134.

(34) Malinoski, J. M.; Brookhart, M. *Organometallics* **2003**, *22*, 5324.

(35) Hanley, P. S.; Hartwig, J. F. *J Am Chem Soc* **2011**, *133*, 15661.

(36) Tolman, C. A. *J Am Chem Soc* **1970**, *92*, 2956.

(37) Tolman, C. A.; Seidel, W. C.; Gosser, L. W. *J Am Chem Soc* **1974**, *96*, 53.

(38) (a) Tolman, C. A. *Chem Rev* **1977**, *77*, 313(b) Musco, A.; Kuran, W.; Silvani, A.; Anker, M. W. *Journal of the Chemical Society, Chemical Communications* **1973**, 938(c) Kuran, W.; Musco, A. *Inorganica Chimica Acta* **1975**, *12*, 187(d) Mann, B. E.; Musco, A. *Journal of the Chemical Society, Dalton Transactions* **1975**, 1673.

(39) Clarke, M. L.; Heydt, M. *Organometallics* **2005**, *24*, 6475.

(40) Halpern, J.; Phelan, P. F. *J Am Chem Soc* **1972**, *94*, 1881.

(41) Matsumoto, M.; Yoshioka, H.; Nakatsu, K.; Yoshida, T.; Otsuka, S. *J Am Chem Soc* **1974**, *96*, 3322.

(42) Brady, R.; De Camp, W. H.; Flynn, B. R.; Schneider, M. L.; Scott, J. D.; Vaska, L.; Werneke, M. F. *Inorg Chem* **1975**, *14*, 2669.

(43) Frech, C. M.; Milstein, D. *J Am Chem Soc* **2006**, *128*, 12434.

(44) Carr, N.; Dunne, B. J.; Mole, L.; Orpen, A. G.; Spencer, J. L. *Journal of the Chemical Society, Dalton Transactions* **1991**, 863.

(45) (a) Johnson, L. K.; Killian, C. M.; Brookhart, M. *J Am Chem Soc* **1995**, *117*, 6414(b) Johnson, L. K.; Mecking, S.; Brookhart, M. *J Am Chem Soc* **1996**, *118*, 267.

(46) Deng, L.; Woo, T. K.; Cavallo, L.; Margl, P. M.; Ziegler, T. *J Am Chem Soc* **1997**, *119*, 6177.

(47) Ledford, J.; Shultz, C. S.; Gates, D. P.; White, P. S.; DeSimone, J. M.; Brookhart, M. *Organometallics* **2001**, *20*, 5266.

(48) Gagne, M. R.; Stern, C. L.; Marks, T. J. *J Am Chem Soc* **1992**, *114*, 275.

(49) van Leeuwen, P. W. N. M.; Kamer, P. C. J.; Reek, J. N. H.; Dierkes, P. *Chem Rev* **2000**, *100*, 2741.

(50) Sowa, J. R.; Zanotti, V.; Facchin, G.; Angelici, R. J. *J Am Chem Soc* **1992**, *114*, 160.

(51) Miedaner, A.; Haltiwanger, R. C.; DuBois, D. L. *Inorg Chem* **1991**, *30*, 417.

(52) (a) Curtis, C. J.; Miedaner, A.; Ellis, W. W.; DuBois, D. L. *J Am Chem Soc* **2002**, *124*, 1918(b) Raebiger, J. W.; Miedaner, A.; Curtis, C. J.; Miller, S. M.; Anderson, O. P.; DuBois, D. L. *J Am Chem Soc* **2004**, *126*, 5502(c) Nimlos, M. R.; Chang, C. H.; Curtis, C. J.; Miedaner, A.; Pilath, H. M.; DuBois, D. L. *Organometallics* **2008**, *27*, 2715.

(53) Kranenburg, M.; Kamer, P. C. J.; van Leeuwen, P. W. N. M. *European Journal of Inorganic Chemistry* **1998**, *1998*, 25.

(54) Johns, A. M.; Utsunomiya, M.; Incarvito, C. D.; Hartwig, J. F. *Journal of the American Chemical Society* **2006**, *128*, 1828.

(55) Kranenburg, M.; Kamer, P. C. J.; van Leeuwen, P. W. N. M.; Vogt, D.; Keim, W. *Journal of the Chemical Society, Chemical Communications* **1995**, 2177.

(56) Marcone, J. E.; Moloy, K. G. *J Am Chem Soc* **1998**, *120*, 8527.

(57) Zuidema, E.; van Leeuwen, P. W. N. M.; Bo, C. *Organometallics* **2005**, *24*, 3703.

(58) Kohara, T.; Yamamoto, T.; Yamamoto, A. *Journal of Organometallic Chemistry* **1980**, *192*, 265.

(59) Brown, J. M.; Guiry, P. J. *Inorganica Chimica Acta* **1994**, *220*, 249.

(60) Calhorda, M. J.; Brown, J. M.; Cooley, N. A. *Organometallics* **1991**, *10*, 1431.

(61) Kranenburg, M.; Kamer, P. C. J.; van Leeuwen, P. W. N. M. *European Journal of Inorganic Chemistry* **1998**, *1998*, 155.

(62) Fujita, K.-i.; Yamashita, M.; Puschmann, F.; Alvarez-Falcon, M. M.; Incarvito, C. D.; Hartwig, J. F. *J Am Chem Soc* **2006**, *128*, 9044.

(63) Carr, N.; Dunne, B. J.; Orpen, A. G.; Spencer, J. L. *Journal of the Chemical Society, Chemical Communications* **1988**, 926.

(64) Mole, L.; Spencer, J. L.; Carr, N.; Orpen, A. G. *Organometallics* **1991**, *10*, 49.

(65) Anderson, G. K.; Lumetta, G. J. *Organometallics* **1985**, *4*, 1542.

(66) Dekker, G. P. C. M.; Elsevier, C. J.; Vrieze, K.; Van Leeuwen, P. W. N. M. *Organometallics* **1992**, *11*, 1598.

(67) Dekker, G. P. C. M.; Elsevier, C. J.; Vrieze, K.; van Leeuwen, P. W. N. M.; Roobeek, C. F. *Journal of Organometallic Chemistry* **1992**, *430*, 357.

(68) (a) Bryndza, H. E.; Calabrese, J. C.; Wreford, S. S. *Organometallics* **1984**, *3*, 1603(b) Bryndza, H. E. *Organometallics* **1985**, *4*, 406.

(69) Ogasawara, M.; Takizawa, K.-i.; Hayashi, T. *Organometallics* **2002**, *21*, 4853.

(70) Clark, T. J.; Rodezno, J. M.; Clendenning, S. B.; Aouba, S.; Brodersen, P. M.; Lough, A. J.; Ruda, H. E.; Manners, I. *Chemistry – A European Journal* **2005**, *11*, 4526.

(71) Schweizer, S.; Becht, J.-M.; Le Drian, C. *Advanced Synthesis & Catalysis* **2007**, *349*, 1150.

(72) Evans, L. A.; Fey, N.; Harvey, J. N.; Hose, D.; Lloyd-Jones, G. C.; Murray, P.; Orpen, A. G.; Osborne, R.; Owen-Smith, G. J. J.; Purdie, M. *J Am Chem Soc* **2008**, *130*, 14471.

(73) Gusev, O. V.; Peganova, T. y. A.; Kalsin, A. M.; Vologdin, N. V.; Petrovskii, P. V.; Lyssenko, K. A.; Tsvetkov, A. V.; Beletskaya, I. P. *Organometallics* **2006**, *25*, 2750.

(74) Tani, K.; Tanigawa, E.; Tatsuno, Y.; Otsuka, S. *Journal of Organometallic Chemistry* **1985**, *279*, 87.

(75) Anet, F. A. L.; Bavin, P. M. G. *Canadian Journal of Chemistry* **1957**, *35*, 1084.

(76) Hess, B. A.; Bailey, A. S.; Boekelheide, V. *J Am Chem Soc* **1967**, *89*, 2746.

(77) van der Veen, L. A.; Keeven, P. H.; Schoemaker, G. C.; Reek, J. N. H.; Kamer, P. C. J.; van Leeuwen, P. W. N. M.; Lutz, M.; Spek, A. L. *Organometallics* **2000**, *19*, 872.

(78) (a) Oita, K.; Gilman, H. *J Am Chem Soc* **1957**, *79*, 339(b) Chang, V. H. T.; Corey, J. Y. *Journal of Organometallic Chemistry* **1980**, *190*, 217(c) Kranenburg, M.; van der Burgt, Y. E. M.; Kamer, P. C. J.; van Leeuwen, P. W. N. M.; Goubitz, K.; Fraanje, J. *Organometallics* **1995**, *14*, 3081.

(79) McMurry, J. E.; Krepski, L. R. *The Journal of Organic Chemistry* **1976**, *41*, 3929.

(80) Bronger, R. P. J.; Kamer, P. C. J.; van Leeuwen, P. W. N. M. *Organometallics* **2003**, *22*, 5358.

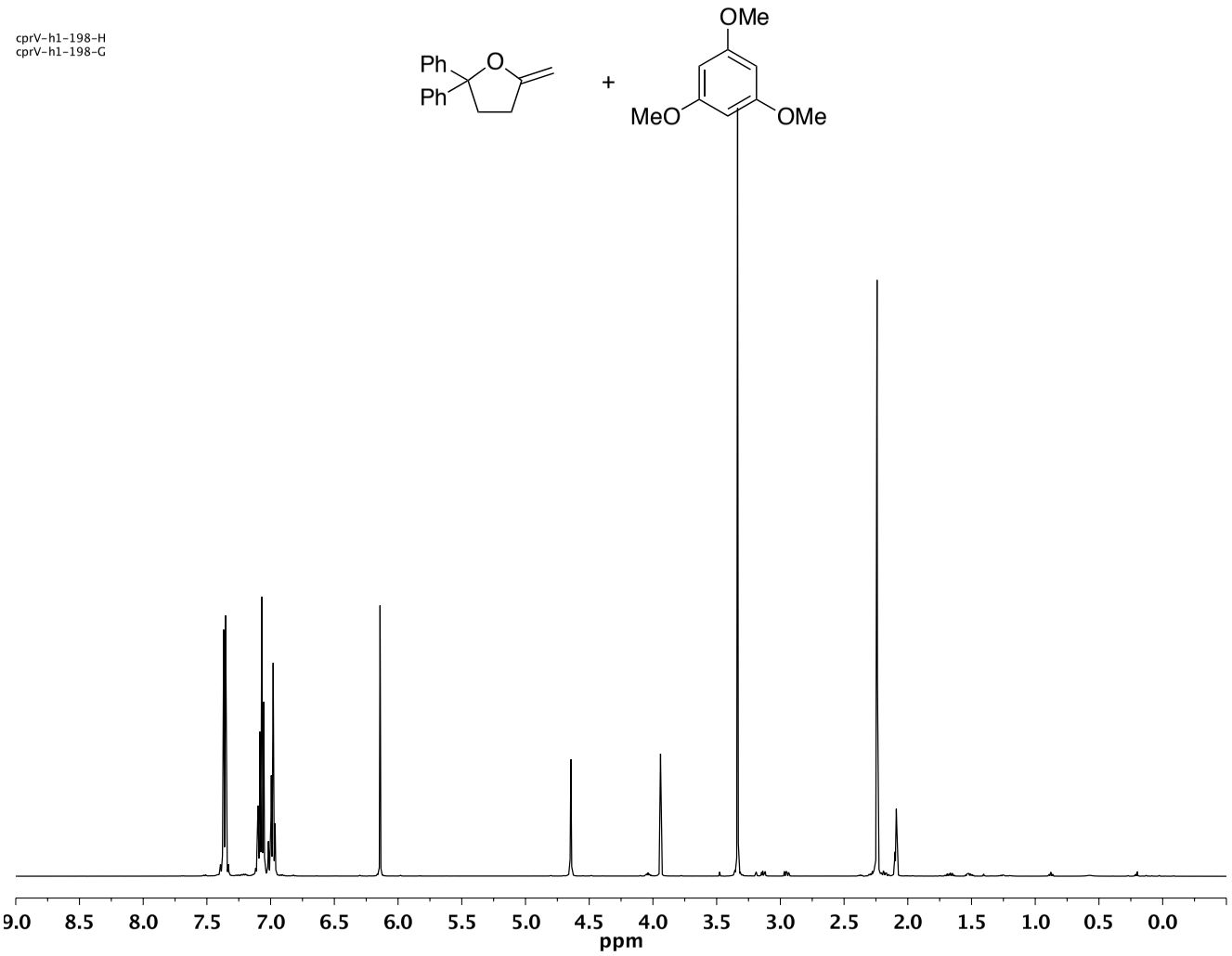
(81) Ricken, S.; Osinski, P. W.; Eilbracht, P.; Haag, R. *Journal of Molecular Catalysis A: Chemical* **2006**, *257*, 78.

(82) Antonio, Y.; Barrera, P.; Contreras, O.; Franco, F.; Galeazzi, E.; Garcia, J.; Greenhouse, R.; Guzman, A.; Velarde, E.; Muchowski, J. M. *The Journal of Organic Chemistry* **1989**, *54*, 2159.

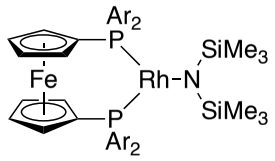
(83) Terao, Y.; Satoh, T.; Miura, M.; Nomura, M. *Bulletin of the Chemical Society of Japan* **1999**, *72*, 2345.

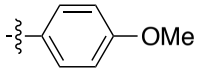
(84) (a) Busacca, C. A.; Raju, R.; Grinberg, N.; Haddad, N.; James-Jones, P.; Lee, H.; Lorenz, J. C.; Saha, A.; Senanayake, C. H. *The Journal of Organic Chemistry* **2008**, *73*, 1524(b) Busacca, C. A.; Lorenz, J. C.; Grinberg, N.; Haddad, N.; Hrapchak, M.; Latli, B.; Lee, H.; Sabila, P.; Saha, A.; Sarvestani, M.; Shen, S.; Varsolona, R.; Wei, X.; Senanayake, C. H. *Org Lett* **2005**, *7*, 4277.

## 3.4 NMR Spectra and Kinetic Data.

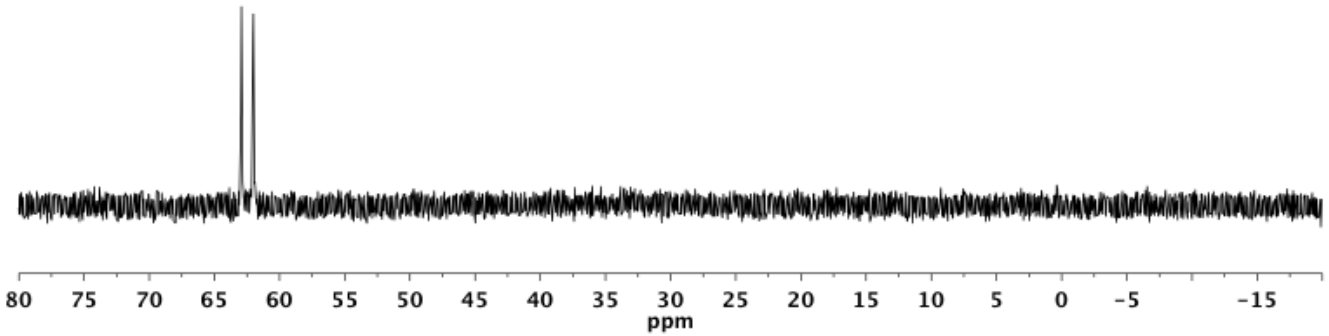

cprV-h1-198-H
cprV-h1-198-G
Ph
Ph
O
+
OMe
MeO
OMe
9.0
8.5
8.0
7.5
7.0
6.5
6.0
5.5
5.0
4.5
4.0
3.5
3.0
2.5
2.0
1.5
1.0
0.5
0.0
ppm

cprIII-p31-21-4a
P31 TRIPHENYLPHOSPHATE PARAMETERS

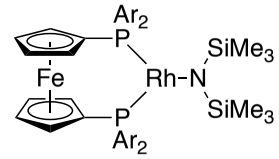


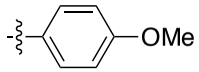

Ar = 


**2a**



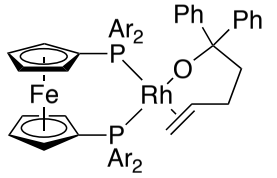
cprlll-h1-50a
cprlll-h1-48c

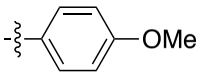



Ar = 

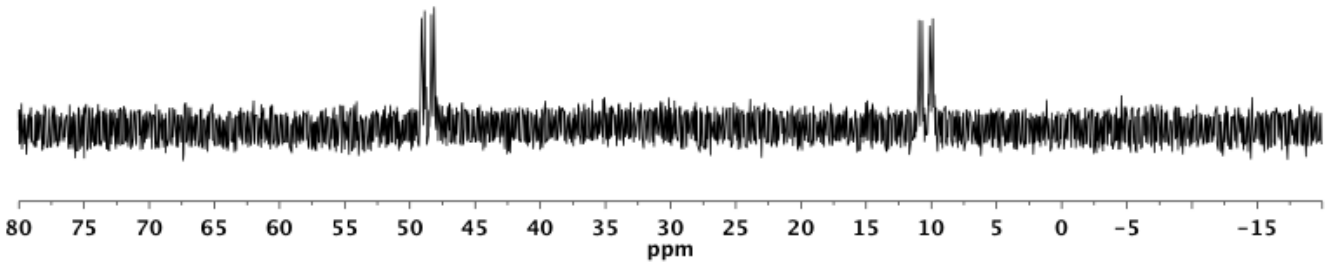

**2a**

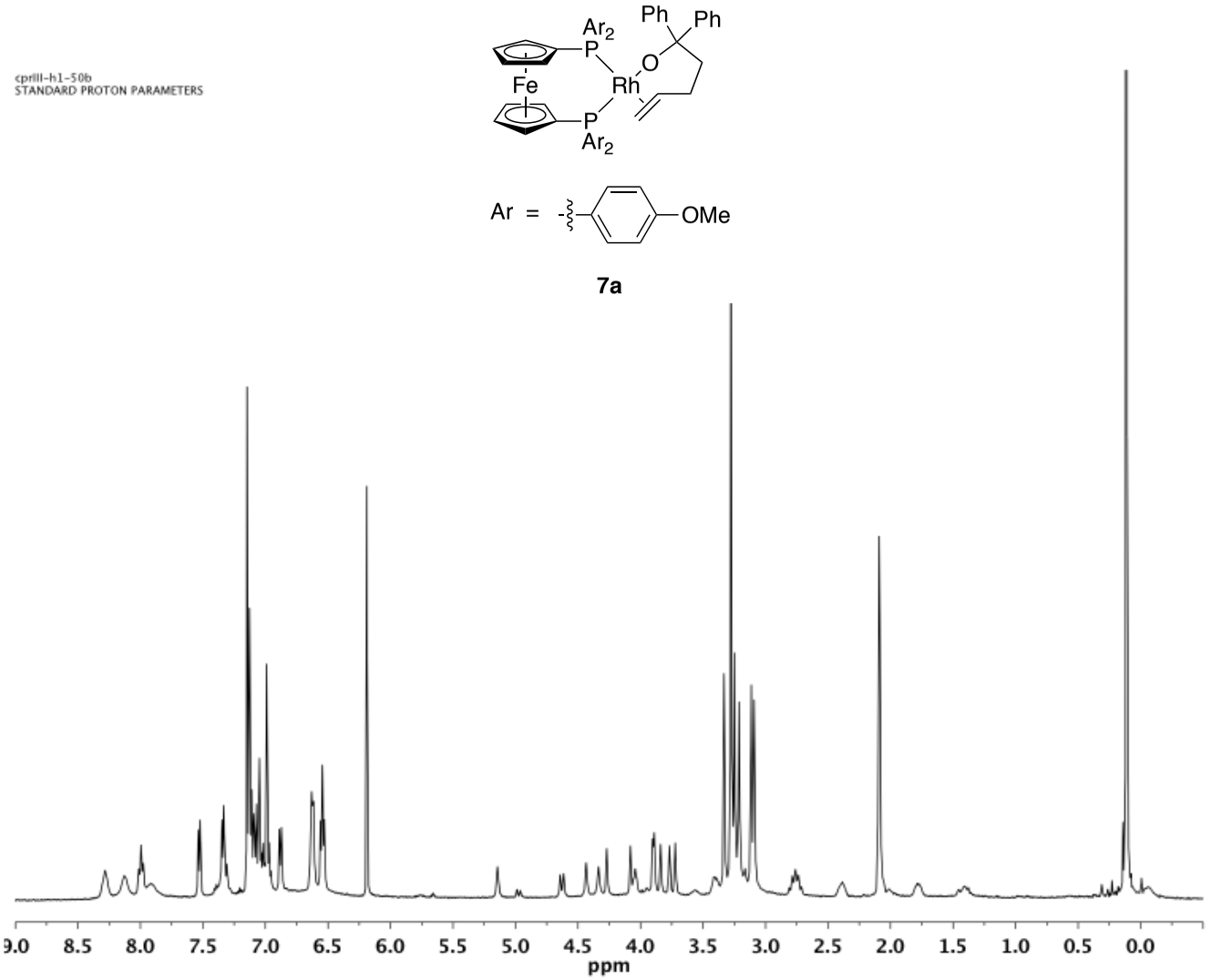
cprIII-p31-21-4b
P31 TRIPHENYLPHOSPHATE PARAMETERS

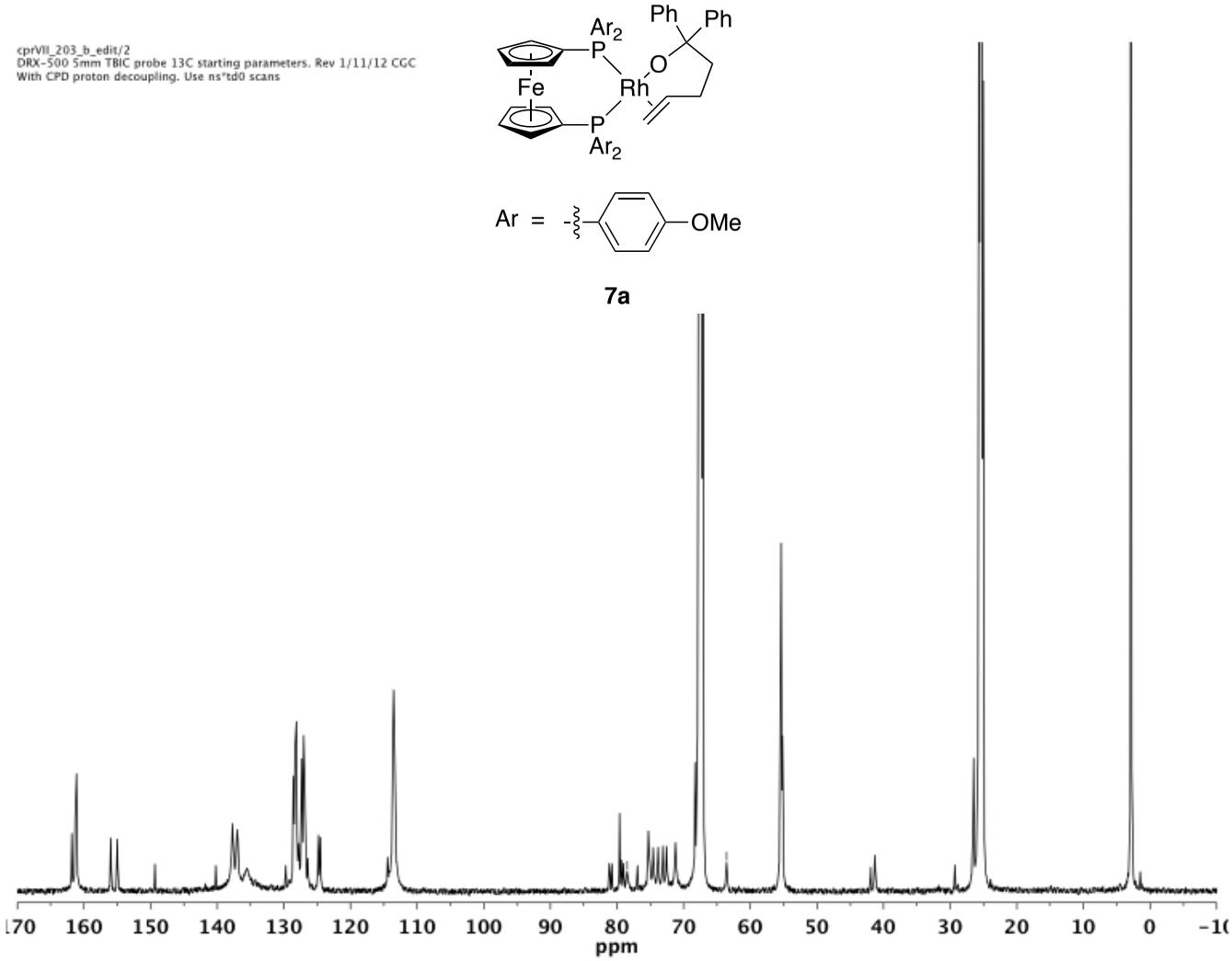



Ar = 

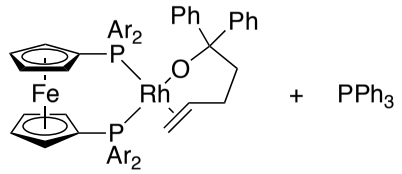

**7a**



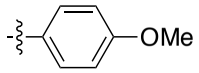

cprIII-h1-50b
STANDARD PROTON PARAMETERS
Ar2
P
Fe
Rh
O
Ph
Ph
P
Ar2
Ar =
OMe
7a
9.0
8.5
8.0
7.5
7.0
6.5
6.0
5.5
5.0
4.5
4.0
3.5
3.0
2.5
2.0
1.5
1.0
0.5
0.0
ppm


cprVII_203_b_edit/2
DRX-500 5mm TBIC probe 13C starting parameters. Rev 1/11/12 CGC
With CPD proton decoupling. Use ns*td0 scans
Ar2
P
Fe
P
Ar2
Rh
O
Ph
Ph
Ar =
OMe
7a
170 160 150 140 130 120 110 100 90 80 70 60 50 40 30 20 10 0 -10
ppm

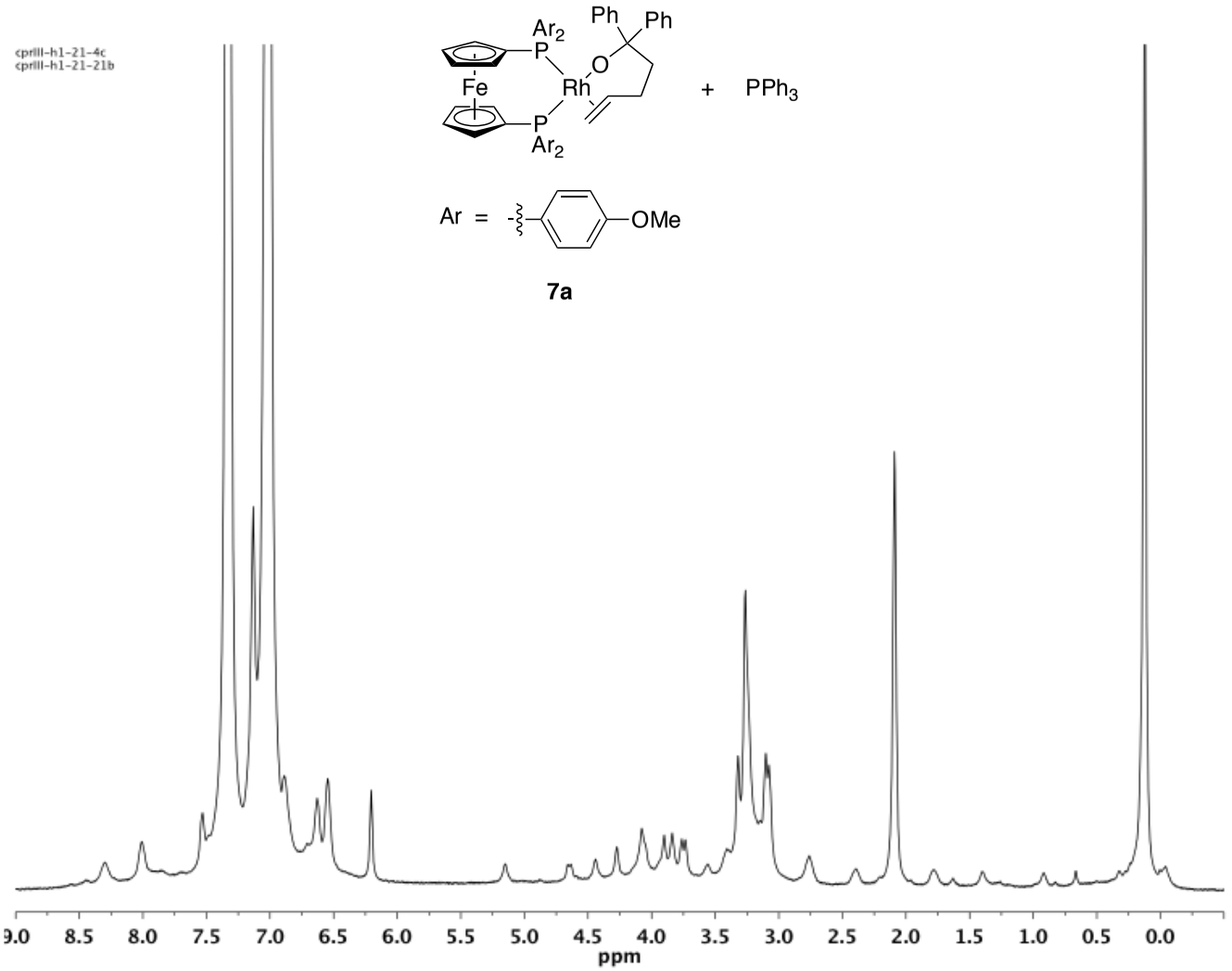
cprIII-p31-21-4c
P31 TRIPHENYLPHOSPHATE PARAMETERS




+ $PPh_3$

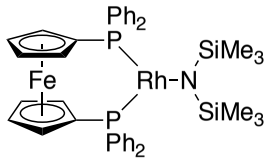
Ar = 


**7a**

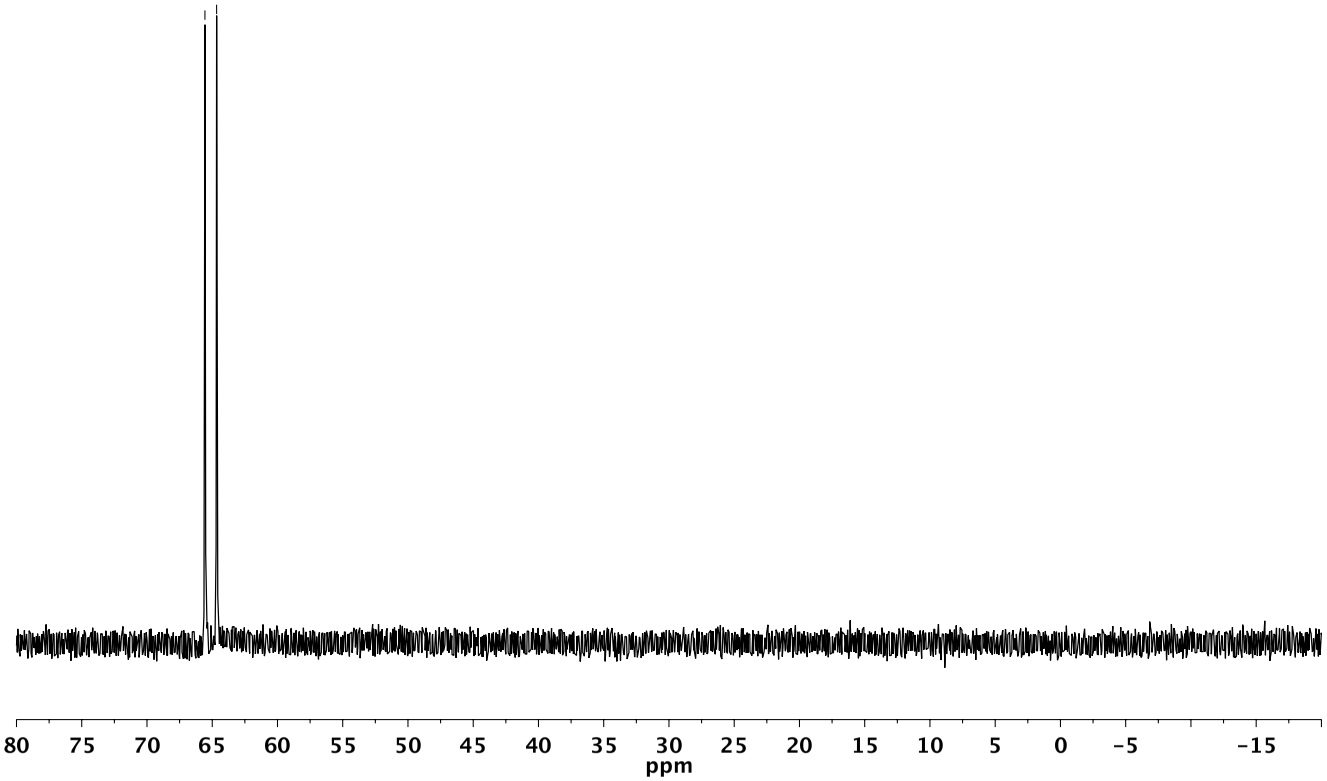

cprIII-h1-21-4c
cprIII-h1-21-21b
Ar2
P
Fe
P
Ar2
Rh
O
Ph
Ph
+ PPh3
Ar = OMe
7a
9.0 8.5 8.0 7.5 7.0 6.5 6.0 5.5 5.0 4.5 4.0 3.5 3.0 2.5 2.0 1.5 1.0 0.5 0.0
ppm

cprIII-p31-25a
P31 TRIPHENYLPHOSPHATE PARAMETERS

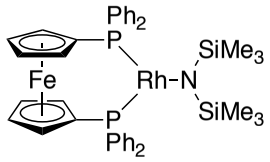
65.56
64.66



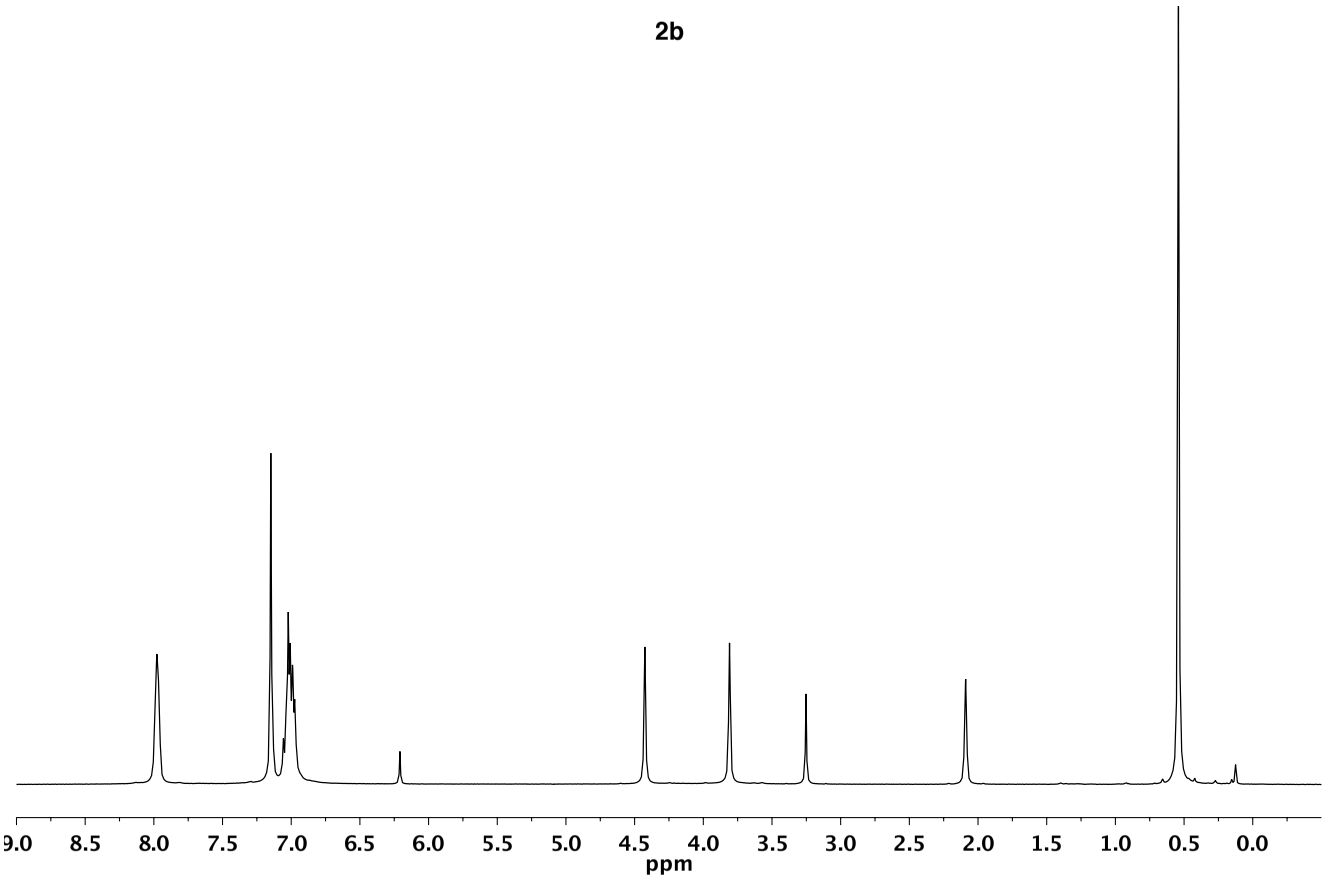

**2b**



cprIII-h1-25a
STANDARD PROTON PARAMETERS

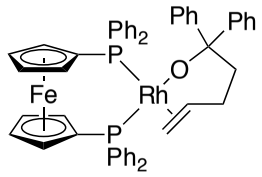



**2b**



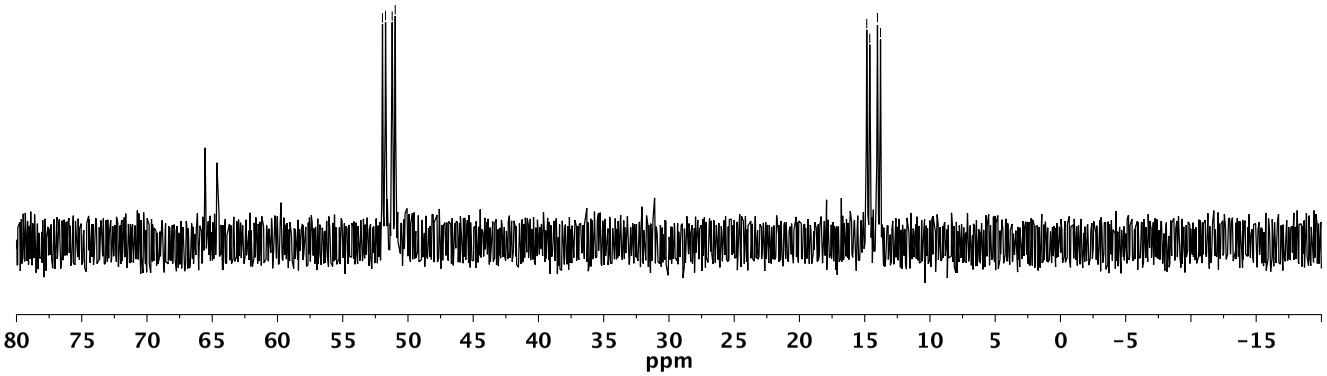
cprlll-p31-25b
cprlll-p31-25b

51.95
51.72
51.21
50.98

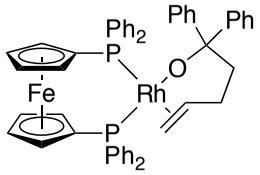



14.84
14.61
14.02
13.79

**7b**

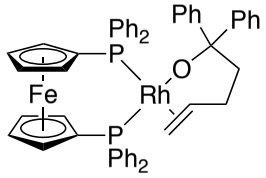


cprlll-h1-25b
STANDARD PROTON PARAMETERS

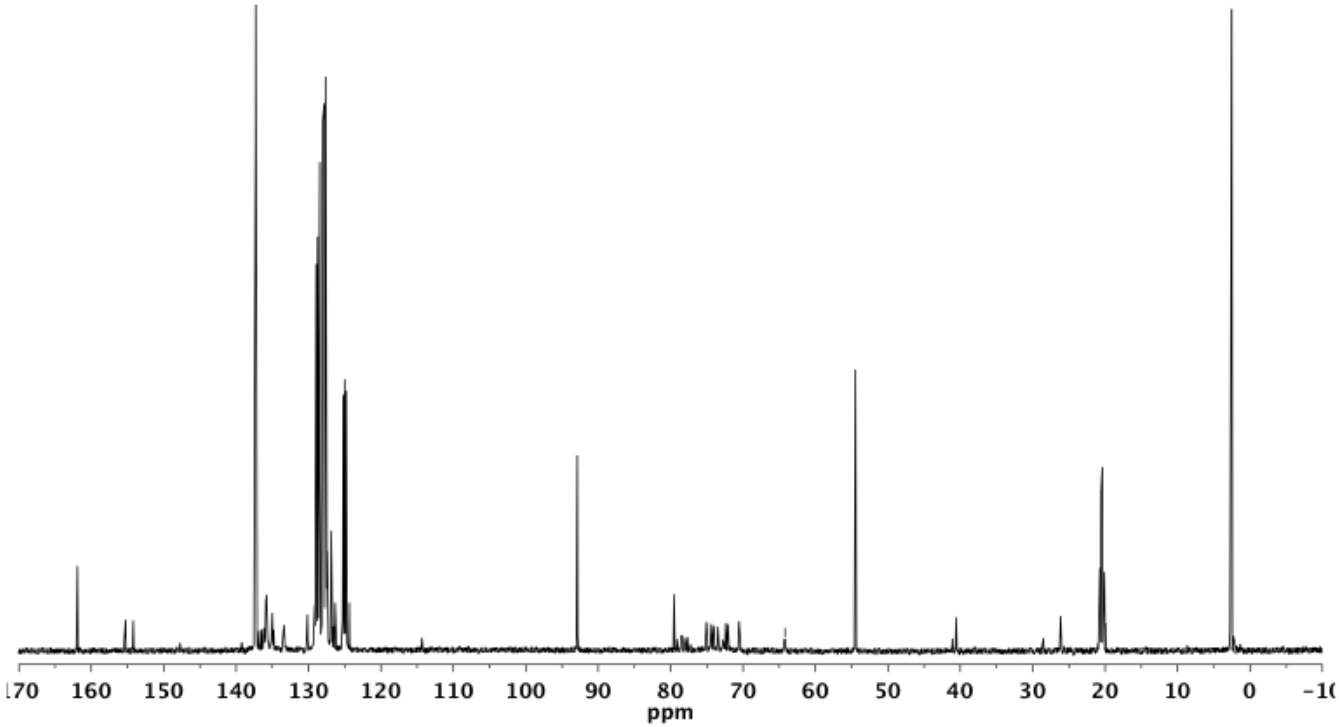



**7b**

cprlll-c13-55b
STANDARD CARBON PARAMETERS

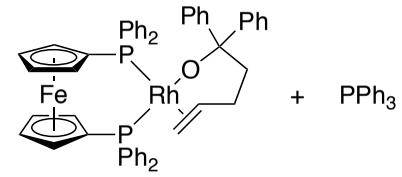



**7b**



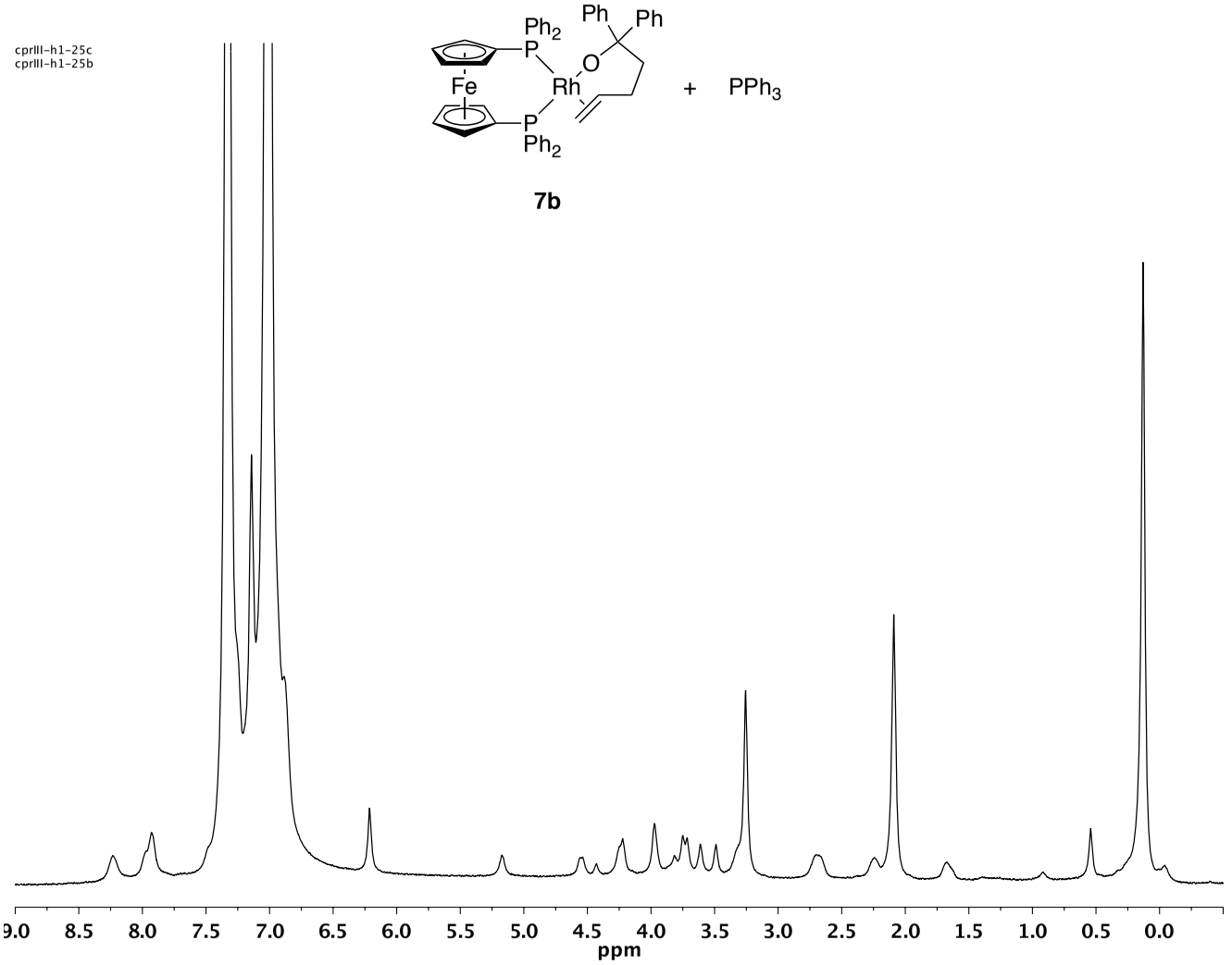
cprIII-p31-25c
P31 TRIPHENYLPHOSPHATE PARAMETERS

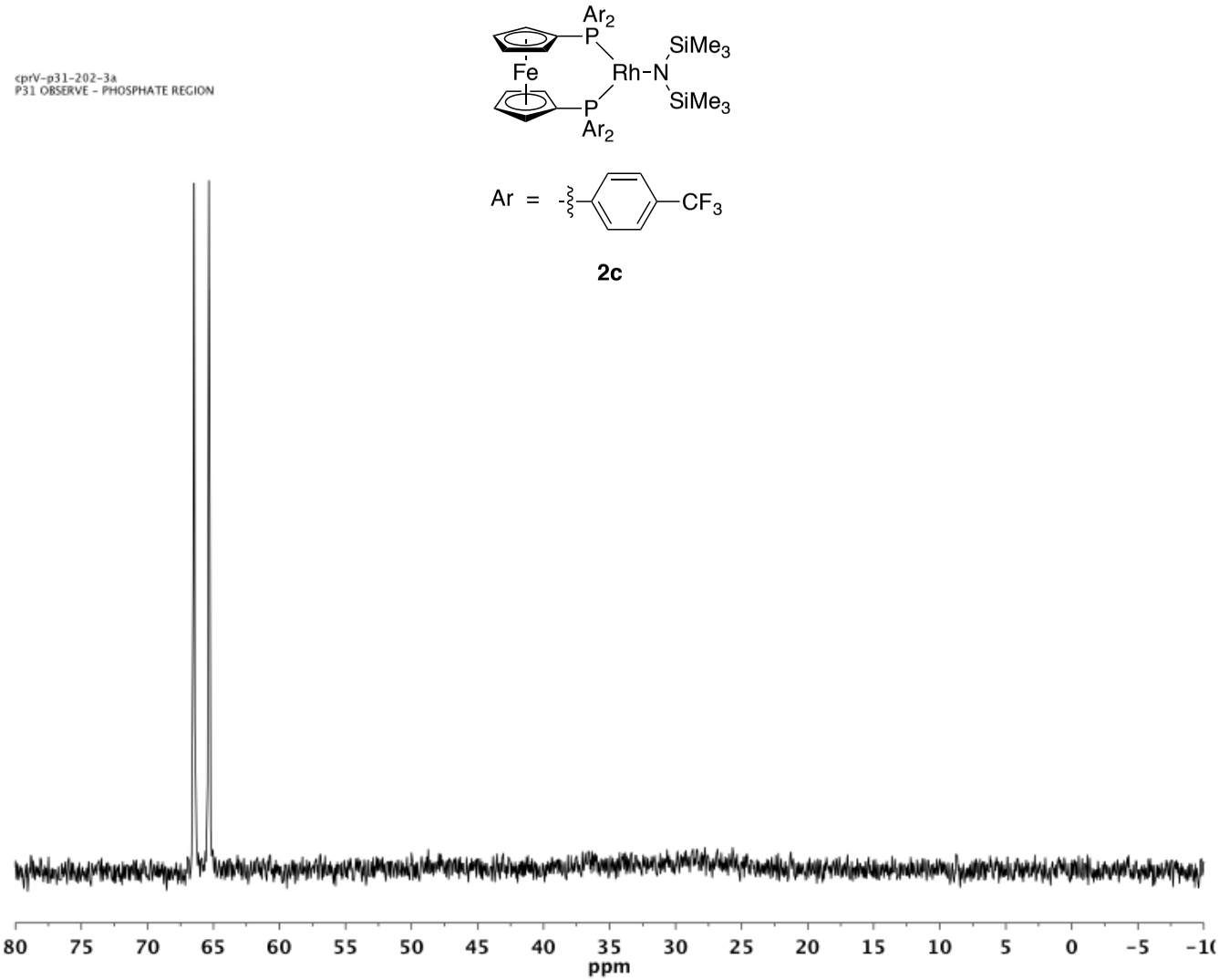
51.96
51.73
51.21

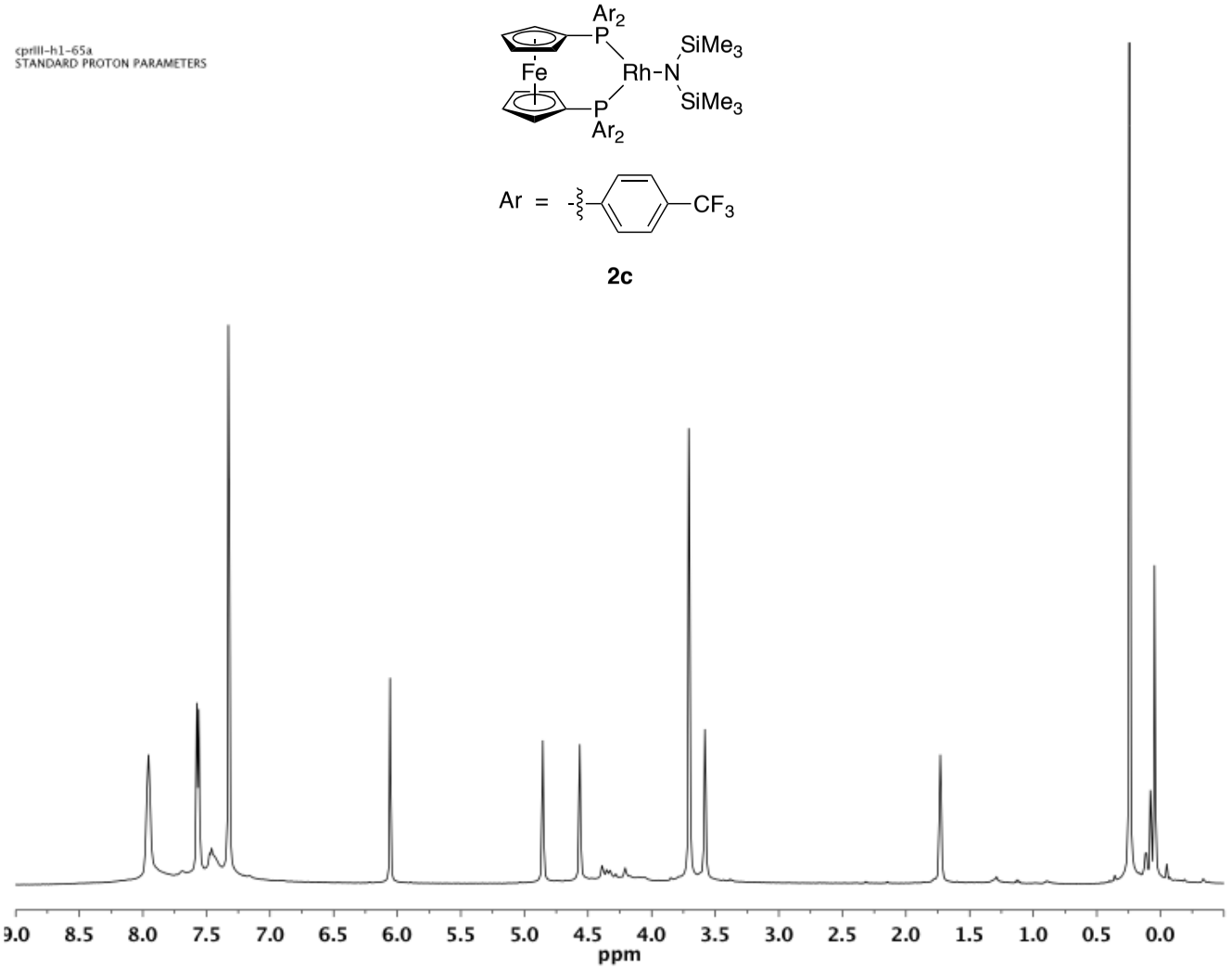



+ $PPh_3$

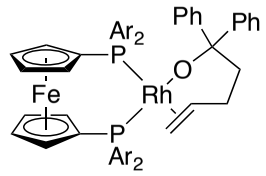
**7b**

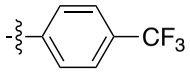

cprlll-h1-25c
cprlll-h1-25b
Ph2
P
Fe
Rh
O
Ph
Ph
P
Ph2
+ PPh3
7b
9.0 8.5 8.0 7.5 7.0 6.5 6.0 5.5 5.0 4.5 4.0 3.5 3.0 2.5 2.0 1.5 1.0 0.5 0.0
ppm


cprV-p31-202-3a
P31 OBSERVE - PHOSPHATE REGION
Ar2
P
Fe
Rh-N
SiMe3
SiMe3
P
Ar2
Ar =
CF3
2c
80
75
70
65
60
55
50
45
40
35
30
25
20
15
10
5
0
-5
ppm

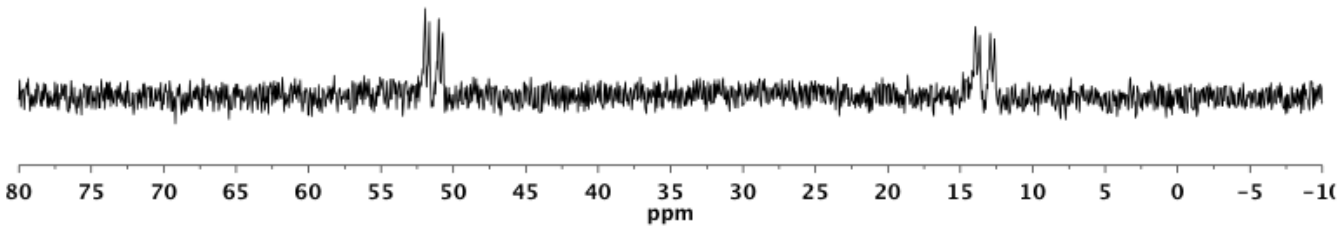

cprIII-h1-65a
STANDARD PROTON PARAMETERS
Ar2
P
Fe
Rh-N
SiMe3
SiMe3
P
Ar2
Ar =
CF3
2c
9.0
8.5
8.0
7.5
7.0
6.5
6.0
5.5
5.0
4.5
4.0
3.5
3.0
2.5
2.0
1.5
1.0
0.5
0.0
ppm

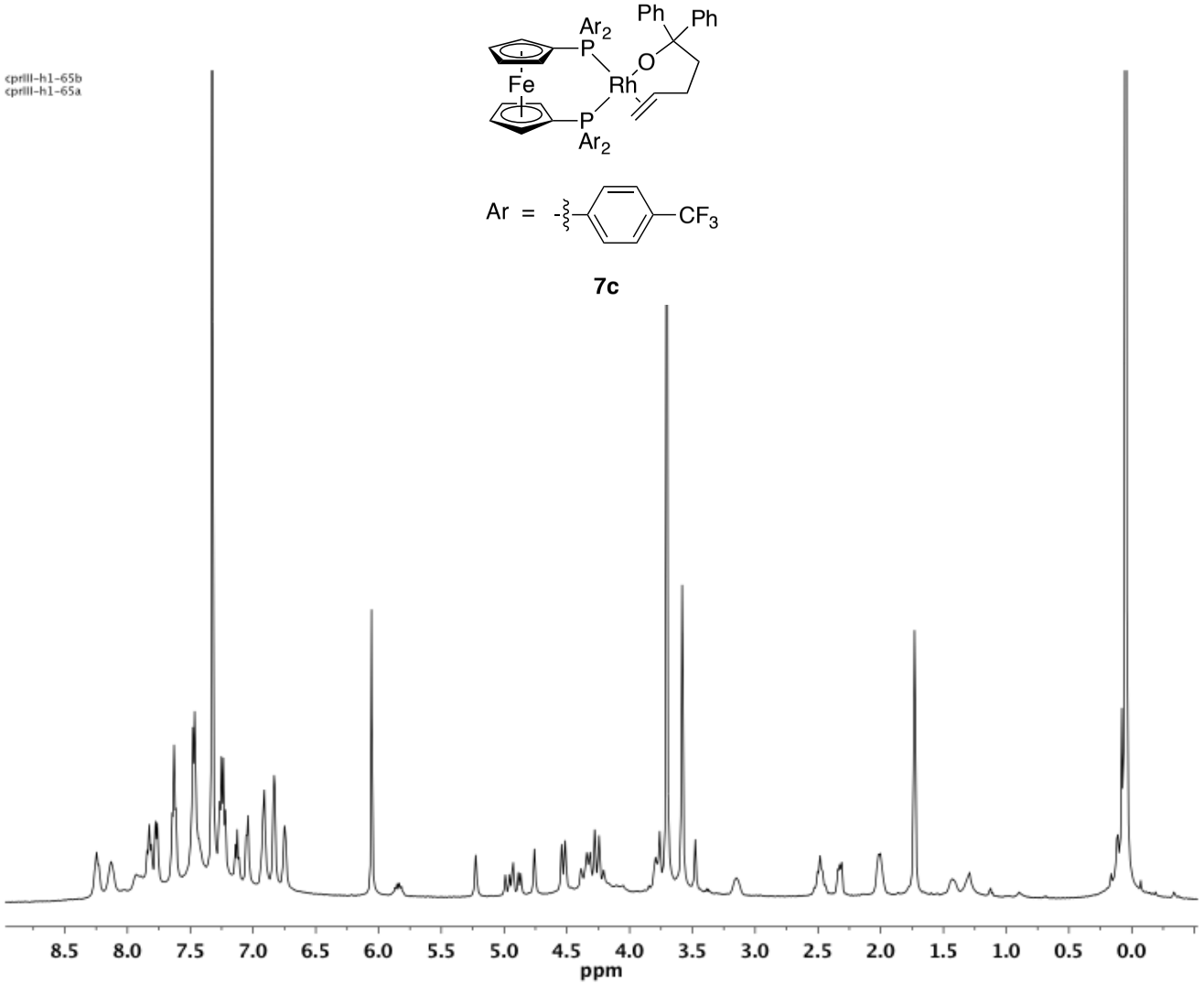
cprV-p31-202-3b
cprV-p31-202-3a



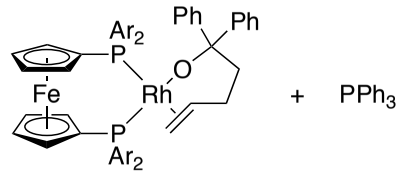

Ar = 


**7c**

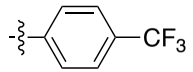



cprIII-h1-65b
cprIII-h1-65a
Ar2
P
Fe
Rh
O
Ph
Ph
P
Ar2
Ar = -
CF3
7c
8.5
8.0
7.5
7.0
6.5
6.0
5.5
5.0
4.5
4.0
3.5
3.0
2.5
2.0
1.5
1.0
0.5
0.0
ppm

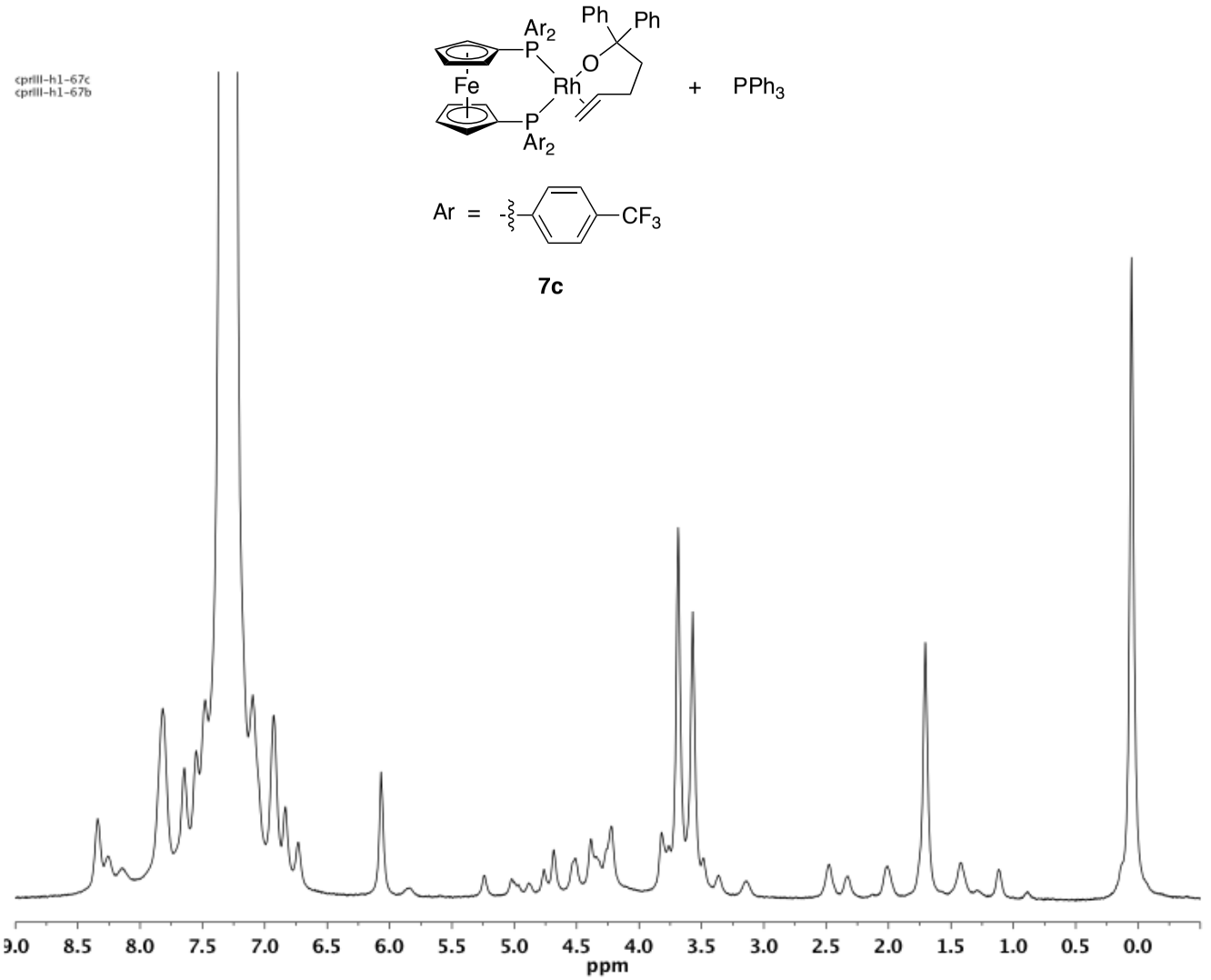
cprV-p31-202-3c
cprV-p31-202-3b

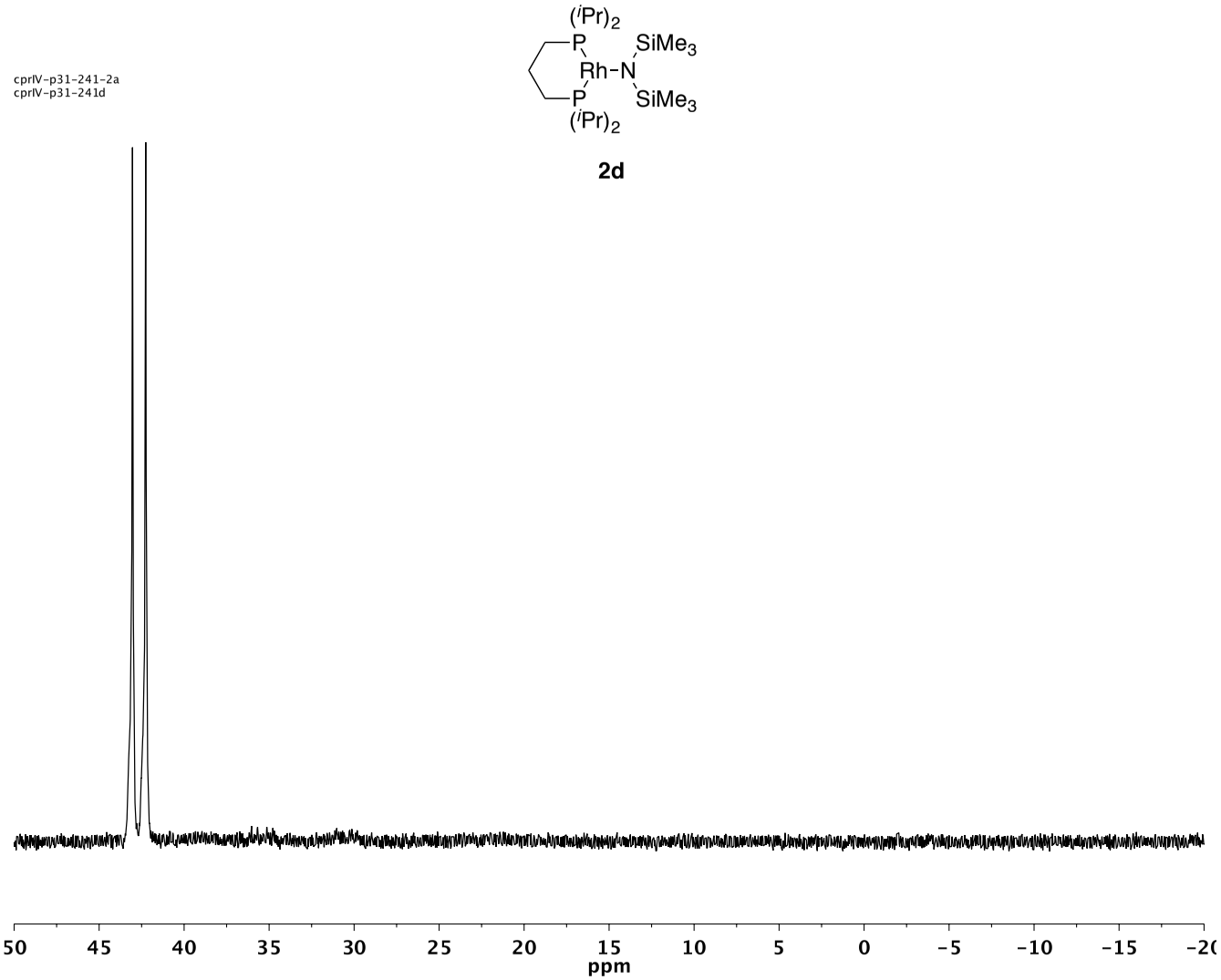



+ $PPh_3$

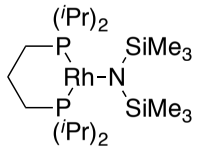
Ar =  $CF_3$

**7c**

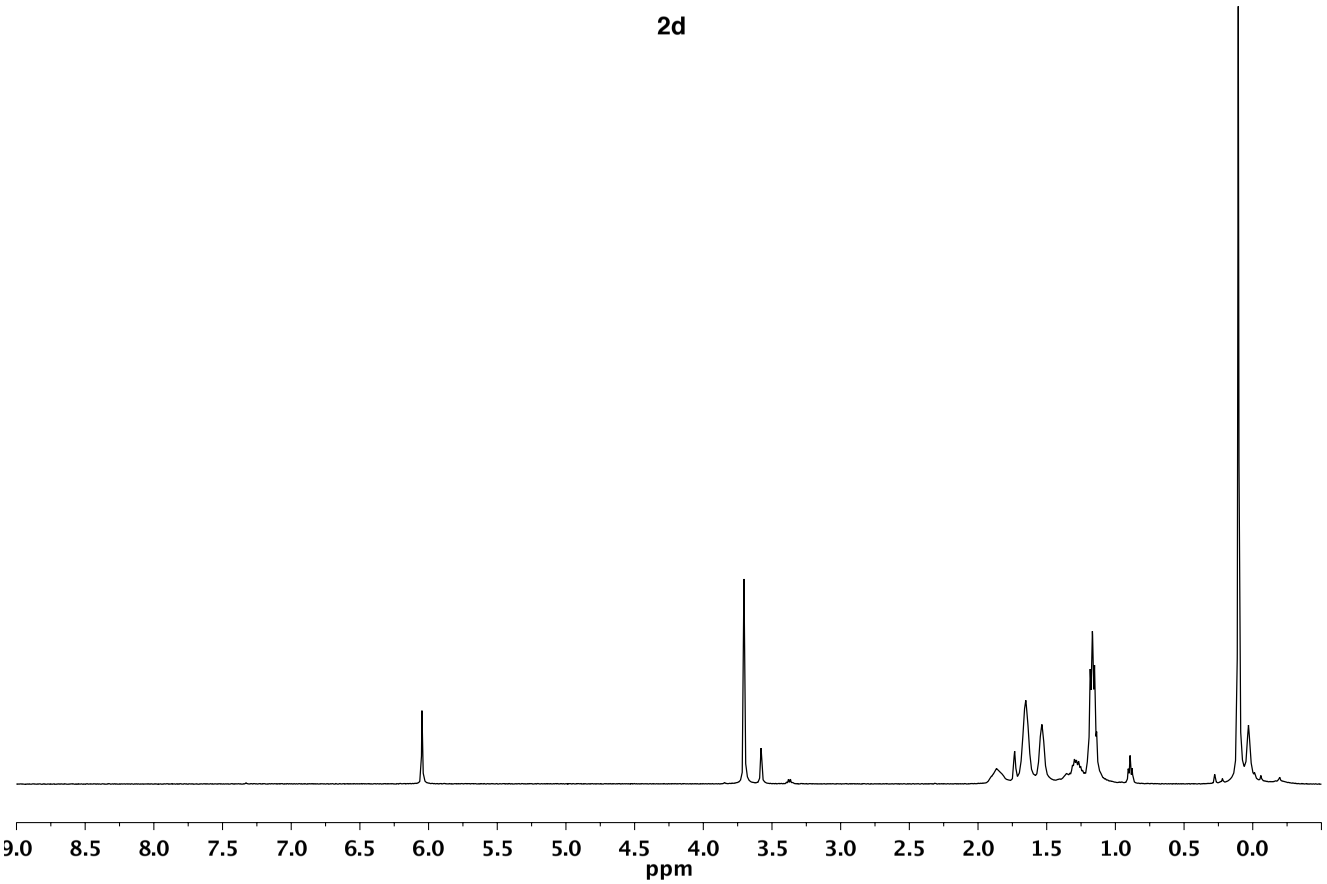

cprIII-h1-67c
cprIII-h1-67b
Ar2
P
Fe
Rh
O
Ph
Ph
+ PPh3
Ar = CF3
7c
9.0 8.5 8.0 7.5 7.0 6.5 6.0 5.5 5.0 4.5 4.0 3.5 3.0 2.5 2.0 1.5 1.0 0.5 0.0
ppm


cprIV-p31-241-2a
cprIV-p31-241d
(iPr)2
P
SiMe3
Rh-N
P
SiMe3
(iPr)2
2d
50
45
40
35
30
25
20
15
10
5
0
-5
-10
-15
-20
ppm

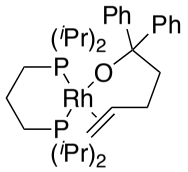
cprIV-h1-241a
STANDARD PROTON PARAMETERS



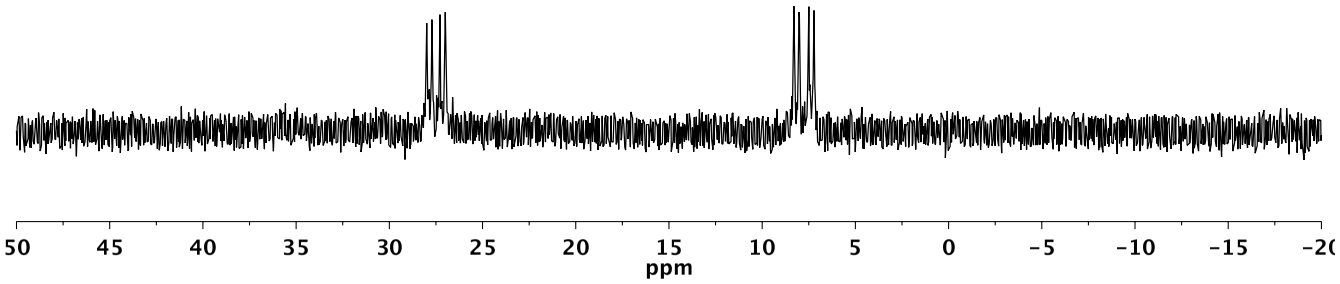

**2d**



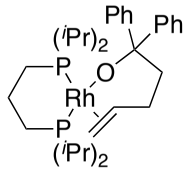
cprIV-p31-241-2b
cprIV-p31-241-2a




**7d**

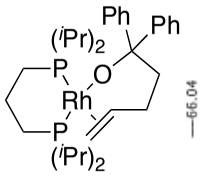


cprIV-h1-241b
cprIV-h1-241a

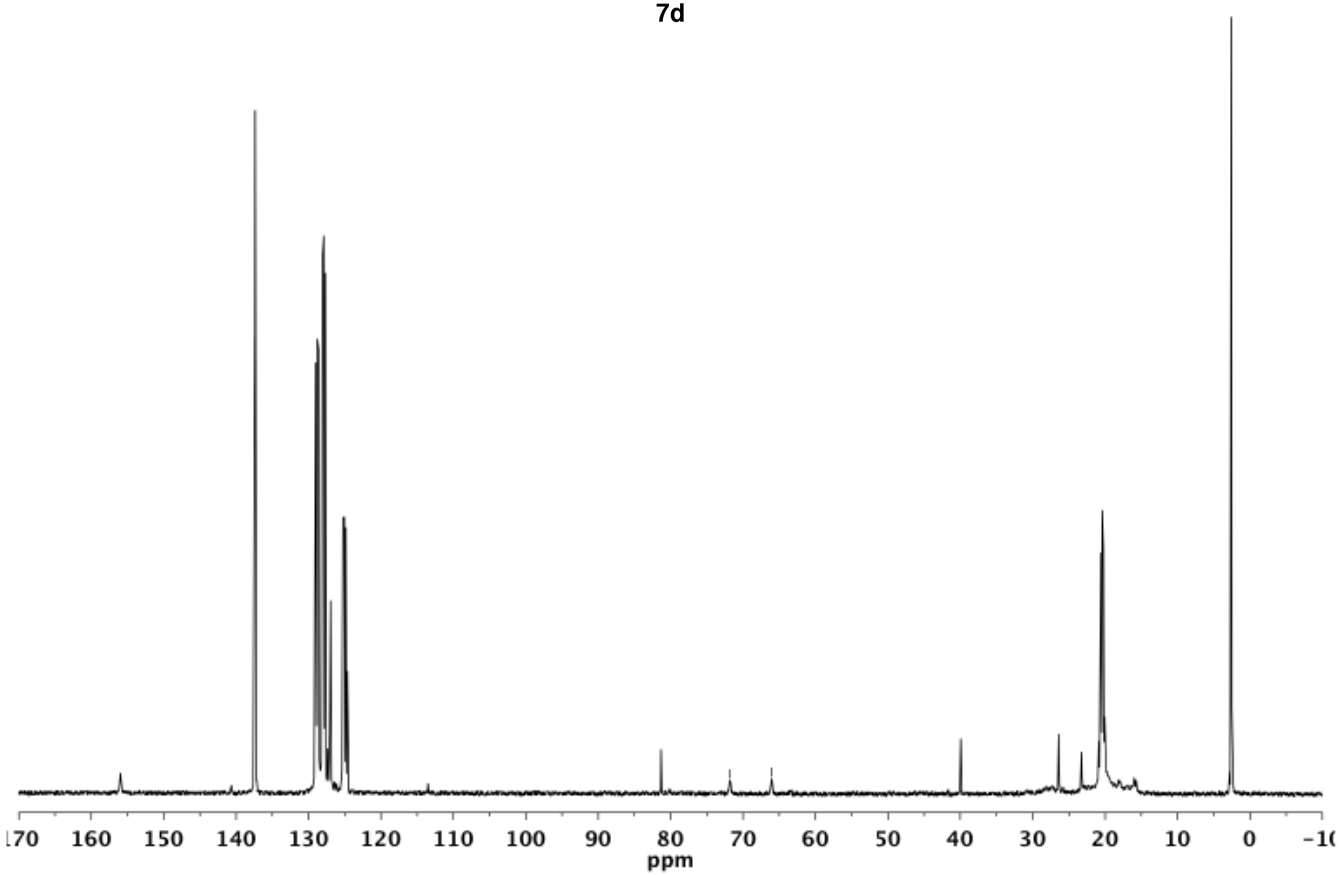



**7d**

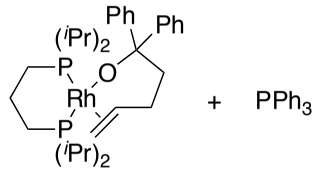
cprVIII_DiPrPP_Rh_alkoxo_alkene/3
DRX-500 5mm ZBO probe 13C starting parameters. Rev 6/12/12 CGC
With CPD proton decoupling. Use ns*td0 scans




**7d**

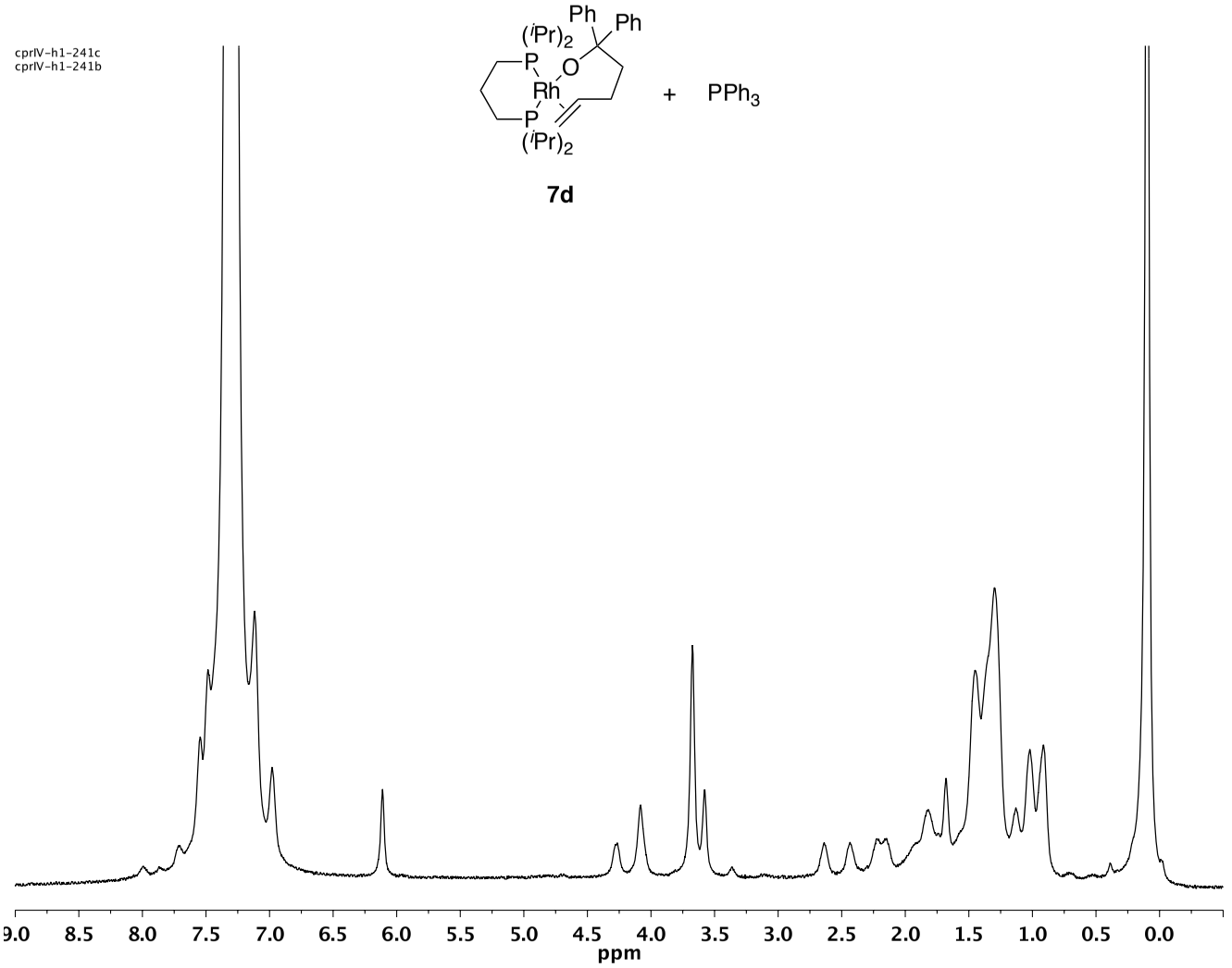


cprIV-p31-241-2c
cprIV-p31-241-2a

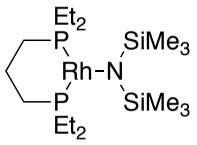



**7d**

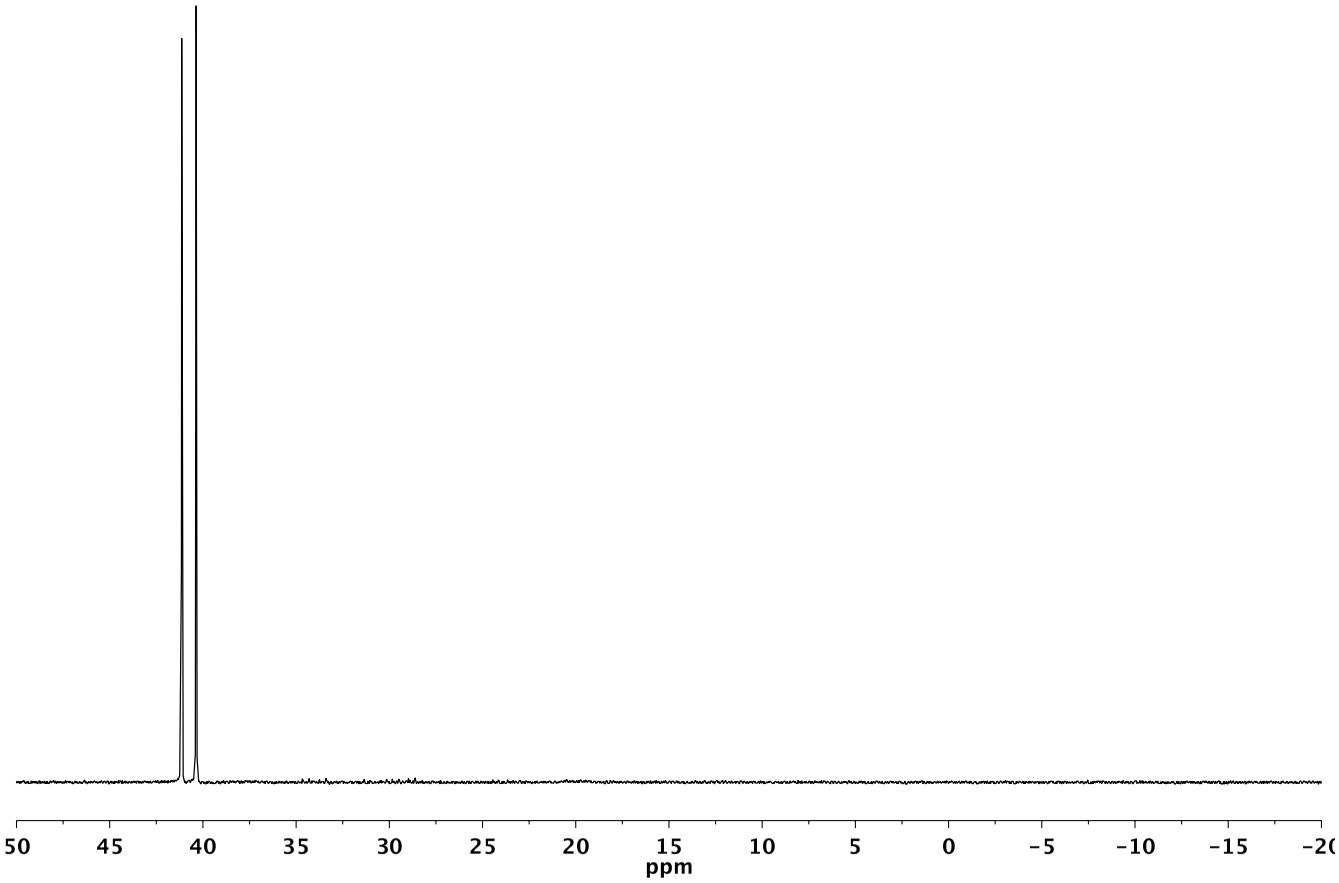
+ $PPh_3$

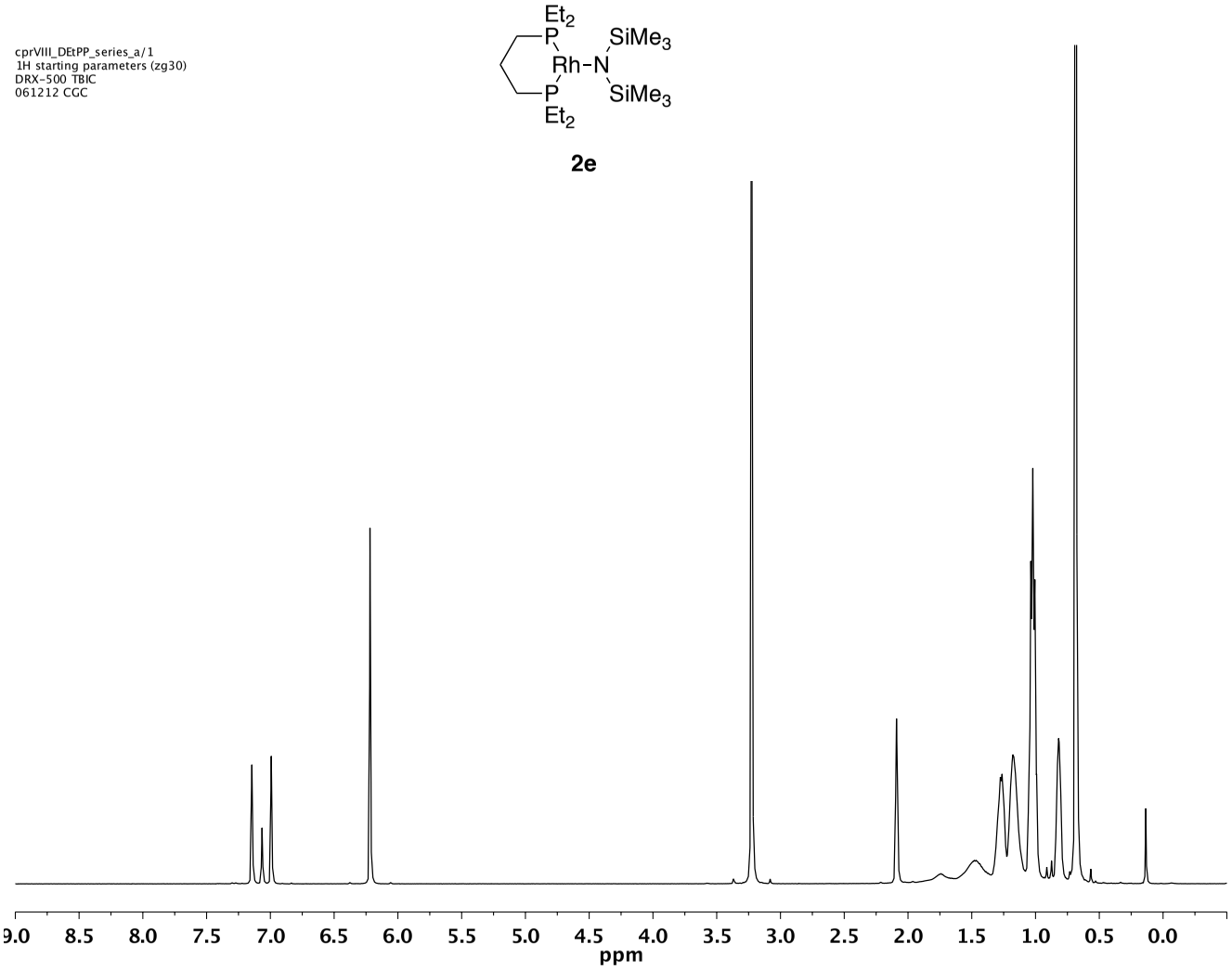

cprIV-h1-241c
cprIV-h1-241b
Ph
Ph
(iPr)2
P
O
Rh
P
(iPr)2
+ PPh3
7d
9.0
8.5
8.0
7.5
7.0
6.5
6.0
5.5
5.0
4.5
4.0
3.5
3.0
2.5
2.0
1.5
1.0
0.5
0.0
ppm

cprVIII_DEtPP_series_a/2
DRX-500 5mm ZBO probe 31P starting parameters
Use ns*d0. PMeO3 set to 1.67 ppm
6/12/12 CC revised

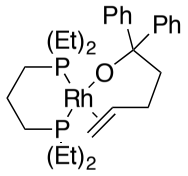



**2e**

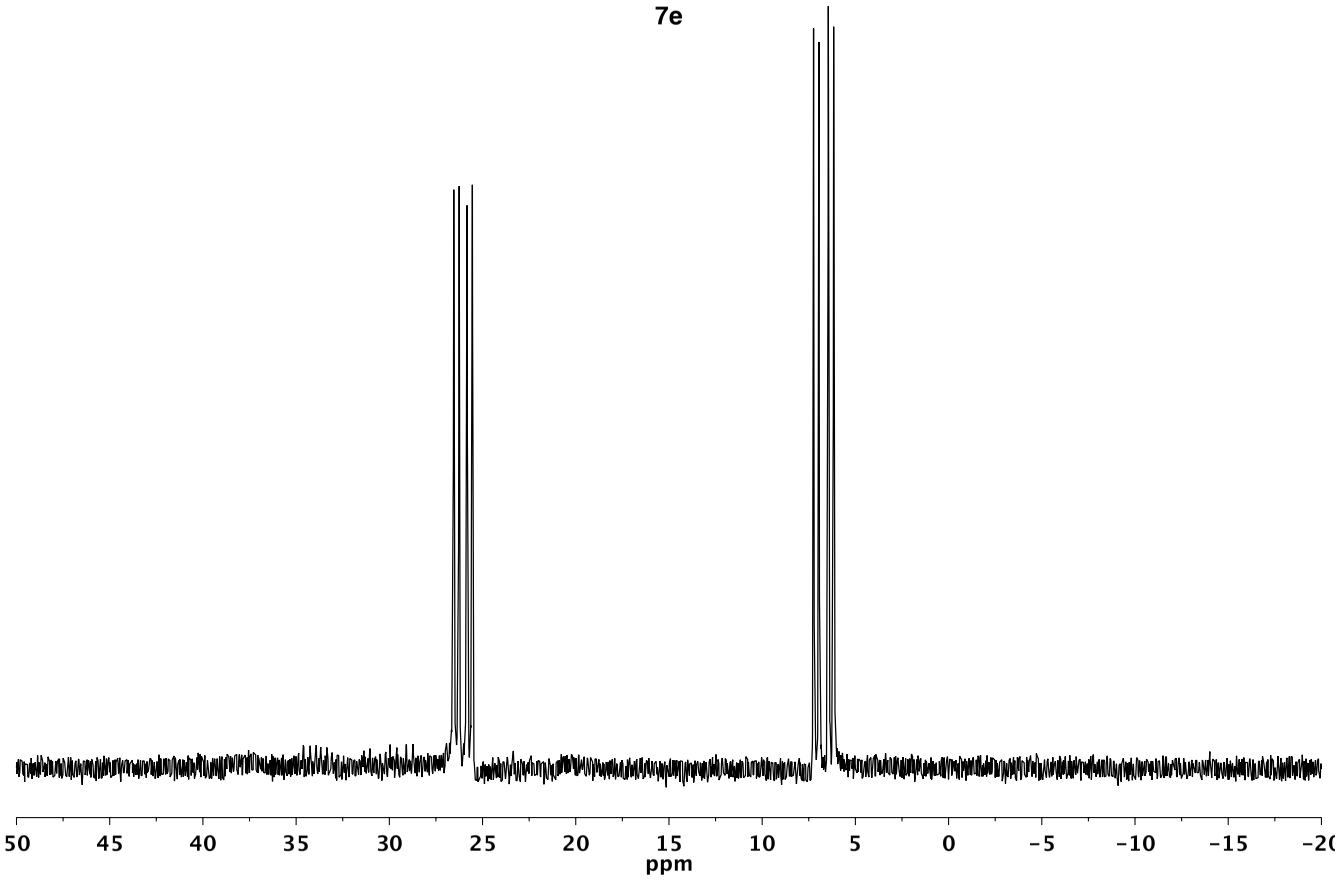



cprVIII_DEtPP_series_a/1
1H starting parameters (zg30)
DRX-500 TBIC
061212 CGC
Et2
P
SiMe3
Rh-N
P
SiMe3
Et2
2e
9.0
8.5
8.0
7.5
7.0
6.5
6.0
5.5
5.0
4.5
4.0
3.5
3.0
2.5
2.0
1.5
1.0
0.5
0.0
ppm

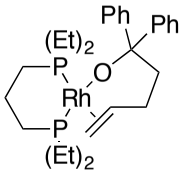
cprVIII_DEtPP_series_b/2
DRX-500 5mm ZBO probe 31P starting parameters
Use ns*d0. PMeO3 set to 1.67 ppm
6/12/12 CC revised



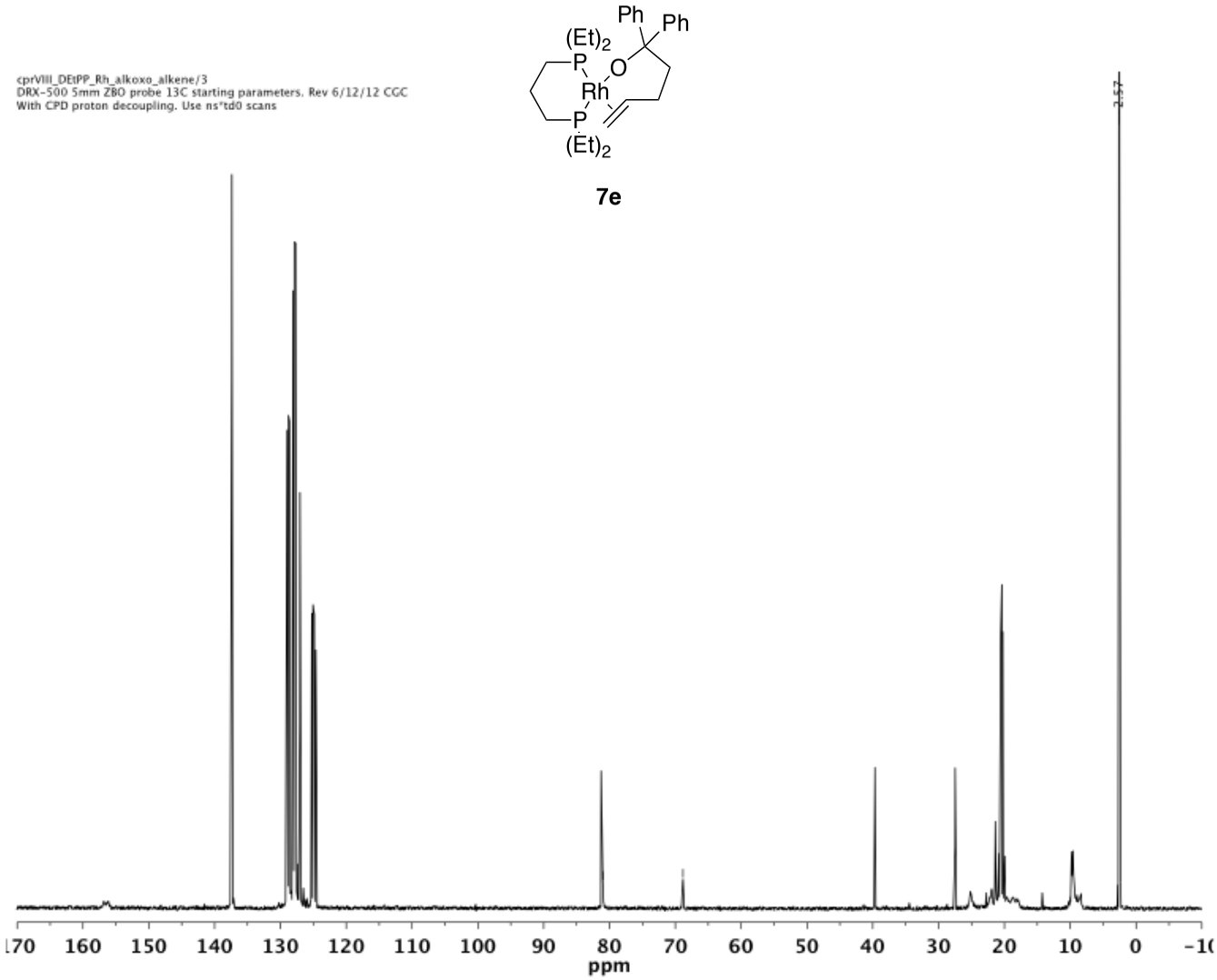

**7e**



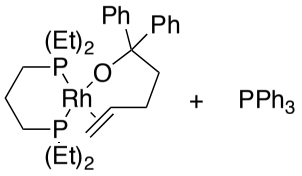
cprVIII_DEtPP_series_b/1
1H starting parameters (zg30)
DRX-500 TBIC
061212 CGC




**7e**

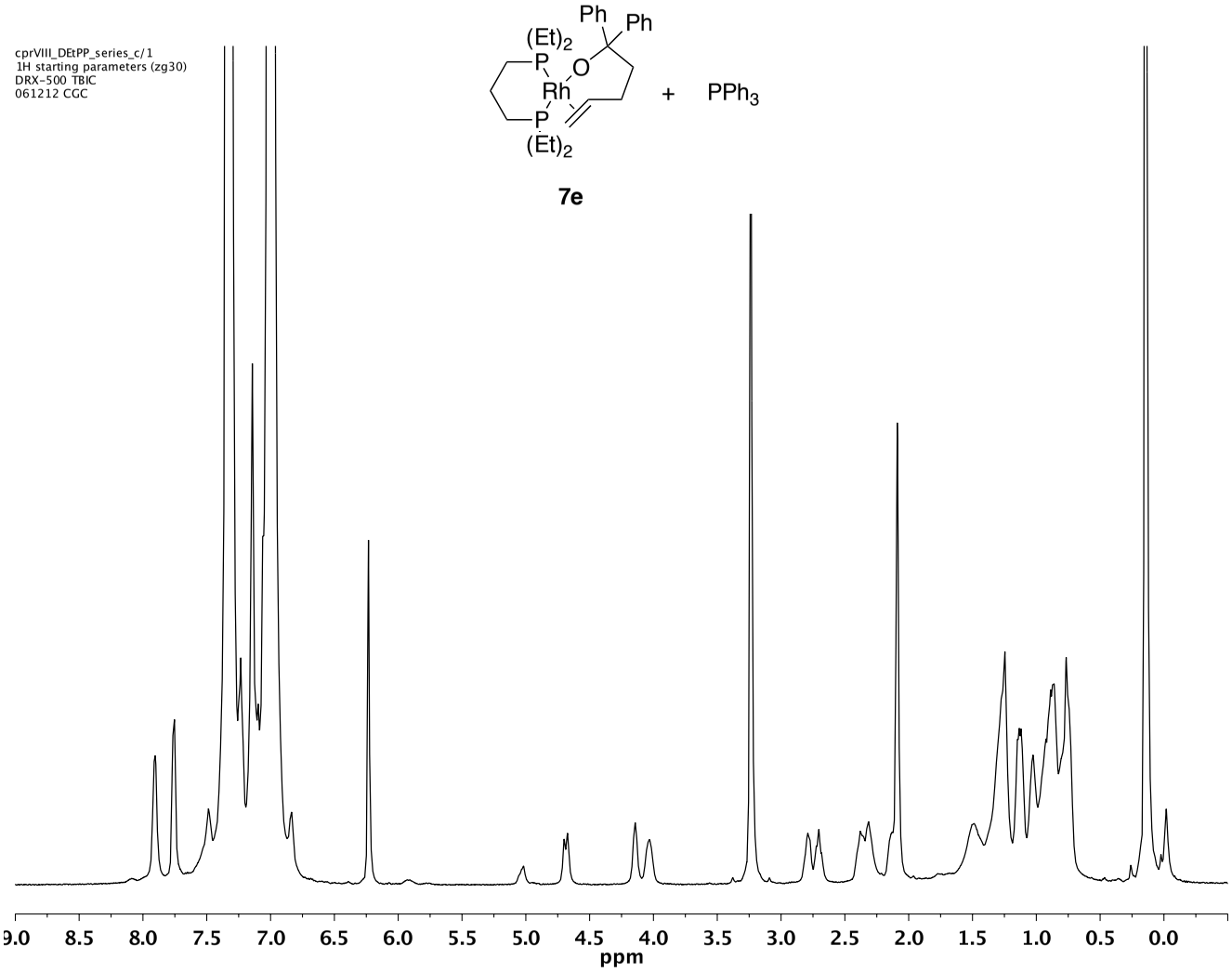

cprVIII_DEtPP_Rh_alkoxo_alkene/3
DRX-500 5mm ZBO probe 13C starting parameters. Rev 6/12/12 CGC
With CPD proton decoupling. Use ns*td0 scans
Ph
Ph
(Et)2
P
O
Rh
P
(Et)2
7e
2.57
170 160 150 140 130 120 110 100 90 80 70 60 50 40 30 20 10 0 -10
ppm

cprVIII_DEtPP_series_c/2
DRX-500 5mm ZBO probe 31P starting parameters
Use ns*d0. PMeO3 set to 1.67 ppm
6/12/12 CC revised

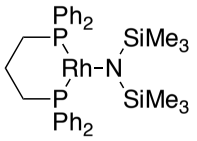



+ $PPh_3$

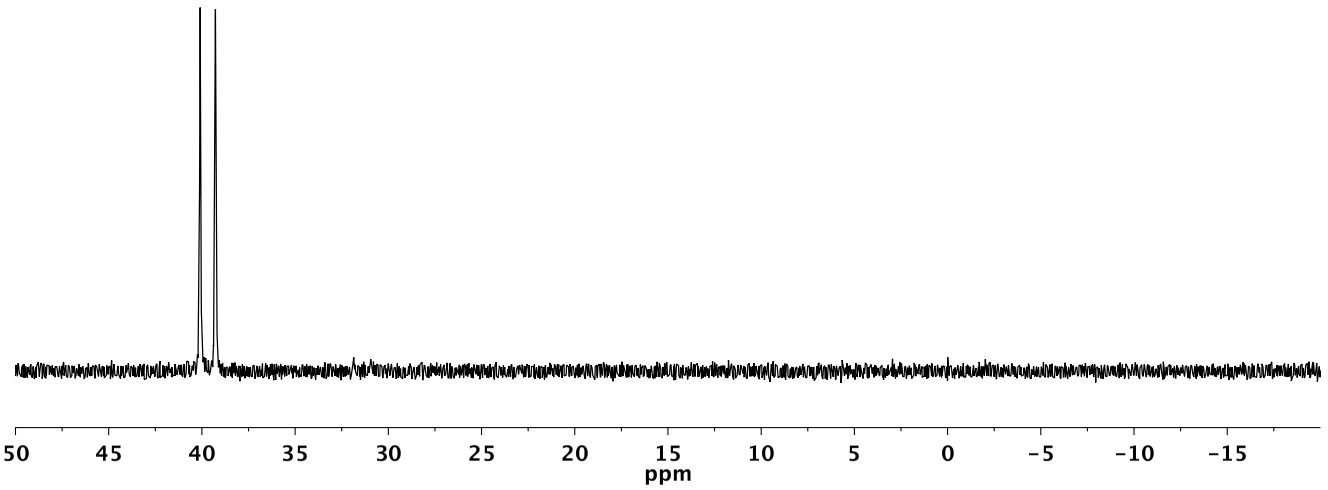
**7e**


cprVIII_DEtPP_series_c/1
1H starting parameters (zg30)
DRX-500 TBIC
061212 CGC
Ph
Ph
(Et)2
P
O
Rh
P
(Et)2
+ PPh3
7e
9.0
8.5
8.0
7.5
7.0
6.5
6.0
5.5
5.0
4.5
4.0
3.5
3.0
2.5
2.0
1.5
1.0
0.5
0.0
ppm

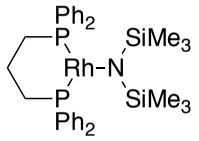
cprVIII_54_a/2
DRX-500 5mm ZBO probe 31P starting parameters
Use ns*d0. PMeO3 set to 1.67 ppm
6/12/12 CC revised



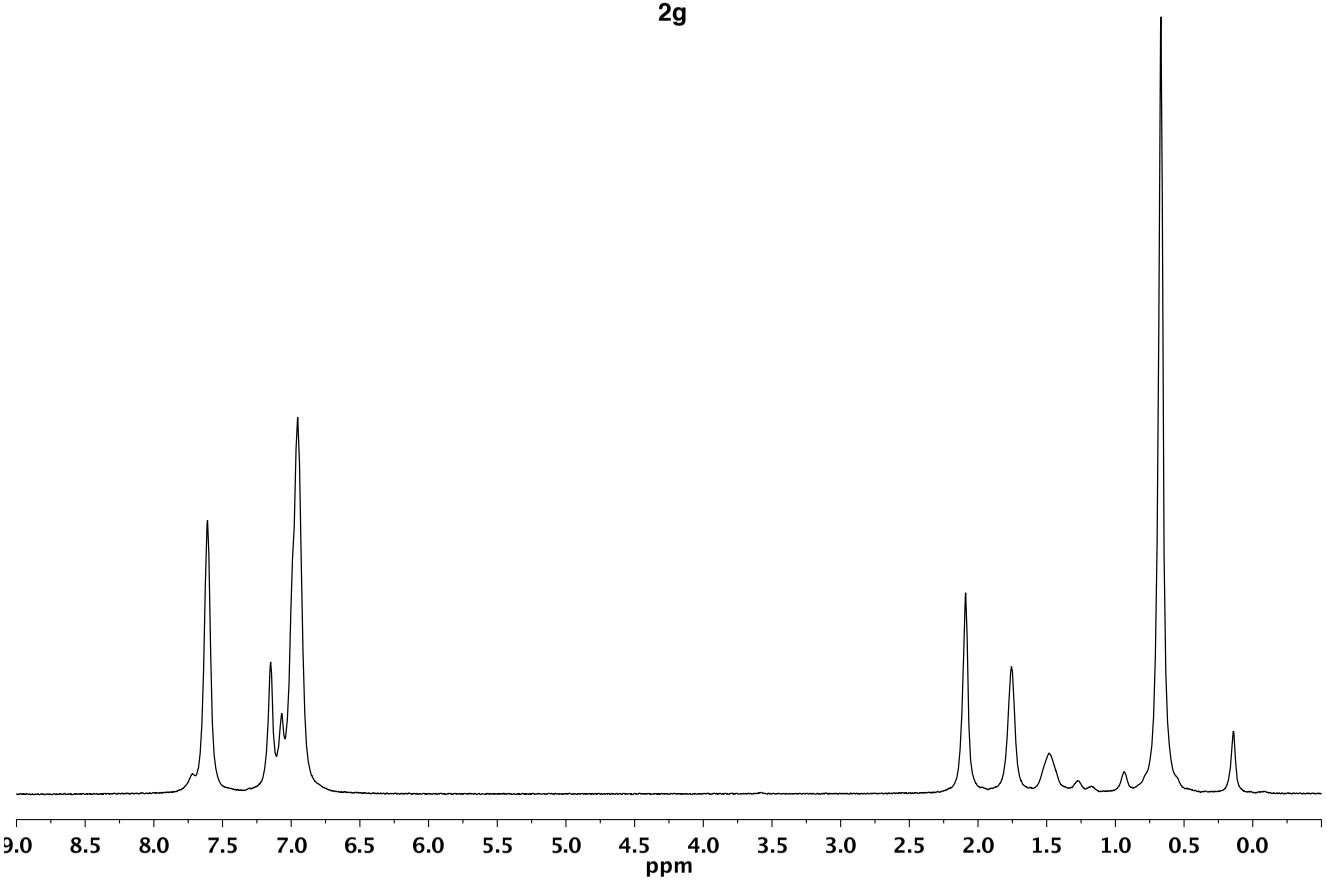

**2g**



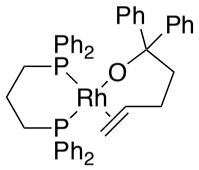
cprVIII_54_a/1
1H starting parameters (zg30)
DRX-500 TBIC
061212 CGC



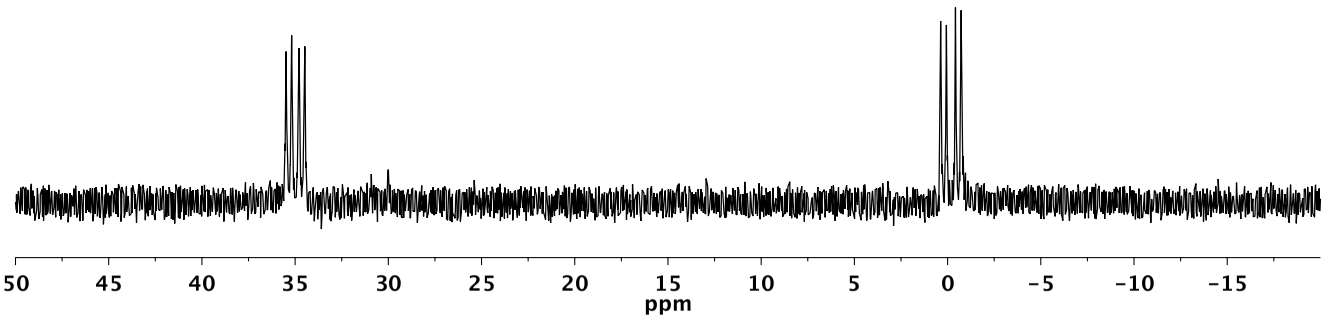

**2g**



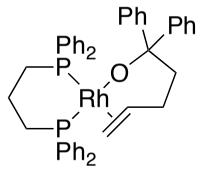
cprVIII_54_b/2
DRX-500 5mm ZBO probe 31P starting parameters
Use ns*d0. PMeO3 set to 1.67 ppm
6/12/12 CC revised




**7g**

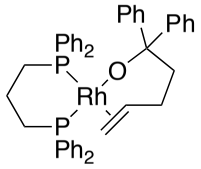


cprVIII_54_b/1
1H starting parameters (zg30)
DRX-500 TBIC
061212 CGC

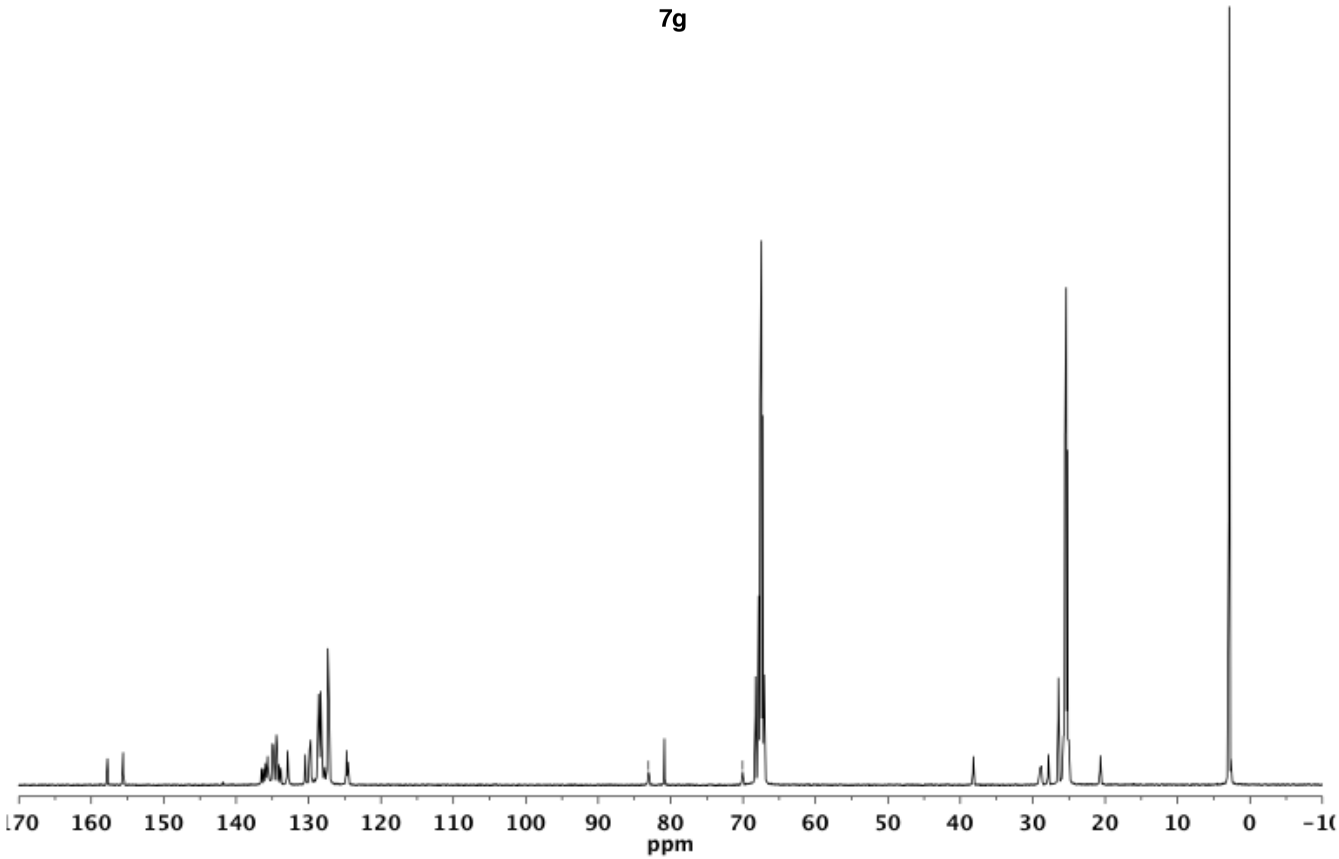



**7g**

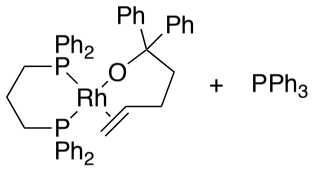
cprVII_189_b/2
DRX-500 5mm TBIC probe 13C starting parameters. Rev 1/11/12 CGC
With CPD proton decoupling. Use ns*td0 scans




**7g**

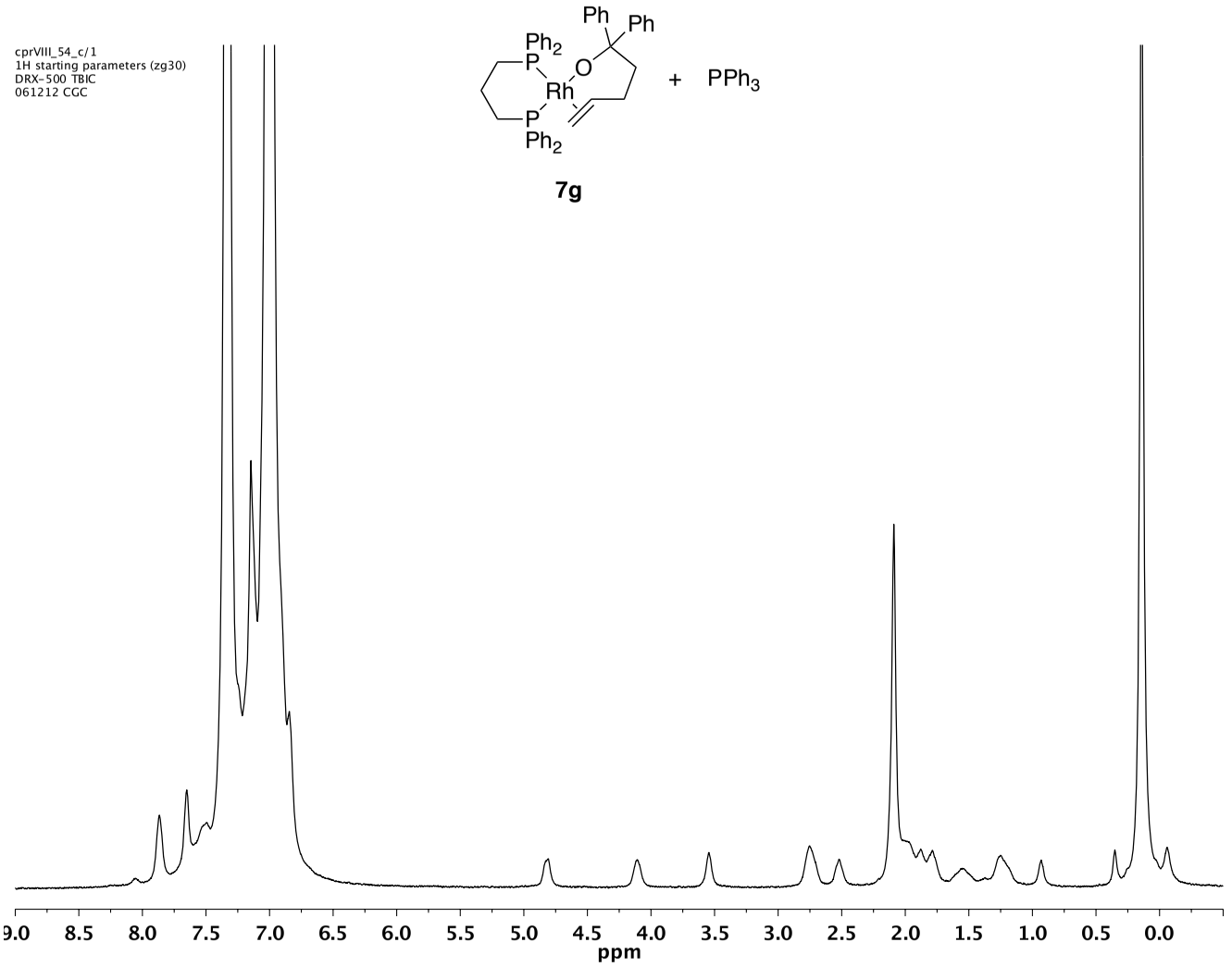


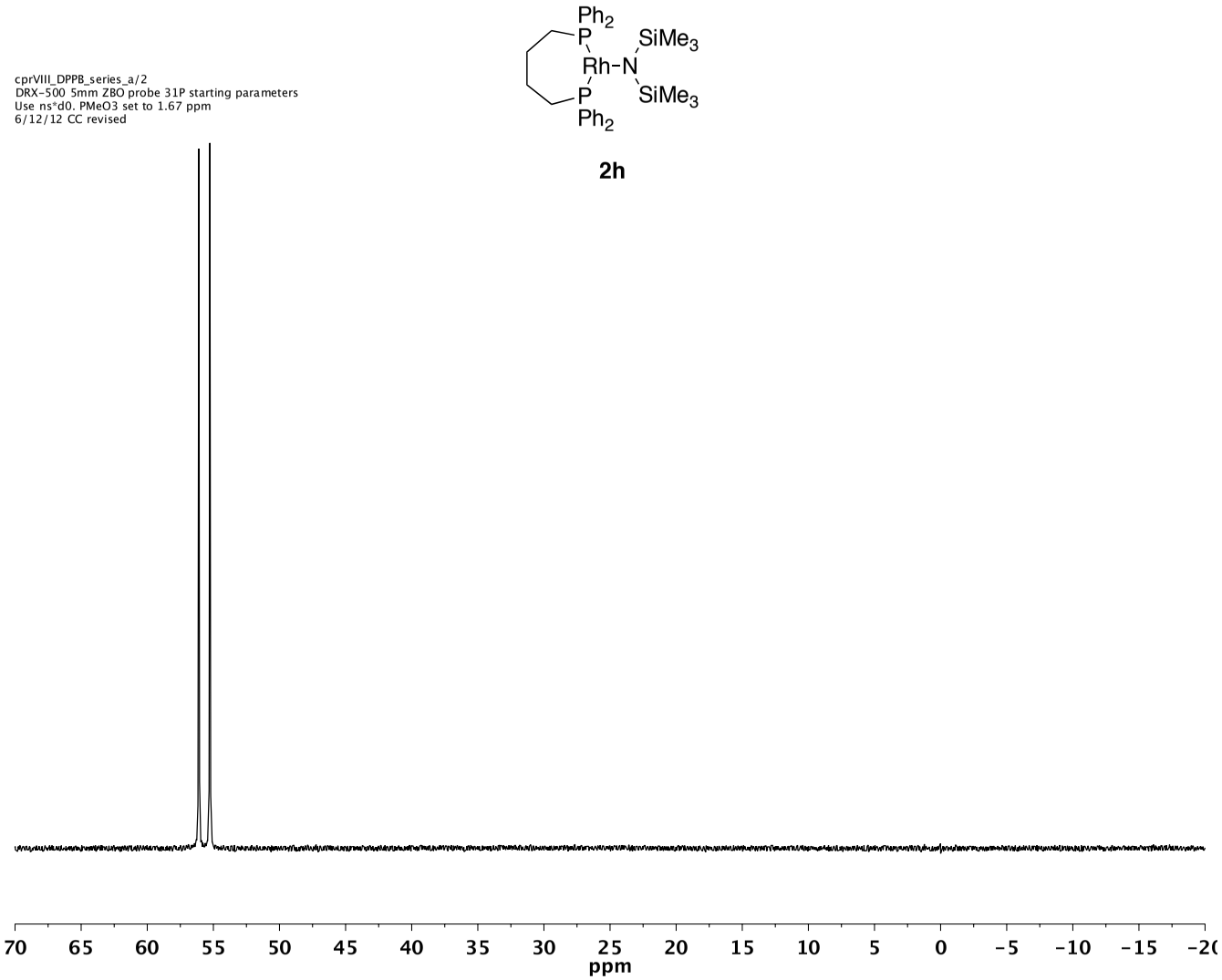
cprVIII_54_c/2
DRX-500 5mm ZBO probe 31P starting parameters
Use ns*d0. PMeO3 set to 1.67 ppm
6/12/12 CC revised

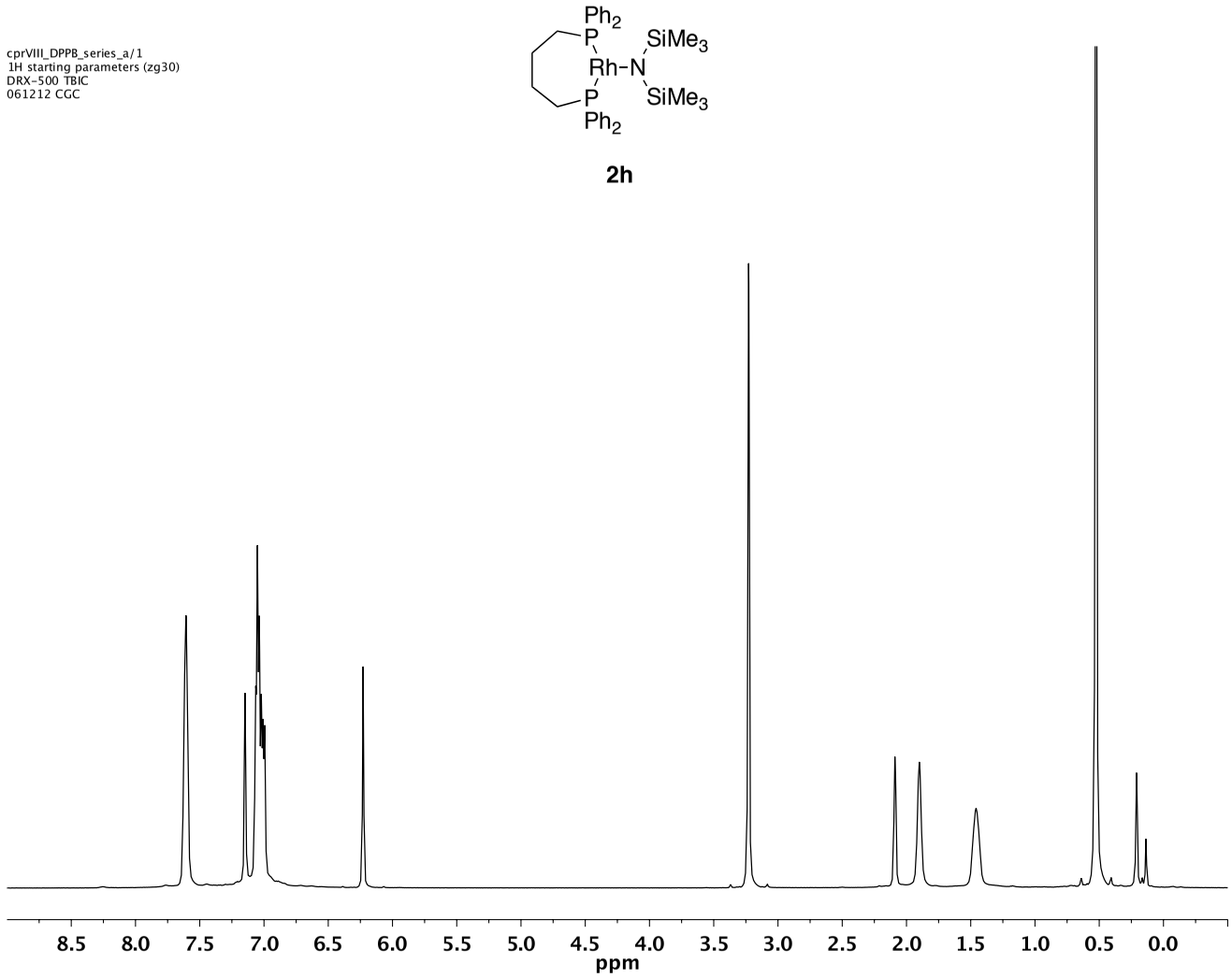



+ $PPh_3$

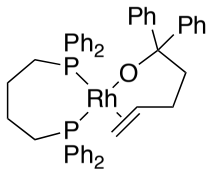
**7g**


cprVIII_54_c/1
1H starting parameters (zg30)
DRX-500 TBIC
061212 CGC
Ph
Ph
Ph2
P
O
Rh
P
Ph2
+ PPh3
7g
9.0
8.5
8.0
7.5
7.0
6.5
6.0
5.5
5.0
4.5
4.0
3.5
3.0
2.5
2.0
1.5
1.0
0.5
0.0
ppm

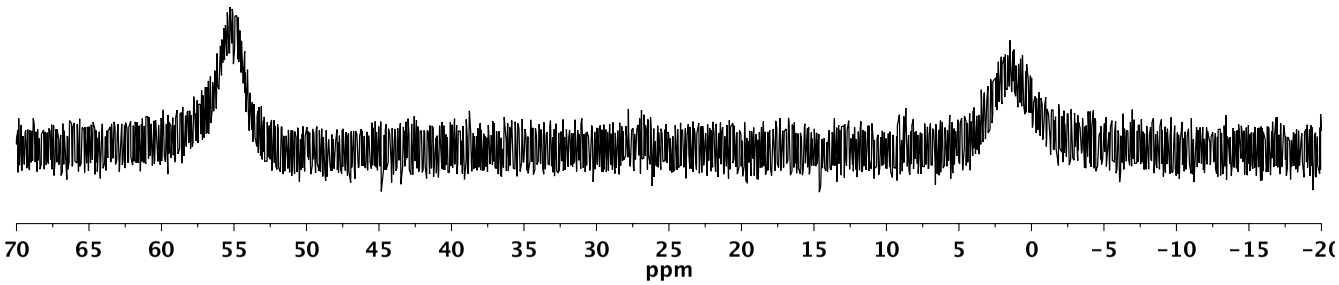

cprVIII_DPPB_series_a/2
DRX-500 5mm ZBO probe 31P starting parameters
Use ns*d0. PMeO3 set to 1.67 ppm
6/12/12 CC revised
Ph2
P
SiMe3
Rh-N
P
SiMe3
Ph2
2h
70 65 60 55 50 45 40 35 30 25 20 15 10 5 0 -5 -10 -15 -20
ppm

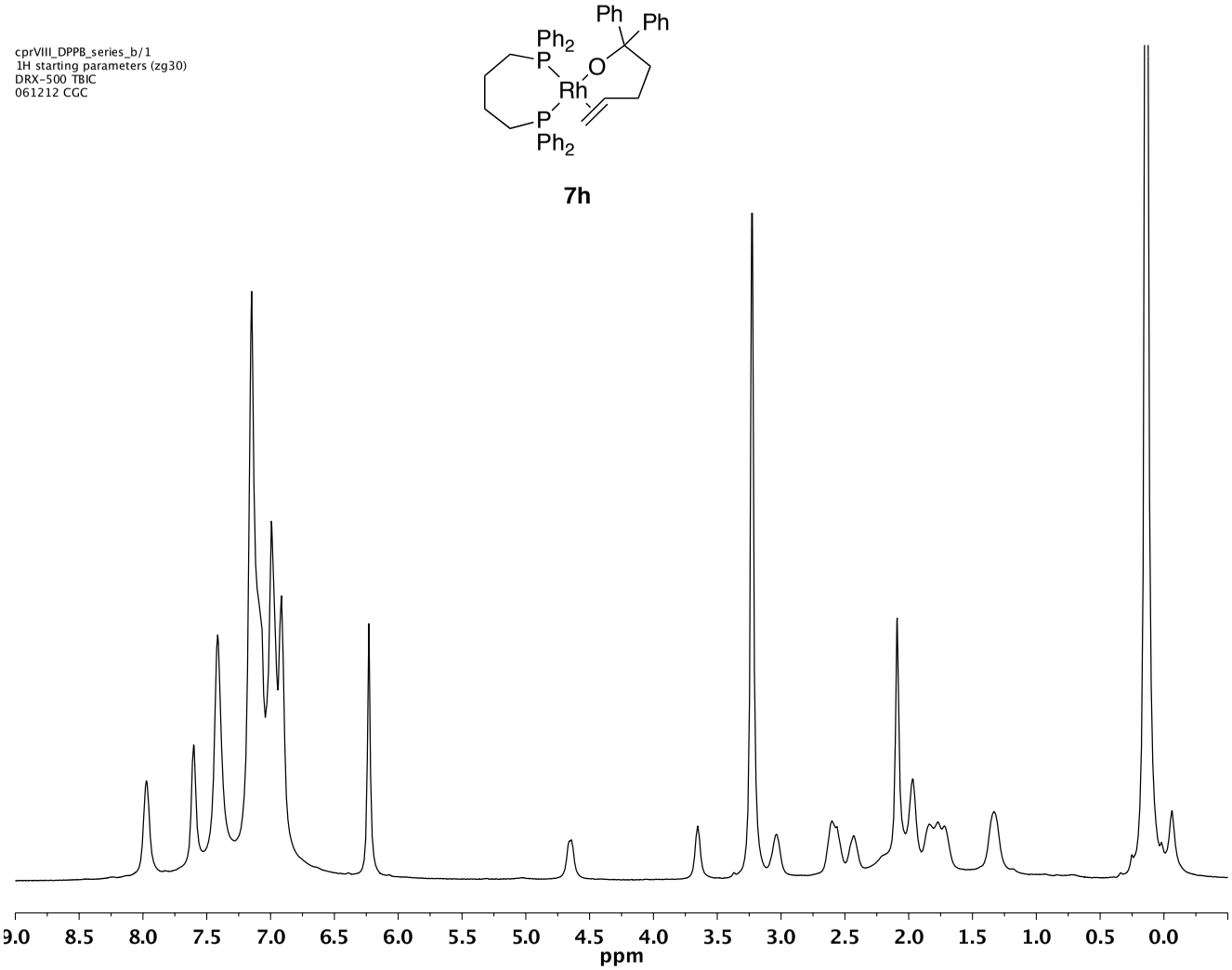

cprVIII_DPPB_series_a/1
1H starting parameters (zg30)
DRX-500 TBIC
061212 CGC
Ph2
P
SiMe3
Rh-N
P
SiMe3
Ph2
2h
8.5
8.0
7.5
7.0
6.5
6.0
5.5
5.0
4.5
4.0
3.5
3.0
2.5
2.0
1.5
1.0
0.5
0.0
ppm

cprVIII_DPPB_series_b/2
DRX-500 5mm ZBO probe 31P starting parameters
Use ns*d0. PMeO3 set to 1.67 ppm
6/12/12 CC revised

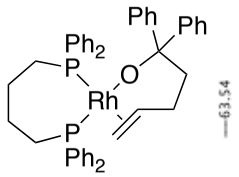



**7h**

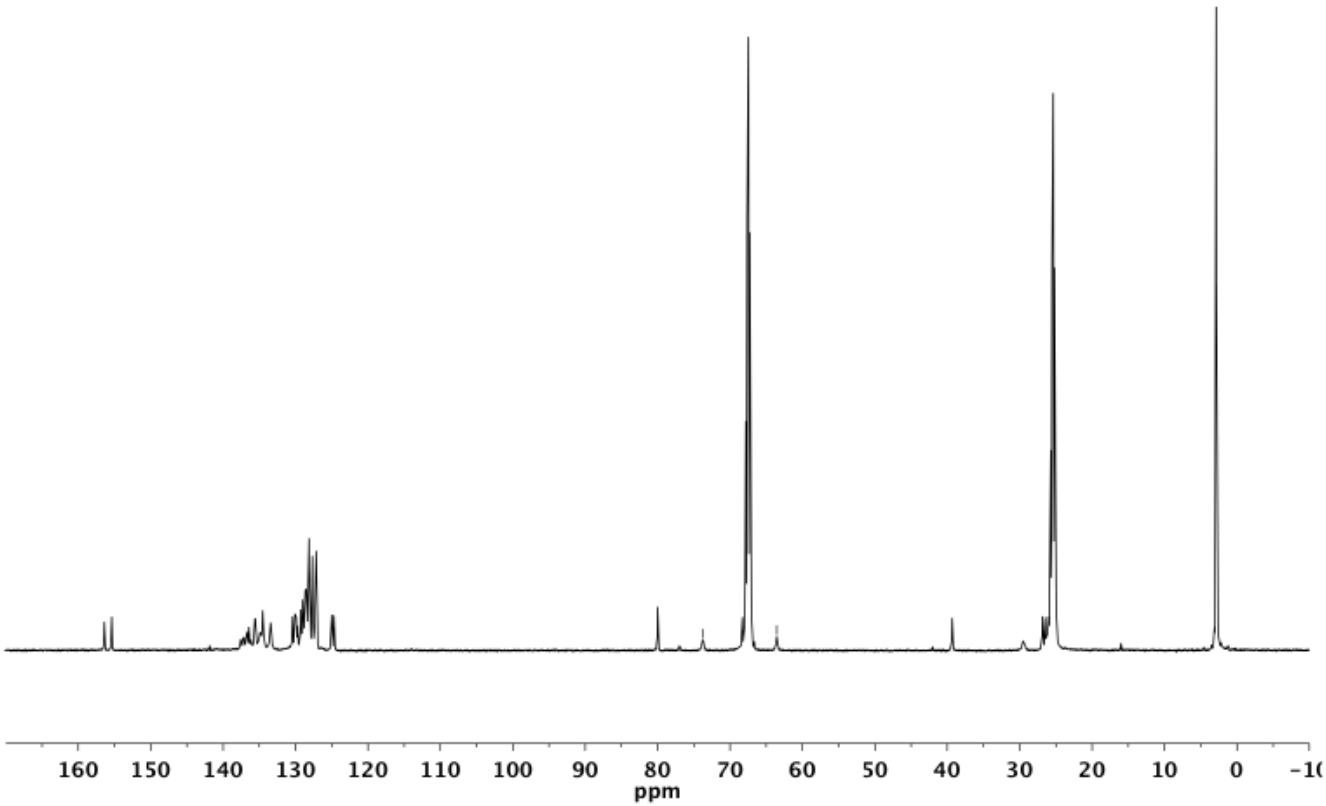



cprVIII_DPPB_series_b/1
1H starting parameters (zg30)
DRX-500 TBIC
061212 CGC
Ph
Ph
Ph2
P
O
Rh
P
Ph2
7h
9.0
8.5
8.0
7.5
7.0
6.5
6.0
5.5
5.0
4.5
4.0
3.5
3.0
2.5
2.0
1.5
1.0
0.5
0.0
ppm

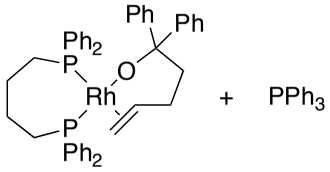
cprVII_188_b/2
DRX-500 5mm TBIC probe 13C starting parameters. Rev 1/11/12 CGC
With CPD proton decoupling. Use ns*td0 scans




**7h**

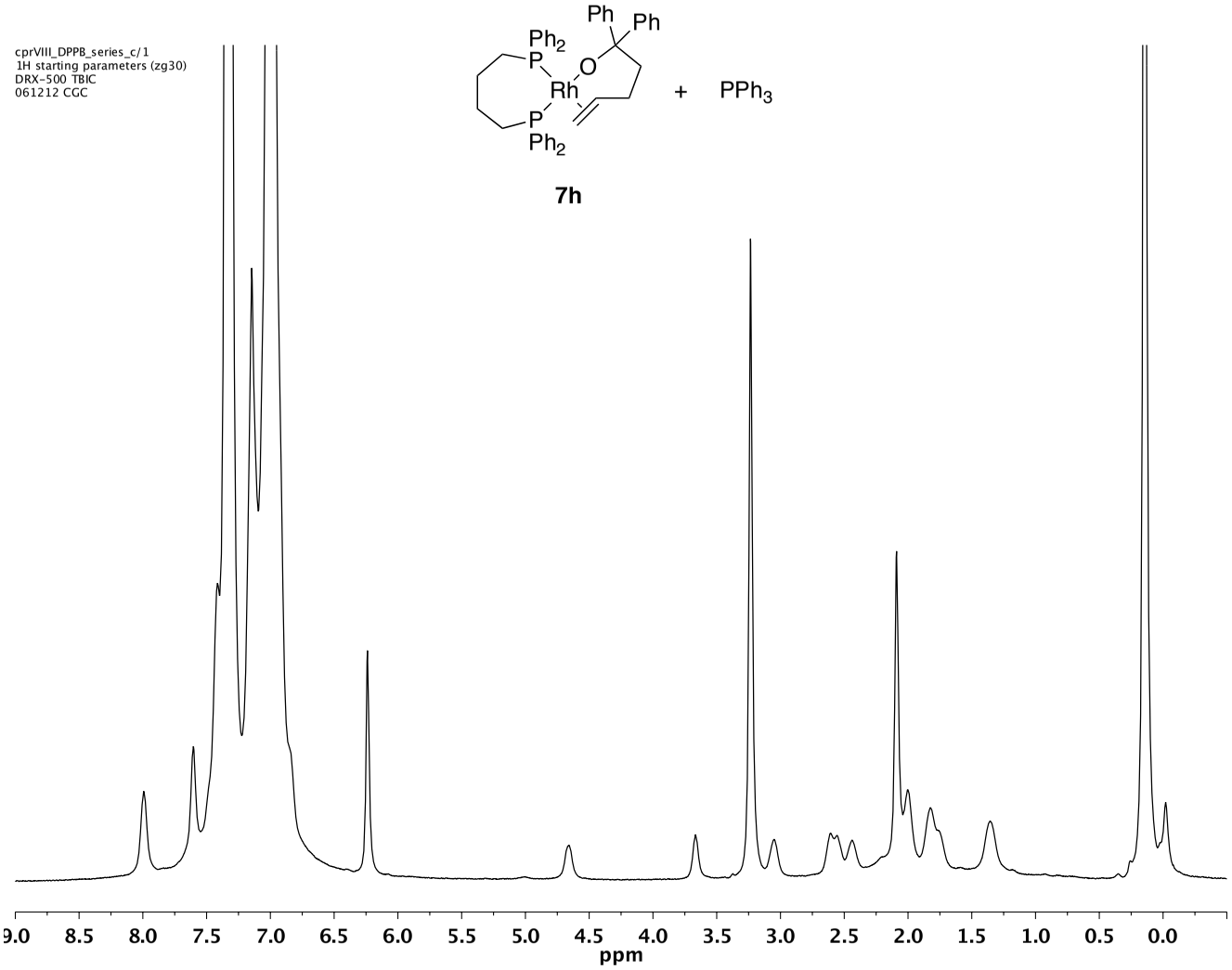


cprVIII_DPPB_series_c/2
DRX-500 5mm ZBO probe 31P starting parameters
Use ns*d0. PMeO3 set to 1.67 ppm
6/12/12 CC revised

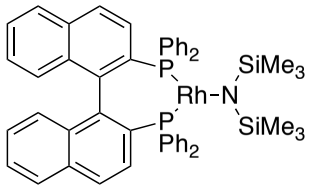



+ $PPh_3$

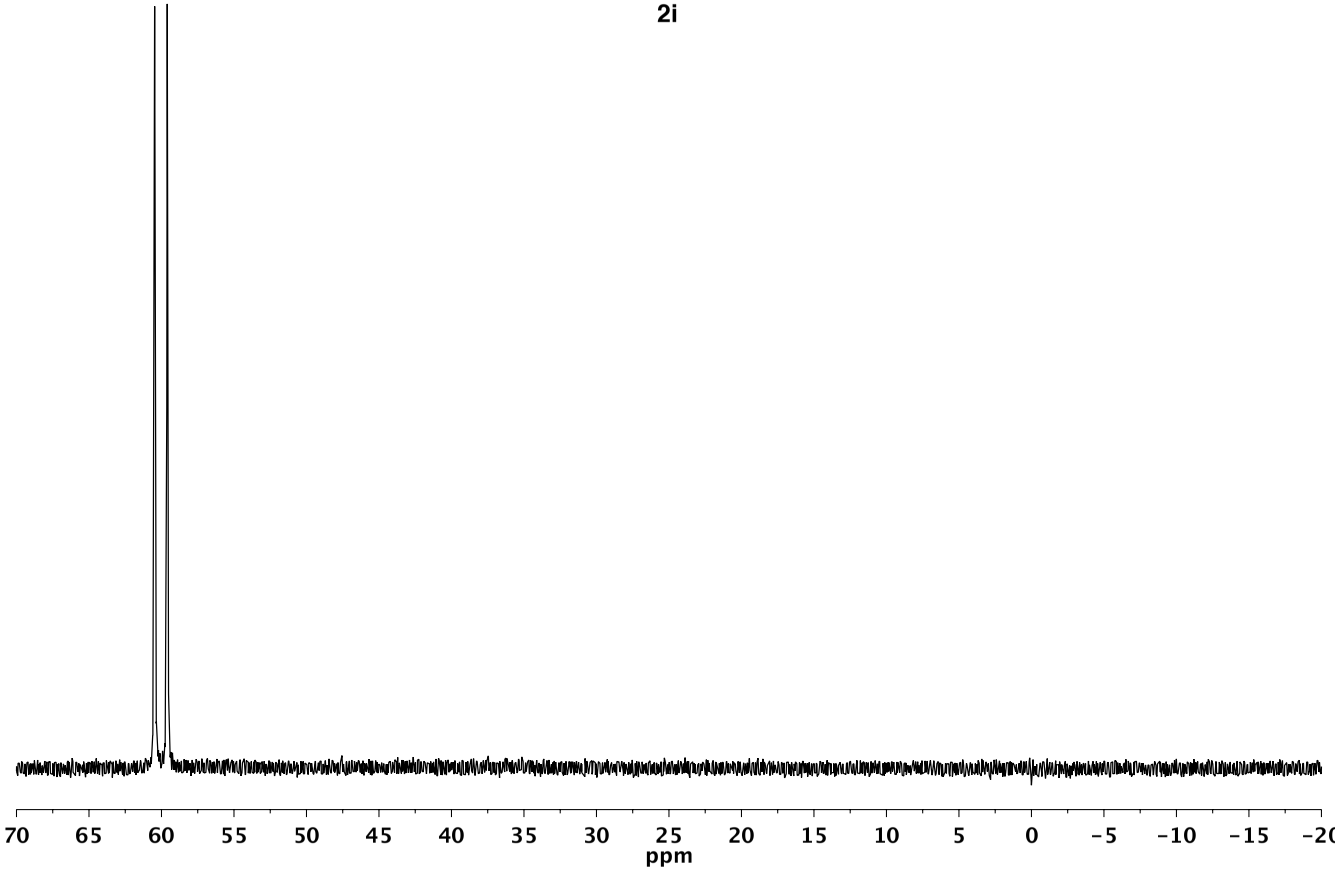
**7h**


cprVIII_DPPB_series_c/1
1H starting parameters (zg30)
DRX-500 TBIC
061212 CGC
Ph
Ph
Ph2
P
O
Rh
P
Ph2
+ PPh3
7h
9.0 8.5 8.0 7.5 7.0 6.5 6.0 5.5 5.0 4.5 4.0 3.5 3.0 2.5 2.0 1.5 1.0 0.5 0.0
ppm

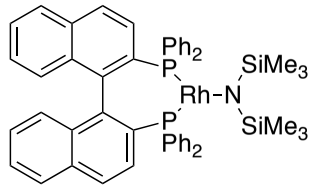
cprVIII_BINAP_series_a/2
DRX-500 5mm ZBO probe 31P starting parameters
Use ns*d0. PMeO3 set to 1.67 ppm
6/12/12 CC revised



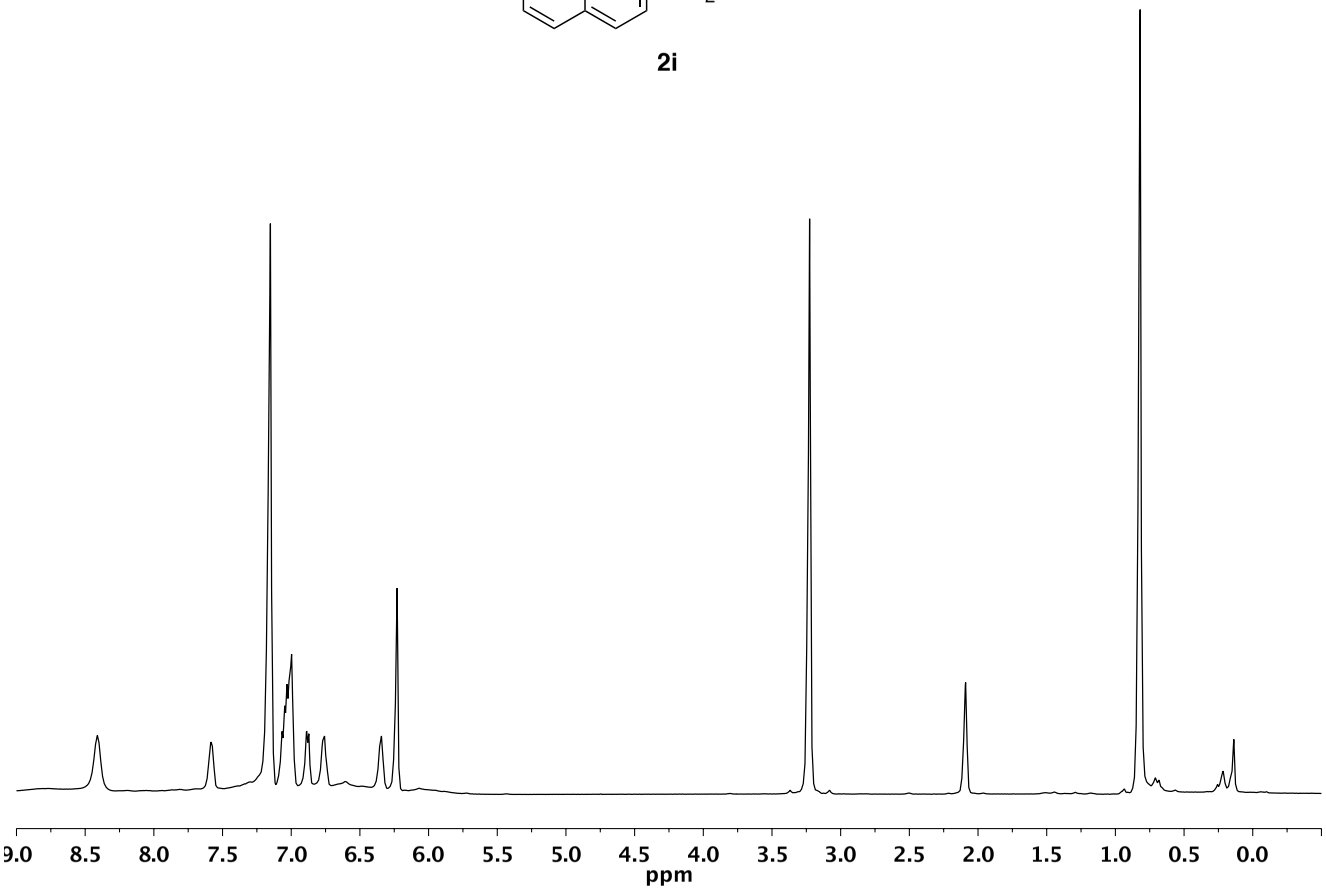

**2i**



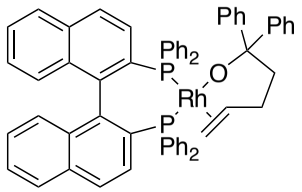
cprVIII_BINAP_series_a/1
1H starting parameters (zg30)
DRX-500 TBIC
061212 CGC



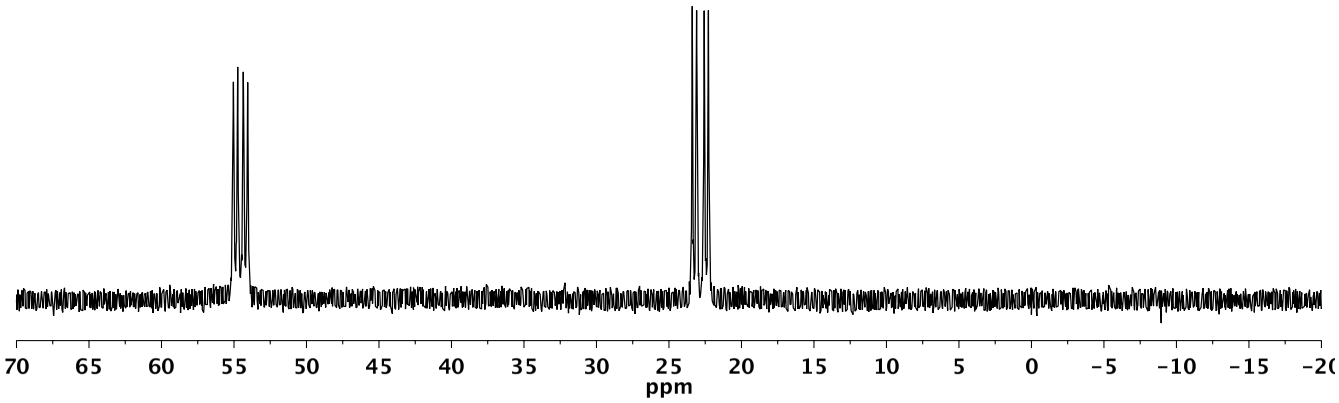

**2i**

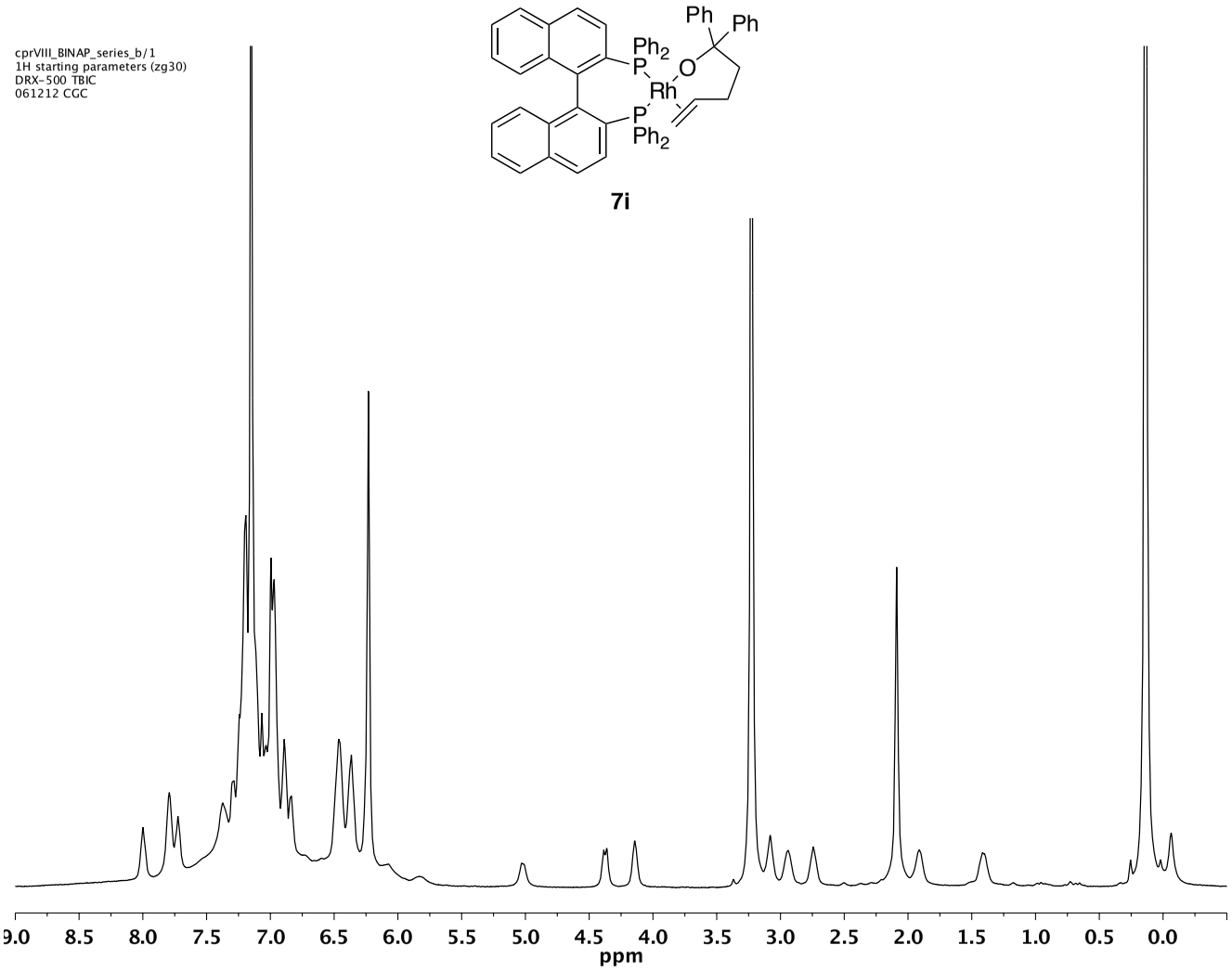


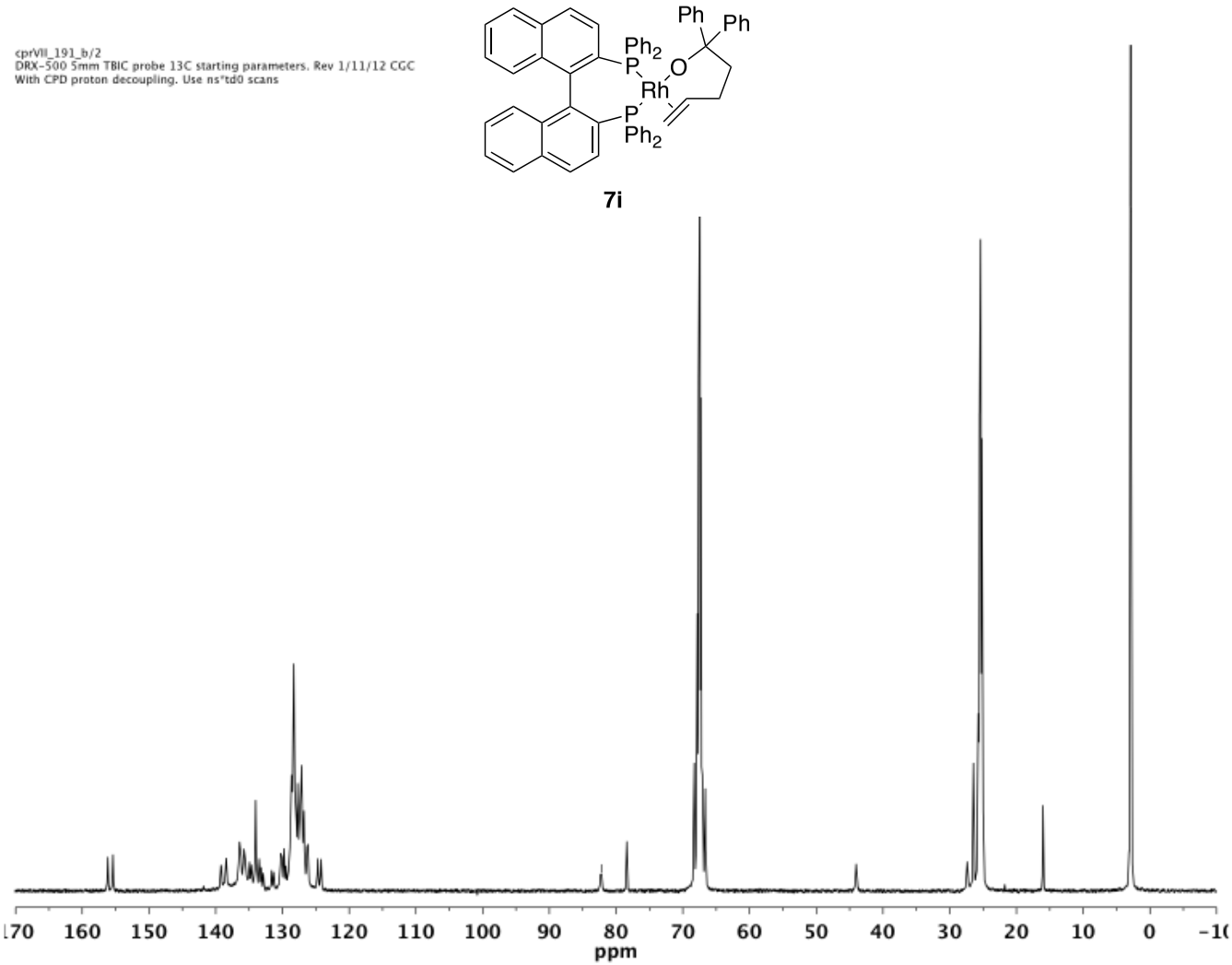
cprVIII_BINAP_series_b/2
DRX-500 5mm ZBO probe 31P starting parameters
Use ns*d0. PMeO3 set to 1.67 ppm
6/12/12 CC revised



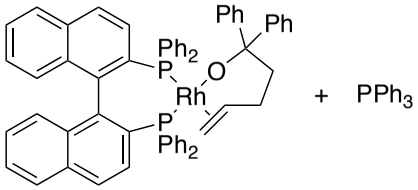

**7i**




cprVIII_BINAP_series_b/1
1H starting parameters (zg30)
DRX-500 TBIC
061212 CGC
Ph
Ph
Ph2
P
O
Rh
P
Ph2
7i
9.0
8.5
8.0
7.5
7.0
6.5
6.0
5.5
5.0
4.5
4.0
3.5
3.0
2.5
2.0
1.5
1.0
0.5
0.0
ppm

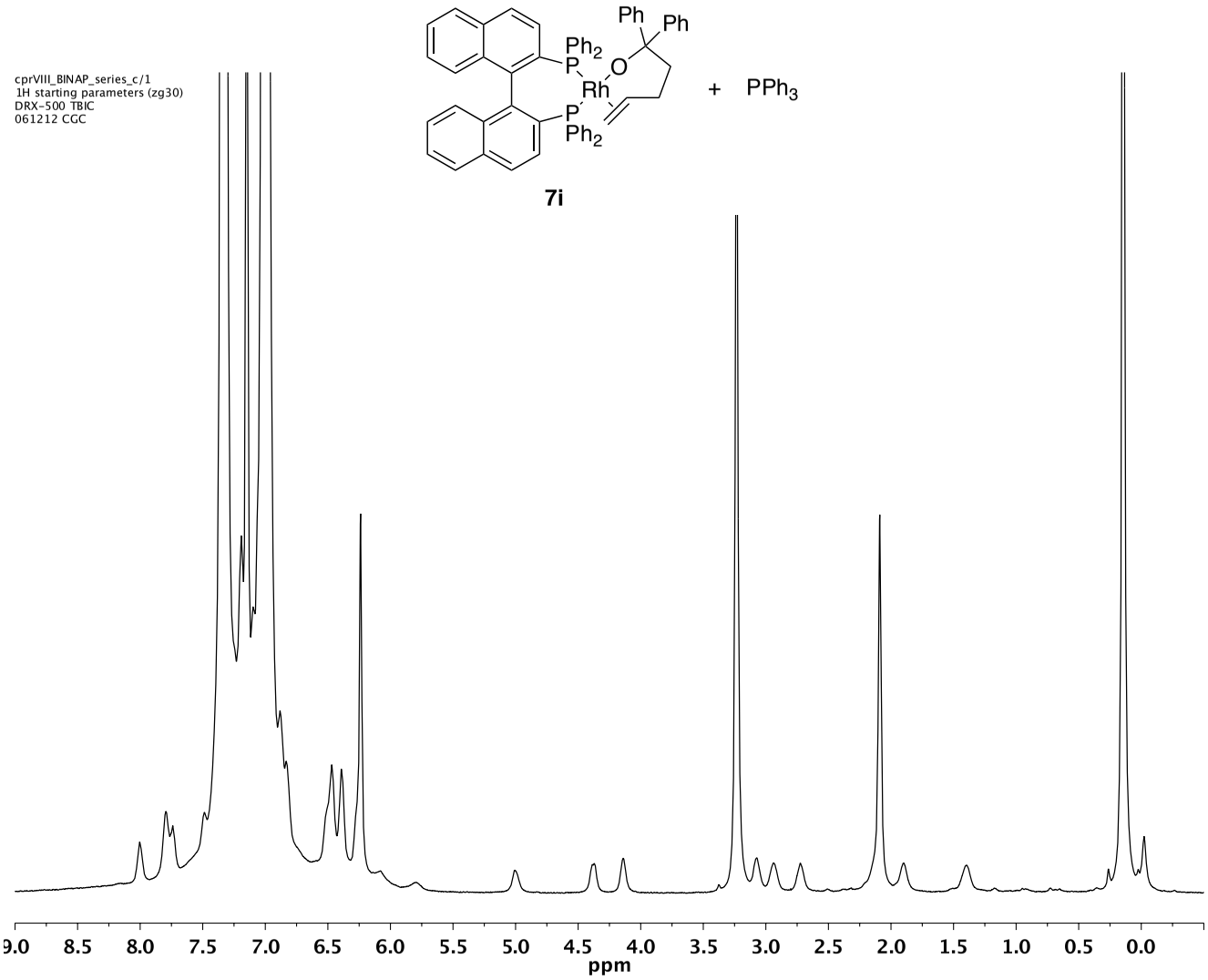

cprVII_191_b/2
DRX-500 5mm TBIC probe 13C starting parameters. Rev 1/11/12 CGC
With CPD proton decoupling. Use ns*td0 scans
Ph
Ph
Ph2
P
O
Rh
P
Ph2
7i
170
160
150
140
130
120
110
100
90
80
70
60
50
40
30
20
10
0
-10
ppm

cprVIII_BINAP_series_c/2
DRX-500 5mm ZBO probe 31P starting parameters
Use ns*d0. PMeO3 set to 1.67 ppm
6/12/12 CC revised

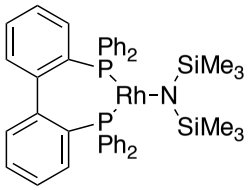



**7i**

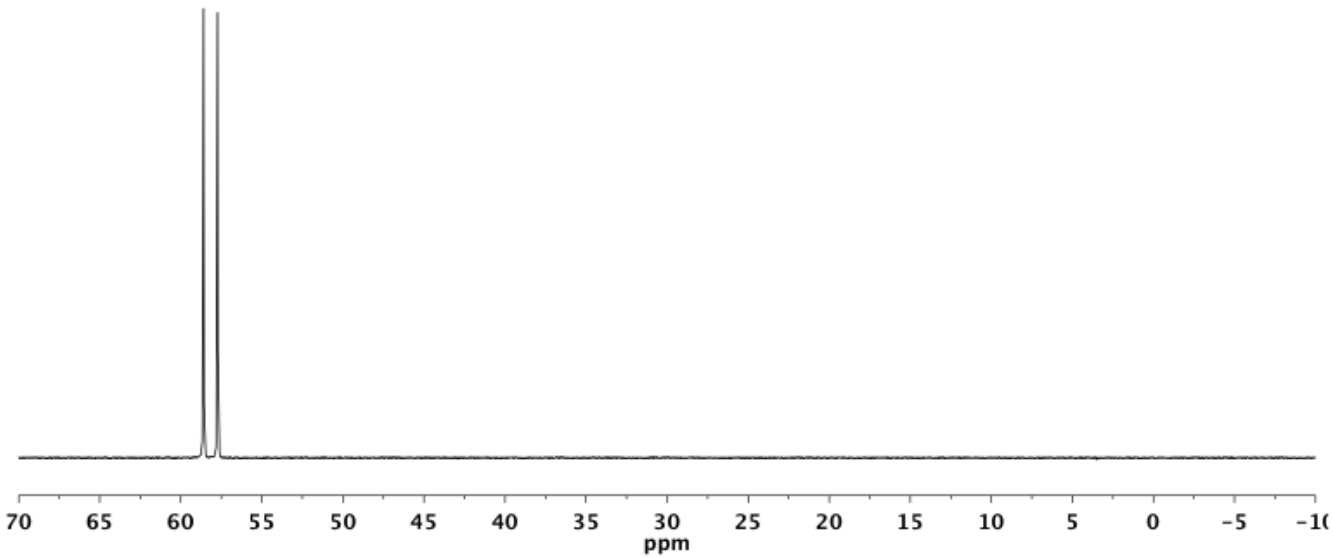
+ $PPh_3$

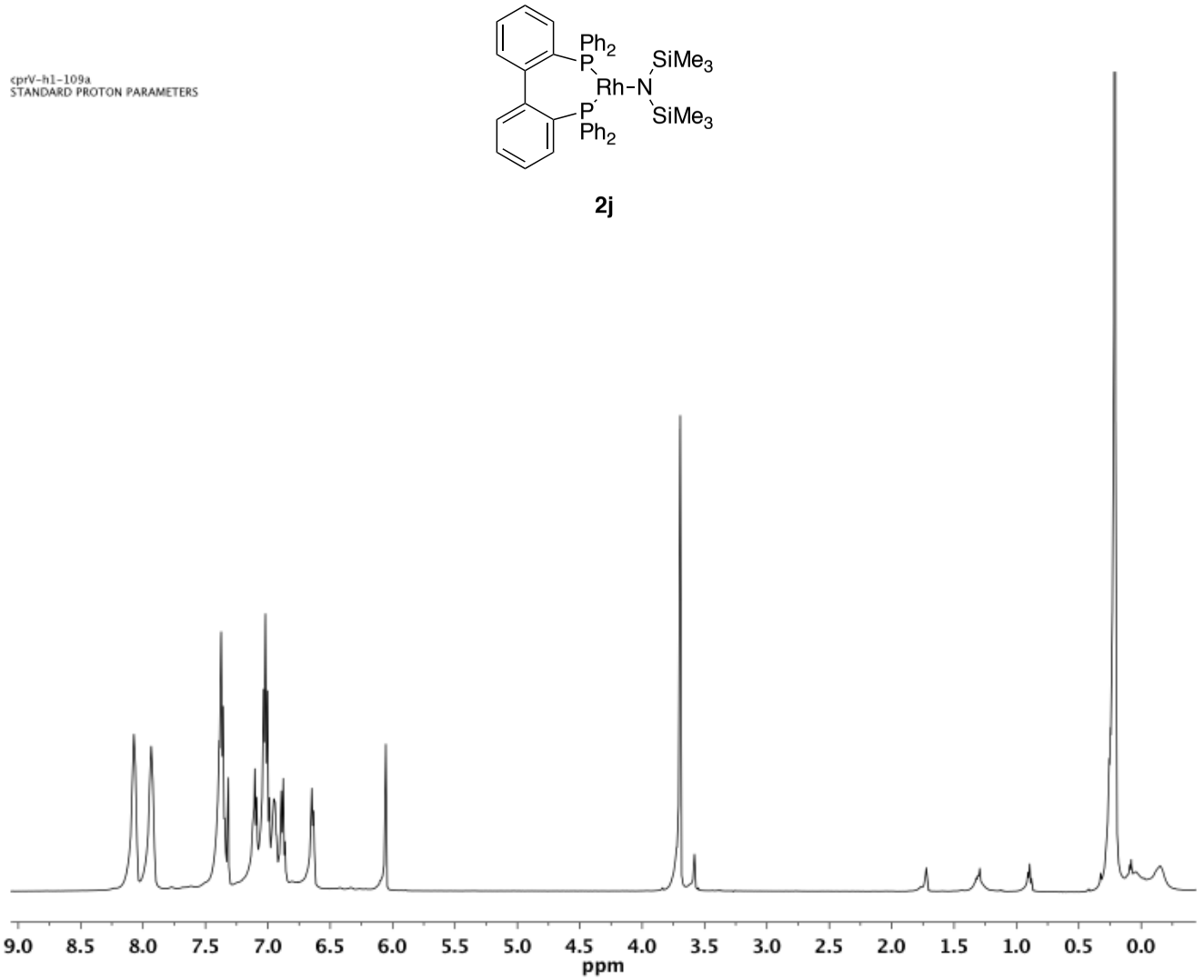

cprVIII_BINAP_series_c/1
1H starting parameters (zg30)
DRX-500 TBIC
061212 CGC
Ph
Ph
Ph2
P
O
Rh
P
Ph2
+ PPh3
7i
9.0
8.5
8.0
7.5
7.0
6.5
6.0
5.5
5.0
4.5
4.0
3.5
3.0
2.5
2.0
1.5
1.0
0.5
0.0
ppm

cprVII_193_a/3
DRX-500 5mm ZBO probe 31P starting parameters
Use ns*d0. PMeO3 set to 1.67 ppm
1/11/12 CC revised

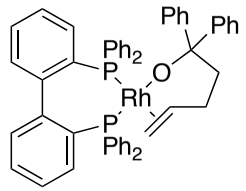



**2j**

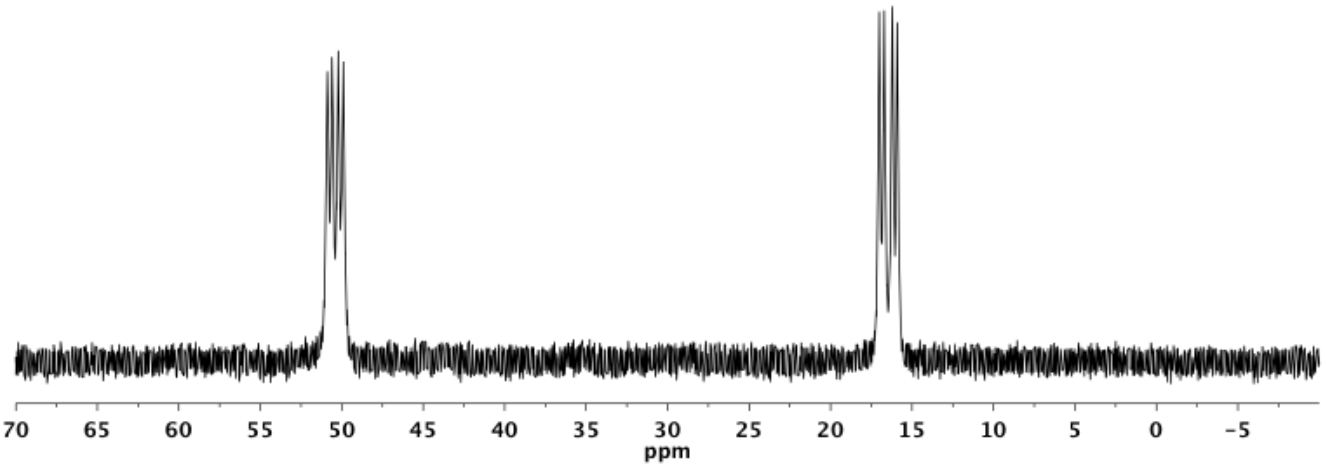


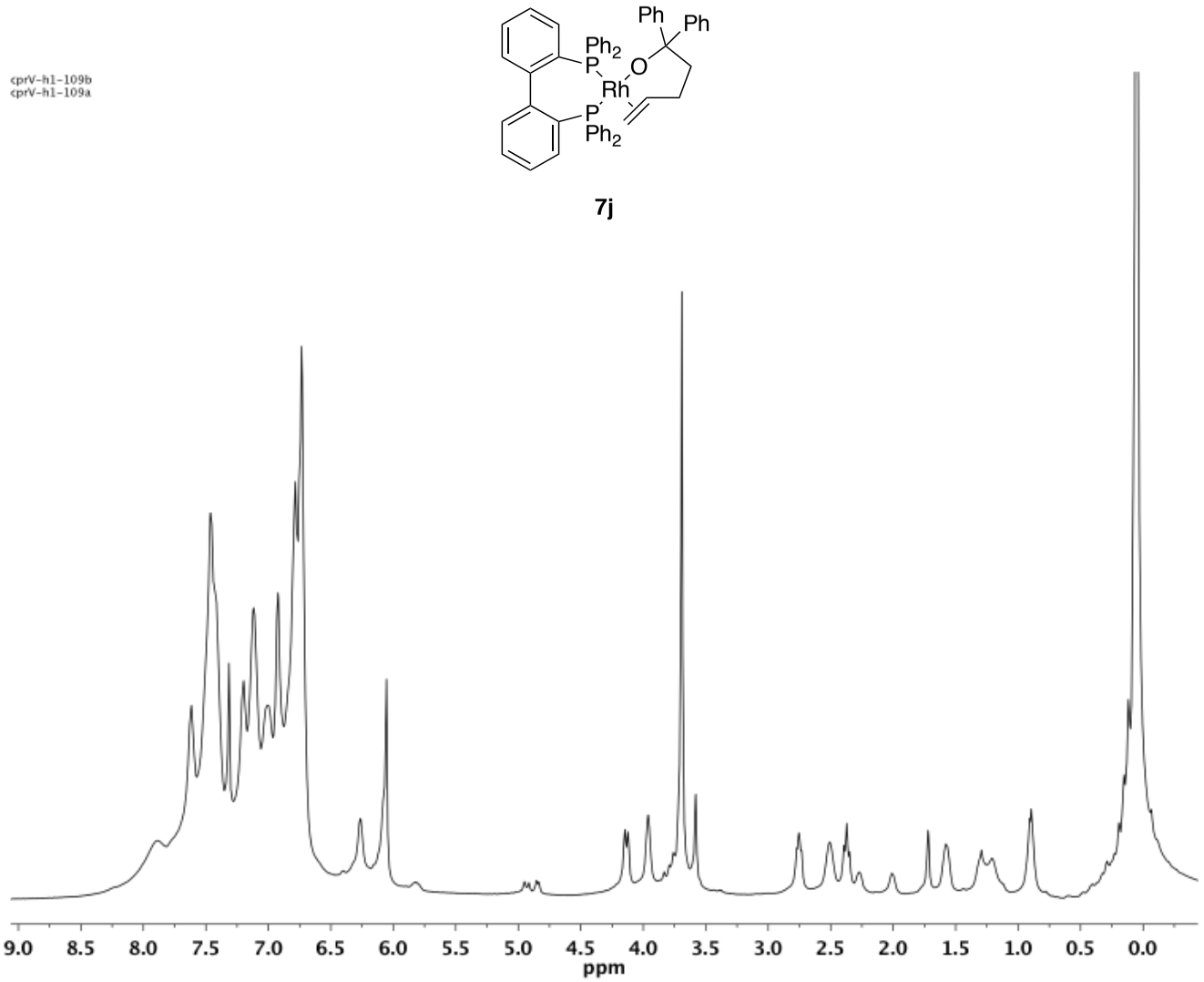

cprV-h1-109a
STANDARD PROTON PARAMETERS
Ph2
P
Rh-N
SiMe3
SiMe3
P
Ph2
2j
9.0
8.5
8.0
7.5
7.0
6.5
6.0
5.5
5.0
4.5
4.0
3.5
3.0
2.5
2.0
1.5
1.0
0.5
0.0
ppm

cprVII_193_b/3
DRX-500 5mm ZBO probe 31P starting parameters
Use ns°d0. PMeO3 set to 1.67 ppm
1/11/12 CC revised

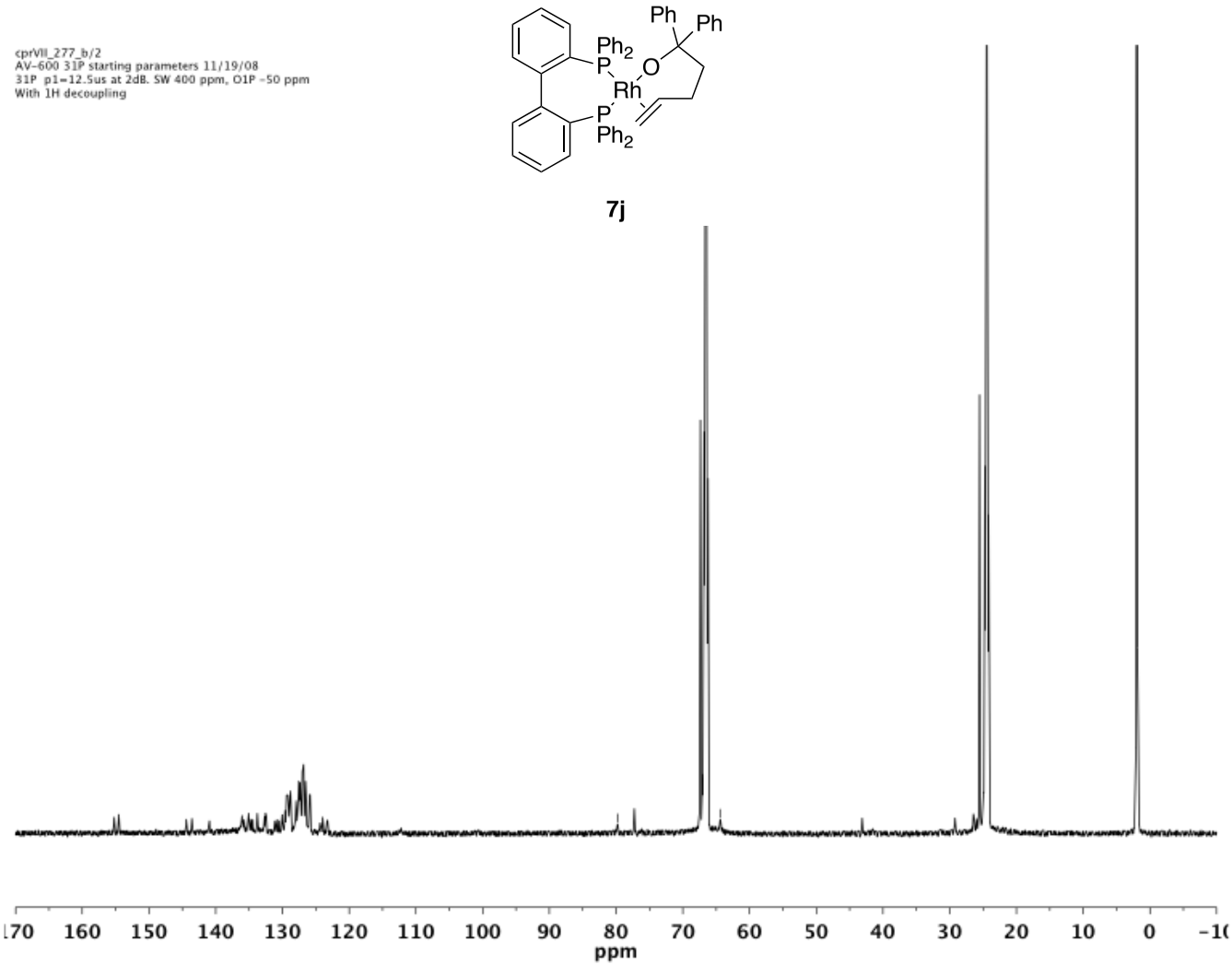


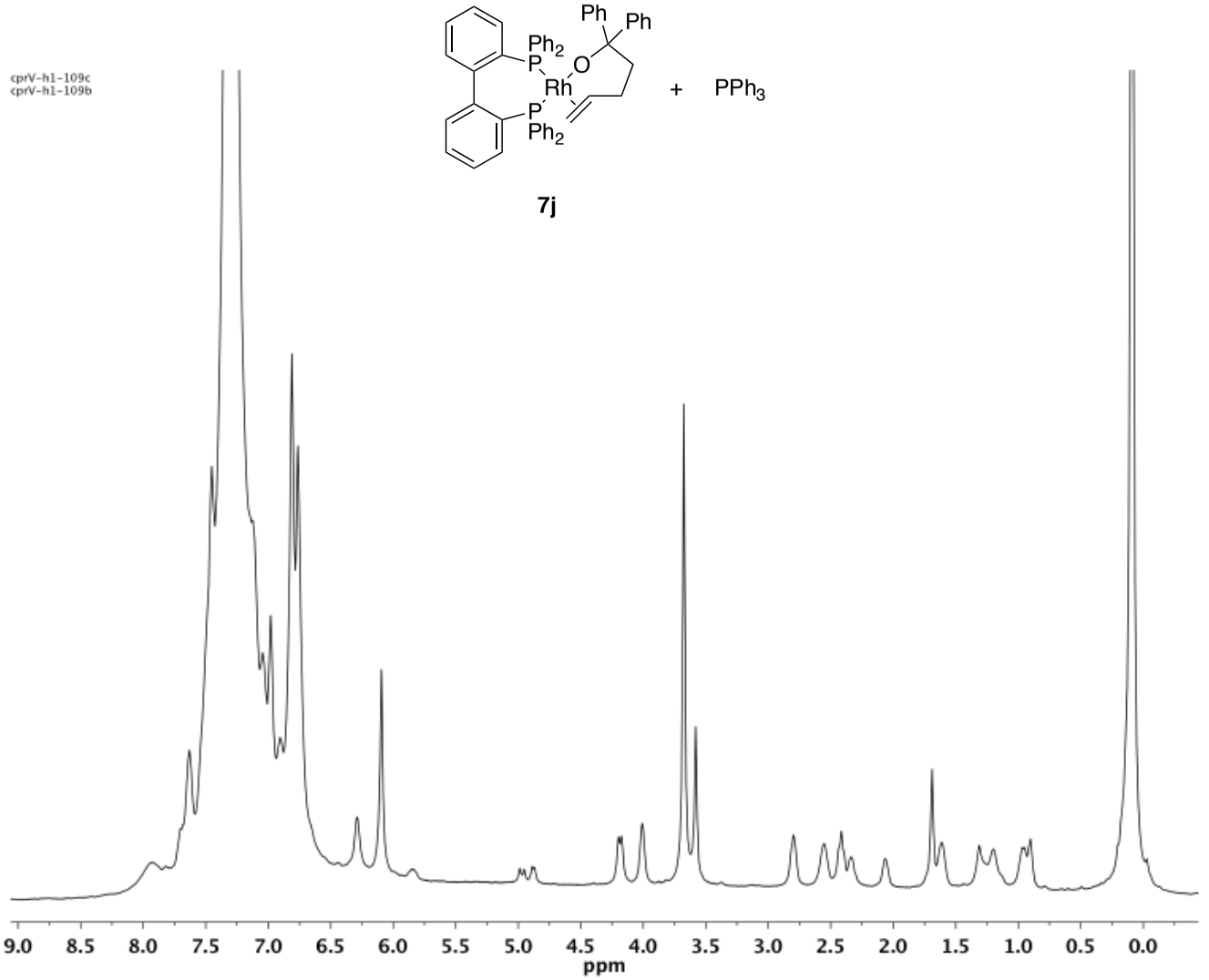

**7j**



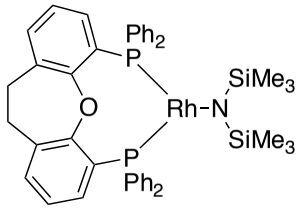

cprV-h1-109b
cprV-h1-109a
Ph
Ph
Ph2
P
O
Rh
P
Ph2
9.0
8.5
8.0
7.5
7.0
6.5
6.0
5.5
5.0
4.5
4.0
3.5
3.0
2.5
2.0
1.5
1.0
0.5
0.0
ppm

**7j**

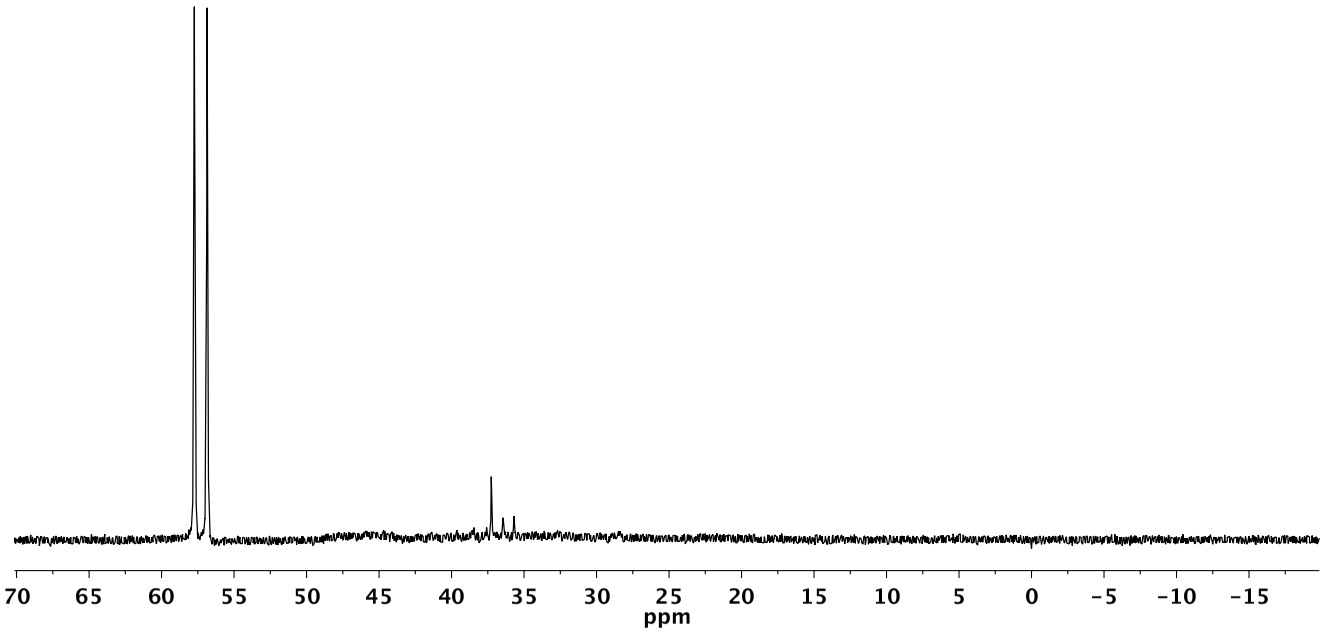

cprVII_277_b/2
AV-600 31P starting parameters 11/19/08
31P p1=12.5us at 2dB. SW 400 ppm, O1P -50 ppm
With 1H decoupling
Ph
Ph
Ph2
P
O
Rh
P
Ph2
7j
170
160
150
140
130
120
110
100
90
80
70
60
50
40
30
20
10
0
-10
ppm


cprV-h1-109c
cprV-h1-109b
Ph
Ph
Ph2
P
O
Rh
P
Ph2
+ PPh3
7j
9.0
8.5
8.0
7.5
7.0
6.5
6.0
5.5
5.0
4.5
4.0
3.5
3.0
2.5
2.0
1.5
1.0
0.5
0.0
ppm

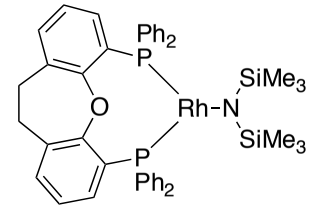
cprVIII_Homoxantphos_series_a/2
DRX-500 5mm ZBO probe 31P starting parameters
Use ns*d0. PMeO3 set to 1.67 ppm
6/12/12 CC revised




**2k**

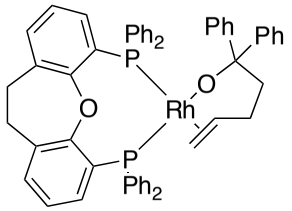


cprV-h1-108a
STANDARD PROTON PARAMETERS

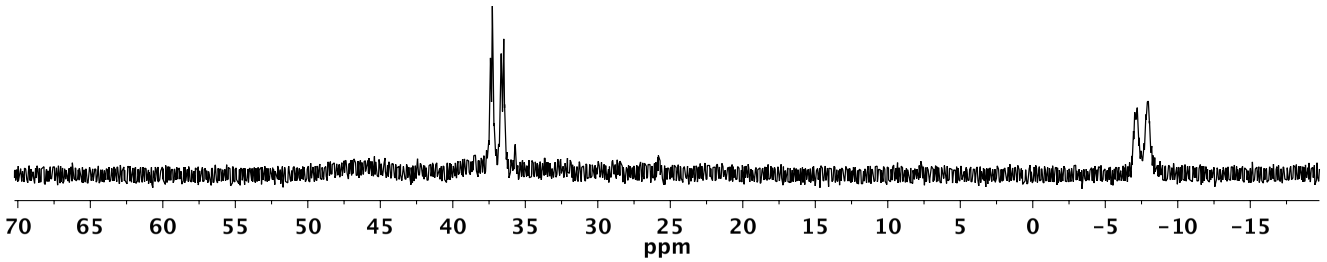



**2k**

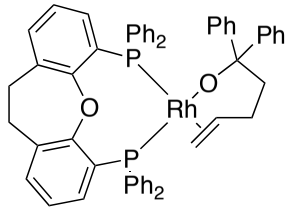
cprVIII_Homoxantphos_series_b/2
DRX-500 5mm ZBO probe 31P starting parameters
Use ns*d0. PMeO3 set to 1.67 ppm
6/12/12 CC revised



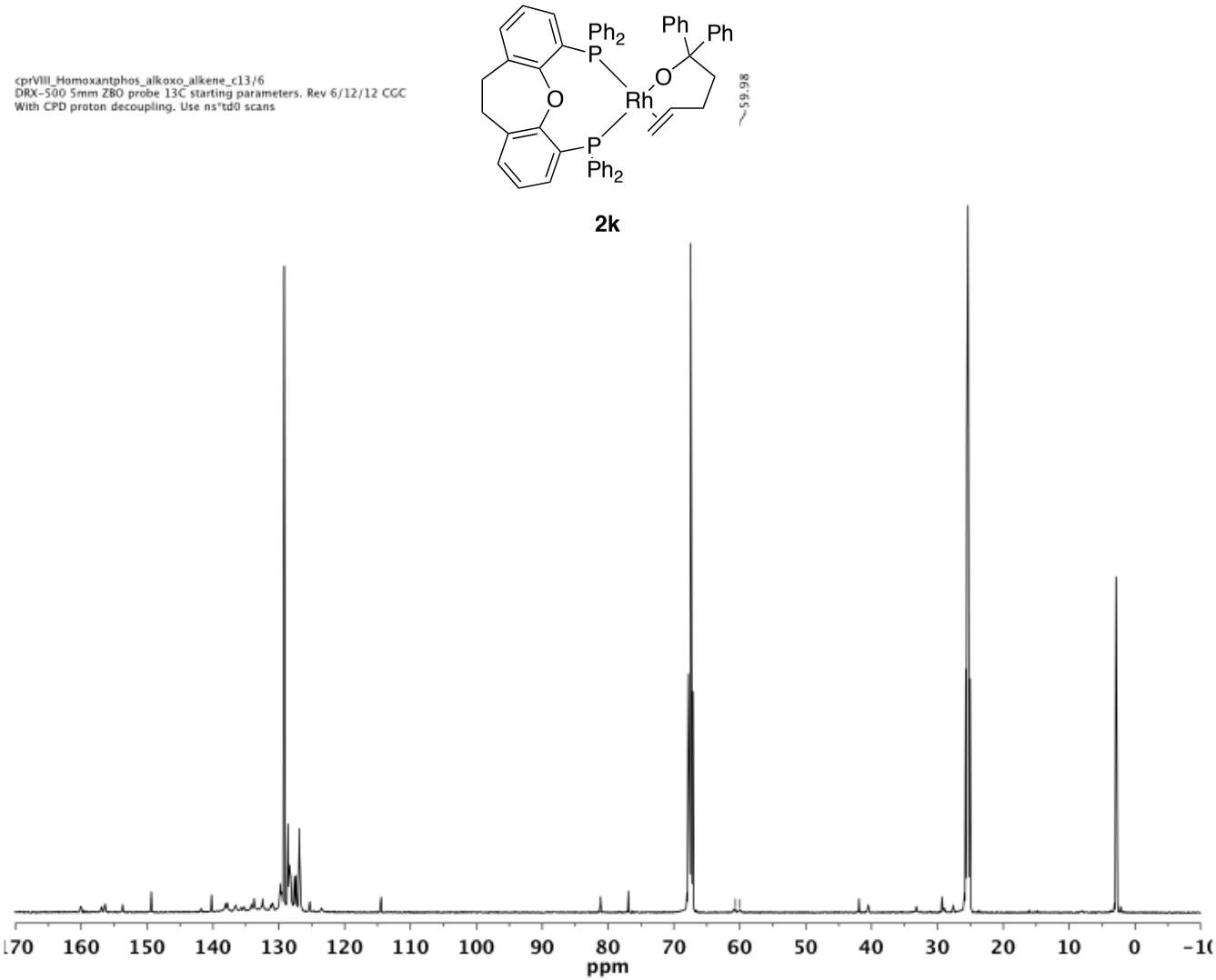

**2k**



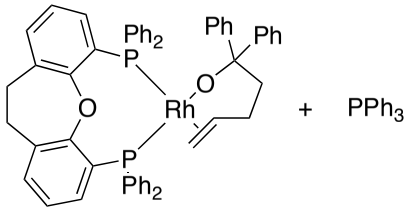
cprV-h1-108b
cprV-h1-108a




**2k**

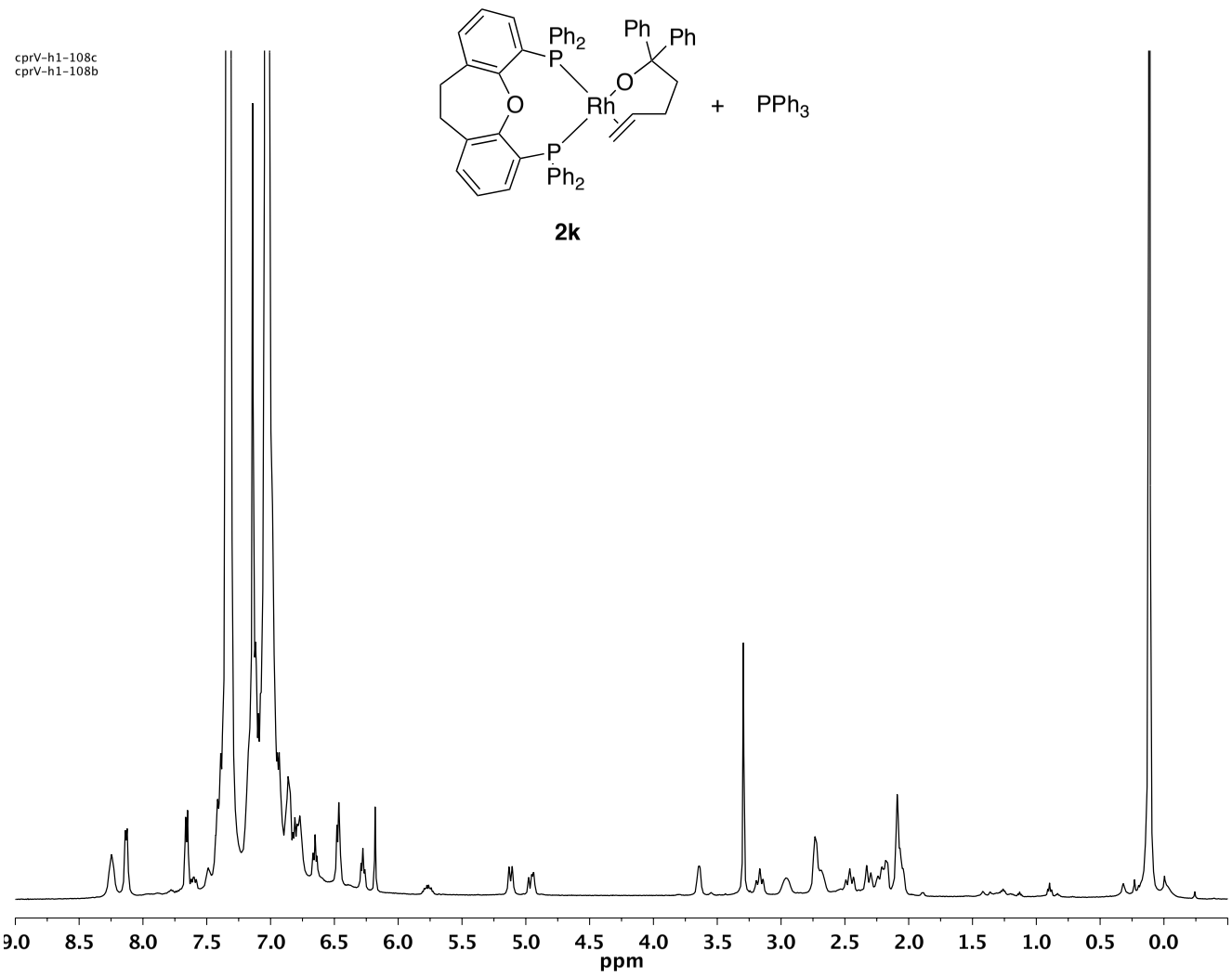

cprVIII_Homoxantphos_alkoxo_alkene_c13/6
DRX-500 5mm ZBO probe 13C starting parameters. Rev 6/12/12 CGC
With CPD proton decoupling. Use ns*td0 scans
Ph2
P
O
Rh
P
Ph2
O
Ph
Ph
~59.98
2k
170
160
150
140
130
120
110
100
90
80
70
60
50
40
30
20
10
0
-10
ppm

cprVIII_Homoxantphos_series_c/2
DRX-500 5mm ZBO probe 31P starting parameters
Use ns*d0. PMeO3 set to 1.67 ppm
6/12/12 CC revised

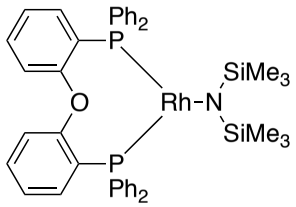



+ $PPh_3$

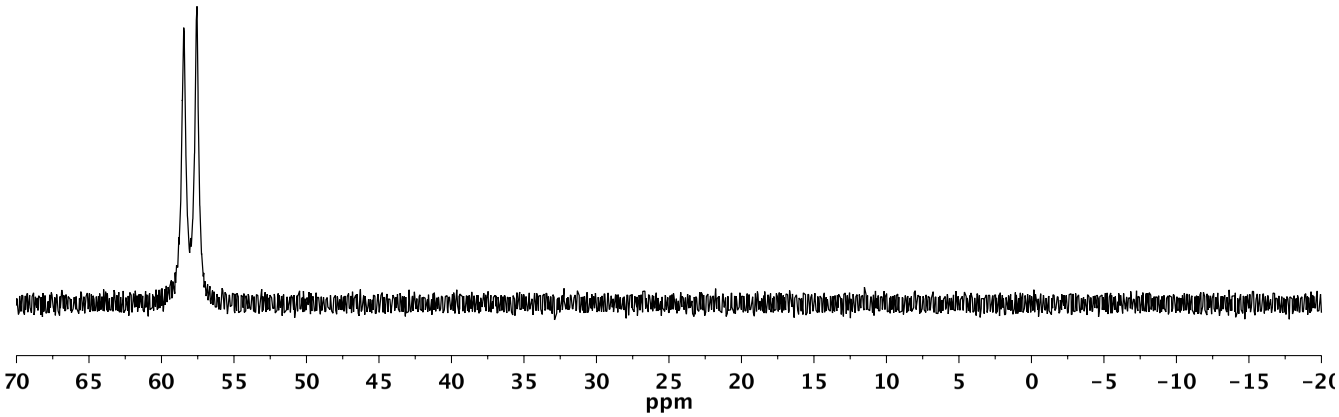
**2k**


cprV-h1-108c
cprV-h1-108b
Ph2
P
Ph
Ph
O
Rh
O
+
PPh3
P
Ph2
2k
9.0
8.5
8.0
7.5
7.0
6.5
6.0
5.5
5.0
4.5
4.0
3.5
3.0
2.5
2.0
1.5
1.0
0.5
0.0
ppm

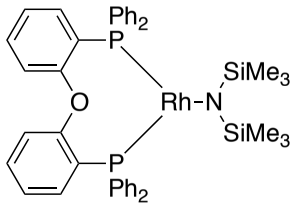
cprIII-p31-33a
P31 TRIPHENYLPHOSPHATE PARAMETERS




**2l**

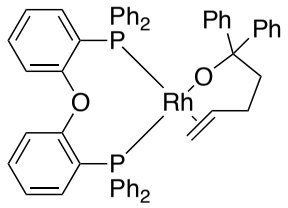


cprIII-h1-33a
STANDARD PROTON PARAMETERS

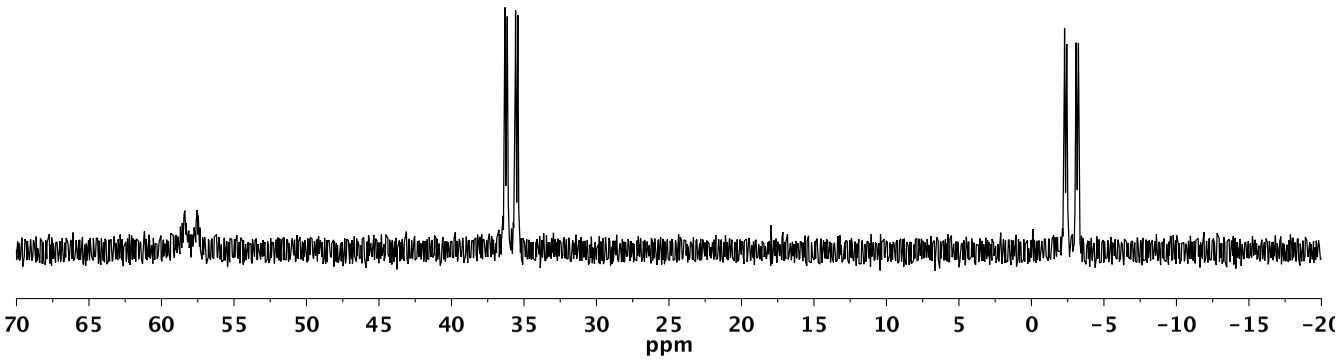



**2l**

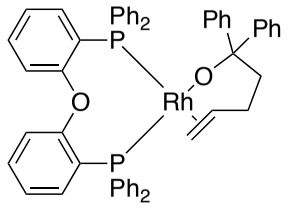
cprlll-p31-33b
cprlll-p31-33a




**7l**

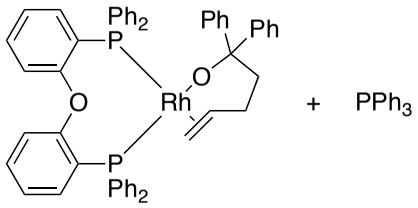


cprlll-h1-33b
cprlll-h1-33a

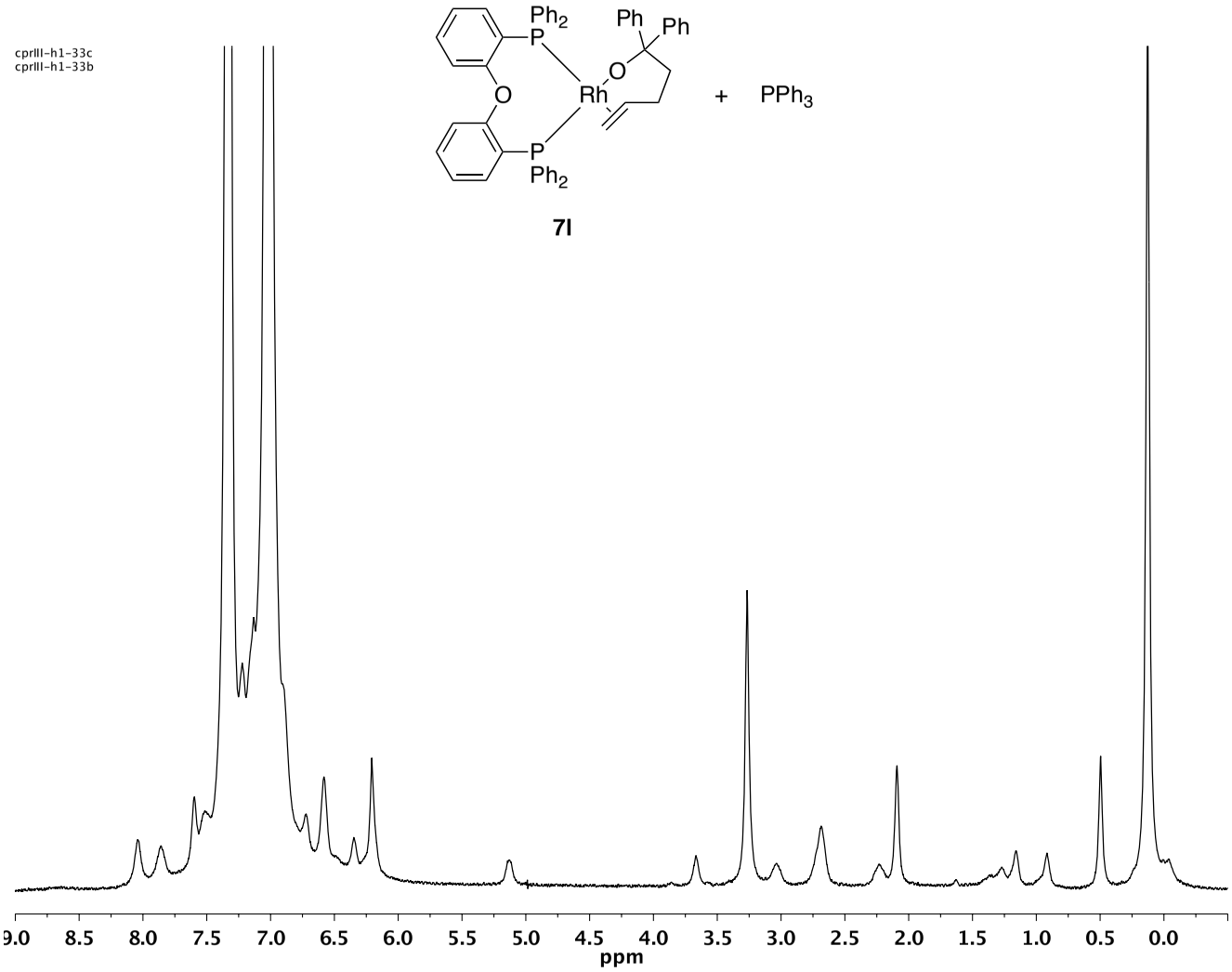



**7l**

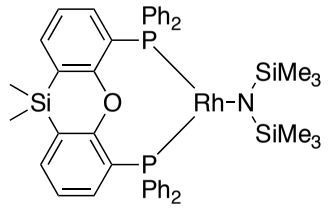
cprlll-p31-33c
P31 TRIPHENYLPHOSPHATE PARAMETERS



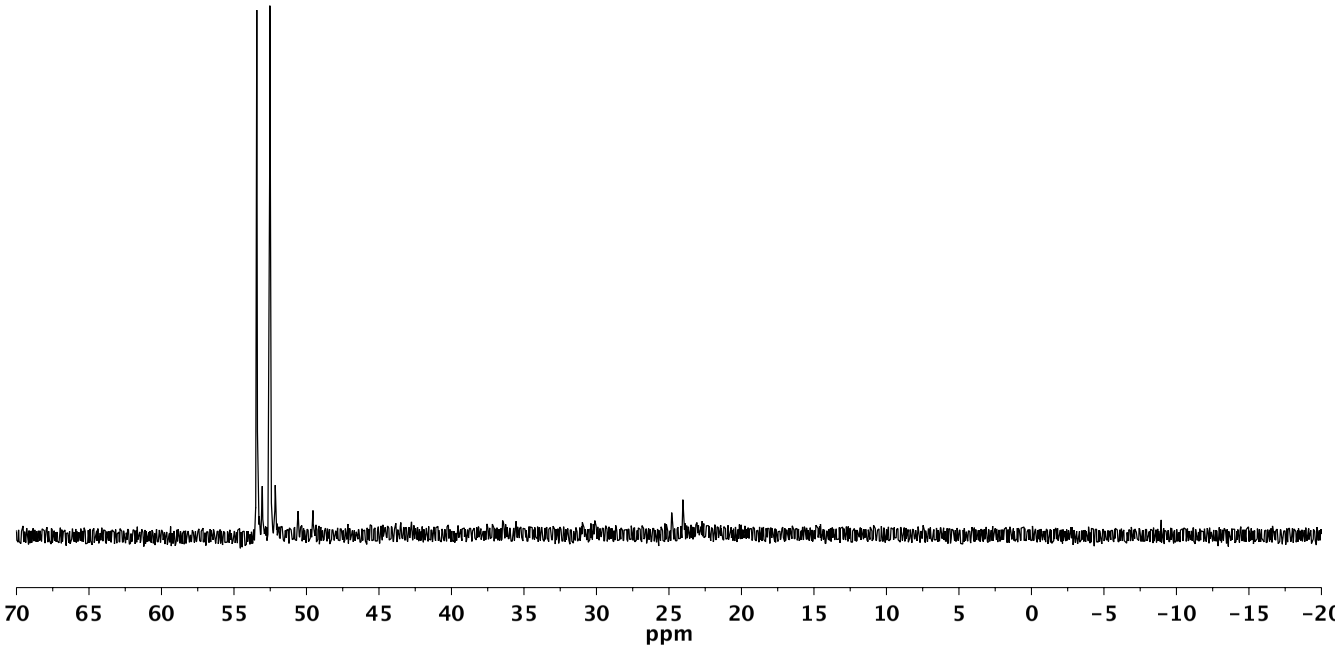

7l + $PPh_3$


cprlll-h1-33c
cprlll-h1-33b
Ph2
P
Ph
Ph
O
O
Rh
+ PPh3
P
Ph2
7l
9.0
8.5
8.0
7.5
7.0
6.5
6.0
5.5
5.0
4.5
4.0
3.5
3.0
2.5
2.0
1.5
1.0
0.5
0.0
ppm

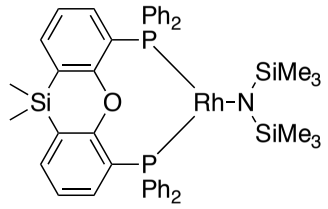
cprVIII_Sixantphos_series_a/2
DRX-500 5mm ZBO probe 31P starting parameters
Use ns*d0. PMeO3 set to 1.67 ppm
6/12/12 CC revised



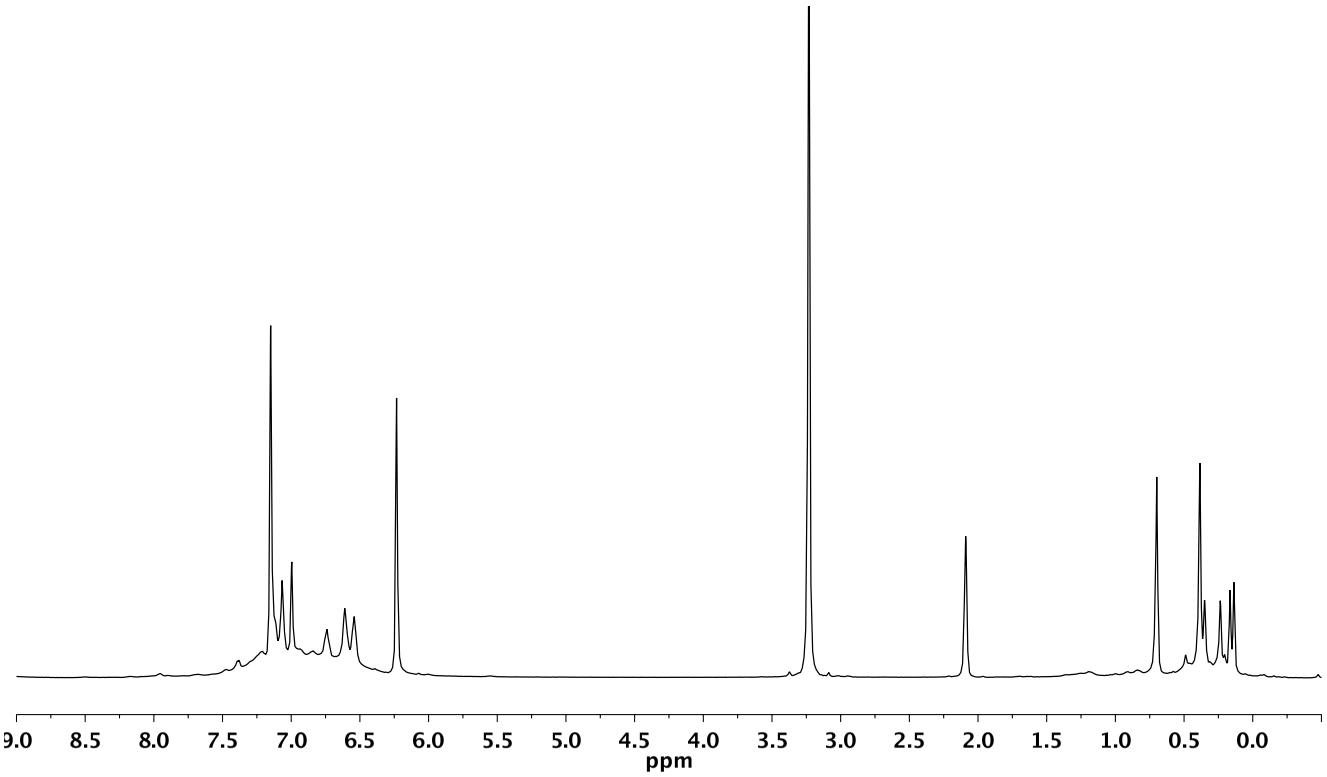

**2m**



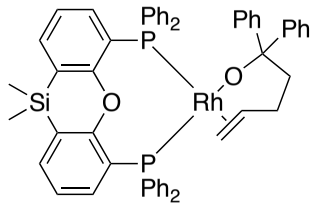
cprVIII_Sixantphos_series_a/1
1H starting parameters (zg30)
DRX-500 TBIC
061212 CGC



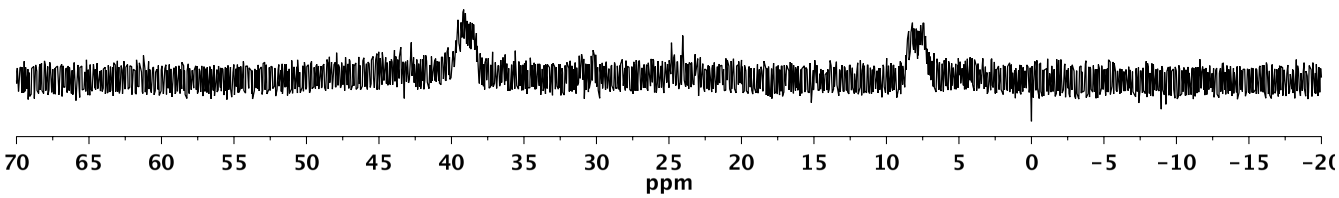

**2m**

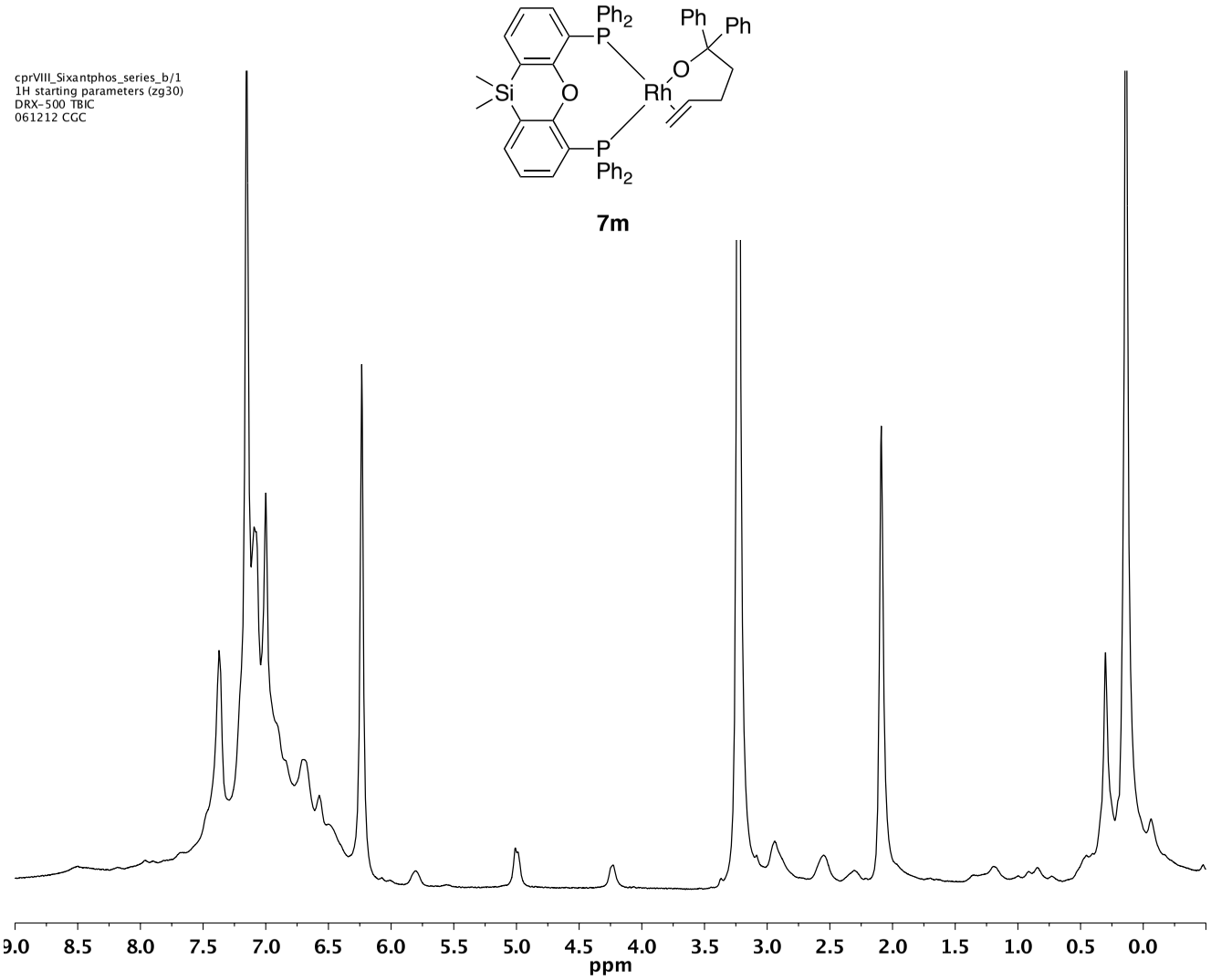


cprVIII_Sixantphos_series_b/2
DRX-500 5mm ZBO probe 31P starting parameters
Use ns*d0. PMeO3 set to 1.67 ppm
6/12/12 CC revised

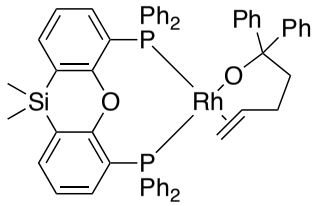



**7m**

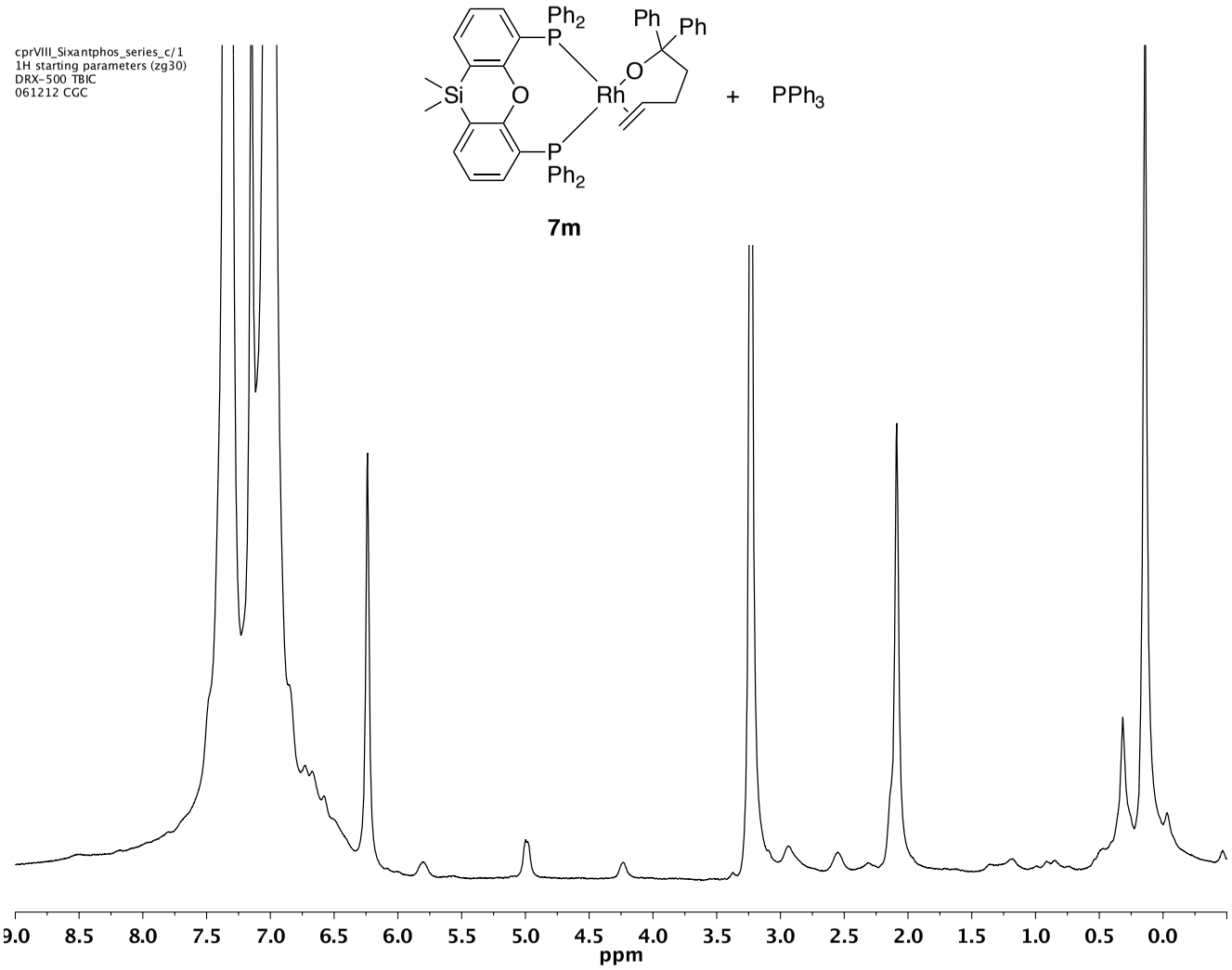


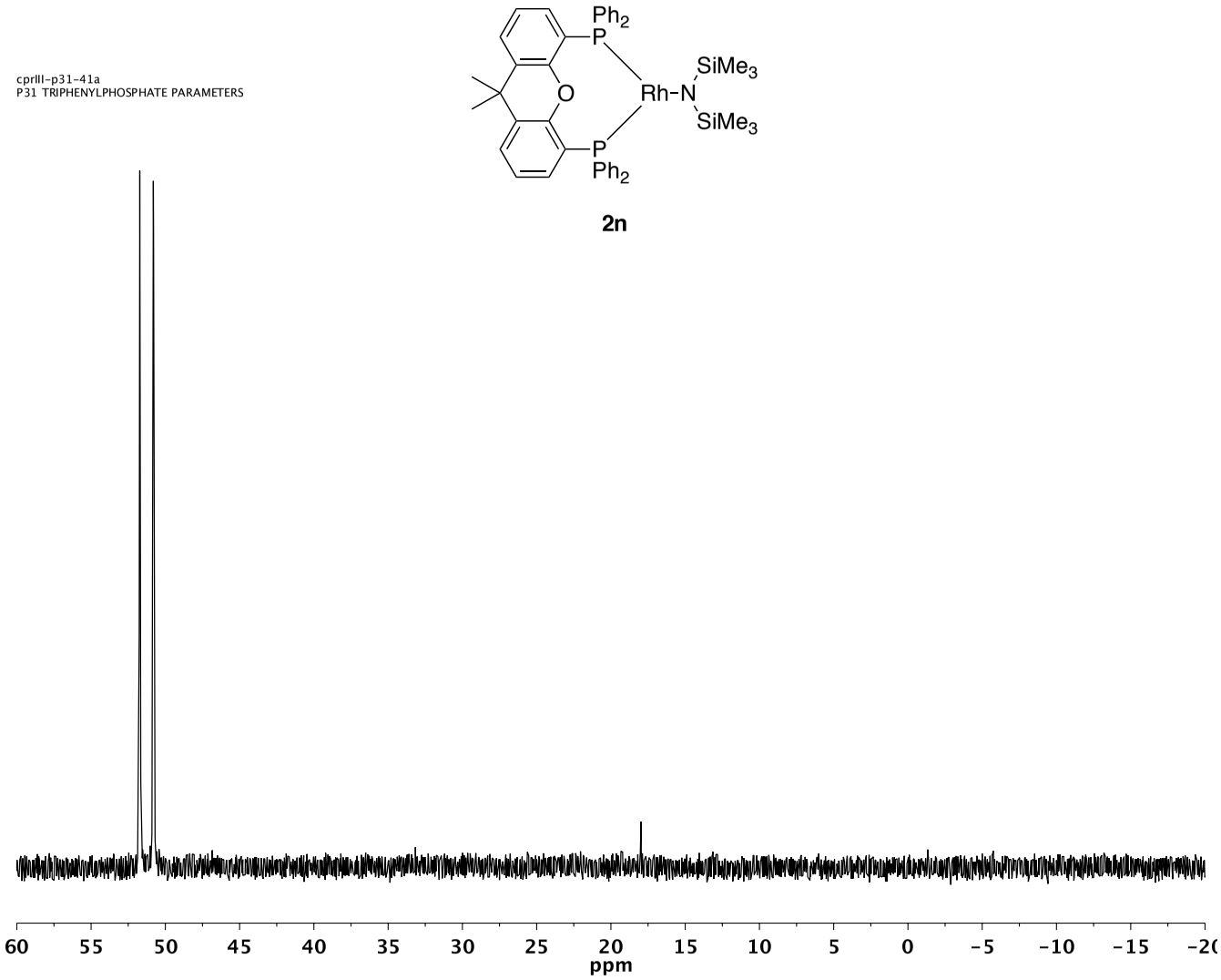

cprVIII_Sixantphos_series_b/1
1H starting parameters (zg30)
DRX-500 TBIC
061212 CGC
Ph2
P
Ph
Ph
O
Si
O
Rh
P
Ph2
7m
9.0
8.5
8.0
7.5
7.0
6.5
6.0
5.5
5.0
4.5
4.0
3.5
3.0
2.5
2.0
1.5
1.0
0.5
0.0
ppm

cprVIII_Sixantphos_series_c/2
DRX-500 5mm ZBO probe 31P starting parameters
Use ns*d0. PMeO3 set to 1.67 ppm
6/12/12 CC revised

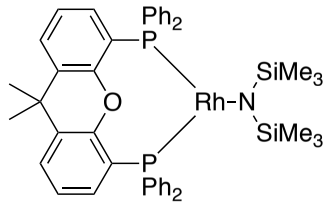



**7m** + $PPh_3$

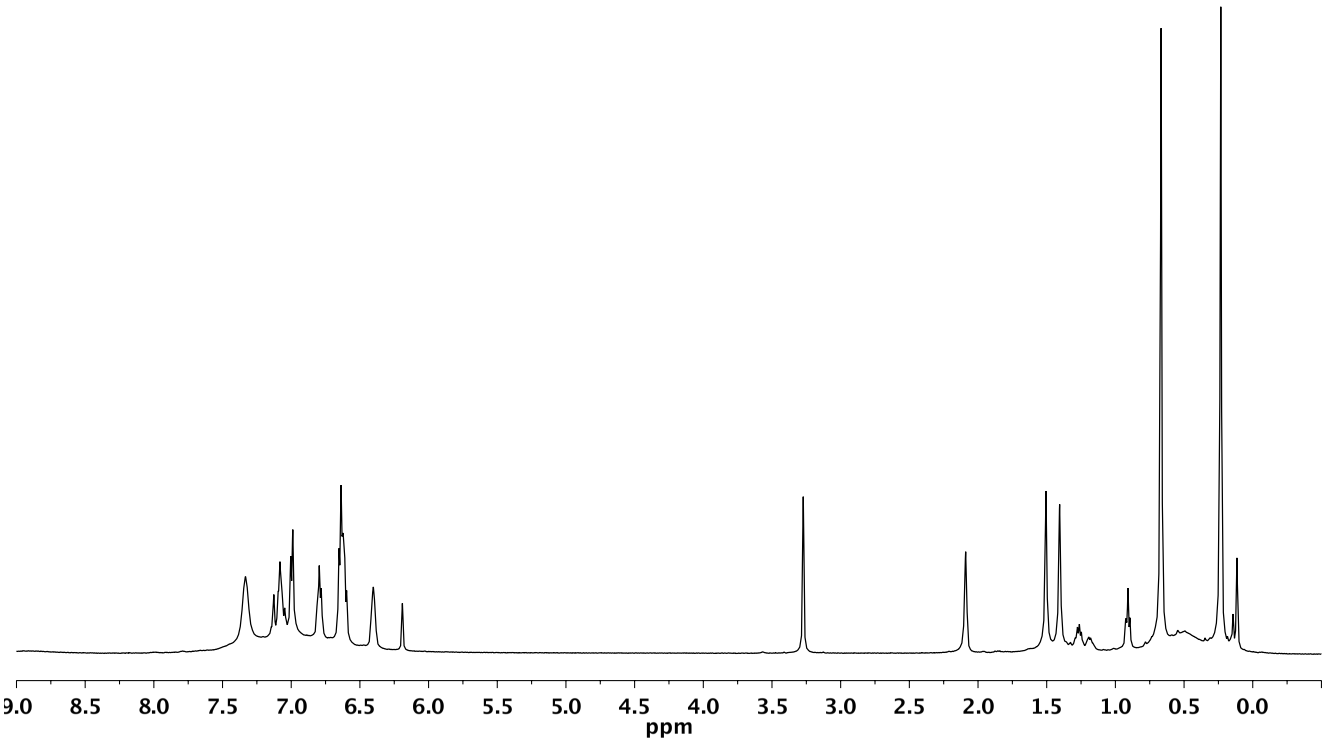

cprVIII_Sixantphos_series_c/1
1H starting parameters (zg30)
DRX-500 TBIC
061212 CGC
Ph2
P
Ph
Ph
Si
O
Rh
O
P
Ph2
+ PPh3
7m
9.0 8.5 8.0 7.5 7.0 6.5 6.0 5.5 5.0 4.5 4.0 3.5 3.0 2.5 2.0 1.5 1.0 0.5 0.0
ppm


cprIII-p31-41a
P31 TRIPHENYLPHOSPHATE PARAMETERS
Ph2
P
O
Rh-N
SiMe3
SiMe3
P
Ph2
2n
60
55
50
45
40
35
30
25
20
15
10
5
0
-5
-10
-15
-20
ppm

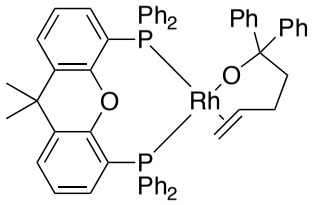
cprIII-h1-41a
STANDARD PROTON PARAMETERS



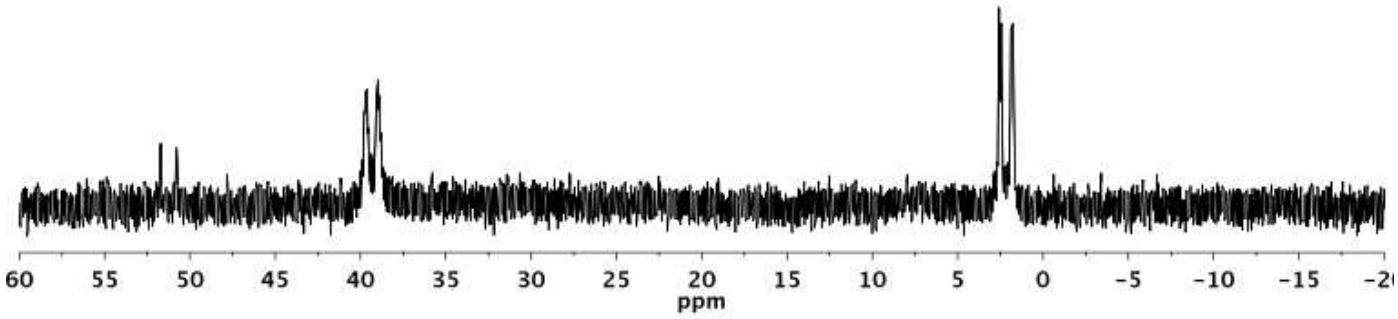

**2n**



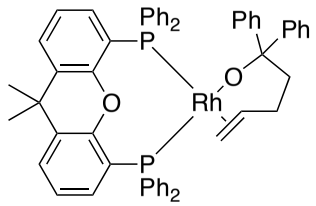
cprlll-p31-41b
cprlll-p31-41a




**7n**

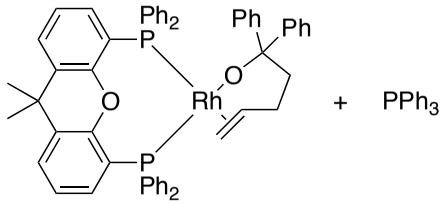


cprlll-h1-41b
cprlll-h1-41a



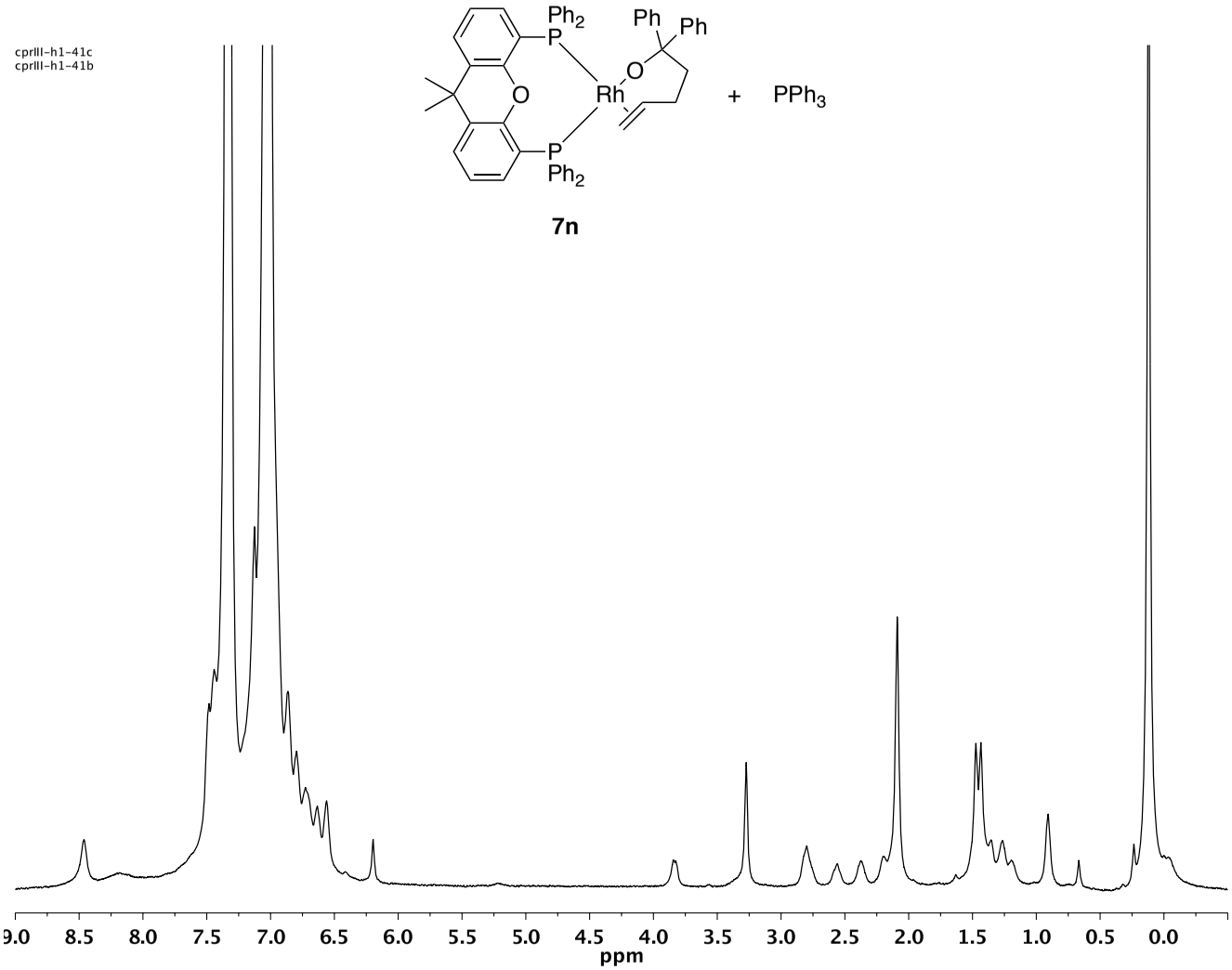

**7n**

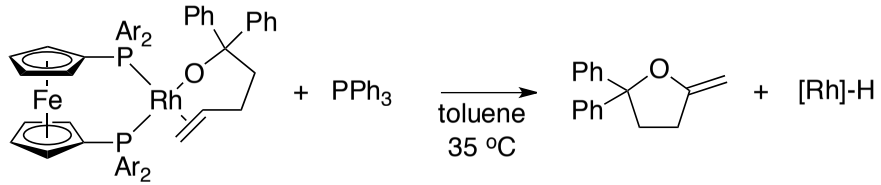
cprlll-p31-41c
cprlll-p31-41b

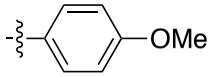



**7n**

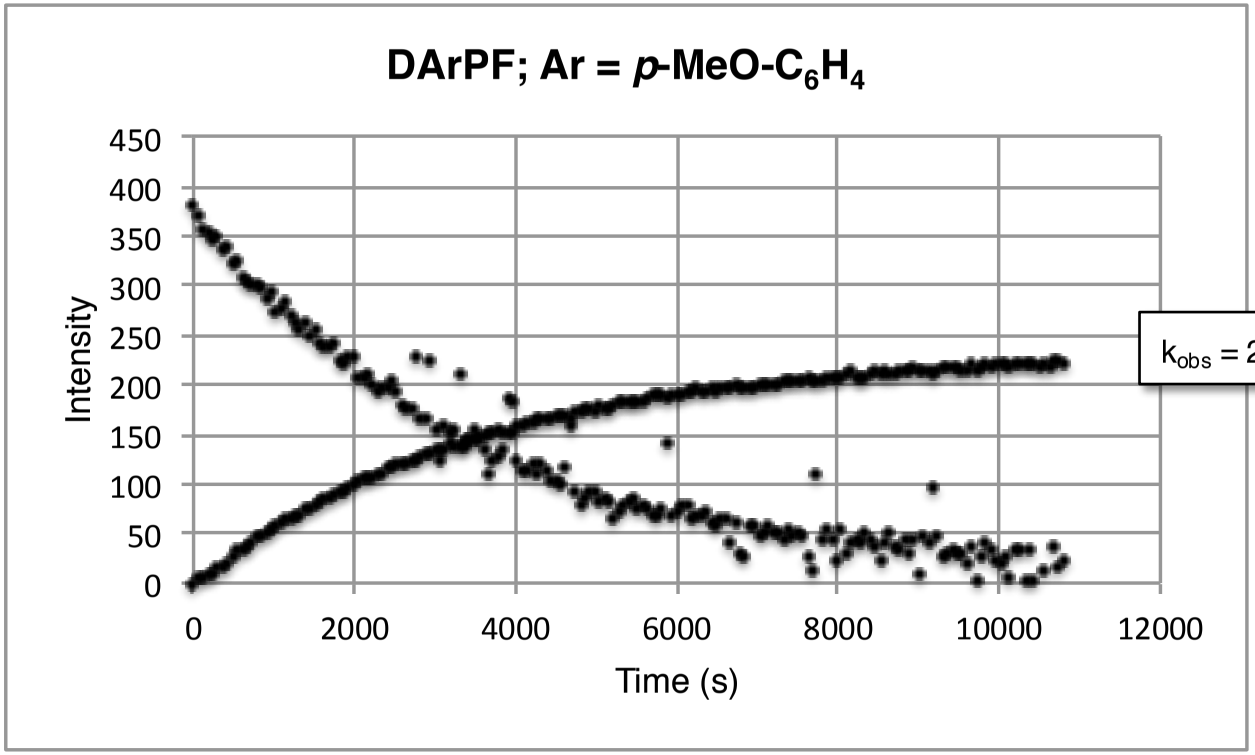
+ $PPh_3$

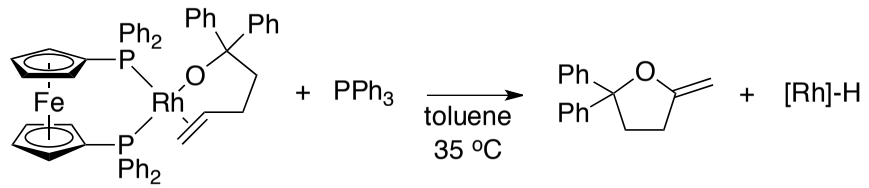

cprIII-h1-41c
cprIII-h1-41b
Ph2
P
Ph
Ph
O
O
Rh
P
Ph2
+ PPh3
7n
9.0 8.5 8.0 7.5 7.0 6.5 6.0 5.5 5.0 4.5 4.0 3.5 3.0 2.5 2.0 1.5 1.0 0.5 0.0
ppm


Ar2
P
Fe
Rh
O
Ph
Ph
P
Ar2
+ PPh3
toluene
35 °C
Ph
Ph
O
+ [Rh]-H

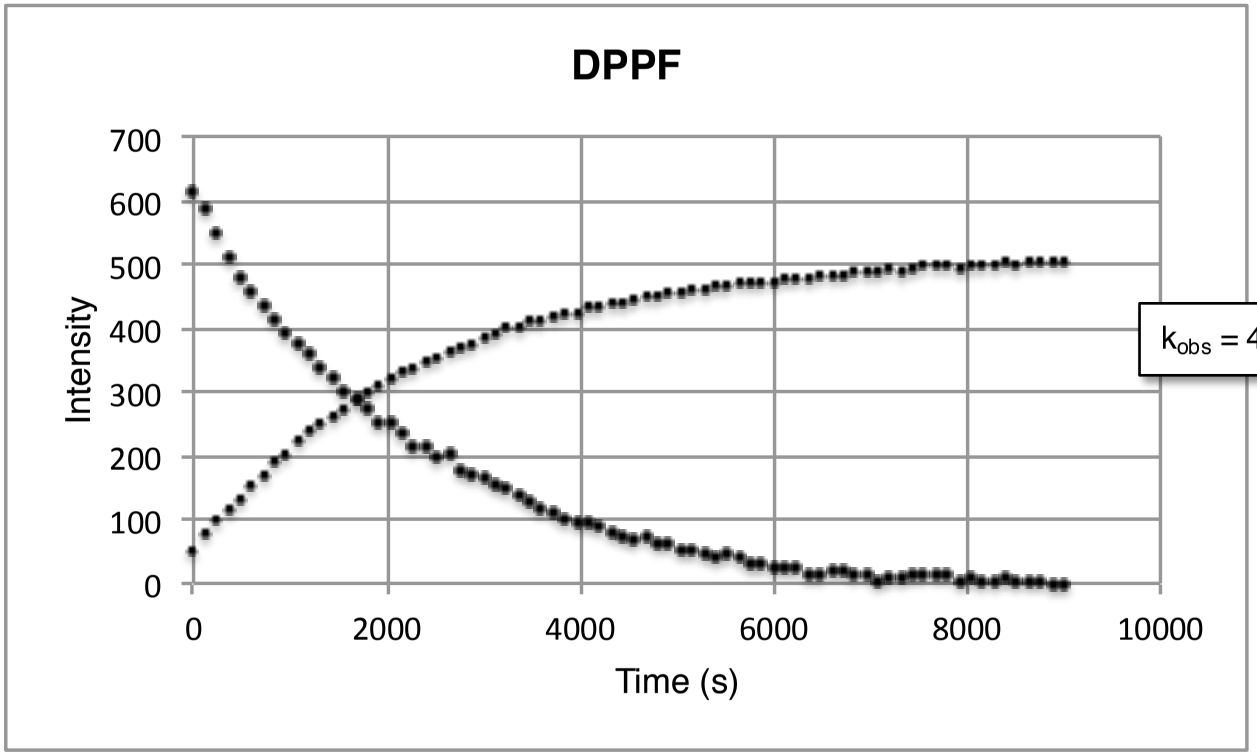
Ar = 
OMe

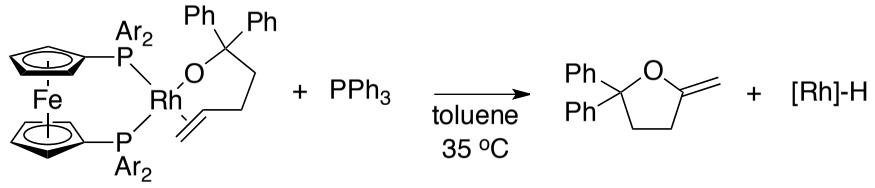
**7a**

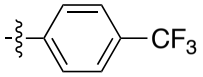

DArPF; Ar = p-MeO-C6H4
Intensity
450
400
350
300
250
200
150
100
50
0
0
2000
4000
6000
8000
10000
12000
Time (s)
kobs = 2.8 x 10-4 s-1


Ph2
P
Fe
Rh
O
Ph
Ph
P
Ph2
+ PPh3
toluene
35 °C
Ph
Ph
O
+ [Rh]-H

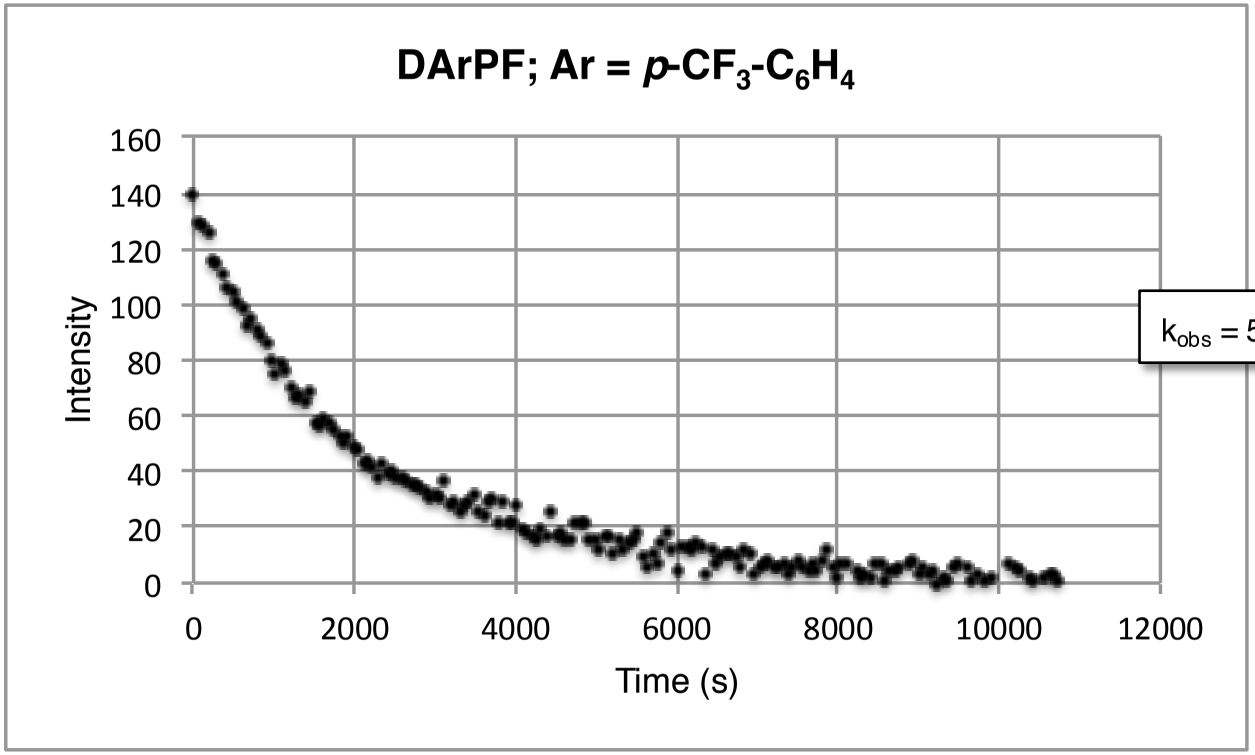
**7b**

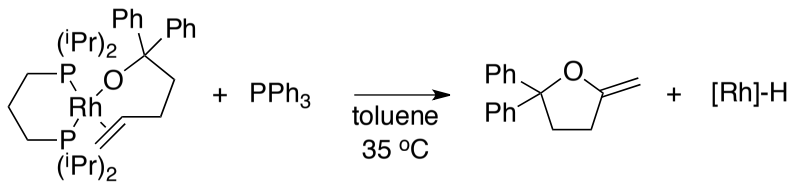

DPPF
Intensity
Time (s)
0
100
200
300
400
500
600
700
0
2000
4000
6000
8000
10000
kobs = 4.2 x 10-4 s-1


Ar2
P
Fe
Rh
O
Ph
Ph
P
Ar2
+ PPh3
toluene
35 °C
Ph
Ph
O
+ [Rh]-H

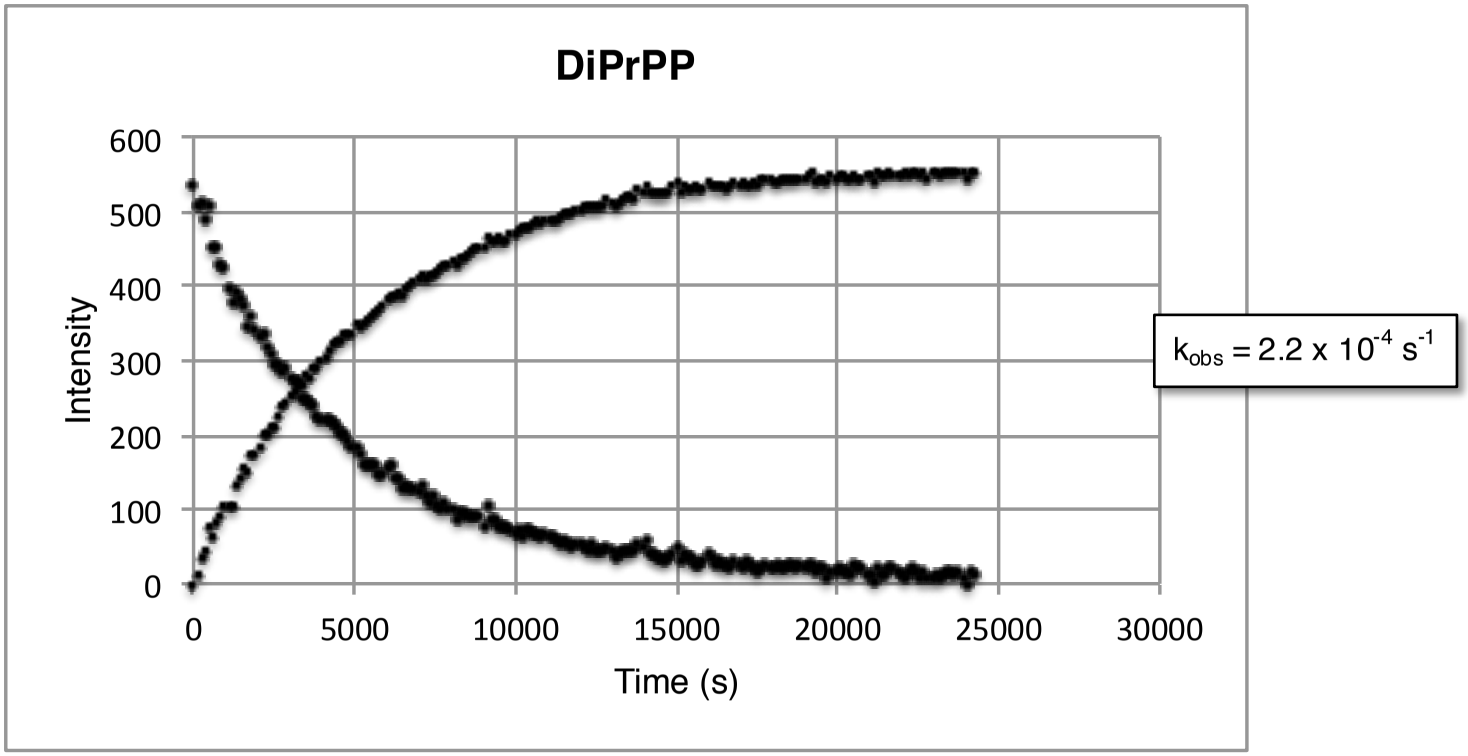
Ar = 
CF3

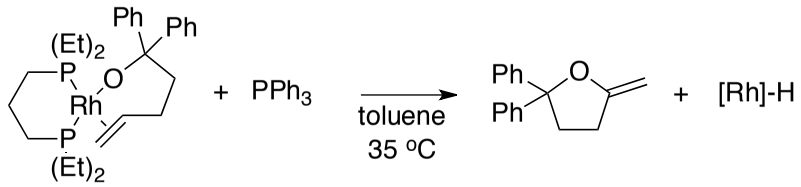
**7c**


DArPF; Ar = p-CF3-C6H4
Intensity
160
140
120
100
80
60
40
20
0
0
2000
4000
6000
8000
10000
12000
Time (s)
kobs = 5.6 x 10-4 s-1

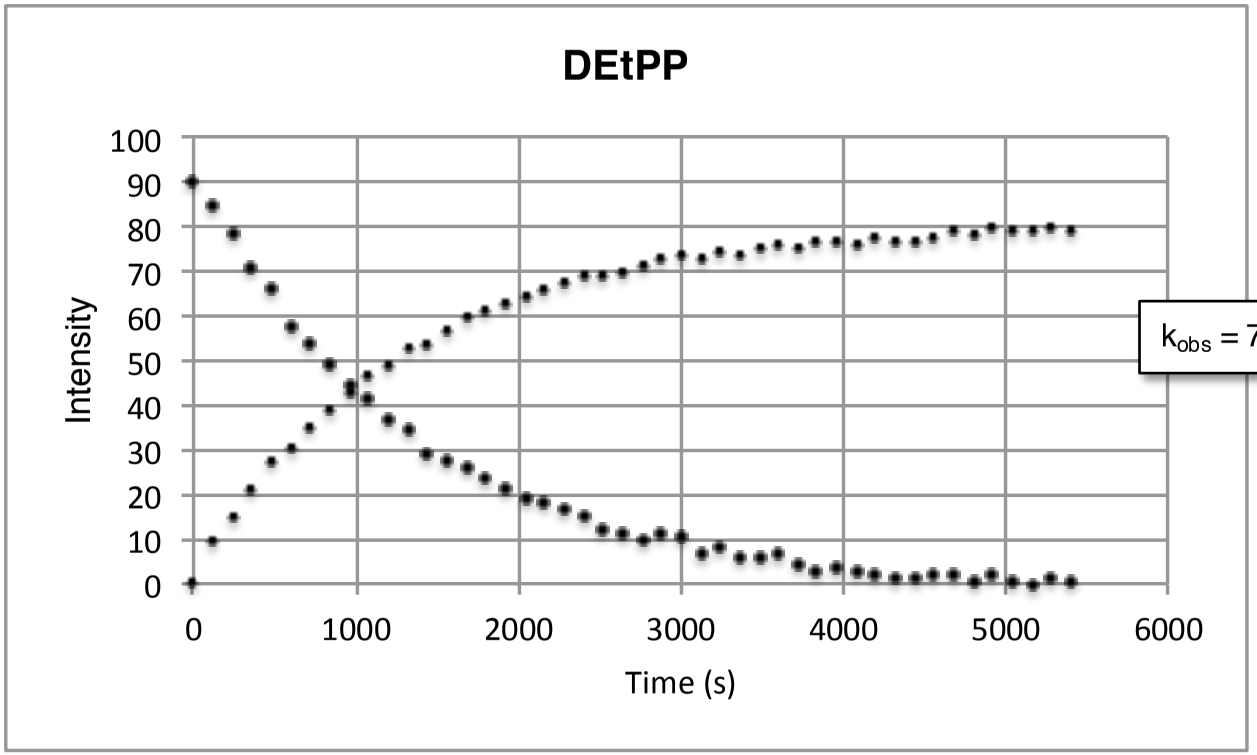

Ph
Ph
(iPr)2
P
O
Rh
P
(iPr)2
+ PPh3
toluene
35 °C
Ph
Ph
O
+ [Rh]-H

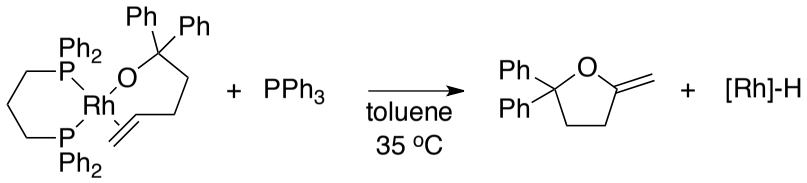
**7d**


DiPrPP
Intensity
600
500
400
300
200
100
0
0
5000
10000
15000
20000
25000
30000
Time (s)
$k_{obs}$ = 2.2 x $10^{-4}$ $s^{-1}$

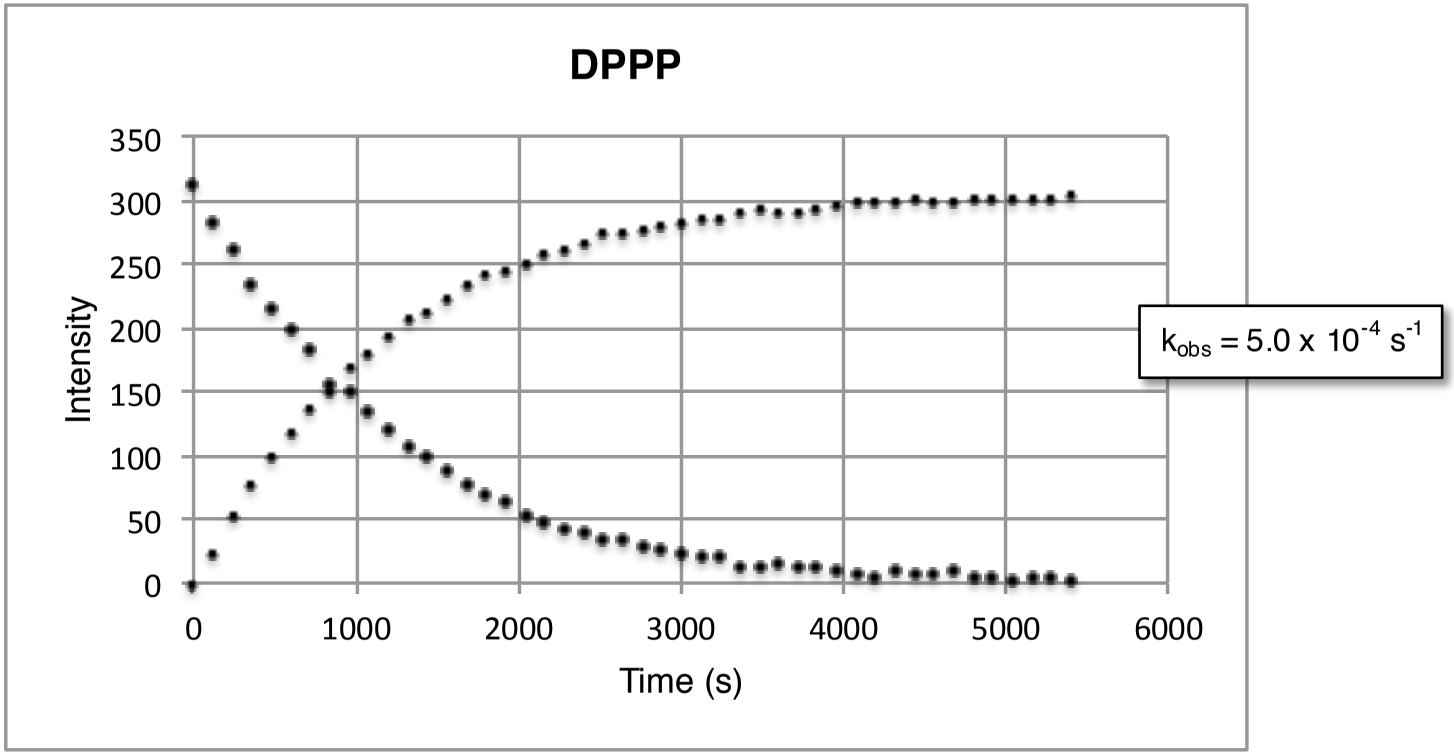

Ph
Ph
(Et)2
P
O
Rh
P
(Et)2
+ PPh3
toluene
35 °C
Ph
Ph
O
+ [Rh]-H

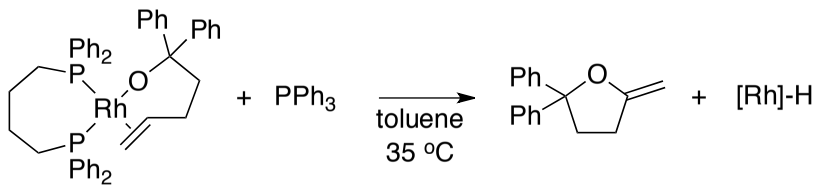
**7e**


DEtPP
Intensity
100
90
80
70
60
50
40
30
20
10
0
0
1000
2000
3000
4000
5000
6000
Time (s)
$k_{obs}$ = 7.5 x $10^{-4}$ $s^{-1}$

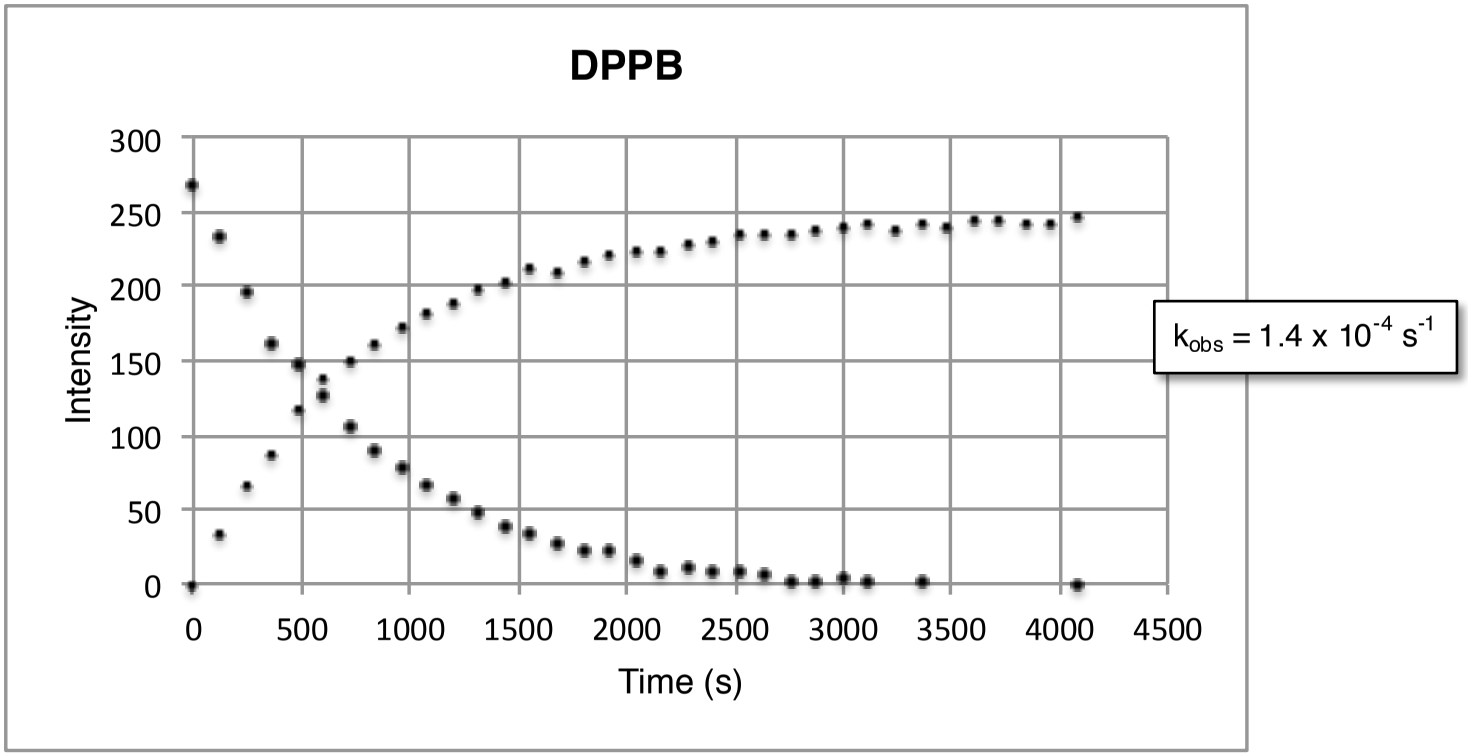

Ph
Ph
Ph2
P
O
Rh
P
Ph2
+ PPh3
toluene
35 °C
Ph
Ph
O
+ [Rh]-H

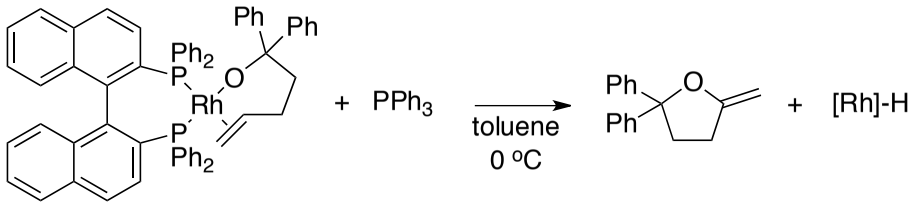
**7g**


DPPP
Intensity
350
300
250
200
150
100
50
0
0
1000
2000
3000
4000
5000
6000
Time (s)
$k_{obs} = 5.0 \times 10^{-4}\ s^{-1}$

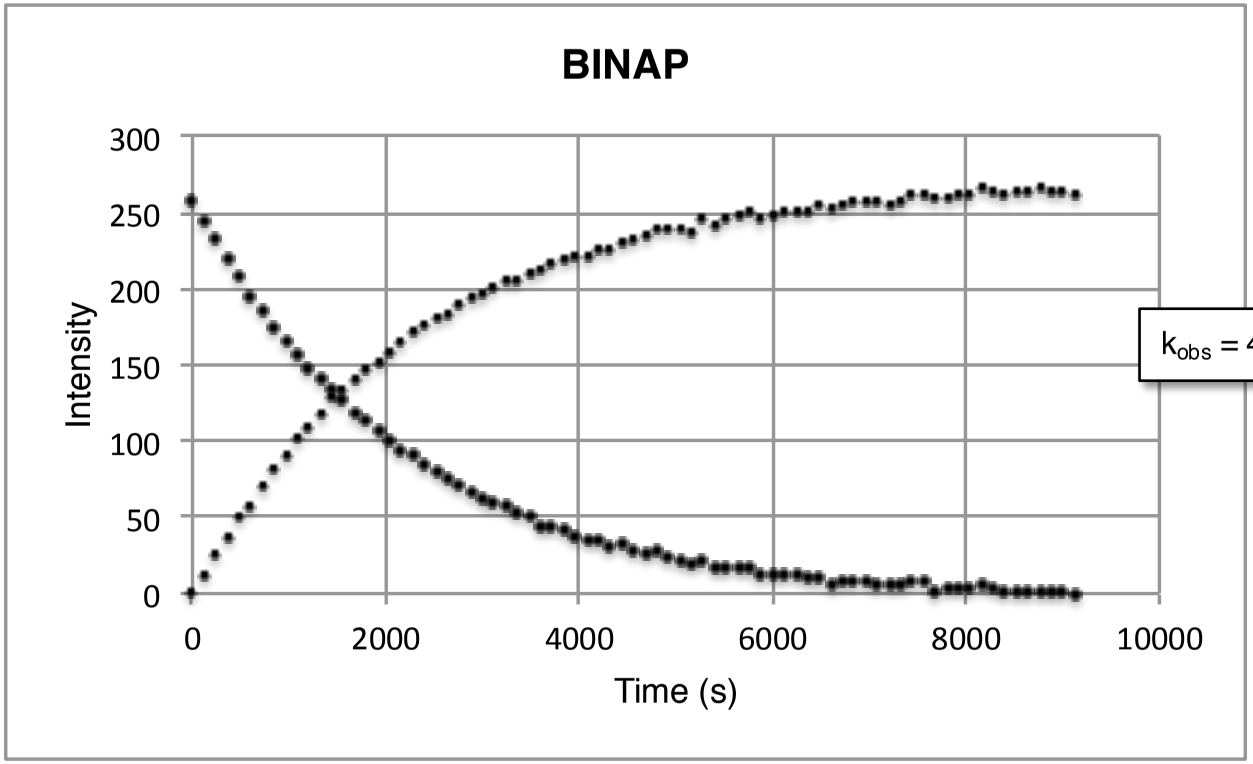

Ph
Ph
Ph2
P
O
Rh
P
Ph2
+ PPh3
toluene
35 °C
Ph
Ph
O
+ [Rh]-H

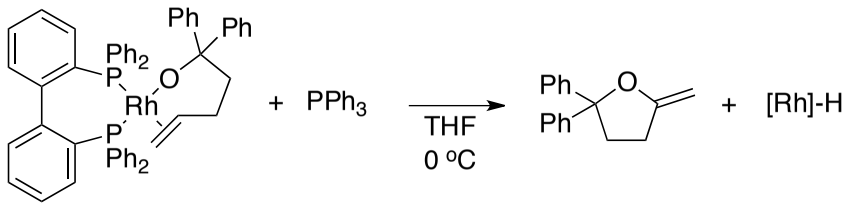
**7h**


DPPB
Intensity
300
250
200
150
100
50
0
0
500
1000
1500
2000
2500
3000
3500
4000
4500
Time (s)
$k_{obs}$ = 1.4 x $10^{-4}$ $s^{-1}$

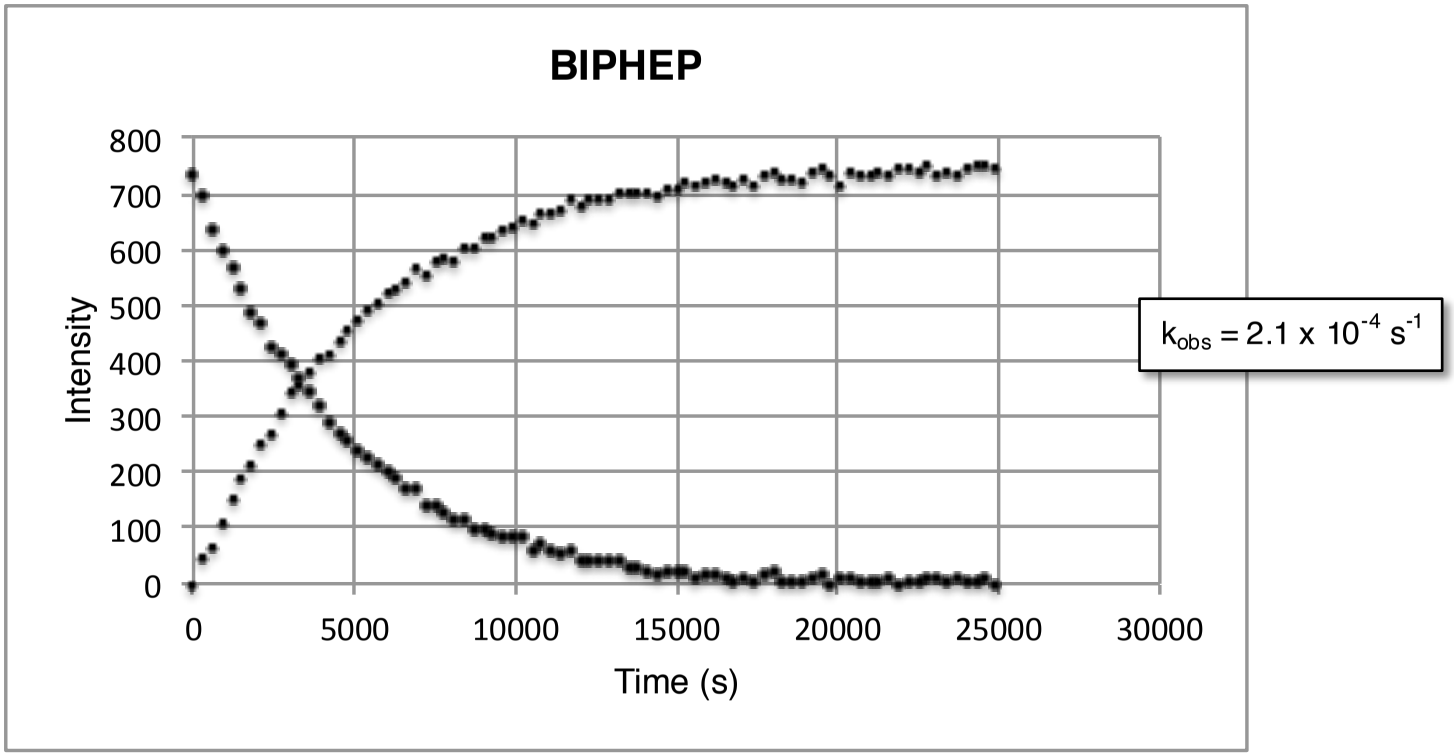

Ph
Ph
Ph2
P
O
Rh
P
Ph2
+ PPh3
toluene
0 °C
Ph
Ph
O
+ [Rh]-H

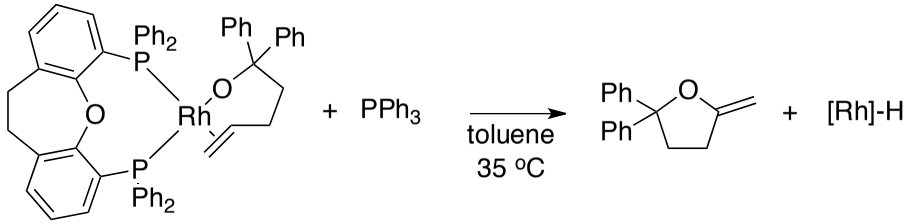
**7i**


BINAP
Intensity
300
250
200
150
100
50
0
0
2000
4000
6000
8000
10000
Time (s)
$k_{obs}$ = 4.5 x $10^{-4}$ $s^{-1}$

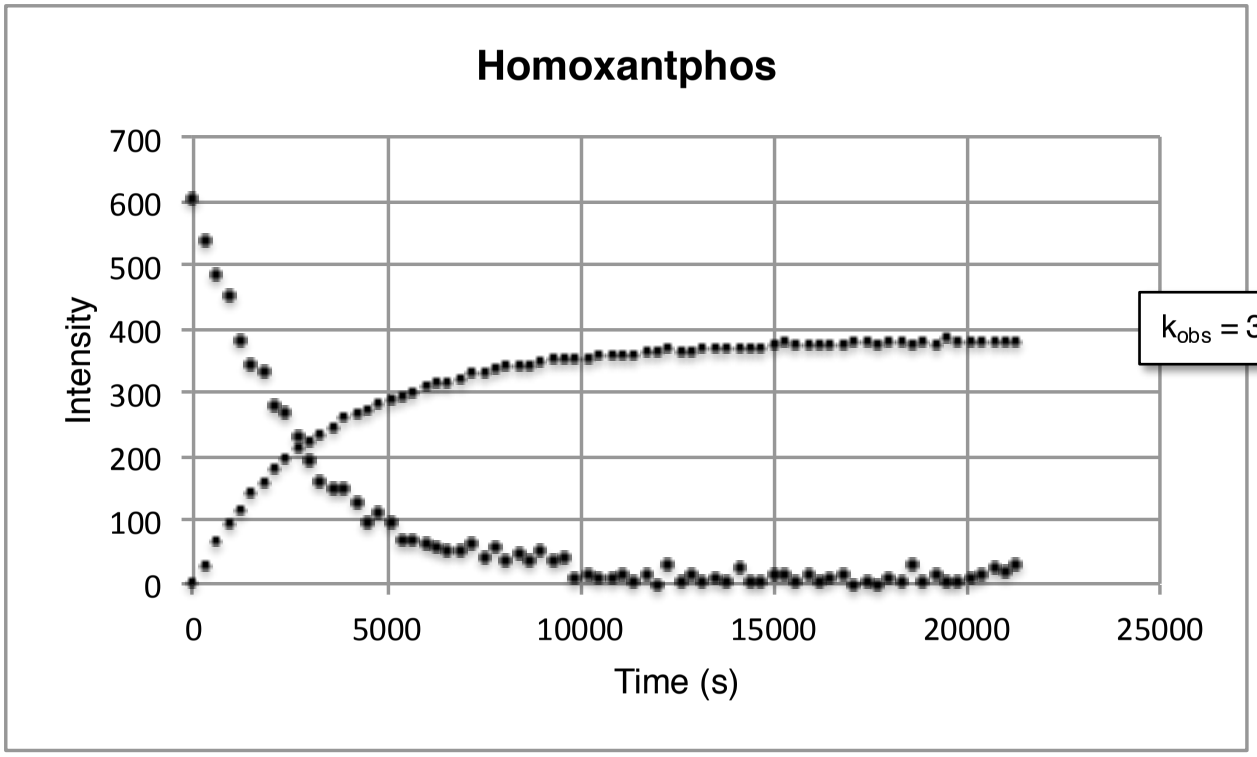

Ph
Ph
Ph2
P
O
Rh
P
Ph2
+ PPh3
THF
0 °C
Ph
O
Ph
+ [Rh]-H

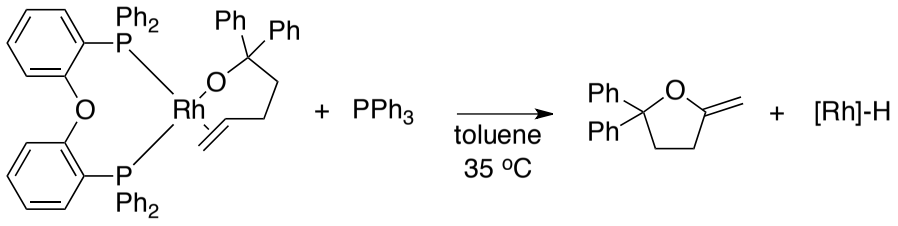
**7j**


BIPHEP
Intensity
800
700
600
500
400
300
200
100
0
0
5000
10000
15000
20000
25000
30000
Time (s)
$k_{obs}$ = 2.1 x $10^{-4}$ $s^{-1}$

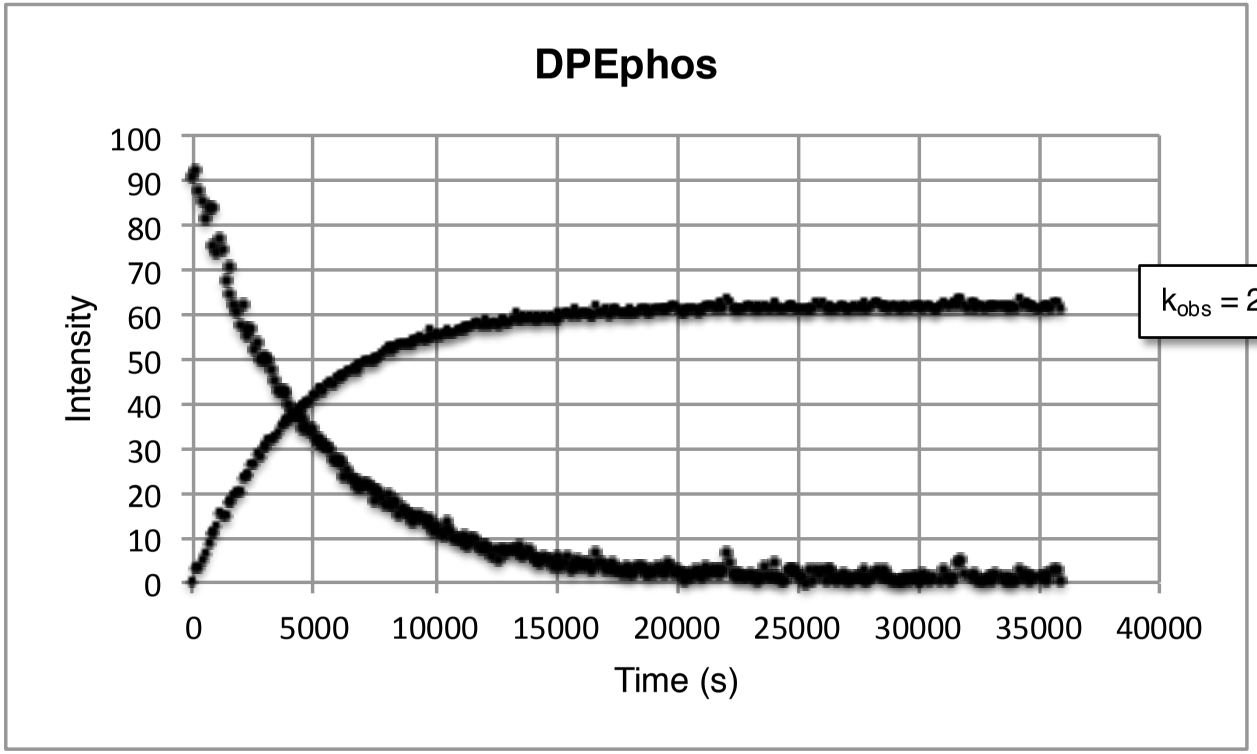

Ph2
P
Ph
Ph
O
Rh
O
P
Ph2
+ PPh3
toluene
35 °C
Ph
Ph
O
+ [Rh]-H

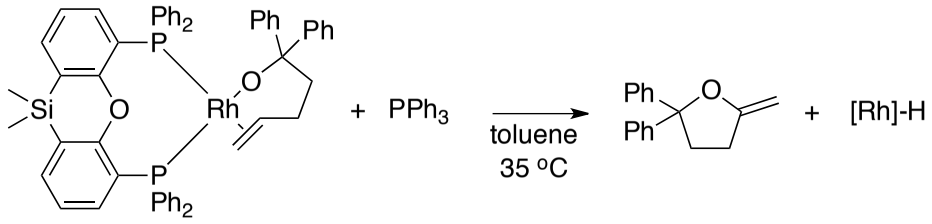
**7k**


Homoxantphos
Intensity
700
600
500
400
300
200
100
0
0
5000
10000
15000
20000
25000
Time (s)
$k_{obs} = 3.2 \times 10^{-4}\ s^{-1}$

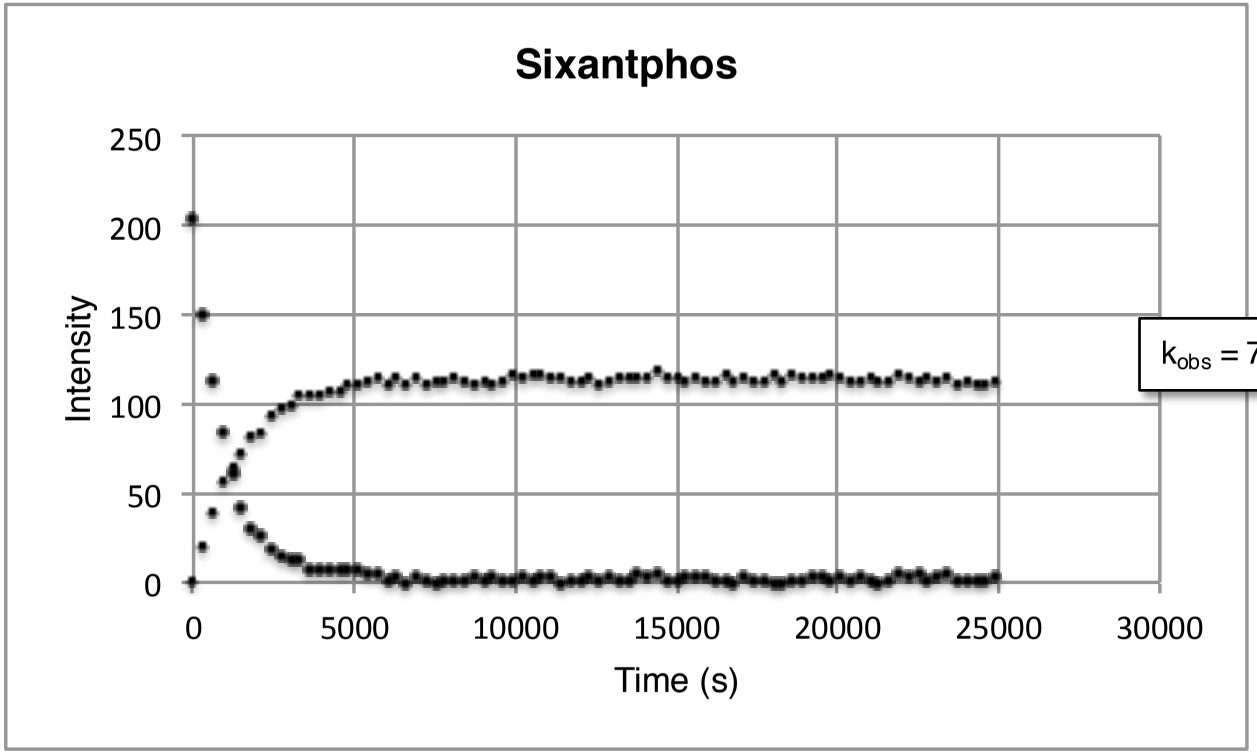

Ph2
P
Ph
Ph
O
O
Rh
P
Ph2
+ PPh3
toluene
35 °C
Ph
Ph
O
+ [Rh]-H

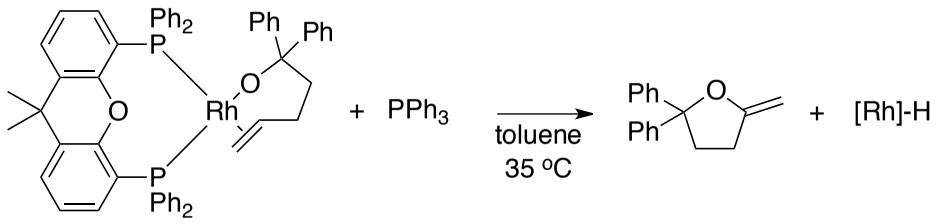
**7l**


DPEphos
Intensity
100
90
80
70
60
50
40
30
20
10
0
0
5000
10000
15000
20000
25000
30000
35000
40000
Time (s)
kobs = 2.2 x 10-4 s-1

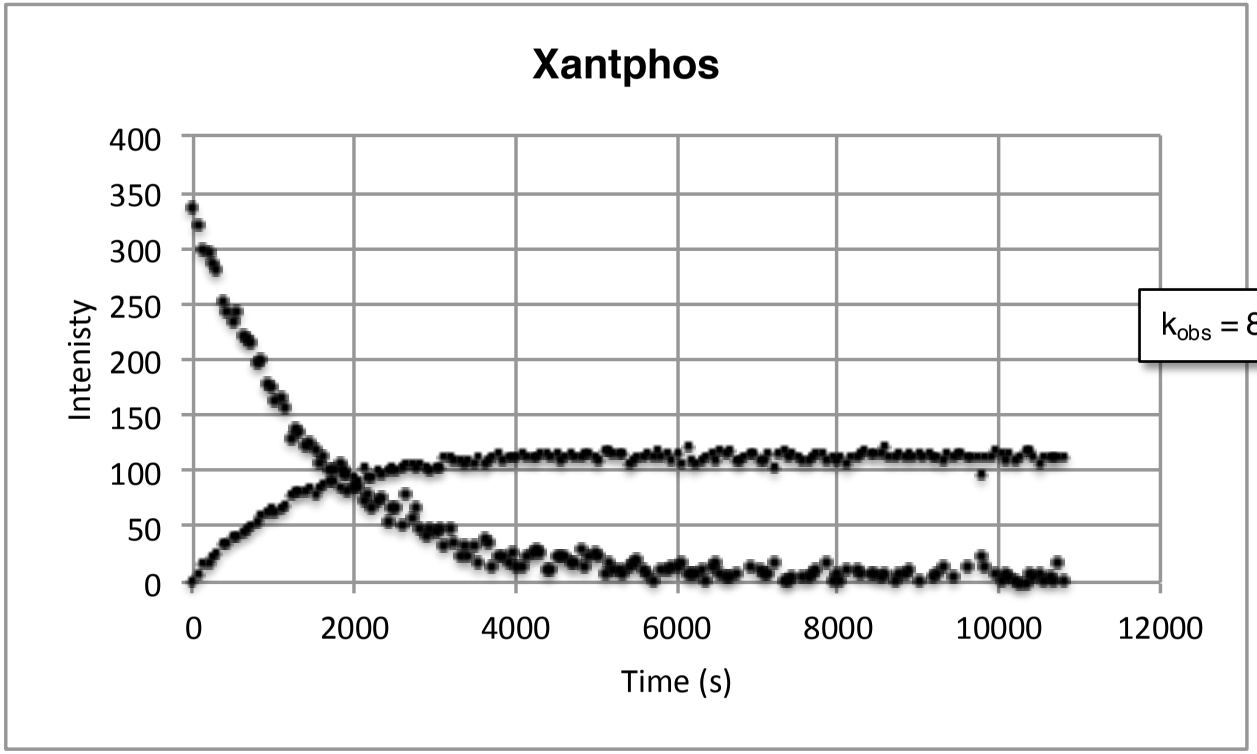

Ph2
P
Ph
Ph
O
Si
O
Rh
P
Ph2
+ PPh3
toluene
35 °C
Ph
Ph
O
+ [Rh]-H

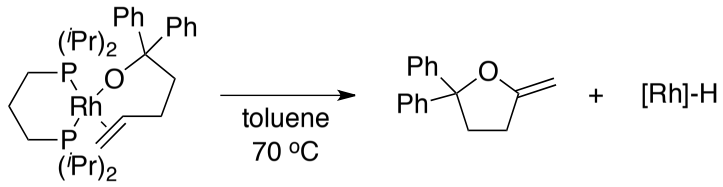
**7m**


Sixantphos
250
200
150
100
50
0
Intensity
0
5000
10000
15000
20000
25000
30000
Time (s)
$k_{obs}$ = 7.2 x $10^{-4}$ $s^{-1}$

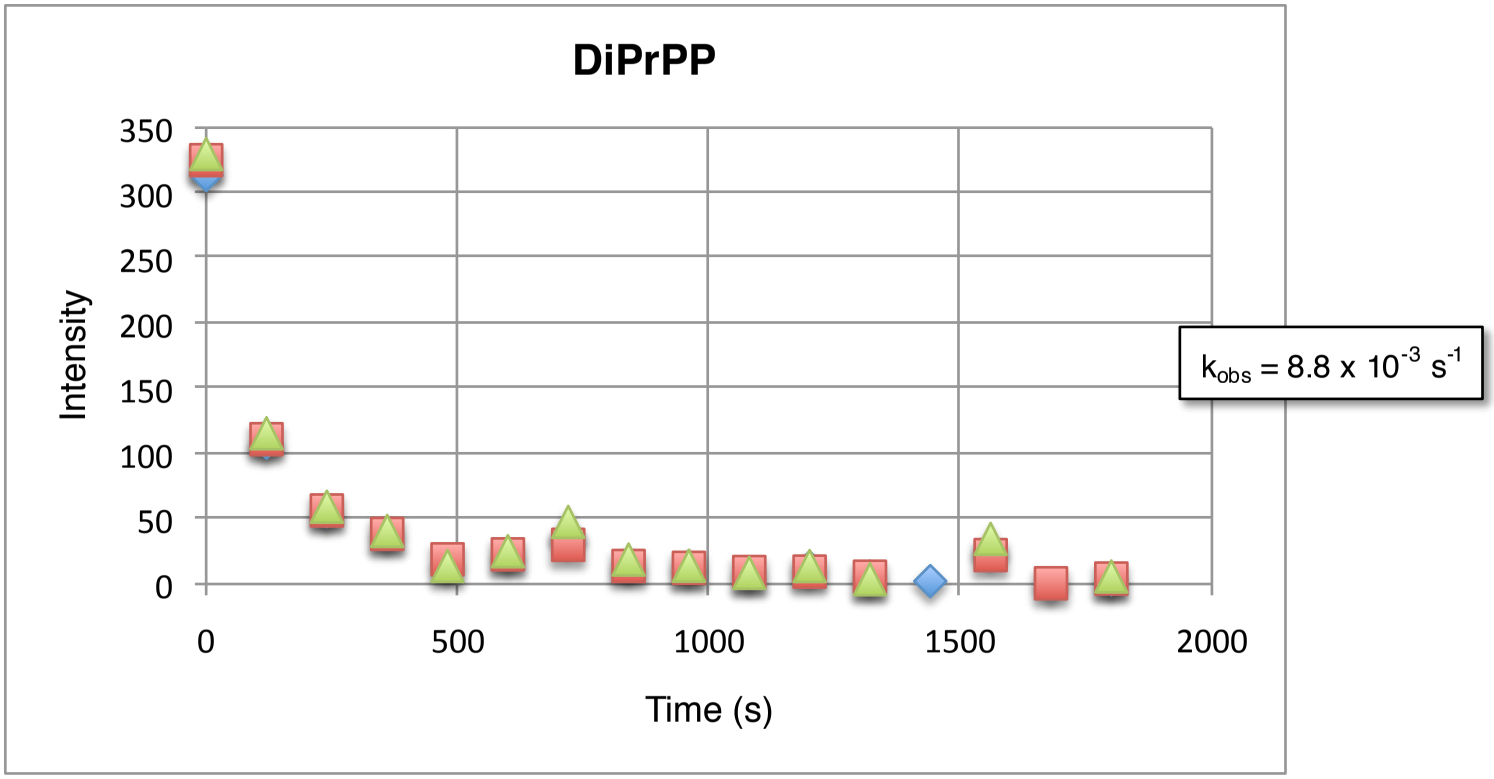

Ph2
P
Ph
Ph
O
Rh
O
P
Ph2
+ PPh3
toluene
35 °C
Ph
Ph
O
+ [Rh]-H

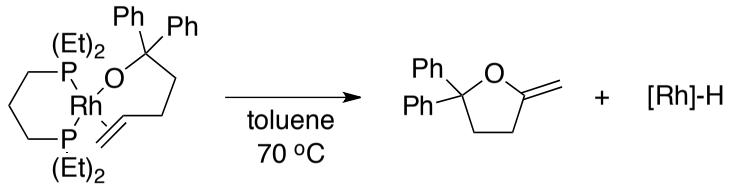
**7n**


Xantphos
Intenisty
400
350
300
250
200
150
100
50
0
0
2000
4000
6000
8000
10000
12000
Time (s)
$k_{obs}$ = 8.0 x $10^{-4}$ $s^{-1}$

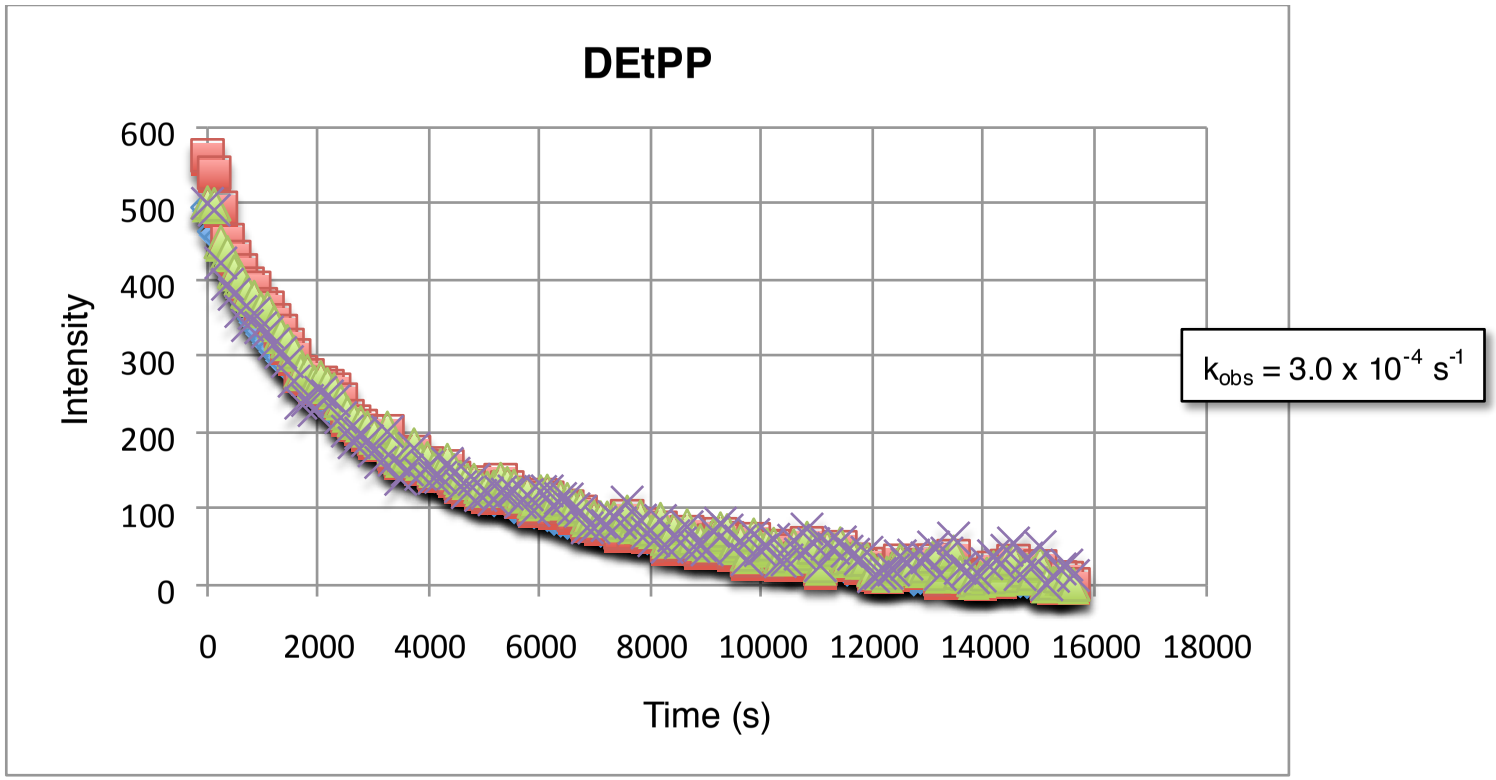

Ph
Ph
(iPr)2
P
O
Rh
P
(iPr)2
toluene
70 °C
Ph
Ph
O
+
[Rh]-H

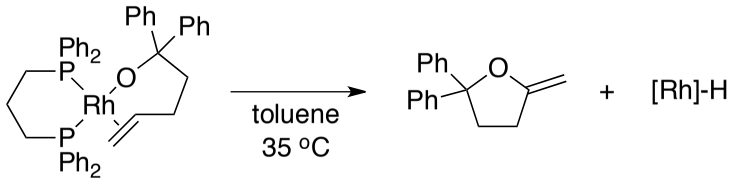
**7d**


DiPrPP
Intensity
350
300
250
200
150
100
50
0
0
500
1000
1500
2000
Time (s)
$k_{obs}$ = 8.8 x $10^{-3}$ $s^{-1}$

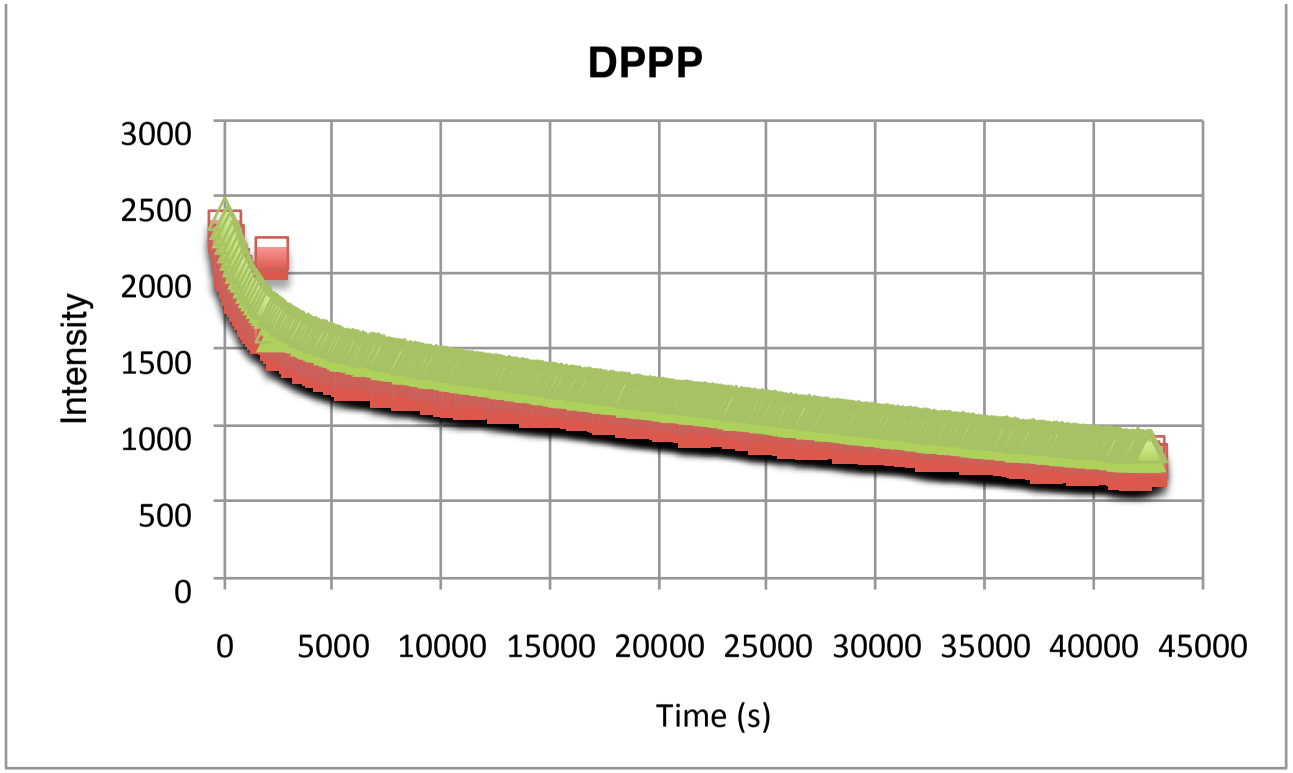

Ph
Ph
(Et)2
P
O
Rh
P
(Et)2
toluene
70 °C
Ph
Ph
O
+
[Rh]-H

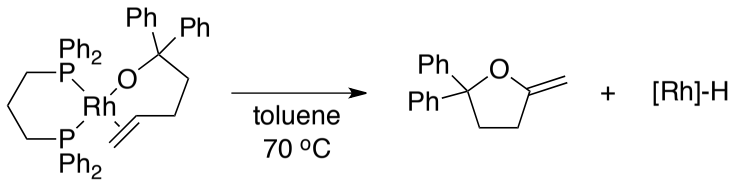
**7e**


DEtPP
600
500
400
300
200
100
0
Intensity
0
2000
4000
6000
8000
10000
12000
14000
16000
18000
Time (s)
$k_{obs}$ = 3.0 x $10^{-4}$ $s^{-1}$

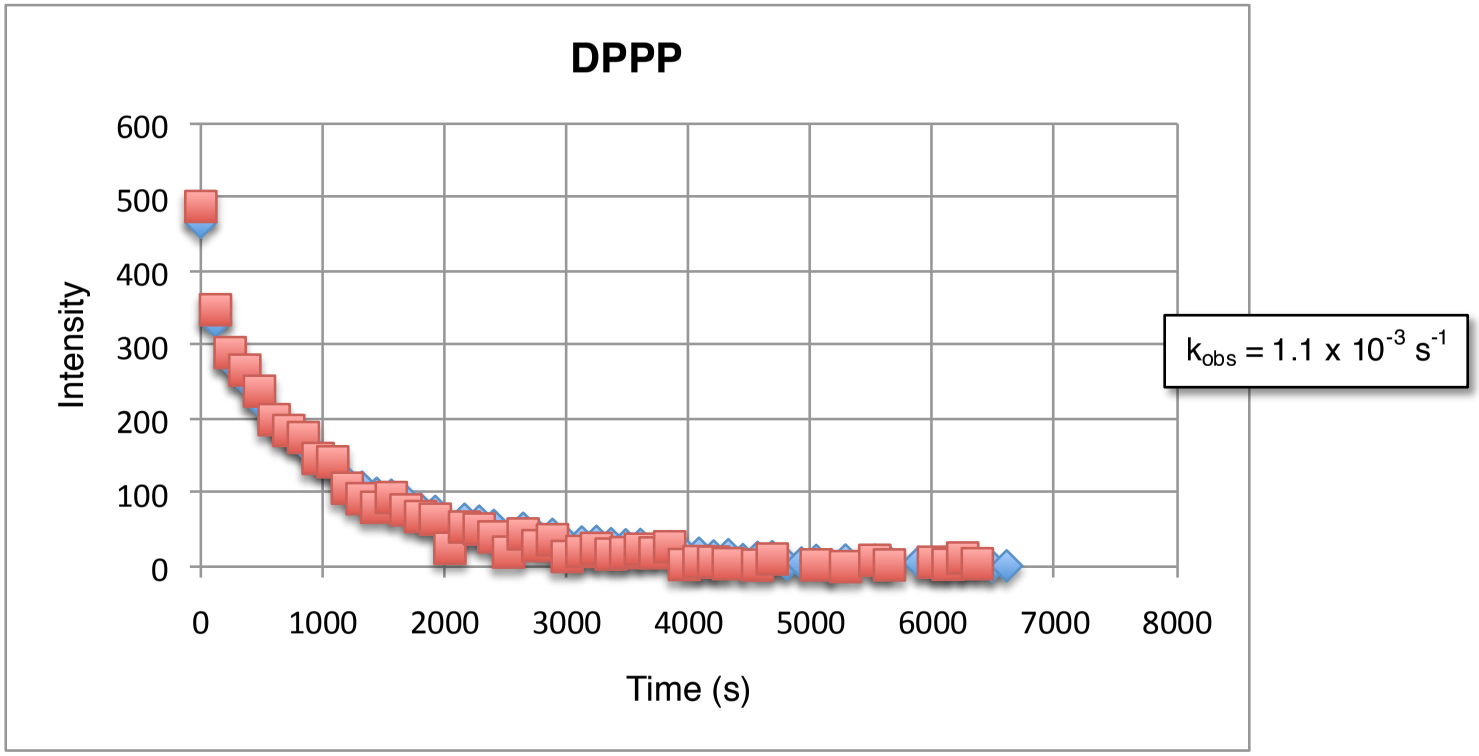

Ph
Ph
Ph2
P
O
Rh
P
Ph2
toluene
35 °C
Ph
Ph
O
+
[Rh]-H

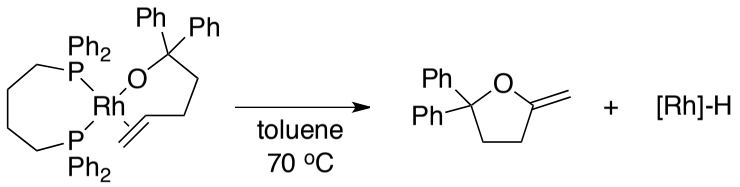
**7g**


DPPP
Intensity
3000
2500
2000
1500
1000
500
0
0
5000
10000
15000
20000
25000
30000
35000
40000
45000
Time (s)

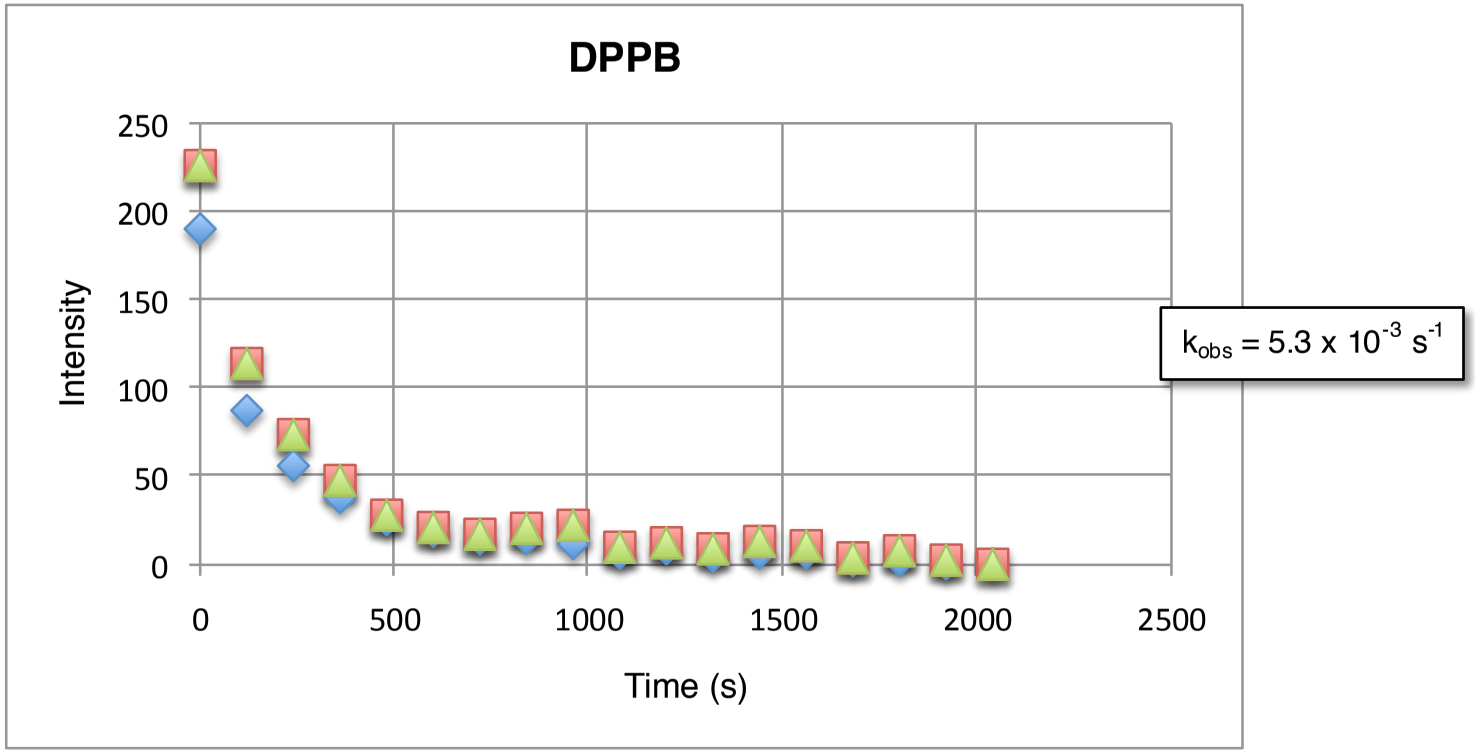

Ph
Ph
Ph2
P
O
Rh
P
Ph2
toluene
70 °C
Ph
Ph
O
+
[Rh]-H

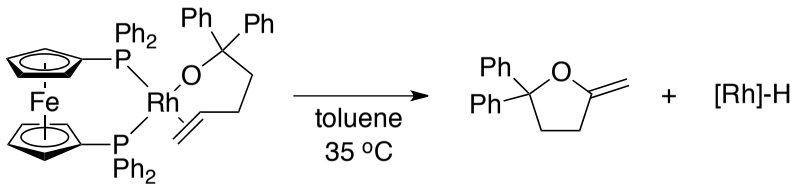
**7g**


DPPP
Intensity
600
500
400
300
200
100
0
0
1000
2000
3000
4000
5000
6000
7000
8000
Time (s)
$k_{obs}$ = 1.1 x $10^{-3}$ $s^{-1}$

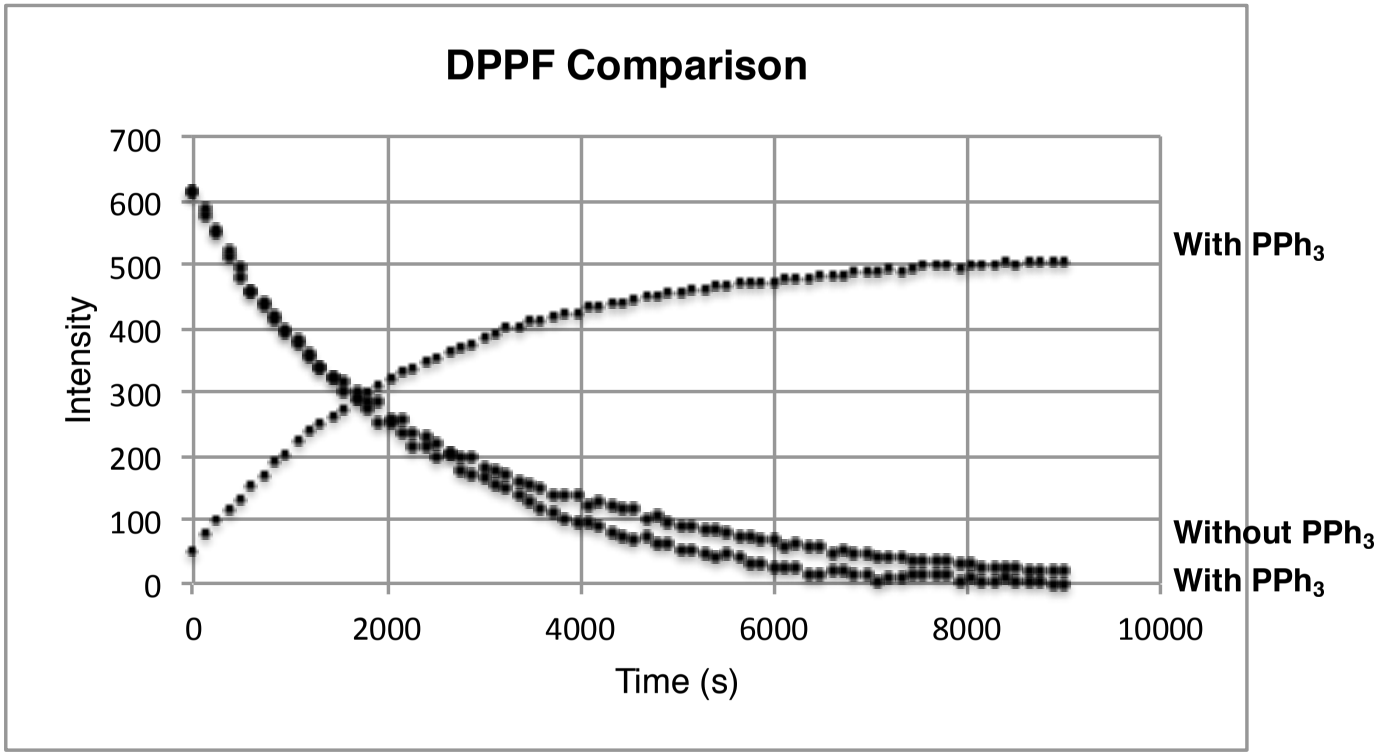

Ph
Ph
Ph2
P
O
Rh
P
Ph2
toluene
70 °C
Ph
Ph
O
+
[Rh]-H

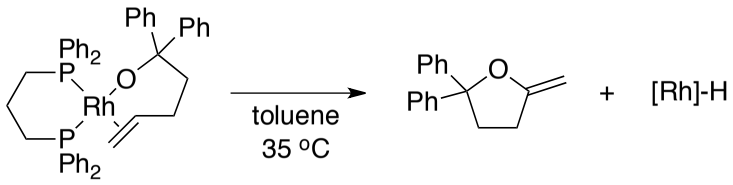
**7h**


DPPB
Intensity
250
200
150
100
50
0
0
500
1000
1500
2000
2500
Time (s)
$k_{obs}$ = 5.3 x $10^{-3}$ $s^{-1}$

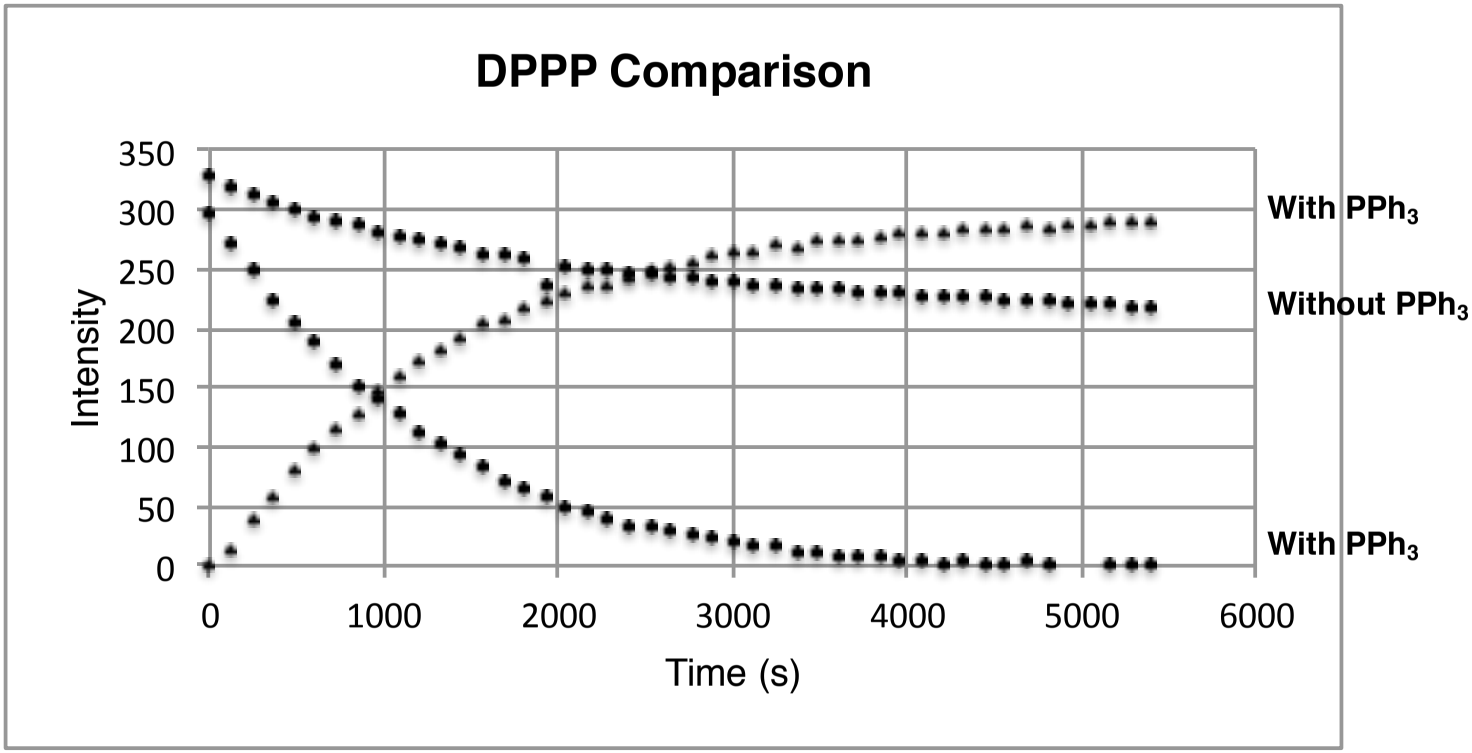

Ph2
P
Fe
Rh
O
Ph
Ph
P
Ph2
toluene
35 °C
Ph
Ph
O
+
[Rh]-H

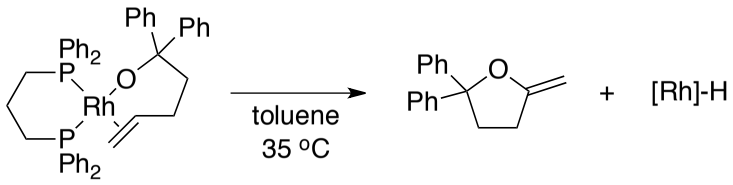
**7b**


DPPF Comparison
Intensity
700
600
500
400
300
200
100
0
0
2000
4000
6000
8000
10000
Time (s)
With PPh3
Without PPh3
With PPh3

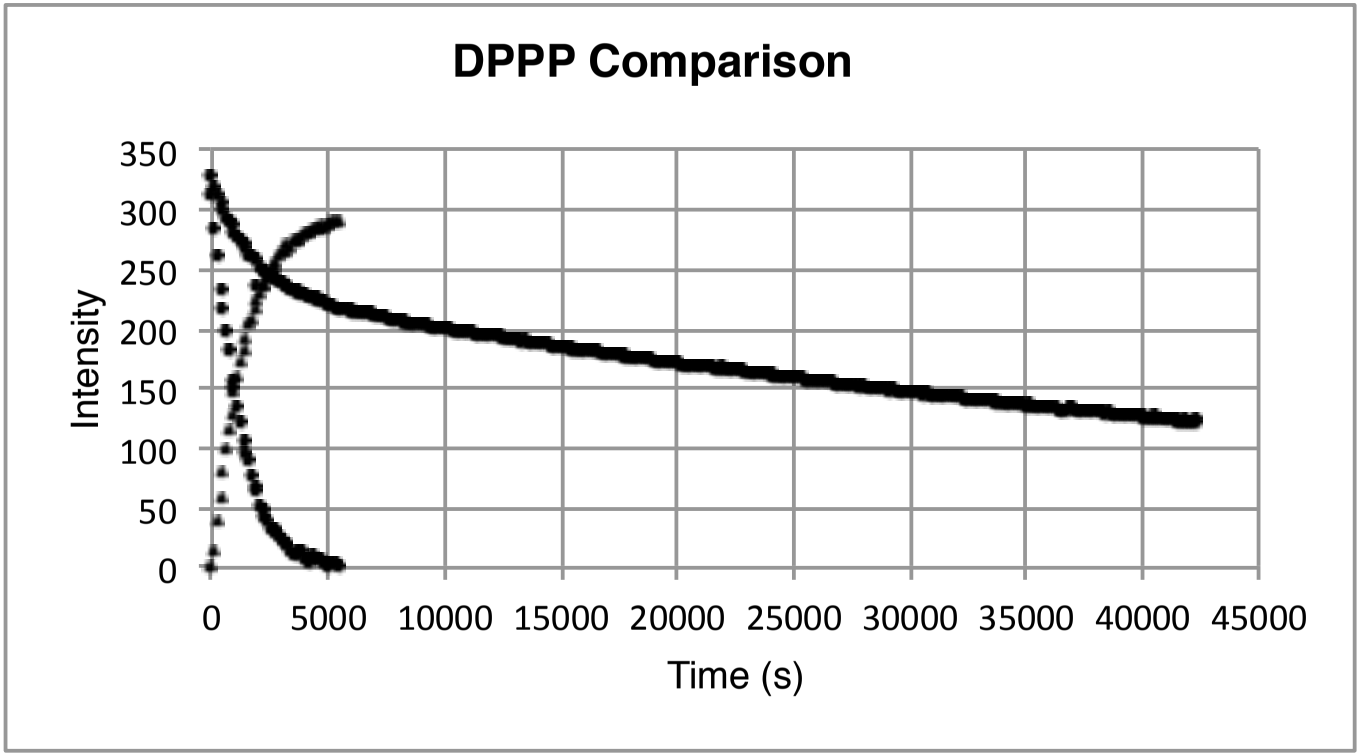

Ph
Ph
Ph2
P
O
Rh
P
Ph2
toluene
35 °C
Ph
Ph
O
+
[Rh]-H

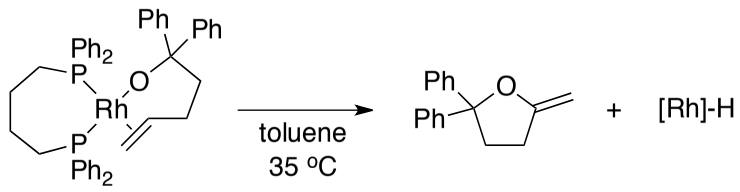
**7g**


DPPP Comparison
Intensity
350
300
250
200
150
100
50
0
0
1000
2000
3000
4000
5000
6000
Time (s)
With PPh3
Without PPh3
With PPh3

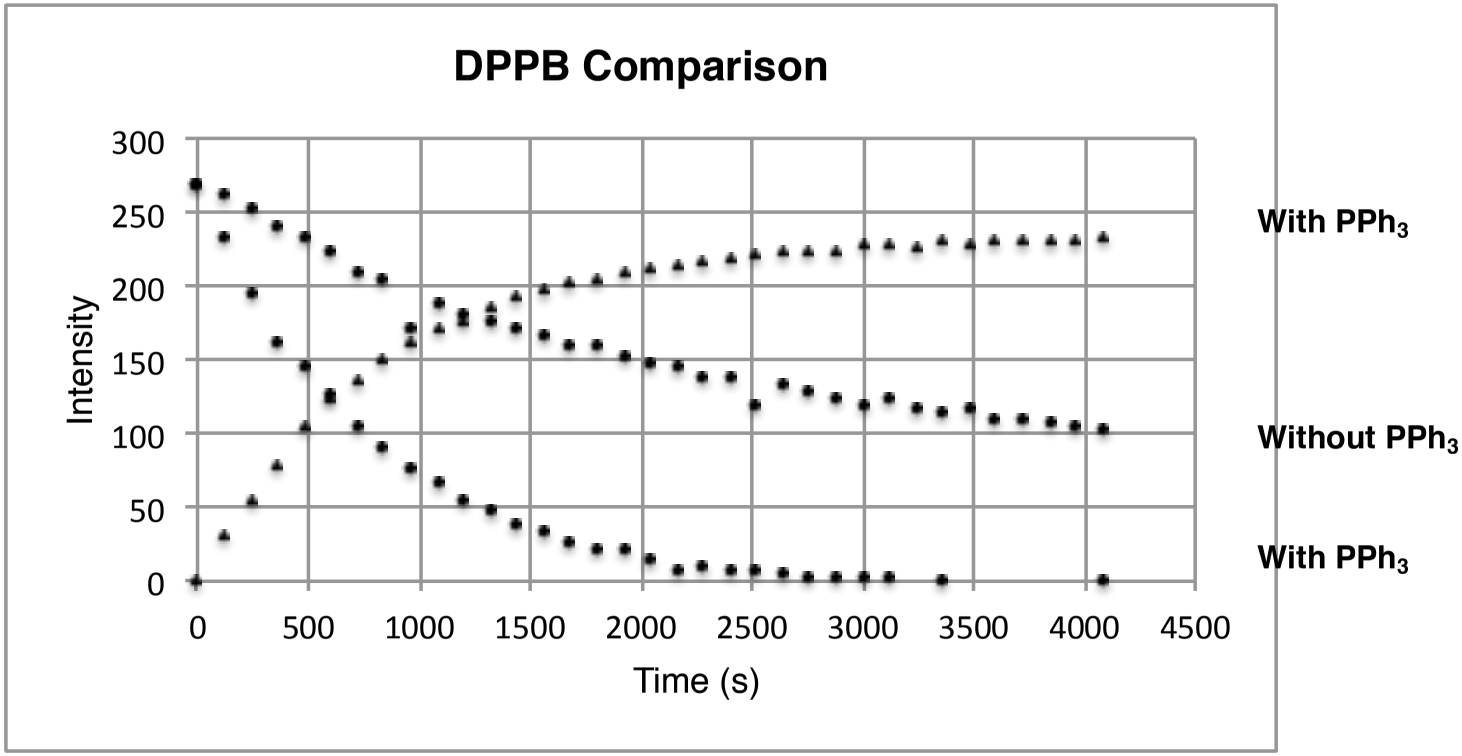

Ph
Ph
Ph2
P
O
Rh
P
Ph2
toluene
35 °C
Ph
Ph
O
+
[Rh]-H

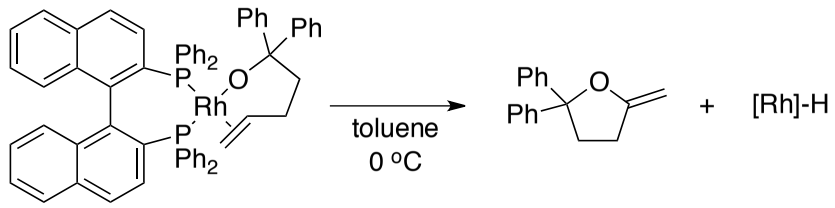
**7g**


DPPP Comparison
Intensity
350
300
250
200
150
100
50
0
0
5000
10000
15000
20000
25000
30000
35000
40000
45000
Time (s)

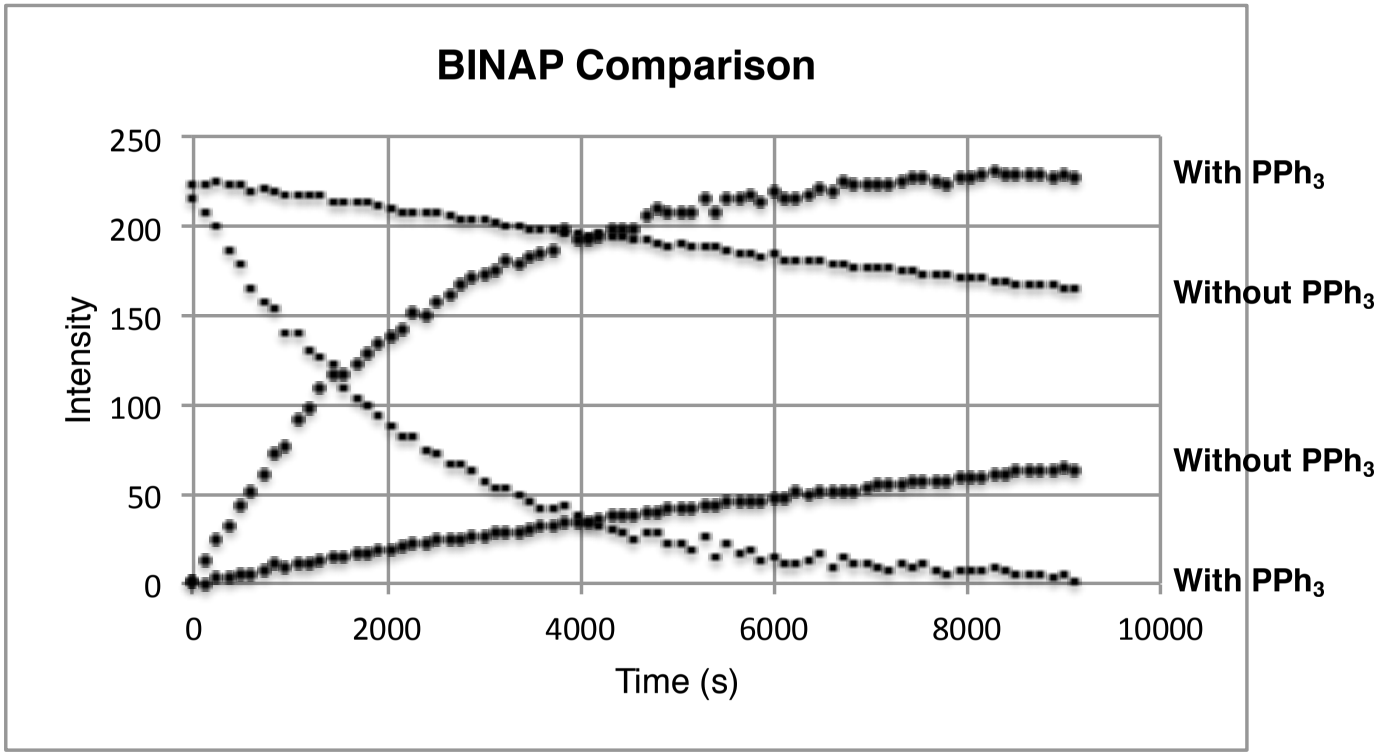

Ph
Ph
Ph2
P
O
Rh
P
Ph2
toluene
35 °C
Ph
Ph
O
+
[Rh]-H

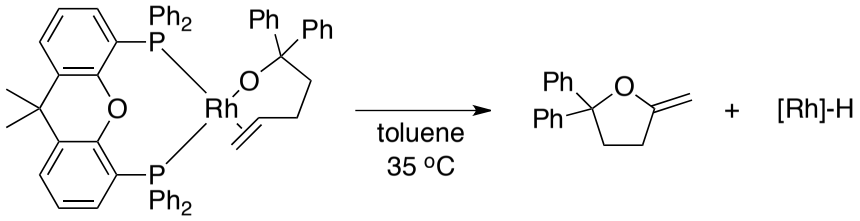
**7h**


DPPB Comparison
Intensity
300
250
200
150
100
50
0
0
500
1000
1500
2000
2500
3000
3500
4000
4500
Time (s)
With PPh3
Without PPh3
With PPh3

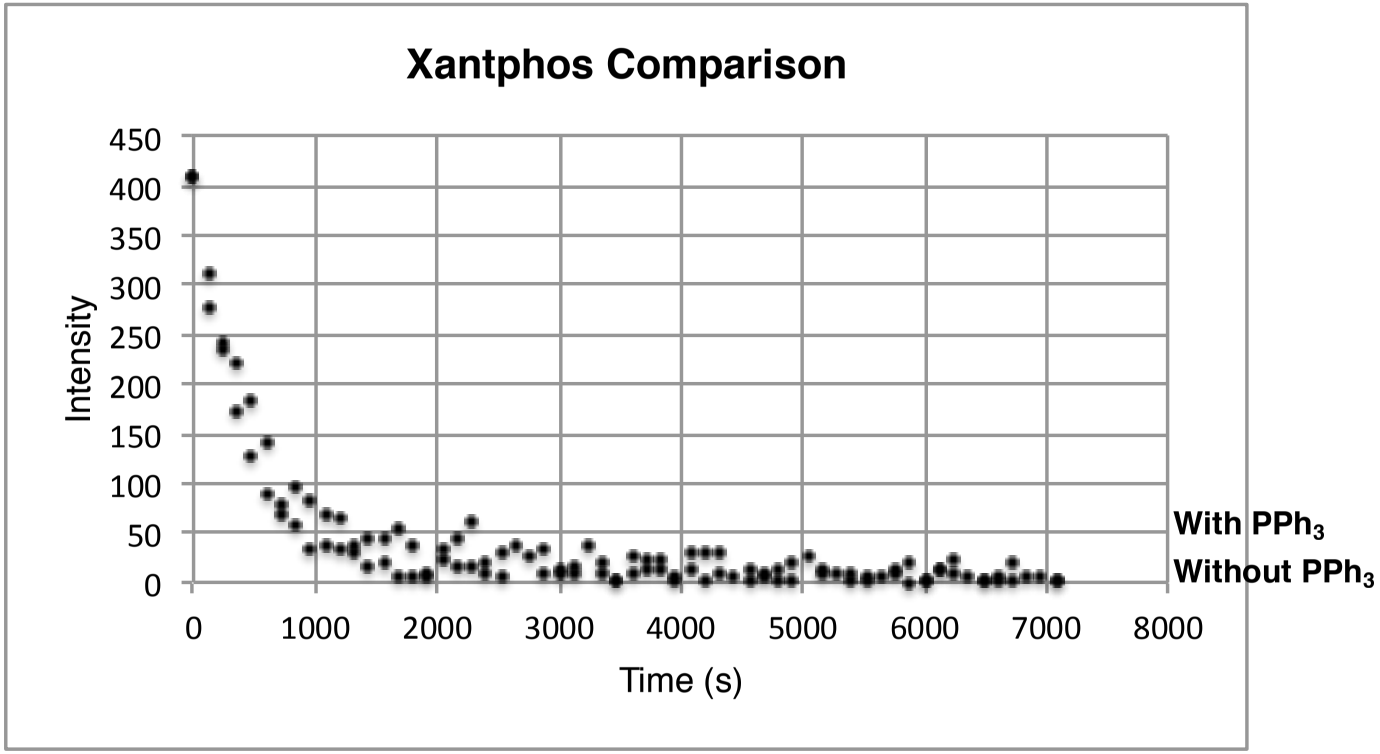

Ph
Ph
Ph2
P
O
Rh
P
Ph2
toluene
0 °C
Ph
Ph
O
+
[Rh]-H

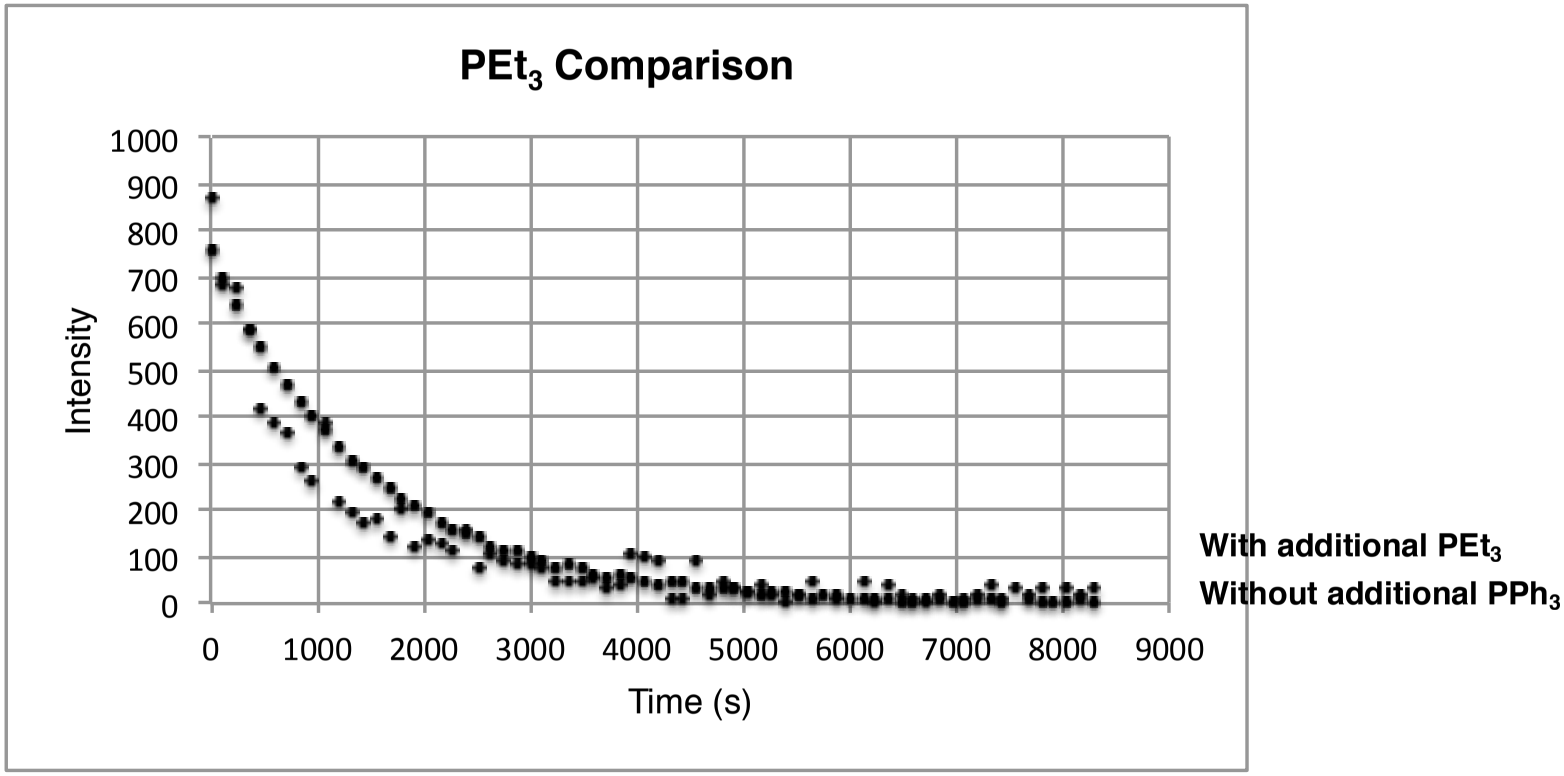
**7i**

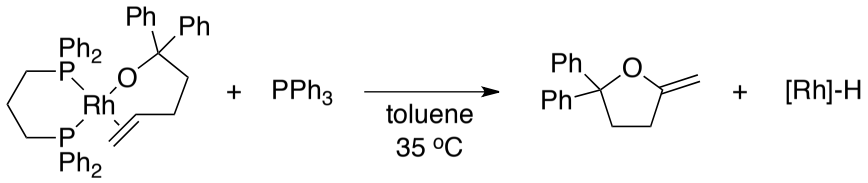

BINAP Comparison
250
200
150
100
50
0
Intensity
0
2000
4000
6000
8000
10000
Time (s)
With PPh3
Without PPh3
Without PPh3
With PPh3


Ph2
P
Ph
Ph
O
Rh
O
P
Ph2
toluene
35 °C
Ph
Ph
O
+
[Rh]-H

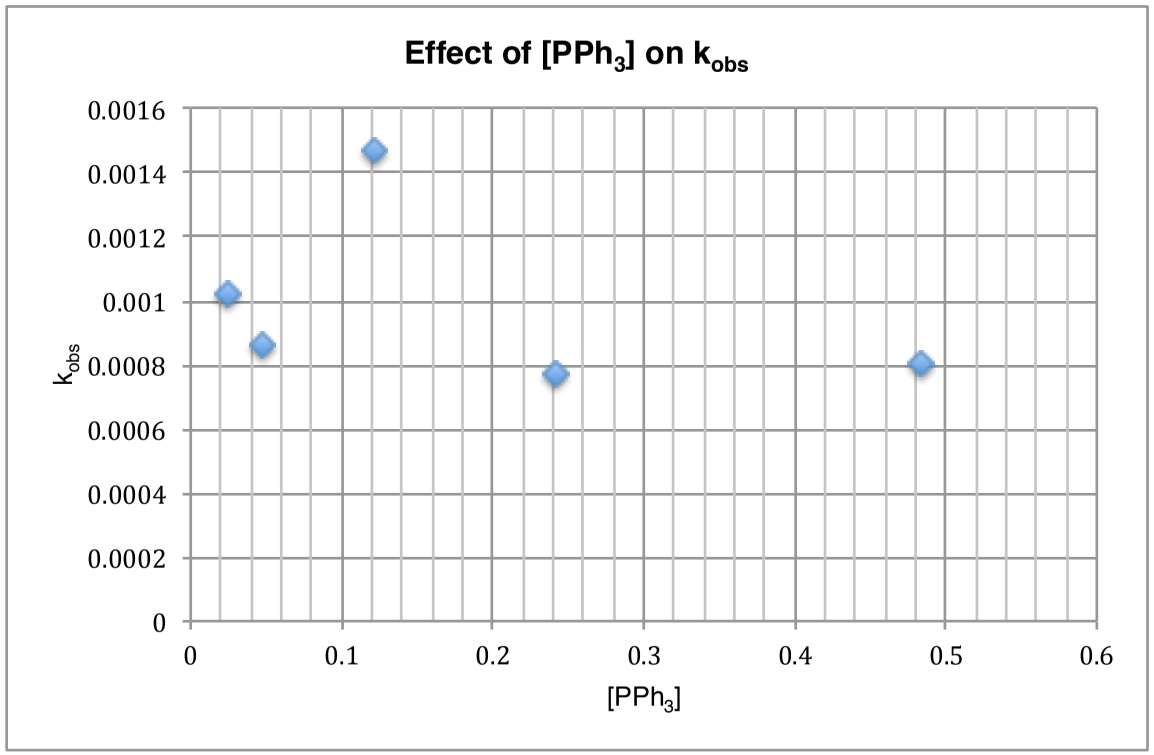
**7n**

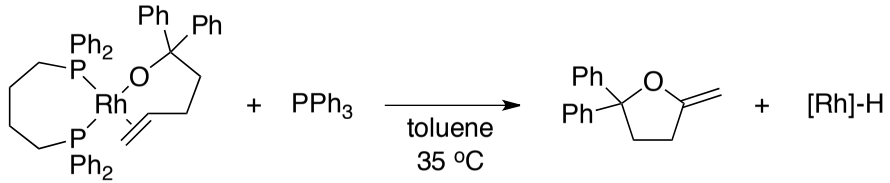

Xantphos Comparison
Intensity
450
400
350
300
250
200
150
100
50
0
0
1000
2000
3000
4000
5000
6000
7000
8000
Time (s)
With PPh3
Without PPh3


PEt3 Comparison
Intensity
1000
900
800
700
600
500
400
300
200
100
0
0
1000
2000
3000
4000
5000
6000
7000
8000
9000
Time (s)
With additional PEt3
Without additional PPh3

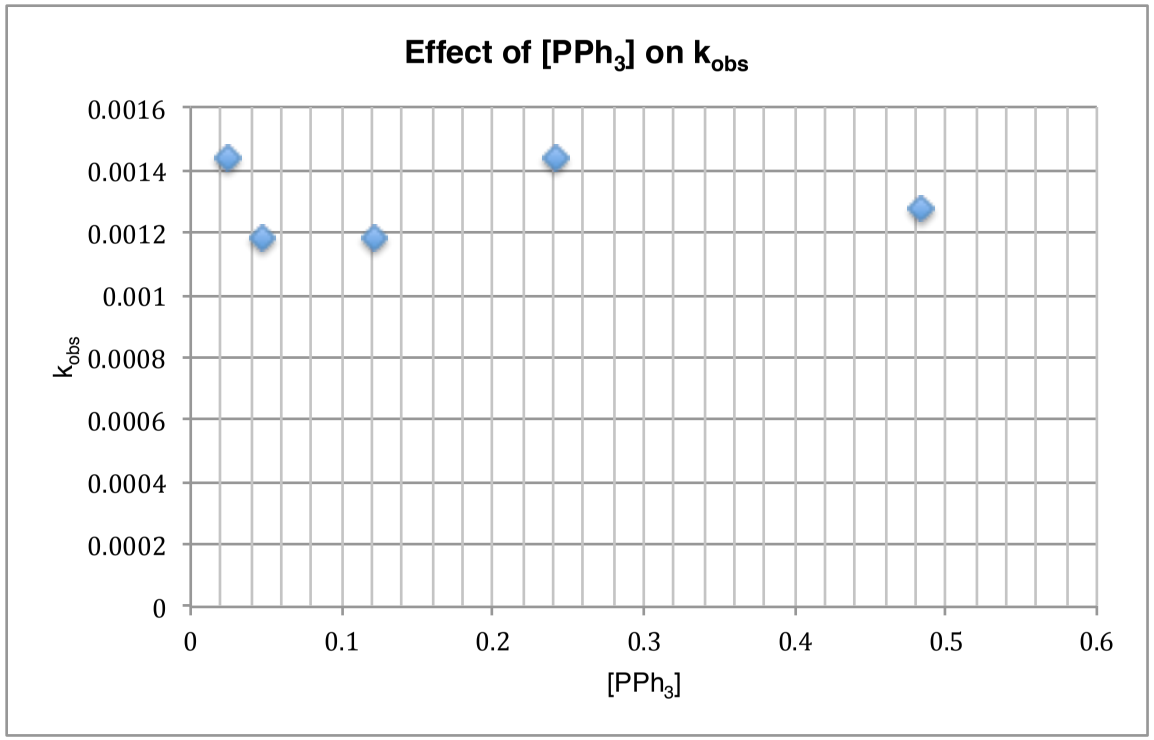

Ph
Ph
Ph2
P
O
Rh
P
Ph2
+ PPh3
toluene
35 °C
Ph
O
Ph
+ [Rh]-H

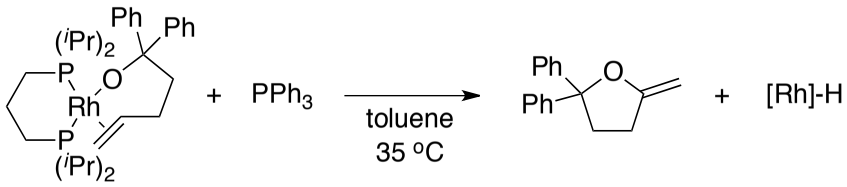
**7g**


Effect of [PPh3] on kobs
0.0016
0.0014
0.0012
0.001
0.0008
0.0006
0.0004
0.0002
0
kobs
0
0.1
0.2
0.3
0.4
0.5
0.6
[PPh3]

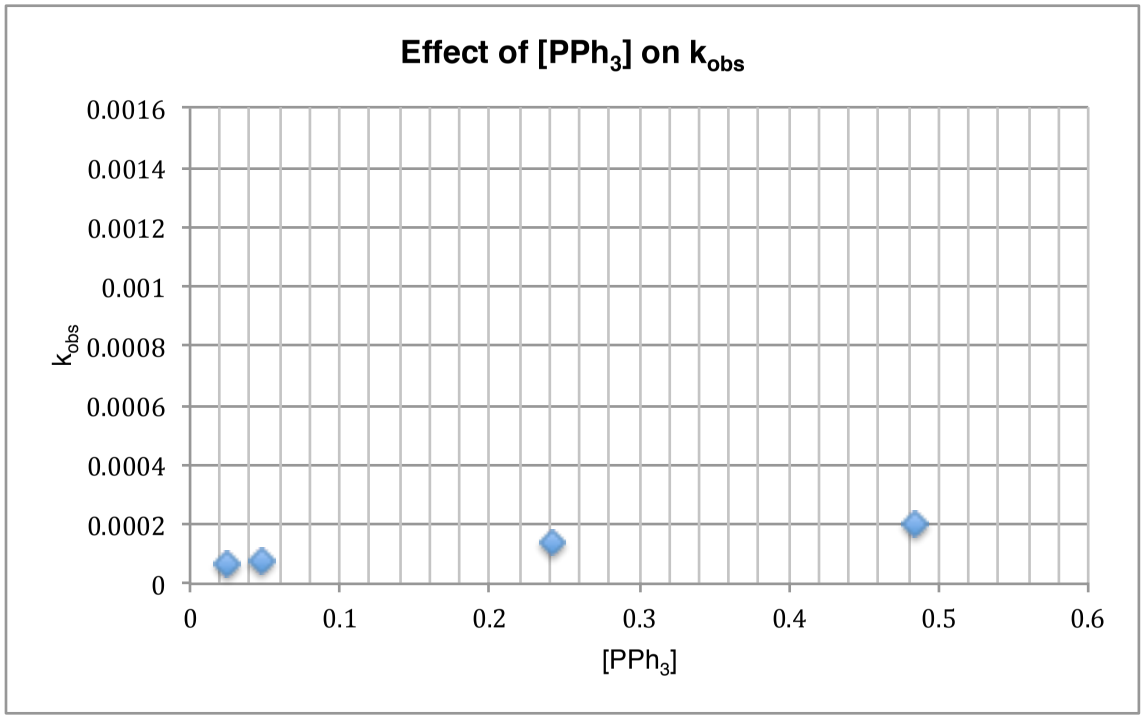

Ph
Ph
Ph2
P
O
Rh
P
Ph2
+ PPh3
toluene
35 °C
Ph
Ph
O
+ [Rh]-H

**7h**


Effect of [PPh3] on kobs
0.0016
0.0014
0.0012
0.001
0.0008
0.0006
0.0004
0.0002
0
kobs
0
0.1
0.2
0.3
0.4
0.5
0.6
[PPh3]


Ph
Ph
(iPr)2
P
O
Rh
P
(iPr)2
+ PPh3
toluene
35 °C
Ph
Ph
O
+ [Rh]-H

**7d**


Effect of [PPh3] on kobs
kobs
0.0016
0.0014
0.0012
0.001
0.0008
0.0006
0.0004
0.0002
0
0
0.1
0.2
0.3
0.4
0.5
0.6
[PPh3]

## CHAPTER 4: The Reactions of Less Electron-Rich Rhodium Alkoxo Alkene Complexes

### 4.1 Background

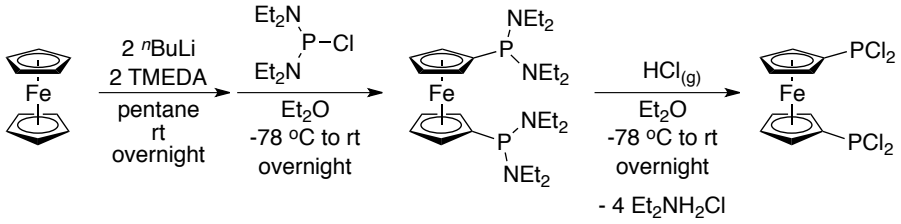
The final chapter of this thesis focuses on efforts to develop new ligands for the promotion of alkene insertions into metal-alkoxo bonds. Studies on the effects of ancillary ligand properties on the rates for alkene insertions into rhodium-alkoxo bonds were performed previously (Chapter 3) and indicate that less electron-rich ligands and ligands with binaphthyl and biphenyl backbones promote faster rates for alkene insertions into rhodium-alkoxo bonds than other ancillary ligands. Consequently, less electron-rich phosphorus ligands and ligands with binaphthyl backbones investigated. Initial efforts began with a phosphonite derivative of DPPF and progressed to 1,1'-bis[bis(trifluoromethyl)phosphino]ferrocene, phosphonite and phosphite derivatives of BINAP, and finally 2,2'-bis[bis(trifluoromethyl)phosphino]binaphthyl.

Phosphites and phosphonites have been reported as ancillary ligands for rhodium-catalyzed hydroformylations and nickel-catalyzed hydrocyanations. Perfluoroalkyl phosphines have been applied to a few metal-mediated reactions, but are less commonly encountered. For rhodium-catalyzed hydroformylations, the rate-limiting step is thought to be CO dissociation from an 18-electron, 5-coordinate rhodium diphosphine (or bis(monophosphine)) dicarbonyl hydrido complex. Less electron-rich ancillary ligands are thought to promote CO dissociation from the dicarbonyl hydrido complex. For nickel-catalyzed hydrocyanations, the rate-limiting step is thought to be C-CN reductive elimination from a nickel(II) cyano alkyl complex formed by alkene insertion into a nickel-hydrido bond. Less electron-rich phosphites and phosphonites are thought to promote C-CN reductive elimination. In the present case, less electron-rich phosphonites, phosphites, and perfluoroalkyl phosphines are targeted to promote faster rates for alkene insertions into rhodium-alkoxo bonds.

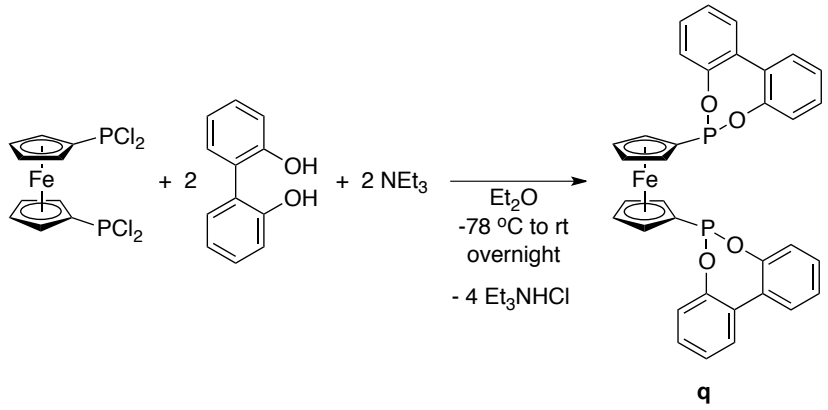
### 4.2 Present Research: The Reactions of Rhodium Diphosphonite, Diphosphite, and Bis-Bis(Trifluoromethyl) Phosphino Complexes.

#### 4.2.1 Synthesis and Reactivity of Rhodium Diphosphonite Chloride Complex, **1q**.

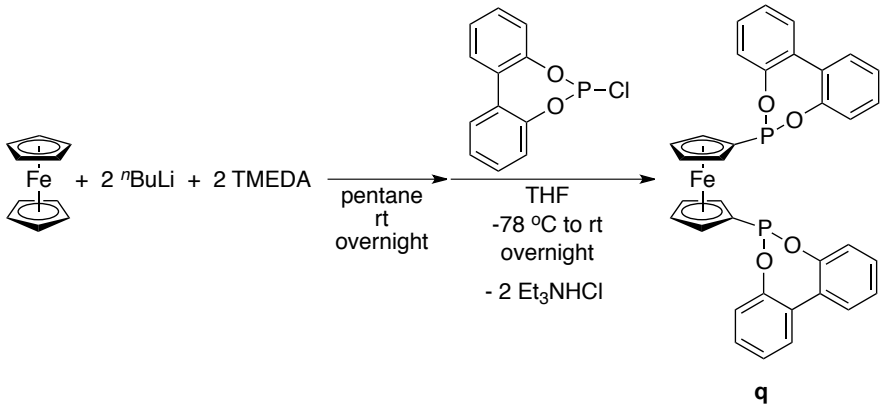
Studies began with the synthesis of 1,1'-bis(dibenzo[*d*,*f*][1,3,2]dioxaphosphepin-6-yl)-ferrocene, **q**. Bunel reported the same ligand in a patent for transition metal-catalyzed hydroformylations of conjugated dienes to alkenals. The compound can be synthesized either by the addition of 2,2'-biphenol to 1,1'-bis(dichlorophosphino)ferrocene (Scheme 276) or by the addition of 2,2'-biphenylylene phosphorochloridite to the TMEDA adduct of 1,1'-dilithioferrocene (Scheme 277).




**Scheme 275: Synthesis of 1,1'-bis(dichlorophosphino)ferrocene**

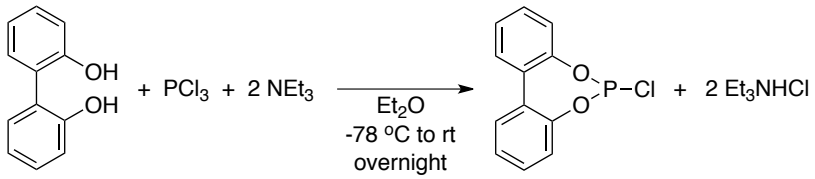



**Scheme 276: Synthesis of 1,1'-bis(dibenzo[*d,f*][1,3,2]dioxaphosphepin-6-yl)-ferrocene, q. via the addition of 2,2'-biphenol to 1,1'-bis(dichlorophosphino)ferrocene**



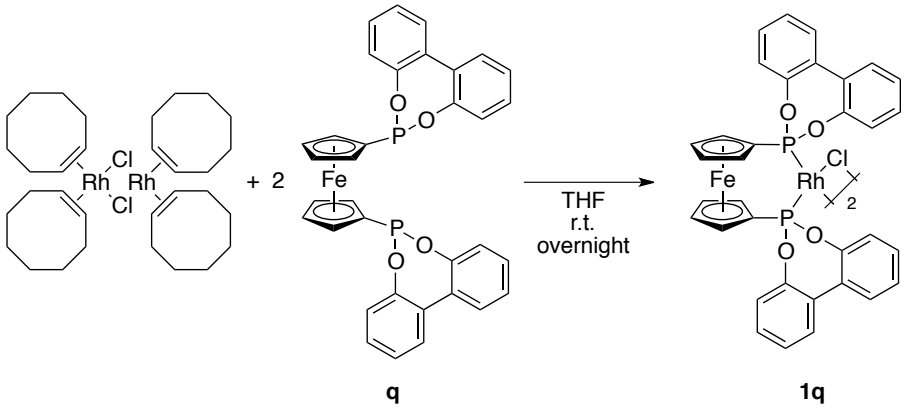

**Scheme 277: 1,1'-bis(dibenzo[*d,f*][1,3,2]dioxaphosphepin-6-yl)-ferrocene, q, via the addition of 2,2'-biphenylylene phosphorochloridite to the TMEDA adduct of 1,1'-dilithioferrocene**

The TMEDA adduct of 1,1'-dilithioferrocene was synthesized by the addition of $^{n}$BuLi and TMEDA to ferrocene (Scheme 277). 2,2'-Biphenylylene phosphorochloridite was synthesized by the addition of 2,2'-biphenol to $PCl_3$ (Scheme 278).



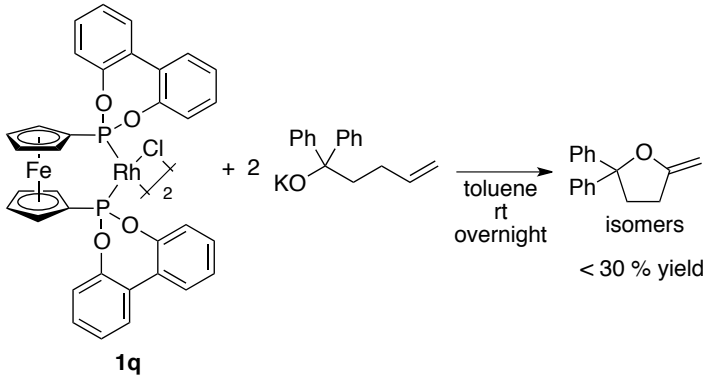

**Scheme 278: Synthesis of 2,2'-biphenylylene phosphorochloridite via the addition of 2,2'-biphenol to $PCl_3$.**

Rhodium diphosphonite chloride complex, **1q**, was synthesized by the addition of 1,1'-bis(dibenzo[*d,f*][1,3,2]dioxaphosphepin-6-yl)-ferrocene, **q**, to $[Rh(COE)_2(\mu\text{-}Cl]_2$ (Scheme 279).




**Scheme 279: Synthesis of rhodium chloride complex, 1q, via the addition of ,1'-bis(dibenzo[*d,f*][1,3,2]dioxaphosphepin-6-yl)-ferrocene, q, to $[Rh(COE)_2(\mu\text{-}Cl]_2$**

Attempts to isolate the rhodium diphosphonite silylamido complex of 1,1'-bis(dibenzo[*d,f*][1,3,2]dioxaphosphepin-6-yl)-ferrocene were unsuccessful. Consequently, the rhodium diphosphonite alkoxo alkene complex of 1,1'-bis(dibenzo[*d,f*][1,3,2]dioxaphosphepin-6-yl)-ferrocene, **q**, was accessed by the addition of potassium 1,1-diphenyl-4-pentenyl-1-alkoxide to rhodium diphosphonite chloride complex, **1q**. Preliminary reactions were conducted at room temperature. Analysis of the product solutions of these reactions by GC and GC/MS indicate the formation of furan products low to moderate yield (Scheme 280).

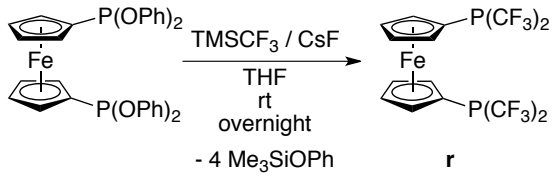



**Scheme 280: The reaction of diphosphnoite complex 1q with the potassium salt of 1,1-diphenyl-4-pentenyl-1-ol. Furan isomers were generated in low yields.**

Attempts to observe the alkoxo alkene complex of 1,1'-bis(dibenzo[*d,f*][1,3,2]dioxaphosphepin-6-yl)-ferrocene by NMR spectroscopy were unsuccessful. NMR spectra ($^1H$ and $^{31}P$) collected at -50 °C reveal poorly resolved signals. NMR spectra ($^1H$ and $^{31}P$) collected at -35 °C reveal the formation of new species. A significant amount of alkene isomerization is observed. Difficulties following the reactions by NMR spectroscopy and the low yields of furan products eventually prompted the investigation of other ligands.

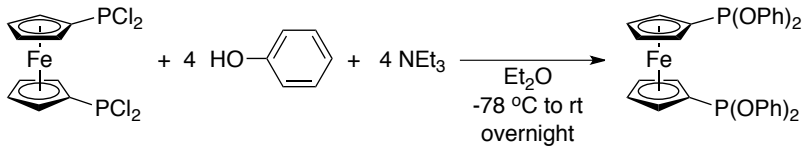
### 4.2.2 Synthesis and Reactivity of Rhodium 1,1'-Bis[bis(trifluoromethyl)phosphino]ferrocene Complex, **1r**.

1,1'-Bis[bis(trifluoromethyl)phosphino]ferrocene, **1r** was synthesized according to literature procedures by the addition of $TMSCF_3$, and CsF to 1,1'-bis(diphenoxyphosphino)ferrocene (Scheme 281).[169]



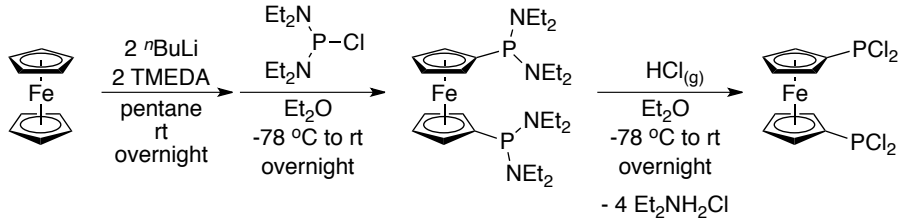

**Scheme 281: Synthesis of 1,1'-Bis[bis(trifluoromethyl)phosphino]ferrocene, r, via the addition of $TMSCF_3$ and CsF to 1,1'-bis(diphenoxyphosphino)ferrocene.**

The reaction was performed at room temperature in THF. 1,1'-Bis(diphenoxyphosphino)ferrocene was synthesized by the addition of phenol to 1,1'-bis(dichlorophosphino)ferrocene (Scheme 282).



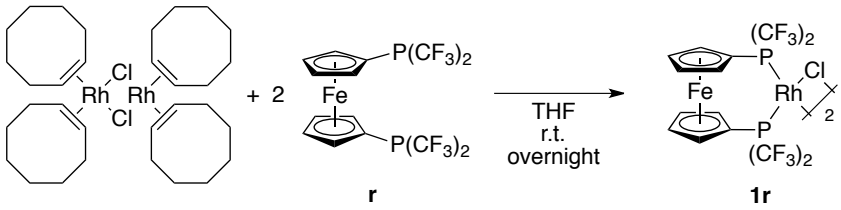

**Scheme 282: Synthesis of 1,1'-bis(diphenoxyphosphino)ferrocene via the addition of phenol to 1,1'-bis(dichlorophosphino)ferrocene**

1,1'-Bis(dichlorophosphino)ferrocene was synthesized in three steps from ferrocene, $^{n}$BuLi/TMEDA, $(Et_2N)_2PCl$, and HCl(g) (Scheme 283).




**Scheme 283: Synthesis of 1,1'-bis(dichlorophosphino)ferrocene.**

1,1'-Bis[bis(trifluoromethyl)phosphino]ferrocene rhodium chloride (**1r**) was synthesized by the addition of 1,1'-bis[bis(trifluoromethyl)phosphino]ferrocene (**r**) to $[Rh(COE)_2(\mu\text{-}Cl]_2$ (Scheme 284).

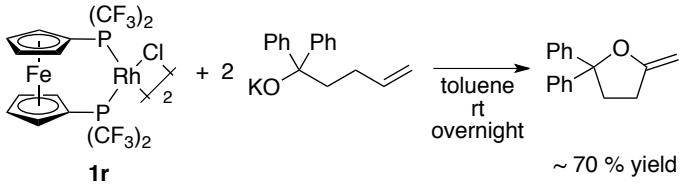



**Scheme 284: Synthesis of 1,1'-bis[bis(trifluoromethyl)phosphino]ferrocene rhodium chloride, 1r.**

The silylamido complex 1,1'-bis[bis(trifluoromethyl)phosphino]ferrocene could not be isolated. As a result, the reaction of with rhodium diphosphine chloride complex **1r** with potassium 1,1-diphenyl-4-pentenyl-1-alkoxide was performed.

Preliminary reactions between **1r** and the potassium salt of 1,1-diphenyl-4-penten-1-ol were performed at room temperature. The product solutions were analyzed by GC and GC/MS. The data from these reactions suggest that furan products form in approximately 70 % yield (Scheme 285). Consequently, the reactions of **1r** with potassium 1,1-diphenyl-4-pentenyl-1-alkoxide were investigated by low temperature NMR spectroscopy. Solutions

formed by the addition of potassium 1,1-diphenyl-4-pentenyl-1-alkoxide to **1r** show no signs of alkene coordination. Disappearance of the uncoordinated alkene signals starts to occur at -35 °C.

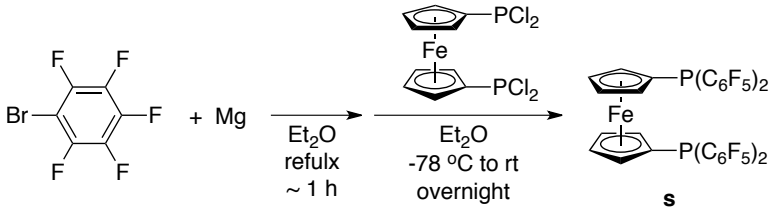



**Scheme 285: Reaction of 1,1'-bis[bis(trifluoromethyl)phosphino]ferrocene rhodium chloride complex 1r with the potassium salt of 1,1-diphenyl-4-pentenyl-1-ol. Furan isomers were generated in moderate to good yields.**

The products formed by the addition of potassium 1,1-diphenyl-4-pentenyl-1-alkoxide to **1r** and the reactions that follow are unclear.

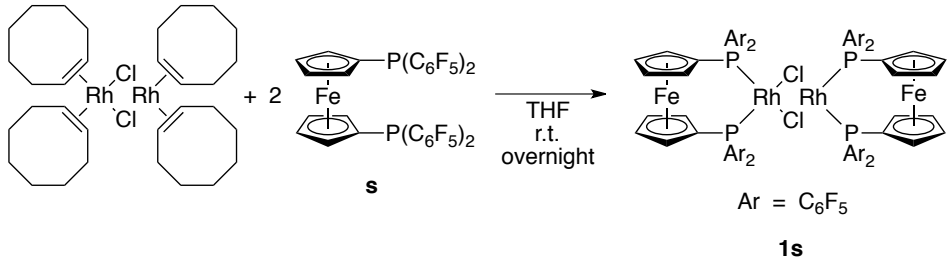
### 4.2.3 Synthesis and Reactivity of Rhodium Chloride Complex, **1s**.

1,1'-Bis[bis(pentafluorophenyl)phosphino]ferrocene was synthesized according to literature procedures by the addition of pentafluorophenylmagnesium bromide to 1,1'-bis(dichlorophosphino)ferrocene (Scheme 286). The procedures were reported by Beletskaya and co-workers. 1,1'-Bis(dichlorophosphino)ferrocene was synthesized in three steps from ferrocene, $^{n}$BuLi/TMEDA, $(Et_2N)_2PCl$, and HCl(g) (Scheme 283).



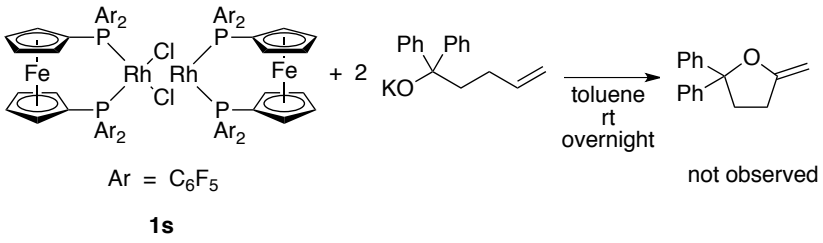

**Scheme 286: Synthesis of 1,1'-bis[bis(pentafluorophenyl)phosphino]ferrocene via the addition of pentafluorophenylmagnesium bromide to 1,1'-bis(dichlorophosphino)ferrocene**

Rhodium diphosphine chloride complex, **1s**, was synthesized by the addition of 1,1'-Bis[bis(pentafluorophenyl)phosphino]ferrocene to $[Rh(COE)_2(\mu\text{-}Cl)]_2$ (Scheme 287).




**Scheme 287: Synthesis of 1,1'-Bis[bis(pentafluorophenyl)phosphino]ferrocene rhodium chloride, 1s.**

Attempts to isolate the rhodium diphosphonite silylamido complex of 1,1'-bis(dibenzo[*d,f*][1,3,2]dioxaphosphepin-6-yl)-ferrocene were unsuccessful. Consequently, the reactions of potassium 1,1-diphenyl-4-pentenyl-1-alkoxide with rhodium diphosphine chloride complex, **1s** were examined (Scheme 288).

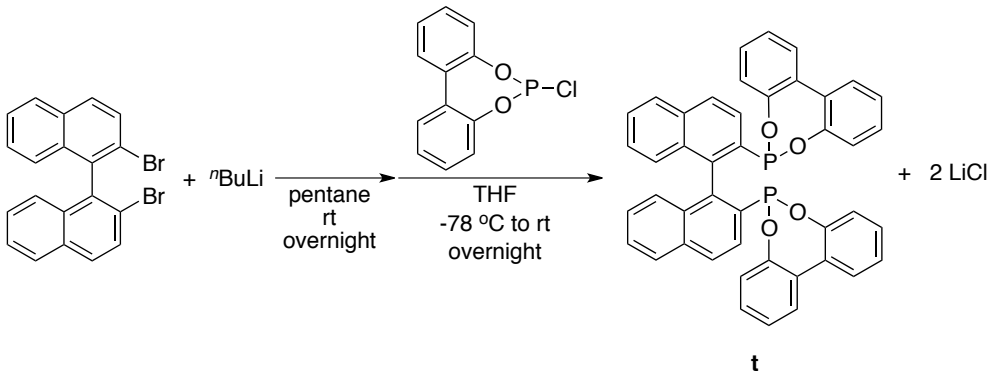



**Scheme 288: Reaction of 1,1'-bis[bis(pentafluorophenyl)phosphino]ferrocene rhodium chloride complex 1s with the potassium salt of 1,1-diphenyl-4-pentenyl-1-ol. No signs of furan isomers were observed in the product solutions.**

Preliminary reactions between potassium 1,1-diphenyl-4-pentenyl-1-alkoxide and **1s** were performed at room temperature and analyzed by GC and GC/MS. The data from these reactions indicate that furan products are not formed. The reactions of **1s** were not investigated further.

### 4.2.4 Synthesis and Reactivity of Rhodium Diphosphonite Chloride Complex, **1t**.

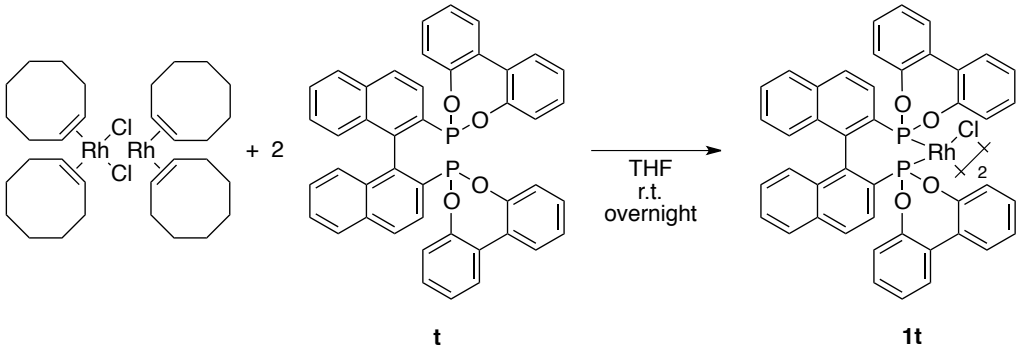
Synthesis of 2,2'-bis(dibenzo[*d*,*f*][1,3,2]dioxaphosphepin-6-yl)-binaphthyl, **t**, was achieved by the addition of 2,2'-biphenylylene phosphorochloridite to 2,2'-dilithiobinaphthyl (Scheme 289).




**Scheme 289: Synthesis of ,2'-bis(dibenzo[*d*,*f*][1,3,2]dioxaphosphepin-6-yl)-binaphthyl via the addition of 2,2'-biphenylylene phosphorochloridite to 2,2'-dilithiobinaphthyl.**

The compound was previously unreported. 2,2'-Dilithiobinaphthyl was synthesized in situ by the addition of $^{n}$BuLi 2,2'-dibromobinapthyl. 2,2'-Biphenylylene phosphorochloridite was synthesized by the addition of 2,2'-biphenol to $PCl_3$ (Scheme 278).

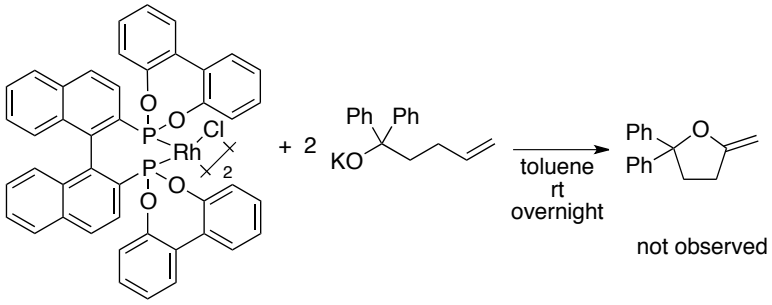
The rhodium chloride complex of 2,2'-bis(dibenzo[*d*,*f*][1,3,2]dioxaphosphepin-6-yl)-binaphthyl, **t**, was synthesized by the addition of 2,2'-bis(dibenzo[*d*,*f*][1,3,2]dioxaphosphepin-6-yl)-binaphthyl, **t**, to $[Rh(COE)_2(\mu\text{-}Cl]_2$ (Scheme 290).




t 1t

**Scheme 290: Synthesis of 2,2'-bis(dibenzo[*d,f*][1,3,2]dioxaphosphepin-6-yl)-binaphthyl rhodium chloride, 1t.**

Attempts to isolate the silylamido complex of 2,2'-bis(dibenzo[*d,f*][1,3,2]dioxaphosphepin-6-yl)-binaphthyl were unsuccessful. Consequently, the reactions of **1t** and the potassium salt of 1,1-diphenyl-4-penten-1-ol to **1t** were examined for the formation of furan products (Scheme 291). Preliminary reactions were performed at room temperature. The data suggest that 5-methylene-2,2-diphenyl tetrahydrofuran did not form.



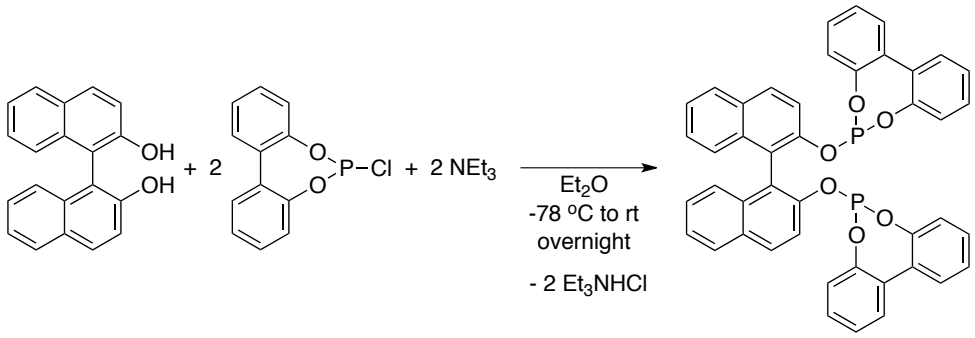

1t

**Scheme 291: Reaction of 2,2'-bis(dibenzo[*d,f*][1,3,2]dioxaphosphepin-6-yl)-binaphthyl rhodium chloride, 1t, with the potassium salt of 1,1-diphenyl-4-pentenyl-1-ol. No signs of furan isomers were observed in the product solutions.**

Reactions performed at lower temperatures (-50 °C) suggest that the alkene does not coordinate to the metal center. Isomerization of the unsaturated alcohol or alkoxide was observed at -35 °C. The data suggest that alkene isomerization is faster than furan formation. The mechanisms for alkene isomerization and furan formation are uncertain. Alkene insertion is presumed to occur by alkene insertion into the rhodium-hydrido bond of a rhodium hydrido complex and subsequent β-hydride elimination. Furan formation is thought to occur by alkene insertion into the rhodium alkoxo bond of a rhodium alkoxo complex. The generation of a rhodium hydrido complex may occur by alkene insertion into a rhodium alkoxo bond by β-hydride elimination. These reactions wee not investigated. Instead, the reactions of rhodium diphosphites were examined.

### 4.2.5 Synthesis and Reactivity of Rhodium Diphosphite Chloride Complex, **1u**.

2,2'-Bis[(1,1'-biphenyl-2,2'-diyl)phosphite]- 1,1'-binaphthyl, **u**, was synthesized by the addition of 2,2'-biphenylylene phosphorochloridite to 2,2'-binaphthol (Scheme 292).[170]

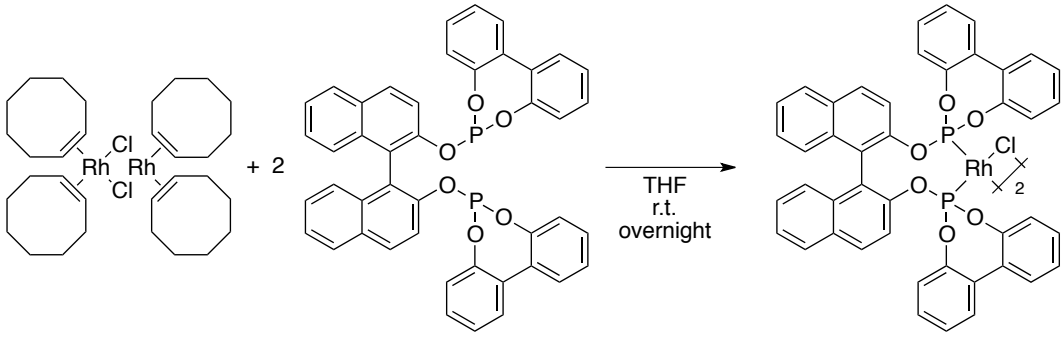



**u**

**Scheme 292: Synthesis of 2,2'-bis[(1,1'-biphenyl-2,2'-diyl)phosphite]- 1,1'-binaphthyl, u via the addition of 2,2'-biphenylylene phosphorochloridite to 2,2'-binaphthol**

The reaction was conducted at -78 °C in the presence of $NEt_3$.

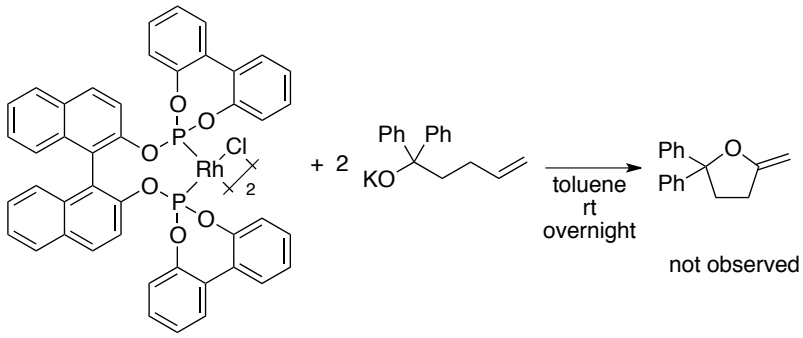
The rhodium chloride complex of 2,2'-bis[(1,l'-biphenyl-2,2'-diyl)phosphite]- l,l'-binaphthyl, **1u**, was synthesized by the addition of 2,2'-bis[(1,l'-biphenyl-2,2'-diyl)phosphite]- l,l'-binaphthyl, **u**, to $[Rh(COE)_2(\mu\text{-}Cl]_2$ (Scheme 293).




**u** **1u**

**Scheme 293: The synthesis of 2,2'-bis[(1,1'-biphenyl-2,2'-diyl)phosphite]- 1,1'-binaphthyl rhodium chloride, 1u.**

Attempts to isolate the rhodium silylamido complex of 2,2'-bis[(1,l'-biphenyl-2,2'-diyl)phosphite]- l,l'-binaphthyl, **2u**, were unsuccessful. Consequently, the reactions of rhodium diphosphite chloride complex, **1u** with potassium salt of 1,1-diphenyl-4-penten-1-ol were examined (Scheme 294). Preliminary reactions were conducted at room temperature. The data from these reactions suggest that furan products did not form. The results mirror those obtained for the reactions of rhodium diphosphonite complex **1t**. The reactions were not investigated further.

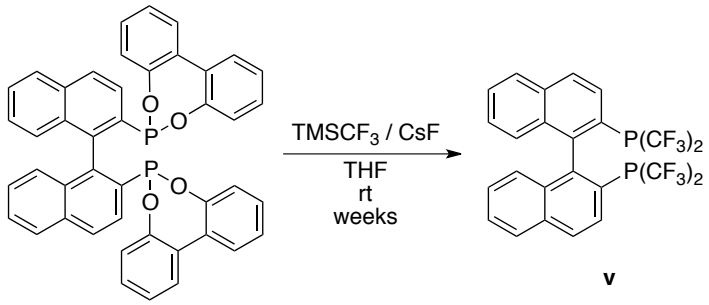



**1u**

**Scheme 294: Reaction of 2,2'-bis[(1,1'-biphenyl-2,2'-diyl)phosphite]- 1,1'-binaphthyl rhodium chloride, 1u, with the potassium salt of 1,1-diphenyl-4-pentenyl-1-ol. No signs of furan isomers were observed in the product solutions.**

### 4.2.6 Synthesis and Reactivity of Rhodium 2,2'-Bis[bis(trifluoromethyl)phosphino]-1,1'- binaphthyl Complex, **1v**.

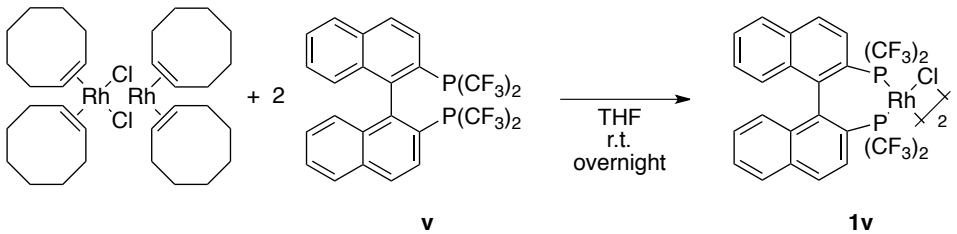
The last ligand investigated in this study was 2,2'-bis[bis(trifluoromethyl)phosphino]-1,1'-binaphthyl, **v**. The compound was synthesized by the addition of Ruppert's reagent and CsF to 2,2'-bis(dibenzo[*d,f*][1,3,2]dioxaphosphepin-6-yl)-binaphthyl, **t** (Scheme 295).




**t** **v**

**Scheme 295: Synthesis of 2,2'-bis[bis(trifluoromethyl)phosphino]-1,1'-binaphthyl, v, t via the addition of TMSCF3 and CsF to 2,2'-bis(dibenzo[*d,f*][1,3,2]dioxaphosphepin-6-yl)-binaphthyl, t.**

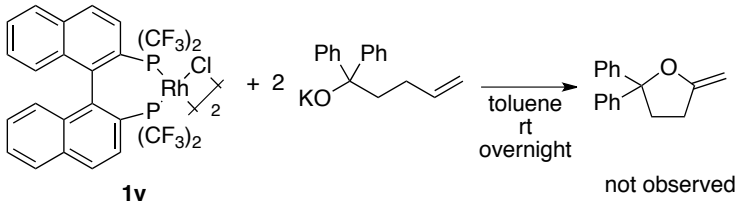
The reaction was performed in THF at room temperature and monitored by $^{31}P$ and $^{19}F$ NMR spectroscopy. The reaction took approximately 1 week to complete. The compound was previously unreported. Rhodium diphosphite chloride complex, **1v**, was synthesized by the addition of 2,2'-bis[bis(trifluoromethyl)phosphino]-1,1'-binaphthyl, **v** to $[Rh(COE)_2(\mu\text{-}Cl]_2$ (Scheme 296).




**v** **1v**

**Scheme 296: Synthesis of 2,2'-bis[bis(trifluoromethyl)phosphino]-1,1'-binaphthyl rhodium chloride complex 1v.**

Attempts to isolate the rhodium silylamido complex of 2,2'-bis[(1,l'-biphenyl-2,2'-diyl)phosphite]- l,l'-binaphthyl, **2v**, were unsuccessful. Consequently, the reactions of rhodium diphosphite chloride complex, **1v** with potassium salt of 1,1-diphenyl-4-penten-1-ol were examined (Scheme 294). Preliminary reactions were conducted at room temperature. The data from these reactions suggest that furan products did not form. The results mirror those obtained for the reactions of rhodium diphosphonite complex **1t** and **1u**. The reactions were not investigated further.




**Scheme 297: Reaction of 2,2'-bis[bis(trifluoromethyl)phosphino]-1,1'-binaphthyl rhodium chloride complex, 1v, with the potassium salt of 1,1-diphenyl-4-pentenyl-1-ol. Furan isomers were not observed in the product solution.**

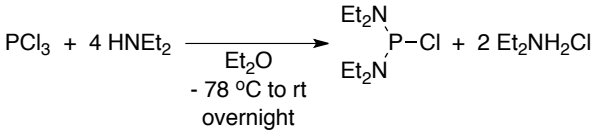
### 4.2.7 Summary and Conclusions

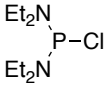
The reactions of rhodium chloride complexes **1q-v** with potassium 1,1-diphenyl-4-pentenyl-1-alkoxide highlight some of the difficulties associated designing ligands for a specific reaction. Even small changes in the ligand architecture can have large effects on the observed rates and yields. More complex ligand descriptors (or parameters) may eventually be able to account for the more subtle changes that occur upon changing different parts of a ligand, but until then, the rational design of ancillary ligands will most likely remain a challenge.

The reactions of rhodium chloride complexes **1q-v** with potassium 1,1-diphenyl-4-pentenyl-1-alkoxide also underscore some of the difficulties associated with observing rhodium alkoxo alkene complexes.

## 4.3 Experimental

### 4.3.1 Synthesis of bis(diethylamino)chlorophosphine, $(Et_2N)_2PCl$.[171]



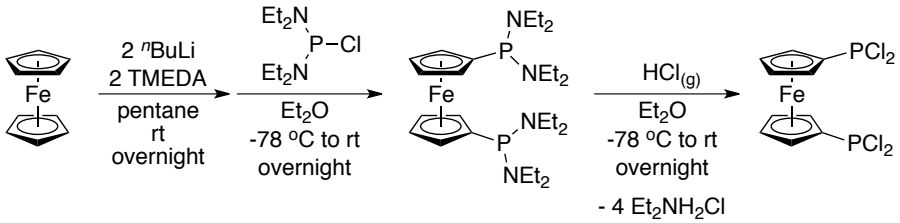

Bis(diethylamino)chlorophosphine, $(Et_2N)_2PCl$, was synthesized according to literature procedures. A solution of $PCl_3$ (50 ml, 78.5 g, 0.572 mol, 1 equiv.) in $Et_2O$ (dry, 200 ml) was prepared in a 1 L three neck flack equipped with a magnetic stir bar, two rubber septa and a 24/40-to-barb flow control adapter attached to a Schlenk manifold by a rubber hose. The flask was placed in a dry ice / acetone bath. Diethyl amine (distilled from sodium, 236 ml, 167 g, 2.29 mol, 4 equiv.) was added drop-wise to the solution of $PCl_3$ at -78 °C. Additional $Et_2O$ (dry, 200 ml) was added to the flask to ensure stirring, the flask was slowly warmed to room temperature, and the resulting solution was stirred overnight. A white precipitate formed. The heterogeneous solution was filtered through a glass frit into a second 1 L three neck flask equipped with a magnetic stir bar, a septum and a 24/40-to-barb flow control adapter (the flask was purged of air and moisture and placed under an $N_2$ atmosphere). The collected solid ($Et_2NH_2Cl$) was washed with additional $Et_2O$ (100 ml total), and the collected filtrate concentrated under vacuum to yield a yellow oil. The crude product was distilled under vacuum to yield a colorless oil (50 ml, 50 g, 0.238 mol, 42 % yield).

$^1$H NMR: (499.9 MHz, toluene- $d_8$) δ 3.09 (m, 4H), 2.96 (m, 4H), 0.95 (t, broad, $J^{H-H}$ = 7 Hz, 12H).

$^{13}C\{^1H\}$ NMR: (125.7 MHz, toluene- $d_8$) δ 40.9 ($J^{C-P}$ = 18 Hz), 13.6 ($J^{C-P}$ = 5 Hz)

$^{31}P\{^1H\}$ NMR: (202.4 MHz, toluene- $d_8$) δ 152.7

### 4.3.2 Synthesis of 1,1'-bis(dichlorophosphino)ferrocene.[171]




Ferrocene (4.76 g, 45.6 mmol, 1 equiv.) was weighed in a 20 ml vial and transferred to a 250 ml Schlenk flask. The Schlenk flask was equipped with a magnetic stir bar, sealed with a septum, and connected to a Schlenk manifold (by a rubber hose). The flask was purged of air by successively applying vacuum and dry $N_2$ (3x), and then placed under an $N_2$ atmosphere. Dry pentane (100 ml) was added to the Schlenk flask via syringe. The resulting solution was stirred at room temperature. A solution of $^n$BuLi in hexanes (35.2 ml, 1.6 M, 56.3 mmol, 2.2 equiv.) was added slowly to the ferrocene solution. A solution of TMEDA (distilled from sodium, 8.4 ml, 6.6 g, 56

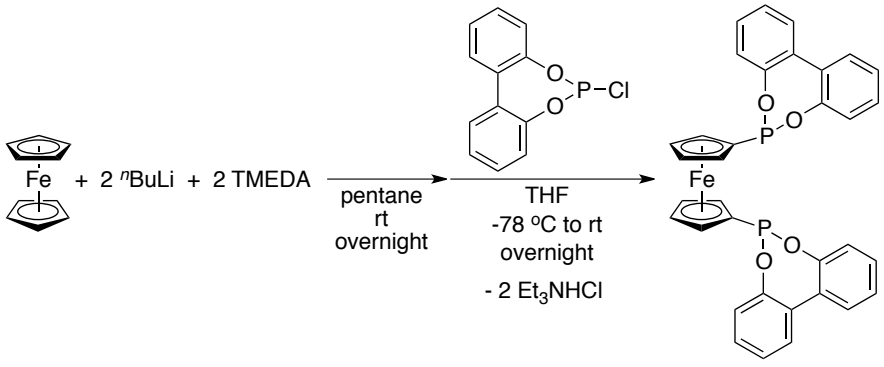
.4 mmol, 2.2 equiv.) in pentane (30 ml) was added slowly to the mixture of ferrocene and $^n$BuLi. The resulting solution was stirred overnight at room temperature under an $N_2$ atmosphere. An orange solid precipitated. The solution was placed in a dry ice / acetone bath and cooled to -78 °C. Bis(diethylamino)chlorophosphine, $(Et_2N)_2PCl$ (11.9 g, 56.5 mmol, 2.2 equiv.), was weighed inside a glovebox in a 20 ml vial. The compound was dissolved in approximately 20 ml of dry THF and loaded into a 50 ml syringe. A rubber septum was placed on the needle of the syringe and the syringe was removed from the glovebox. The solution of $(Et_2N)_2PCl$ in THF was added slowly to the solution of 1,1'-dilithioferrocene / 2 TMEDA at -78 °C. The dry ice / acetone bath was removed and the reaction was allowed to stir at room temperature overnight. The resulting solution was filtered through celite into a second 250 ml Schlenk flask equipped with a magnetic stir bar and a filter stick. The filter stick was removed from the Schlenk flask under a high $N_2$ pressure and replaced with a rubber septum. The solvent was then removed from the filtrate under vacuum. The crude product, 1,1'-bis[bis(diethylamino)phosphino]ferrocene ($Fe[C_5H_4P(NEt_2)_2]_2$), was carried on to the next step without further purification.

The residue obtained by the reaction of ferrocene, $^n$BuLi, TMEDA, and $(Et_2N)_2PCl$ was placed under an $N_2$ atmosphere and dissolved in dry $Et_2O$ (100 ml). The solution was cooled to -78 °C by placing the Schlenk flask into a dry ice / acetone bath. Anhydrous HCl(g) was bubbled through the solution at -78 °C for approximately 2 hours. The reaction was slowly warmed to room temperature and then stirred overnight. A white-yellow precipitate formed. The heterogeneous solution was filtered through celite into a third 250 ml Schlenk flask. The collected solid was washed with additional dry $Et_2O$ (3 x 20 ml). The collected filtrate was concentrated under vacuum to yield an orange solid (6.88 g, 17.7 mmol, 69 % yield). The compound was used as obtained.

$^1$H NMR: (399.9 MHz, toluene-$d_8$) δ 4.18 (s, 4H), 4.04 (s, 4H).

$^{31}$P{$^1$H} NMR: (161.9 MHz, toluene-$d_8$) δ 163.8.

### 4.3.3 Synthesis of 1,1'-bis(dibenzo[*d,f*][1,3,2]dioxaphosphepin-6-yl)-ferrocene, **q**.




**q**

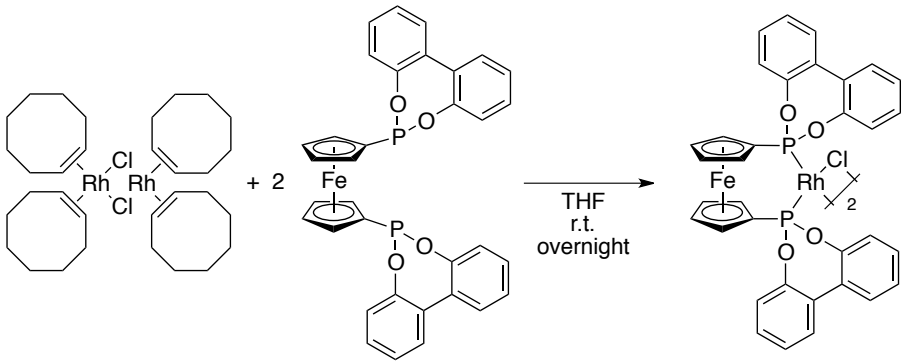
1,1'-bis(dichlorophosphino)ferrocene (1.0 g, 2.6 mmol, 1 equiv.) was weighed inside a glovebox in a 20 ml vial. 2,2'-Biphenol (1.1 g, 5.9 mmol, 2.3 equiv.) was weighed inside a glovebox in a 20 ml vial. The 1,1'-bis(dichlorophosphino)ferrocene was dissolved in $Et_2O$ (20 ml) and transferred to a 100 ml Schlenk flask equipped

with a magnetic stir bar. The 2,2'-biphenol was dissolved in $Et_2O$ (20 ml) and transferred to a 50 ml syringe. The Schlenk flask was sealed off from the box atmosphere (with a rubber septum) and removed from the glovebox. The flask was connected to a Schlenk manifold. The rubber hose connecting the Schlenk flask to the manifold was purged with $N_2$ and vacuum. The Schlenk flask then opened to $N_2$ and placed in a dry ice / acetone bath. A septum was placed on the syringe containing the weighed 2,2'-biphenol, and the syringe was removed from the glovebox. The 2,2'-biphenol solution was added to the -bis(dichlorophosphino)ferrocene solution at -78 °C. $NEt_3$ (1.6 ml, 1.16 g, 11.5 mmol, 4.5 equiv.) distilled from $CaH_2$ was added to the mixture of -bis(dichlorophosphino)ferrocene and 2,2'-biphenol in $Et_2O$ at -78 °C. The resulting solution was slowly warmed to room temperature and stirred overnight. A white precipitate formed. The heterogeneous solution was filtered through celite into a 250 ml Schlenk flask. The collected solid was washed with dry $Et_2O$ (3 x 20 ml). The filtrate was concentrated under vacuum (after removing the filter stick used to remove the precipitated $Et_3NHCl$ from the reaction solution and replacing it with a rubber septum under high $N_2$ pressure). An orange solid was collected. The solid residue was dissolved in benzene and filtered through celite again, inside the glovebox. The filtrate was collected and frozen. The frozen benzene was removed under vacuum. The resulting orange solid was used as obtained (1.2 g, 2.0 mmol, 76 % yield).

$^1$H NMR: (399.9 MHz, toluene-$d_8$) δ 7.46 (dd, J = 7 Hz, J = 2 Hz, 4H), 7.34-7.22 (m, 8H), 6.97 (dd, J = 7 Hz, J = 2 Hz, 4H), 4.56 (s, broad, 4H), 4.39 (s, broad, 4H) ppm.

$^{31}$P{$^1$H} NMR: (161.9 MHz, $CD_2Cl_2$) δ 191.62 ppm.

### 4.3.4 Synthesis of rhodium diphosphonite chloride complex, **1q**.




**q** **1q**

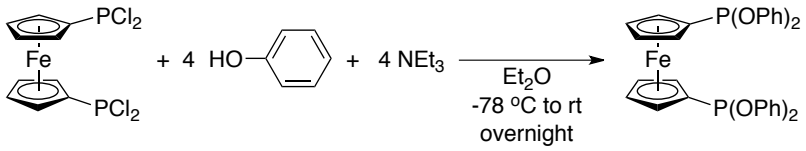
$[Rh(COE)_2(\mu\text{-}Cl)]_2$ (117 mg, 0.163 mmol, 1 equiv.) was weighed inside a glovebox in a 20 ml vial. 1,1'-Bis(dibenzo[*d*,*f*][1,3,2]dioxaphosphepin-6-yl)-ferrocene, **q**, (201 mg, 0.327 mmol, 2 equiv.) was weighed inside the same glovebox in a 3 ml vial. The weighed 1,1'-bis(dibenzo[*d*,*f*][1,3,2]dioxaphosphepin-6-yl)-ferrocene was dissolved in 2 ml of dry THF and transferred to the vial containing the weighed $[Rh(COE)_2(\mu\text{-}Cl)]_2$ An additional, 2-3 ml of dry THF was added to the reaction vial. A magnetic stir bar was added to the vial. The vial was capped and the reaction was stirred overnight at room temperature. The resulting solution was concentrated under vacuum.

Dry $Et_2O$ (10 ml) was added to the vial to precipitate a yellow solid. The heterogeneous solution was filtered on a glass frit. The collected solid was washed with additional $Et_2O$ (3 x 5 ml), transferred to a tared 20 ml vial, and dried under vacuum. The resulting solid was used as collected (138 mg, 0.092 mmol, 56 % yield).

$^1$H NMR: (399.9 MHz, THF-$d_8$) δ 7.46 (m, 4H), 7.30 (m, 4H), 7.16 (m 8H), 4.96 (s, broad, 4H), 4.36 (s, broad, 4H) ppm.

$^{31}$P{$^1$H} NMR: (161.9 MHz, THF-$d_8$) δ 176.1 (d, J = 268 Hz) ppm.

### 4.3.5 Synthesis of 1,1'-bis(diphenoxyphosphino)ferrocene.[169]



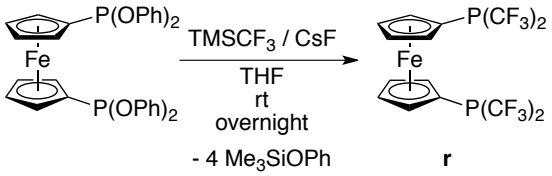

1,1'-bis(dichlorophosphino)ferrocene (2.0 g, 5.2 mmol, 1 equiv.) was weighed inside a glovebox in a 20 ml vial. Phenol (2.4 g, 25.5 mmol, 4.9 equiv.) was weighed inside a glovebox in a 20 ml vial. The 1,1'-bis(dichlorophosphino)ferrocene was dissolved in $Et_2O$ (15 ml) and transferred to a 250 ml Schlenk flask equipped with a magnetic stir bar. Additional $Et_2O$ (40 ml) was added to the Schlenk flask. The phenol was dissolved in $Et_2O$ (20 ml) and transferred to a 50 ml syringe. The Schlenk flask was sealed off from the box atmosphere (with a rubber septum) and removed from the glovebox. The flask was connected to a Schlenk manifold. The rubber hose connecting the Schlenk flask to the manifold was purged with $N_2$ and vacuum. The Schlenk flask then opened to $N_2$ and placed in a dry ice / acetone bath. A septum was placed on the syringe containing the weighed phenol, and the syringe was removed from the glovebox. The phenol solution was added to the -bis(dichlorophosphino)ferrocene solution at -78 °C. $NEt_3$ (1.6 ml, 1.16 g, 11.5 mmol, 4.5 equiv.) distilled from $CaH_2$ was added to the mixture of -bis(dichlorophosphino)ferrocene and phenol in $Et_2O$ at -78 °C. The resulting solution was slowly warmed to room temperature and stirred overnight. A white precipitate formed. The heterogeneous solution was filtered through celite into a 250 ml Schlenk flask. The collected solid was washed with dry $Et_2O$ (3 x 20 ml). The filtrate was concentrated under vacuum (after removing the filter stick used to remove the precipitated $Et_3NHCl$ from the reaction solution and replacing it with a rubber septum under high $N_2$ pressure). An orange solid was collected. The solid residue was dissolved in benzene and filtered through celite again, inside the glovebox. The filtrate was collected and frozen. The frozen benzene was removed under vacuum. The resulting orange solid was used as obtained (2.4 g, 3.9 mmol, 75 % yield).

$^1$H NMR: (400 MHz, $CD_2Cl_2$) δ 7.38 (s, broad, 8H), 7.22 (s, broad, 12H), 4.75 (s, broad, 4H), 4.64 (s, broad, 4H) ppm.

$^{13}$C{$^1$H} NMR: (162 MHz, $CD_2Cl_2$) δ 155.7, 130.1, 120.6, 79.8 (m), 72.6, 71.8 (m) ppm.

$^{31}$P{$^1$H} NMR: (162 MHz, , $CD_2Cl_2$) δ 162.3 ppm.

### 4.3.6 Synthesis of 1,1'-bis[bis(trifluoromethyl)phosphino]ferrocene, **r**.[169]



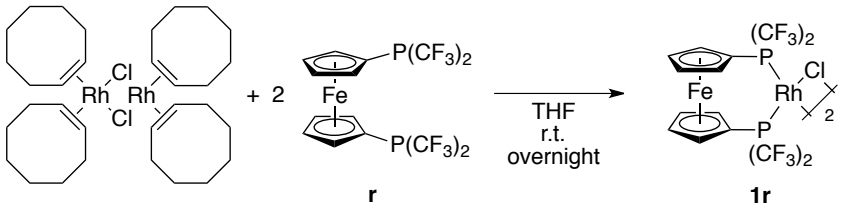

1,1'-bis(diphenoxyphosphino)ferrocene (0.84 g, 1.4 mmol, 1 equiv.) was weighed inside a glovebox in a 20 ml vial. The compound was dissolved in $Et_2O$ (20 ml) and transferred to a 100 ml Schlenk flask. The Schlenk flask was equipped with a magnetic stir bar and sealed from the box atmosphere with a rubber septum. The flask was removed from the glovebox and connected to a Schlenk manifold. The rubber hose connecting the Schlenk flask to the manifold was purged of $O_2$ and moisture by applying vacuum and $N_2$ successively 3 times. The Schlenk flask was opened to $N_2$. Cesium fluoride (0.93 g, 6.1 mmol, 4.5 equiv.) was weighed inside the glovebox in a 3 ml vial. Dry THF (2 ml) was added to the cesium fluoride, and the resulting solution was loaded into a 6 ml syringe with a 16 gauge needle. A septum was placed on the needle and the syringe containing the weighed cesium fluoride was removed from the glovebox. The cesium fluoride solution was added to the solution of 1,1'-bis(diphenoxyphosphino)ferrocene at room temperature. Ruppert's reagent, $TMSCF_3$, (1.04 ml, 1.0 g, 7.0 mmol, 5.2 equiv.) was loaded into a syringe and added slowly to the solution of 1,1'-bis(diphenoxyphosphino)ferrocene and CsF (caution: the resulting reaction is exothermic and possibly autocatalytic). The resulting solution was stirred overnight at room temperature. The solvent was removed under vacuum. A dark orange solid precipitated. The solid was removed by filtration and washed with hexanes. The filtrate was collected and placed in a freezer. Additional solid precipitated and was collected by filtration. The combined solids were dried under vacuum (0.548 g, 1.05 mmol, 77 % yield).

$^1$H NMR: (399.9 MHz, $C_6D_6$) δ 4.09 (d, J = 1 Hz, 4H), 3.97 (d, J = 1 Hz, 4H).

$^{19}$F{$^1$H} NMR: (376 MHz, $C_6D_6$) δ -54.2 (d, $J^{F-P}$ = 74 Hz).

$^{31}$P{$^1$H} NMR: (161.9 MHz, $C_6D_6$) δ -4.95 (septet, $J^{P-F}$ = 74 Hz).

### 4.3.7 Synthesis of 1,1'-bis[bis(trifluoromethyl)phosphino]ferrocene rhodium chloride, **1r**.



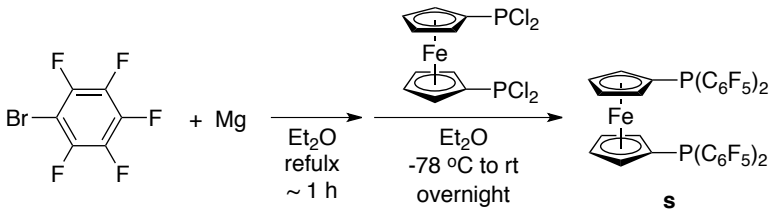

$[Rh(COE)_2(\mu\text{-}Cl)]_2$ (367 mg, 0.511 mmol, 1 equiv.) was weighed inside a glovebox in a 20 ml vial. 1,1'-Bis[bis(trifluoromethyl)phosphino]ferrocene, **r**, (533 mg, 1.02 mmol, 2 equiv.) was weighed inside the same

glovebox in a 3 ml vial. The weighed 1,1'-bis[bis(trifluoromethyl)phosphino]ferrocene was dissolved in 2 ml of dry THF and transferred to the vial containing the weighed $[Rh(COE)_2(\mu\text{-}Cl)]_2$ An additional, 2-3 ml of dry THF was added to the reaction vial. A magnetic stir bar was added to the vial. The vial was capped and the reaction was stirred overnight at room temperature. The resulting solution was concentrated under vacuum. Dry pentane (10 ml) was added to the vial to precipitate a yellow solid. The heterogeneous solution was filtered on a glass frit. The collected solid was washed with additional pentane (3 x 5 ml), transferred to a tared 20 ml vial, and dried under vacuum. The resulting solid was used as collected (204 mg, 0.154 mmol, 30 % yield).

$^1$H NMR: (500 MHz, $C_6D_6$) δ 4.34 (s, 8H), 3.66 (s, 8H) ppm.

$^{31}P\{^1H\}$ NMR: (202 MHz, $C_6D_6$) δ 67.25 (m) ppm.

### 4.3.8 Synthesis of 1,1'-bis[bis(pentafluorophenyl)phosphino]ferrocene, **s**.[161]

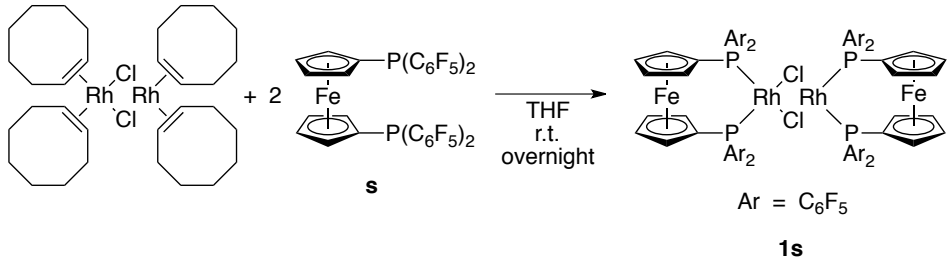



A 250 ml Schlenk flask was charged with magnesium turnings (0.38 g, 15.6 mmol, 6 equiv.) and a magnetic stir bar and purged of air and moisture by applying vacuum and $N_2$ successively, 3 times. The Schlenk flask was placed under an $N_2$ atmosphere. Dry $Et_2O$ (60 ml) was added to the flask by syringe. A solution of bromopentafluorobenzene (1.29 ml, 2.55 g, 10.3 mmol, 4 equiv.) in dry $Et_2O$ (20 ml) was prepared in a separate 50 ml Schlenk flask under an $N_2$ atmosphere and slowly cannulated in the flask containing the weighed magnesium. The solution began to reflux. The rate of addition was adjusted so that a gentle reflux was maintained. The solution became black. The solution was heated to 35 °C for an additional 15 minutes, then cooled to -78 °C by placing the Schlenk flask in a dry ice / acetone bath. A solution of 1,1'-bis(dichlorophosphino)ferrocene (1.0 g, 2.58 mmol, 1 equiv.) in dry $Et_2O$ (30 ml) was prepared inside a nitrogen-filled glovebox. The solution was loaded into a 60 ml syringe and removed from the glovebox (the syringe was stoppered with a rubber septum). The solution of 1,1'-bis(dichlorophosphino)ferrocene in $Et_2O$ was slowly added to the solution of pentafluorophenylmagensium bromide at -78 °C. The resulting solution was stirred overnight. The dry ice / acetone bath was allowed to warm to room temperature. Methanol (2 ml) was added to the reaction solution. The solvent was removed under vacuum. The Schlenk flask was brought into a nitrogen-filled glovebox. The residue from the reaction was dissolved in pentane and filtered through celite. The pentane solution was concentrated to approximately 1 ml total and place in the freezer. A yellow solid precipitated from solution. The solution was decanted and the collected solid was transferred to a tared 20 ml vial and dried under vacuum (0.28 g, 0.31 mmol, 12 % yield).

$^1$H NMR: (499.4MHz, toluene-$d_8$) δ 4.44 (s, broad, 4H), 4.15 (s, broad, 4H) ppm.

$^{31}P\{^1H\}$ NMR: (202 MHz, toluene-$d_8$) δ -54.7 (broad) ppm.

### 4.3.9 Synthesis of rhodium diphosphine complex, **1s**.



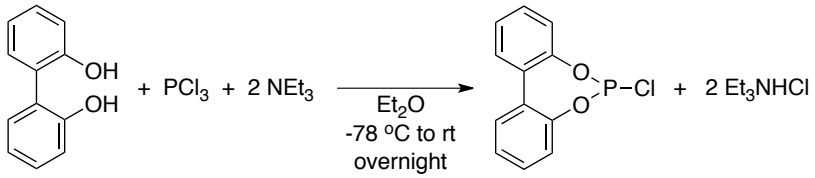

$[Rh(COE)_2(\mu\text{-}Cl)]_2$ (50 mg, 0.070 mmol, 1 equiv.) was weighed inside a glovebox in a 20 ml vial. 1,1'-Bis[bis(pentafluorophenyl)phosphino]ferrocene, **s**, (128 mg, 0.140 mmol, 2 equiv.) was weighed inside the same glovebox in a 3 ml vial. The weighed 1,1'-bis[bis(pentafluorophenyl)phosphino]ferrocene was dissolved in 2 ml of dry THF and transferred to the vial containing the weighed $[Rh(COE)_2(\mu\text{-}Cl)]_2$ An additional, 2-3 ml of dry THF was added to the reaction vial. A magnetic stir bar was added to the vial. The vial was capped and the reaction was stirred overnight at room temperature. The resulting solution was concentrated under vacuum. Dry pentane (10 ml) was added to the vial to precipitate a yellow solid. The heterogeneous solution was filtered on a glass frit. The collected solid was washed with additional pentane (3 x 5 ml), transferred to a tared 20 ml vial, and dried under vacuum. The resulting solid was used as collected (68 mg, 0.032 mmol, 46 % yield).

$^1$H NMR: (400 MHz, THF-$d_8$) δ 4.61 (s, 8H), 4.38 (s, 8H) ppm.

$^{19}$F NMR: (376 MHz, THF-$d_8$) δ -126.02, -152.72, -163.31 (t, J = 20 Hz) ppm.

$^{31}$P{$^1$H} NMR: (162 MHz, THF-$d_8$) δ 16.36 (J = 218 Hz) ppm.

### 4.3.10 Synthesis of 2,2'-Biphenylylene phosphorochloridite.



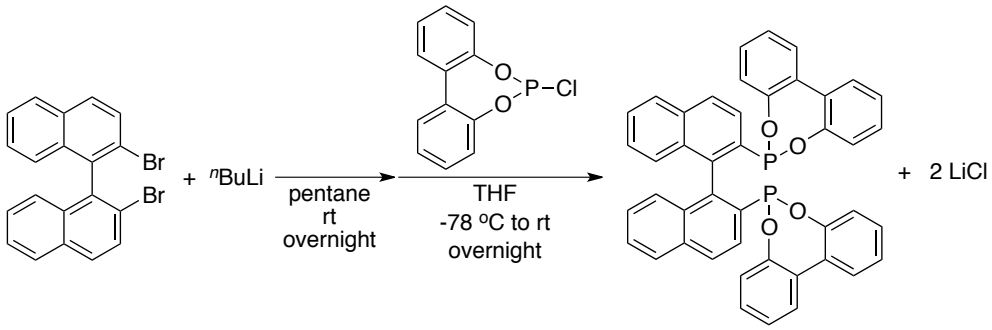

A 250 ml Schlenk flask, equipped with a magnetic stir bar was removed from an oven and connected to a Schlenk manifold and purged of $O_2$ and moisture by successively applying vacuum and $N_2$ (3x). The Schlenk flask was opened to $N_2$, then charged with $PCl_3$ (6.35 ml, 10 g, 72.8 mmol, 1 equiv.) and toluene (80 ml). 2,2'-Biphenol (13.6 g, 73.0 mmol, 1 equiv.) was weighed inside a glovebox in a 20 ml vial and dissolved in dry toluene (20 ml). The resulting 2,2'-biphenol solution was loaded into a 25 ml syringe. A rubber septum was placed on the needle of the syringe to isolate the contents from the box atmosphere, and the syringe was removed from the glovebox. The 2,2'-biphenol solution was slowly added to the $PCl_3$ solution at room temperature. The reaction flask was placed in

a dry ice / acetone bath. $NEt_3$ (20.3 ml, 14.7 g, 146 mmol, 2 equiv.), distilled from CaH2 was loaded into a 25 ml syringe and added slowly to the solution of $PCl_3$ and 2,2'-biphenol at -78 °C. The reaction was slowly warmed to room temperature and stirred overnight. A white precipitate ($Et_3NHCl$) formed. The heterogeneous solution was filtered through celite into a second 250 ml Schlenk flask, purged of $O_2$ and moisture beforehand and equipped with a magnetic stir bar. The collected solid was washed with additional toluene (3 x 20 ml). The filter stick was removed from the second Schlenk flask under a high pressure of $N_2$ and replaced with a rubber septum. The collected filtrate was concentrated under vacuum to yield a white solid (17.5 g, 69.8 mmol, 96 % yield).

$^1$H NMR: (399.9 MHz, THF-$d_8$) δ 7.57 (dd, J = 8 Hz, J = 2 Hz, 2H), 7.44 (triplet of doublets, J = 8Hz, J = 2 Hz, 2H), 7.38 (t, broad, J = 8 Hz, 2H), 7.26 (d, broad, J = 8 Hz, 2H) ppm.

$^{31}$P{$^1$H} NMR: (161.9 MHz, THF-$d_8$) δ 176.8.

### 4.3.11 Synthesis of 2,2'-bis(dibenzo[*d*,*f*][1,3,2]dioxaphosphepin-6-yl)-binaphthyl, **t.**




**t**

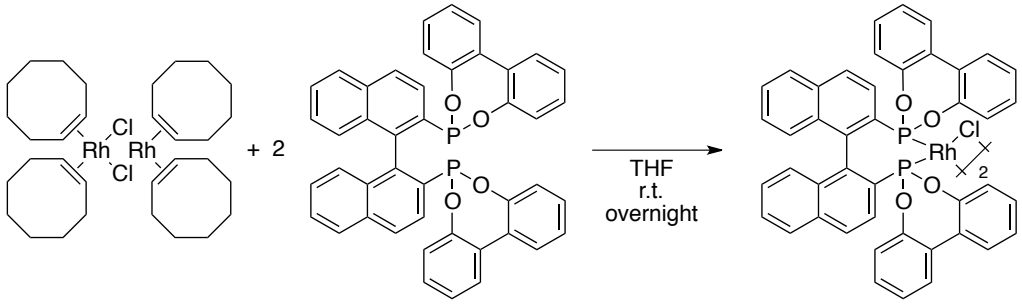
2,2'-Dibromo-1,1'-binaphthyl (1.0 g, 2.4 mmol, 1 equiv.) was weighed inside a glovebox in a 20 ml vial. The majority of the weighed solid was transferred to a 100 ml Schlenk flask as a solid. The remainder of the weighed 2,2'-dibromo-1,1'-binaphthyl was transferred to the 100 ml Schlenk flask with the aid of added pentane (~ 20 ml total). Additional pentane (~ 20 ml) was added to the flask. The flask was equipped with a magnetic stir bar. The 2,2'-dibromo-1,1'-binaphthyl solution was stirred inside the glovebox at room temperature. A solution of $^n$BuLi in hexanes (1.6 M, 3.8 ml, 6.1 mmol, 2.5 equiv.) was added to 2,2'-dibromo-1,1'-binaphthyl at room temperature. The flask was sealed with a rubber septum, and the resulting solution was stirred overnight inside the glovebox at room temperature. A white precipitate persisted throughout the reaction. The Schlenk flask was removed from the glovebox and connected to a Schlenk manifold. The hose connecting the flask to the manifold was purged of $O_2$ and moisture by successively applying vacuum and $N_2$. The hose was then place under a positive $N_2$ atmosphere and the Schlenk flask opened to $N_2$. The flask was placed in a dry ice / acetone bath. 2,2'-Biphenylylene phosphorochloridite (1.6 g, 6.4 mmol, 2.6 equiv.) was weighed inside the glovebox in a 20 ml vial. The weighed 2,2'-biphenylylene phosphorochloridite was dissolved in 10 ml of pentane and loaded into a 25 ml syringe. A rubber septum was placed on the end of the needle of the syringe, and the syringe was removed from the

glovebox. The solution of 2,2'-biphenylylene phosphorochloridite was added slowly to the solution of 2,2'-dilithiobinaphthyl at -78 °C. The reaction was warmed to room temperature and stirred overnight. The solvent was removed under vacuum. The residual solid was dissolved in benzene (60 ml) and filtered through celite into a 250 ml Schlenk flask equipped with a magnetic stir bar and purged of $O_2$ and moisture. The collected solid was washed with additional benzene (3 x 10 ml). The filter stick on the 250 ml Schlenk flask was replaced with a rubber septum under a high $N_2$ pressure. The benzene solvent was removed under vacuum to yield a white solid. (0.50 g, 0.73 mmol, 30 % yield).

$^1$H NMR: (399.9 MHz, toluene-$d_8$) δ 7.30 (d, J = 8 Hz, 2H), 7.17 (dd, J = 8 Hz, J = 2 Hz, 2H), 7.12-7.01 (overlapping signals, m, 8H), 7.00-6.83 (overlapping signals, m, 16H) ppm.

$^{31}$P{$^1$H} NMR: (161.9 MHz, toluene-$d_8$) δ 145.62.

### 4.3.12 Synthesis of rhodium diphosphonite chloride complex, **1t**.



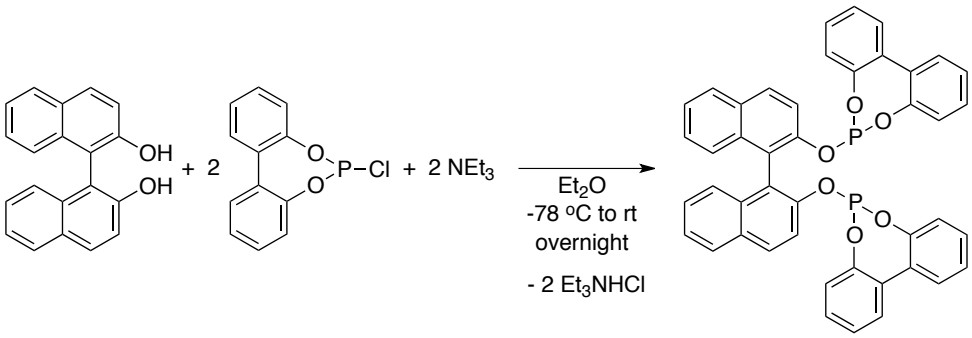

**t** **1t**

$[Rh(COE)_2(\mu\text{-}Cl)]_2$ (200 mg, 0.279 mmol, 1 equiv.) was weighed inside a glovebox in a 20 ml vial. 2,2'-Bis(dibenzo[*d*,*f*][1,3,2]dioxaphosphepin-6-yl)-binaphthyl, **t,** (381 mg, 0.558 mmol, 2 equiv.) was weighed inside the same glovebox in a 3 ml vial. The weighed 2,2'-bis(dibenzo[*d*,*f*][1,3,2]dioxaphosphepin-6-yl)-binaphthyl was dissolved in 2 ml of dry THF and transferred to the vial containing the weighed $[Rh(COE)_2(\mu\text{-}Cl)]_2$ An additional, 2-3 ml of dry THF was added to the reaction vial. A magnetic stir bar was added to the vial. The vial was capped and the reaction was stirred overnight at room temperature. The resulting solution was concentrated under vacuum. Dry $Et_2O$ (10 ml) was added to the vial to precipitate a yellow solid. The heterogeneous solution was filtered on a glass frit. The collected solid was washed with additional $Et_2O$ (3 x 5 ml), transferred to a tared 20 ml vial, and dried under vacuum. The resulting solid was used as collected (413 mg, 0.252 mmol, 90 % yield).

$^1$H NMR: (399.9 MHz, $CD_2Cl_2$) δ 7.54 (s, broad, 8H), 7.49 (d, J= 8 Hz, 2H), 7.41 (d, J = 8 Hz, 4H), 7.38-7.16 (overlapping signals, m, 32H), 7.12 (d, J = 7Hz, 4H), 6.95 (d, J = 7 Hz, 2H) 6.67 (m, 4H) ppm.

$^{31}$P{$^1$H} NMR: (202 MHz, $CD_2Cl_2$) δ 131.87 (d, J = 306 Hz) ppm.

### 4.3.13 Synthesis of 2,2'-bis[(1,1'-biphenyl-2,2'-diyl)phosphite]- 1,1'-binaphthyl, **u**.



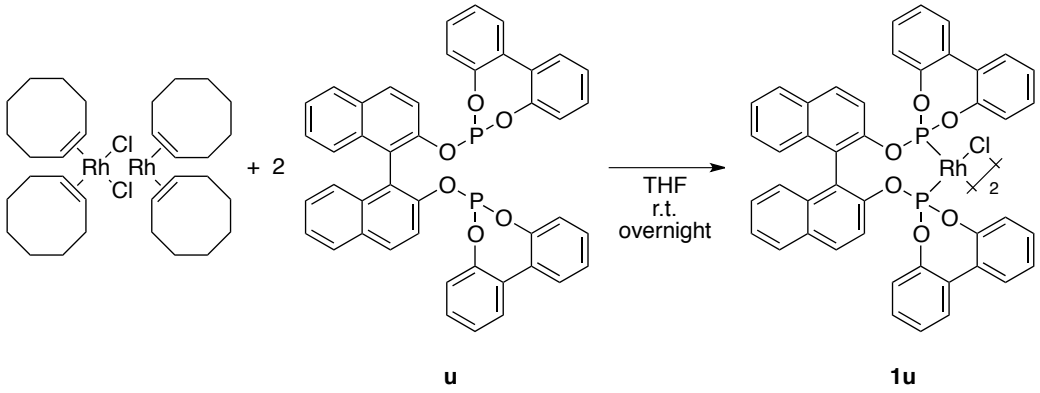

**u**

2,2'-Binaphthol (1.55 g, 5.4 mmol, 1 equiv.) was weighed inside a glovebox in a 20 ml vial. The majority of the weighed solid was transferred to a 100 ml Schlenk flask as a solid. The remainder of the weighed 2,2'-binaphthol was transferred to the 100 ml Schlenk flask with the aid of added toluene (~ 20 ml total). Additional toluene (~ 20 ml) was added to the flask. The flask was equipped with a magnetic stir bar, and was sealed with a rubber septum. The Schlenk flask was then removed from the glovebox and connected to a Schlenk manifold. The hose connecting the flask to the manifold was purged of $O_2$ and moisture by successively applying vacuum and $N_2$. The hose was place under a positive $N_2$ atmosphere and the Schlenk flask opened to $N_2$. 2,2'-Biphenylylene phosphorochloridite (1.6 g, 6.4 mmol, 2.6 equiv.) was weighed inside the glovebox in a 20 ml vial. The weighed 2,2'-biphenylylene phosphorochloridite was dissolved in 10 ml of toluene and loaded into a 25 ml syringe. A rubber septum was placed on the end of the needle of the syringe, and the syringe was removed from the glovebox. The solution of 2,2'-biphenylylene phosphorochloridite was added slowly to the solution of 2,2'-binaphthol at room temperature. The reaction flask was placed in a dry ice / acetone bath. $NEt_3$ (2.14 ml, 1.7 g, 16.5 mmol, 3 equiv.), distilled from $CaH_2$ was loaded into a 6 ml syringe and added to the solution of 2,2'-biphenylylene phosphorochloridite and 2,2'-binaphthol. The reaction was warmed to room temperature and stirred overnight. The resulting solution was filtered through celite into a 250 ml Schlenk flask equipped with a magnetic stir bar and purged of $O_2$ and moisture. The collected solid was washed with additional toluene (3 x 10 ml). The filter stick on the 250 ml Schlenk flask was replaced with a rubber septum under a high $N_2$ pressure. The toluene solvent was removed under vacuum to yield a white solid. (1.4 g, 1.96 mmol, 36 % yield).

$^1$H NMR: (499.9 MHz, THF-$d_8$) δ 8.06 (d, J = 9 Hz, 2H), 7.96 (d, J = 8 Hz, 2H), 7.53 (d, J = 9 Hz, 2H), 7.38 (m, 2H) 7.32-7.15 (overlapping signals, m, 8H), 7.10 (m, 4H), 7.06 (triplet of doublets, J = 8 Hz, J = 1Hz, 2H), 6.99 (triplet of doublets, J = 8 Hz, J = 2 Hz, 2H), 6.59 (m, 2H), 6.36 (d, J = 8 Hz, 2H) ppm.

$^{31}$P{$^1$H} NMR: (161.9 MHz, THF-$d_8$) δ 144.26 ppm.

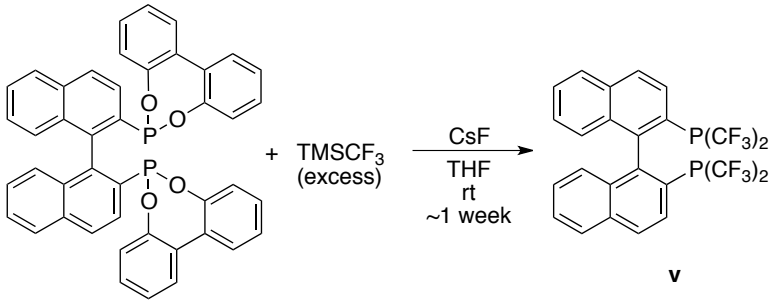
### 4.3.14 Synthesis of rhodium diphosphite chloride complex, **1u**.




**u** **1u**

$[Rh(COE)_2(\mu\text{-}Cl)]_2$ (200 mg, 0.279 mmol, 1 equiv.) was weighed inside a glovebox in a 20 ml vial. 2,2'-Bis[(1,1'-biphenyl-2,2'-diyl)phosphite]- 1,1'-binaphthyl, **u,** (398 mg, 0.557 mmol, 2 equiv.) was weighed inside the same glovebox in a 3 ml vial. The weighed 2,2'-bis[(1,1'-biphenyl-2,2'-diyl)phosphite]- 1,1'-binaphthyl was dissolved in 2 ml of dry THF and transferred to the vial containing the weighed $[Rh(COE)_2(\mu\text{-}Cl)]_2$ An additional, 2-3 ml of dry THF was added to the reaction vial. A magnetic stir bar was added to the vial. The vial was capped and the reaction was stirred overnight at room temperature. The resulting solution was concentrated under vacuum. Dry $Et_2O$ (10 ml) was added to the vial to precipitate a yellow solid. The heterogeneous solution was filtered on a glass frit. The collected solid was washed with additional $Et_2O$ (3 x 5 ml), transferred to a tared 20 ml vial, and dried under vacuum. The resulting solid was used as collected (415 mg, 0.243 mmol, 87 % yield). The complex was insoluble in all solvents tried.

### 4.3.15 Synthesis of 2,2'-Bis[bis(trifluoromethyl)phosphino]-1,1'-binaphthyl, **v**.




**t** **v**

2,2'-Bis[bis(trifluoromethyl)phosphino]-1,1'-binaphthyl, **u**, was synthesized in two steps from 2,2'-dibromo-1,1'-binaphthhyl (5.0 g, 12.1 mmol, 1 equiv.), $^n$BuLi (1.6 M in hexanes, 16.7 ml, 26.7 mmol, 2.2 equiv.), 2,2'-biphenylylene phosphorochloridite (9.1 g, 36.3 mmol, 3 equiv.), $TMSCF_3$ (10.8 ml, 10.4 g, 73.1 mmol, 6.0

equiv.), and CsF (0.74 g, 4.9 mmol, 0.40 equiv.). In this case, no efforts were made to isolate the 2,2'-bis(dibenzo[*d*,*f*][1,3,2]dioxaphosphepin-6-yl)-binaphthyl (**t**) formed by the reactions of 2,2'-dibromo-1,1'-binaphthhyl, $^{n}$BuLi, and 2,2'-biphenylylene phosphorochloridite.

2,2'-Bis(dibenzo[*d*,*f*][1,3,2]dioxaphosphepin-6-yl)-binaphthyl, **t**, was synthesized according to the procedures described above. The crude product was dissolved in $Et_2O$ (60 ml) and transferred to a 250 ml Schlenk flask equipped with a magnetic stir bar and purged of $O_2$ and moisture (the Schlenk flask was connected to a Schlenk manifold and placed under an $N_2$ atmosphere). Cesium fluoride (0.74 g, 4.9 mmol, 0.40 equiv.) weighed inside the glovebox in a 3 ml vial. Dry THF (2 ml) was added to the cesium fluoride, and the resulting solution was loaded into a 6 ml syringe with a 16 gauge needle. A septum was placed on the needle and the syringe containing the weighed cesium fluoride was removed from the glovebox. The cesium fluoride solution was added to the solution of 2,2'-bis(dibenzo[*d*,*f*][1,3,2]dioxaphosphepin-6-yl)-binaphthyl (**t**) at room temperature. Ruppert's reagent, $TMSCF_3$ (10.8 ml, 10.4 g, 73.1 mmol, 6.0 equiv.), was loaded into a syringe and added slowly to the solution of 2,2'-bis(dibenzo[*d*,*f*][1,3,2]dioxaphosphepin-6-yl)-binaphthyl (**t**) and CsF at room temperature (caution: the resulting reaction is exothermic and possibly autocatalytic). The resulting solution was stirred for approximately 1 week at room temperature. The reaction became dark brown. The progress of the reaction was monitored by $^{31}$P and $^{19}$F NMR spectroscopy. When the reaction was complete, the solvent was removed under vacuum. The residual solid was dissolved in hexanes and passed through a column of silica gel. The colorless product was collected, concentrated, crystallized from MeOH, and dried under vacuum (3.6 g, 6.1 mmol, 50 % overall yield).

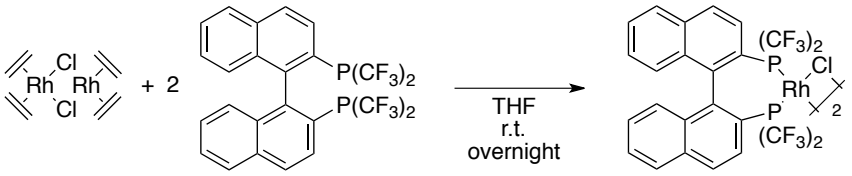
$^{1}$H NMR: (499.9 MHz, $CDCl_3$) δ 7.95 (d, *J* = 8 Hz, 2H), 7.89 (d, *J* = 9 Hz, 2H), 7.85 (d, *J* = 9 Hz, 2H), 7.52 (t, *J* = 8 Hz, 2H), 7.33 (t, *J* = 8 Hz, 2H), 7.13 (d, *J* = 9 Hz, 2H) ppm.

$^{13}$C{$^{1}$H} NMR: (125.6 MHz, toluene-$d_8$) δ 137.3, 133.5, 132.6, 130.2, 130.0, 128.5, 127.6, 126.5, 126.0, 122.9 ppm.

$^{19}$F NMR (376 MHz, THF) δ -52.52 (dd, $J^{F-F}$ = 7 Hz, $J^{F-P}$ = 82 Hz), -53.75 (dd, $J^{F-F}$ = 7 Hz, $J^{F-P}$ = 81 Hz).

$^{31}$P NMR (162 MHz, THF) δ -7.86 (septet, J = 82 Hz).

### 4.3.16 Synthesis of 2,2'-Bis[bis(trifluoromethyl)phosphino]-1,1'-binaphthyl rhodium chloride complex **1v**.




**v** **1v**

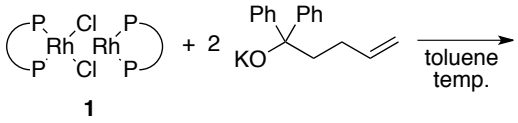
$[Rh(C_2H_4)_2(\mu\text{-}Cl)]_2$ (100 mg, 0.257 mmol, 1 equiv.) was weighed inside a glovebox in a 20 ml vial. 2,2'-Bis[bis(trifluoromethyl)phosphino]-1,1'-binaphthyl, **v**, (304 mg, 0.515 mmol, 2 equiv.) was weighed inside the same glovebox in a 3 ml vial. The weighed 2,2'-bis[bis(trifluoromethyl)phosphino]-1,1'-binaphthyl was dissolved in 2 ml of dry THF and transferred to the vial containing the weighed $[Rh(COE)_2(\mu\text{-}Cl)]_2$ An additional, 2-3 ml of dry THF was added to the reaction vial. A magnetic stir bar was added to the vial. The vial was capped and the reaction was

stirred overnight at room temperature. The resulting solution was concentrated under vacuum. Dry $Et_2O$ (10 ml) was added to the vial to precipitate a tan solid. The heterogeneous solution was filtered on a glass frit. The collected solid was washed with additional $Et_2O$ (3 x 5 ml), transferred to a tared 20 ml vial, and dried under vacuum. The resulting solid was used as collected (207 mg, 0.142 mmol, 55 % yield).

$^1$H NMR: (399.9 MHz, toluene-$d_8$) δ 7.61 (d, broad, J = 9 Hz, 2H), 7.53 (d, broad, J = 8 Hz, 2H), 7.41 (d, broad, J = 9 Hz, 2H), 7.17-7.07 (overlapping signals, broad, 6H) ppm.

$^{31}$P{$^1$H} NMR: (161.9 MHz, toluene-$d_8$) δ 78.5 (m, broad) ppm.

### 4.3.17 Preliminary reactions of rhodium chloride complexes, **1q-v**.




Rhodium chloride complexes **1q-v** were weighed inside a glovebox in a 3 ml vial (0.009 mmol). The complexes were dissolved in either toluene or THF (0.4 ml) and transferred to a screw cap NMR tube. The NMR tubes were capped with septum-bearing caps. 1,1-Diphenyl-4-penten-1-ol and KH were weighed inside a glovebox in a 3 ml vials (0.018 mmol). The alcohol was dissolved in either toluene or THF (0.1 ml) and transferred to the vial containing the weighed KH. The reagents were mixed together using a 250 μL syringe. The product was loaded into the 250 μL syringe and the syringe was stoppered with a rubber septum. The syringe and NMR tube were removed from the box. The NMR tube was placed in a dry ice / acetone bath. An NMR probe was cooled to -50 °C. The potassium alkoxide solution was syringed into the screw cap NMR tube. The NMR tube was shaken briefly to mix the two reagents. NMR spectra ($^1$H and $^{31}$P) were collected at -50 °C. The NMR tube was returned to the dry ice / acetone bath. The NMR probe was warmed to the appropriate temperature and set-up to collect a series of $^1$H NMR spectra over the course of the next several hours. The NMR tube was returned to the NMR probe and spectra were collected every 2-5 minutes for the next several hours or until the reactions were complete.

References


(1) (a) Muller, T. E.; Beller, M. *Chem Rev* **1998**, *98*, 675(b) Muller, T. E.; Hultzsch, K. C.; Yus, M.; Foubelo, F.; Tada, M. *Chem Rev* **2008**, *108*, 3795.

(2) (a) Gagne, M. R.; Marks, T. J. *J Am Chem Soc* **1989**, *111*, 4108(b) Gagne, M. R.; Stern, C. L.; Marks, T. J. *J Am Chem Soc* **1992**, *114*, 275(c) Giardello, M. A.; Conticello, V. P.; Brard, L.; Gagne, M. R.; Marks, T. J. *J Am Chem Soc* **1994**, *116*, 10241(d) Li, Y. W.; Marks, T. J. *Organometallics* **1996**, *15*, 3770(e) Hong, S.; Marks, T. J. *Accounts Chem Res* **2004**, *37*, 673.

(3) The rate expressions for the intermolecular hydroaminations of alkenes show a first order dependence on catalyst concentration a first order dependence on alkene concentration and a zero-order dependence on amine concentration.

(4) Manna, K.; Kruse, M. L.; Sadow, A. D. *Acs Catal* **2011**, *1*, 1637.

(5) Crimmin, M. R.; Casely, I. J.; Hill, M. S. *J Am Chem Soc* **2005**, *127*, 2042.

(6) Dunne, J. F.; Fulton, D. B.; Ellern, A.; Sadow, A. D. *J Am Chem Soc* **2010**, *132*, 17680.

(7) Tobisch, S. *Chem-Eur J* **2011**, *17*, 14974.

(8) (a) Walsh, P. J.; Baranger, A. M.; Bergman, R. G. *J Am Chem Soc* **1992**, *114*, 1708(b) Baranger, A. M.; Walsh, P. J.; Bergman, R. G. *J Am Chem Soc* **1993**, *115*, 2753.

(9) Kim, H.; Lee, P. H.; Livinghouse, T. *Chemical Communications* **2005**, 5205.

(10) (a) Bexrud, J. A.; Beard, J. D.; Leitch, D. C.; Schafer, L. L. *Org Lett* **2005**, *7*, 1959(b) Thomson, R. K.; Bexrud, J. A.; Schafer, L. L. *Organometallics* **2006**, *25*, 4069.

(11) Allan, L. E. N.; Clarkson, G. J.; Fox, D. J.; Gott, A. L.; Scott, P. *J Am Chem Soc* **2010**, *132*, 15308.

(12) Reznichenko, A. L.; Hultzsch, K. C. *Organometallics* **2009**, *29*, 24.

(13) Knight, P. D.; Munslow, I.; O'Shaughnessy, P. N.; Scott, P. *Chemical Communications* **2004**, 894.

(14) Gribkov, D. V.; Hultzsch, K. C. *Angew Chem Int Edit* **2004**, *43*, 5542.

(15) Coulson, D. R. *Tetrahedron Lett* **1971**, 429.

(16) Casalnuovo, A. L.; Calabrese, J. C.; Milstein, D. *J Am Chem Soc* **1988**, *110*, 6738.

(17) (a) Hesp, K. D.; Stradiotto, M. *Org Lett* **2009**, *11*, 1449(b) Hesp, K. D.; Tobisch, S.; Stradiotto, M. *J Am Chem Soc* **2010**, *132*, 413.

(18) (a) Cochran, B. M.; Michael, F. E. *J Am Chem Soc* **2008**, *130*, 2786(b) Michael, F. E.; Cochran, B. M. *J Am Chem Soc* **2006**, *128*, 4246.

(19) Beller, M.; Eichberger, M.; Trauthwein, H. *Angewandte Chemie-International Edition in English* **1997**, *36*, 2225.

(20) (a) Takemiya, A.; Hartwig, J. F. *J Am Chem Soc* **2006**, *128*, 6042(b) Utsunomiya, M.; Kuwano, R.; Kawatsura, M.; Hartwig, J. F. *J Am Chem Soc* **2003**, *125*, 5608.

(21) Liu, Z.; Hartwig, J. F. *J Am Chem Soc* **2008**, *130*, 1570.

(22) Liu, Z. J.; Yamamichi, H.; Madrahimov, S. T.; Hartwig, J. F. *J Am Chem Soc* **2011**, *133*, 2772.

(23) Julian, L. D.; Hartwig, J. F. *J Am Chem Soc* **2010**, *132*, 13813.

(24) Ambuehl, J.; Pregosin, P. S.; Venanzi, L. M.; Ughetto, G.; Zambonelli, L. *Journal of Organometallic Chemistry* **1978**, *160*, 329.

(25) (a) Palumbo, R.; Derenzi, A.; Panunzi, A.; Paiaro, G. *J Am Chem Soc* **1969**, *91*, 3874(b) Panunzi, A.; Derenzi, A.; Paiaro, G. *J Am Chem Soc* **1970**, *92*, 3488(c) Panunzi, A.; Derenzi, A.; Palumbo, R.; Paiaro, G. *J Am Chem Soc* **1969**, *91*, 3879.

(26) (a) Brunet, J.-J.; Chu, N. C.; Diallo, O. *Organometallics* **2005**, *24*, 3104(b) Brunet, J. J.; Cadena, M.; Chu, N. C.; Diallo, O.; Jacob, K.; Mothes, E. *Organometallics* **2004**, *23*, 1264.

(27) (a) Karshtedt, D.; Bell, A. T.; Tilley, T. D. *J Am Chem Soc* **2005**, *127*, 12640(b) Mcbee, J. L.; Bell, A. T.; Tilley, T. D. *J Am Chem Soc* **2008**, *130*, 16562.

(28) Wang, X.; Widenhoefer, R. A. *Organometallics* **2004**, *23*, 1649.

(29) Bender, C. F.; Widenhoefer, R. A. *J Am Chem Soc* **2005**, *127*, 1070.

(30) (a) Lober, O.; Kawatsura, M.; Hartwig, J. F. *J Am Chem Soc* **2001**, *123*, 4366(b) Kawatsura, M.; Hartwig, J. F. *J Am Chem Soc* **2000**, *122*, 9546(c) Utsunomiya, M.; Hartwig, J. F. *J Am Chem Soc* **2003**, *125*, 14286(d) Johns, A. M.; Utsunomiya, M.; Incarvito, C. D.; Hartwig, J. F. *Journal of the American Chemical Society* **2006**, *128*, 1828(e) Minami, T.; Okamoto, H.; Ikeda, S.; Tanaka, R.; Ozawa, F.; Yoshifuji, M. *Angew Chem Int Edit* **2001**, *40*, 4501.

(31) Nettekoven, U.; Hartwig, J. F. *J Am Chem Soc* **2002**, *124*, 1166.

(32) Pawlas, J.; Nakao, Y.; Kawatsura, M.; Hartwig, J. F. *J Am Chem Soc* **2002**, *124*, 3669.

(33) (a) Zhang, J. L.; Yang, C. G.; He, C. *J Am Chem Soc* **2006**, *128*, 1798(b) Kovacs, G.; Ujaque, G.; Lledos, A. *J Am Chem Soc* **2008**, *130*, 853(c) Han, X. Q.; Widenhoefer, R. A. *Angew Chem Int Edit* **2006**, *45*, 1747.

(34) Rosenfeld, D. C.; Shekhar, S.; Takemiya, A.; Utsunomiya, M.; Hartwig, J. F. *Org Lett* **2006**, *8*, 4179.

(35) (a) Utsunomiya, M.; Hartwig, J. F. *J Am Chem Soc* **2004**, *126*, 2702(b) Takaya, J.; Hartwig, J. F. *J Am Chem Soc* **2005**, *127*, 5756.

(36) Hegedus, L. S.; Allen, G. F.; Waterman, E. L. *J Am Chem Soc* **1976**, *98*, 2674.

(37) Hegedus, L. S.; Allen, G. F.; Bozell, J. J.; Waterman, E. L. *J Am Chem Soc* **1978**, *100*, 5800.

(38) Hegedus, L. S.; McKearin, J. M. *J Am Chem Soc* **1982**, *104*, 2444.

(39) Rönn, M.; Bäckvall, J.-E.; Andersson, P. G. *Tetrahedron Lett* **1995**, *36*, 7749.

(40) Larock, R. C.; Hightower, T. R.; Hasvold, L. A.; Peterson, K. P. *The Journal of Organic Chemistry* **1996**, *61*, 3584.

(41) (a) Brice, J. L.; Harang, J. E.; Timokhin, V. I.; Anastasi, N. R.; Stahl, S. S. *J Am Chem Soc* **2005**, *127*, 2868(b) Kotov, V.; Scarborough, C. C.; Stahl, S. S. *Inorg Chem* **2007**, *46*, 1910(c) Stahl, S. S. *Angewandte Chemie International Edition* **2004**, *43*, 3400.

(42) Liu, G. S.; Stahl, S. S. *J Am Chem Soc* **2007**, *129*, 6328.

(43) Pugin, B.; Venanzi, L. M. *J Am Chem Soc* **1983**, *105*, 6877.

(44) Bozell, J. J.; Hegedus, L. S. *The Journal of Organic Chemistry* **1981**, *46*, 2561.

(45) Hosokawa, T.; Takano, M.; Kuroki, Y.; Murahashi, S.-I. *Tetrahedron Lett* **1992**, *33*, 6643.

(46) Timokhin, V. I.; Anastasi, N. R.; Stahl, S. S. *J Am Chem Soc* **2003**, *125*, 12996.

(47) Timokhin, V. I.; Stahl, S. S. *J Am Chem Soc* **2005**, *127*, 17888.

(48) Brunet, J. J.; Commenges, G.; Neibecker, D.; Philippot, K.; Rosenberg, L. *Inorg Chem* **1994**, *33*, 6373.

(49) Hintermann, L. *Top Organometal Chem* **2010**, *31*, 123.

(50) Dang, T. T.; Boeck, F.; Hintermann, L. *J Org Chem* **2011**, *76*, 9353.

(51) (a) Hori, K.; Kitagawa, H.; Miyoshi, A.; Ohta, T.; Furukawa, I. *Chem Lett* **1998**, 1083(b) Oe, Y.; Ohta, T.; Ito, Y. *Chemical Communications* **2004**, 1620(c) Oe, Y.; Ohta, T.; Ito, Y. *Synlett* **2005**, 179.

(52) Komeyama, K.; Morimoto, T.; Nakayama, Y.; Takaki, K. *Tetrahedron Lett* **2007**, *48*, 3259.

(53) Qian, H.; Han, X. Q.; Widenhoefer, R. A. *J Am Chem Soc* **2004**, *126*, 9536.

(54) Yang, C. G.; He, C. *J Am Chem Soc* **2005**, *127*, 6966.

(55) Yang, C.-G.; Reich, N. W.; Shi, Z.; He, C. *Org Lett* **2005**, *7*, 4553.

(56) (a) Yu, X. H.; Seo, S.; Marks, T. J. *J Am Chem Soc* **2007**, *129*, 7244(b) Dzudza, A.; Marks, T. J. *Org Lett* **2009**, *11*, 1523(c) Seo, S. Y.; Yu, X. H.; Marks, T. J. *J Am Chem Soc* **2009**, *131*, 263(d) Dzudza, A.; Marks, T. J. *Chem-Eur J* **2010**, *16*, 3403(e) Weiss, C. J.; Marks, T. J. *Dalton T* **2010**, *39*, 6576.

(57) Hosokawa, T.; Maeda, K.; Koga, K.; Moritani, I. *Tetrahedron Lett* **1973**, *14*, 739.

(58) Hosokawa, T.; Ohkata, H.; Moritani, I. *Bulletin of the Chemical Society of Japan* **1975**, *48*, 1533.

(59) Hosokawa, T.; Miyagi, S.; Murahashi, S.; Sonoda, A. *The Journal of Organic Chemistry* **1978**, *43*, 2752.

(60) Hayashi, T.; Yamasaki, K.; Mimura, M.; Uozumi, Y. *J Am Chem Soc* **2004**, *126*, 3036.

(61) Trend, R. M.; Ramtohul, Y. K.; Stoltz, B. M. *J Am Chem Soc* **2005**, *127*, 17778.

(62) Hosokawa, T.; Hirata, M.; Murahashi, S.-I.; Sonoda, A. *Tetrahedron Lett* **1976**, *17*, 1821.

(63) Larock, R. C.; Hightower, T. R. *The Journal of Organic Chemistry* **1993**, *58*, 5298.

(64) Note: Other mechanisms for metal-catalyzed aminations and alkoxylations of alkenes include nucleophilic attacks onto cooridnated alkenes, nucleophilic attacks onto η6-arene complexes, nucleophilic attacks onto η3-benzyl and η3-allyl complexes, [2+2] cycloadditions of metal-imido complexes, and non-insertive proton coupled additions of amido ligands to alkenes

(65) (a) Cowan, R. L.; Trogler, W. C. *Organometallics* **1987**, *6*, 2451(b) Cowan, R. L.; Trogler, W. C. *J Am Chem Soc* **1989**, *111*, 4750.

(66) Ryu, J. S.; Li, G. Y.; Marks, T. J. *J Am Chem Soc* **2003**, *125*, 12584.

(67) Zhao, P. J.; Krug, C.; Hartwig, J. F. *J Am Chem Soc* **2005**, *127*, 12066.

(68) Hoover, J. M.; DiPasquale, A.; Mayer, J. M.; Michael, F. E. *J Am Chem Soc* **2010**, *132*, 5043.

(69) (a) Hanley, P. S.; Markovic, D.; Hartwig, J. F. *J Am Chem Soc* **2010**, *132*, 6302(b) Hanley, P. S.; Hartwig, J. F. *J Am Chem Soc* **2011**, *133*, 15661.

(70) (a) Neukom, J. D.; Perch, N. S.; Wolfe, J. P. *J Am Chem Soc* **2010**, *132*, 6276(b) Neukom, J. D.; Perch, N. S.; Wolfe, J. P. *Organometallics* **2011**, *30*, 1269.

(71) White, P. B.; Stahl, S. S. *J Am Chem Soc* **2011**, *133*, 18594.

(72) Tsutsui, H.; Narasaka, K. *Chem Lett* **1999**, 45.

(73) Helaja, J.; Gottlich, R. *Chemical Communications* **2002**, 720.

(74) (a) Ney, J. E.; Wolfe, J. P. *Angew Chem Int Edit* **2004**, *43*, 3605(b) Lira, R.; Wolfe, J. P. *J Am Chem Soc* **2004**, *126*, 13906(c) Ney, J. E.; Wolfe, J. P. *J Am Chem Soc* **2005**, *127*, 8644(d) Yang, Q. F.; Ney, J. E.; Wolfe, J. P. *Org Lett* **2005**, *7*, 2575(e) Bertrand, M. B.; Neukom, J. D.; Wolfe, J. P. *J Org Chem* **2008**, *73*, 8851.

(75) Liu, G. S.; Stahl, S. S. *J Am Chem Soc* **2006**, *128*, 7179.

(76) Desai, L. V.; Sanford, M. S. *Angew Chem Int Edit* **2007**, *46*, 5737.

(77) (a) Du, H. F.; Yuan, W. C.; Zhao, B. G.; Shi, Y. *J Am Chem Soc* **2007**, *129*, 7496(b) Du, H. F.; Yuan, W. C.; Zhao, B. G.; Shi, Y. A. *J Am Chem Soc* **2007**, *129*, 11688(c) Du, H. F.; Zhao, B. G.; Shi, Y. *J Am Chem Soc* **2007**, *129*, 762(d) Zhao, B. G.; Du, H. F.; Cui, S. L.; Shi, Y. A. *J Am Chem Soc* **2010**, *132*, 3523.

(78) Muniz, K.; Hovelmann, C. H.; Streuff, J. *J Am Chem Soc* **2008**, *130*, 763.

(79) (a) Bryndza, H. E.; Calabrese, J. C.; Wreford, S. S. *Organometallics* **1984**, *3*, 1603(b) Bryndza, H. E. *Organometallics* **1985**, *4*, 406.

(80) Zhao, P. J.; Incarvito, C. D.; Hartwig, J. F. *J Am Chem Soc* **2006**, *128*, 9642.

(81) unpublished results.

(82) (a) Wolfe, J. P.; Rossi, M. A. *J Am Chem Soc* **2004**, *126*, 1620(b) Hay, M. B.; Hardin, A. R.; Wolfe, J. P. *J Org Chem* **2005**, *70*, 3099(c) Hay, M. B.; Wolfe, J. P. *J Am Chem Soc* **2005**, *127*, 16468.

(83) (a) Hatano, M.; Ito, O.; Suzuki, S.; Ishihara, K. *The Journal of Organic Chemistry* **2010**, *75*, 5008(b) Zhao, P.; Incarvito, C. D.; Hartwig, J. F. *J Am Chem Soc* **2006**, *128*, 9642.

(84) Kondo, T.; Tsunawaki, F.; Sato, R.; Ura, Y.; Wada, K.; Mitsudo, T.-a. *Chem Lett* **2003**, *32*, 24.

(85) (a) Dragoli, D. R.; Burdett, M. T.; Ellman, J. A. *J Am Chem Soc* **2001**, *123*, 10127(b) Schomaker, J. M.; Travis, B. R.; Borhan, B. *Org Lett* **2003**, *5*, 3089(c) Nicolai, S.; Waser, J. *Org Lett* **2011**, *13*, 6324(d) Bartoli, G.; Bosco, M.; Dalpozzo, R. *Tetrahedron Lett* **1985**, *26*, 115.

(86) Pei, T.; Wang, X.; Widenhoefer, R. A. *J Am Chem Soc* **2002**, *125*, 648.

(87) (a) Perlmutter, P.; Selajerern, W.; Vounatsos, F. *Organic & Biomolecular Chemistry* **2004**, *2*, 2220(b) Hoover, J. M.; DiPasquale, A.; Mayer, J. M.; Michael, F. E. *J Am Chem Soc* **2010**, *132*, 5043.

(88) (a) Luedtke, A. E.; Timberlake, J. W. *The Journal of Organic Chemistry* **1985**, *50*, 268(b) Miller, R. D.; Goelitz, P. *The Journal of Organic Chemistry* **1981**, *46*, 1616.

(89) (a) Marcelis, A. T. M.; Van der Plas, H. C.; Harkema, S. *The Journal of Organic Chemistry* **1985**, *50*, 270(b) House, H. O.; Manning, D. T.; Melillo, D. G.; Lee, L. F.; Haynes, O. R.; Wilkes, B. E. *The Journal of Organic Chemistry* **1976**, *41*, 855(c) Logothetis, A. L. *J Am Chem Soc* **1965**, *87*, 749.

(90) (a) Xie, Q.; Denton, R. W.; Parker, K. A. *Org Lett* **2008**, *10*, 5345(b) Ashby, E. C.; Park, B.; Patil, G. S.; Gadru, K.; Gurumurthy, R. *The Journal of Organic Chemistry* **1993**, *58*, 424(c) Juaristi, E.; Jimenez-Vazquez, H. A. *The Journal of Organic Chemistry* **1991**, *56*, 1623.

(91) (a) Ashby, E. C.; Deshpande, A. K.; Doctorovich, F. *The Journal of Organic Chemistry* **1993**, *58*, 4205(b) Ashby, E. C.; Coleman, D. *The Journal of Organic Chemistry* **1987**, *52*, 4554.

(92) (a) Kirchhoff, J. H.; Netherton, M. R.; Hills, I. D.; Fu, G. C. *J Am Chem Soc* **2002**, *124*, 13662(b) Netherton, M. R.; Fu, G. C. *Angewandte Chemie International Edition* **2002**, *41*, 3910(c) Hills, I. D.; Netherton, M. R.; Fu, G. C. *Angewandte Chemie International Edition* **2003**, *42*, 5749.

(93) Hartwig, J. F. *Organotransition Metal Chemistry; From Bonding to Catalysis*; 1 ed.; University Science Books: Sausalito, CA, 2010.

(94) Farina, V.; Krishnan, B. *J Am Chem Soc* **1991**, *113*, 9585.

(95) (a) Farina, V.; Kapadia, S.; Krishnan, B.; Wang, C.; Liebeskind, L. S. *The Journal of Organic Chemistry* **1994**, *59*, 5905(b) Amatore, C.; Bahsoun, A. A.; Jutand, A.; Meyer, G.; Ndedi, N.; Ricard, L. *J Am Chem Soc* **2003**, *125*, 4212.

(96) Korenaga, T.; Ko, A.; Uotani, K.; Tanaka, Y.; Sakai, T. *Angewandte Chemie International Edition* **2011**, *50*, 10703.

(97) Tolman, C. A. *Inorg Chem* **1972**, *11*, 3128.

(98) Thompson, W. H.; Sears, C. T. *Inorg Chem* **1977**, *16*, 769.

(99) Amatore, C.; Carre, E.; Jutand, A.; M'Barki, M. A. *Organometallics* **1995**, *14*, 1818.

(100) Amatore, C.; Jutand, A.; Meyer, G. *Inorganica Chimica Acta* **1998**, *273*, 76.

(101) (a) Abis, L.; Sen, A.; Halpern, J. *J Am Chem Soc* **1978**, *100*, 2915(b) Halpern, J. *Accounts Chem Res* **1982**, *15*, 332.

(102) Jones, W. D.; Kuykendall, V. L. *Inorg Chem* **1991**, *30*, 2615.

(103) Negishi, E.-i.; Takahashi, T.; Akiyoshi, K. *Journal of Organometallic Chemistry* **1987**, *334*, 181.

(104) Ariafard, A.; Yates, B. F. *Journal of Organometallic Chemistry* **2009**, *694*, 2075.

(105) Culkin, D. A.; Hartwig, J. F. *Organometallics* **2004**, *23*, 3398.

(106) Korenaga, T.; Abe, K.; Ko, A.; Maenishi, R.; Sakai, T. *Organometallics* **2010**, *29*, 4025.

(107) Hamann, B. C.; Hartwig, J. F. *J Am Chem Soc* **1998**, *120*, 3694.

(108) Mann, G.; Hartwig, J. F. *Tetrahedron Lett* **1997**, *38*, 8005.

(109) Mann, G.; Shelby, Q.; Roy, A. H.; Hartwig, J. F. *Organometallics* **2003**, *22*, 2775.

(110) The rate constant for the reductive elimination of 4-(3,5-di-tert-butylphenoxy)-benzonitrile from Pd(DPPF)(Ar1)(OAr2) (Ar1 = p-CN-C6H4; Ar2 = 3,5-(tBu)2-C6H3) at 105 °C is 1.0 x 10-4 s-1. The rate constant for the reductive elimination of 4-(3,5-di-tert-butylphenoxy)-benzonitrile from Pd(p-CF3-DPPF)(Ar1)(OAr2) (Ar1 = p-CN-C6H4; Ar2 = 3,5-(tBu)2-C6H3) at 105 °C is 2.0 x 10-4 s-1.

(111) Casalnuovo, A. L.; RajanBabu, T. V.; Ayers, T. A.; Warren, T. H. *J Am Chem Soc* **1994**, *116*, 9869.

(112) Goertz, W.; Keim, W.; Vogt, D.; Englert, U.; D. K. Boele, M.; A. van der Veen, L.; C. J. Kamer, P.; W. N. M. van Leeuwen, P. *Journal of the Chemical Society, Dalton Transactions* **1998**, 2981.

(113) Unruh, J. D.; Christenson, J. R. *Journal of Molecular Catalysis* **1982**, *14*, 19.

(114) Moser, W. R.; Papile, C. J.; Brannon, D. A.; Duwell, R. A.; Weininger, S. J. *Journal of Molecular Catalysis* **1987**, *41*, 271.

(115) van der Veen, L. A.; Boele, M. D. K.; Bregman, F. R.; Kamer, P. C. J.; van Leeuwen, P. W. N. M.; Goubitz, K.; Fraanje, J.; Schenk, H.; Bo, C. *J Am Chem Soc* **1998**, *120*, 11616.

(116) Hegedüs, C.; Madarász, J.; Gergely, I.; Szöllo˝sy, Á.; Monsees, A.; Riermeier, T.; Bakos, J. *Tetrahedron: Asymmetry* **2004**, *15*, 2507.

(117) RajanBabu, T. V.; Ayers, T. A. *Tetrahedron Lett* **1994**, *35*, 4295.

(118) Montelatici, S.; van der Ent, A.; Osborn, J. A.; Wilkinson, G. *Journal of the Chemical Society A: Inorganic, Physical, Theoretical* **1968**, 1054.

(119) Halpern, J.; Okamoto, T. *Inorganica Chimica Acta* **1984**, *89*, L53.

(120) (a) RajanBabu, T. V.; Ayers, T. A.; Casalnuovo, A. L. *J Am Chem Soc* **1994**, *116*, 4101(b) Gergely, I.; Hegedüs, C.; Szöllősy, Á.; Monsees, A.; Riermeier, T.; Bakos, J. *Tetrahedron Lett* **2003**, *44*, 9025(c) Herseczki, Z.; Gergely, I.; Hegedüs, C.; Szöllősy, Á.; Bakos, J. *Tetrahedron: Asymmetry* **2004**, *15*, 1673.

(121) Wu, H.-C.; Hamid, S. A.; Yu, J.-Q.; Spencer, J. B. *J Am Chem Soc* **2009**, *131*, 9604.

(122) Jacobsen, E. N.; Zhang, W.; Guler, M. L. *J Am Chem Soc* **1991**, *113*, 6703.

(123) Palucki, M.; Finney, N. S.; Pospisil, P. J.; Güler, M. L.; Ishida, T.; Jacobsen, E. N. *J Am Chem Soc* **1998**, *120*, 948.

(124) Burger, B. J.; Santarsiero, B. D.; Trimmer, M. S.; Bercaw, J. E. *J Am Chem Soc* **1988**, *110*, 3134.

(125) Malinoski, J. M.; Brookhart, M. *Organometallics* **2003**, *22*, 5324.

(126) Hanley, P. S.; Hartwig, J. F. *J Am Chem Soc* **2011**, *133*, 15661.

(127) Tolman, C. A. *J Am Chem Soc* **1970**, *92*, 2956.

(128) Tolman, C. A.; Seidel, W. C.; Gosser, L. W. *J Am Chem Soc* **1974**, *96*, 53.

(129) (a) Tolman, C. A. *Chem Rev* **1977**, *77*, 313(b) Musco, A.; Kuran, W.; Silvani, A.; Anker, M. W. *Journal of the Chemical Society, Chemical Communications* **1973**, 938(c) Kuran, W.; Musco, A. *Inorganica Chimica Acta* **1975**, *12*, 187(d) Mann, B. E.; Musco, A. *Journal of the Chemical Society, Dalton Transactions* **1975**, 1673.

(130) Clarke, M. L.; Heydt, M. *Organometallics* **2005**, *24*, 6475.

(131) Halpern, J.; Phelan, P. F. *J Am Chem Soc* **1972**, *94*, 1881.

(132) Matsumoto, M.; Yoshioka, H.; Nakatsu, K.; Yoshida, T.; Otsuka, S. *J Am Chem Soc* **1974**, *96*, 3322.

(133) Brady, R.; De Camp, W. H.; Flynn, B. R.; Schneider, M. L.; Scott, J. D.; Vaska, L.; Werneke, M. F. *Inorg Chem* **1975**, *14*, 2669.

(134) Frech, C. M.; Milstein, D. *J Am Chem Soc* **2006**, *128*, 12434.

(135) Carr, N.; Dunne, B. J.; Mole, L.; Orpen, A. G.; Spencer, J. L. *Journal of the Chemical Society, Dalton Transactions* **1991**, 863.

(136) (a) Johnson, L. K.; Killian, C. M.; Brookhart, M. *J Am Chem Soc* **1995**, *117*, 6414(b) Johnson, L. K.; Mecking, S.; Brookhart, M. *J Am Chem Soc* **1996**, *118*, 267.

(137) Deng, L.; Woo, T. K.; Cavallo, L.; Margl, P. M.; Ziegler, T. *J Am Chem Soc* **1997**, *119*, 6177.

(138) Ledford, J.; Shultz, C. S.; Gates, D. P.; White, P. S.; DeSimone, J. M.; Brookhart, M. *Organometallics* **2001**, *20*, 5266.

(139) van Leeuwen, P. W. N. M.; Kamer, P. C. J.; Reek, J. N. H.; Dierkes, P. *Chem Rev* **2000**, *100*, 2741.

(140) Sowa, J. R.; Zanotti, V.; Facchin, G.; Angelici, R. J. *J Am Chem Soc* **1992**, *114*, 160.

(141) Miedaner, A.; Haltiwanger, R. C.; DuBois, D. L. *Inorg Chem* **1991**, *30*, 417.

(142) (a) Curtis, C. J.; Miedaner, A.; Ellis, W. W.; DuBois, D. L. *J Am Chem Soc* **2002**, *124*, 1918(b) Raebiger, J. W.; Miedaner, A.; Curtis, C. J.; Miller, S. M.; Anderson, O. P.; DuBois, D. L. *J Am Chem Soc* **2004**, *126*, 5502(c) Nimlos, M. R.; Chang, C. H.; Curtis, C. J.; Miedaner, A.; Pilath, H. M.; DuBois, D. L. *Organometallics* **2008**, *27*, 2715.

(143) Kranenburg, M.; Kamer, P. C. J.; van Leeuwen, P. W. N. M. *European Journal of Inorganic Chemistry* **1998**, *1998*, 25.

(144) Kranenburg, M.; Kamer, P. C. J.; van Leeuwen, P. W. N. M.; Vogt, D.; Keim, W. *Journal of the Chemical Society, Chemical Communications* **1995**, 2177.

(145) Marcone, J. E.; Moloy, K. G. *J Am Chem Soc* **1998**, *120*, 8527.

(146) Zuidema, E.; van Leeuwen, P. W. N. M.; Bo, C. *Organometallics* **2005**, *24*, 3703.

(147) Kohara, T.; Yamamoto, T.; Yamamoto, A. *Journal of Organometallic Chemistry* **1980**, *192*, 265.

(148) Brown, J. M.; Guiry, P. J. *Inorganica Chimica Acta* **1994**, *220*, 249.

(149) Calhorda, M. J.; Brown, J. M.; Cooley, N. A. *Organometallics* **1991**, *10*, 1431.

(150) Kranenburg, M.; Kamer, P. C. J.; van Leeuwen, P. W. N. M. *European Journal of Inorganic Chemistry* **1998**, *1998*, 155.

(151) Fujita, K.-i.; Yamashita, M.; Puschmann, F.; Alvarez-Falcon, M. M.; Incarvito, C. D.; Hartwig, J. F. *J Am Chem Soc* **2006**, *128*, 9044.

(152) Carr, N.; Dunne, B. J.; Orpen, A. G.; Spencer, J. L. *Journal of the Chemical Society, Chemical Communications* **1988**, 926.

(153) Mole, L.; Spencer, J. L.; Carr, N.; Orpen, A. G. *Organometallics* **1991**, *10*, 49.

(154) Anderson, G. K.; Lumetta, G. J. *Organometallics* **1985**, *4*, 1542.

(155) Dekker, G. P. C. M.; Elsevier, C. J.; Vrieze, K.; Van Leeuwen, P. W. N. M. *Organometallics* **1992**, *11*, 1598.

(156) Dekker, G. P. C. M.; Elsevier, C. J.; Vrieze, K.; van Leeuwen, P. W. N. M.; Roobeek, C. F. *Journal of Organometallic Chemistry* **1992**, *430*, 357.

(157) Ogasawara, M.; Takizawa, K.-i.; Hayashi, T. *Organometallics* **2002**, *21*, 4853.

(158) Clark, T. J.; Rodezno, J. M.; Clendenning, S. B.; Aouba, S.; Brodersen, P. M.; Lough, A. J.; Ruda, H. E.; Manners, I. *Chemistry – A European Journal* **2005**, *11*, 4526.

(159) Schweizer, S.; Becht, J.-M.; Le Drian, C. *Advanced Synthesis & Catalysis* **2007**, *349*, 1150.

(160) Evans, L. A.; Fey, N.; Harvey, J. N.; Hose, D.; Lloyd-Jones, G. C.; Murray, P.; Orpen, A. G.; Osborne, R.; Owen-Smith, G. J. J.; Purdie, M. *J Am Chem Soc* **2008**, *130*, 14471.

(161) Gusev, O. V.; Peganova, T. y. A.; Kalsin, A. M.; Vologdin, N. V.; Petrovskii, P. V.; Lyssenko, K. A.; Tsvetkov, A. V.; Beletskaya, I. P. *Organometallics* **2006**, *25*, 2750.

(162) Tani, K.; Tanigawa, E.; Tatsuno, Y.; Otsuka, S. *Journal of Organometallic Chemistry* **1985**, *279*, 87.

(163) Anet, F. A. L.; Bavin, P. M. G. *Canadian Journal of Chemistry* **1957**, *35*, 1084.

(164) Hess, B. A.; Bailey, A. S.; Boekelheide, V. *J Am Chem Soc* **1967**, *89*, 2746.

(165) van der Veen, L. A.; Keeven, P. H.; Schoemaker, G. C.; Reek, J. N. H.; Kamer, P. C. J.; van Leeuwen, P. W. N. M.; Lutz, M.; Spek, A. L. *Organometallics* **2000**, *19*, 872.

(166) (a) Oita, K.; Gilman, H. *J Am Chem Soc* **1957**, *79*, 339(b) Chang, V. H. T.; Corey, J. Y. *Journal of Organometallic Chemistry* **1980**, *190*, 217(c) Kranenburg, M.; van der Burgt, Y. E. M.; Kamer, P. C. J.; van Leeuwen, P. W. N. M.; Goubitz, K.; Fraanje, J. *Organometallics* **1995**, *14*, 3081.

(167) McMurry, J. E.; Krepski, L. R. *The Journal of Organic Chemistry* **1976**, *41*, 3929.

(168) Bronger, R. P. J.; Kamer, P. C. J.; van Leeuwen, P. W. N. M. *Organometallics* **2003**, *22*, 5358.

(169) Velazco, E. J.; Caffyn, A. J. M.; Le Goff, X. F.; Ricard, L. *Organometallics* **2008**, *27*, 2402.

(170) Hariharasarma, M.; Lake, C. H.; Watkins, C. L.; Gray, G. M. *Organometallics* **1999**, *18*, 2593.

(171) Punji, B.; Mague, J. T.; Balakrishna, M. S. *Inorg Chem* **2007**, *46*, 10268.